Introduction to SOFT SOIL GEOTECHNIQUE

Content, Context and Application

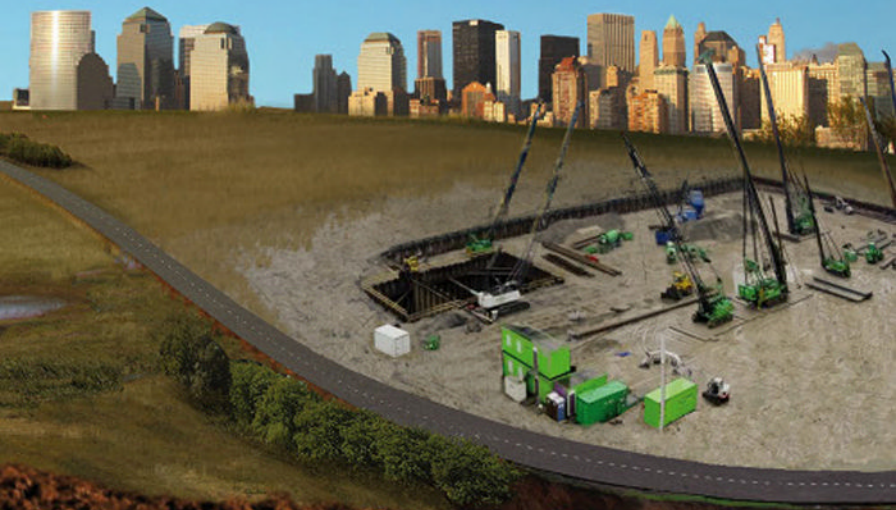

FRANS BARENDS

INTRODUCTION TO SOFT SOIL GEOTECHNIQUE

Content, Context and Application

This page intentionally left blank

INTRODUCTION TO SOFT SOIL GEOTECHNIQUE

Content, Context and Application

Frans B. J. Barends
Technical University Delft / Deltares
May 2011

IOS Press

Deltares provided financial sponsorship for this publication

© 2011 The author and IOS Press. All rights reserved

ISBN 978-1-60750-788-8 (print)
ISBN 987-1-60750-789-5 (online)

Publisher
IOS Press BV
Nieuwe Hemweg 6b
1013 BG Amsterdam
The Netherlands
Tel: +31-20-688 3355
Fax: +31-20-687 0019
Email: info@iospress.nl
www.iospress.nl

LEGAL NOTE
The author and the publisher are not responsible for the use that might be made of the information in this book.

PRINTED IN THE NETHERLANDS

FOREWORD

All over the world, habitable space in deltas and river basins is under increasing pressure from economic expansion, growing populations, subsidence and the impacts of climate change. It is expected that, within 40 years from now, about 80 percent of all people will live in deltaic regions. The Netherlands is a typical example of such an area. The geological stratification consists of typical soft to very soft soils, especially in the western part of the country. More than half of the country is located below sea level, the surface of the land is flat, and the groundwater table is extremely high. In these areas particularly it is important to understand the complex behaviour of the subsoil, consisting of soft soils, like organic clays, loose sand deposits and peat. Keeping the water separated from the land is a continuous challenge. It is important to search for solutions that draw on the potential of the coastal system, that enhance safety in densely populated coastal areas, and that minimise the ecological impact. Building and maintaining infrastructure in these areas is quite challenging. Expert knowledge of soil mechanics and geotechnical engineering is essential to reduce the risks inherent to construction on and in deltaic areas.

Soil mechanics and geotechnical engineering. Theory and practice. Both are equally important in order to create a safe and sustainable living environment for us and our (grand)children. Both theory and practice can be found in this publication. In the first part, starting from the fundamental side, the ins and outs of the complicated multi-phase material which we call soil, are explained and summarised. In the second and third part this theoretical knowledge is further developed and used to analyse a large number of specific soil-related problems, like slope stability, earth retaining structures, foundations, ground improvement, environmental impact, underground construction, coastal engineering, dike technology and so on.

The author has been active in this field for the past 40 years, well connected on the one hand to the scientific world of soil mechanics and on the other hand to the (geotechnical) engineering practice. With this book, the author has left a legacy of his wide knowledge and expertise to the younger professionals. It is particularly valuable for the geotechnical engineer of the 21st century, living and working in deltaic areas.

Peter van den Berg
Deltares, Director Geo-Engineering

This page intentionally left blank

CONTENTS PAGE

Introduction 1

PART I FUNDAMENTALS AND CONCEPTS

1 A history of geotechnical achievements 5

2 Characteristics of soils
a Geological data 25
b Gravimetric-volumetric data 26
c Atterberg limits 28
d Structure of granular soils 30
e Strength and stiffness aspects 32
Applications 32

3 Soil investigation
a Site investigation 37
b Laboratory testing 42
c Physical model testing strategy 46
Applications 50

4 Soil and groundwater
a Vertical soil stress 51
b Groundwater flow 52
c Boiling, heave and piping 59
Applications 62

5 Uniaxial stress and strain
a Stress and strain 69
b Strain concept 70
c Uniaxial compressibility 72
Applications 73

6 Creep and consolidation
a Time-dependency 77
b Creep 78
c One-dimensional consolidation 80
d Multi-dimensional consolidation 84
e Method of the transient leakage factor 86
Applications 88

7 Triaxial stress and strain
a Continuum mechanics 93
b Mohr-Coulomb model 96
c Coefficient of earth pressure 97
d Triaxial cell 99
e Undrained strength 101
f The *A* and *B* factor 102
Applications 104

PART II METHODOLOGY AND TOOLS

8 Uncertainty and reliability
a Uncertainty in geotechnical engineering 109
b Partial safety factors 116
c Eurocode 7 and the observational method 119
d Risk approach and visualising the unseen 121
e Risk management process: GeoQ 124
f Expertise and experience: GeoBrain 126
Applications 129

9 Observation and prediction
a Physical simulation 133
b Constitutive models 135
c Aspects of numerical simulation 143
d A visco-plastic analytical element method 149
Applications 157

PART III DESIGN AND CONSTRUCTION

10 Stability of slopes
a Limit analysis 163
b Slide on long slopes (micro-stability) 164
c Slide on short slopes (macro-stability) 167
Applications 171

11 Stability of earth-retaining structures
a Gravity walls 176
b Embedded walls 179
c Slurry walls 182
d Reinforced walls 183
Applications 184

12 Footings and pile foundations
a Bearing capacity of footings 189
b Bearing capacity of pile foundations 193
c Deformation of foundations 199
d Dynamic soil response 201
Applications 207

13 Methods of ground improvement
a Gravity displacement methods 211
b Replacement methods 212
c Mass improvement 213
d Stiff inclusions 218
e Bio-chemical treatment 223
Applications 224

14 Environmental engineering
a Physical-chemical characteristics of soil 227
b Physical-chemical processes in soil 230
c Bio-chemical processes in soil 233
d Heat / cold transport in soil 234
e Land subsidence 239
Applications 247

15 Underground engineering
a Deep building pits 249
b Soft ground tunnel-boring techniques 252
c A cylindrical cavity in a uniform infinite soil 254
d A horizontal cylindrical cavity in a uniform semi-infinite soil 258
e Tunnel boring design and construction 260
f Unseen leakage 263
Applications 264

16 Coastal engineering
a Hydro-geodynamics 267
b Waves on seabed 271
c Waves on breakwaters 281
d A liquefaction model 286
e Squeezing 290
Applications 290

17 Dike engineering
a Deltas in the world 295
b History of Dutch dike engineering 297
c Philosophy of water defence 301
d State of the art 309
e Latest developments 312

ANNEX

I Answers to the applications 321
II Recommended literature 337
III About the author 339
IV Symbols, standards, units, keywords 345
V Name index 347
VI Subject index 351

This page intentionally left blank

INTRODUCTION

Geotechnique comprises any aspect of geotechnical and environmental engineering in the areas of soil and rock mechanics, including material behaviour, analysis and interpretation, design, construction and monitoring. In this book, the focus is on the behaviour of soft soils, notably sand, silt, clay and peat.

The book reviews basic aspects of soil mechanics such as laboratory and field-testing, stresses and strains, deformation and strength, and groundwater effects, including environmental aspects. It touches upon a wide range of applications of soil mechanics in construction: prediction of settlements, bearing capacity of shallow and deep foundations, piles and footings, stability of earth retaining structures, analysis of slope stability, principles of soft-ground tunnelling, ground improvement techniques, and coastal and reservoir engineering. Fundamental aspects of physical and numerical models and their application, codes of practice and guidelines, principles of risk management for handling uncertainty and reliability, and a structural involvement of experience are discussed. At the end of each chapter exercise applications are available; answers are compiled at the end.

Besides content and application, this book deals with the context, the society around the geotechnical engineer. Building with soil has uncertainties, significantly more than for example steel or concrete. In the field of geotechnique this is a fact, but for society these larger risks are not obvious. It creates tension: the ratio of the engineer versus the emotion of people (public and politicians). Media usually magnify damage beyond realistic proportions, which unfairly spoils the geotechnical image. The engineer has therefore to deal with public perception and clear transparency, and so creating proper social support for his indispensable contribution. This aspect gets proper attention.

The text of this introductory book is based on a wide range of comprehensive textbooks and some trendsetting articles and reports, which are mentioned in the reference list, and where appropriate the author has added examples and elaborations from his own experience. Specific references are not compiled. Occasionally, the name of a specialist is mentioned. The reader who is looking for more information may consult the Internet or send a request to the author at: frans.barends@deltares.nl.

ACKNOWLEDGEMENT

The careful review and support of Evert den Haan, particularly on settlement, creep and ground improvement, the support of Hans Teunissen on localisation, the suggestions by Hideo Sekiguchi, Frits van Tol, Wijbren Epema, Gerard Kruse, Hans Sellmeijer, Thomas Bles and Andre van Hoven, and the applications try-out by Bernard van der Kolk are gratefully acknowledged.

Delft, May 2011
Frans B. J. Barends

This page intentionally left blank

Part I

Fundamentals and Concepts

This page intentionally left blank

1 A HISTORY OF GEOTECHNICAL ACHIEVEMENTS

This chapter describes a history of geotechnical achievements, not exhaustive and to some extent with a Dutch focus. The author is fully aware that similar interesting and memorable achievements may exist in other countries.

Before two thousand years

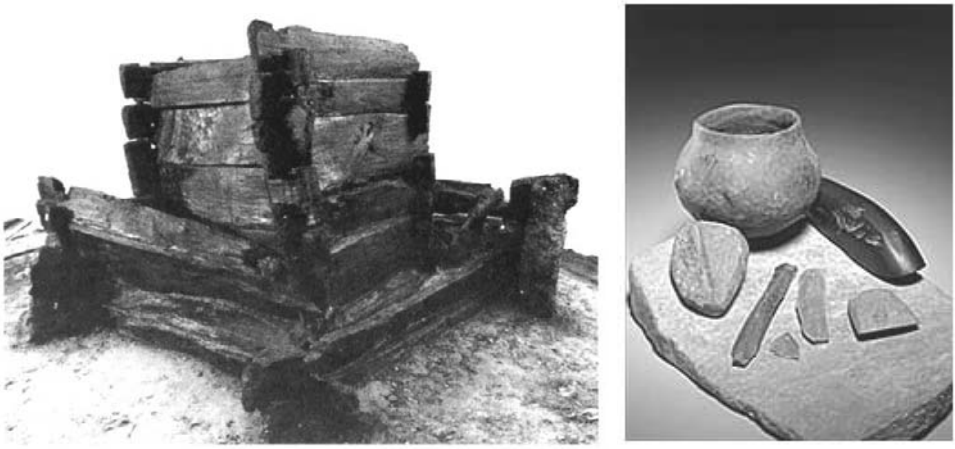

Figure 1.1 Prehistoric water well structure; stone and bone equipment.

About 15 years ago, a prehistoric water well was found near Erkelenz, north of Aachen, in Germany, dug about 7000 years ago by early farmers, members of the so-called band-ceramics culture. It was the early Stone Age. The saw and the wheel were not yet invented. Oak trees were dragged to the fertile loess plateau and with stone axes 200 branches were cut in 3-metre length, 50 cm wide and 15 cm thick. For the connection notches were carved by using animal bones as chisels. For the construction of the 15 metres deep well smart engineering and a perfectly organised cooperation were required. This structure is probably the oldest known underground construction (Fig 1.1). It is a fine example of prehistoric geotechnical engineering.

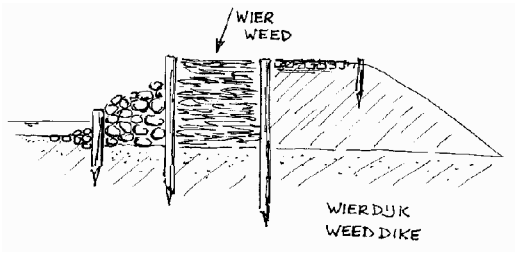

Figure 1.2 Dutch historic sea dike design

Six thousand years ago the oldest known dam at Jawa in Jordan was built with a true stone revetment. 4600 years ago the Kafara Dam near Cairo was constructed to tame the river Nile. This earthen gravity dam nicely fulfilled two functions, stability by side dikes and imperviousness by a central filling (Kerisel). This practice of function separation is found in two thousand year old sea dikes along the Dutch coast (Fig 1.2). The front consists of stones to form a revetment against currents and wave attack; the backside is a massive earth fill of stacked sods providing stability and the centre part exists of compacted seaweed, all compartments flanked by palisades. The seaweed appears to be very durable and when found today its colour is white.
Four millennia ago the Sumerians built an enormous temple mount of sand with geotextiles of woven reed: the Ziggurat at Aqar Quf. Sumerians, and also Aztecs and Venetians understood that weak soils become stronger when surcharged. In many old cultures, complex underground water supply tunnels were installed, sometimes many kilometres long. They are called qanat, the origin of our word for canal. These tunnels are still in use in Iran and Morocco. It requires special ground engineering skills to construct and maintain such delicate and crucial systems. The Greek made their footing foundations earthquake resilient by applying iron clamps embedded in lead (antirust).

Figure 1.3 Remains of the sluices of the old Ma'arib dam

The Great Dam of Ma'arib (or Marib) was one of the engineering wonders of the ancient world and a central part of the south Arabian civilization. The site of the great Dam of Marib is south-west of the ancient city of Marib, once the capital of the Kingdom of Saba'a, believed to be the kingdom of the legendary Queen of Sheba. The Sabaens built the dam to capture the periodic monsoon rains, which from nearby mountains irrigate the land. Archaeological findings suggest that simple earth dams and a canal network were constructed as far back as 2000 BC. The building of the first Marib dam began somewhere between 1750 BC and 1700 BC. The dam was of packed earth, triangular in cross section, 580 metre in length

and 4 metres high. It ran between two groups of rocks on either side of the river and was linked to the rock with substantial stonework (Fig 1.3).

The dam's position allowed for a spillway and sluices between the northern end of the dam and the cliffs to the west. Around 500 BC the dam height was increased to 7 metres, the upstream slope (the water face) was reinforced with a cover of stones, and irrigation was extended to include the southern side as well as the northern side. After the Kingdom of Sheba, possession of the dam came to the Himyarites in around 115 BC, who undertook further reconstruction, raising it to 14 metres high with extensive water works at both the northern and southern ends with five spillway channels, two masonry-reinforced sluices, a settling pond, and a 1000 metre canal to a distribution tank. These works, completed in 325 AD, allowed the irrigation of 100 km^2. The dam suffered numerous breaches and the maintenance work became increasingly burdensome. Around 570, the dam was again overtopped, and this time left unrepaired. The final destruction of the dam is noted in the Qur'an and the consequent failure of the irrigation system provoked the migration of 50,000 people to the present emirate El Fujeira.[1]

According to the Romans stiff soil is masculine and soft soil is feminine. Archimedes[2] is considered a mastermind and mathematician, inventor of many mechanical principles, in particular the buoyancy force, important in geotechnics.

Vitruvius[3], author of Architectura (discovered in the 15th century) wrote in Fermitas about soil densification, installation machines for piles, iron

---

[1] In 1986 a new 38 m high, 763 m long, earth dam located 3 km upstream of the ruins of the old Ma'arib dam was completed across the Wadi Dhana, creating a storage capacity of 400 million cubic metres.

[2] Archimedes 287 BC – 212 BC, Greek mathematician, physicist, and inventor. His reputation in antiquity was based on several mechanical contrivances, e.g., Archimedes' screw; which he is alleged to have invented. One legend states that during the Second Punic War he protected his native Syracuse from the besieging armies of Marcus Claudius Marcellus for three years by inventing machines of war, e.g., various ballistic instruments and mirrors that set Roman ships on fire by focusing the sun's rays on them. In modern times, however, he is best known for his work in mathematics, mechanics, and hydrostatics. In mathematics, he calculated that the value of π is between 3,1408 and 3,1429, devised a mathematical exponential system to express extremely large numbers, proved that the volume of a sphere is two thirds the volume of a circumscribed cylinder, and, in calculating the areas and volumes of various geometrical figures, carried the method of exhaustion invented by Eudoxus of Cnidus far enough in some cases to anticipate the invention (17th cent.) of the calculus. One of the first to apply geometry to mechanics and hydrostatics, he proved the law of the lever entirely by geometry and established Archimedes' principle. In another legendary story, the ruler Hiero II of Syracuse requested him to find a method for determining whether a crown was pure gold or alloyed with silver. Archimedes realised, as he stepped into a bath, that a given weight of gold would displace less water than an equal weight of silver (which is less dense than gold); and he is said, in his excitement at his discovery, to have run home naked, shouting Eureka! (I've found it! I've found it!). A Roman soldier killed him, supposedly while absorbed in mathematics.

[3] Marcus Vitruvius Pollio (ca 90 BC – ca 20 BC) Roman architect. He wrote the oldest extant Western treatise on architecture De Architectura or the Ten Books. An invaluable document of Roman and Greek architectural history and building practices; its discovery in

reinforcement of wooden piles, manufacture of concrete (= growing together) from pozzolan sand with chalk from heated limestone. The Romans built their Coliseum on an enormous concrete plate placed in a dug lake. They were also the best road builders with 90 thousand km primary roads (viae consulares) and 200 thousand km secondary roads (viae vicinales). Emperor Nero built a 40 m high stone reservoir dam that resisted 13 centuries.

Since the last glacier the sea level rose and the landscape in the former Netherlands underwent drastic changes. Also the groundwater levels rose and soils were covered partly with peat. When the land temporarily drowned clay and sand layers were deposited. Dunes took shape and permanent settlements of fishermen occurred near eutrophic river mouths. Two thousand years ago, possibilities for inhabitation improved and many small farming communities lived at the edges of peat lands and along creeks in the inland. Such a fairway of that time was the Gantel, which ran from the river Maes to the Old Rhine along Delft. The Romans canalised the bedding so that navigation and trade could flourish.

The first millennium of our era

In the third century AD, due to wetting of the area, political instability (the Romans had left) and epidemics (malaria), the Dutch population left to eastern and southern sand soils. Excessive peat growth created a real morass in the western part. Thereafter, land clearing and building were regulated and executed by monasteries and by armies of serfs of kings and landlords. When desiccation rose again, land developments increased by installation of dewatering systems, stimulated by duke Dirk II, the largest landowner. Frisian emigrants were encouraged to come to western Holland by offering a piece of land with tax duty (tied farmers). At the end of the first millennium larger cities developed together with professional communities (guilds) and farmers corporations.

Siphons were built to promote dewatering during low tides. In Valkenburg, Schiedam-Kethel and Vlaardingen valve-sluices (see Fig 17.2a) are found dating from the first century. A dam of clay and sods riveted by palisades provided water retainment. Dikes were built to protect the plane lowlands against high river waters (Fig 1.2). The peat lands were mined for turf (heating, cooking) and salt production, and in 800 AD this caused a dramatic land loss. Our present-day lakes and lowlands are mainly the result of human action.[4]

---

the early 15th century ushered in the revival of the classical orders in Italian Renaissance architecture.

[4] When mining peat, the land was divided into long strokes with ditches at both sides that dewatered to a larger channel (wetering), which ended in a creek. Villages arose as wisps at the edges of the plots. By dewatering the land subsided sometimes meters under seal level. Mounds and dikes were erected which caused the soft soil underneath to compact but also covered the peat against oxidation. Subsidence and wetting made agriculture impossible. The lands became pastures and meadows. Now, some areas are lovely nature reserves.

The period 1000 to 1600 AD

Chronicles, archives of old towns, and the history profile of glaciers tell us that the years 1176-1200 and 1226-1250 belong to the very warm periods in Europe. The summers of 1473 and of the years during 1536-1540 were the warmest ever. During these summers, tropical heat lasted nine months! The year 1540 was called the Great Sun Year. Crops desiccated. The air was thick with ash, dust and smoke from burning fields, woods, and many villages. Rivers dried up. In Paris people crossed the Seine without wetting their feet. The water became polluted, undrinkable. Water mills stopped and there was no bread. Insects could not find food and attacked the people in towns, who suffered from hunger, dysentery, heart attack and sun stroke. In 1562, the famous painter Pieter Breughel was probably inspired by this hazard when painting the background of his Triumph of Death (Fig 1.4). The Dutch peat lands dried, rotted and oxidised, and the wetlands subsided.

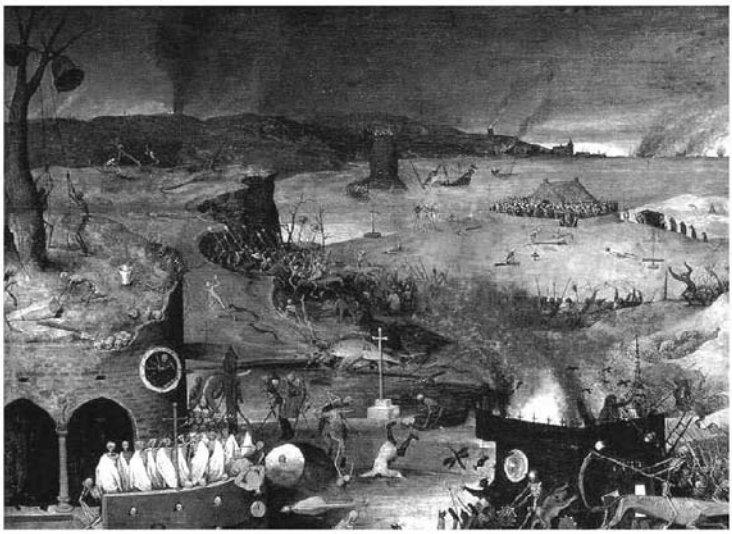

Figure 1.4 Pieter Breughel, Triumph of Death

The Dutch population increased steadily and new land was needed. Landowners saw their property and wealth increase. In the 15th century contractor's companies came into being, which executed both private and public works on commercial basis. Swamps and peat lands were reclaimed en masse, and new land was taken from the sea step by step, e.g. the present island Goeree (Fig 1.5), originally a small sandbank, grew by steadily reclaiming the sea mud planes. Nature steered the process. Due to consequent subsidence and diminishment of water storage capacity more water troubles occurred. Injudicious measures and insubordinate dike building caused large floods (1421 Saint Elisabeth flood, 1530 Saint-Felix flood, 1570 All-Hallows flood), which took hundreds of drowned and large devastations. Complete villages disappeared with all hands. Waterboards were installed and the need for technology, control systems and cooperation rose. Commerce (Hanze) made Holland rich and farmers organised themselves in free and powerful communities. Heavy defence works fortified cities and harbours and the construction of many churches started in this period where often the tower in

property of the town formed a symbol for the prosperity and success. There was a competition between cities for the tallest.

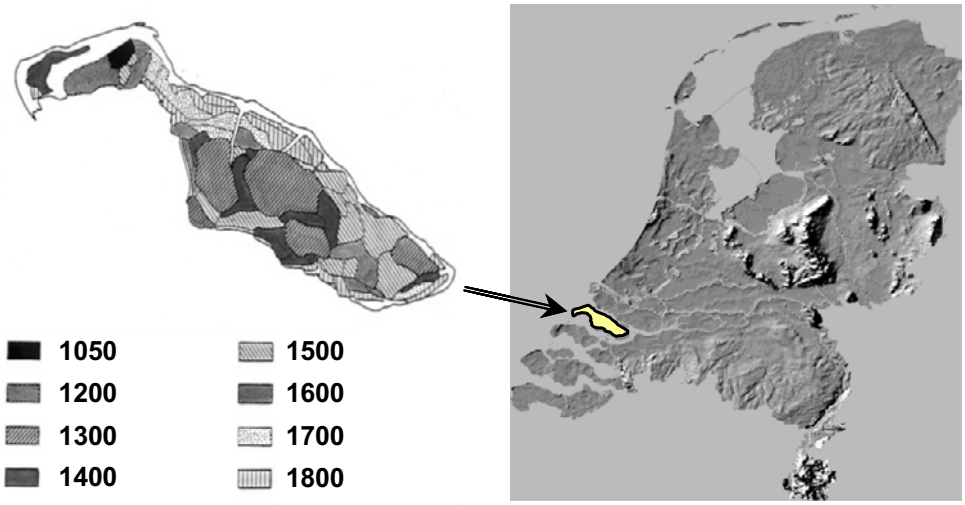

Figure 1.5 Land reclamation a process of centuries

In Europe a small elite of talented and renowned architects built the monumental castles, pompous churches, rich palaces and massive monasteries. These artists met regularly and exchanged their ideas on new construction methods, because a failure would also destroy a career. Building assignments always were a challenge, as through these principals looked for eternal respect and remembrance.

Figure 1.6a Historic raft foundation

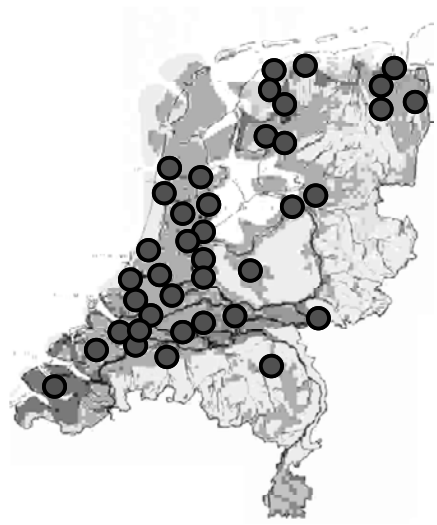

Figure 1.6b Oblique towers in Holland

Towers were not only a city's pride but also for rich and mighty families. The Tower of Pisa is probably the best known. The construction of it is characteristic and the consequences are characteristic for many such towers.[5] Also in Holland so many towers were erected. The foundation usually consists of a raft of heavy wooden beams placed just under groundwater level (Fig 1.6a), packed in manure (conservation). Sometimes a ground improvement was applied, particularly suitable for soft soils (see Fig 13.10). The construction process advanced slowly, and unavoidable settlements did not cause damage worth mentioning in the masonry, because the mortar of that time contained chalk and could follow slow deformations (creep). Differential settlements did however cause inclinations, which could hardly be avoided. Holland counts more than 50 oblique towers (Fig 1.6b), some of which collapsed and a few of which have been successfully put straight (Montelbaan Tower in Amsterdam in 1610, the Lawrence Church tower in Rotterdam in 1654, and the church tower of Nijland in 1866).

Fascinating is the construction of a 60 metre deep water well in Orvieto (Italy). The well has a double wall with in between a spiral staircase. Etruscans used to build their settlements on mountaintops for protection and therefore needed deep-water wells for water provision, in particular during siege.

Around 1650, the Taj Mahal was built ordered by Mughal emperor Shah Jahan for his beloved wife Mumtaz Mahal, who died in 1631 at the birth of her 14th child. The foundation of this huge monument, partly erected with white marble decorated with marvellous branded motifs of semiprecious stone, in perfect symmetry, is very competently based on cylindrical wells. An area of roughly three acres in the soft bedding of the river Agra was excavated, filled with dirt to reduce seepage, and levelled at 50 metres above riverbank. In the tomb area, wells were dug and filled with stone and rubble to form the footings of the tomb. The advantage of well foundations is that the cylindrical pits can be created top down, their fill can be relatively stiff and they usually settle more or less regularly.

The period 1600 to 1800 AD

Amazing achievements where made in the past when so little was known compared to what we do know to day. In Rotterdam, in 1620, the Lawrence Church Tower was lower than the church tower of Delft. This was not acceptable and a two stories wooden building was placed on top to make it 30 cm higher. It was cheap

---

[5] The early construction of the bell tower of Pisa took place during 1173-1178. The underground (a prehistoric embankment) made the foundation of masonry and mortar and the four stories on top lean towards north (opposite to present). During 1272-1278 the construction continued with elegant marble covering and with eight stories a height of 51 meters was achieved. The tower leaned south and settlements were estimated to reach 2 meter. During 1360-1370 the bell gallery was completed and the height reached 58 meter. The weight amounted 145 MN and the obliqueness was then probably 2º (is at present about 5º). During 1985-2001 a 14th Italian Pisa Tower conservation commission under leadership of Jamiolkowski succeeded to relieve the inclination by carefully extracting small amounts of soil underneath the uplifted side of the tower while the tower weight caused the soil to be compressed again and straightened it for about 1º, sufficient to prevent the sudden buckling collapse, which is thought otherwise to have been imminent.

wood, Dutch avidity, and soon rotted. In 1646 the top was replaced by expensive and heavy marble. The architect's warning in 1620 not to add heavy load for the tower's stability was forgotten. In 1650, a windstorm made the tower lean (3.5 feet off plumb). It was decided to put the tower straight and Claes Jeremiasz Persoons, a master stonemason, succeeded in doing so, earning eternal fame. With the newest pile driving machines, by hand, 500 wooden piles of 12m length were driven just outside the existing foundation into a sand layer at 17 metre deep, next by horse power and heavy iron chains the tower was put straight - so it is written - and finally new brick-work buttresses, still visible to day, (Fig 1.7) carry the tower. How Persoons moved and twisted this heavy tower remains a miracle.

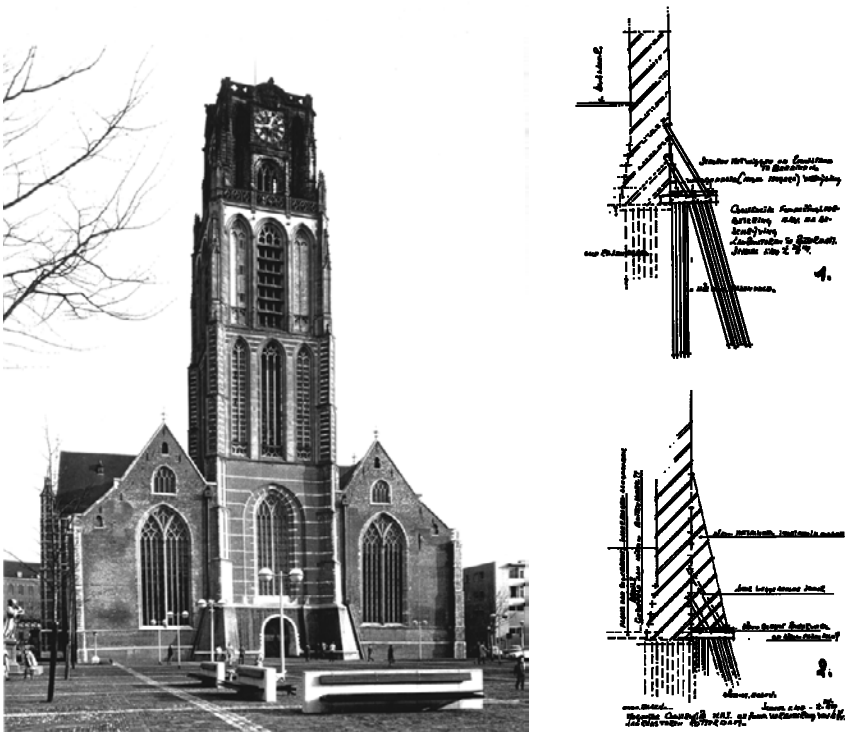

Figure 1.7 Putting a heavy church tower straight in 1655

The trade by sea with the orient was flourishing. Cities required good connection with the sea, asking for high river levels. On the contrary, farmers and landowners demanded protection against high waters. To support solving this level contest, the Dutch ruler, Prince Maurits, founded the institutionalisation (diploma) of geometricians and fortress builders (military engineers). In 1583, Simon Stevin, a famous Flemish mathematician and excellent military engineer, started for this purpose the Duytsche Mathematique at the university of Leiden. By this innovation the water regulation by precise levelling became possible. Geometrician Cruquius was one of the pioneers in making detailed river maps and the spirit level instrument developed by Huygens was of great importance. Hydraulic problems

got focus but it was yet too early for consistent scientific theories. Water mills with great capacity took care of drying large lakes.

In the Dutch golden age (17th century) the VOC[6]-ships brought besides spices, porcelain, silk and exotic wares also a sub-tropical wood-worm, unknown before in the area, that ravaged the wooden water-defence structures (Fig 1.8) within a few years. As a consequence, avoiding the use of local wood, dike design changed drastically into sloping embankments with solid surface protection. Dike builders flattened slopes and applied rigid revetments (twined brushwood blankets with stones). Calamities promoted the insight in redistributions of river courses (1744 dikes collapsed and the river Merwede inundated vast areas), but it was yet also too early for a really holistic approach.

Figure 1.8 Old river dike structure (Ruysdael's painting: Wijk bij Duurstede ~ 1645)

In 1648, the town hall of Amsterdam – since 1808 the royal palace – is constructed on 13,659 wooden piles, passing through the soft Holocene top layer into a stiff sand deposit. It was a symbol of the power and status of Amsterdam at the climax of its Golden Century (Fig 1.9). This monumental building stands firm still today thanks to a solid foundation, long wooden piles driven by the modern equipment of that time under the groundwater table into the stable deep sand layer.

[6] VOC: Dutch East India Company established in 1602.

Reinard Woltman (~1755-~1840) followed mathematics and hydraulics at the Academic Gymnasium of Hamburg, and studied dike building at the university of Kiel. He visited Göttingen, Frankfurt, Straßburg, Paris, Cherbourg, London and Haarlem in his search for knowledge. He wrote several books (e.g. Hydraulische Architektur) that gave him international prestige and he was involved in various important river and canal projects (Elbe, Hamburg). He also played a prominent role in ground mechanics of that time, i.e. by developing a theory for earth pressure, independent from Coulomb. He introduced the friction angle, which he related to the natural angle of repose. In carefully designed physical tests, he verified his theory by measuring earth pressures on a retaining wall, and concluded that the lower pressures found are due to soil friction. With these findings he was ahead of his time, but his work is not generally known.

Figure 1.9 The town hall of Amsterdam in 1673

In 1775, Charles-Augustin Coulomb developed the friction law, a theoretical model for the equilibrium of soil, distinguishing active and passive earth pressure. It was a portal to a new era in ground engineering and his work was a real breakthrough that supported later the work of Rankine (1855), Boussinesq (1882), Sokolovski (1954), and many others.

The period 1800 to 1940 AD

The urbanisation of western Netherlands and the economic industrialisation stimulated innovations in the application of new materials and construction methods (concrete, large roofs). Large contractors and municipalities promoted the development of new foundation techniques. From 1900, railway disasters and flood calamities contributed to the scientification of soil mechanics. The circle of Mohr

is formulated in 1822 (Mohr was a German civil engineer, professor of mechanics at Stuttgart Polytechnic). Dutch governmental engineers were invited by the Japanese emperor (Ming dynasty) to assist in the regulation of complex water management problems and land reclamation. They introduced the NAP[7], a central geodetic reference level that worked well in the Netherlands. Also in Germany this was adopted and still in use.

In 1918, the State Courant reports the act about closure and land winning of the South Sea (plan Lely), a great engineering project. In 1919 the execution started: a 2.4 km long dike from North-Holland to Wieringen (1924 completed) and a 30 km dike from Wieringen to Friesland (1932 completed). For five new polders ring dikes were constructed: Wieringer Lake (1929), North-East Polder (1940), East Flevoland (1956), South Flevoland (1967) and Markerwaard (1975). Except the last one, these new lands contain at present urban conglomerates, nature reserves, road and railway connections, agricultural lands and pastures. In the mean time, the need for land for food for a growing population is outdated by modernisation and intensification. Some outstanding achievements related to the geotechnical profession are listed next.

- 1808 The Overtoom sluice in Amsterdam is constructed by a consortium, for the first time after an open tendering,
- 1818 The first patented shield tunnel in London (Marc Brunel).
- 1825 After the invention of the steam engine by James Watt, Stephenson succeeded to make a steam locomotive, which allowed large-scale transport.
- 1838 Application of a pile drilling machine that can be handled by one single man.
- 1839 The first railway line in Holland, Amsterdam-Haarlem; a national project for modernisation of transport.
- 1841 First application of the pneumatic caisson method (Triger, France).
- 1842 Nasmyth invents the steam hammer.
- 1846 Alexandre Collin shows the relation of strength of clay with water content: water negates cohesion. He also shows that the slip surface of a slope failure runs according to a cycloid. Petterson and Fellenius rediscovered his work in 1956.
- 1850 Systematic ground investigation via borings became standard (the function of Boring Master).
- 1853 Darcy discovers his law of groundwater flow for the design of a fountain in a park in Dijon.
- 1857 Rankine studied extreme stress states. Due to internal friction a range of admissible stress fields exists, marked by active and passive states.
- 1860 Dutch Railway Law. The government takes the railway development in hand, because soft soil conditions made it difficult (peat and clay).
- 1860 Mechanisation of building; invention of (modern) concrete.

1866 A simple carpenter, Fedde Albertus Hokwerda, put straight a dangerously leaning church tower of the village Nijland in the Province Friesland of the

[7] NAP stands for Normaal Amsterdam Peil, or Amsterdam Ordnance Datum, adopted in the Netherlands around 1684. Since 1955 in use in many other countries (Normalnull).

Netherlands, applying a method of carefully extracting soil underneath the uplifted edge and letting the soil compact by the tower's weight. The newspaper of those days reported: By him a new proof is provided that only then the work attains its full value, when the hand that works is steered by a head that thinks. He was honoured by the churchwardens for his idea and persistence and obtained an annual fee of 5 guilders, raised at retirement to 52 guilders, enough to live in humble comfort. It is remarkable how courageous and skilful the profession was 150 years ago. It is good to notice that today the same attitude exists, e.g. in saving the Pisa Tower (see John Burland). Methods survive generations, sometimes unnoticed. The church tower of Nijland, unmoved since, remains nicely upright.

- 1868 Menck (Germany) built the first drilling steam car.
- 1874 Application of the pneumatic caisson method for the northern abutment of the Old Willem Bridge in Rotterdam.
- 1875 Cullman's method for slope stability
- 1879 Dramatic slope failure in Berlin.
- 1883 Ground freezing applied in mining.
- 1883 Discovery that friction increases with density in sands.
- 1885 Reynolds discovers dilatancy in sands.
- 1885 Boussinesq theoretically solves the point load problem.
- 1888 Kötter develops curved line earth pressure characteristics
- 1889 Difficulties with excessive creep of the foundation blocks of the large roof of the central railway station in Amsterdam are overcome.
- 1890 The first concrete caisson invented by Kraus (Chili).
- 1891 The first application of a screw pile for the railway bridge Konigsberg-Labiauer (Germany).
- 1892 Flamant solves the line load problem.
- 1892 Railway embankment failure at Beek-Elsloo (no casualties). The public trust in the safety of rail transport was shocked. It caused vivid discussion in the Parliament and a serious collision between geologists and geotechnicians.
- 1894 Honigman applies heavy fluid (bentonite) for bore hole stability.
- 1894 The first concrete foundation pile applied by consulting bureau Hennebique.
- 1898 Kraus invents the hollow concrete tilting caisson for hydraulic engineering.
- 1898 First application of a dewatering cell system for sewer works in the Hague.
- 1900 Electric pile driving car (France).
- 1901 Application of caissons in the quay wall of Rotterdam by consulting bureau Hennebique.
- 1903 Hackstroh suggests using gunpowder explosions for soil densification.
- 1905 Caisson Law: protection of labourers against the caisson disease.
- 1909 Large slope failure during construction of the Panama Canal.
- 1910 Resal shows the importance of cohesion. Cohesion could not be measured, which resulted in overestimation of the design strengths and stability.
- 1910 Von Kármán performs the first triaxial test on marble and sand stone, at high ambient pressures.
- 1911 Sweden, Atterberg defines a protocol for water content and soil condition (liquid limit and plasticity limit).
- 1915 Fillunger defined effective stress.

- 1916 Flood disaster South Sea; start of the project Closure Dike.
- 1916 Fellenius designs a circular slip method for the determination of slope stability, after a large quay wall collapse in Gothenbourg. His method has been improved by Taylor, Bishop, Morgenstern, Price, Spencer, and Janbu.
- 1916 A phosphate factory in Amsterdam is founded on hollow concrete piles (de Waal pile).
- 1917 Weight cone penetration test (Sweden).
- 1917 Westergaard considered elastic pile top displacement.
- 1918 Failure of the railway embankment in Weesp (41 killed). This catastrophe leads to the installation of a committee on the bearing capacity of soil with members Lely, Hackstroh, van den Thoorn and Keverling Buisman. In 1924, the committee installed three sub-commissions. Keverling Buisman is chairman of the sub-commission for Theoretical Approach of Bearing Capacity of Building Ground and Soil, and member of the sub-commission Investigation of Methods for Experimental Research of Bearing Capacity of Building Grounds.
- 1919 Albert Sybrandus Keverling Buisman (1890-1944) becomes professor in applied mechanics at the Technical University Delft (at the age of 29). He starts the Dutch research of mechanical behaviour of soils. Two of his contributions catch the eye: the creep law for soft soil and the cell test (Fig 1.10), which has been replaced by the triaxial test around 1990. His research was so useful, that assignments from practice increased beyond his capacity. This led to the foundation of the Dutch Laboratory of Soil Mechanics in 1934. Keverling Buisman did not survive WWII.

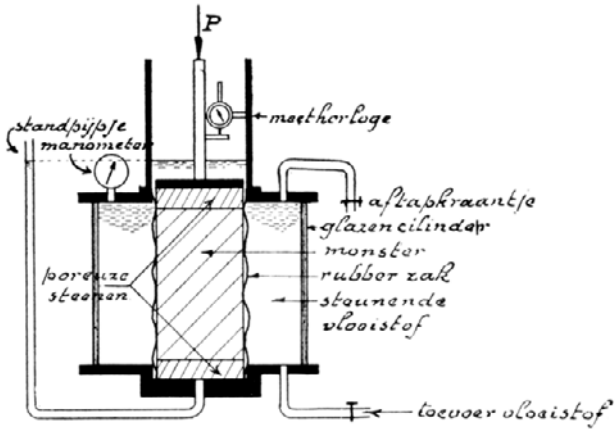

Figure 1.10 The cell test apparatus of Keverling Buisman

- 1920 Discovery of the effect of negative friction on piles.
- 1920 Prandtl's wedge, a theory for strip loading.

1924 After WWI von Kármán took the initiative to organise the First International Congress on Applied Mechanics in Delft, where under leadership of Biezeno and Burgers some selected lectures and about 50 papers illustrated the advancements in the field of applied mechanics and mathematics. The world's first 'scientific society' was founded (IUTAM). It became a blueprint of the new manner of knowledge exchange. Under the more than 200 participants (the French

were absent because of political reasons) many prominent scientists appeared (Fig 1.11). Lectures were presented in English, French and German. Soil behaviour was then a part of applied mechanics, like fluid mechanics, mechanics of materials and constructions and dynamics of oceans and atmosphere. Nadai, Hencky and von Mises gave their view on plasticity, Prandtl explained his wedge, Reissner discussed the horizontal active and passive earth pressure, and von Terzaghi presented his paper "Die Theorie der Hydrodynamische Spannungserscheinungen und Ihr Erdbautechnisches Anwendungsgebiet", in which the principle of effective stress and the consolidation theory were mentioned. He referred to the development of the hydrostatic pressure in a saturated soil sample with time under a static loading by the term hydrodynamic stress. He also elaborated on swell, cohesion and building pit stability, aspects which were mentioned by the ASCE as a problem of national importance. Von Terzaghi referred to his coming book and Buisman was present in the audience.[8] This conference marks the start of soil mechanics.

Figure 1.11 Participants at the 1st IC on Applied Mechanics, Delft

Figure 1.12 Keverling Buisman and Terzaghi, pioneers in geotechnique

[8] Von Terzaghi omitted the prefix von when he left to the States. Buisman omitted in 1924 his first surname Keverling.

- 1925 Terzaghi gave with his book Erdbaumechanik auf Bodenphysikalischer Grundlage a consistent physical and mathematical theory for soil mechanics. He designed the consolidation theory and the logarithmic settlement law, and he experimented with the soil compression test, the standard test of today.
- 1925 Joosten introduces ground injection with water-glass (Na-Silicate) and calcium chloride, suitable for coarse sands.
- 1930 Delmag diesel pile driving machine.
- 1931 Barentsen, governmental engineer, introduces the hand cone penetrometer.
- 1931 CPT. The CPT-value of soil gives information about the consistency of the soil type and represents penetration resistance (at a certain speed) of a standard cone. About the form of the cone (apex) much discussion arose.
- 1933 Proctor apparatus (relation between humidity and density). Proctor developed a tamping apparatus in order to determine at which water content the maximum density can be achieved. It was applied for the first time for an earthen dam in California.
- 1933 Porter experimented with vertical drains to promote consolidation of clays.
- 1937 Fillunger, employed at the Technical University of Vienna, committed suicide with his wife. It followed from a serious conflict with Terzaghi about the professional ethics of Terzaghi, who was accused by Fillunger of false science. Fillunger had written a polemic pamphlet of 50 pages against soil mechanics, in particular against the consolidation theory and Terzaghi. A disciplinary commission examined the case and concurred with Terzaghi. Fillunger wrote a letter with his apology, which he never posted. It is typical that in this scientific battle Fillunger turned out as a pioneer in porous media, since he described in his argumentation the equilibrium of a two-phase porous medium system in a complete and correct way (later referred to as the Biot theory). Earlier, in 1915, Fillunger had already formulated the effective stress principle. Fillunger's work was not recognised due to the sad circumstances (de Boer, Géotechnique 1996)

The recent period, till 2008

1936 The 1st International Conference on Soil Mechanics and Foundation Engineering in Harvard, and the establishment of the ISSMFE, the International Society of Soil Mechanics and Foundation Engineering. Around 2000 the name part Foundation was changed in Geotechnical as to incorporate environmental geotechnics.[9] At the conference, 206 delegates attended from 20 countries.

1934 On the 15th of February in Delft, the Laboratory of Ground Mechanics (LGM) was founded. Geuze and Pesman were the first engineers. Huizinga, the first director, employed every engineer he could find, for example Nanninga, Plantema, de Nie, van Mierlo and later, de Josselin de Jong.

Huizinga and Geuze played an important role in the organisation of the 2nd ICSMFE in 1948 in Rotterdam (596 delegates), and they strongly supported the

[9] At present the ISSMGE counts over 16,000 members from more that 70 countries. Besides regular conferences, it is active through the establishment of many technical committees and task forces, attracting young and old engineers, scientists and practicioners.

further development of the International Society of Soil Mechanics and Foundation Engineering, which had its origins in the 1st ICSMFE, in 1936.

Until 1960 geotechnical investigation and consultancy was concentrated at LGM, the Municipality Works Departments of Rotterdam and Amsterdam, and the Dutch Railways. Thereafter, the profession had become more common and commercially interesting, which gave rise to consultancy and research bureaus. Small site investigation firms conquered the housing market. The field of LGM moved from advice to applied research. Large contractors established soil mechanics departments. In 1962 Fugro was founded. It specialised in off-shore together with Heerema, and became a global player in size. In the eighties automatisation commenced, which gave a boost to micro-electronics in devices and numerical simulation.

Figure 1.13 The staff of LGM in 1936

- 1934 LGM's first large project, the Maes tunnel.
- 1934 Oedometer.
- 1934 Cone penetration test (CPT).
- 1935 deep CPT.
- 1935 Shear apparatus.
- 1935 Keverling Buisman discovers that clay subjected to loading ever compacts. He developed the creep law for soft soils, which he called secular settlement that appears proportional to the logarithm of time.
- 1936 1st Int Soil Mech Congress in Cambridge. Keverling Buisman presented his creep law, which was received sceptically. Later Mitchell proved on purely physical principles it was right.

- 1936 Cell test of Keverling Buisman (Fig 1.11). In a cell, a cylindrical sample surrounded by an impervious membrane is supported by water pressure at the side and loaded on top. In this way a three-dimensional stress-strain behaviour and the slip-shear behaviour can be observed and measured. Keverling Buisman also developed a hollow cylinder cell test with a double membrane.
- 1937 Large-scale application of the Franki pile for the Maes tunnel.
- 1938 Relation CPT and pile bearing capacity.
- 1939 Barkan invents the vibration drill method.
- 1941 Relation CPT and blow count (the blow count is the number of blows required to hammer a pile 25 mm deeper).
- 1942 Biot publishes the complete equations for two-phase mechanics in porous media (he did it actually already in 1935 in an obscure journal).
- 1942 Opening of the Maes tunnel. The project started in 1937.
- 1942 Ackermann's sampler.
- 1942 Koppejan combines the theory of Terzaghi and Keverling Buisman.
- 1943 Application of Rütteldrückverfahren, a vibrating needle, for soil densification for the foundation of a submarine bunker in Rotterdam.
- 1947 Mechanical sleeve cone of Vermeiden.
- 1948 2nd Int Soil Mech Congress in Rotterdam. Rotterdam was chosen during the first conference because of pioneering work of the Dutch.
- 1948 Bakker invents the electrical cone test. The shaft friction of cone rods could not anymore disturb the CPT measurements
- 1949 Establishment of NSSMFE.
- 1952 Begemann invents the mechanical sleeve cone test.
- 1952 Koppejan designs the pile bearing capacity rule (the 4D-8D rule).

Figure 1.14 The Van Brienenoord bridge in 1959, crossing the largest Rhine branch

- 1953: Flood disaster in South-West Netherlands, many drowned, huge damage. As a consequence the Delta works project starts that shortens the coastline

drastically and improves the flood safety to a socially acceptable norm. The project is finished in 1985 (see Chapter 17).

- 1955 Inclinometer.
- 1957 Opening of the Velser Tunnel for traffic and trains. The project started in 1934, delayed during WWII and restarted in 1952. The open building pit method was used (staffel-well dewatering).
- 1957 Triaxial apparatus (UK), actively promoted by Bishop and Henkel.
- 1957 De Josselin de Jong describes the double sliding mechanism.
- 1959 Opening of the Van Brienenoord Bridge in Rotterdam. Span 1320 metre and headroom of 24 metre. The southern abutment is founded on very soft soil. It still creeps.
- 1960 Tan Tjong Kie explains clay settlements is due to electrical charges on broken edges of clay particles.
- 1960 Rise of geotechnical consultant bureaus.
- 1960 Verstraeten invents the Fundex pile and the Tubex pile.
- 1961 Continuous soil sampler of Begemann.
- 1961 Introduction of automatisation in the geotechnique by de Leeuw. Use was made of TUDelft's computer, the Zebra, which worked with lamps and diodes and relied on 8-locks telegraph tapes. One of the first calculation models was for slope stability (the circle method of Bishop) and ground stress distribution based on Boussinesq's solution, resulting in the Tables of de Leeuw.
- 1962 Fugro is founded in Leidschendam. In 1970 it specialised in off-shore geotechnics. At present, it is one of the largest consultant firms worldwide.
- 1962 Flood calamity in Hamburg, 312 drowned, 120,000 in danger.
- 1964 First application of grout anchors for a temporary sheet piling in Sas van Gent.
- 1965 Three-dimensional consolidation (Biot, de Josselin de Jong, Gibson, Verruijt).
- 1966 Opening of the Coen Tunnel.
- 1966 Opening of the Schiphol Tunnel.
- 1967 Opening of the Benelux Tunnel.
- 1967 Electrical friction sleeve CPT of Fugro.
- 1968 Opening of the IJ Tunnel.
- 1968 Opening of the North-South Metroline, Rotterdam.
- 1969 Opening of the Heinenoord Tunnel.
- 1969 Use of standard computer models for geotechnical design.
- 1969 Fugro develops with SHELL the Sea Cow, a CPT and boring machine for open sea.
- 1970 In Japan pile driving in large cities is forbidden because of damage and annoyance, in favour of the newly developed screw piles.
- 1972 20 ton ballast truck for field survey.
- 1972 Fugro applies the Sea Calf for penetration tests at sea up to 180 metre depth. Also wire-CPT with the Wison was a success.
- 1973 Density meter (nuclear).
- 1973 Opening pipe line tunnel, Holland's Deep.
- 1973 Opening water transport tunnel, Amsterdam-Rijn Canal.
- 1975 Introduction of computer terminals.

- 1975 Opening of the Vlake Tunnel.
- 1977 Opening of the Drecht Tunnel.
- 1977 Opening of the Kil Tunnel.
- 1977 Opening of the Prinses Margriet Tunnel.
- 1978 Opening of the Schiphol Railway Tunnel.
- 1980 Opening of the Botlek Tunnel.
- 1981 Opening of the Gouwe Aqueduct.
- 1981 Opening of the East Metroline, Amsterdam.
- 1982, IUTAM Granular Mechanics, in Delft. As in 1924 at the first IUTAM conference on applied mechanics, where the profession of geotechnical engineering got a boost by finding roots in mathematics and physics, this IUTAM conference on granular mechanics gave a strong impulse to the profession by advanced numerical methods, allowing to further develop complex geometries and complicated material behaviour.

Figure 1.15 IUTAM Granular Mechanics Conference, Delft, 1982

- 1983 Opening the Hem Railway Tunnel.
- 1985 Opening the Spijkenisse Metrotunnel.
- 1985 The first personal computer (PC) is in use, at purchased for Fl. 25,000.
- 1986 Computer models Mserie, DIANA, PLAXIS.
- 1986 Opening the East-West Metroline, Rotterdam.
- 1987 Geo-environmental field devices in use for large-scale soil cleansing.
- 1988 Opening of the water transport tunnel, Hartelkanaal.
- 1990 Opening of the Zeeburger Tunnel.
- 1990 Opening of the Zuidwillemsvaart Syphon.
- 1990 Development of computer networks.
- 1991 Den Haan develops the abc settlement model.
- 1992 Opening of the Noord Tunnel.
- 1992 Opening of the Grouw Aqueduct.

- 1992 Earthquake near Roermond, magnitude 5.8; minor landslides, sandboils and embankment failures; 125 M€ damage.
- 1995 The lower river branches risk flooding. 200.000 people evacuated.
- 1996 The River Maes inundates large areas, causing huge damage to the recent built residences in the original river bedding. Since dike construction is not an option, the vision 'space for water' gains ground. A long kept tradition of always fighting the water erodes.
- 1996 Opening of the Willems Railway Tunnel.
- 1999 Opening of the 2nd Heinenoord Tunnel.
- 1999 The Dutch organise the 12th ECSMGE, in Amsterdam.
- 2000 Whiffin invents biotechnology as a new ground improvement technique.
- 2002 New concepts Biogrout en Biosealing successful.
- 2003 Opening of the Western Scheldt Tunnel.
- 2007 GeoBrain (structured use of experience) wins an innovation award.
- 2007 Official introduction of Eurocode 7.
- 2008 GeoDelft (former LGM) merges with Delft Hydraulics, parts of TNO and some Governmental departments into Deltares, a knowledge institute of 900 FTE, with the slogan: enabling delta life.

application 1.1

Probably the most oblique tower in the Netherlands is the 35 metre high Walfridus Church Tower at Bedum (North Netherlands), so to say 2611 mm off plumb. The evaluation of obliqueness is not unambiguous. It can be deduced from the height *h* and the yield *u* on top. For the Walfridus Tower it is 4.266º (the Pisa Tower is 5.296º, at present). However, the height measured from the ground surface is not correct, since the rotation point A is not necessarily located there. This point is determined by the resultant *R* of the vertical ground pressure and the deformation of the tower. Failure (tumbling) occurs when the gravity centre *Z* the vertical line through *A* (and *R*) crosses. The height of the Walfriduskerk is 60% of the one of the Pisa Tower. Thus, it will not tumble soon. A greater danger may be the pressures in the masonry at the leaning side, which should be determined by detailed mechanical analysis.

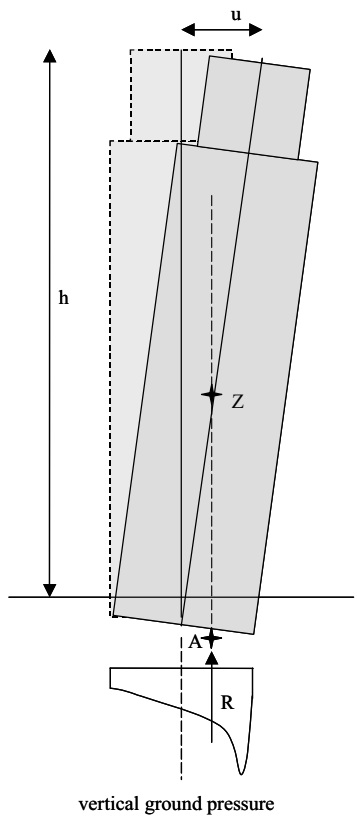

2 CHARACTERISTICS OF SOILS

Interaction between earth materials and environment produces various kinds of sediments, which are deposited and precipitated as minerals in many different sedimentary basins. Eventually, they are subjected to processes of diagenesis, i.e. physical, chemical and biological processes, which bring about compaction, cementation, crystallisation, weathering and other modifications to the original sediments. The study on earth's sediments and environment of the past and the present is of great significance, because it is essential to predict the changes of earth's environment in the future and project knowledge of one location to another geologically similar location. This knowledge is important for geotechnical engineering.

Geotechnical engineering comprises any aspect of geotechnics (soil mechanics and foundation engineering) and geo-environmental engineering in the areas of soil and rock mechanics. Some years ago, the name geotechnical engineering has been adopted by the professional society ISSMGE as to include environmental engineering aspects.

Geotechnical engineering is considered a branch of civil engineering and it deals with the behaviour of earth materials using principles of engineering geology, soil mechanics, rock mechanics and geohydrology to determine the relevant physical, mechanical and chemical properties, to evaluate stability of slopes and deposits, to assess risks posed by site conditions, to design earthworks and foundations and to monitor site conditions, earthwork and foundation construction, and the effects to the environment.

In civil engineering, geological principles are used, either related to rock or to unlithified material, which comes from more recent deposits studied in Quaternary geology, including soils. Rock mechanics is the science of the mechanical behaviour of rock and rock masses, e.g. mechanics related with the response of rock and rock masses to the force fields of their physical environment. Soil mechanics is a discipline that applies principles of engineering mechanics, e.g. kinematics, dynamics, fluid mechanics, and mechanics of material, to predict the mechanical behaviour of soils. A geotechnical engineer determines and designs the type of foundations, earthworks and subgrades required for the intended man-made structures to be built, including shallow and deep foundations, retaining structures, embankments, tunnels, dikes, levees, channels, reservoirs, storage of hazardous waste and sanitary landfills. Geotechnical engineering is also related to coastal and ocean engineering, involving the design and construction of wharves, marinas, jetties and anchor systems for offshore structures.

In this book, the focus is on soft soil in an engineering context, e.g. sand, clay, silt and peat. These soils are classified according to a classification system, based on the outcome of a number of (simple) classification tests, performed on disturbed or undisturbed soil samples.

A GEOLOGICAL DATA

The majority of geological data come from research on solid earth materials, which are classified in two categories: rock and soil (particles). Table 2.1 shows

the geological strength description of clays and silts (tested by fingers), and sands and rocks (tested by hand or hammer).

TABLE 2.1 GEOLOGICAL STRENGTH

clay and silt					
very sof	soft	firm	stiff	very stiff	hard
undrained shear strength clays (kN/m^2)					
10	20	40	60	80	100
squeeze		mould	indent		tick

sand and rock					
very weak	weak	stiff	strong	very strong	extremely strong
unconfined compressive strength (MN/m^2)					
0.5	1	5	10	50	100	200
crumble	crush	scratch	peel	notch	chip

B GRAVIMETRIC-VOLUMETRIC DATA

Soil is a multiphase system, containing a volume V_s of solids (grains), a volume V_w of fluid (water) and a volume V_a of gas (air), with a total volume V. The fluid and/or gas fills the pore space volume V_p in between a complex structure of grains (grain skeleton). In Table 2.2 common symbols used to define the phase content are compiled.

Many soils consist of a mixture of sand, silt, clay and organic material. The organic material typically has a specific gravity of 1.4. In peat soils the organic content is so high that the specific solid gravity G_s is noticeably influenced

$$1/G_s \approx OC/1.4 + (1-OC)/2.65 \qquad (2.1)$$

where OC is the mass proportion of organic material to total solids. OC varies from 1 in pure peat to approximately 0.2 in very clayey peat, with G_s increasing correspondingly. For soft organic soils G_s can not be simply assumed but must be determined in the laboratory.

TABLE 2.2a GRAVIMETRIC / VOLUMETRIC DATA

n	porosity	$= V_p/V$	$= e/(1+e)$
e	voids ratio	$= V_p/V_s$	$= n/(1-n)$
v	specific volume	$= 1+e$	$= 1/(1-n)$
s	saturation degree	$= V_w/V_p$	
w	water content	$= W_w/W_s$	$= se/G_s$
γ_w	unit weight of water	$= W_w/V_w$	
γ_s	unit weight of solid	$= W_s/V_s$	
G_s	specific (solid) gravity	$= \gamma_s/\gamma_w$	
γ	wet unit weight (solids plus water)	$= W/V$	$= (1+w)G_s\gamma_w/(1+e)$
γ_d	dry unit weight (solids)	$= W_s/V$	$= \gamma/(1+w)$
γ'	submerged unit weight (solids)	$= \gamma - \gamma_w$	
D_r	relative density	$= (e_{max} - e) / (e_{max} - e_{min})$	

TABLE 2.2b SPECIFIC (SOLID) GRAVITY G_S

sand or silt			*clay*	
quartz	2.65		kaolinite	2.65
K-feldspars	2.54 – 2.57		montmorillonite	2.75
Na-Ca-feldspars	2.62 – 2.76		illite (mica)	2.84

Particle size distribution

A useful method for classification of granular soils is by particle size distribution obtained by sieving oven-dried (disturbed) soil following a standard procedure. The amount of material retained in each of the sieves is expressed in a percentage of the total weight of the original dried sample and represented in a graph on logarithmic diameter scale. The presentation of a well-graded and a poorly graded soil by a standard particle size distribution is shown in Fig 2.1.

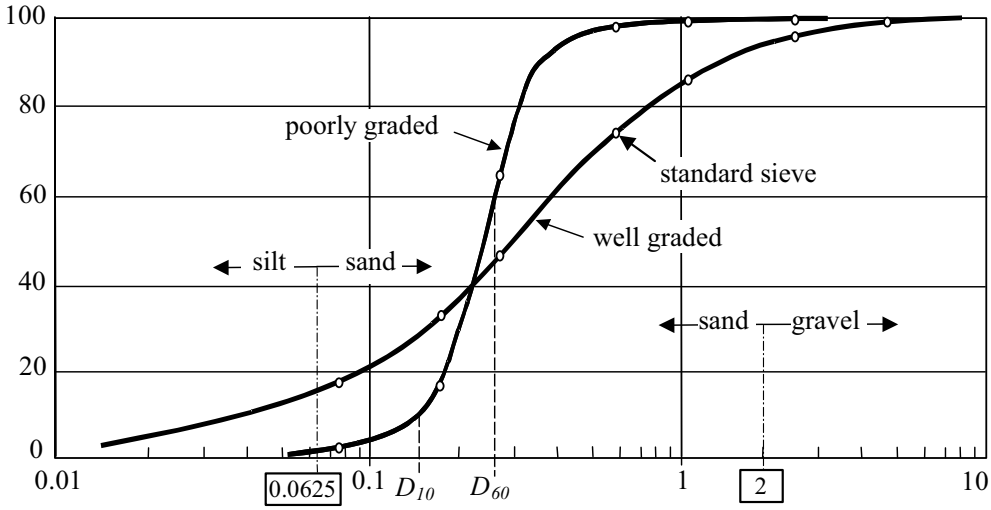

Figure 2.1 Particle grain-size distribution graph (D in mm)

By definition, D_x represents the diameter for which x% of the graded material is less than that diameter. In Fig 2.1, D_{60} of the poorly graded material is 0.25 mm, and D_{10} is 0.13 mm (i.e. 10% of the grains has a diameter less than 0.13 mm). A soil is considered uniformly graded when the uniformity coefficient $U = D_{60}/D_{10}$ is less than 2. For the poorly graded material in Fig 2.1, $U = 0.25/0.13 = 1.92$, and thus uniformly graded. Fines less than 16 μm are determined with sedimentation tests (Hydrometer) after organic material such as peat has been removed.

Internationally accepted soil classification by particle-size ranges is shown in Table 2.3.

TABLE 2.3 CLASSIFICATION BY PARTICLE SIZE D_{50}

fine-graded			
clay	silt		
colloids	fine	medium	coarse
2	6	20	50
μm			

coarse-graded								
sand			gravel				stone	
fine	medium	coarse	fine	medium	coarse		cobbles	boulders
0.1	0.3	0.5	2	6	20	60	0.15	1.00
mm							m	

C ATTERBERG LIMITS

Atterberg limits are useful for classifying fine cohesive soils. They are based on soil consistency as determined by its actual water content w, and four stages are distinguished: liquid state, plastic state, semi-solid state and solid state, their boundaries being the Atterberg limits: liquid limit, plastic limit and shrinkage limit.

The liquid limit is defined as the water content w_l at which a V-shaped groove in a soil-cake in a standardised cup will just close after 25 drops from 10 mm height. The soil behaves as clotted cream. The plastic limit is the water content w_p at which it is just possible to roll a sample into a continuous thread with a uniform diameter of 3 mm. The soil starts to break and crumble. An alternative method is the fall-cone test, for the determination of the liquid and the plastic limit, while a predetermined penetration is sought for a standardised cone of given weight and apex angle. The shrinkage limit is the water content w_s during drying to the air at which air begins to enter the pores and density does not increase further.

From these measures the following classification numbers are determined: the plasticity index $I_p=w_l - w_p$ and the liquidity index $I_l=(w - w_p)/I_p$. The particle's surface, which attracts the water, is a dominating factor for these limits. Soils with similar I_p and I_l show similar mechanical behaviour.

The plasticity chart, devised by Casagrande, plots I_p as a function of w_l. The A-line separates clays (above) from silts (below), and the value of w_l itself determines the degree of plasticity of the soil. Many clays plot on a line more or less parallel to the A-line, approximately 5 - 15% above it. Organic soils and peat tend to have extremely high plasticity and plot to the right of the A-line.

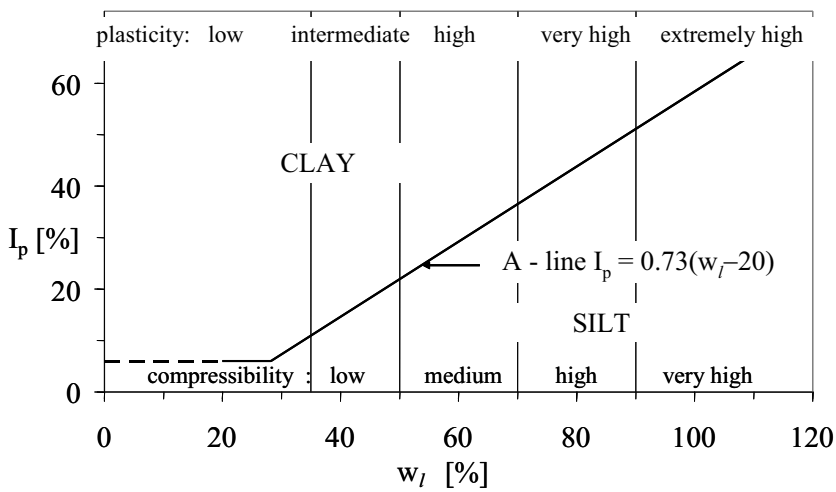

Figure 2.2 Plasticity chart after Casagrande

The correlation of the compression index C_c of clay with Atterberg values are demonstrated by various authors

$$C_c = a(c - b) \tag{2.2}$$

	a	b	c		a	b	c
Terzaghi and Peck (normal clay)	0.009	10	w_l	*Schofield and Wroth*	1.325	0.0	I_p
Skempton (remoulded clay)	0.007	7	w_l	*Nishida*	0.54	0.35	e_0
Hough	0.01	9.2	w	*Rendon-Herrero*	0.30	0.27	e_0
Azzouz	0.01	5	w				

Two practical correlations between the liquidity index and the undrained shear strength c_u (Wroth and Wood) and the internal friction angle ϕ (Jamiolkowski et al.) are shown in Fig 2.3.

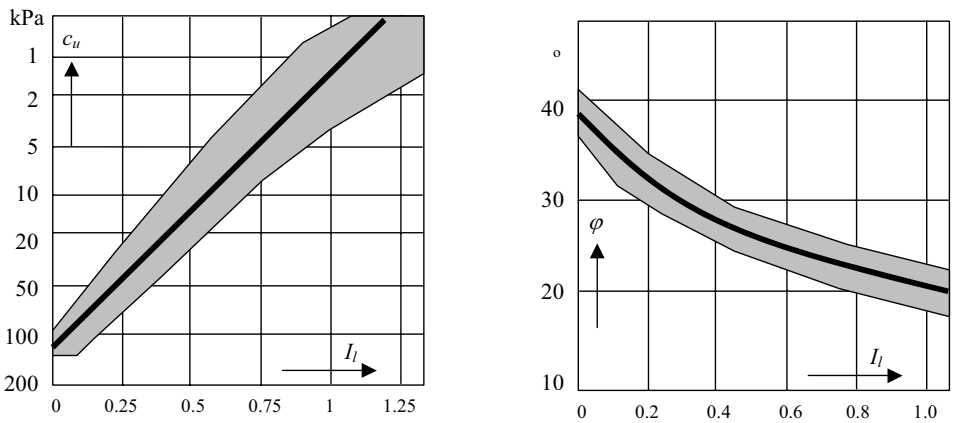

(a) *(b)*

Figure 2.3 Empirical correlations

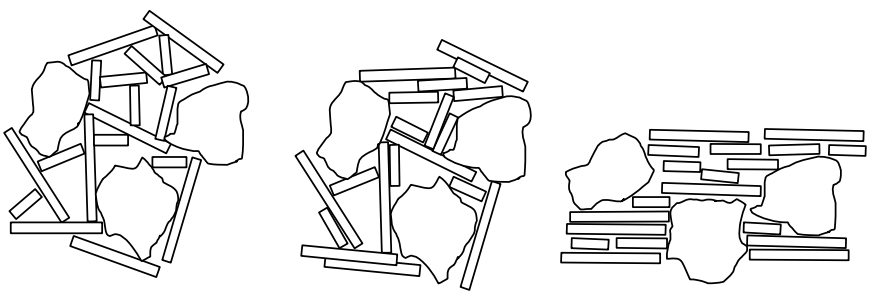

(a) flocculated (salty) (b) non-flocculated (fresh) (c) remoulded (dispersed)

Figure 2.4 Schematic soil structures

D STRUCTURE OF GRANULAR SOIL

One distinguishes sedimentary soil, being transported by water, air, ice, gravity or organisms, changing properties during that process and finally deposited, and residual soil, resulting from rock weathering and accumulated in place. Peat soils either accumulate in place (sedentary) or are dispersed by erosion and deposited, often together with mineral soil. Soils may change their constitution due to stress (gravity), time (ageing), water, environment (salty/fresh) and other disturbance (cementation, bioactivity), see Fig 2.4. A notorious example of the effect of chemical change is the cause of the Rissa landslide in April 1978. The structure of soil depends on its origin, history and environment, and can be classified by compaction and consistency.

Compaction and consistency

Grain texture (fabric), shape and the surface roughness (or roundness) are important for internal friction and compaction features. The compaction of sand also depends on the relative density D_r, i.e. the particle distribution and the packing (voids between large particles may be filled with smaller particles: well-graded). The consistency of cohesive soil (clay) depends on water content, flocculation and electrical forces, and is expressed in terms of undrained shear strength c_u. The corresponding qualitative classification is shown in Table 2.4.

TABLE 2.4 CLASSIFICATION OF SAND AND CLAY

compaction of granular soils	
classification	D_r
very loose	0 – 15
loose	15 – 35
medium dense	35 – 65
dense	65 – 85
very dense	85 – 100

consistency of cohesive soils	
classification	c_u [kPa]
very soft	< 10
soft	10 – 25
medium firm	25 – 50
stiff	50 – 100
hard	> 100

Peat

Peat differs from sand and clay by its high organic content *OC*, in the form of an open fibre structure with little inorganic material ('ash'). In the botanic origin of the fibres one distinguishes between water plants, reed, sedge, wood, moss, rushes and heather. The fibres may contribute substantially to the shear resistance, depending on their orientation, weathering and length (usually between 0.25 and 4.0 mm). The fibre orientation may give a directional dependent friction and cohesion value (anisotropy).

Clay

Most common clays are kaolinite, illite and montmorillonite. Kaolinite or Chinese clay is the result of erosion of minerals of granite. The structure is a two layered system of silica and gibbsite. It shows little swell and has a relatively low plasticity. Illite is structured according to a three layered system of silica-gibbsite-silica. It is slightly weaker than kaolinite and shows little swell. Montmorillonite is most common and is a product of further weathering of illite. It is an important

element in bentonite. It cracks in dry periods, can absorb much water, and swells significantly in wet periods; this particularly counts for natrium-montmorillonite.

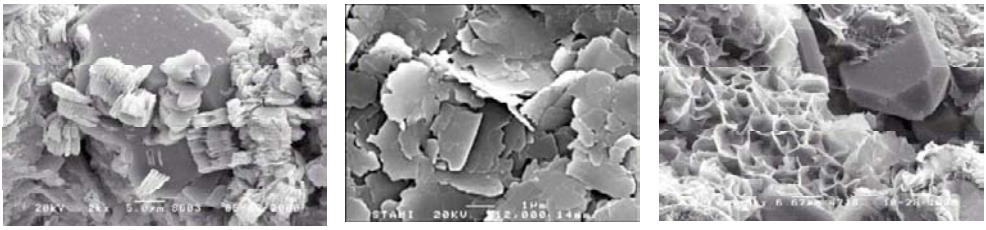

(a) kaolinite *(b) illite* *(c) montmorillonite*

Figure 2.5 Clay structure (electron-microscope)

Classification

A common system uses two letters to classify a soil sample on a first visual interpretation (borehole log), the first relates to the soil type and the second to the constitution, see Table 2.5. Sometimes more than one letter are used for the soil constitution.

TABLE 2.5 CLASSIFICATION SYSTEM

soil type		*soil constitution*	
gravel	G	well graded	W
sand	S	poorly graded	P
silt	M	silty	M
clay	C	clayey	C
organic	O	low plasticity	L
peat	Pt	high plasticity	H

Permeability

In sandy soils the permeability may vary depending on the particle size, the content of fines and the grain-size distribution (see Fig 2.1 and 2.4). For clays the permeability is related to the free water space (non-hydrated) and it is usually small. The range of permeability for various soil types and tests is shown in Table 2.6.

The variation in permeability can be large due to natural heterogeneity and stratification in the field. Air intrusion (unsaturated soil), gas bubbles (methane) or fine fraction have a large impact as well. A distinction is made between hydraulic permeability k [m/s] used in geotechnics and geohydrology, and intrinsic permeability κ [m^2] used for multiple pore fluids, and their relation is $k = \kappa\gamma_w/\mu$. Here, μ is the dynamic pore-water viscosity. Many empirical expressions exist for the permeability, such as $\kappa = 0.005D_{15}^2Tn^3/(1-n)^2$, where T is the so-called tortuosity[10], expressing the pore-space geometrical complexity. Here, the diameter

[10] Tortuosity is a property of a curve being twisted, having many turns. In porous media, its value can be related to the square of the ratio of curve ends and curve length distance and it varies between 0.3 and 0.8 (Bear, 1972).

fraction D_{15} is a suitable measure for the average pore size cross section. The permeability is a constitutive parameter applied in Darcy's law, which describes fluid flow in porous media (groundwater flow).

TABLE 2.6 PERMEABILITY VALUES, CLASSIFICATION AND TESTS

k [m/s]	1	10^{-2}	10^{-4}	10^{-6}	10^{-8}	10^{-10}
drainage	good			moderate	poor	
class	large	moderate	small	very small	relatively impervious	
soil type	boulders	gravel	clean sand	silty sand	clay	
test		pumping test, constant head test		falling head test, oedometer		
			monopole or dipole cone		piezometer	
correlation	grain size distribution			density	clay index	

The hydraulic permeability of the poorly graded sand, of which the grain size distribution is presented in Fig 2.1, can be estimated using the empirical formula for the intrinsic permeability, assuming the porosity n is 40% and the tortuosity T is 0.5. The kinematic viscosity of water is $\nu = \mu/\rho_w = 10^{-6}$ m^2/s. Elaboration gives $\kappa = 0.005\ D_{15}^2\ T\ n^3/(1-n)^2 = 0.005\ (0.15\text{x}10^{-3})^2\ 0.5\ (0.4)^3/(1-0.4)^2 = 10^{-11}$ m^2. Hence, the hydraulic permeability becomes $k = \kappa\gamma_w/\mu = \kappa g/\nu = 10^{-11}\text{x}10/10^{-6} = 10^{-4}$ m/s. The well-graded sand of Fig 2.1 has D_{15} = 0.06 mm, which for similar porosity leads to $k = 1.6\text{x}10^{-5}$ m/s. Significantly less than the poorly graded sand, though D_{50} is higher. For the well graded sand the pores between coarse grains is filled up by smaller grains, creating a less pervious porous structure.

The electrical conductivity of saturated soils, where the pore fluid is conducting and the porous matrix is non-conducting, allows to determine the tortuosity of the porous structure, by comparing the electric conductivity of an electrolyte in a porous medium with the bulk conductivity of the electrolyte. In reservoir engineering this ratio is referred to by the formation factor F. In literature, empirical relations are mentioned, such as $F = T^{m_1} n^{m_2}$, where n is the porosity, and m_1 and m_2 are empirical factors. For uniform equal spheres, Maxwell found $F = (3-n)/2n$. Then, a dense packing (cubic) gives $n = 0.4764$ and a loose packing (rhombohedra) gives $n = 0.2596$, so that one finds $2.64 < F < 5.28$ and for $m_1 = -0.8$ and $m_2 = -1$, the tortuosity becomes $0.67 < T < 0.75$.

Finally, the permeability is essential for contaminant and heat transport through porous media, since it takes place by convection (pore water flow). The transport is also affected by adsorption to/in the grains (retardation) and chemical decay, and heat disperses by conduction (non-conservative).

E STRENGTH AND STIFFNESS ASPECTS

The behaviour of soil masses is described by strength and stiffness parameters. The most relevant are: stress-strain modulus, elasticity or Young's modulus E [Pa], the shear modulus G [Pa], Poisson's ratio ν, the angle of internal friction ϕ [^{o}] , soil cohesion c [Pa], undrained shear strength c_u [Pa], dilation angle ψ [^{o}], compression index C_c, creep or secondary compression index C_α and the coefficient of consolidation c_v [m^2/s]. Aspects of non-linear, anisotropic and irreversible behaviour requires additional parameters, such as the over-consolidation ratio

OCR, ageing, chemical processes, and the distinction between unloading and reloading. These parameters are used in so-called constitutive models, which are invented to describe soil behaviour, when loaded, in terms of deformation and failure. A wide variety of constitutive models exists for one-dimensional swell/compaction or settlement. Generally accepted constitutive and/or rheological models for multi-dimensional behaviour are Hooke's model (linear elasticity), Mohr-Coulomb model, CamClay model, Soft-Soil model, Hardening-Soil model, and Hypoelastic model (see Chapter 9).

application 2.1

What is SMW?
SMW: silty sand well-graded
Estimate I_p from Fig 2.2 for soil type CML.
CML: low plasticity silty clay, I_p around 7 - 10.

application 2.2

Prove that $\gamma_w(G_s+e)/v$ represents the unit weight of saturated soil (see Table 2.1). Consider a volume V of saturated soil, i.e. $V = V_s + V_p$. The pore volume V_p is saturated with water, thus $V_w = V_p$. The weight of solids is $W_s = \gamma_s V_s = \gamma_w G_s V_s$ and the weight of pore water is $W_w = \gamma_w V_p$. Together, the total weight is $W = W_s + W_w = \gamma_w(G_s V_s + V_p)$. With $V_s/V = 1/(1+e) = v^{-1}$ and $V_p/V = e/(1+e) = e/v$, the unit weight of the saturated soil becomes

$$\gamma = W/V = (W_s + W_w)/V = W_s(1+w)/V =$$

$$= \gamma_w(G_s V_s + V_p)/V = \gamma_w(G_s V_s/V + V_p/V) = \gamma_w(G_s + e)/v$$

By weighing the saturated soil W of a soil sample and determining its total volume V, and next drying the soil sample in an oven and weighing the solids and determining their volume by means of a pycnometer, i.e. W_s and V_s, water content w, specific gravity G_s and specific volume $v = 1+e$ are determined. It is a standard laboratory test.

The unit weight of semi-saturated soils is $\gamma_w(G_s + se)/v$, with s the saturation degree. Is the standard test sufficient to also calculate the saturation degree, in the case of semi-saturated soil?

application 2.3

A specific volume of dry sand and water are measured separately and together after pouring the soil in the water (otherwise trapped air causes a saturation of about 75%). Data is given in Fig 2.6. The purpose is to determine various soil properties. Adopt g = 10 m/s^2 and γ_w = 10 kN/m^3. The particle size distribution curve gives D_{50} = 160 μm (fine sand), and U = 1.5 (uniform sand).

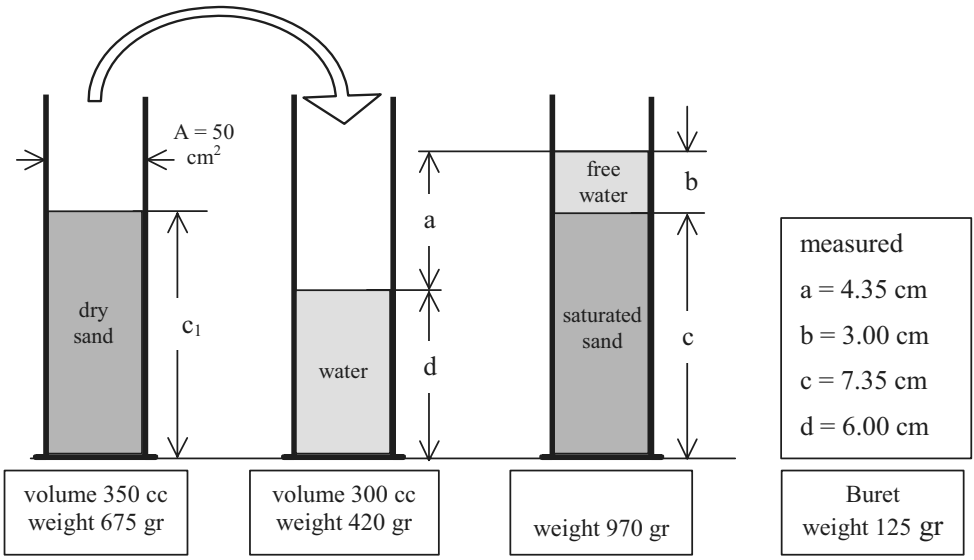

Figure 2.6 Simple classification test (laboratory)

The unit weight of dry sand is

$$\gamma_d = (675 - 125) / 350 = 1.57 \text{ gr/cc} = 15.7 \text{ kN/m}^3$$

Volume of grains and replaced water provide porosity

$$dA = bA + ncA \quad \rightarrow \quad 6 = 3 + 7.35\, n \quad \rightarrow \quad n = 0.408$$

Weight of the saturated sand gives the unit weight of solids γ_s and the wet unit soil weight γ

$$bA\gamma_w + cA((1 - n)\gamma_s + n\gamma_w) = 970\text{-}125 \text{ gr} \quad \rightarrow \quad \gamma_s = 2.505 \text{ gr/cc} = 25.05 \text{ kN/m}^3$$

$$\gamma = (1 - n)\gamma_s + n\gamma_w = 1.89 \text{ gr/cc} = 18.9 \text{ kN/m}^3$$

Consider the sand grains as uniform spheres with diameter D_{50} = 160 μm = 160x10^{-6} m. Then, the so-called specific surface[11] (grain surface/grain volume) becomes $S = 6/D_{50}$ = 3.75x10^4 m^{-1}. For the volume of 350 cc, the total granular volume is $V_s = (1 - n)$ 350 = 207.2 cc = 207.2x10^{-6} m^3 and the total inner surface becomes SV_s = 3.75x10^{4}x207.2x10^{-6} = 7.77 m^2.

The number of equivalent particles in 350 cc becomes 350x10^{-6}/(πD_{50}^3) = 27.2x10^6. So, 30 cm^3 of sand with D_{50} of 160 μm contains 27.2 million particles with a surface of 7.77 square metre! Soil consists of many particles, many intergranular contacts, which determine the shear resistance, and a relatively large internal surface, which determines the permeability.

---

[11] The volume of a sphere is $V = \pi D^3/6$; the surface is $A = \pi D^2$. Hence, $S = A/V = 6/D$.

application 2.4

Explain which soil is characterised by CMH.

application 2.5

According to standard testing of a semi-saturated soil sample, the total weight W, the bulk volume V and, after drying, the solids weight W_s and its volume V_s are determined. Is this sufficient to determine also the saturation degree? If yes, describe how it is related to these measurements.

application 2.6

A semi-saturated soil sample has been tested in the laboratory; the following results are obtained: Bulk mass 160 gram, bulk volume 125 cm^3, dry mass of 110 gram and the net volume of solids 65 cm^3. What was the porosity n, the water content w, and the saturation degree s? What is the specific solid's gravity G_s, and give an indication of the organic content. Then give an indication of the type of soil we are dealing with.

application 2.7

What are the answers on the previous question if bulk mass 193 gram, bulk volume 100 cm^3, dry mass of 158 gram and the net volume of solids 60 cm^3?

application 2.8

A soil sample is tested. The site condition is porosity $n = 0.52$ and saturation $s = 0.85$. The liquidity limit is found for $n = 0.55$ and $s = 0.88$, and the plastic limit for $n = 0.5$ and $s = 0.8$. The specific gravity is $G_s = 2.65$. Is the sample clay or silt, and what is the range of its undrained strength?

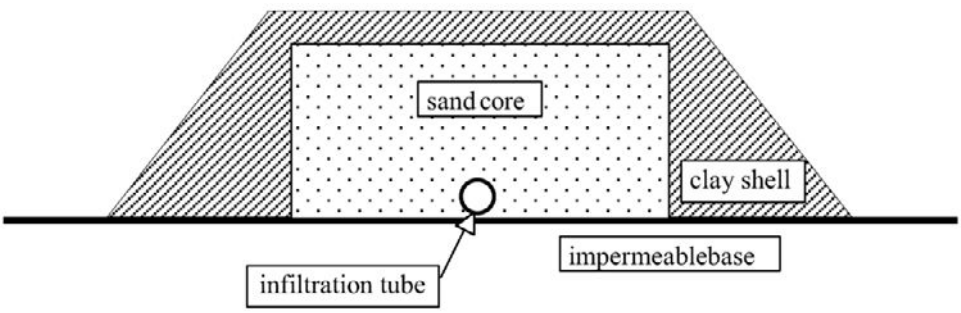

Figure 2.7

application 2.9

An embankment consists of a rectangular sand core covered by an impermeable clay shell (Fig 2.7). The sand is neither dry nor completely wet. A certain amount of water (1 m^3 per 1 m embankment length) is stored in the core by pumping water

into it through an infiltration tube. The water saturates the sand as it rises. Calculate the ultimate position of the phreatic level. How thick should the top impermeable clay cover be to resist the final gas pressure?

Unit weight of sand core $\gamma = 19.5$ kN/m^3, initial water content of sand core $w_0 = 15\%$, unit weight of sand solids $\gamma_s = 26.5$ kN/m^3, unit weight of clay shell $\gamma = 18$ kN/m^3, width resp. height of sand core 10m, 5m, amount of water entering the core 1m^3 / m.

Hint: Calculate dry porosity, initial degree of saturation, initial free porosity, volume necessary to accommodate incoming water. Initial gas pressure = 100 kPa. Use Boyle's gas law.

3 SOIL INVESTIGATION

A SITE INVESTIGATION

Site investigations are determined by their need and impact, related to project requirements, to the specific site and its environment, and to practical and economic limitations. Structural aspects, considered for a site investigation, comprise unequal structural units, the related grid system (columns), location of stabilizing elements (elevator shafts, walls, long elements), foundation levels, temporary structures (building pit), and loading schemes and allowable displacements of all these elements. For offshore structures (platforms and pipelines) and line infrastructural elements, such as roads, railways, dikes and pipelines, site investigation and laboratory testing are required to detect the geological and geotechnical variability (heterogeneity) along the track. In hazard-prone areas (earthquakes, landslides, floods) special tests are required. All aspects of hindrance (sound, vibration, traffic, pollution), fills and excavations, effects on neighbouring buildings and infrastructure, on water and groundwater regimes, during construction and afterwards should be considered. As for practical and economic limitations, it must be stated unfortunately that soil investigations, particularly for large and more complex projects, are usually insufficient. The soil-related probability of damage or stagnation during construction is generally underestimated, and national evaluation studies, e.g. by Littlejohn (1991) and Cummings and Kenton (2004), show that a better quality of site investigation could create considerable savings. The geotechnical engineer should be involved from earlier stages in a project and be more capable of convincing the client about the necessity of proper soil investigation.

Reconnaissance survey

Overall topographic and geological maps, stratigraphic investigation techniques (echo-sounding and seismic survey, geo-electric, electromagnetic, and bathymetric survey, borehole logs, SPT and CPT) are applied to obtain a schematization of the subsoil. For the Standard Penetration Test (SPT) the number of blows N required to push a standard rod 30 cm in the soil is measured. A typical value of N for normal sand is 20 and for normal clay 5. For the Cone Penetration Test (CPT), a standard cone is pushed into the soil with a moderate constant velocity while measuring the tip resistance q_c and the sleeve friction, separately. The point resistance allows distinguishing sands and clay or peat. The ratio between side friction and point resistance represents the friction number, which gives an indication to distinguish between clay and peat. A piezometer at the tip gives information about the local permeability; even thin silt or clay layers in sand are detectable. Usually, the hole caused by CPTs is not sealed off, except in the case of polluted soils (DNAPLs) or when leakage could be a problem (artesian situations). The sealing is performed by a environmental-friendly bentonite.

In some cases, special tests are required (density probe, vane test, plate bearing test, CBR-test, dilatometer, piezometer, pumping test, pore-pressure meter, pressure meter, vibration test, specific chemical probes). An example of a standard site investigation is shown in Fig 3.1: a boring and a CPT.

The main purpose is the determination of the subsoil stratification, i.e. the layering, and to measure the physical and mechanical constitution of stiff and weak soil layers. In principle, only a limited number of local soil properties can be measured directly, and most of the required properties must be determined indirectly, by empirical correlation and additional laboratory testing on carefully obtained samples. Since soil is heterogeneous by nature and the scale of heterogeneity (correlation length) differs largely for various properties, a site investigation provides only limited information and engineering experience plays a major role in the interpretation of the data obtained.

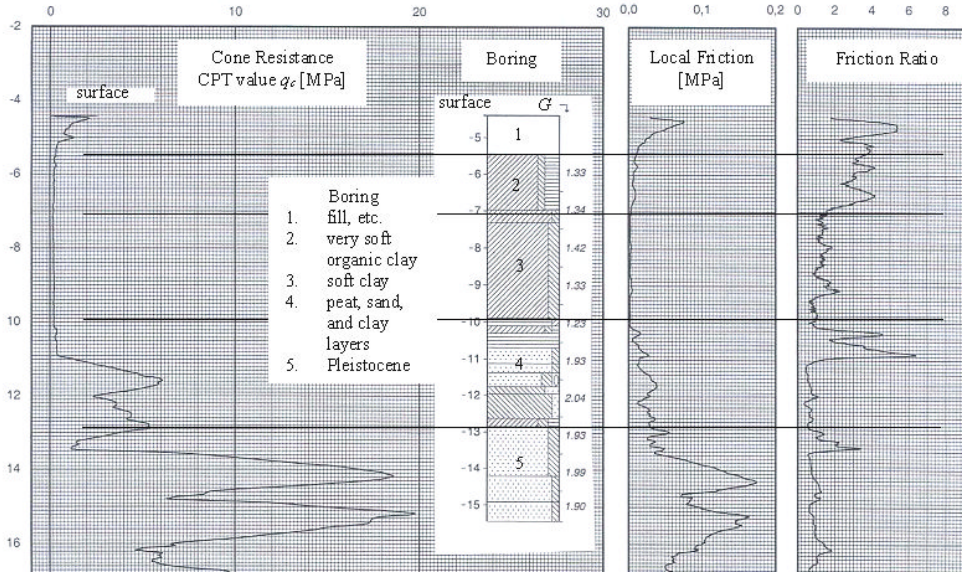

Figure 3.1a CPT test and schematised soil profile from a boring

In addition to the mechanical and electronic cones, a variety of other CPT-deployed tools have been developed over the years to provide additional information. One common tool advanced during CPT testing is a geophone set to gather seismic shear wave and compression wave velocities.

The Delft continuous sampler is used for obtaining high quality samples of soft cohesive soils. The system is pushed into the ground using standard CPT equipment, while the sample being fed automatically into an impervious nylon sleeve (Fig 3.1b). Next, the sample within the sleeve is inserted into a thin-walled plastic inner tube filled with a supporting fluid of bentonite. The upper end of the nylon sleeve is fixed to the top cap of the sample, which is connected through a tension cable to a fixed point at ground surface. In this manner up to 10m continuous sampling can be achieved. High horizontal stresses may cause sleeve breakage.

Ground radar is a non-destructive site investigation technique that uses electromagnetic waves to visualize the layering of the shallow subsurface. An emitting antenna radiates an electromagnetic wave front, which is transmitted in the subsoil. It reflects at inhomogeneities, such as a sand-clay interface, recorded in

the receiver antenna. The non-reflecting part penetrates deeper into the soil. The reach of the ground radar depends on the electric resistance of the subsoil and the frequency. Common frequencies are 50 to 2500 MHz. The distinction depends on the wave celerity *c* and the frequency *f*; an object much smaller than *c/f* can not be detected. So, for high frequencies the accuracy is large, but the reach is small. The method is particular suitable for determining asphalt thickness, detecting obstacle and groundwater levels. It works very well in dry soils and ice, rather well in wet soils (fresh water) and frozen soil, not well in clay or peat, and in soils containing brackish or salty water.

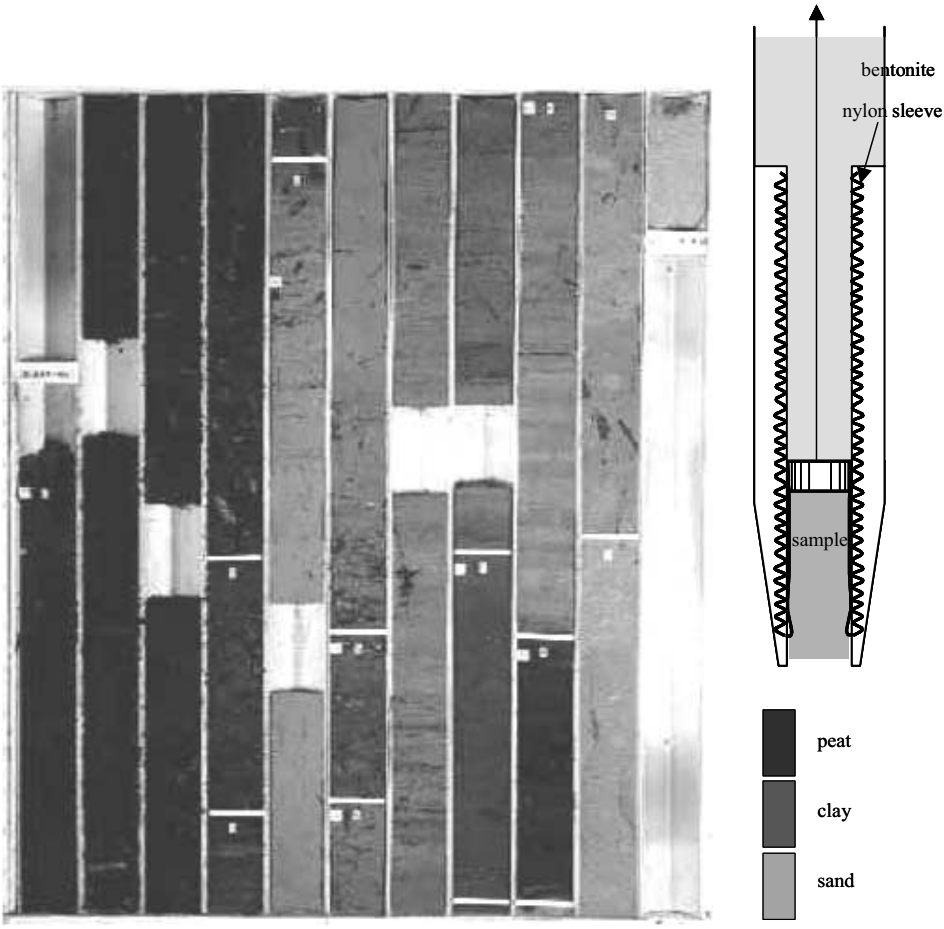

Figure 3.1b. Soil profile from a boring by the Delft Continuous Sampler, 10.2 m long

A pressiometer probe can measure stiffness properties of soils. Mounted on a standard cone penetrometer, the pressiometer consist of flexible membrane protected by a thin laminated metal cover, which during testing is expanded by nitrogen gas pressure at a given rate, while displacement sensors record the deformation. At a certain maximum, the pressure is kept constant and creep and plasticity is measured. From the obtained results the elastic shear modulus, the

initial soil pressure and the (shear) failure pressure can be determined (but initial pressure is affected by the probe penetration itself).

Monitoring of vertical deformation in the subsoil is possible by an extensometer. Packer-anchors are fixed (by grout) in a boring, at various levels. A hollow pipe in the anchor allows transmission of fibreglass rods, which are fixed at other anchors (maximum 6), allowing vertical deformation recording at various levels. At the surface, sensors register the displacements of the fibres. Data can be collected locally or remotely via GSM. An inclinometer is used to measure the horizontal displacement at different levels. It consists of a plastic pipe, in which the inclinometer rolls along grooves, while recording deviations of the vertical that are caused by deformations of the vertical pipe due to horizontal soil movements.

Soil quality survey

Interactions between surface water, groundwater and ground particles are complex. Consequently, groundwater pollution, sometimes referred to as groundwater contamination, is not easily classified. In particular, groundwater aquifers (permeable sand layers) are susceptible to organic (sulphur dioxide, ammonia, nitrates and phosphates, heavy metals) and inorganic (detergents, food processing waste, insecticides and herbicides, hydrocarbons, industrial solvents, cosmetics, medicines) substances from sources that are related to surface water bodies, heat, industrial spill or ongoing releases of chemical or radionuclide contaminants or by waste and agricultural fertilizers, which infiltrate into the subsoil and initiate physical, chemical and/or biological reactions. The pollution manifests itself as a contaminated plume or floating thin lenses, such as dense nonaqueous phase liquids (DNAPLs). The movement of the plume, a plume front, can be part of a geohydrological transport model or groundwater model. Analysis of ground and groundwater contamination focusses on the soil characteristics, site geology and the nature of the contaminants. A series of tests for the groundwater status is defined in the Water Framework Directive (2000/60/EC) and Groundwater (Daughter-)Directive (2006/118/EC). In situ testing includes boring (sampling for further lab testing) and specially equipped cone penetrometers, e.g. measuring volatile substances, electrical resistance, chemical characteristics and a realistic view by a micro-camera.

Special CPT-probes such as laser-induced fluorescence, X-ray fluorescence, soil conductivity/resistance, and cameras for capturing video imaging are also increasingly advanced in conjunction with the CPT probe. The camera probe is a soil investigation technique that uses a standard soil penetrometer to visualise record images of the subsoil, retrieved by a lamp, a mirror and the camera itself, which focuses at the soil aside through a sapphire-glass window of 35 mm^2. The camera is connected to a video recorder and a monitor via an electrical signal cable. Images show the soil at high resolution, clearly exposing grain size and colour. As images can be magnified up to 100 times on the monitor, the camera also acts as a microscope, providing information that cannot be seen by the naked eye.

The water-probe measures the local electric resistance of the pore water in a small cell with a volume of 5 ml. The ground-probe measures the electrical resistance of the bulk soil. Combining both results provide information about the

local density (sands). The ground-probe contains two sets of electrodes, one for the current and one for measurement. In an EM-investigation, electromagnetic induction is used to measure the electrical conductivity of the subsoil from the surface. A transmission coil on one side of the instrument sends an alternating current with a fixed frequency into the soil, which creates a primary magnetic field in the subsoil. This induces small currents in the subsoil that in turn create a secondary magnetic field. A receiving coil records the secondary magnetic field and the primary field. From these data the electrical conductive capacity of the subsoil can be found, which represents an average value of the electrical conductive capacity of the layered subsoil.

The groundwater-sampling probe has an externally located filter element. During penetration of the probe pressurised nitrogen gas is applied to the filter, keeping it free of incoming water and/or soil particles. At the measuring location, groundwater is let entering the sampling chamber, where the electric resistance, the *pH* and the temperature are being measured. Next the nitrogen gas expels the water and the probe can advance to the following location. As an addition/alternative, the groundwater can be fed through a set of anaerobic flow cells, where several physical/chemical parameters can be measured.

The determination of hydrocarbon pollution in soils (DNAPLs) is performed by lightening the soil through a sapphire glass window with UV light, mounted in a standard CPT probe. The fluorescent hydrocarbon reflects the light, which is detected by a photo-multiplication tube and registered via an electric cable to a data-acquisition system.

Monitoring

The goal of geotechnical monitoring is the development and maintenance of sensor network and remote observation (e.g. InSAR) technologies for early warning systems, which detect technical and environmental factors that affect safety and health, and which make it possible to forecast failures. A detection system for failure mechanisms might be cheaper and safer than the alternative: over-dimensioning. Monitoring will increase the understanding of mechanical soil behaviour.

Developments in communication and sensor technology have advanced so far that it seems possible to utilise it to effectively support the management and monitoring of construction works and their functioning in an economically efficient manner. Acoustic sensors may detect the noise that (sandy) soils produce when deforming. However, most of the recently developed sensor and communication technology (e.g. optic fibres, wireless LAN), needs to be tested under field circumstances, to prove their robustness, suitability and efficiency.

Determining real failure processes is still a research field in development. Strength depends on a number of parameters, which are hard to determine. Numerical calculation methods for strengths and performance suffer from significant uncertainty between calculated and actual strength. Monitoring supports such models, fed by real time data from sensors and remote observation, when calculating the short and long time future of the structure and reporting if immediate safety issues are at stake.

Intensive monitoring of the strength and performance reduces costly over-dimensioning, enables transparent and reproducible decision-making during imminent calamities, enables determination of the effectiveness of innovative construction technologies, and plays an eminent role in the observational method (Eurocode 7).

B LABORATORY TESTING

For most standard laboratory tests in geotechnical practice internationally accepted test procedures are available. These laboratory tests are suitable to determine the following

- soil classification (already discussed before);
- permeability (constant head test, falling head test);
- compressibility and creep (oedometer, swelling test);
- strength properties (shearbox, triaxial test);
- compaction (density tests);
- chemical constitution tests.

Permeability

For granular soils the constant head method is applied for determining the sample permeability k (see Fig 4.2). For cohesive less-permeable soils the falling head method is suitable (see Fig 4.3). For this method the applied stress state is important and consideration of different loading stages is sometimes required (see also oedometer test). The in-situ permeability of soils, in particularly in sand and silt formations, is often determined by site investigation (pumping test, piezocone, monopole sounding).

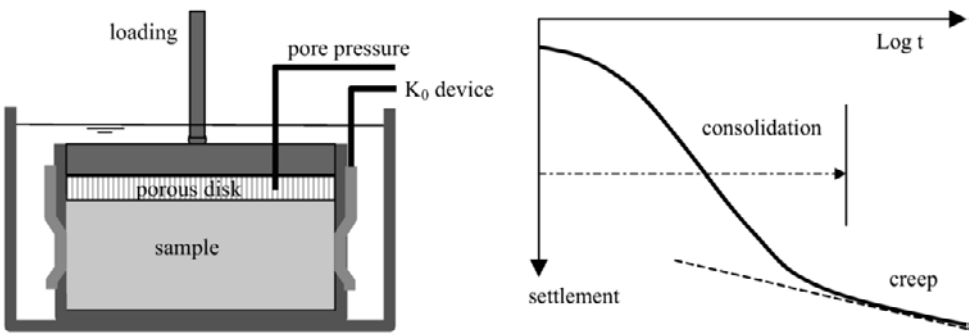

Figure 3.2 Oedometer with K_0 facility

Oedometer and swelling test

The oedometer is used to determine the uniaxial deformation of a soil sample. It is particularly suitable to soft and less pervious soils (silt, clay, peat). In principle, four parameters are determined: consolidation coefficient c_v (the v refers to vertical), the coefficient of vertical volume strain m_v or the compressibility index C_c, the vertical permeability k, and the creep index C_α. A variety of testing equipment and procedures exist. Most commonly, incremental loading is applied, with the load being doubled each subsequent step (Load Increment Ratio = 1).

More recent procedures use piston control to obtain the Constant Rate of Strain (CRS) test, the Constant Rate of Loading (CRL) test, the Constant Gradient test (CG), the Constant Pore Pressure Ratio test (CPR), and recently the K_0-CRS compression test (Fig 3.2), which allows to measure the horizontal stress changes during the test.

There are various methods to determine the uniaxial deformation parameters from the measurements. The c_v value can be obtained by Taylor's method, Casagrande's method, Sridharan-Prakash' method, and Asaoka's method (see Chapter 6). Approximate values for the elasticity modulus E can be obtained from the CPT value q_c, according to

$$E = aq_c \tag{3.1a}$$

Here, a is < 1 for peat, 1 – 2.5 for (silty) sand, 3 – 6 for clayey sand, or 3 – 8 for soft clay. An alternative value for E is, incorporating the typically non-linear soil behaviour

$$E = \frac{1.5\sigma'_v}{(1-n)C_c} \tag{3.1b}$$

Here σ_v' is an estimate of the vertical effective soils stress, and n the porosity. A typical value for the compressibility index C_c may be 0.005 for sand, 0.1 for clay and 0.3 for peat.

Some clays are known to heave (swell) when they become saturated, which may involve considerable forces. Measuring the free swell in the oedometer is called the simple swelling test, and measuring the vertical load required to prevent swell during saturation is called the swelling pressure test. The swelling process may require a considerable time to reach final stage.

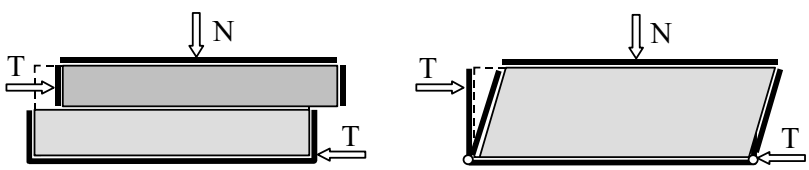

(a) *(b)*

Figure 3.3 Direct Shear and Direct Simple Shear Box

Shear box test

The shear strength of soil is a crucial parameter for soil stability (failure). It is related to the friction capacity between soil particles. Several shear tests are available to evaluate the shear strength, such as under direct shear DS and direct simple (uniform) shear DSS conditions (Fig 3.3). The normal force N and the shear force T can be approximated by a uniform normal stress σ and shear stress τ. The test outcome is presented as an envelope, known as the Mohr-Coulomb failure line, in the σ'-τ stress plane, which determines the stability limit in terms of cohesion c and internal friction angle φ. The state of stress in the DS test is clearly highly non-

uniform. The DSS test was developed to improve on the DS test, but also it suffers from non-uniformity by the lack of shear stress on the vertical faces. Since frictional soil can fail in two modes (double sliding), the failure state in a DSS test is not necessarily unique. It depends on the actual stress state (horizontal stress/vertical stress), see Chapter 9.

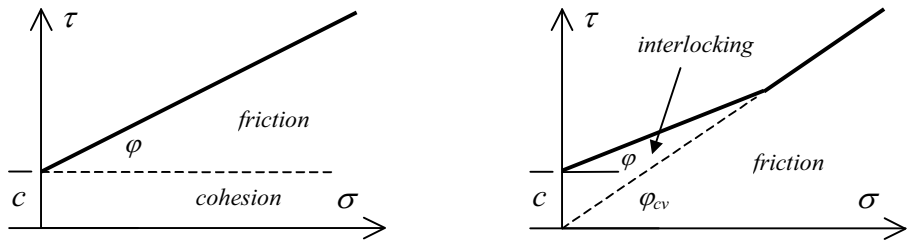

(a) Terzaghi's concept *(b) Taylor's concept*

Figure 3.4 Mohr-Coulomb model

The Mohr-Coulomb model is widely in use in geotechnical engineering. Terzaghi suggested for clay a concept based on cohesion, independent of normal stress, and friction (Fig 3.4a). Taylor suggested, based on shear box tests on sand, a different (peak strength) model. His concept does not include cohesion but interlocking (related to dilation or asperity theory), which decreases with normal stress (Fig 3.4b), and friction following φ_{cv}, the angle of repose of drained granular soil. These two concepts led to a serious debate on true friction and true cohesion, and whether or not cohesion exists, lasting to the present day. In stiff clay, interlocking develops just as in dense sand, but the increased shear resistance is mainly a result of the work required to suck in water. Localised weakened shear surfaces develop and strength is subsequently reduced. According to Schofield, Coulomb (1773) supported by Rankine (1857) stated that disturbed soils do not possess cohesion. In design, it is safe not to count on cohesion. Normally consolidated clay, the consolidation stress of which is above or equal to the yield stress, is known not to possess cohesion, unless significant cementation of particles and/or particle aggregates is involved.

Triaxial test

The triaxial test apparatus (see Fig 3.5) allows measuring axial and horizontal deformations of a cylindrical soil sample wrapped in an impervious membrane under varying vertical loading (called deviator stress, see later) and a supporting ambient cell fluid pressure. Also the pore pressure in the sample (usually at the bottom) can be measured. From triaxial test data various constitutive parameters can be determined, such as elasticity E_{50}, cohesion c, friction angle φ, and dilation angle ψ. The various stages in triaxial testing (impose cell pressure, impose a vertical loading step or a certain deformation, etc.) and the choice to allow the sample to drain (consolidate) or not during a stage provide for different approaches. One distinguishes CU (consolidated under uniform cell pressure load and undrained during a loading step), CD (consolidated-drained) and UU

(unconsolidated-undrained) under stress or strain controlled compression or extension. Triaxial behaviour is discussed in Chapter 7.

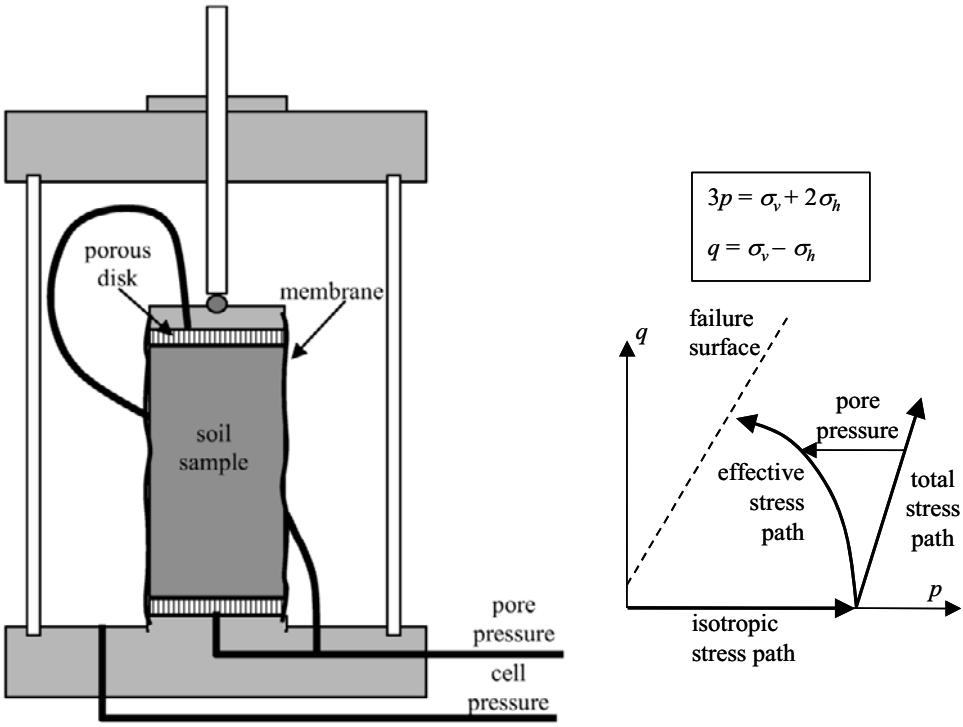

Figure 3.5 Triaxial test apparatus and the pq-diagram for a triaxial compression test

Density tests

An important method for soil improvement is densification, and three methods are distinguished: mechanical densification, preloading and dewatering. Specific laboratory tests are designed to evaluate the effect in the field.

The porosity n or the voids ratio e is an essential parameter, which determines the matrix density. For granular soils the density is expressed by the relative density D_r but it is often not very accurate. The minimum density of sand can be determined by the dry method (carefully depositing oven-dried sand) or the sedimentation (floating) method in water. The critical density of sand refers to the density, for which there is no volume change when subjected to shear deformation. A strain-controlled shear test is applied to measure the volume change during shear deformation. Dense granular soils may show an initial increase (dilatancy) of volume during shear and loose soils a decrease (contraction), which is related to properties of a granular skeleton. For large deformation the soil attains the critical density. Since during dilation or contraction of saturated soil the pore volume changes, pore water pressure changes may occur, which may increase or decrease soil stability. This is of particular importance, when assessing liquefaction of sand or undrained shear strength of clay (contraction), see Chapter 16.

MATRIX A		*innovation cycle (tools)*			
geotechnical fields		*empirical*	*experience*	*theoretical*	
main field	*specific item*	*experimental model-facilities*	*field data & monitoring*	*prediction & calculation model*	*M (S)*
transportation infrastructure	airfields, roads, railways, tunnels, bridges, pipelines	86	93	82	87(5)
foundation engineering	building pits, underground building, piling, monuments	68	82	81	77(8)
hydro-geotechnics	offshore, harbours, dredging, dikes, dams, reclamation	88	84	86	86(1)
geo-ecology	waste disposals, industry plants, reservoirs, groundmixing	74	88	79	80(5)
M (S)		79(9)	87(5)	82(3)	83(5)

C PHYSICAL MODEL TESTING STRATEGY

In 2000 a workshop was held on the role of experimental research for the international geotechnical world. 34 prominent researchers[12] contributed and 20 of them participated in a brainstorm session. The main goal of the workshop was a statement on the role of experimental modelling, the scientific value of experimental R&D, and the usefulness of unique experimental model-facilities. Two scans were elaborated: matrix A about the importance of innovation for specific geotechnical fields and matrix B about the estimated value of specific experimental model-facilities for the identified geotechnical fields.

Each participant gave a value (1=low, 2=mediate, or 3=high) expressing the importance from personal experience or from a national point of view. These values are accumulated and transferred to percentages (0%=useless, 100%=perfectly useful), in Matrix A above, and per category the mean value (M) and the standard deviation (S, in brackets).

[12] Austria (Heinz Brandl), Belgium (William van Impe), Denmark (Jørgen Steenfelt), France (Jacques Garnier, Samuel Amar), Germany (Helmut Kobus, Manfred Nussbaumer, Hocine Oumeraci, Pieter Vermeer), Greece (Michael Kavvadas, Andreas Anagnostopoulos), Hungary (Emöke Imre), Ireland (Trevor Orr, Eric Farell), Italy (Henrico Brignoli, Michael Jamiolkowski), Japan (Hideo Sekiguchi, Kenji Ishihara), Netherlands (Frans Barends (organizer), Ben Veltman, Arnold Verruijt), Norway (Knut Andersen, Suzanne Lacasse), Portugal (Antonio Gomes Correia, Pedro Sêco e Pinto), Romania (Iacinto Manoliu), Russia (Viacheslav Ilychev), Spain (Eduardo Alonso, Cesar Sagaseta), Sweden (Ulf Bergdahl, Rainer Massarch, Bengt Rydell), Switzerland (Sarah Springman), Turkey (Ergün Togrol), UK (Frans Molenkamp, Neils Taylor), USA (Gholamreza Mesri).

score	*TRANSPORTATION INFRASTRUCTURE* *aspects*	*shaking table*	*compact devices*	*large element test*	*dedicated element test*	*centrifuge test*	*test-site*	*monitoring*
11	soft-soil improvement	0	2	4	1	4	12	11
11	reliable soil properties	0	3	8	10	0	12	3
8	embankment settlement	0	0	2	1	7	12	13
8	landslides, slopes	0	0	4	2	9	6	14
7	deformation by tunnelling	0	0	0	2	14	2	13
7	serviceability limit state	0	2	2	5	3	4	8
7	HSL settlement dynamics	0	1	4	6	4	5	9
4	seismic effects on buried structures	← *not evaluated*						
3	plasto dynamics							
2	ship and ice collision							
2	use of materials outside the limits							
1	road widening							
1	bridge abutments							

score	*FOUNDATION ENGINEERING* *aspects*	*shaking table*	*compact devices*	*large element test*	*dedicated element test*	*centrifuge test*	*test-site*	*monitoring*
14	environmental effect of deep foundations	0	0	1	6	8	4	17
12	coupled foundation-superstructure behaviour	2	0	0	7	10	1	10
12	reliable ground properties	0	3	8	9	0	10	6
8	serviceable limit state	0	2	0	6	5	7	11
6	water table lowering effect (settlement)	← *not evaluated*						
6	specific pile foundations							
5	foundations on soft soil							
5	dynamic loading (sheet pile, deep/shallow foundations)							
3	pile group effect (horizontal, vertical)							
3	deep excavation, slope stability							
1	stress rotation effect on security							
1	reuse foundations, ULS and SLS change							

score	*HYDRO-GEOTECHNICS* *aspects*	*shaking table*	*compact devices*	*large element test*	*dedicated element test*	*centrifuge test*	*test-site*	*monitoring*
11	capacity under cyclic loading	7	4	3	9	9	1	3
8	dynamic structure-foundation interaction	12	0	1	3	9	1	3
7	interaction water-soil (incl. semi-saturated)	0	4	2	9	6	6	6
6	slope failure by rain and/or water	0	2	3	2	5	8	14
6	safety old dikes (internal erosion and decay)	0	1	4	0	5	6	16
6	underwater slope stability	1	0	1	5	11	4	10
5	embankments of soft soil							
5	offshore structure anchors							
4	cracking in earth and rock-fill dams							
4	filtration criteria							
3	measures to ensure clean water						← *not evaluated*	
3	shallow foundations							
2	avalanches, moraine creep							
2	seismic behaviour breakwaters							
2	deep-water soil investigation							

score	*GEO-ECOLOGY* *aspects*	*shaking table*	*compact devices*	*large element test*	*dedicated element test*	*centrifuge test*	*test-site*	*monitoring*
14	monitoring leakage	0	2	2	1	2	7	15
11	remediation contaminated soils	0	4	4	1	5	8	9
10	rehabilitation old waste disposal sites	0	1	4	1	1	9	8
10	stability waste disposal	2	1	3	3	7	6	7
8	two-phase flow in heterogeneous media	0	3	5	5	6	0	7
6	assessment of characteristic values							
6	detection pollution in heterogeneous media							
6	effect of natural hazards on waste disposals						← *not evaluated*	
2	use of geo-radar in waste detection							
1	dynamic effects in two-phase flow							
1	interplay geotechnics and geology							

The outcome is remarkable. Experimental model-facilities, field monitoring and calculation models all obtain a high score. The mean value and corresponding standard deviation show that in all cases the outcome is significant and rather

unanimous. It shows the generic potential of the geotechnical tools. A more close inspection on the role of facilities was worked out for the four geotechnical field: (1) transportation infrastructure, (2) foundation engineering, (3) hydro-geotechnics, and (4) geo-ecology. From more than 200 geotechnical aspects, 22 specific aspects were selected by ranking and the corresponding appropriateness of the various experimental facility applications were evaluated by counting votes. Details are given per geotechnical field in the previous tables.

From about 100 facilities in total 6 specific unique experimental model-facilities and 1 for field data & monitoring were selected, relevant for further evaluation.

experimental model-facilities	LET: large element tests; heterogeneous and coarse materials DET: dedicated element tests; small strain, dynamic and cyclic properties BIN: comprehensive and compact facilities for testing and calibrations SHA: shaking tables for dynamic and earthquake research CEN: centrifuge models; small- and large-capacity facilities TES: test sites and portable in-situ labs
field data & monitoring	MON: intelligent monitoring systems; extensive, on-line, and automatic, related to projects or maintenance of structures

Each participant assigned per aspect not more than two facilities as most appropriate. The result is shown in Matrix B. By multiplying the aspect priority, given to the specific problem or innovation for each main field, with the number of votes given to the selected facilities, a balanced weight is found to evaluate the usefulness of the various facilities. For example, the results show that geo-centrifuges are required mostly for investigation in the field of transportation infrastructure for embankments, landslides and tunnelling, in foundation engineering for deep foundation and coupled structure-foundation behaviour, in hydro-geotechnics for underwater slopes, cyclic and dynamic interaction, and in geo-ecology for stability of waste disposal, two phase flow and behaviour of contaminated soils.

MATRIX B	SHA	BIN	LET	DET	CEN	TES	MON
main geotechnical field	*experimental unique model-facilities*						*projects*
transport infrastructure	0	4	12	12	17	25	30
foundation engineering	2	3	7	21	18	16	33
hydro-geotechnics	12	6	7	16	23	12	24
geo-ecology	1	8	12	7	14	23	35
total (facilities)	5%	7%	14%	20%	26%	28%	-

The general results are expressed in percentages per geotechnical field in Matrix B. The bottom row shows the scientific score for the various experimental model-facilities. Field data and monitoring are also involved during the construction process and structural maintenance, and as such not quite a model-facility. In fact, field monitoring focuses on the serviceability state (function), while modelling commonly on ultimate limit state (failure). In general, about 1/3 of the geotechnical effort should be devoted to field data collection and structure monitoring, and 2/3 to experimental modelling by unique facilities. A well-balanced geotechnical laboratory should be equipped for test-sites (28%), centrifuge testing (26%),

dedicated element testing (20%), large element testing (14%), compact sets for testing and calibration (7%), and shaking table testing (5%).
The main conclusions are

- Unique experimental model-facilities are important instruments for research and for complex situations in practice.
- Resources and efforts should be divided in a well-balanced way over field monitoring, experimental modelling and calculation model development. It appears that each needs comparable investment and attention.
- Only when results of experimental modelling are better integrated in required developments and innovations, will a significant step forward be possible with regard to durability and reliability of geotechnical achievements.
- Unique experimental model-facilities are expensive in character, because permanent specialised staffs are required. Therefore, it is recommended that a special task in an international context is reserved for "main geotechnical centres" in developed countries.

application 3.1

What is the essential difference between cohesion in Terzaghi's concept and interlocking in Taylor's concept?

application 3.2

Two shear tests are applied in practice: direct shear and simple shear. What do you prefer? Explain why.

application 3.3

In the triaxial test there is a cell pressure p and an additional loading stress q. Show that this loading induces a maximum shear stress in the sample equal to $q/2$.

application 3.4

A housing project is to be built over expansive clays in a dry climate. Due to thermal osmosis, moisture will be drawn towards the soil under the houses as its temperature drops. What effects might this have on the foundations? Devise a laboratory test to determine these effects. With which soil parameters would you characterise this behaviour?

application 3.5

What is the essential difference between SPT and CPT and in which soils is SPT preferred?

4 SOIL AND GROUNDWATER

A VERTICAL SOIL STRESS

Terzaghi's effective stress principle

Intergranular soil forces at micro scale are averaged over the soil bulk surface and referred to as intergranular normal stress σ'' and intergranular shear stress τ''. Saint-Venant's principle permits to state that an individual grain completely surrounded by a uniform water pressure u carries everywhere inside the same pressure u. Hence, on any cross section through a granular fabric (arrangement of grains) the pore pressure u is present in the pores and in the grains, i.e. uniform over a bulk surface. This allows to add the intergranular stress σ'' and the pore pressure u into a total normal stress $\sigma = \sigma'' + u$. Since the pore water does not convey shear stress, the total shear stress becomes $\tau = \tau''$.

If the pore water partly surrounds the grains, i.e. if the intergranular contact areas are large (deep sand formations) or in unsaturated soil, the normal pressure inside the grains generated by the pore fluid will be less than u.

Soil deformations are related to rearrangements and compression of the granular fabric. It is convenient to have a stress that directly relates to deformations. Terzaghi (after Fillunger) defined such stress, the effective stress σ'. When the grains are relatively incompressible[13] the deformations will not involve changes at the granular contacts (indenting) and then $\sigma' = \sigma''$. However, when grains compression is involved, as a consequence the pore water becomes involved, and $\sigma' \neq \sigma''$. In any bulk cross section in the soil the total normal stress σ becomes

$$\sigma = \sigma' + \chi u \qquad \text{with} \qquad 0 < \chi < 1 \tag{4.1a}$$

For deep soil layers, χ is related to the Biot coefficient, and for unsaturated flow χ is related to the pF value. In saturated soils with relatively incompressible grains and relatively small intergranular contact areas $\chi = 1$, and Terzaghi's effective stress principle holds

$$\sigma = \sigma' + u \tag{4.1b}$$

Formula (4.1b) allows to separate granular deformation and pore water flow in a simple way, in terms of partial stresses, i.e. the effective stress σ' and pore pressure u, in more dimensions. Pore pressures are affected by and may induce groundwater flow. Effective stress changes induce soil deformation (rearrangements of the granular fabric), which changes the porosity and affects the pore pressure. This interconnected system is the core of soil mechanics, i.e. equilibrium and deformation behaviour.

---

[13] Order of magnitudes of compressibility factors in m^2/N: water 0.5×10^{-9}, sand grain (silicate) $\sim 10^{-11}$, granite $\sim 10^{-13}$, water with small air bubbles $\sim 10^{-6}$, granular fabric (sand, clay) $\sim 10^{-6}$.

Vertical stress and pore pressure

Soil stresses are generated by weight (gravity) and loading. The vertical total normal stress σ_v in a horizontal layer increases with depth, according to (positive z is downwards)[14]

$$\sigma_v = z\gamma \tag{4.2}$$

Here, γ is the volumetric (total) soil weight, composed of specific weight of grains γ_s and pore water weight γ_w , incorporating saturation degree s, specific air weight γ_a and porosity n.

$$\gamma = (1 - n)\gamma_s + sn\gamma_w + (1 - s)n\gamma_a \tag{4.3}$$

In soil mechanics, the air or any other gas plays usually a minor role. The groundwater or pore pressure u however plays an important role and in stagnant groundwater it increases with depth, according to

$$u = z\gamma_w \tag{4.4}$$

Soil particles when submerged in groundwater loose some weight (Archimedes' law or buoyancy force[15]), which affects their intergranular stress. In soil mechanics, one adopts a hypothetical stress to express the average intergranular stress, referred to by effective stress. For the vertical component it becomes with (4.3), disregarding γ_a

$$\sigma_v' = z\gamma' \quad \text{with} \quad \gamma' = (1 - n)\gamma_s - (\chi - sn)\gamma_w = \gamma - \chi\gamma_w \tag{4.5}$$

which for $s = 1$ and $\chi = 1$ gives $\gamma' = (1 - n)(\gamma_s - \gamma_w)$, exactly the submerged grain unit weight.

For a saturated soil with relatively incompressible grains, fluctuations in a (horizontal) free water level will not affect the effective vertical stress when fully submerged. Thus, effective stresses in a sea bottom do not change due to sea waves. However, fluctuations of a (horizontal) groundwater table will affect the vertical effective stress because of the buoyancy. Large groundwater table lowering may therefore cause noticeable land subsidence.

B GROUNDWATER FLOW

Occurrence

Water penetrates the soil from rain, rivers, lakes, etc., accumulates in the pores and evaporates through heat and plants. This is the field of geohydrology. One

---

[14] Common in geotechnics, stress is defined positive for pressure, throughout this book.

[15] The pore pressure increases linearly according to volumetric water weight: $z\gamma_w$, but the gravity force due to the mass of pore water increases only with $nz\gamma_w$. Archimedes' law covers the difference $z(1 - n)\gamma_w$.

distinguishes the unsaturated zone and the saturated zone (pores are completely filled with water). The water pressure in the soil, the pore pressure, is affected by atmospheric pressure, gravity and pore water flow. The theoretical surface where the pore pressure equals the atmospheric pressure is called the phreatic surface or free water table, above which is the so-called capillary zone (height h_c), a semi-saturated zone supported by water-grain attraction (molecular adhesion). The capillary zone in sand or peat is in the order of some decimetres, and in clays it can be metres. In the unsaturated zone isolated areas of hanging saturated soil may occur, so-called pendular pore water, with an independent pressure field. These zones do not affect the coherent groundwater area, but may affect local soil behaviour.

In geohydrology, formations (sand) that provide for groundwater flow are called aquifers, layers (clay) that allow minor groundwater flow are called aquitards, and impermeable formations (rock, salt) are called aquicludes. Natural processes, such as roots, worms and leaching, cause soil formation changes. Hence, clays at the surface may have a permeability equal to sand. Sands may suffer internal erosion or internal migration of their finer particles. Suffosion or suffusion refers to the process of extracting of fine soil components and increasing permeability. Colmation is the opposite process where fines are blocking the pores and permeability decreases.

Groundwater head

When placing an open-end pipe (piezometer) in the saturated zone at a certain depth z, the groundwater will penetrate in the pipe up to a level where its weight counterbalances the actual pore pressure u at the pipe tip. This rise expressed as pressure head h_p reads in formula

$$h_p = u/\gamma_w \tag{4.6}$$

The position of the pipe tip is measured from a certain reference and it is called elevation head h_e. The water level in the piezometer is measured from the same reference and called potential head or total head h (often written as potential ϕ). During field measurement the reference is the ground surface. Here, the z-direction is usually taken positive pointing down. Thus, the potential head is equal to the elevation head h_e minus the pressure head (Fig 4.1a), in formula

$$\phi = h = h_e + h_p = -z + u/\gamma_w \tag{4.7}$$

Since the potential head contains information about local pore pressure and includes stagnant hydrostatics[16], it is suitable to detect with it groundwater flow behaviour in terms of local pressure and flow. Lines (or surfaces in 3D) of equal

[16] If the potential does not vary in z-direction, i.e. $\partial\phi/\partial z = 0$, it follows $\partial(z-u/\gamma_w)/\partial z = 0$, or $u = \gamma_w(z-c)$. Here constant c is related to the position where $u = 0$, the groundwater table. Thus, $\partial\phi/\partial z = 0$ reflects hydrostatic pressure.

potential head are called equipotentials. In 2-dimensions, groundwater flow can be visualised by orthogonal flow and equipotential lines (Fig 4.1a).

Gradient

The difference of measured potential head measured at two specific locations A and B, referred to as potential drop, will generate groundwater flow. The corresponding local gradient is defined as (when distance l_{AB} tends to zero)

$$i = (h_B - h_A) / l_{BA} = dh/ds \qquad (4.8)$$

where s is measured along the flow direction (here s is seepage path coordinate, not to be confused with saturation degree). Since the free water table is also a flow line, its inclination represents a local gradient i, which indicates flow along the free water table.

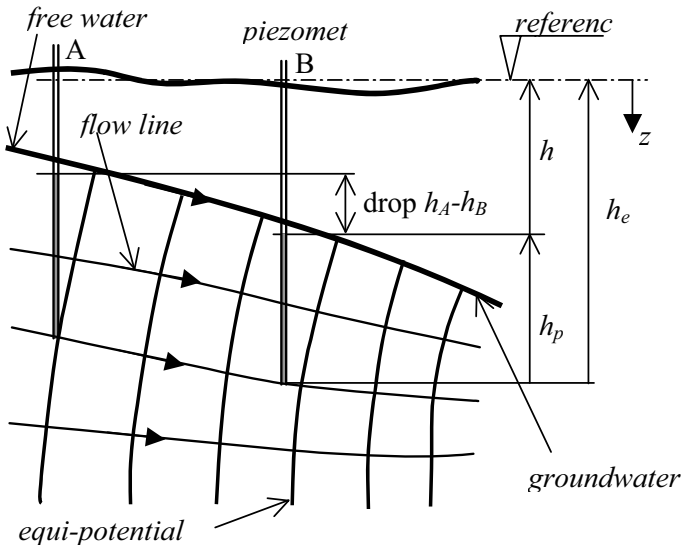

Figure 4.1a Principles of groundwater flow; phreatic aquifer (vertical cross section)

Darcy's law

The average true velocity of the groundwater in the pores is expressed by v [m/s]. At microscopic scale the actual velocity varies strongly. Large pores convey most, and fine pores less. There are also stagnant pores (dead-end pores). Material (solvents, fines, small gas bubbles, heat) carried by this flow will therefore disperse, while sometimes being absorbed, released or trapped in blocking pores (clogging or colmation). This process is important for ground(water) quality control. Convective transport by groundwater flow is related to the true pore-water velocity (see Chapter 14).

The bulk velocity, averaged over a total soil surface, referred to as specific discharge or seepage velocity q [m/s], is related to the true pore-water velocity v according to (n is the porosity)

$$q = vn \tag{4.9}$$

Local flow of groundwater is related to the local gradient according to Darcy's law[17]

$$q = -k\, dh/ds \quad \text{or} \quad q_x = -k\partial h/\partial x,\ q_y = -k\partial h/\partial y,\ q_z = -k\partial h/\partial z \tag{4.10}$$

where k [m/s] is the hydraulic permeability. By measuring or calculating dh/ds everywhere in the soil one can establish the groundwater flow pattern and by using (4.7) the local pore pressure u.

Method of squares

For 2D flow in a homogeneous soil (k is constant), Darcy's law can be expressed by the stream function Ψ or the so-called flow-potential $\Phi = k\phi$, (here ϕ is written in stead of h)

$$q_x = -k\partial\phi/\partial x = -\partial\Phi/\partial x = -\partial\Psi/\partial y \tag{4.11a}$$

$$q_y = -k\partial\phi/\partial y = -\partial\Phi/\partial y = +\partial\Psi/\partial x \tag{4.11b}$$

Mass conservation $\partial q_x/\partial x + \partial q_y/\partial y = 0$ leads then to $\nabla^2\Phi = 0$. Because Φ is a scalar, it is single-valued, which implies $\partial(\partial\Phi/\partial x)/\partial y = \partial(\partial\Phi/\partial y)/\partial x$. Using (4.11), this yields $\nabla^2\Psi = 0$. Thus, Φ and Ψ are scalar harmonic functions, either of which can be used to characterise a groundwater flow field.

Equation (4.11) holds for any orthogonal system and by rotating (x,y) to (s,n), where s is the direction of the flow vector q (Fig 4.1b), one obtains

$$q_s = q = -\partial\Phi/\partial s = -\partial\Psi/\partial n \quad \text{and} \quad q_n = 0 = -\partial\Phi/\partial n = +\partial\Psi/\partial s \tag{4.12}$$

Interpretation of $\partial\Phi/\partial n = 0$ implies $\Phi =$ constant along n-direction. $\partial\Psi/\partial s = 0$ leads to $\Psi =$ constant along s-direction. Therefore, the flow field can be visualised by a curved orthogonal network with lines $\Phi =$ constant (equipotential lines) and lines $\Psi =$ constant (flow lines), see Fig 4.1b.

Interpretation of $-\partial\Phi/\partial s = -\partial\Psi/\partial n$ (in 4.12) leads for finite increments to $\Delta\Phi/\Delta s = \Delta\Psi/\Delta n$. Choosing locally equal steps, i.e. $\Delta s = \Delta n$, gives $\Delta\Phi = \Delta\Psi$, everywhere in the flow field. Thus, each potential flow field possesses a unique value $\Delta\Phi$, everywhere, which only depends on the sketched square flow net, i.e. the choice of the step Δs. This is the magic of the method of squares.

The unique value $\Delta\Phi$ can be found from boundary conditions. If from one boundary with known potential head ϕ_1 (that boundary is an equipotential) there are

---

[17] If the fluid density varies, equilibrium is covered by the law: $q = -(\kappa/\mu)(\partial u/\partial s - \gamma_w)$, where κ is the intrinsic permeability and μ the dynamic pore fluid viscosity. For constant density: $q = -(\kappa\gamma_w/\mu)(\partial u/\gamma_w\partial s - 1) = -k\partial h/\partial s$.

N subsequent other equipotential lines to reach the other boundary with known potential head ϕ_2, then $\Delta\Phi = k(\phi_2-\phi_1)/N$. Hence, also $\Delta\Psi = k(\phi_2-\phi_1)/N$.

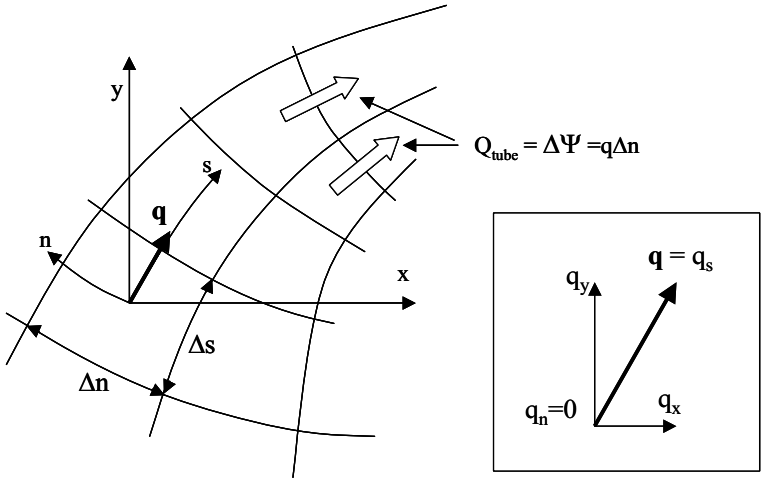

Figure 4.1b Principle of square flow net

From (4.12), the local discharge, expressed in finite differentials, is $q = -\Delta\Psi/\Delta n$. This implies $q\Delta n = -\Delta\Psi = k(\phi_1-\phi_2)/N$. If the 2D flow field reflects groundwater flow in a layer with thickness B (perpendicular to the (s,n)-plane), the meaning of $qB\Delta n$ is the discharge Q_{tube} through the tube bounded by two subsequent streamlines. Thus, $Q_{tube} = -B\Delta\Psi$ is a constant: through every flow tube in the sketched square net the same amount of flow occurs. If the total flow field counts M flow tubes, then the total discharge in m^3/s becomes

$$Q = MkB(\phi_1-\phi_2)/N \qquad (4.13)$$

By just sketching a flow field and counting the number of flow tubes M and equipotential intervals N, the total discharge can be estimated by formula (4.13). One needs not to be an artist; for a rough drawing, the resulting Q will be accurate within 20%.

Model tests

The essential parameter for groundwater flow is the permeability k. It can be determined in the laboratory or in the field. In the laboratory, for sandy soils a cylinder test is performed (Fig 4.2). The sandy sample, height L and cross-section A, is placed on a permeable raster and subjected to a constant water drop H. The cylinder test was first performed by Darcy, published in 1856. Darcy found a discharge Q proportional to HA/L, or $Q = kHA/L$. With the definition of the specific discharge $q = Q/A$, the formula becomes $q = k(H/L)$, known as Darcy's law. Here H/L is the water-head gradient, usually represented as $-d\phi/dz$ or $-dh/ds$ or i. The minus sign indicates flow runs to the lower pressure. Note that effective stresses is affected by the drag force of the flowing pore fluid (see page 63).

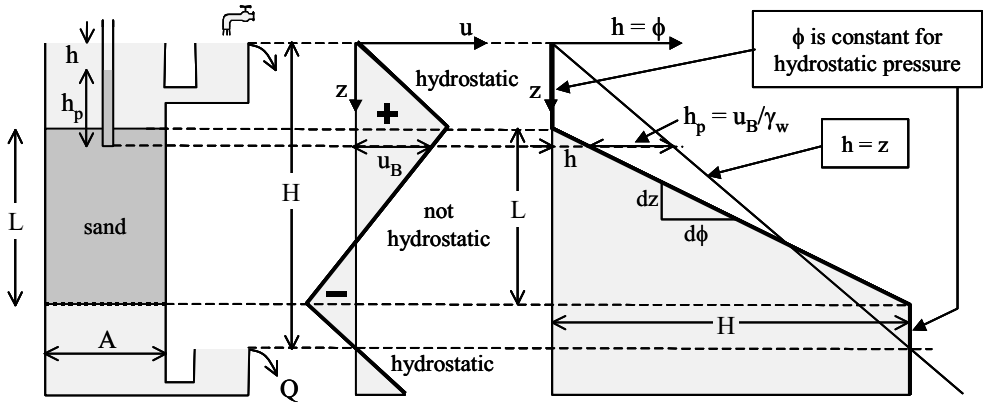

Figure 4.2 Darcy permeability test and corresponding pressure and potential head distribution.

For less permeable soils the cylinder test takes too long and the falling head test is applied (Fig 4.3). The tube cross-section a is very small compared to the sample cross-section A so that tiny changes in the volume are easily observed.

A = Cross-section of soil sample
a = Cross-section of tube
L = Height of soil sample
V = Change of volume between time t_0 and time t
h_0 = Height of water table at time t_0
h_t = Height of water table at time t

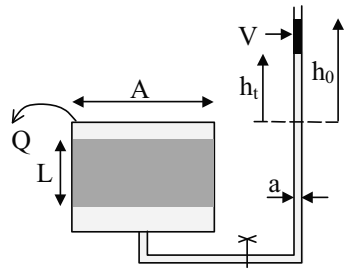

Figure 4.3 Falling head test

In the falling head test the water table h in the tube varies in time. Initially, at $t = t_0$, the water table is $h(t_0) = h_0$. V is the volume of water that leaves the tube during Δt, while the water table drops from h_0 to h_t at $t = t_0 + \Delta t$. So, $V = a(h_0 - h_t) = -a\Delta h$. The same amount of water flows through the soil sample. Thus $Q = -a\Delta h/\Delta t$, which gives, with Darcy's law applied to the sample, $Q = -a\Delta h/\Delta t = kAh_t/L$ (assuming that $\Delta h << h_0$). This leads to $\Delta h/h_t = (KA/aL)\Delta t$. Integration gives $h_t = h_0 \exp[-(kA/aL)(t - t_0)]$. Thus, the permeability is found by measuring h_0, h_t and Δt, according to

$$k = aL \ln(h_0/h_t) / A\Delta t \qquad (4.14)$$

In the field, the permeability can be determined by measuring the local groundwater head using observation pipes. A geological profile can help to recognise a specific groundwater regime or reservoir, which is essential for a proper interpretation of groundwater head observations. A particular field test concerns the permeability of the soil surface, i.e. to determine the drainage capacity under conditions of heavy rain or free surface flow. An open-end pipe is placed

vertically partly in the soil and a certain amount of water is poured in the pipe. The initial free water head h_0 in the pipe and the time t required for the penetration of all the water provides an approximate value for the local permeability $k \approx 0.7h_0/t$. Note, that this value includes impurities. The pipe toe should not reach the groundwater or a relatively impervious layer, i.e. the outflow at the pile toe into the ground must not be blocked.

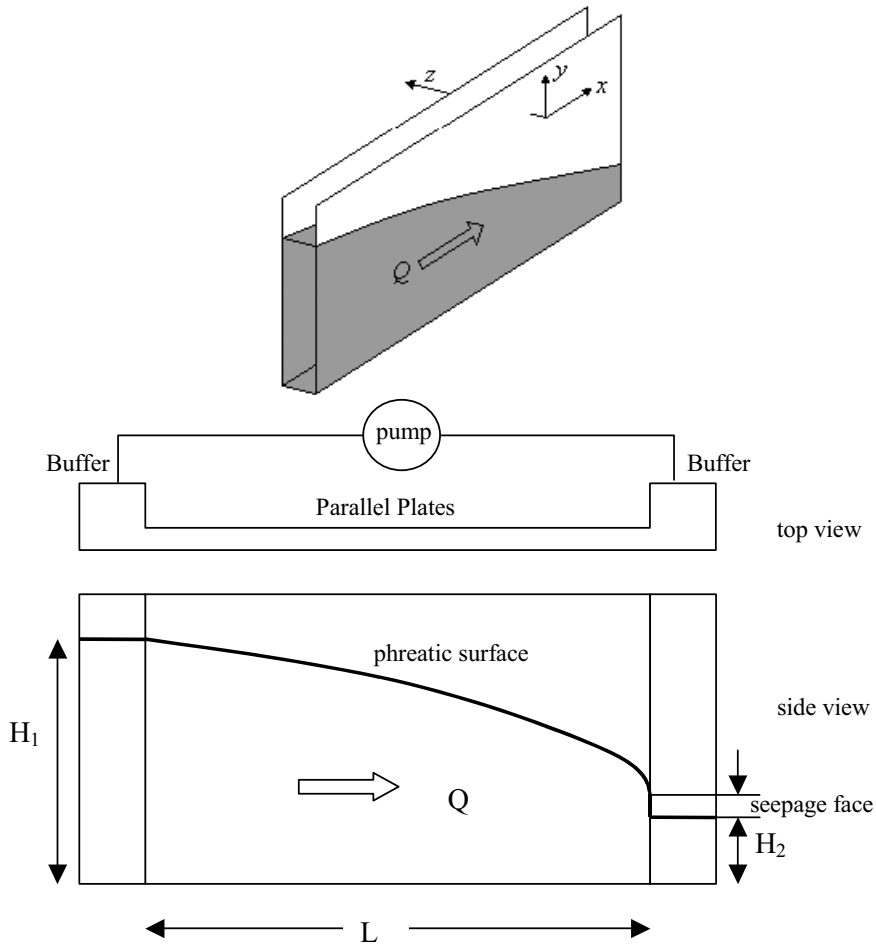

Figure 4.4 The Hele-Shaw model, applied for free-surface groundwater flow

Two dimensional flow in a homogeneous porous medium can be simulated by flow between two flat parallel plates, separated by a small distance d, (see Fig 4.4). The experiment was originally carried out by Hele-Shaw in 1898. For flow of a viscous fluid (no turbulence: Hagen-Poiseuille flow), the corresponding intrinsic permeability is $k = gd^2/12\nu$ with ν the kinematic viscosity (for water of 25°, $\nu = 10^{-6}$ m^2/s). The analogy between two dimensional groundwater flow and the flow between parallel plates enables the study of two-dimensional groundwater flow problems, since gravity influences the flow in the same way as in permeable soils. Hence, with the Hele-Shaw model the flow of moving surfaces is possible, either

the free water table or interfaces between fluids (multiple fluid flow, such as fresh and salt water). The Hele Shaw model is an ideal method to visualise effects. It is, however, not suitable to simulate transport by flow in heterogeneous fields.

A typical example is the free surface flow through the model (Fig 4.4). The outcome is the well known Dupuit formula for flow through earthen dams (B is the length of the dam)

$$Q = Bk\,(H_1^2 - H_2^2)/2L \qquad (4.15)$$

This formula includes the aspect of vertical flow components and the seepage face (see Fig 4.4).

Heterogeneity and anisotropy

Since the soil structure and constitution may vary in space, the corresponding permeability will vary, which is referred to as heterogeneity. Different values for permeability are given in Table 2.6.

When the soil structure shows a different pattern in horizontal and vertical direction, the flow for similar gradients is not the same in different directions. This is called anisotropy. For horizontally sedimented soils in delta areas, anisotropy is given by the ratio of horizontal and vertical permeability, e.g. $k_h/k_v = 3$. In heterogeneous substrata the groundwater flow and corresponding groundwater pressures are not easily obtained. User-friendly computer programs are available to determine the groundwater flow pattern. Comprehensive computer programs provide modules to calculate the groundwater pressures as a part of a total analysis.

C BOILING, HEAVE AND PIPING

Boiling

Granular soils subjected to upward vertical flow can become a mud (heavy fluid). This process of fluidisation is used in laboratory tests to make low-density sand. When fluidised, the sand lost it strength and one refers to its constitution by the quick or boiling condition. It is also called liquefaction, which is further outlined in Chapter 16. The vertical equilibrium of such soil is described by

$$\frac{\partial \sigma_v}{\partial z} = \frac{\partial(\sigma_v' + u)}{\partial z} = \gamma = \gamma' + \gamma_w \qquad (4.16)$$

Here, γ' is the submerged weight of the soil. Using (4.7) and (4.8) the pore pressure gradient can be expressed by

$$\frac{\partial u}{\partial z} = \gamma_w (1 + i) \qquad (4.17)$$

Here, $i = \partial h/\partial z$ is the potential gradient. From (4.16) and (4,17) one finds for the effective stress $\sigma_v' = (\gamma' - i\gamma_w)z$. The factor $i\gamma_w$ is the seepage force per volume and it causes the effective stress to vanish at any value of z, when $i = i_c = \gamma'/\gamma_w$, the so-

called critical gradient. For sands this value is about 1. In clay, the limited permeability and cohesion prevent a uniform gradient to occur before swell and consolidation have taken place. Here heave is more likely. Peat may be permeable, but boiling is less likely due to fibres, which allow for tensile stresses. However, peat is light and it may break under upward groundwater gradients.

Heave

Heave is uplift of semi-pervious cover layers and structures due to excessive groundwater pressure. Similar voids may also arise under piled structures (tunnels, pipelines, sewer lines) due to soil compaction (consolidation). Under high pore pressures heave may cause fissures in the layer above or at the construction interface, through which water may freely flow. It may cause erosion (colmation or washing out of fines), when the local gradient i exceeds a certain value. The common remedy is to place a weight (a filter of coarser material) on top or cast up the zone around the leak with sand bags to create a small water pond in order to suppress the gradient. Filters are designed using filter rules (see Chapter 16).

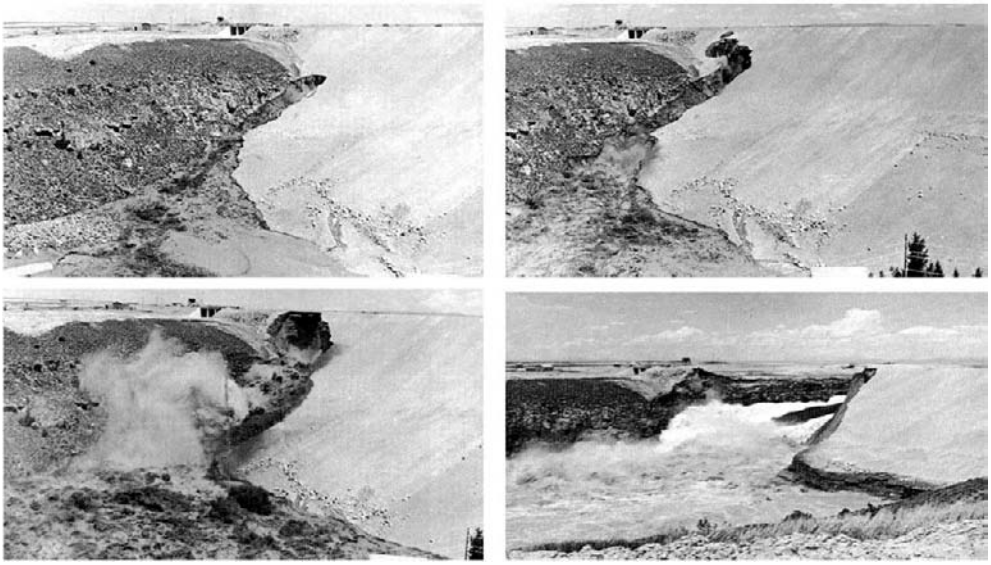

Figure 4.5 Piping failure of the Teton dam in 1976; pictures taken about every 30 minutes

Piping

Piping is a process of erosive channel formation in granular soil layers by seepage. A distinction is made between reservoir-dam piping and river-dike piping. Reservoir-dam piping concerns erosion in the cohesive dam core (clay) at constant water-level drop. It is an important failure mechanism (Fig 4.5). River-dike piping deals with erosion of non-cohesive soils (sand) under and at the toe of the dike at high river-water levels (Fig 4.6). It is considered a serious failure mechanism of flood retaining systems. Piping commonly starts at the downstream side, often with heave and cracking of the cover layer at high water pressures. The corresponding groundwater flow conveys sand grains, creating a cavity (pipe) underneath the

levee, which grows from the downstream side to the upstream side. Continued erosion may finally lead to instability and failure of the levee.

Figure 4.6 Start of retrograde erosion piping and a full-scale piping test

A few design rules are available to estimate the probability of piping, such as the empirical model of Bligh and the semi-analytical model of Sellmeijer

Bligh (1910) $\Delta H < L / C$ *(4.18a)*

Sellmeijer (1989) $\Delta H < abcL\,(0.68 - 0.10\ln(\eta\, b))$ *(4.18b)*

with $a = (Z/L)^{\frac{0.28}{(Z/L)^{2.8}-1}}$, $b = D_{70}/(\kappa L)^{1/3}$, $c = \eta\,\dfrac{\gamma_s - \gamma_w}{\gamma_w}\dfrac{\sin(\theta+\alpha)}{\cos\theta}$

Here, ΔH is the hydraulic drop, L the minimum seepage length, C an empirical factor (18 for fine, 15 for medium, 12 for coarse sand, 7 for gravel), a is a geometry factor, b a sand scaling factor, c a sand grain equilibrium factor, θ the rolling resistance angle of the sand grains, α the slope of the pipe, η a drag force factor (coefficient of White), κ the intrinsic permeability of the sand layer, D_{70} the 70% value of the grain distribution, and Z the thickness of the sand layer. Some large-scale tests on one type of sand have been conducted for validation. The suggested model (4.18b) has been validated on the base of extensive physical tests and it is incorporated in a practical numerical FEM design tool. Full-scale experiments have shown that piping failure is time-dependent. Dike breach may occur within several hours after pipes reach the upstream side (Fig 4.6).

For a particular geological situation (Fig 4.7a), the variation in geometry has been elaborated by an artificial neural-network (ANN), a self-learning approach. The chosen network contained 5 input nodes (Z_i/L and the permeability ratio), 50 hidden nodes and 1 output node (F). After 18674 calculations (90% training, 10% check) the trained network prediction for the check showed an excellent match (Fig 4.7b). The result is a simple formula

$$\Delta H < F\, bcL^{4/3} Z_1^{-1/3} \qquad (4.18c)$$

where F is the geometry factor, which is instantly provided by the trained network after input of the geometric measurements. Applying self-learning methods for a quick evaluation of (geometric) variations is a promising new approach.

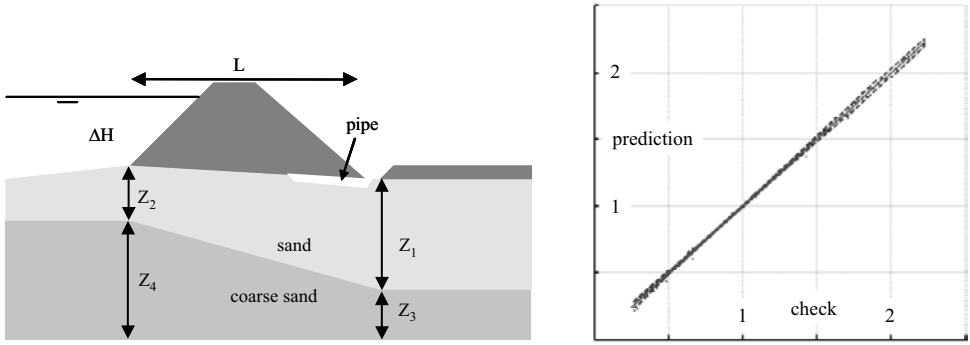

(a) (b)

Figure 4.7 ANN for a specific geological schematisation (Sellmeijer)

application 4.1

Consider a sand layer of H = 10 m thick and water table h about 1 m under the ground surface. The known properties of soil and groundwater are: γ_s = 25.3 kN/m^3, γ_w = 10 kN/m^3, γ_d = 14.6 kN/m^3, n = 0.42, h_c = 0.3 m. A corresponding vertical soil pressure diagram is shown in Fig 4.8. Next, the question is what effect a groundwater lowering of Δh = 1 m may have on soil stress and corresponding deformation of the soil.

Lowering the groundwater table with Δh will decrease the pore pressure with $\Delta u = \gamma_w \Delta h$ and increase the vertical effective stress with $\Delta\sigma_v'$. Using the effective stress principle for general saturated soil (s = 1, χ = 1), it provides the following elaboration

$$\sigma_v = \sigma_v' + u = \gamma(z-h+h_c) + \gamma_d(h-h_c) \quad \rightarrow$$

$$\sigma_v' = \gamma(z-h+h_c) + \gamma_d(h-h_c) - \gamma_w(z-h)$$

$$= \gamma'(z-h) + (1-n)\gamma_s h + (\gamma-(1-n)\gamma_s)h_c = ((1-n)\gamma_s - \gamma')h + \gamma' z + (\gamma-(1-n)\gamma_s)h_c$$

$$= (1-n)\gamma_w h + \gamma' z + (\gamma-(1-n)\gamma_s)h_c$$

This result shows that a lowering of the groundwater table by Δh gives an increase of the vertical effective stress by

$$\Delta\sigma_v' = (1-n)\gamma_w \Delta h$$

which is precisely the buoyancy force of a soil height of Δh, i.e. the solid volume $(1-n)\Delta h$ times γ_w.

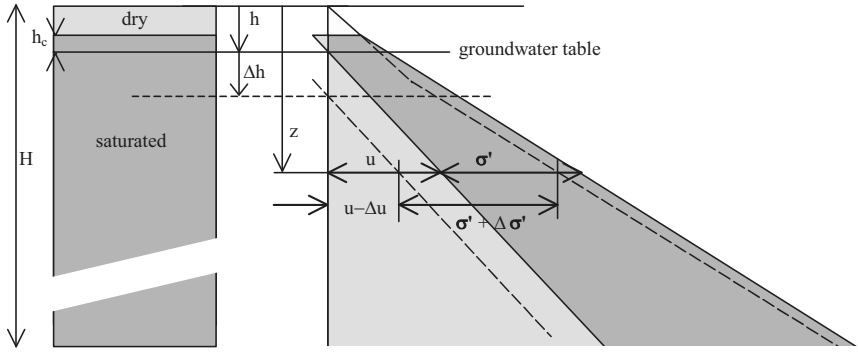

Figure 4.8 Groundwater pressure and effective stress

For the present case, the increase of vertical effective stress (in the saturated zone) becomes $\Delta\sigma_v' = (1–0.42)\text{x}10\text{x}1 = 5.8$ kPa. The increase of effective stress causes compression, which results in ground settlement at the surface (land subsidence). The average soil elasticity is estimated, using (3.1b) and adopting $C_c = 0.005$

$$E = 1.5\sigma_v'/((1–n)C_c) \approx 1.5(½H\gamma')/((1–n)C_c) = 0.75H\,(1–n)(\gamma–\gamma_w)/\,((1–n)C_c)$$

$$= 0.75H\,(\gamma–\gamma_w)/C_c = 0.75\text{x}10(18.9–10)/0.005 = 13350 \text{ kPa}$$

The corresponding local vertical strain due to the vertical effective stress increase becomes

$$\varepsilon_v = \Delta\sigma_v'/E = (5.8 / 13350) = 0.00043$$

The settlement S equals the induced strain over the entire saturated soil layer height (the drying zone itself contributes for 50%)

$$S = (H – (h + ½\Delta h))\ \varepsilon_v = (10 – (1 + 0.5))\ 0.00043 = 3.6 \text{ mm}$$

which is practically insignificant.

However, for a soft clay layer with similar dimensions and a compression index $C_c = 0.1$, the corresponding settlement due to 1 m groundwater table lowering would be in the order of 7 cm, which is not insignificant.

For submerged soil a change in the free water level would not give rise to any change in effective stress, since there is no Archimedes effect. Is this also valid, when the pore water contains gas bubbles? What happens in clay soil with large h_c reaching the surface, after lowering?

application 4.2

Consider an open end tube placed partly in unsaturated soil (Fig 4.9). At time $t = 0$, it is quickly filled with a water volume $V = h_0 A$ m^3, which will infiltrate in the soil (the air in the pores can escape at the tube tip without hindrance). The time t_e

required to let all water infiltrate is determined. At time t in the interval $(0\,,\,t_e)$, the specific discharge is $q = k(h–d)/d$. Conservation of mass states that the total volume of water remains unchanged; so, $\partial V = 0 = (\partial h + n\partial d)A$, or $\partial h = –n\partial d$. The velocity of the infiltrating waterfront is $v = q/n = \partial d/\partial t$ (d is the coordinate of the moving front). Thus $\partial t = n\partial d/q$ and integration, according to ${}_0\int^{t_e}\partial t = {}_{h0}\int^{0} n\partial d/q$, yields after some elaborations $kt_e = h_0\, f(n)$, with $f(n) = (1+n\log(n)/(1–n))/(1–n)$. Noticing that f is about 0.7 for $0.3 < n < 0.4$, the final result becomes a simple formula to estimate the permeability of an unsaturated soil layer in the field: $k = 0.7\, h_0/t_e$. Make a sketch of $f(n)$ versus n. What is the effect of the capillary head?

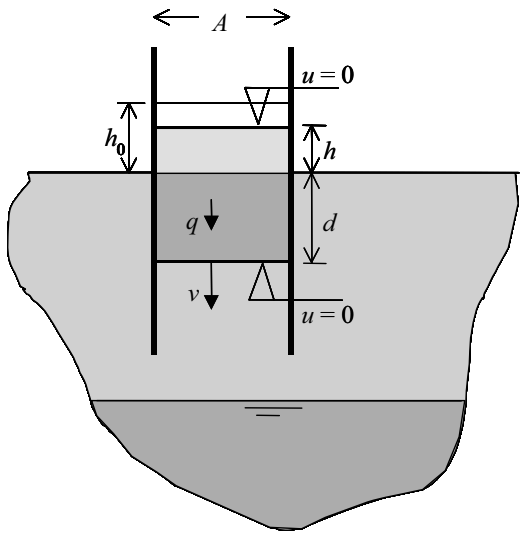

Figure 4.9 Field infiltration test

application 4.3

Consider a horizontal confined aquifer, i.e. a sandy layer with thickness B and on top and underneath a relatively impervious layer. Somewhere a building pit is required, the depth of which reaches in the sandy layer, and in order to create a dry excavation with a surrounding of sheet piling, some pumping wells are being applied. In the aquifer a natural seepage flow exists. The horizontal flow pattern is calculated and visualised using a square net of flow lines and equipotentials, shown in Fig 4.10. Making use of the geohydrological conditions, the use of three wells is suitable to create a more or less equal drawdown at the proposed location of the building pit.

The theory of square flow net provides a practical formula to determine the local discharge using (4.13). Given k = 10 m/day and layer thickness B = 5 m, the discharge of the large scale virtual well (Fig 4.10a) becomes $Q = 4kB(2.0–0.8)/3$ = 80 m^3/day. Note, that $M = 4$ (use all the flow lines towards the well) and that Δh and N are related (the drop over the chosen intervals). The discharges of the real wells (Fig 4.10b) can be determined in the same way.

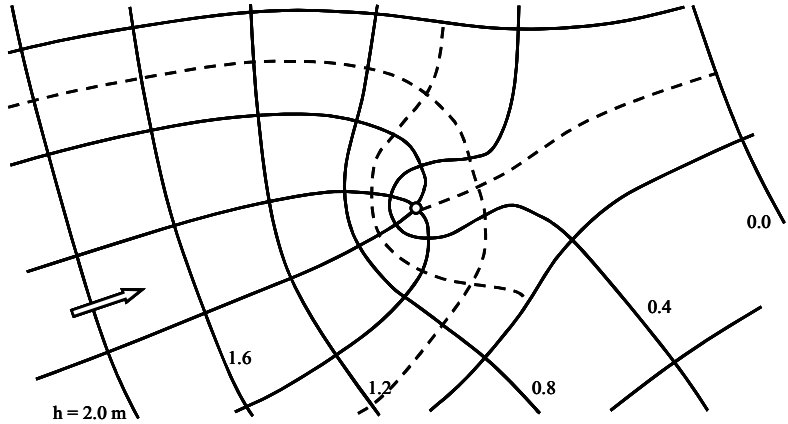

(a) large scale

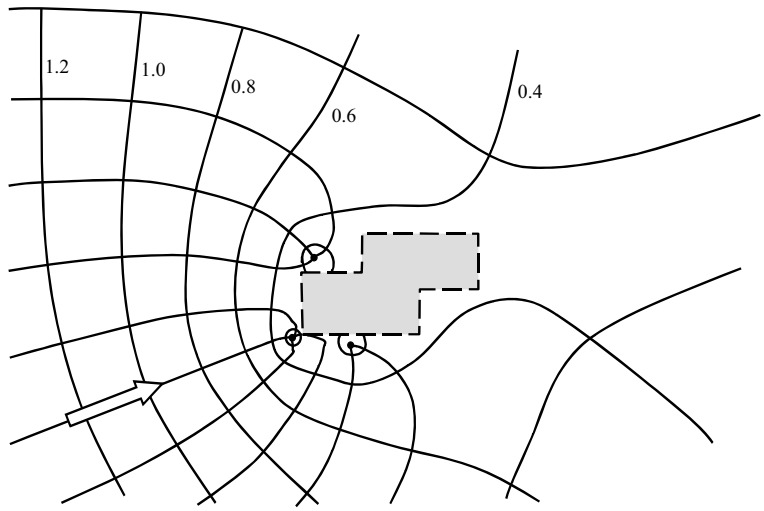

(b) detailed

Figure 4.10 Pumping system for a building pit (horizontal view)

application 4.4

Consider a river embankment. The subsoil consists of three layers, from top to bottom: a semi-pervious sandy clay layer (aquitard) with a height of $D = 2.5$ m, then a permeable sandy layer (aquifer) with a height of $H = 10$ m, and next an impervious clay layer (aquiclude), which seals off the groundwater flow. The dike is considered impervious. The geometry is shown in Fig 4.11.

At three locations (A, B and C) a piezometer measures the groundwater pressure in the aquifer (sand layer), for high water level: $h_A = 4$ m, $h_B = 2$ m, $h_C = 0$ m (h_C is taken as reference, fixed water level in the hinterland behind the dike). The length $L_1 = 50$ m, the length L_2 is so long as to render the groundwater head at location C practically unaffected by the seepage flow in the aquifer. The permeability of the sand is $k_h = 10^{-4}$ m/s and of the top clay $k_v = 10^{-6}$ m/s. Determine the seepage under the dike Q_h and the leakage through the aquitard (top clay layer) Q_v.

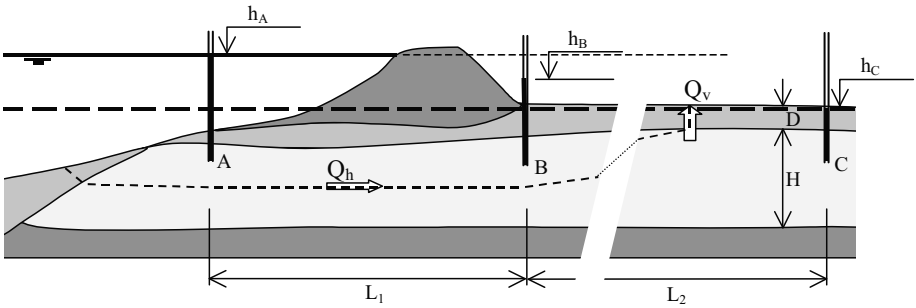

Figure 4.11 Groundwater flow in a coastal or riverbank zone

In the aquifer, in zone AB, the groundwater flow is horizontal and in the zone BC nearly horizontal (the deviation is in the order of $k_v/k_h < 1\%$); see the dashed flowline in Fig 4.11, which breaks at the interface. In zone AB the groundwater-pressure gradient is $i = (h_B - h_A)/L_1 = -0.04$, the corresponding seepage velocity is $q_h = -k_h i = 4\text{x}10^{-6}$ m/s, and therefore the total seepage under the dike becomes $Q_h = q_h H = 4\text{x}10^{-5}$ m^3/sm (about 3.5 m^3 per day per meter dike length).

In the zone BC, the groundwater leaks slowly vertically through the top clay layer. Since after location C no effect is supposed, all the seepage Q_h must vanish by leakage in the zone BC. In average the potential head in zone BC is $h_v = (h_B - h_C)/2 = 1$ m. The average (vertical) drop over the top clay layer is therefore 1 m, the corresponding gradient is $i_v = -h_v/D = -0.4$, and the average vertical seepage in the clay becomes $q_v = -i_v k_v = 0.4\text{x}10^{-6}$ m/s. Therefore, the total leakage becomes $Q_v = q_v L_2$, which must be equal to Q_h. Thus $L_2 = Q_h/q_v = 100$ m.[18]

The pore pressure at the sand-clay interface, at location B, applying (4.7), is $u_B = (D+h_B)\gamma_w = 45$ kPa. It exceeds the local vertical soil stress σ_{vB}, which is equal to the local soil weight per m^2, which, if for the clay $\gamma = 16$ kN/m^3 is adopted, leads to $\sigma_{vB} = \gamma D = 40$ kPa, at the interface. Hence, the clay layer will be lifted up (heave) and a thin gap filled with water will occur at the interface, its length in the order of 25 m, in the present case. Since the pore pressure in this gap is limited by the local soil weight, the potential head reduces to $h_B = (\sigma_{vB}/\gamma_w - D) = 1.5$ m (this is the value one would measure). The occurrence of uplift affects the dike stability, since local shear resistance will be significantly reduced.

Which river height would just not cause any uplift at the leeside of the dike? So, is the stability of the dike affected by this river level?

application 4.5

A cofferdam has been constructed (see Fig 14.12) with two anchored walls AB and CD and a fill with coarse clean sand. Estimate the permeability and the variance (see Table 2.6). Determine from the sketched groundwater flow pattern

[18] The leakage factor $\lambda = \sqrt{(k_h HD/k_v)}$ is for the present case 54 m. A typical leakage zone would be $3\lambda = 162$ m. The value L_2 of 100 m differs because of the simplifications.

the total leakage (discharge Q) through the structure and the corresponding variance. What value for Q would you suggest to the client?

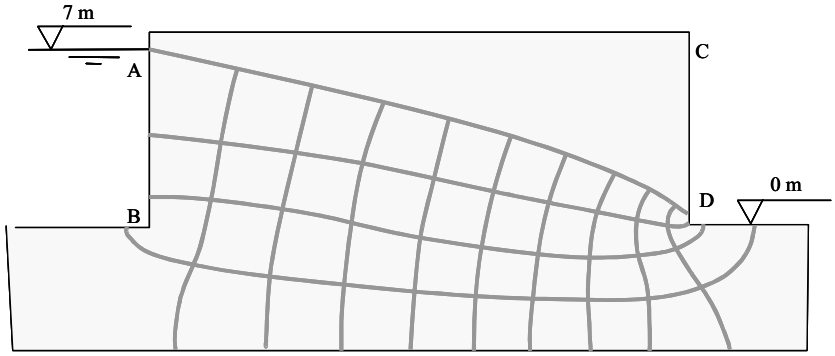

Figure 4.12 Groundwater flow in a coffer dam

application 4.6

A dike retains a water level of 5m. The soil consists of silty sand. The permeability of the dike material and the underground is similar: k = 1 m/day. The groundwater table along DC reaches the ground surface. Determine from the sketched groundwater flow pattern (Fig 4.13) the total leakage (discharge Q per m length of the dike) through the dike and the underground. What is the potential head along flow line FE (groundwater table), and along seepage face line ED?

If the layer ABCD is peat with identical permeability as silty sand and a wet unit weight of 11 kPa/m, what will happen in point A? Suggestion: determine the pore pressure and total vertical stress in point A?

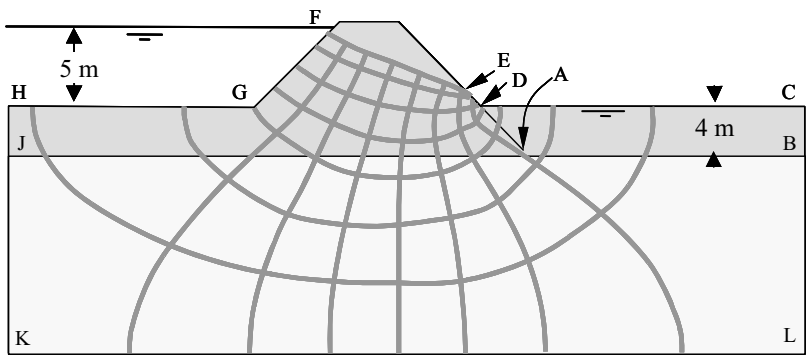

Figure 4.13 Groundwater flow in a dike and underground

application 4.7

A permeability test on sand with wet unit weight 20 kN/m^3 is shown in the Fig 4.14a. Make a graph of the vertical pore pressure and determine the corresponding vertical effective stress (γ_w = 10 kN/m^3) versus height. The graph is shown in Fig 4.14b. The pressure height in the pipes is 35 cm, yielding actual pore pressure of 0.35 kPa. Total weight equals the height of water and soil, resulting in total stress

σ. The effective stress σ' is just the difference of total stress and the actual pore pressure.

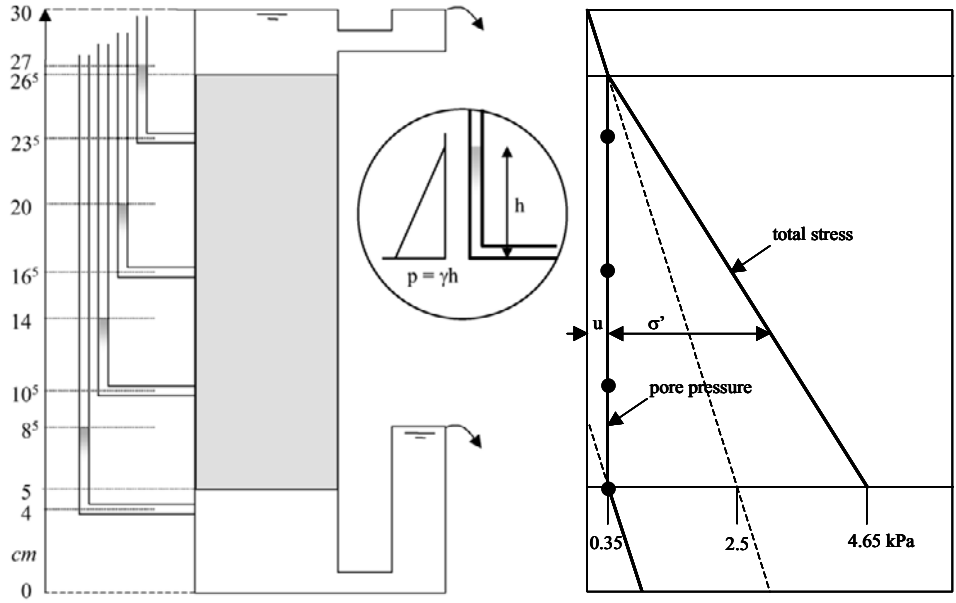

(a) permeability test *(b) stress field*

Figure 4.14 Permeability test interpretation

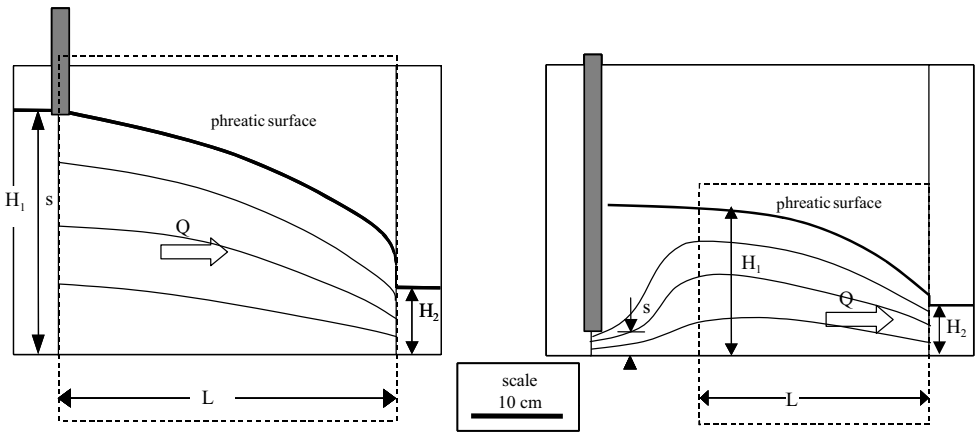

Figure 4.15 Hele Shaw box tests

application 4.8

Two tests are performed with the Hele Shaw model (Fig 4.15). The formula of Dupuit can be assigned to the area indicated (dashed box). Sketch a graph of the effect of relative discharge (Q_{test2}/Q_{test1}) versus relative opening (s_{test2}/s_{test1}) by determining three points (two are obvious, and one is to be determined by the two tests). What does this result tell you about a leak in a wall?

5 UNIAXIAL STRESS AND STRAIN

A STRESS AND STRAIN

Material behaviour in soils is expressed by effective stress σ' and strain ε.[19] Their ratio is called stiffness, and the slope of the stress-strain curve is the elasticity modulus E (Fig 5.1). If the curve is independent of the loading history, the material is called elastic, and when E is constant it is linear-elastic, characterised by Hooke's law.

$$\sigma' = E\varepsilon \tag{5.1}$$

Sometimes a linear value is used for a certain stress range: the tangent or secant modulus. Usually, soil is dependent on loading history. Unloading and reloading differ from earlier behaviour (marked by the preloading or preconsolidation pressure). Soil may show creep (less in sand, more in clay) and/or relaxation, gain strength and stiffness with time (ageing, preconsolidation ratio), and the elasticity may depend on the loading rate (stiffer for faster loading). For larger strains soil behaviour may yield and develop hardening, plasticity or softening, or it may break in a more brittle way (soft rock).

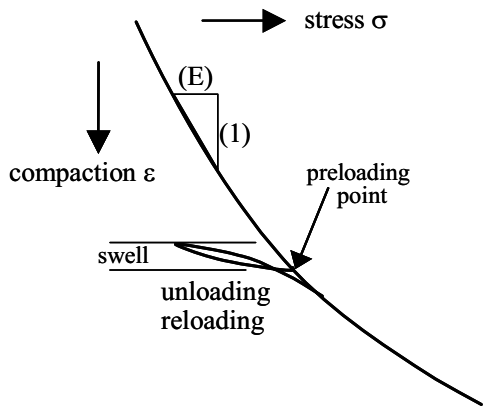

Figure 5.1 Uniaxial stress-strain curve

In principle soil mechanics includes multiple dimensions. Triaxial strains are defined as follows

$$\boldsymbol{\varepsilon} = (\varepsilon_x, \varepsilon_y, \varepsilon_z) \quad \text{and} \quad \boldsymbol{\sigma}' = (\sigma_x', \sigma_y', \sigma_z') \quad \text{in the directions } (x, y, z) \tag{5.2a}$$

[19] Common in geotechnics: strain is defined positive for compaction; stress is defined positive for pressure, throughout this book. As strain is related to porosity, this definition leads to an extra minus sign: $-\mathrm{d}n = (1-n)\mathrm{d}\varepsilon_v$.

$$\boldsymbol{\varepsilon} = E^{-1} \begin{vmatrix} 1 & -\nu & -\nu \\ -\nu & 1 & -\nu \\ -\nu & -\nu & 1 \end{vmatrix} \boldsymbol{\sigma}'^{T} \qquad (5.2b)$$

where ν is the Poisson ratio. For laterally confined compression $\varepsilon_x = \varepsilon_y = 0$, and the corresponding stresses become $\sigma_x' = \nu(\sigma_y' + \sigma_z')$ and $\sigma_y' = \nu(\sigma_x' + \sigma_z')$. If also $\sigma_x' = \sigma_y' = \sigma_h'$ (axi-symmetric, horizontal effective stress) and $\sigma_z' = \sigma_v'$ (vertical effective stress) then

$$\sigma_h' = \sigma_v'(\nu/(1-\nu)) = K_0\,\sigma_v' \quad \text{and so} \quad K_0 = \nu/(1-\nu) \qquad (5.3)$$

The parameter K_0 is the stress ratio σ_h'/σ_v'. In undisturbed soils one may adopt for the Poisson ratio the value 0.3, which gives for laterally confined compression $K_0 \approx 0.5$. In reality, K_0 depends on the geological loading history and rises during unloading. It varies from place to place. The corresponding vertical strain for laterally confined undisturbed soil becomes, employing (5.2)

$$\varepsilon_v = E^{-1}(\sigma_z' - \nu(\sigma_x' + \sigma_y') = ((1-2\nu K_0)/E)\sigma_v' = \alpha\sigma_v' \qquad (5.4)$$

Here, α is the laterally confined compressibility coefficient. Formula (5.4) is, in fact, valid for small increments $d\sigma_v'$ and $d\varepsilon_v$, since soil behaviour is typically nonlinear. Tests have revealed, that this nonlinear character can be expressed by a power law (after Janbu), according to

$$d\varepsilon_v = \alpha\, d\sigma_v' \quad \text{with} \quad \alpha = \eta(\sigma_v')^{-m} \qquad (5.5)$$

where η, a compressibility index, is an empirical constant dependent on soil type. Formula (5.5) expresses that soil stiffness increases with depth. For sand one may find $1/3 < m < 2/3$, for (soft) rock $0 < m < 1/3$, and for cohesive soils $m \approx 1$. Unloading and reloading correspond to stiffer response than virginal loading, i.e. two to ten times stiffer. In the case of a preloaded soil the maximum preloaded stress is 'remembered' (named preconsolidation pressure, preloading point or yield stress) and reloading beyond the actual stress must be considered in two parts: reloading and virginal loading, each with its own stiffness (Fig 5.1).

B STRAIN CONCEPT

Soil strain is determined in the laboratory, for example in the oedometer, by measuring the compaction or settlement. When subjected to a load step $\Delta\sigma'$ a surface settlement Δh of the surface is noticed (usually, after some time). Reference can be made to the original sample height h_0 (linear strain) or for a strain increment to the actual height h (natural strain), in formula[20]

[20] dh and Δh are positive for extension. Since strain is positive for compression, an extra minus sign is involved.

$$\varepsilon_l = -\Delta h/h_0 \quad \text{and} \quad d\varepsilon = -dh/h \tag{5.6}$$

Elaboration yields the following relation between the natural and linear strain concept[21]

$$-d\varepsilon = dh/h = d(h/h_0)/(h/h_0) = d(\ln(h/h_0)) = d(\ln((h_0 + \Delta h)/h_0)) = d(\ln(1 - \varepsilon_l))$$

$$\rightarrow \quad \varepsilon = -\ln(1 - \varepsilon_l) \tag{5.7}$$

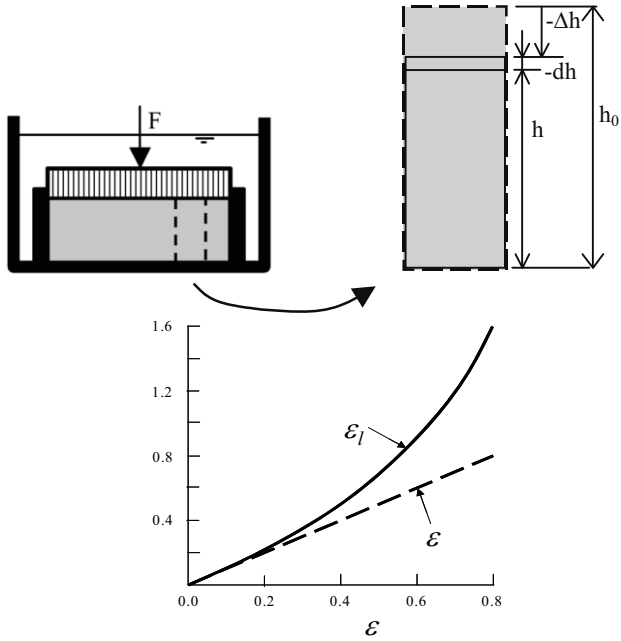

Figure 5.2 Uniaxial compression and strain concept.

For small strains (less than 20%) linear and natural strain are practically similar. For large strains, which may occur in soft soils, natural strain should be applied.

The original German(-Austrian) approach is based on measuring the voids ratio $e = n/(1-n)$, the ratio between pore volume and solid volume, based on the idea that deformation should be related only to the change of pore volume (solid grains are relatively stiff), i.e. the fabric (arrangement of grains) changes and this causes deformation. Using the fact that the total soil volume V can be expressed in terms of voids ratio and volume of solids V_s, according to $V_s = (1-n)V = V/(1+e)$, the relation between voids ratio and natural strain becomes for uniaxial compression, using a similar development as for (5.7) and incompressible soil grains (V_s = constant),

$$-d\varepsilon = dh/h = dV/V = d((1+e)V_s)/((1+e)V_s) =$$

[21] Alternative method: $\varepsilon = -\int_{h_0}^{h} h^{-1} dh = -\int_{h_0}^{h} d\ln(h) = -\ln(h/h_0) = -\ln(1-\varepsilon_l)$.

$$= d(1+e)/(1+e) = d\ln((1+e)/(1+e_0))$$

$$\rightarrow -\varepsilon = \ln((1+e)/(1+e_0)) = \ln(v/v_0) \qquad (5.8a)$$

Here, $v = 1+e$ is the specific volume (i.e. total volume relative to solids volume). Note, that for the reference $e = e_0$, a reference strain is chosen, according to $\varepsilon = 0$. With (5.7) one obtains

$$(1-\varepsilon_l) = (1+e)/(1+e_0) = v/v_0 \quad \text{or} \quad \varepsilon_l = (e_0 - e)/(1+e_0) \qquad (5.8b)$$

C UNIAXIAL COMPRESSIBILITY

Elaboration of the laterally confined compressibility in soft soils ($m \approx 1$), expressed by (5.5), using natural strain (5.7), leads to[22]

$$d\varepsilon = (\eta/\sigma')d\sigma' = (\eta/(\sigma'/\sigma_0')d(\sigma'/\sigma_0') = \eta\, d\ln(\sigma'/\sigma_0') = d\ln((\sigma'/\sigma_0')^{\eta}) \qquad (5.9)$$

which becomes after integration (defining $\varepsilon = 0$ at $\sigma' = \sigma_0'$)

$$\varepsilon = \eta \ln(\sigma'/\sigma_0') \quad \text{or} \quad \sigma'/\sigma_0' = \exp(\varepsilon/\eta) \qquad (5.10)$$

It shows a hardening behaviour (at higher stress soil is less compressible). In terms of linear strain the elaboration of (5.9) using (5.7) yields

$$(1-\varepsilon_l) = (\sigma'/\sigma_0')^{-\eta} = (1+\Delta\sigma'/\sigma_0')^{-\eta} \qquad (5.11)$$

This formula is powerful, because, while based on large strain concept (natural strain approach), it is expressed in terms of linear strain (displacement with respect to original state) and the corresponding stress increment, both easily conceivable values. For small strains (less than 10%) the difference between natural strain and linear strain can be disregarded, and from (5.10) one may obtain Terzaghi's compression law

$$\varepsilon_l = \eta \ln(\sigma'/\sigma_0') = \eta \ln(1+\Delta\sigma'/\sigma_0') = 2.3\eta\, {}^{10}\log(1+\Delta\sigma'/\sigma_0') \qquad (5.12)$$

For a small load step a linear approximation is obtained (Hooke's law), similar to (5.4)

$$\varepsilon_l = (\eta/\sigma_0')\,\Delta\sigma' = \alpha\Delta\sigma' \quad \text{with} \quad \alpha = \eta/\sigma_0' \quad \text{as a constant} \qquad (5.13)$$

The original British-American approach, measuring the strain in terms of the voids ratio e, leads to an empirical formula, according to

$$\Delta e = -C_c\, {}^{10}\log(1+\Delta\sigma'/\sigma_0') \qquad (5.14)$$

---

[22] Suffix v for *vertical* has been left out.

Using (5.8), one finds $\Delta\varepsilon_l = -\Delta e/(1+e_0)$, so that from (5.14) one obtains

$$\Delta\varepsilon_l = \varepsilon_l = (C_c/(1+e_0))\ {}^{10}\log(1+\Delta\sigma'/\sigma_0') \qquad (5.15)$$

Comparison of (5.15) and (5.12) yields a relation between the original empirical compression index C_c and the theoretical index η, according to

$$C_c = 2.3\,\eta\,(1+e_0) = 2.3\,\eta\,v_0 \qquad (5.16)$$

The compression index C_c is extensively measured and reported in literature. Some values are given in Table 5.1.

TABLE 5.1 RANGE OF COMPRESSION INDEX VALUES FOR VARIOUS SOILS

soil type	*C_c value*		*soil type*	*C_c value*
gravel	0.002 – 0.009		clay	0.126 – 1.360
sand	0.002 – 0.020		sandy clay	0.069 – 0.756
silty sand	0.005 – 0.019		organic clay	0.420 – 1.690
loam	0.030 – 0.170		peat (preloaded)	0.900 – 1.800
sandy loam	0.055 – 0.092			

In many textbooks, unloading and reloading behaviour is expressed by C_c', also referred to by recompression or swelling index. It is usually 2 to 5 times less than C_c, or even smaller.

The representation of the compressibility index C_c with regard to voids ratio e_0 and ${}^{10}\log$ is historic. As a reference, the voids ratio incorporates the solids volume, which was considered a stable factor, and in the early times only ${}^{10}\log$-graphic paper was available for outlining test results. It is nowadays convenient to use measured data directly, like η in particular, because $C_c/(1+e_0)$ shows less variation than C_c itself.

Settlement of soils is the accumulated vertical displacement at the ground surface, and it is related to strain summed for each layer, according to

$$S = \int \varepsilon_l\, dz \qquad (5.17)$$

As stated before, when using (5.11) the natural strain concept is satisfied. It applies for large strains as well, and so does (5.17).

In conclusion, for small strains one may use (5.12), for small load steps (5.13), and for large strains one should use (5.11). Using (5.11) avoids missing the advantage of large strain concept. The compression index or compressibility coefficient is easily converted using the relation mentioned in (5.16).

application 5.1

Consider a stratified soil consisting of sand, clay, sandy clay, peat and stiff sand. The groundwater table and some specific soil properties are given in Table 5.2. When loaded by 100 kPa, the settlement S is calculated and the effect of using the linear and the natural strain concept is evaluated.

TABLE 5.2a DATA PROVIDED

	height H [m]	porosity n	weight γ [kN/m^3]	C_c
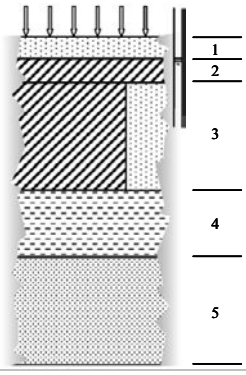	1	0.40	20	0.006
	1	0.42	17	0.76
	5	0.40	18	0.12
	3	0.51	12	1.5
	5	0.38	21	0.003

TABLE ELABORATION FOR $\Delta\sigma = \Delta\sigma' = 100$ KPA

layer	e_0	η	σ_0 kPa	u kPa	σ'_0 kPa	ε_1	S m	remark
1	0.667	0.00157	20	0	10	0.004	0.004	(1)
2	0.724	0.192			20	0.344	0.320	(3)
			37	10	27	0.297		
3	0.667	0.0312			27	0.048	0.192	
			127	60	67	0.029		
4	1.041	0.320			67	0.292	0.852	(4)
			163	90	73	0.276		
5	0.613	0.00081			73	0.0007	0.003	
			268	140	128	0.0005		
							1.371	
remark	$n/(1-n)$	using (5.16)	$\Sigma\gamma z$ at the interface		$\sigma_0 - u$	using (5.12) at interface	(2)	

Remarks

- The strain is determined at the top and the bottom of each layer, but at the ground surface $\sigma'_0 = 0$ and the formula fails. Therefore, the value in the middle of the layer is used.
- The settlement, using (5.17) in each layer, is approximated by $H(\varepsilon_1^{top} + \varepsilon_1^{bottom})/2$.[23]
- The strain in layer 2 is larger than 10% and (5.11) should be used which gives a settlement contribution of $H(\varepsilon_1^{top} + \varepsilon_1^{bottom})/2 = 1(0.291+0.257)/2 = 0.274$ m.

[23] Stresses due to weight are (sectionally) linear with depth. Corresponding strain increases nonlinearly with stress. The settlement (accumulated strain) should in fact be elaborated accordingly, but it is cumbersome.

- The strain in layer 4 is larger than 10% and (5.11) should be used which gives a settlement contribution of $H(\varepsilon_1^{top} + \varepsilon_1^{bottom})/2 = 3(0.253+0.241)/2 = 0.741$ m.
- With the large strain concept the total settlement S becomes 1.241 m. The linear strain concept overestimates the settlement when large strain occurs, in this case with 9.5%. In fact, one should use (5.11) instead of (5.12) and the best result is obtained automatically.

application 5.2

A fill, which imposes a load of 50 kN/m^2, compresses a clay layer of 5 m thick. The wet unit weight of the clay is $\gamma = 15$ kN/m^3 and the compressibility index of the clay is $\eta = 0.2$. Give an estimate of the final settlement by considering only stresses at the mid-height of the layer. Next, refine this estimate by considering two equally thick sublayers, each 2.5 m thick.

application 5.3

Does an equal numerical value of natural strain respectively linear strain correspond to greater, equal or less compression for the natural strain case?

application 5.4

To how much (linear) compression does a natural strain of 120% correspond?

application 5.5

An oil tank is built at a site containing a soft sublayer, which was preloaded before construction (Fig 5.3). The preload equals the full tank load. How much will the tank settle on its first filling to full tank load? Assume stresses at mid-height of the soft material as representative for the whole layer. Sand fill: Thick 2m, $\gamma = 20$ kN/m^3, $\gamma_d = 16$ kN/m^3. Soft sublayer: Thickness 5m, $\gamma = 16$ kN/m^3, $C_c'/(1+e_0) = 0.01$, $C_c/(1+e_0) = 0.1$. Full tank load: 100 kPa. Phreatic level: 1m below surface

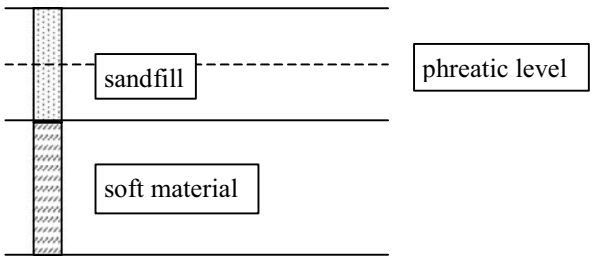

Figure 5.3

application 5.6

A soft layer with compressibility coefficient $C_c/(1+e_0)$ and unit weight γ'_1 dips slightly through stiffer soil (unit weight γ'_2) as shown (Fig 5.4). Give an expression for the compression due to this layer as function of the horizontal position x. Quantify the compression at left, centre and right, and explain the trend. Use H =

100m, h = 30m, L = 1000m, $C_c/(1+e_0)$ = 0.1, γ'_1 = 18 kN/m^3, γ'_2 = 20 kN/m^3, $\Delta\sigma$ = 50kPa.

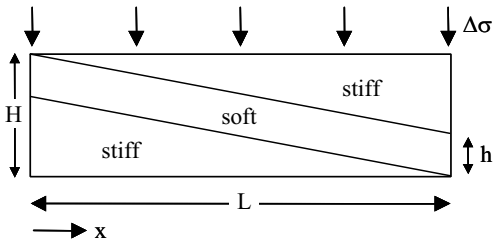

Figure 5.4

application 5.7

A soft clay site is to be prepared for development by applying a surcharge sand fill of 2m thick (Fig 5.5). Determine the final level of the sand fill relative to N.A.P. Thickness soft clay is 6m. Groundwater level: 1m below surface (Fig 5.5). The wet unit weight soft clay is 14 kN/m^3. The dry unit weight sand: 16 kN/m^3. Take: η = 0.15 and n = 40%. NAP: basic level (standard).

Hint. Take an average value of initial effective stress at one-third depth in the soft clay. Perform two calculation cycles, the first without submergence correction, the second with submergence correction based on the first calculation. Then average both results.

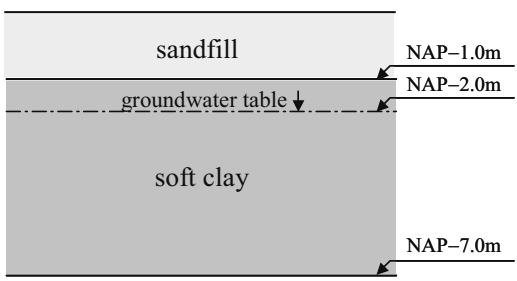

Figure 5.5

6 CREEP AND CONSOLIDATION

A TIME-DEPENDENCY

Time-rate effects are observed in clay and peat, referred to by creep, relaxation and consolidation. Creep is the strain increment under sustained constant stress. Relaxation is the stress reduction under sustained constant strain. Consolidation in soft soil is the dissipation of excess pore pressures with time, involving groundwater flow (drainage) and deformation. Ageing is used to express that soil gains strength with creep/relaxation. In sand these time-rate effects are less significant. If in saturated and laterally confined soil the volume reduction by creep occurs, outflow of pore water is required. The corresponding hydraulic gradients are quite small (in the so-called secondary phase, after primary consolidation). However, if drainage is restricted, for example in the centre of a thick soft layer, creep may cause increase of pore pressure.

A general uniaxial stress-strain relation, following the concept of (5.10), allows these time-rate phenomena to be visualised as shown in Fig 6.1, referred to by the abc-model (after Den Haan).[24]

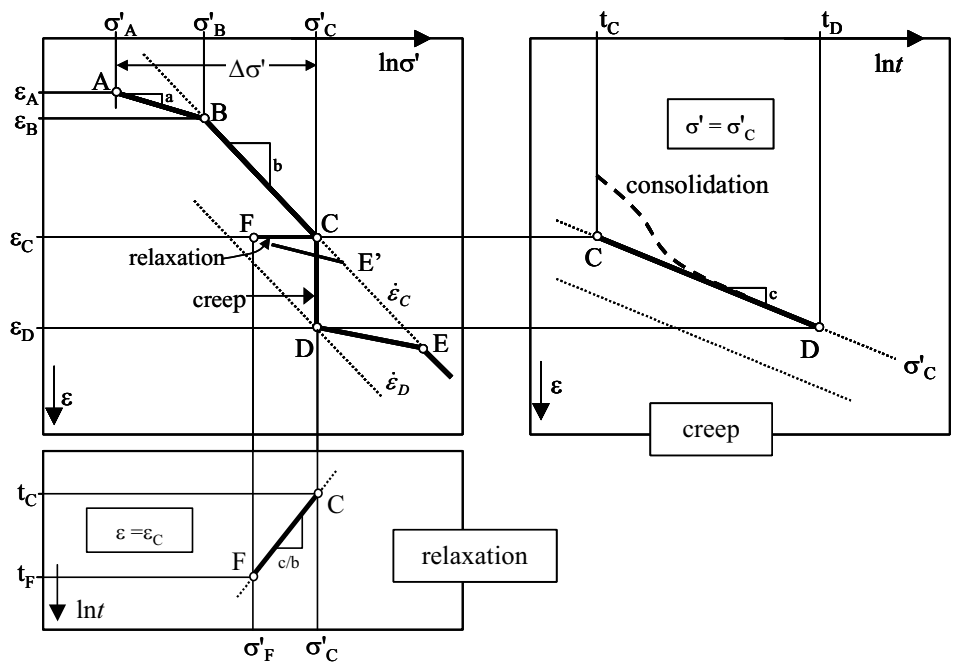

(a) (b)

Figure 6.1 Model for uniaxial deformation

[24] In 1972, Garlanger defined a similar relation: $e = e_0 - C_r\log(\sigma'_B/\sigma'_A) - C_c\log(\sigma'/\sigma'_B) - C_\alpha\log((t+t_i)/t_i)$, where e is the voids ratio, σ'_B the preconsolidation pressure, C_r is the recompression index, C_c the inelastic-compression index, C_α the creep index (secondary compression), t the elapsed time and t_i a reference time (intrinsic time).

As shown in Fig 6.1, soil is subjected to a loading step $\Delta\sigma' = \sigma'_C - \sigma'_A$.[25] The branch AB (elastic) is reloading with a recompressibility index a and σ'_B is the so-called preconsolidation stress (ultimate historic loading, preloading pressure). The branch BC (elasto-plastic) is virginal compression or inelastic compression with compressibility index b (similar to η, see Chapter 5). When thereafter strain is sustained, relaxation will occur, branch CF (visco-elastic). When the stress is sustained, strain may further develop by creep, branch CD (visco-plastic). If a new load step is applied, the state will move to the line BC first, along branch DE (creep) or FE' (relaxation). The increase from σ'_C to σ'_E due to creep is called ageing effect, after Bjerrum, i.e. by time during relaxation or creep soil strength has increased. In this regard, the stress point σ'_E is referred to as preconsolidation pressure, since it is not related to historic over-loading. The effect of ageing is similar as preloading.

B CREEP

Creep occurs when strain continues under constant effective stress. Its rate decreases with time and when projected against *ln(t)*, a straight line is found; the corresponding creep index is c (Fig 6.1b). Similarly, when strain is kept constant, stress will attenuate with time (relaxation) and when projected against *ln(t)*, also a straight line may be found with an index proportional to c/b (Fig 6.1a, lower part).

The abc-model or isotache model

In the uniaxial compression model it is suggested that creep can be visualised in the stress-strain plot of Fig 6.1a by straight lines each with a specific constant creep rate (dotted lines). They are called isotache lines. The model is also referred to as the isotache model. Similarly, in the strain-time plot of Fig 6.1b, it is found that for most soft soils the creep develops with the same compression index c, independent of pressure.

A compression creep index C_α is usually mentioned in literature. The relation with the index c is based on the way of measurement, identical to (5.16)

$$C_\alpha = 2.3\, c\,(1+e_0) = 2.3\, c\, v_0 \qquad (6.1)$$

TABLE 6.1 COMPRESSION CREEP INDEX VALUES

soil type	C_α *value*
gravel	0.0
sand	0.0
loam	0.002

soil type	C_α *value*
preconsolidated clay	< 0.005
normally consolidated clay	0.005 – 0.05
organic soils, peat	0.05 – 0.5

[25] In the oedometer test the loading is applied in successive steps, one a day. Consolidation causes the sudden loading step to be transferred by a gradual pore pressure reduction to a gradual effective stress increase. The period of (primary) consolidation takes about 1 hr in the oedometer test.

The ratio $C_\alpha/C_c = c/b$ will usually be in the range 0.025 – 0.10, the higher values pertaining to more compressible soils, such as peat. The total strain by the loading step $\Delta\sigma'$ is supposed to be a superposition of natural strains, and using (5.7), (5.8) and (5.10), it leads to a compact formula in terms of specific stress increments.[26]

$$\varepsilon_D - \varepsilon_A = (\varepsilon_B - \varepsilon_A) + (\varepsilon_C - \varepsilon_B) + (\varepsilon_D - \varepsilon_C)$$

$$= +a\,ln(\sigma'_B/\sigma'_A) + b\,ln\,(\sigma'_C/\sigma'_B) + c\,ln(t_D/t_C)$$

$$\rightarrow \quad \varepsilon = \ln[(\sigma'_B/\sigma'_A)^a\,(\sigma'_C/\sigma'_B)^b\,(t_D/t_C)^c]$$

$$\rightarrow \quad 1 - \varepsilon_l = v_D/v_A = (\sigma'_B/\sigma'_A)^{-a}\,(\sigma'_C/\sigma'_B)^{-b}\,(t_D/t_C)^{-c} \qquad (6.2)$$

During strain development in branch BC, the strain rate is considered a constant. During creep (branch CD) strain continues with attenuating strain rate. The creep time-frame of $t_C = t_i$ and $t_D = t_i + t$, where t is the time from C to D, is not related to the moment of loading, see Fig 6.1b. In fact t_i is unknown. The creep time is referred to as *intrinsic time*, according to which creep proceeds logarithmically at constant stress. In any creep process, after some time, the difference of intrinsic time and loading time t becomes insignificant, i.e. $t_D = t$. Historically, the creep effect is determined empirically, with $t_C = 1$ day and $t_D = 10^4$ days ≈ 27 years, an appropriate period when considering the maintenance period (life-cycle) of a geotechnical structure (road, dam, foundation).

An alternative way to consider creep is by associating it to the strain rate itself. The strain rate is expressed by $\varepsilon_{,t} = c/t$ which gives $t = c/\varepsilon_{,t}$. This leads to $\ln(t_D/t_C) = \ln(\varepsilon_{C,t}/\varepsilon_{D,t})$. So, expressing the right-hand graph of Fig 6.1 not in terms of $\ln(t)$, but by $\ln(\varepsilon_{,t})$ avoids the problem of intrinsic time and time frame difference.

Although formula (6.2) is expressed in terms of linear strain ε_l, the formula is fully based on the concept of natural strain. It therefore properly reflects convective and large-strain aspects. The formulation in terms of linear strain makes it convenient for practical use, as it can be directly related to measurements in terms of linear strain.

Formula (6.2) corresponds to a non-linear Maxwell material. A Maxwell material is a visco-elastic material having both elastic and viscous properties. It is named for James Clerk Maxwell who proposed the model in 1867. The Maxwell model can be represented by a purely viscous damper and a purely elastic spring connected in series. In this configuration, under an applied axial stress, the total stress σ and the total strain ε can be defined as follows: $\sigma = \sigma_S = \sigma_D$ and $\varepsilon = \varepsilon_S + \varepsilon_D$, where the subscript D indicates the stress/strain in the damper and the subscript S indicates the stress/strain in the spring. Taking the derivative of total strain with respect to time, we obtain:

---

[26] The 2nd line of (6.2) states $\varepsilon = \ln(\sigma'/\sigma'_A)^a$ for $\sigma' < \sigma'_B$ and $\varepsilon = \ln[(\sigma'_B/\sigma'_A)^a\,(\sigma'/\sigma'_B)^b]$ for $\sigma'_B < \sigma' < \sigma'_C$.
The 3rd of (6.2) states $1 - \varepsilon_l = (\sigma'/\sigma'_A)^{-a}$ for $\sigma' < \sigma'_B$ and $1 - \varepsilon_l = (\sigma'_B/\sigma'_A)^{-a}\,(\sigma'/\sigma'_B)^{-b}$ for $\sigma'_B < \sigma' < \sigma'_C$

$$\varepsilon_{,t} = \varepsilon_{S,t} + \varepsilon_{D,t} = \sigma_{,t}/E + \sigma/\mu \qquad (6.2a)$$

where E is the elastic modulus and μ is the material coefficient of viscosity. This model describes the damper as a Newtonian fluid and models the spring with Hooke's law. In the comparison with (6.2) one may notice the non-linearity, in fact that the strain $a\ln(\sigma'_B/\sigma'_A)$ corresponds to the strain σ/E, and that the strain $b\ln(\sigma'_C/\sigma'_B) + c\ln(t_D/t_C)$ is related to the strain rate σ/μ. In 1948, the Dutch pioneer in soil mechanics Keverling Buisman referred for the first term (spring) to direct strain and for the term $c\,ln(t_D/t_C)$ to secular strain (dashpot), as it is may last for ages. Some years later, Koppejan suggested that the creep term should be stress-dependent and modified the material coefficient c. In Den Haan's model (6.2) Maxwell's dashpot constitutes a visco-plastic behaviour, where both a stress-independent (viscosity) and a stress-dependent (plasticity) feature, the term $b\ln(\sigma'_C/\sigma'_B)$, play a role, and by doing so giving credit to Keverling Buisman and Koppejan.

Ageing

Age dependency is reflected in the preconsolidation pressure σ'_E, embodying the creep history from the latest loading stress σ'_C (see Fig 6.1), The following relation expresses the increase of the preconsolidation pressure due to ageing

$$c\ln(\frac{t_D}{t_C}) + a\ln(\frac{\sigma'_E}{\sigma'_C}) = b\ln(\frac{\sigma'_E}{\sigma'_C}) \quad \text{or} \quad \frac{\sigma'_E}{\sigma'_C} = (\frac{t_D}{t_C})^n = (\frac{\varepsilon_{D,t}}{\varepsilon_{D,t}})^n \qquad (6.2b)$$

$$\text{with} \quad n = \frac{C_\alpha}{C_c - C_r} \approx \frac{C_\alpha}{C_c} = \frac{c}{b}$$

There are many factors that affect the secondary compression (creep) index C_α, such as temperature, intrinsic time t_i, remoulding, loading rate, shear stress and consolidation stress.

C ONE-DIMENSIONAL CONSOLIDATION

Because loading of fine-grained soils causes an increase of pore pressures (excess pore pressures), silts and clays undergo a process of consolidation, during which the pore water is slowly squeezed out. After this period (for thick layers it takes years) compression ceases and the soil is fully consolidated. Soil is normally consolidated when the actual state corresponds to full consolidation. Soil is overconsolidated (or preconsolidated) when the actual state of stress is less than imposed sometime in the past. The state of stress is then commonly characterised by the overconsolidation ratio $OCR = \sigma_{\text{historic max}}/\sigma_{actual}$. From Fig 6.1, it can be understood that relaxation and creep induce an $OCR > 1$. So, deposited clays gain some strength with time (ageing). It gives many clays a moderate overconsolidation ratio $1 < OCR < 2$.

Consolidation model

At the beginning of consolidation, the response to a sudden load step $\Delta\sigma$ is a sudden increase in pore pressure Δu (excess pore pressure).[27] During the consolidation process, the response to loading by excess pore pressures is gradually transferred to the granular skeleton (effective stresses), until the excess pore pressures have vanished (end of consolidation). Compression or settlement related to these effective stress increments shows up as a time-dependent process.[28] Thereafter, compression may yet continue at a reduced rate with time, which is referred to as creep, since the state of effective stress is sustained after consolidation.

During creep soil compacts as well, and the corresponding decreasing pore volume may give rise to pore pressure increase, which will play a role when the drainage capacity is very small (clay). Even so, during consolidation, creep will take place as an independent phenomenon. In standard soil mechanics, however, the process of consolidation and creep are considered separate and successive. As a simplification, consolidation is called primary compression and creep secondary compression.

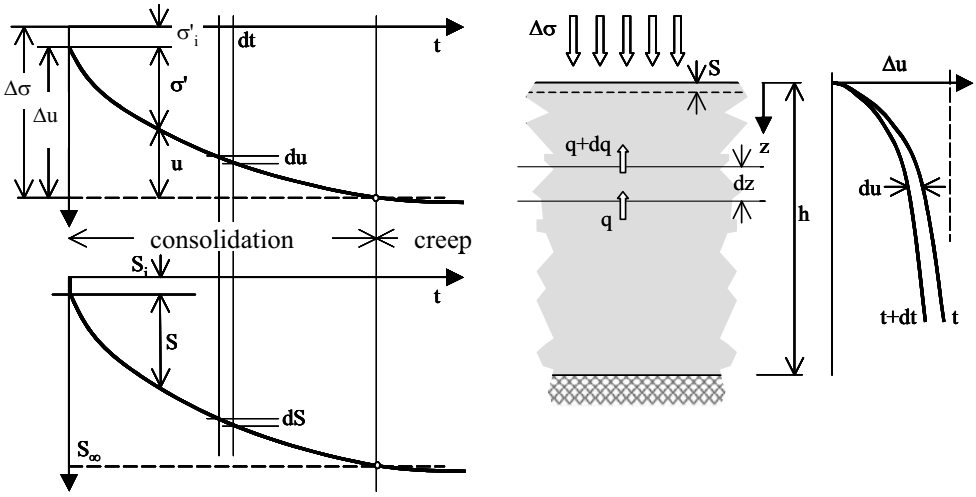

Figure 6.2 Consolidation process

When performing an oedometer test, the sample may not be fully saturated and the response to a sudden load step $\Delta\sigma$ may give an immediate settlement S_i which is due to compressibility of the pore fluid, as it provokes an immediate increase of effective stress σ_i. At the end of consolidation, when all excess pore pressures have

[27] In laterally confined conditions and for incompressible pore water and solid grains, the initial state $\Delta u = \Delta\sigma$ holds. In two and three-dimensional situations initially $\Delta u < \Delta\sigma$ usually applies.

[28] Terzaghi noticed this effect on the slow settlement of structures after being built. In his first article in 1924, he named the apparent stress that caused it effective stress.

vanished, the settlement is denoted by S_∞. In practice, one adopts the so-called degree of consolidation U, which is defined in terms of settlement, according to

$$U = (S - S_i)/(S_\infty - S_i) \tag{6.3}$$

The beginning of consolidation is then expressed by $U = 0\%$ and the end by $U = 100\%$.

The elaboration of the uniaxial consolidation process (after Terzaghi) is as follows. During dt the decrease of pore pressure $-du$ in segment dz results in an increase of effective stress $d\sigma'$, and the corresponding volume compaction of the segment dz is therefore[29] $-\alpha dzdu = -\alpha(\partial u/\partial t)dzdt$, which must be equal to the volume of expelled water dq during dt of segment dz, which is $(\partial q/\partial z)dzdt$. This leads to $(\partial q/\partial z) + \alpha(\partial u/\partial t) = 0$, at every dt and dz. Inserting Darcy's law $q = -(k/\gamma_w)(\partial u/\partial z - \gamma_w)$ provides the consolidation equation in terms of pore pressure u, according to

$$c_v \partial^2 u/\partial z^2 = \partial u/\partial t \quad \text{with} \quad c_v = k/(\gamma_w \alpha) \ [\mathrm{m^2/s}] \tag{6.4}$$

Here, c_v is the consolidation coefficient, assuming uniform and constant permeability and compressibility (homogenous soil layer). In reality, during the consolidation process, when with compaction the pore volume decreases, the permeability and the compressibility will decrease. It is sometimes stated that the consolidation coefficient, being proportional to k and reciprocal to α, will be yet more or less a constant. Applying the relation between the pore pressure u and the settlement S according to (4.1), (5.4) and (5.17), and solving (6.4) for the oedometer test, assuming that c_v is a constant, the following expression for the degree of consolidation U is obtained

$$U = 1 - (8/\pi^2)\, \Sigma_j \{ \exp[-(2j-1)^2 T_v \pi^2/4] / (2j-1)^2 \} \quad \text{with} \quad T_v = c_v t/h^2 \tag{6.5}$$

Here, h is the sample height. For large times, $T_v > 0.2$, the higher order terms (for $j > 1$) vanish and (6.5) reduces to

$$U = 1 - (8/\pi^2) \exp(-T_v \pi^2/4) \tag{6.6}$$

For small time, $T_v < 0.2$, (6.5) is parabolic with time and can be approximated by

$$U = (4T_v/\pi)^{0.5} \tag{6.7}$$

It appears that for $T_v = 0.2$ the degree of consolidation U becomes 50.5%, and for $T_v = 2$ it becomes 99.4%. That implies that consolidation is practically completed for

$$T_v = T_{hd} = 2\, h^2/c_v \tag{6.8}$$

---

[29] $\sigma = \sigma' + u;\ 0 = d\sigma = d\sigma' + du;\ du = -d\sigma' = -d\varepsilon/\alpha;\ dV = dzd\varepsilon = \alpha dzd\sigma' = -\alpha dudz$

Here, T_{hd} is referred to as the hydrodynamic period. Equations (6.6) and (6.7) show that the consolidation process is a function of $c_v\ t/h^2$, in which the layer thickness h appears quadratic. Therefore, scaling has a pronounced (quadratic) effect: the hydrodynamic period of a layer twice thicker becomes four times longer.

Determination of c_v from oedometer test (Asaoka's method)

From the measured settlements observed in an oedometer test, the consolidation coefficient c_v, the (linear) compressibility α and the permeability k can be determined. Beside numerical methods, which may cover non-linear aspects, graphical methods are often applied in practice, such as the square-root method (Taylor), the log-time method (Casagrande), the hyperbola method (Sridharan and Prakash), and the settlement method (Asaoka). Casagrande's empirical method distinguishes the initial, primary and secondary phase of consolidation, Tayler's method is based on (6.7) and is appropriate for the early phase of the consolidation process, and Sridharan and Prakash' method covers the middle part of consolidation. Asaoka's method is based on (6.6) and is not applicable for the early phase of the consolidation. For details of these methods, reference is made to standard textbooks.

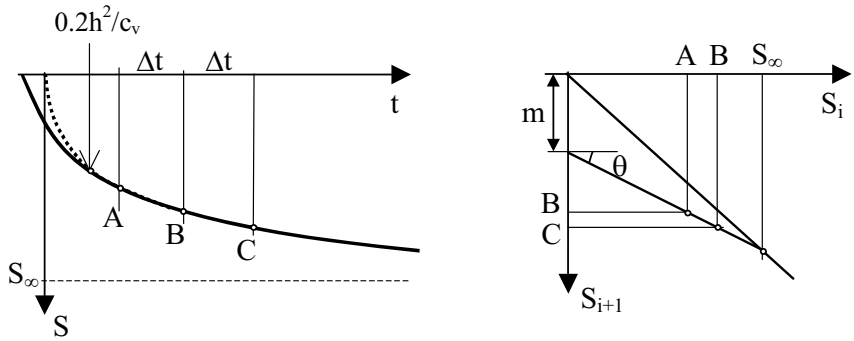

(a) *(b)*

Figure 6.3 Asaoka's method

Asaoka's method is explained next. The settlement S is measured during successive times. Three subsequent values are selected in an appropriate part of the data at equal time intervals Δt, providing that $t > 0.2h^2/c_v$ (to be checked afterwards), and they are depicted in a special manner, shown in Fig 6.3b. By measuring θ and m from the graph, the following material parameters can be found

$$c_v = 4h^2(1-\tan\theta)/(\pi^2\Delta t) \tag{6.9a}$$

$$\alpha = m/(\Delta\sigma h(1-\tan\theta)) \tag{6.9b}$$

And from (6.4) the permeability can now be determined: $k = c_v\alpha\gamma_w$.

D MULTI-DIMENSIONAL CONSOLIDATION

The specific solution of consolidation problems in three dimensions requires advanced mathematics. For a first estimation of the order of magnitude of the effects induced by consolidation, a simple method is suggested (Verruijt). Consider a general porous medium with volume V and surface $S = A_1 + A_2$ (Fig 6.4), where A_1 is a drained surface (pore pressure is constant $u = 0$) and A_2 is closed surface (no flow condition). Adopting a volumetric approach, i.e. volume strain ε and mean effective stress σ' are related through a bulk modulus K: $\sigma' = K\varepsilon$, the general storage equation, expressed by

$$-(\gamma_w/k)\ \nabla\cdot q = \nabla\cdot\nabla u = (\gamma_w/k)\ \partial\varepsilon/\partial t = (\gamma_w/k)\ \partial\sigma'/\partial t = (1/c_v)\ \partial(u - \sigma)/\partial t \qquad (6.10)$$

Here, the consolidation coefficient reads $c_v = kK/\gamma_w$.[30] Equation (6.10) is integrated over the entire volume

$$\iiint[\nabla\cdot\nabla u = (1/c_v)(\partial u/\partial t - \partial\sigma/\partial t)]\ dV$$

$$\iiint[\nabla\cdot\nabla u]\ dV = (1/c_v)\ (\ \iiint[\partial u/\partial t]\ dV - \iiint[\partial\sigma/\partial t]\ dV\ ) \qquad (6.11)$$

which requires the solution of three specific integrals. The second integral yields with the introduction of a volume average pore pressure P

$$\iiint[\partial u/\partial t]\ dV = \partial\ [\iiint u\ dV]\ /\partial t = V\ \partial\ [\iiint u\ dV/V]\ /\partial t = V\ \partial P/\partial t \qquad (6.12)$$

The third integral in (6.11) is assumed to be zero, by considering the cases where at time $t = 0$ a sudden loading is applied, which is kept constant during the consolidation process. Hence $\partial\sigma/\partial t = 0$, and the third term vanishes. The first integral in (6.11) expresses the groundwater flow, since

$$\iiint[\nabla\cdot\nabla u]\ dV = -(\gamma_w/k)\ \iiint[\nabla\cdot q]\ dV \qquad (6.13)$$

where $\nabla\cdot q$ is the net outflow out of a unit volume. It can be understood that in the absence of singularities (point sources and wells) the compatibility of unit volumes composing the entire volume, requires the flow at the boundaries to be in accordance with the local flow. Mathematically this is equivalent to Gauss' divergence theorem

$$\iiint[\nabla\cdot q]\ dV = \iint q\cdot dA$$

where q represents the boundary flux (q is perpendicular to boundary element dA). This boundary integral can be approximated by assuming a pore pressure gradient at the boundary, according to an arbitrary parabolic shape of the actual

---

[30] The compressibility of the pore fluid β can be included by adopting $c_v = kK/(\gamma_w + n\beta K)$. Note, that the bulk modulus is involved and not the laterally confined compressibility α

pore pressure field in the entire volume (Fig 6.4). The maximum pore pressure is caused by a sudden jump at $t = 0$ and decaying with time. This parabolic shape is characterised by a maximum pressure u_m at an average distance L_1 (drainage length) from the drained border A_1. The relation between the average pressure P and the maximum pressure u_m for a 2D parabolic shape is $P = {}^2/_3\, u_m$.

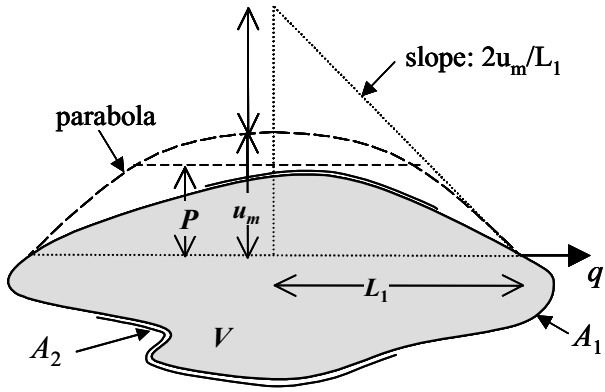

Figure 6.4

Introduction of Darcy's law yields at the border A_1 for a parabola $q = 2\,(k/\gamma_w)u_m/L_1 = 3\,(k/\gamma_w)P/L_1$. The integral (6.13) can now be evaluated

$$\iint q\cdot dA = \iint q\cdot dA_1 = \iint [3(k/\gamma_w)P/L_1]\, dA_1 = 3(k/\gamma_w)P/L_1 \iint dA_1 = 3(k/\gamma_w)P\, A_1/L_1$$

Thus

$$\iiint [\nabla\cdot\nabla u]\, dV = -3P\, A_1/L_1 \qquad (6.14)$$

and equation (6.11) becomes with (6.12) and (6.14)

$$-3P\, A_1/L_1 = (V/c_v)\, \partial P/\partial t \qquad (6.15)$$

With the introduction of a second length scale $L_2 = V/A_1$ called the hydraulic radius (it is related to the drainage capacity of the considered volume) this equation becomes

$$P = -\,\theta\, \partial P/\partial t \quad \text{with} \quad \theta = L_1L_2/(3c_v) \qquad (6.16)$$

The general solution, assuming $P = P_0$ at $t = 0$, yields[31]

$$P = P_0 \exp[-\,t/\theta] = P_0 \exp[-\,3c_v t/L_1L_2] \qquad (6.17)$$

---

[31] For an axi-symmetric parabolic shape the factor $P = {}^1/_2\, u_m$ leading $P/P_0 = \exp[-4ct/L_1L_2]$, and for a spherical symmetry $P = {}^2/_5\, u_m$ giving $P/P_0 = \exp[-\,5c_v t/L_1L_2]$. But for a wick drain it becomes $P/P_0 \approx \exp[-\,0.25c_v t/L_1L_2]$

It is important to notice the distinction between the two length scales:
- L_1 is a relevant flow path, connecting the location of maximum pressure to the drained border.
- L_2 is the hydraulic radius, related to the drainage capacity (volume and drained surface).

In the operator $\nabla\cdot\nabla$ one may recognise these length scales. The gradient ∇ is related to the flow path L_1 and the divergence $\nabla\cdot$ is related to the hydraulic radius L_2. For proper estimation of the hydrodynamic period in situations of multi-dimensional consolidation problems, the determination of L_1 and L_2 is crucial and requires some experience. Shortening both length scales by using vertical drains, properly placed, a soft soil may consolidate much faster. In the one-dimensional oedometer test both lengths are equal to the sample height h, and from here the quadratic rule for scaling the consolidation period by the square of the layer thickness originates. In multi-dimensional situations the drainage capacity L_2 and the characteristic seepage length L_1 are not necessarily equal.

The simple method represents a powerful tool for the estimation of the general behaviour of the consolidation process in any specific situation, while taking care of boundary and initial conditions in a consistent way.

E METHOD OF THE TRANSIENT LEAKAGE FACTOR

In deltas the common soil stratification consists of permeable sand layers (aquifers) and semi-permeable clay layers (aquitards). In the case where the system contains one aquifer and one aquitard, it is referred to as semi-confined aquifer (Fig 6.5a). The aquitard contributes to the groundwater flow in the aquifer by leakage, which for steady situations is determined by the leakage factor $\lambda = \sqrt{(kDC)}$, where kD is the aquifer transmissivity (horizontal permeability times height) and $C = d/k'$ the hydraulic resistance of the aquitard (height over vertical permeability). In unsteady situations the leakage is affected by consolidation in the aquitard and storage in the aquifer. Unsteady situations occur in pumping tests and under dikes and embankments during temporary high water levels. An elegant method to account for unsteady effects is the transient leakage factor (Barends).

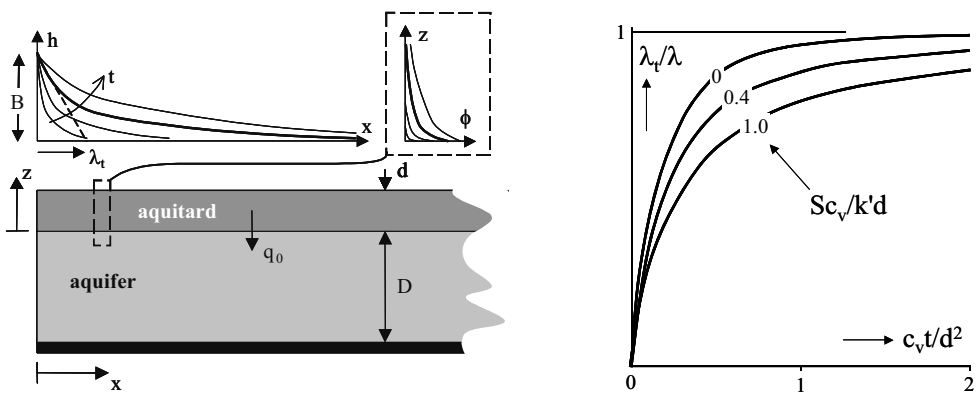

(a) semi-confined aquifer system *(b) the transient leakage factor*

Figure 6.5 a semi-confined aquifer

The consolidation process in the aquitard is described in terms of the potential head ϕ by

$$c_v \frac{\partial^2 \phi}{\partial z^2} = \frac{\partial \phi}{\partial t} \tag{6.18a}$$

Here c_v is the consolidation coefficient of the aquitard. The porous flow in the aquifer is described in terms of the potential head h by

$$\frac{\partial^2 h}{\partial x^2} = (S\frac{\partial h}{\partial t} + q_0)/kD \tag{6.18b}$$

Here, S is the storativity, k the permeability and D the height of the aquifer. The actual leakage from the aquitard at the interface $z = 0$ is expressed by q_0. Compatibility of the processes at the interface is guaranteed by

$$h = \phi \quad \text{and} \quad q_0 = -k'\frac{\partial \phi}{\partial z} \quad \text{at} \quad z = 0 \tag{6.18c}$$

Using Laplace Transform with the Laplace transform coordinate s, (6.18a) becomes

$$c_v \frac{\partial^2 \overline{\phi}}{\partial z^2} = s\overline{\varphi} \quad \text{and} \quad \overline{h} = \overline{\phi} \;\; at\, z = 0, \quad \overline{h} = 0 \quad \text{at} \quad z = d \tag{6.19}$$

which provides

$$\overline{\phi} = \overline{h}\;\frac{\sinh((d-z)\sqrt{s/c_v})}{\sinh(d\sqrt{s/c_v})},$$

$$\overline{q}_0 = -k'\left[\frac{\partial \overline{\phi}}{\partial z}\right]_{z\downarrow 0} = k'\sqrt{s/c_v}\,\coth(d\sqrt{s/c_v}) \tag{6.20}$$

Inserting this in the Laplace transform of (6.18b) yields

$$\frac{\partial^2 \overline{h}}{\partial x^2} = (sS\overline{h} + k'\sqrt{s/c_v}\,\coth(d\sqrt{s/c_v}))/kD = \overline{h}/\lambda_s^{\,2} \qquad \text{with} \tag{6.21}$$

$$\lambda_s = \lambda\left[\frac{sSd}{k'} + d\sqrt{\frac{s}{c_v}}\,\coth(d\sqrt{\frac{s}{c_v}})\right]^{-0.5}$$

A boundary condition is imposed at the aquifer: a unit-step load B at time $t = 0$ at $x = 0$ ($h = B$ for $t > 0$ and $h = 0$ for $t < 0$) , and the aquifer is supposed to be long. The corresponding solution of (6.21) becomes

$$\bar{h} = \frac{B}{s}\exp(-\frac{x}{\lambda_s}) \tag{6.22}$$

The real solution can be found by Laplace Inverse Transform, but it is complex. The so-called Simple Method is applied, which is easy and quite accurate for this consolidation problem (error less than 3%). It states that $s\bar{h} = h$ for $s = 1/2t$, which results in

$$h = B\exp(-\frac{x}{\lambda_t}) \quad \text{and} \quad \phi = h\,\frac{\sinh((d-z)/\sqrt{2tc_v})}{\sinh(d/\sqrt{2tc_v})} \quad \text{with} \tag{6.23}$$

$$\lambda_t = \lambda\left[\frac{Sd}{2tk'} + \frac{d}{\sqrt{2tc_v}}\coth(\frac{d}{\sqrt{2tc_v}})\right]^{-0.5}$$

Here, λ_t is the transient leakage factor. For large time[32], λ_t becomes equal to the steady leakage factor λ, see Fig 6.5b. Solution (6.23) shows that the storage in the aquifer proceeds with $t^{0.5}$ and that consolidation in the aquitard proceeds with $t^{0.25}$, much slower. Since for shallow sand layers the storage effect is less than the consolidation effect of adjacent clay layers, this has implications for the response of sand-clay systems to time-dependent loading (see Chapter 8, Fig 8.4).

For varying boundary conditions (B is not a constant) convolution can be used with solution (6.23)

$$h = \int_0^t \frac{\partial B}{\partial \tau}\exp(-\frac{x}{\lambda_{t-\tau}})\,d\tau \tag{6.24}$$

This method has been validated by field tests and is implemented in the Dutch guideline for dike design.

application 6.1

Consider a three-layer system: sand, clay and silty clay. Characteristic properties are given (Table 6.2). The groundwater table is at the top of the clay layer. The question is to determine the settlement due to a loading of 100 kPa and the creep thereafter for a period of 27 years (~ 10^4 days). The preconsolidation load is 50 kPa.

---

[32] $x\coth(x)$ tends to 1 for $x \rightarrow 0$

TABLE 6.2a DATA PROVIDED

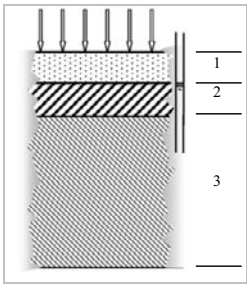

H [m]	n	weight [kN/m^3]		C_r	C_c	C_α
		γ_d	γ			
1	0.40	16.0	20	0.001	0.006	0.0
1	0.42	12.8	17	0.12	0.76	0.005
5	0.35	14.0	18	0.04	0.14	0.002

TABLE 6.2b ELABORATION, $\Delta\sigma = \Delta\sigma' = 100$ KPA, PRECONSOLIDATION STRESS 50 KPA

layer	e_0	a	b	c	σ_A kPa	u kPa	σ'_A kPa	σ'_B kPa	σ'_C kPa	ε_1	S_{total} m	S_{creep} m
1	0.667	0.0003	0.0016	0	8	0	8	58	108	0.0015	0.001	0.0
2	0.724	0.0303	0.1917	0.0013	16	0	16	66	116	0.1500	0.143	0.010
					33	10	23	73	123	0.1363		
3	0.538	0.0113	0.0395	0.0006	33	10	23	73	123	0.0382	0.160	0.025
					123	60	63	113	163	0.0260		
											total 0.305	total 0.035
remark					1		2	2	2	3	4	5

Use the following remarks (Table 6.2b)

1. The total stress at each layer interface (top and bottom); for the first layer in the middle.
2. See Fig 6.1. See also Table 5.2b.
3. Formula (6.2) is applied: $\varepsilon_1 = 1 - v_D/v_A. = 1 - (..)^{-a}\,(..)^{-b}\,(..)^{-c}$
4. The total settlement S (reloading, virginal loading and creep) in each layer is approximated by $H(\varepsilon_1^{top}+\varepsilon_1^{bottom})/2$, except for the first layer.
5. The settlement due to the creep component only after 27 years (10^4 days) is shown separately (last column of Table 6.3). For example, for layer 2 (top) one finds, applying (6.2)

$$S_{creep} = H\,\varepsilon_{1\,creep}^{top} = H\,\varepsilon_{1\,total}^{top} - H\,\varepsilon_{1\,elastic+plastic}^{top} =$$

$$H(1-(\sigma'_B/\sigma'_A)^{-a}\,(\sigma'_C/\sigma'_B)^{-b}\,(t_D/t_C)^{-c}) - H(1-(\sigma'_B/\sigma'_A)^{-a}\,(\sigma'_C/\sigma'_B)^{-b})$$

$$= H(\sigma'_B/\sigma'_A)^{-a}\,(\sigma'_C/\sigma'_B)^{-b}\,(1-(t_D/t_C)^{-c})$$

$$= 1(66/16)^{-0.0303}(116/66)^{-0.1917}(1-(10^4)^{-0.0013}) = 0.0102 \text{ m}$$

It appears that, in this case, the creep in total is about 12% of the primary (elasto-plastic) settlement. What would be the result when layer 2 and 3 are switched?

application 6.2

Consider a normally consolidated saturated clay layer of 10 m thick. On top a sand layer must be placed of 3 m thick (γ_d = 15 kN/m^3) for a road construction, which invokes consolidation in the clay. The works have to wait for the consolidation to be finished. The question is whether it is economic to install a vertical-drain system in the clay (drain distance *1.5* m), given that cost for installation is 250 €/m^2 and delay of works by consolidation costs 25 €/m^2 per year (note, m^2 refers to ground surface).

A soil sample is taken at a depth of 3 m. Characteristic properties are porosity n = 0.40 and saturated unit weight γ = 18 kN/m^3. It is tested in an oedometer (h = 0.02 m). The initial condition, reflecting the field condition, is σ_0'= 3x(18-10) = 24 kPa, which is met by preloading the sample. Next, the loading is applied corresponding the sand layer weight $\Delta\sigma$ = 3x15 = 45 kPa. The observed settlements in the oedometer are as follows (time t in seconds, settlement S in mm).

TABLE 6.3a

t	10	20	30	40	60	120	240	600	1200	1800	3600	7200
S	0.70	0.82	0.89	0.94	1.05	1.27	1.57	2.01	2.30	2.40	2.58	2.75

Asaoka's method is applied. By interpolation two sets of three successive measurements are selected (first one at t_0), the first set more in the beginning and the second set more at the end of the process. The corresponding graphs, according to Fig 6.3, yield for $\Delta\sigma$= 45 kPa the following values.

TABLE 6.3b

	Δt	t_0	S_A	S_B	S_C	S_∞	m	θ	c_v	α	k
	s	s	mm	mm	mm	mm	mm	°	m^2/s	m^2/kN	m/s
1st trial	400	200	1.46	2.01	2.24	2.40	1.42	20	2.6x10^{-7}	2.5x10^{-3}	6.5x10^{-9}
2nd trial	600	600	2.01	2.31	2.40	2.42	1.72	15	2.0x10^{-7}	2.6x10^{-3}	5.2x10^{-9}

These 2nd trial results show that $0.2h^2/c_v$ = 400 s. Since t_0 is smaller, the 1st trial is less appropriate (Asaoka's method is not applicable for t < 400 s). The hydrodynamic period (99.4% completion of consolidation) is $t = T_{hd} = 2h^2/c_v$ = 4000 s. Therefore, the last two measured settlements are mainly due to creep. At 50% consolidation (t = 400) the actual effective stress reaches $\sigma'_{50\%}$ = 24 + 0.5x45 = 46.5 kPa. An approximate value for the (virginal) compression index becomes $b = \eta = \alpha\sigma'_{50\%}$ = 0.12. The last two measurements provide a value for the creep index (difference in strain divided by logarithm of time interval): c = (0.00275/0.02 – 0.00258/0.02) / ln(3600/7200) = 0.012.

In the field, practical completion of consolidation will take $t > T_{hd} = 2h^2/c_v$ = 2 10^2/(2.0 10^7) = 10^9 s = 31.7 year! Application of vertical drains – taking for h the mutual drain distance as seepage path – will reduce the hydrodynamic period to about $T_{hd} = 2h^2/c_v$ = 2 1.5^2/(2.0x10^{-7}) = 0.71 year. Delay of 30 years will cost 750 €/m^2, and vertical drains 250 €/m^2. A vertical-drain system is therefore preferred.

Settlement, using the non-linear compression according to (6.2), adopting for the top a separate clay layer of 1 m thick and evaluation in the middle (to avoid the zero stress state at the ground surface), leads to 0.99 m, and creep in 25 years would add another 0.22 m, giving then a total settlement of 1.21 m.

application 6.3

A 5m layer of clay is consolidating under a surface load. Drainage is to the surface. Settlement is monitored. 1m, 1.2m and 1.35m are measured after 60, 90 and 120 days respectively. Predict the hydrodynamic period. Predict the final settlement.

application 6.4

A road embankment was placed 50 years ago on soft soil, and its settlement in the last 10 years was 0.05 m. Determine the creep index c of the soft soil, if its thickness is 10 m.

application 6.5

A clay layer in a planned industrial site is too soft for use so it is to be covered by sand. The sand compresses the clay and gradually settles, thereby becoming partially submerged under the groundwater table and so reducing the load on the clay.

Clay data: layer 6 m thick, lies at surface, underlain by dense sand, wet unit weight 15 kN/m^3, saturated, groundwater table at surface, compressibility indices $a = 0.01$, $b = 0.1$, $c = 0.005$, yield stress 25 kPa. Sand data: dry unit weight equals 16 kN/m^3, porosity 40%, thickness 2 m. $\gamma_w = 10$ kN/m^3.

Find a maximum value of the settlement (Z_{max}) of the clay layer after 10^4 days by neglecting the gradual submergence of the load. Find a minimum value of the settlement (Z_{min}) of the clay layer after 10^4 days by assuming immediate submergence to the value of Z_{max}.

Hints: Consolidation effects may be disregarded. Take the stresses at 1/3 of the layer depth as representative for the whole layer.

application 6.6

A Roman road built over a peat moor was eventually abandoned around 200 AD At that time the road level was 20 cm above the moor. The moor adjacent to the road grew upward by accumulation of dead plant material with a rate of 0.5 mm/year. Does consolidation plays a role in this problem? By how many years did the peat level reach the road level without considering creep. By how many years did soil creep hasten this event? Assume a peat layer of 3 m thick, having a c-value of 0.0225.

application 6.7

What is the relation between the recompression index C_r and the isotache parameter a.

application 6.8

What will be the transient leakage factor of (6.23) if the aquifer has two adjacent aquitards, one on top and one at the bottom?

application 6.9

What is the consolidation zone in the clay at the sand-clay interface in Fig 6.5a for a loading period of one week, if $c_v = 10^{-6}$ m^2/s and $d = 4$ m? And what is the storage effect in Fig 6.5b, if $S = 0.001$ and $k' = 10^{-7}$ m/s?

7 TRIAXIAL STRESS AND STRAIN

A CONTINUUM MECHANICS

In mechanics the principles of equilibrium and compatibility are considered, i.e. forces and displacements (or stresses and strains), and their connection through constitutive laws. Equilibrium requires directional balance of forces and rotational balance of moments, and compatibility requires displacements without loss or gain of material (connected material remains connected during deformation). A one-dimensional relation of stress and strain is shown in Fig 5.1. Concepts for stresses and strains can be developed quite precisely, but constitutive models, which define their mutual relation, are based on rather empirical laws. Soil stiffness increases with regard to volumetric compression (characterised by the bulk modulus *K*) and decreases with regard to shear strain (characterised by the shear modulus *G*). It is therefore common in soil mechanics to distinguish between isotropic (volumetric) and deviatoric (shear) stresses and strains. A specific material behaviour, important in soil mechanics, is the yield point, i.e. the stress where the elastic response changes to plastic straining, usually marked by an abrupt change in the slope of the stress-strain curve. Deviatoric stress may show a peak (curve A in Fig 7.1b), for sands due to high density, interlocking, cementation, etc., and for clays due to overconsolidation, interlocking, etc.

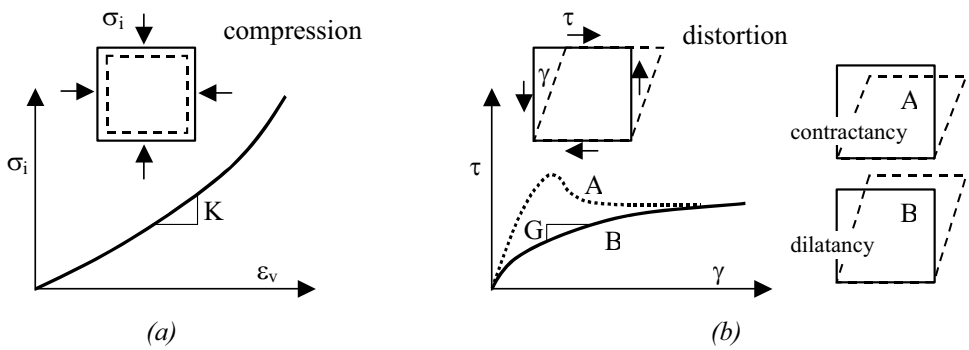

Figure 7.1 Stress-strain behaviour for compression and distortion

Soil is even more complex. Except for cemented soils, it cannot sustain tension. Saturated soils undergo volumetric changes when pore water is squeezed out or sucked in. Sometimes a loose granular structure may collapse into a denser one (contraction), or dense sand becomes loose (dilatancy). Some soils exhibit brittle failure; others more plastic. Microscopic elements (organic matter) may influence soil stiffness and strength significantly (peat, organic clay).

Several so-called constitutive models exist, which approximate the soil behaviour during triaxial (multi-dimensional) loading. This is the field of continuum mechanics. Such models try to link the three-dimensional (effective) stress state to the corresponding strain state by a specific set of parameters. Here, a distinction must be made between stiffness (deformation) and strength (failure). For sand or clay one may use the Mohr-Coulomb model or the CamClay model

(see Chapter 9). Relevant parameters are measured in laboratory tests under controlled conditions, and sometimes validated in the field. These parameters are then used in numerical simulation models.

The triaxial stress and strain states are tensors. Their direction and size change with orientation in such a manner that the internal equilibrium (of related forces) and the internal compatibility (of related displacements) are satisfied. The triaxial stress-strain relation is formulated as follows

$$\begin{vmatrix} \sigma_{xx} & \sigma_{xy} & \sigma_{xz} \\ \sigma_{yx} & \sigma_{yy} & \sigma_{yz} \\ \sigma_{zx} & \sigma_{zy} & \sigma_{zz} \end{vmatrix} = \boldsymbol{S} \begin{vmatrix} \varepsilon_{xx} & \varepsilon_{xy} & \varepsilon_{xz} \\ \varepsilon_{yx} & \varepsilon_{yy} & \varepsilon_{yz} \\ \varepsilon_{zx} & \varepsilon_{zy} & \varepsilon_{zz} \end{vmatrix} \quad \text{or} \quad \sigma_{ij} = S_{ijkl}\, \varepsilon_{kl} \qquad (7.1)$$

where σ_{ij} and ε_{ij} are the stress and strain tensor in space. σ_{ii} represents a normal stress and for $i \neq j$, σ_{ij} is a shear stress (usually denoted by τ). ε_{ii} represents a normal strain and for $i \neq j$, ε_{ij} is a shear strain, also denoted by $\gamma = \varepsilon_{ij} + \varepsilon_{ji}$. The modulus S_{ijkl} is a stiffness matrix, which compiles all possible interrelations, 81 in total! Each component may be non-linear. Hence, drastic simplifications are required to assess the triaxial mechanical behaviour in a practical way.

When considering a two-dimensional plane, the third dimension (perpendicular to the considered plane) also plays a role. For example, if strain in the third dimension is prevented (plane strain condition), then for an elastic material the normal stress in the third dimension becomes, using (5.2): $\sigma_3 = \nu\,(\sigma_1+\sigma_2)$, and the isotropic stress becomes: $\sigma_i = (1+\nu)(\sigma_1+\sigma_2)/3$. This may apply for a cross-sectional two-dimensional view of elongate structures such as dikes and embankments. Material properties for soil mechanics are usually obtained in a triaxial test, where the stress symmetry is cylindrical. When interpreting test results sometimes a correction is required to adjust for apparent field conditions.

The stress or strain state can be presented by a Mohr circle, which connects the geometric orientation to the corresponding state. For a two-dimensional situation, it is worked out in Fig 7.2. On the left-hand side (Fig 7.2a) the geometric situation of an elementary soil volume is shown with actual stresses and displacements as they work on the elementary volume. In the middle (Fig 7.2b) a particularly rotated volume is shown subjected to the same state, where for deformations the distortion and for stresses the shear are absent. The corresponding orientations are called principal directions.

If the principal directions, here denoted by angle α for stress and angle β for strain, are identical, the material is said to behave co-axially. It makes the description of the behaviour, i.e. the relation between stresses and strains, easier (the number of components in S_{ijkl} decreases drastically). For sand, however, this is less likely, because of density changes. Non-associativity can be expressed in the so-called dilation angle, usually denoted by ψ, which is related to the difference of α and β, see Chapter 9.

In Fig 7.2c, the state is shown in a compact way. Fulfilling internal compatibility and equilibrium shows that the state for any orientation is a circle (after Mohr), both for strain and stress. Every point on the circle reflects the state in a specific orientation. The direction centre or pole of normals ($DC_{\perp}$) correlates this

orientation in the field and in the Mohr circle. The principal stresses σ_1 and σ_2 and the principal strains ε_1 and ε_2 are represented on the circle without shear and distortion, in direction α and β respectively. For strains, the radius of the Mohr circle is $D_\varepsilon = (\varepsilon_1 - \varepsilon_2)/2$, called the deviator strain, and the free body rotation is expressed by ω. For stresses, the Mohr circle radius is $D_\sigma = (\sigma_1 - \sigma_2)/2$, called the deviator stress.

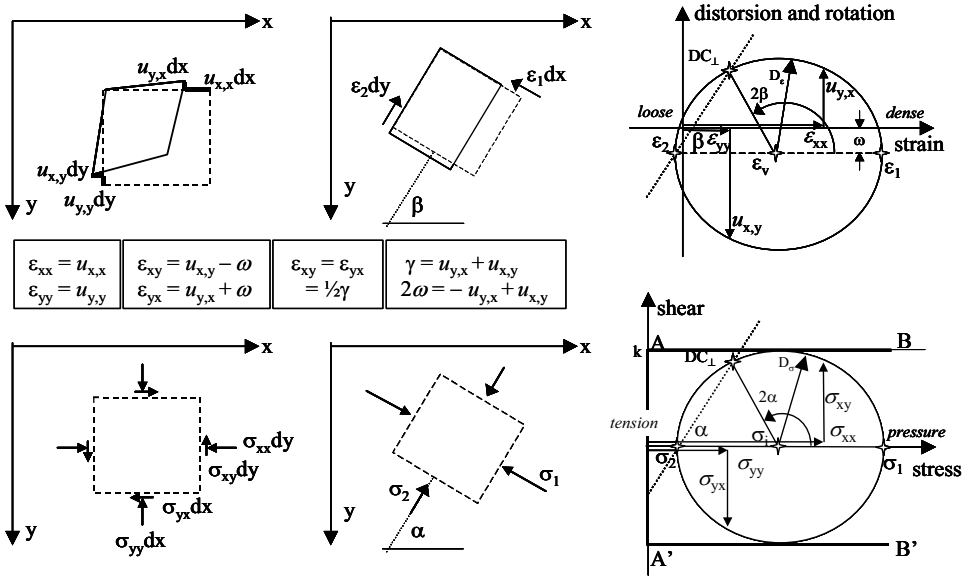

(a) general soil element (b) along principal directions (c) circle of Mohr

Figure 7.2 States of strain and stress ($DC_\perp$: direction centre of surface normals)

The third dimension plays a role, i.e. ε_3 and σ_3. Several specific cases can be considered, e.g. plane strain ($\varepsilon_3 = 0$, $\sigma_3 \neq 0$), plane stress (($\varepsilon_3 \neq 0$, $\sigma_3 = 0$) and axi-symmetry ($\sigma_3 = \sigma_2$). Isotropic strain ε_v (volumetric strain) and isotropic stress σ_i involve the third dimension, and only in special cases the two-dimensional Mohr circle centre correspond to ε_v or σ_i. One usually chooses the major and minor principle effective stress to represent the Mohr circle and its deviator. The state can be fully described by the isotropic stress or strain, the deviator and the principal direction. These parameters, which are invariants for the coordinate axes system usually appear in constitutive models. The free body rotation ω is important for compatibility, not for the local stress-strain behaviour. Its effect is a translation of the strain Mohr circle vertically over ω. The free body rotation should be accounted for in computational models.

A constitutive model (Tresca's model), particularly suited to elasto-plastic behaviour, is shown in Fig 7.2c by the yield envelope BAA'B' for the stress Mohr circle. It states that the stress circle cannot grow beyond the envelope, and the shear stress is limited: $\sigma_{ij} < k$. When the local stress state touches the envelope, plastic deformation occurs and the material completely yields (no strength left). This model is suitable for undrained clay, because increasing normal stress does not

invoke the reduction of volume necessary to increase normal stresses and strength. For undrained clay, parameter k in the Tresca model corresponds to undrained strength s_u or apparent cohesion c_u.

B MOHR-COULOMB MODEL

In the Mohr-Coulomb model, soil behaviour is elasto-plastic. Loading causes elastic deformations, but once stresses reach a yield envelope, indefinite plastic deformation occurs and the soil collapses. This collapse is assumed to occur only in some preferential shear planes, where the local friction resistance is exceeded, similarly as in the friction model of Coulomb.

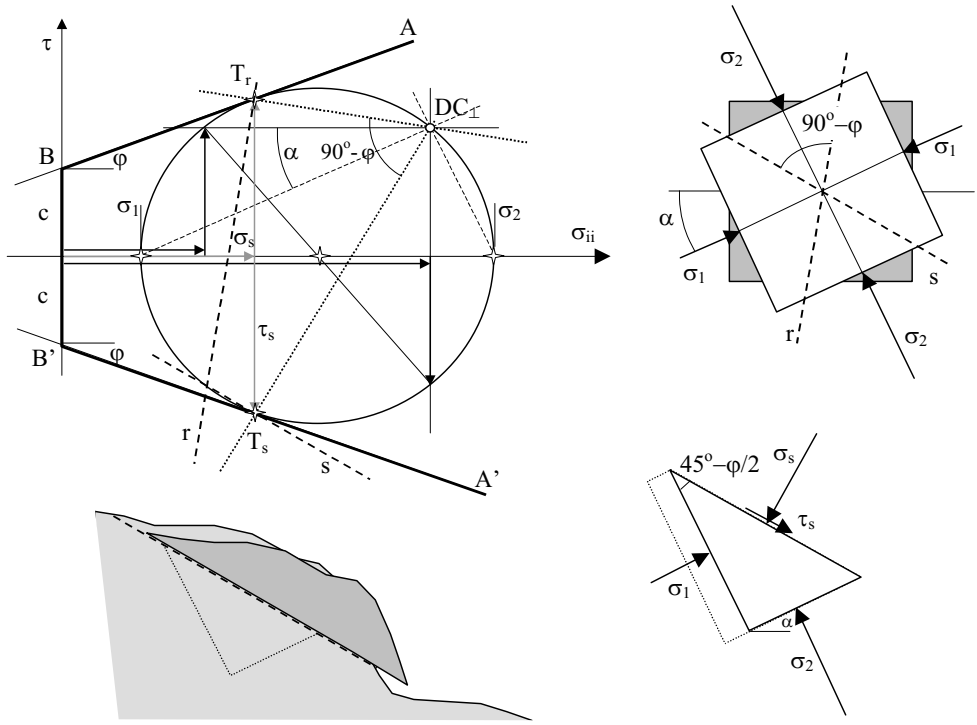

Figure 7.3 Mohr-Coulomb model for a landslide, related stress orientation and equilibrium

These failure shear planes can be shown with the stress Mohr circle as it touches the failure envelope ABB'A', shown in Fig 7.3. Here, in contradiction to Tresca's model, the yield envelope depends on the local isotropic stress level. In the contact points T_s or T_r a critical stress state occurs in a plane parallel to s or r. The critical stress state is formulated by the so-called Mohr-Coulomb failure criterion[33]

$$|\tau_s| = c + \sigma'_s \tan\varphi \qquad (7.2)$$

[33] This expression was originally proposed by Terzaghi, see Fig 3.4.

where the suffix *s* refers to a particular slip plane. In principle, shear strength depends on cohesion, internal friction and the effective stress. In Fig 7.3 the local critical stress state for a landslide along a slip plane (*s*) is worked out for its orientation, and its equilibrium.

The Mohr-Coulomb model is commonly applied for slope stability (straight slip plane or circular slip planes). A landslide occurs when along a failure plane everywhere the stress state is critical. In reality, a slide may involve zones with plasticity and local slip in different directions. It may appear that the Mohr-Coulomb model does not always describe the most critical situation and then other constitutive models should be used.

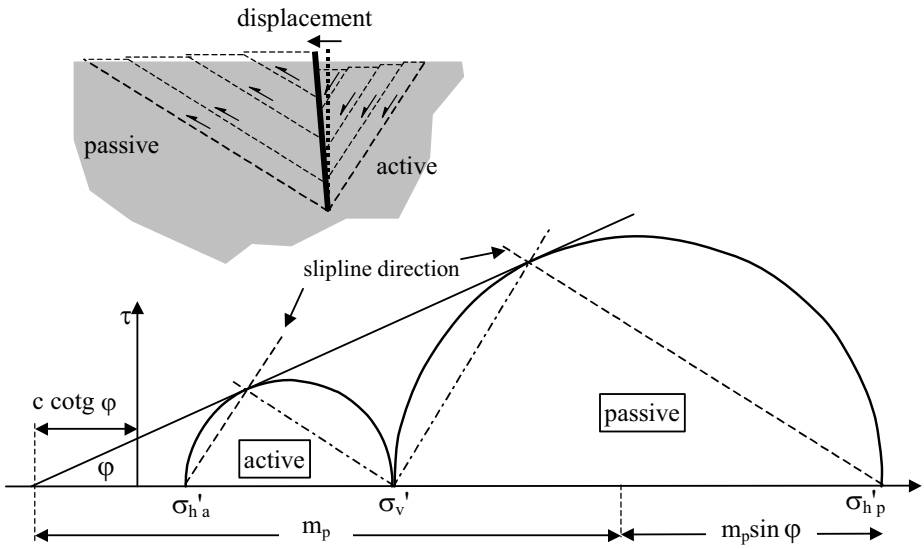

Figure 7.4 Rankine stress states, with cohesion effect (after Bell)

C COEFFICIENT OF EARTH PRESSURE[34]

The horizontal effective stress usually differs from the vertical stress. See for example equation (5.3), which refers to an elastic state without horizontal strain. The ratio of horizontal and vertical stress, expressed by so-called coefficient of earth pressure at rest K_0, is then $\nu/(1-\nu)$, where ν is the Poisson ratio. Instead, one may adopt the correlations for K_0, mentioned in Table 7.1.

Depending on (historic) deformation or actual displacement of the soil, the stress ratio σ_h'/σ_v' can vary significantly. Using the Mohr-Coulomb failure criterion, two limit states can be identified in soil, one with maximum (passive) and one with minimum (active) horizontal stress. In the plastic wedges, as shown in Fig 7.4, shearing resistance is supposed to be fully mobilised. This observation has led to

[34] The earth pressure coefficient is applied for effective stresses. Sometimes, it refers to total stresses, but in case of saturated soil, special care is required for the involvement of pore pressures.

the double-sliding model (see Chapter 9), an extension of the Mohr-Coulomb model.

TABLE 7.1 VALUES FOR K_0

type of soil	*correlation*	*Remark*
sand	$1 - \sin\varphi$	Jaky's formula
clay	$0.19 + 0.23\log(I_p)$	I_p: plasticity index
peat	$0.83 - 0.67OC$	OC: organic matter content (%)

For a given vertical effective stress σ_v', e.g. equal to vertical weight, the passive effective earth pressure σ_h' is found, when soil experiences maximum horizontal compression. The following holds (see Fig 7.4)

$$\sigma_h' + c\,\mathrm{cotg}\varphi = m_p\,(1 + \sin\varphi) \qquad (7.3a)$$

$$\sigma_v' + c\,\mathrm{cotg}\varphi = m_p\,(1 - \sin\varphi) \qquad (7.3b)$$

Elimination of m_p yields

$$\sigma_h' = \sigma_v'\,\frac{1+\sin\varphi}{1-\sin\varphi} + c\,\mathrm{cotg}\phi\,(\frac{1+\sin\varphi}{1-\sin\varphi} - 1) = \sigma_v'\,\frac{1+\sin\varphi}{1-\sin\varphi} + 2c\sqrt{\frac{1+\sin\varphi}{1-\sin\varphi}} \qquad (7.4)$$

And the passive earth pressure becomes

$$\sigma_h' = K_p\sigma_v' + 2c\sqrt{K_p} \quad \text{with} \quad K_p = \frac{1+\sin\varphi}{1-\sin\varphi} = \tan^2(45^\circ + \varphi/2) \qquad (7.5a)$$

In a similar manner, the active earth pressure σ_h is found, when soil experiences minimum horizontal compression. One finds

$$\sigma_h' = K_a\sigma_v' - 2c\sqrt{K_a} \quad \text{with} \quad K_a = \frac{1-\sin\varphi}{1+\sin\varphi} = \tan^2(45^\circ - \varphi/2) \qquad (7.5b)$$

Obviously, $K_a = 1/K_p$. For cohesive soils with $\varphi = 0^\circ$, formula (7.5) yields the following possible variation of σ_h' within the Tresca yield limit k

$$\sigma_v' - 2k < \sigma_h' < \sigma_v' + 2k \qquad (7.6)$$

For non-cohesive soil, $c = 0$, formula (7.5) expresses the Rankine stress states. For example, $\varphi = 30^\circ$ gives with (7.5), dependent on the deformation, the following possible variation of σ_h'

$$\tfrac{1}{3}\sigma_v' < \sigma_h' < 3\sigma_v' \qquad (7.7)$$

Horizontal stresses are important for stability of earth retaining structures (see Chapter 11). The range of some practical values of K_0 is given in Table 7.2.

TABLE 7.2 PRACTICAL VALUES FOR K_0

type of soil	K_0		*type of soil*	K_0
loose sand	0.4 – 0.6		normal clay	0.5 – 0.7
dense sand	0.3 – 0.5		over-consolidated clay	1.0 – 4.0
peat	0.1 – 0.6		compacted clay	0.7 – 2.0

In case of saturated soil, the local pore pressure u plays a role. It can be incorporated by adding it to all effective stresses. In this respect, the coefficient of earth pressure in terms of total stress becomes, by elaboration of equation (7.5a) for $c = 0$ and an apparent total-stress earth pressure coefficient $K_{p,total}$.

$$\sigma_h = \sigma_h' + u = K_p\sigma_v' + u = K_p(\sigma_v) + u(1-K_p)$$

$$\rightarrow \quad K_{p,total} = \sigma_h/\sigma_v = K_p + (1-K_p)u/\sigma_v \qquad (7.5c)$$

which reveals how the pore pressure is involved. For the active state a similar analysis can be made.

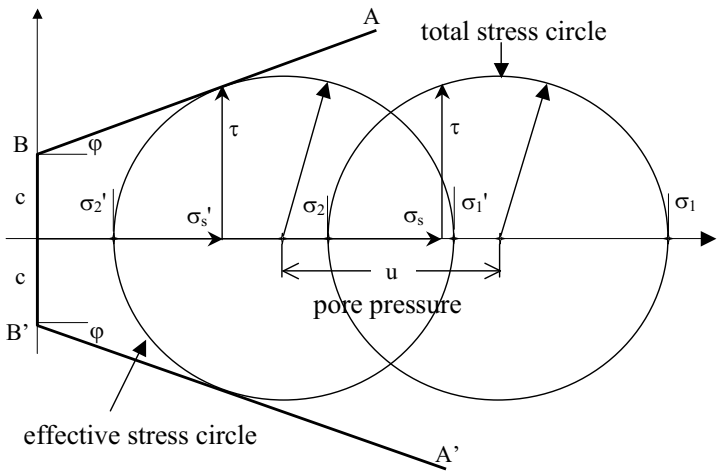

Figure 7.5 Effect of pore pressure for the Mohr-Coulomb model

D TRIAXIAL CELL

In a triaxial cell the stress and strain state have a cylindrical symmetry[35], i.e. in the horizontal direction they are invariant: $\sigma_2 = \sigma_3$ and $\varepsilon_2 = \varepsilon_3$. The vertical and horizontal directions are principal directions (no shear stress and deformation).

The total stress state may be expressed in terms of the deviator stress q and the mean normal stress p, according to

$$q = \sigma_1 - \sigma_2 \quad \text{and} \quad p = (\sigma_1 + 2\sigma_3)/3 \qquad (7.8)$$

[35] In the triaxial compression test the vertical direction is assigned to suffix 1, and horizontal to suffix 2 or 3.

A soil sample is usually saturated and the pore pressure u plays a role. The corresponding effective stresses become, using Terzaghi's effective stress principle (4.1b): $\sigma = \sigma' + u$, leading to

$$q' = q = \sigma_1' - \sigma_2' \quad \text{and} \quad p' = (\sigma_1' + 2\sigma_3')/3 = p - u \tag{7.9}$$

In a Mohr-circle representation the effective stress circle is shifted over u with respect to the total stress circle, while the deviator (radius) does not change (Fig 7.5). Since soil failure is related to effective stresses, the influence of pore pressure has to be accounted for with regard to total stress. It confirms that criterion (7.2) refers to effective stress. In terms of total stresses (7.2) the failure state reads

$$|\tau_s| = c + (\sigma_s - u)\tan\varphi \tag{7.10}$$

A typical undrained triaxial compression test includes two steps: an isotropic consolidated loading stage (until excess pore pressure $u = 0$) at $\sigma_1 = \sigma_2 = \sigma_3$, giving $p_0 = p_0' = \sigma_1$ and $q = 0$, and an undrained loading stage increasing σ_1, giving $p = (\sigma_1+2\sigma_3)/3 = (\sigma_1-\sigma_3+3\sigma_3)/3 = ⅓\, q + \sigma_3$. This relation gives a straight line under a slope of 1/3 as a total stress path in a p-q diagram (path DC in Fig 7.6). Since during loading the pore pressure may change due to volume change under shear deformation, while the undrained condition prevents pore water pressure dissipation, the effective stress path will follow the total stress path by horizontally subtracting this pore pressure change (u). For positive pore pressure generation (path DU) $p' < p$ and $q' = q$ (normal clay, contractant sand). For negative pore pressure generation (path DU') $p' > p$ and $q' = q$ (overconsolidated clay, dilatant sand), as shown in Fig 7.6.

The changes in the K_0 value can be measured in the triaxial cell from dq/dp', using equation (7.8), taking $\sigma_1' = \sigma_v'$, $\sigma_2' = \sigma_3' = \sigma_h'$, and $K_0 = \sigma_h'/\sigma_v'$, it follows that

$$\frac{dq}{dp'} = \frac{3(\sigma_v'-\sigma_h')}{\sigma_v'+2\sigma_h'} = \frac{3(1-K_0)}{1+2K_0} \quad \rightarrow \quad K_0 = (3 - \frac{dq}{dp'})/(3 + 2\frac{dq}{dp'}) \tag{7.11}$$

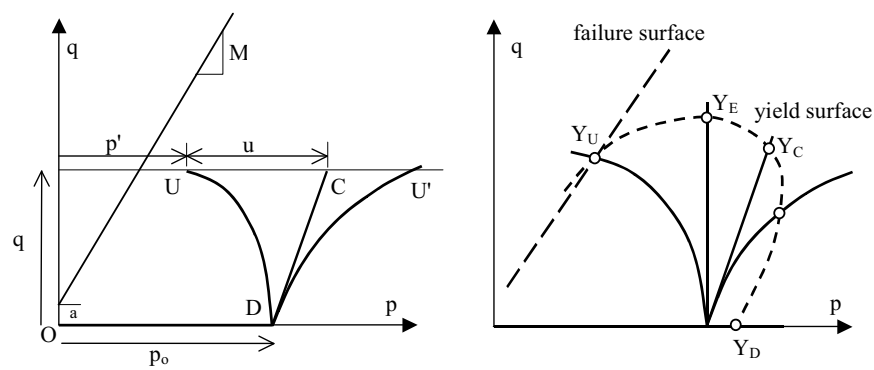

(a) (b)

Figure 7.6 Triaxial cell test in a p-q diagram, and a yield surface

The Mohr-Coulomb failure envelope in the *p-q* diagram is a straight line. The relation with the friction angle φ and the cohesion c is $M = 6\sin\varphi/(3-\sin\varphi)$ and $a/c = 6\cos\varphi/(3-\sin\varphi)$. The friction angle φ can therefore be found from

$$\sin\varphi = 3M/(6+M) \tag{7.12}$$

The yielding of soft soils is more diverse than can be represented by a simple failure criterion. Yielding is defined as a distinct point where the stress-strain curve deflects. These yield points can be investigated in a triaxial cell under different loading conditions, such as isotropic loading (D), one-dimensional compression (C), constant mean stress (E) and undrained triaxial (U). Some corresponding effective stress paths are shown in Fig 7.6b. A yield and a failure surface are used in sophisticated constitutive models, such as in the double sliding theory or the critical state theory, the backbone of the CamClay model (see Chapter 9).

E UNDRAINED STRENGTH

The condition of undrained loading and corresponding undrained strength is of great practical importance in the case of clays and silts, and for saturated sands under rapid loading (earthquake). Soil may fail when induced pore pressures have not been consolidated. During undrained loading shear related volume changes are counterbalanced by additional induced pore pressures that may be positive (contraction) or negative (dilation), affecting actual strength (Fig 7.7).

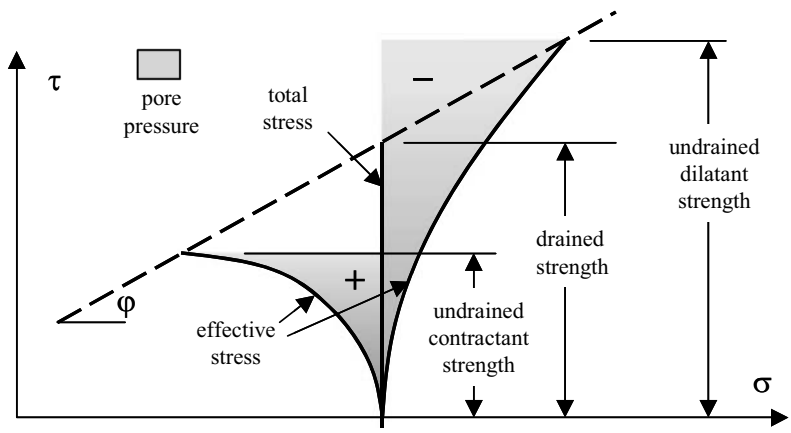

Figure 7.7 Total and effective stress paths in normally consolidated clay under undrained simple shear

For treatment of undrained stability problems in a total stress analysis, simplified expressions for undrained shear strength are used, symbolised by s_u in stead of $|\tau_s|$ from equation (7.2). Values of s_u can be obtained by triaxial CU tests.

Distinction can be made for active (compression) and passive (extension) states. In active loading the shear stresses increase in the same direction as those imposed during consolidation, and generally high undrained strengths are measured (e.g. in triaxial compression tests). In passive loading the shear stresses are reversed

relative to those imposed during consolidation, and relatively low undrained strength results. Active and passive states may even differ more due to (induced) anisotropy. Along slip surfaces of failed embankments active states occur under the crest and passive states near the toe. An average value of $s_u / \sigma_p' = 0.22$ is often assumed for the entire slip surface where σ_p' is the oedometric yield stress of the soil. More complex relationships such as $s_u = s_{u,nc} OCR^{0.8}$ are sometimes used. Correlations of s_u with CPT penetration resistance and SPT blow count also exist. A new development is to use so-called full-flow penetrometers (T-bar or ball) around which the soil closes back. This removes the overburden pressure as a source of penetration resistance and allows for more accurate correlations.

Because the undrained shear strength may vary with depth and highly depends on the mode of shear and time to failure, the choice of a proper value requires experience. One must recognise that the undrained shear strength s_u is not an intrinsic soil parameter.

F THE *A* AND *B* FACTOR

In saturated soil the pore pressure plays an essential role. It affects the normal effective stress, not the shear stress. Because the pore pressure is related to volume change, which equals the pore volume change when assuming rigid solid particles, the following holds for isotropic conditions

$$\varepsilon_v = -\Delta V/V = -\Delta(V_w+V_s)/V = -\Delta V_w/V = -n(\Delta V_w/V_w) = n\beta\Delta u \qquad (7.14)$$

where β is the pore water compressibility, defined by $\beta = -\Delta V_w/V_w\Delta u$. For undrained conditions the soil fabric (granular matrix) undergoes the same volume change[36], which is expressed by

$$\varepsilon_v = \Delta\sigma'/K \qquad (7.15)$$

where σ' is the isotropic effective stress and K the bulk modulus. Using (4.1b): $\sigma = \sigma' + u$, leads to $\varepsilon_v = (\Delta\sigma - \Delta u)/K$, and with (7.14) one obtains

$$\Delta u = \Delta\sigma/(1+n\beta K) = B\Delta\sigma \qquad (7.16)$$

where B is the undrained pore pressure factor (Skempton). For incompressible pore water ($\beta = 0$) this factor becomes $B = 1$, expressing that the response of an undrained soil sample under isotropic loading is letting the pore fluid carry the entire load, so that the corresponding effective stress change is zero. Pore water may contain a minor air fraction, which has however a significant influence on the compressibility, and subsequently $B < 1$. In test procedures, one should incorporate B properly.

[36] Undrained conditions imply no relative motion between pore fluid and grains. Hence, there is volumetric consistency for the pore fluid and the soil matrix.

When loading is not isotropic and shear stress is involved, the situation differs. Accounting for density changes during shear, equation (7.15) can be approximately extended to

$$\varepsilon_v = \Delta\sigma'/K - D\Delta\tau \tag{7.17}$$

where D represents a dilation parameter, i.e. a relation between shear stress change and corresponding volume strain. For $D > 0$, a volume increase (dilatancy) occurs and for $D < 0$ a volume decrease (contraction), see Fig 7.1. Using (7.14) and (4.1b), equation (7.17) gives

$$\Delta u = B(\Delta\sigma - KD\Delta\tau) \tag{7.18}$$

Conditions in a triaxial cell test can be expressed by

$$\Delta p = \Delta\sigma = (\Delta\sigma_1 + 2\Delta\sigma_3)/3 = \Delta\sigma_3 + (\Delta\sigma_1 - \Delta\sigma_3)/3 \quad \text{and}$$

$$2\Delta\tau = \Delta\sigma_1 - \Delta\sigma_3 = \Delta q \tag{7.19}$$

Here, $\Delta\sigma_3$ is the cell pressure and $\Delta\sigma_1 - \Delta\sigma_3$ the vertical load step, both typical triaxial test items. (7.19) render (7.18) into

$$\Delta u = B(\Delta\sigma_3 + A(\Delta\sigma_1 - \Delta\sigma_3)) \quad \text{with} \quad A = (⅓ - ½KD) \tag{7.20}$$

Although A and B are not intrinsic soil parameters, they reflect effects of pore water compressibility and soil dilation, in an approximate way. It also shows that under triaxial conditions the loading is only partly related to the pore water. Expressed in terms of p and q equation (7.20) becomes $\Delta u = B(\Delta p - ½\Delta q\, KD)$. Hence, in an undrained triaxial test, for incompressible pore water ($B = 1$) and no dilation ($D = 0$), $\Delta p' = \Delta p - \Delta u = 0$. In a p-q diagram it shows a stress path under a slope of 1/3 (DC in Fig 7.6). In a p'-q diagram, it corresponds to a vertical effective stress path. When the soil is loose, i.e. $D < 0$, Δu will be larger and the effective stress path will incline to the left (DU in Fig 7.6)); for compressible water ($B < 1$) or dense soil ($D > 0$) the stress path will turn to the right (DU' in Fig 7.6).

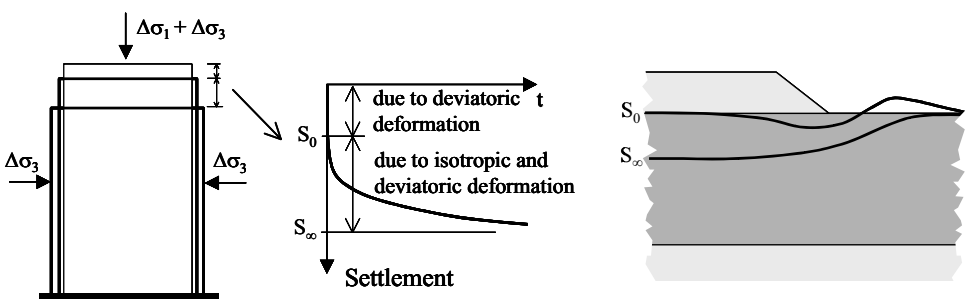

(a) (b) (c)

Figure 7.8 Settlement in a triaxial cell test and at the edge of a land fill

For B = 1 and D = 0, loading may cause an instantaneous volume constrained shear deformation, and if conditions allow shear to develop, yielding an instantaneous settlement S_0. If pore water pressure then dissipates by drainage, this settlement will increase at attenuating rate, according to a consolidation process, as shown in Fig 7.8, ending in a final settlement S_∞. For example, at the edge of a landfill, there will be an instantaneous settlement under the edge and heave beyond the edge, to maintain volume. In the middle, far from the edge, one-dimensional conditions apply, since (rotational) shear deformation is not possible there and hence no immediate settlement occurs.

application 7.1

A slide of a long slope can be predicted by simple tests and observation. In the field, an impression of a probable slip surface angle is obtained by observation: $\varphi_f \approx 35^o$. The vertical stress is approximated on the basis of measured unit soil weight γ = 18 and γ_d = 14.5 kN/m^3. Porosity is 0.35. The groundwater table is 2 metre under the ground level, more or less parallel to the slope. Thus, $u = 10(z–2)$ kPa. A shear test in the laboratory shows: $\varphi = 32^o$ and cohesion c = 5 kPa.

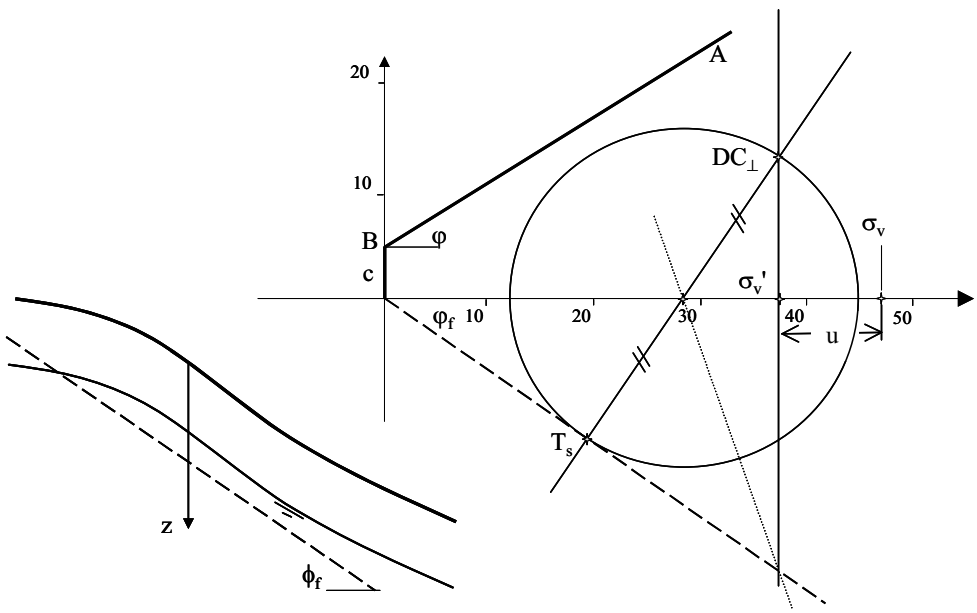

Figure 7.9 Practical evaluation of a potential slope slide

Consider a possible slip plane at a depth of 3 m, assume that the slip plane could occur at $\varphi_f \approx 35^o$ and disregard cohesion at this stage. In fact, this is a direct way to estimate the current stress state. The construction of the corresponding circle of Mohr allows to evaluate the slope stability. The vertical total stress at 3 m depth is σ_v = 47 kPa and the effective stress is σ_v' = 37 kPa. The Direction Centre $DC_\perp$ must lie on the vertical through σ'_v and point T_s must lie on the circle and the assumed failure line under angle 35°. The line through $DC_\perp$ and T_s is perpendicular

to the failure surface, such that its middle (being the centre of the circle) lies on the horizontal coordinate axis. The construction is shown in Fig 7.9 (aided by the dotted line that cuts the line T_s to $DC_\perp$ in half). Laboratory test results (line AB) reveal some reserve strength before failure would occur. Note that groundwater table rise by heavy rain would make the circle move to the left creating failure when touching AB.

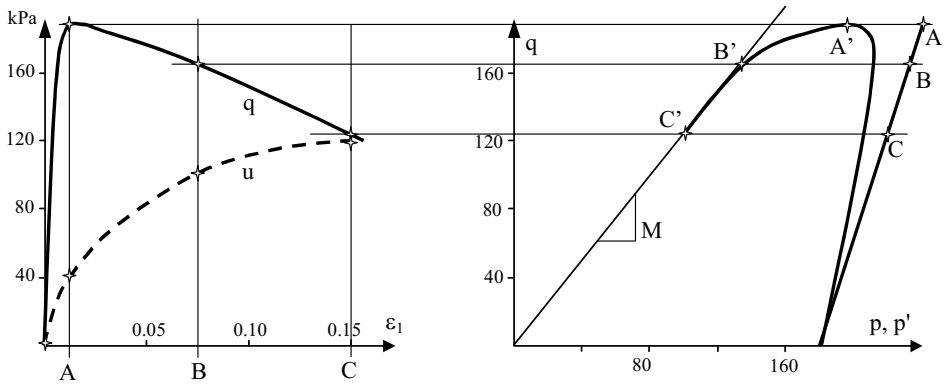

(a) (b)

Figure 7.10 A triaxial test and corresponding total (ABC) and effective (A'B'C') stress paths

application 7.2

A soil sample is tested in a triaxial cell. The first stage of the test is drained (consolidated) under an isotropic stress of 180 kPa; the second is undrained under vertical strain-controlled loading (a constant strain rate is applied). The response, in terms of deviator stress q and pore pressure u, is continuously measured and represented as a function of the vertical strain ε_1 in Fig 7.10a.

At first inspection, it may seem that the sample almost immediately collapses, but a detailed analysis shows that this is not the case. The development of the stress-strain state is evaluated at three distinct states (strain levels A, B and C) in a *p-q* diagram, see Fig 7.10.

TABLE 7.3

	q	ε_1	u	σ_3	σ_3'	σ_1	σ_1'	p	p'	M	φ
	kPa	%	kPa	kPa	kPa	kPa	kPa	kPa	kPa		°
A	190	1.25	40	180	140	370	330	243	203		
B	165	7.5	100	180	80	345	245	235	135	1.22	30.5
C	125	15	120	180	60	305	185	222	102	1.23	30.7
remark	*obtained from the graph*				$\sigma_3 - u$	$q+\sigma_3$	$\sigma_1 - u$	$\Sigma\sigma/3$	$p-u$	q/p'	*(7.13)*

At state A the effective stresses are still high, and the pore pressure is yet low. With time, the pore pressure increases during continuing compression, the effective

stresses become low and the sample fails. For states A, B and C characteristic values are elaborated in the Table 7.3. Fig 7.10 is typical for loose to medium dense sand. In very loose sand pore pressure build-up can continue all the way to the stress origin, in which case liquefaction occurs. Draw the circles of Mohr for state A, B and C.

Application 7.3

The immediate settlement of a saturated soft soil layer being subjected to a fill on top is practically zero, but not at the edges of the fill (Fig 7.8). Why is that?

Application 7.4

Consider application 7.1. How much must the groundwater level rise to create a critical situation (slope instability), according to the laboratory measurements? If the rain has an intensity of 5 cm/day, how long should it rain to reach the critical rise? Data provided: porosity $n = 0.4$, vertical permeability $k_v = 0.08$ m/day.

Application 7.5

If the circle of Mohr touches the failure envelope, the direction of the critical shear plane can be determined. In Fig 7.2 a stress state (circle of Mohr) is given. What are the directions of the critical shear plane (angles in degrees relative to the x-axis)?

Application 7.6

At a given depth in soil the active soil state is defined by a vertical soil stress of 75 kPa and a horizontal stress 15 kPa. The cohesion is 15 kPa. What is the corresponding friction angle and what is the maximum possible horizontal stress (passive state)? Hint: Use a graphical approach.

Application 7.7

Given c = 15 kPa, φ = 35°, Skempton's pore pressure parameter A = 1 (soft normally consolidated clay), Skempton's pore pressure parameter B = 1 (saturated soil), isotropic consolidation pressure p_0' = 100 kPa.

- Draw a graph of the total and effective stress path (tsp resp esp) during undrained triaxial compression.
- Estimate the undrained strength c_u.
- With $B = 0$, repeat in a new graph.
- Comment on the influence of B on c_u.

Part II

Methodology and Tools

This page intentionally left blank

8 UNCERTAINTY AND RELIABILITY

A UNCERTAINTY IN GEOTECHNICAL ENGINEERING

For large projects, where soil mechanics is prominently involved, corresponding construction cost and time seem not well predictable. They usually overrun seriously, and sometimes it goes wrong entirely. Some experts proclaim that sound engineering judgment is of prime importance above a sophisticated approach. Others state that inadequate soil investigation and lack of awareness of this aspect is to blame (Littlejohn), or when looking at various geotechnical failures one may conclude that human error is the culprit. From reviewing building pit failures, it is observed that in 80% of these failure cases relevant knowledge existed but was not available and applicable to the responsible people at the spot in proper time (Van Tol).

Modern societies do not accept anymore that issues, which are recognised for quite some time, are not being properly understood. Investment in knowledge changed from searching scientific truth to actuality and reality. This is a problem especially in geotechnical engineering, since here uncertainty is a unavoidable characteristic, unfortunately not generally recognised and not managed in systematic way. For society, it seems that geotechnical engineering fits in the 'disappointment' part of the hype curve (Fig 8.1).

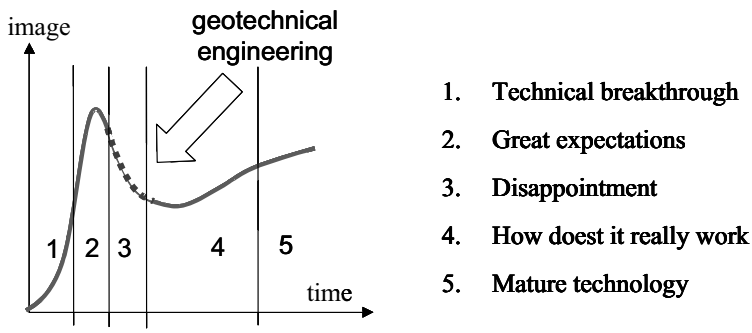

Figure 8.1 The hype curve (after Gartner)

Communicating to outside the technical world, i.e. transparent knowledge transfer, while recognizing the different types of communication, is becoming more essential, in particular with regard to informing others of intrinsic uncertainties and how to address them. And here, the process of contextualization presents a new paradigm (Barends in Terzaghi Oration 2005, Annex III), in which engineers and technical scientists should find their place. The current development of an integral approach in research agendas for the construction sector in a context of knowledge-driven economy, the handling of soil-related uncertainties using the benefits of pore-space engineering, biotechnology (SmartSoil®) and the Internet, and promising innovations, such as a concept for collective brains (GeoBrain) and the process of risk management in geotechnical design and construction (GeoQ) are new challenges that may improve the status of the geotechnical profession.

A crucial issue in society's reaction is the individual risk perception related to the intrinsic uncertainty. It is about emotion and trust. Uncertainty in geotechnical engineering may lead to remarkably high risk, i.e. significant vulnerability in areas prone to hazards. This is commonly not understood nor accepted in society. The geotechnical engineer should better explain the intrinsic uncertainty in geotechnical engineering to the outside world. In this chapter, aspects of geotechnical uncertainties and corresponding limitations and opportunities are elucidated.

Soil investigation

Geo-engineers know that uncertainty of soil properties (stratification and model parameters) is relatively high with regard to other common building materials like concrete and steel. Uncertainty for steel it is not beyond ±5%, for concrete it is about ±15%, for soil it is usually beyond ±50%.

Fig 8.2 shows our limited capability indicating soil conditions by some common site investigation methods using non-destructive techniques (NDT). The success rate of our predictability is not more than 30%! In soils this situation is common, and obviously the engineer dealing with it has to add intuition and experience when defining relevant soil conditions.

NDT	Depth	Piles	Stone	Peat	Clay	Loam	Silt	Sand	Gas
		shaft	*boulder*	*lens*	*lens*	*lens*	*lens*	*bed*	*pocket*
from surface or borehole									
CPT + coring	N – F	+?!	+?!	+	+	+?	+?	+	+
Seismic	M – F	?	?	?	?	?	?	+?	+?
Electromagnetic	N – M	÷	÷	+?	÷	÷	?	?	÷
Ground radar	N	+?	+?	÷	?	÷	÷	?	÷
Geoelectric	M – F	÷	÷	+	+?	?	+?	?	?

Figure 8.2 Capability of site investigation methods in geotechnical engineering.
Legenda: + OK, ? unknown, +? probable, ! damage, ÷ not possible;
N: near (1 to 5 m), M: medium distance (5 to 20 m), F: far (more than 20m).

The range of intrinsic and characteristic soil property values gathered from common field and laboratory tests is well studied. In codes of practice, corresponding partial safety factors are defined related to actual circumstances and related risks (see Table 8.2).

Boundary conditions

When modelling the real geometry, a choice has to be made about dimensions (1D, 2D or 3D), and about the soil stratification. At the borders of chosen domains suitable conditions are to be chosen with regard to groundwater and soil in terms of stresses, fluxes and/or displacements. This also holds to some extent for interfaces within the considered domain; by example, at locations of soil-structure interaction. For non-linear and time-dependent problems the initial state has to be defined. In fact, the determination of the initial state is sometimes more difficult than the actual problem itself.

Fig 8.3a shows the effect of unknown boundary conditions at the edge of a chosen domain: a two-layered (top clay, bottom sand) soil mass with on top a dike subjected to a sudden river level rise. The problem arose as a local pore-pressure

meter (position B) in the lee-side slope of the dike showed an immediate response, which did not comply with the hydrodynamic response period of the clay layer (months).

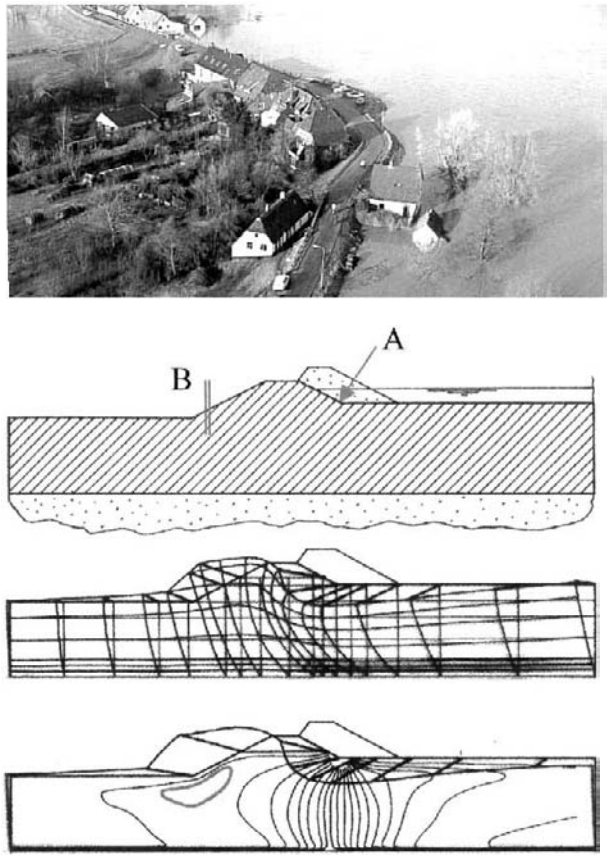

Figure 8.3a Boundary conditions, river dike

This immediate response was modelled by FEM considering two-dimensional linear-elastic consolidation. Various boundary conditions at the sides and bottom have been adopted: fixed, slip, pressure, impermeable, in 6 scenarios. The resulting deformation of the toe of the dike (point A) shows a horizontal deformation for different scenarios varying between 5 and 40 cm and vertical between 1 and 2.5 cm. The immediate pore pressure response did not vary as much (less than 10%). Fig 8.3a shows one such scenario: deformations and excess pore-pressure contours. The immediate response at point B is due to horizontal (total) loading by the river water on the dike, which is reflected in the pore water. The vertical effective stresses are slightly affected (by about 25% due to 2D-effects). So, slope stability was not really at risk. When the river level dropped the excess pore pressures disappeared rapidly. This example reveals that boundary conditions have distinctly different effects on field variables. Particularly deformations are sensitive to subjective choices for unknown boundary conditions.

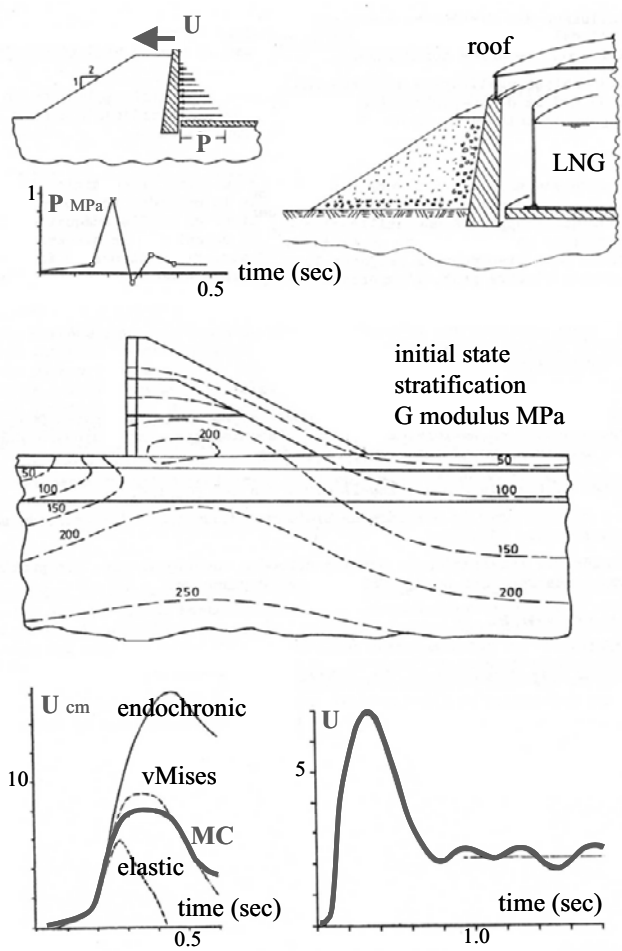

Figure 8.3b Modelling constitutive behaviour, storage tank

Constitutive behaviour

For the improvement of the stability of an LNG reservoir design, in case the inner metallic tank suddenly ruptures, a soil embankment is placed around the outer concrete tank wall. To prevent (explosive) gas escape, the roof structure must remain intact under dynamic forces caused by induced dynamic liquid flow pressures. The critical issue is the maximum horizontal displacement *U* of the roof edge (Fig 8.3b). Structure and soil properties and initial state are chosen and various constitutive soil behaviour models are selected: elastic, von Mises (elasto-plastic, no friction), Mohr-Coulomb (elasto-plastic and friction), and endochronic (visco-elastic including creep). The choice of characteristic parameter values for different constitutive models, based on available soil tests, has been taken identical when appropriate. The results show a wide range of the calculated critical displacement *U* varying from 6 to 16 cm. The residual deformation (just one, the Mohr-Coulomb model, is also shown) varies even more. As in this case there is not yet a structure, practical validation or monitoring is not possible. The client was not pleased with an uncertainty range of a factor 3. Here, it is up to the engineer's

intuition and experience, if any, to decide how to appreciate this outcome and what practical maximum displacement should be adopted for a proper design.

Physical processes

In reality, all possible and relevant physical processes do play a role, always. For a simulation or prediction the engineer has to optimise his approach by making a selection of the dominant processes and disregard physical processes, which are not relevant. It is recommended to support such a choice by an elementary analysis or by specific experiments. A striking example of the effect of choices of physical processes is found in the application of well-functions in geohydrology. For a constant well in a semi-confined aquifer system the Hantush well-function is commonly applied. It encompasses flow and storage in the aquifer and leakage through the adjacent aquitard. The outcome after calibration reveals the production capacity Q and the corresponding area of influence, the leakage factor λ. This approach is applicable for (deep) reservoirs and thin or rigid adjacent aquitards.

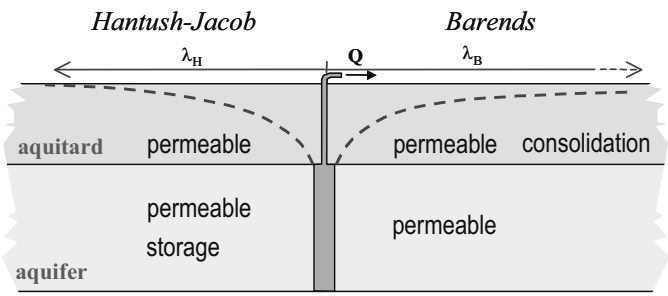

Physical processes; production well in a semi-confined aquifer

Choice	aquifer		aquitard		λ/λ_1
	permeable	storage	permeable	consolidation	
1	yes	yes	no	no	1.00
2	yes	yes	yes	no	1.25
3	yes	no	yes	yes	3.45

well-functions: (1) Theis, (2) Hantush, (3) Barends

Figure 8.4 Pumping test

In shallow regions where semi-permeable aquitards are relatively young deposits, the storage is due to induced consolidation (storage) in the aquitard; storativity of the aquifer is less relevant. By applying a special well-function (Barends) including this consolidation process, the outcome shows a value for λ being about 3.45/1.25 = 2.76 times larger than with the standard Hantush function (see Fig 8.4, Table). That the outcome of a constant well in a shallow semi-confined aquifer system by applying Hantush well-function represents all expected phenomena (storage, flow, leakance), is in fact misleading, since the storage is

adopted in the wrong layer. Fortunately, it has little implication on the production Q, but the influence area λ is largely underestimated.

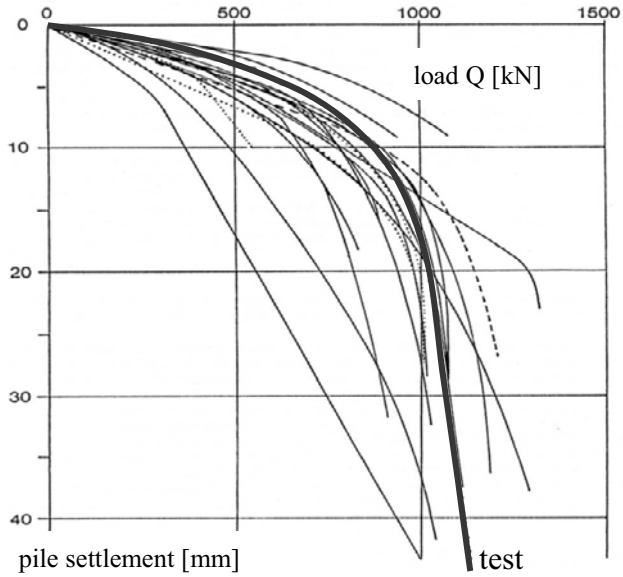

Figure 8.5a Pile load test ESOPT-II 1989 (Van Weele)

Ratio between predicted and measured displacement at 50% of the ultimate bearing capacity (static loading test)

Expert	Pile 1	Pile 2	Pile 3	Pile 4
1	-	0.59	1.32	0.70
2	3.32	0.80	1.53	1.08
3	-	-	-	1.06
4	1.20	1.10	1.29	1.25
5	2.00	1.06	1.38	1.50
6	0.60	0.63	1.35	1.22
7	1.03	0.79	1.26	0.80
8	1.42	1.46	1.04	0.71
9	1.21	0.74	1.41	1.00
Max/Min	5.53	2.32	1.47	1.78
Average	1.54	0.90	1.32	1.04

Figure 8.5b Pile load test ASWTP-4, 1992

Pile load-settlement behaviour

During the Penetration Testing Symposium ESOPT-II, in 1982, a prefabricated prestressed concrete pile (15 m, 0.25x0.25 m^2) was driven and statically loaded till failure. Long before, extensive site and lab investigations had been performed. With the results of these tests, 15 international experts made a prediction, using their best methods and experience. The predictions together with the real result are shown in Fig 8.5a. The predicted pile loading at 10 mm settlement varies from 360 to 1110 kN, and predicted failure load ranged from 600 to 1500 kN.

During the 4th conference of the Application of Stress-Wave Theory to Piles, in 1992, a similar contest was organised. Four concrete piles with different shape were dynamically tested and 9 international experts made a prediction for the static bearing capacity, each using his tool and interpretation method. In Fig 8.5b results are presented. The scatter is striking. The Test Report states that the interpretation method and type of software were more important for the variation in answers than the difference in monitoring systems. Moreover, surprisingly, local experience was not particularly helpful for obtaining more reliable predictions.

Slope stability

In 2008 a large dike on soft clay and peat was tested for slope stability (Fig 8.6). An international prediction contest was organised and 40 independent experts took a chance to estimate at which of the 8 phases the dike would collapse. The collapse occurred in phase 4, The prediction results show (Fig 8.6, Table) that the wide spread is mainly related to engineering choices and that the use of standard or sophisticated models does not make much of a difference.

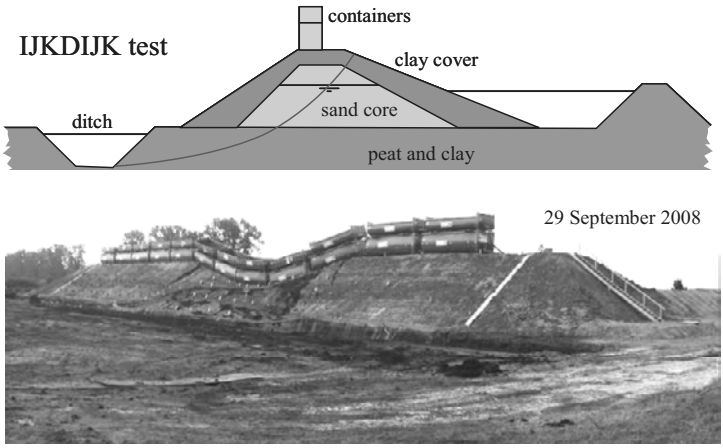

Predictions made by experts of the phase of collapse

Phase	Phase description	Experts	Method
1	before the test	1	-
2	digging the ditch	1	E
3	deepening the ditch	1	-
4	waterfilling sand core	6	E S P
5	emptying the ditch	10	E S
6	filling containers	13	E S P
7	saturating the dike	4	E S
8	no failure	4	E

E: educated guess, S: slip circle analysis, P: FEM (Plaxis)

Figure 8.6 Slope stability test

Sheet piling

In 1993, in Karlsruhe, a sheetpiling test was organised (Wolffersdorff). The behaviour of a strutted sheetpiling retaining 4 m of non-saturate sand was

approached by 43 international experts using FEM, subgrade reaction and other methods to predict deformations, moments and forces. The outcome showed a wide spread: three quarter of the experts obtained an answer beyond 50% of the test result. Those who disregarded capillary cohesion were completely out of range.

In 1999 an anchored sheetpiling test was organised in Rotterdam. 6.5 m of soft clay and peat were retained at high groundwater table. 23 international experts made a prediction for horizontal displacement, plastic hinge and oblique bending, applying FEM and subgrade reaction methods. Results showed again a wide spread: for the displacement, by FEM between 45 and 210 mm and by subgrade reaction between 62 and 173 was calculated, while 107 mm was measured Surprisingly, FEM was less accurate (more parameters had to be guessed). It was observed that data interpretation for parameter values for strength and stiffness varied significantly ($19^o < \varphi < 35^o$, $2 < c < 10$ kPa). Another striking outcome was that different sets of parameter values could produce the same result.

Engineering factor

The examples mentioned above indicate that a significant part of the spread in geotechnical prediction is due to lack of information, different interpretations and subjective choices. If more specific information becomes available, the spread will decrease, but uncertainty about soil stratification, initial state, soil behaviour and boundary conditions remains. We could refer to that as the *engineering factor*, since it is related to individual knowledge and personal experience. For the examples discussed in this chapter, the uncertainty (95% range) varies somewhere between ±0.30% and ±0.70% which is quite large; it is 10 times larger than in steel construction and 3 times more than in concrete design.

B PARTIAL SAFETY FACTOR (ISO 2394)

Structures and foundations on and in soft soils have to be reliable, meeting certain standards of safety and functionality (serviceability and durability). The general risk of failure or malfunctioning of a structure is related for a major part to the soil, both during construction (temporary works) and during usage (permanent works). Soil has a large heterogeneity and a wide variety of failure mechanisms. Prediction models are in principle approximate. By risk analysis proper insight in the possible failure (slip, uplift, squeeze, settling, deforming) of structural elements (dam, embankment, wall, trench, pit, tunnel), and their interaction can be obtained. One considers the ultimate limit state (ULS) and the serviceability limit state (SLS). A collapse of a slope fits ULS and damage of a road surface because of soil deformations SLS.

The reliability of a structure is expressed by $1 - P_f$, where P_f is the probability of failure. The safety is related to risk of malfunctioning, and risk is normally expressed as Risk = Probability of Failure x Consequences. The consequences are a matter that involves feeling of well-being and cannot be determined unambiguously. In this respect, the term safety factor should be conceived as a stability factor, when addressing the probability of failure.

Malfunction can be expressed in terms of a reliability function Z

$$Z = R - S \tag{8.1}$$

where R is the structural resistance (design) and S denotes the effect of actions (loading excitations or solicitation). If $Z < 0$ the construction fails. $Z = 0$ is the limit state. The ratio R/S can be related to an overall safety factor γ_0 (the old-fashioned way). The resistance R depends on various structural elements X_i and the effect of loading S can be composed of different components Y_j. For a specific model approach the method of partial safety factors may express the reliability, as follows

$$R(\ldots, X_i/\gamma_i, \ldots) \,/\, S(\ldots, Y_j\gamma_j, \ldots) \geq \gamma_m \tag{8.2}$$

where γ_i is a material factor, γ_j is a loading factor, and γ_m is a resistance factor related to model factors (design methods for Z). The design approach, which can be adopted, includes either calculations, prescriptive measures, experimental models or the observational method (see Eurocode 7). In applying (8.2) one may choose to lower strength through γ_i (the Resistance Factor Approach) or to increase loads through γ_j (the Load Factor Approach).

Considering normal distributions of X_i and Y_j, one may use the 5% or 95% confidence level with

$$X_i = \mu_i\,(1 - 1.64V_i) \quad \text{and} \quad Y_j = \mu_j\,(1 + 1.64V_j) \tag{8.3}$$

where μ is the respective mean value, V the variation coefficient $(V = \sigma_{sd}/\mu)$ and σ_{sd} the respective standard deviation. V follows from observations, educated guesses or specific codes (see recommendations of the JCSS: Joint Commitee on Structural Safety). Typical values for V are given in Table 8.1.

TABLE 8.1 TYPICAL VALUES FOR THE VARIATION COEFFICIENT

soil property	*range of typical V values*	*recommended V value if tests results are limited*
weight γ	0.01 – 0.10	0.0
compressibility m_v	0.20 – 0.70	0.40
undrained shear strength c_u	0.20 – 0.40	0.30
cohesion c	0.30 – 0.50	0.40
friction $\tan\varphi$	0.05 – 0.15	0.10

When applying the method of partial safety factors, one needs sufficient soil investigation in order to obtain the statistical values μ and σ_{sd} of each characteristic parameter. The interpretation of tests is important; one may choose an average, a global or a local value, related to the situation. The partial safety factor γ_i is based on statistical analysis, according to

$$\gamma_i = 1/(1 - \alpha_i \beta V_i) \quad \text{with} \quad \alpha_i = (\partial Z/\partial X_i)\,\sigma_{sdXi}/\sigma_{sdZ} \tag{8.4}$$

Here, α_i is a relative standard deviation. The factor α_i expresses a weighted contribution, i.e. the relative importance of the considered parameter to the overall reliability. For dominant loading aspects, $\alpha = 0.7$ is adopted and for dominant

strength, 0.8 is usually applied. The reliability coefficient β is related to current norms, i.e. accepted probability of failure. For example $\beta = 3$ is identical to a probability of $P_f = 10^{-3}$. The standard deviation σ_{sdZ} can be found by vectorial summation, for independent variables

$$\sigma_{sdZ}=\sqrt{\Sigma_i[\partial Z/\partial X_i)\sigma_{sdXi}]^2} \qquad (8.5)$$

Applying partial safety factors is referred to as a level I approach, i.e. quasi-probabilistic using characteristic values. More sophisticated methods are the semi-probabilistic approach (level II) using normal distributions and linearisation (mean value or design point approach), and the full-distribution approach (level III) using numerical integration (Monte Carlo approach). In standards and guidebooks more information can be found. Sophisticated methods are usually applied to define partial safety factors.

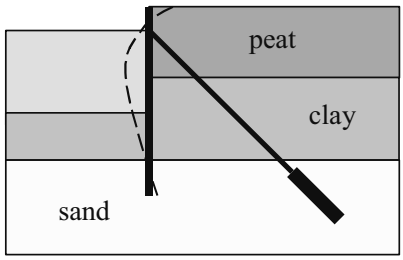

Level III (Monte Carlo)

- shear strength behind the wall is hardly mobilized
- using level I will give a conservative design

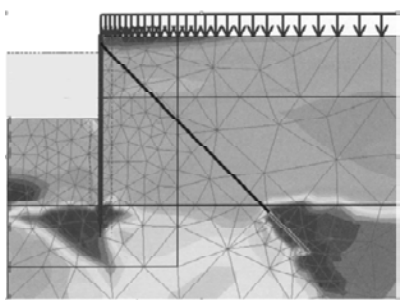

99 calculations
influence factor values

$\alpha_{E\ clay} = 0.878$	$\alpha_{E\ peat} = 0.114$
$\alpha_{\nu\ clay} = 0.320$	$\alpha_{\nu\ peat} = 0.107$
$\alpha_{\varphi\ sand} = 0.064$	$\alpha_{\gamma\ clay} = 0.037$
$\alpha_{\varphi\ clay} = 0.037$	$\alpha_{\gamma\ peat} = 0.174$
$\alpha_{\varphi\ peat} = 0.000$	$\alpha_{c\ clay} = 0.079$
	$\alpha_{c\ peat} = 0.002$

(a) mechanical system and relative shear stress *(b) influence factors*

Figure 8.7 System analysis for mechanical influence factors (Schweckendiek)

Special care is to be taken when applying the level I approach. The suggested partial safety factors may not be representative in characteristic failure modes, since locally the development of the mobilised shear strength may be limited. In that case, the straightforward application of level I approach will result in a conservative design. This effect can be covered in an adjusted α-factor in formula (8.4) after employing proper mechanical analysis, see Fig 8.7.

C EURO CODE 7 AND THE OBSERVATIONAL METHOD

Eurocode

The Eurocode started in 1980 as an initiative of the European Commission and were handed over in 1990 to CEN (Commission for European Standardization). From 2010 the Eurocodes are mandatory. The Eurocodes consist of a general document (Basis of Structural Design) and 9 specific codes. Eurocode 7 (EC7) is for geotechnical design (part 1) and ground investigation and testing (part 2). Specifications are defined in the National Annex. In EC7, three reliability classes (RC) or design approaches (DA) are recognised when using partial safety factors. Seismic effects are covered in EC8.

EC7 design requires a geotechnical structure be verified for the Ultimate Limit States (ULS) in the ground and the structure itself also for the Serviceability Limit States (SLS). ULS requirements comprise overall stability, adequate bearing resistance, adequate sliding resistance, adequate structural capacity, and no combined failure of ground and structure. SLS requirements include no excessive settlement (immediate and delayed), design against heave (immediate and delayed), and design for vibrating loads. The designer should use commonly accepted methods. EC7 subdivides ULS requirements into 5 broad categories and each category has a particular set of partial factor values associated, which should be applied in corresponding design calculations:

- EQU: loss of equilibrium of the structure or the ground, considered as a rigid body, in which the strengths of structural materials and the ground are insignificant in providing resistance;
- STR: internal failure or excessive deformation of the structure or structural elements (footings, piles, basement walls, etc) in which the structural material is significant in providing resistance;
- GEO: failure or excessive deformation of the ground, in which the strength of soil or rock is significant in providing resistance;
- UPL: loss of equilibrium of the structure or the ground due to uplift by water pressure (buoyancy) or other vertical actions;
- HYD: hydraulic heave, internal erosion and piping in the ground caused by hydraulic gradients.

The design approaches differ in combinations of partial safety factors related to actions S, to materials M, and to resistance R. DA1/1 is essentially a STR Limit State approach, DA1/2 essentially a GEO Limit State approach, DA2 an Action and Resistance Factor approach, and DA3 an Action and Material Factor approach.

ULS situations are verified by applying partial factors to the main variables of the calculation model, and by verifying that the fundamental inequality $S \leq R$ is fulfilled, where S denotes the design value of the action effects and R denotes the design value of the resistance. Due to the novelty of Limit State Design in most of the European countries and the wide variety of soil conditions, soil testing and design methods, EC7 allows for one of three different Design Approaches (DA1, DA2 or DA3) when assessing R and S for permanent and variable situations. Table 8.2 summarises the sets of values of the partial factors recommended by EC7. The selection of the mandatory design approach and of the values of the partial factors

are left to the National Annex. So, the outcome of applying EU7 may be different in different countries. Properly applying EC7 and the National Annex needs some guidance/experience.

TABLE 8.2 SUGGESTED PARTIAL FACTORS FOR GEOTECHNICAL ENGINEERING (EC7)

	*Unfavourable actions** S*		*Materials** M*		*Resistance R*
	Permanent γ_G	*Variable* γ_Q	γ_M		γ_R
			$\tan\varphi$, c	c_u	
SLOPES AND EMBANKMENTS					
DA1/1	1.35	1.50	1.00	1.00	1.00
DA1/2	1.00	1.30	1.25	1.40	1.00
DA2	1.35	1.50	1.00	1.00	1.10 – 1.40
DA3	STR: 1.35 GEO: 1.00	STR: 1.50 GEO: 1.30	1.25	1.40	1.00
SPREAD FOUNDATIONS					
DA1/1	1.35	1.50	1.00	1.00	1.00
DA1/2	1.00	1.30	1.25	1.40	1.00
DA2	1.35	1.50	1.00	1.00	1.40
DA3	STR: 1.35 GEO: 1.00	STR: 1.50 GEO: 1.30	1.25	1.40	1.00
RETAINING WALLS					
DA1/1	1.35	1.50	1.00	1.00	1.00
DA1/2	1.00	1.30	1.25	1.40	1.00
DA2	1.35	1.50	1.00	1.00	1.10 – 1.40
DA3	STR: 1.35 GEO: 1.00	STR: 1.50 GEO: 1.30	1.25	1.40	1.00
PILE FOUNDATIONS					
DA1/1	1.35	1.50			1.00 – 1.25
DA1/2	1.00	1.30			1.30 – 1.60
DA2	1.35	1.50			1.10 – 1.15
DA3	STR: 1.35 GEO: 1.00	STR: 1.50 GEO: 1.30	1.25	1.40	1.00 – 1.10

** Favourable actions: if permanent 1.00, if variable 0.00*

*** Partial factor on soil density: 1.00 ; Partial factor on permanent water pressures: 1.00*

Observational method (OM)

When realizing construction projects in or with ground, the Eurocode permits to use the so-called observational method. The method is in accordance with the precaution principle. The Eurocode states[37]

- The complexity of interaction between the ground and the retaining structure sometimes makes it difficult to design a retaining structure in detail before the actual execution begins.

[37] EC7, prEN 1997-1:2004(E), section 2.7 and 9.4

- When prediction of geotechnical behaviour is difficult, it can be appropriate to apply the approach known as the observational method, in which the design is reviewed during the construction.

The Observational Method (OM) in ground engineering is a continuous, managed, integrated, process of design, construction control, monitoring and review that enables previously defined modifications to be incorporated during or after construction as appropriate. All these aspects have to be demonstrably robust. The objective is to achieve greater overall economy without compromising safety (CIRIA). Hence, at the start, the basis is (after Powderham) a design with all possible uncertainty (risks) with sufficient margins (risk analysis) in accordance with actual building codes. The OM then allows adjusting the earlier estimated risks by using an adequate and suitable monitoring (observation) following a predetermined protocol. The purpose is minimising time and cost without danger, and the obtained benefit is distributed amongst partners according to a predefined agreement. For more information see Nicholson et all.

D RISK APPROACH AND VISUALISING THE UNSEEN

In many cases on-site soil investigation is limited and the real subsoil condition remain unseen, which can sometimes lead to risky situations. It is up to the geotechnical engineer to create proper awareness about such circumstances and to suggest and design adequate monitoring and alertness procedures. The expert was traditionally on the site in early times, but nowadays he is more likely to be remote from the site or not involved at all. We should be aware of risk exposure and juridical aspects and bring the expert back to site: the remote observational specialist.

Dealing with risks

Risks are categorised according to the certainty of their occurrence and related consequences (van Staveren). They represent a range with at one end completely uncertain risks and at the other end unambiguously well-defined risks. To risks with a well-defined probability, based on sound scientific proof, the concept of own responsibility or solidarity applies. In juridical terms, the principle of prevention prevails. Somewhere in the range, the uncertainty of the probability and consequence of a risk is so large that it is not possible to have sufficient control. To these risks the principle of precaution prevails. This implies that a proactive policy should be adopted, which is based on presumptions about possible consequential damage without sound scientific proof. Finally, unknown risks exist for which preparation is not possible.

Three aspects are distinguished in the application of the principle of precaution for human activities in the subsoil: scientific uncertainty, damage threshold and reversal of the burden of proof. From a scientific view, natural processes in the underground are uncertain because of complexity, variability, limited transparency and limited knowledge of long-term effects. Therefore, the type and gravity of related damage is unsure. Before mitigating measures can be or (in a juridical sense) must be taken, the potential damage threshold must be determined. Here, the concept of non-negligible damage with regard to the natural environment prevails,

or more precisely, irremediable damage. For the built environment, the criterion is often aesthetic damage, or worse, user damage and structural damage. Because of the lack of knowledge about long-term effects, the determination of an appropriate damage threshold is troublesome. In some cases, a lower boundary can be based on historic evidence, provided the natural system has not changed.

The principle of precaution is combined with the concept of reversal of the burden of proof. The provoker should demonstrate that his mitigation measures exclude or sufficiently reduce the uncertainties and related risks, within his capability and according to the state of art.

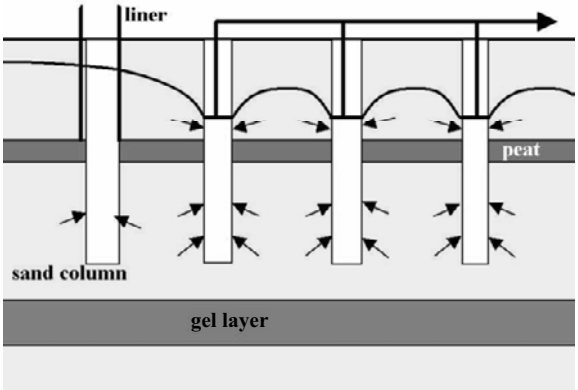

Figure 8.8 Drainage system, tram-tunnel construction, The Hague

Complex tunnelling by on-line monitoring

In the busy shopping centre of The Hague an underground tram station and car parking has been built. The construction consists of two diaphragm walls to a depth of 28 m in mainly sandy soils, a covering roof and internal floors, vertically anchored. Inflow of groundwater during construction was restricted by a jet grout arch (a strut for the diaphragm walls and support against uplift) in some places and a silicate gel layer formed by permeating grouting on other places. Unfortunately, scour from under the arch (sand boils) and local collapse caused a delay of the works. After two years – devoted to judicial disputes more that technical discussions – construction was resumed in 2000 using excess air pressure of 1.14 bar in an air-proof underground building pit, which imposed difficult labour conditions. A heavier floor, additional ballast and anchors were applied to guarantee stability against uplift. Soon it appeared that the dewatering system above the silicate gel layer did not work properly: serious well clogging was occurring. Heave and subsequent excessive deformation of the walls could jeopardize the entire project.

The contractor decided to ask for specialist advice from geotechnicians, geobiologists and geohydrologists. They discovered that due to the long delay gel material had caused a locally high *pH* (Luger). This dissolved organic matter locally that precipitated near the well filters, where the *pH* was lower. The unusual clogging problem was solved by applying smart instrumented sand columns and a temporary isolation system (PVC-liner) making full profit of a thin semi-pervious peat layer (Fig 8.8). About 100 piezometers were installed and the records every 10

min were directly processed and sent to a database, that facilitated direct access to all parties involved: client, contractor, consultant, local authority and insurance company. Easy visualization by coloured maps indicated normal, alert and critical levels, in the last case automatically sending emails and SMSs. This 'dynamic' warning system comprised permanent "virtual" specialist's eye on site and provided the proper conditions to complete the construction safely in 2004.

Lower uncertainty but safe margins shorten construction time[38]

The Betuwe route, a double track freight railway of 160 km connecting Rotterdam harbour with Germany, is completed at 4.5 billion euro in 2007. The embankment of this railway leads into the western part of the Netherlands through an area of extremely soft soils. In particular, consolidation time and residual settlements composed a serious risk to the progress of the project. The high risk profile of the Sliedrecht-Gorinchem section of the Betuwe line, characterised by peat soil, a high water table, a short construction time, various subsidence-sensitive objects in the direct proximity and inflexible links with existing infrastructure (Fig 8.9), formed the start of the formation of the 'Waardse Alliance', a special and new type of alliance between the contractor and the client. Together they took on the challenge to redesign and build this section within the tight time schedule and the appointed budget. Both parties agreed to share the costs of identified risks including unexpected soil conditions and possible damage to existing infrastructures.

Figure 8.9 The new Betuwe line runs close to existing infrastructure; by applying a monitoring concept to the largest risk factor: the subsidence, a new type of PPS contract could be established, leading to significant cost reduction and an excellent project result.

The alliance provided a unique opportunity to optimize the design, to maintain a constant watch on the unseen and to act swiftly to compensate for any unexpected situation. The risk on excessive settlement and instability was controlled by on-line

[38] In his Terzaghi Oration, Barends introduced the slogan: *from uncertain safety to safe uncertainty*, marking the awareness of dealing with large margins in soil mechanics.

monitoring, a well-structured data management system and various fall back scenarios, which allowed for smaller safety margins, a continuous adjustment of extrapolated predictions of the consolidation process and residual settlements, and – most important – a significant shorter construction period. The alliance started in 1999 and completed its task successfully on time, in November 2003, and it achieved a reduction of about 10% of the original project cost. The major part of the success of the project had its origin in a sound risk management strategy for covering the geotechnical aspects. The benefit was shared amongst all the parties involved.

E RISK MANAGEMENT PROCESS: GEOQ

"Transparency of the uncertainty in geotechnical works will facilitate proper risk assessment and risk sharing by use of appropriate forms of contracts, avoiding inflexibility, indecision and time overrun". This statement was one of the conclusions of the Terzaghi Oration 2005. This single sentence not only connects uncertainty to risk assessment, it also adds some essential non-technical aspects, such as risk sharing and contracts, which cannot be neglected for a successful construction project (Van Staveren). Cummings and Kenton reported in 2004 about several case studies of failures in geotechnical engineering, engineering geology and geophysics. Their conclusion is remarkable. It is important, they state, to recognize that almost all completed projects did not fail. Only the most egregious failures get wide public attention. Failures are usually not caused by natural events, such as earthquake, flood or landslide that immediately precede a failure. Failures are caused by human error that allows marginally stable or unstable conditions to exist through substandard investigation, dishonesty and deceit, approval of substandard reports by reviewing agencies, and political influence.

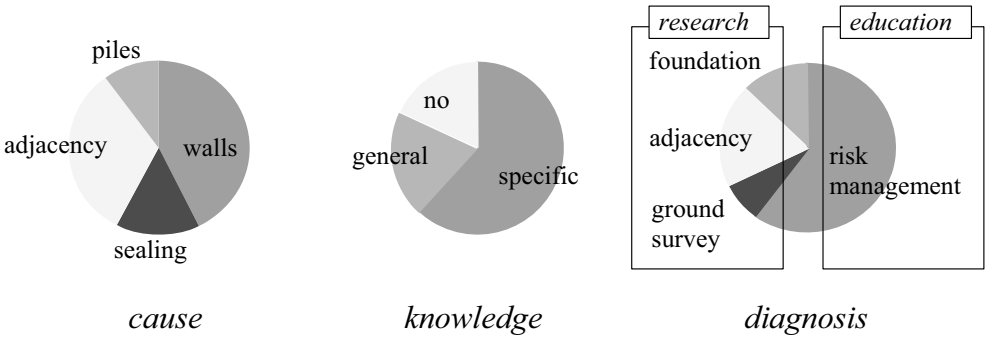

Figure 8.10 Building pit damage; insufficient ground survey (10%), insufficient adjacency survey (20%), missing knowledge (10%), available knowledge not properly applied (60%)

In 2008, Van Tol reviewed 40 cases of building pit damages and his conclusion is that in many cases the required knowledge was available but not applied (Fig 8.10). Proper risk management will make significant savings. In 2011, CUR Build and Infra published Report 232 on Construction Failure, emphasising that presence of proper skill at the construction site and risk awareness of the project

organisation are essential for reduction of failure costs, and that the investment to realise these conditions is not more than 10% of the average failure costs.

Any risk assessment can only be effective, when truly integrated in the entire design and construction process. Still, too often, risk assessment is a rather isolated and spur-of-the-moment exercise, performed by highly specialised professionals during the design phase, for instance. This situation limits the positive impact that risk assessment could have on the final project result, in terms of reliability, safety, and functionality, with acceptable costs and within a reasonable project planning.

Before introducing a flexible and proven risk management process approach, the terms risk and risk management require some attention. A generic definition of the term risk is the product of the likelihood of occurrence of an event and the consequences of that event. Normally these events are hazards, with the potential to have negative effects. Here, risk is considered by definition as potentially harmful (or profitable). Risk management can be simply defined as the overall application of policies, processes and practices dealing with risk. Fig 8.11 presents schematically an example of a structured risk management process approach, the GeoQ approach. It is based on three pillars: (1) a cyclic procedure during construction, (2) proper-in-time data availability in all construction phases, and (3) continuity and transparency of data (particularly the 'soft' data).

The transparant and flexible GeoQ risk management process aims to assure the overall quality of a project, by risk management of ground behaviour in relation to design, construction, operation and maintenance activities. In addition, the risk-driven GeoQ process reveals the need for timely and adequate site characterisation, appropriate design adjustments and effective monitoring. These activities are easily underestimated and often under severe attack by today's business pressures of lowest cost and shortest construction time. The GeoQ approach provides an adaptive framework for managing the risky ground during all phases of a construction project, from the early feasibility phase through to the maintenance phase. A tedious process, but it pays, because uncertainty in soil behaviour is a dominant factor in construction and maintenance.

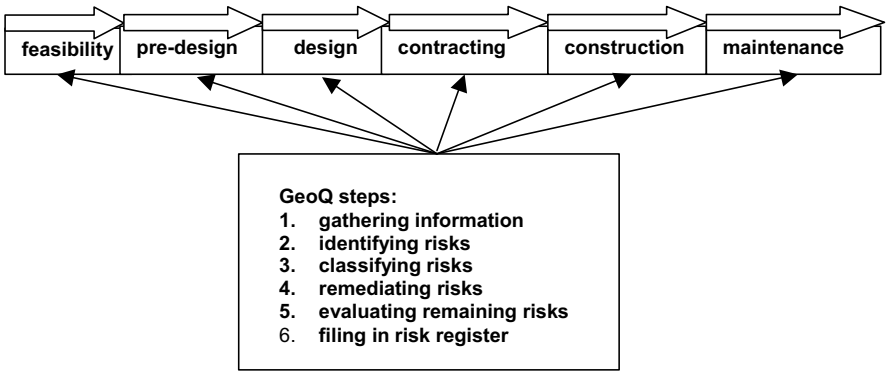

Figure 8.11 The GeoQ risk management process

The GeoQ process consists of six specific risk management steps, which ideally should repeat as a cyclic process in each phase of the project (Fig 8.11)

1. Gathering information;
2. Identifying risks;
3. Classifying risks;
4. Remediating risks;
5. Evaluating the remaining risks;
6. Filing all relevant risk information in a risk register.

The first step is about gathering all relevant project information. Sources are for instance geological maps, existing borings, and CPT results. The second step is about identifying risks (and opportunities). What risks can be expected, in the current and next project stages? During the third step all identified risks are classified. This can be done qualitatively, semi-quantitatively or quantitatively, depending on the required accuracy, in relation to the associated costs, in the particular project phase. Also the impact of the risk, in case of risk occurrence, needs to be judged, preferably in terms of costs, time, quality, safety and, to an increasing extent, even the reputation of the project to its stakeholders.

In the fourth risk management step the most suitable risk-remediating measures are selected and implemented. These risk-response strategies include taking the risk, addressing the risk, transferring the risk or eliminating (or exploiting) the risk. The fifth step involves the evaluation of the resulting risk profile, preferably with all relevant parties involved. In this stage, it should be verified whether the remaining risk profile, as a result of the risk control measures, is acceptable to the responsible and affected project participants. Finally, in the sixth GeoQ step all gathered and analysed risk management information is properly stored in a risk register. It should be ready for transfer and serve as a basis in the risk management process of the remaining project phases. This risk register should be part of the bidding documents in the contracting phase. The contractor can base the bid price on the risk register and use it as a basis for his own risk management during construction. In addition, the risk register may serve as a basis for the risk allocation or sharing in the contracting phase.

It is interesting and promising to realise that this and similar structured risk management approaches are proliferating into the global construction community. An example is The Joint Code of Practice for Risk Management of Tunnel Works in the UK, which is the result of an initiative of the Association of British Insurers (ABI), in order to reduce the probabilities of losses and the size of the claims. To further professionalize our dealing with uncertainty and reliability, it is our challenge to embrace the concepts of risk management, and to make it common use in day-to-day construction activities.

In 2010, a Risk Scan on five of the top 20 largest Dutch infrastructure projects has been elaborated (Bles), the subject of which is the GeoQ approach (previously mentioned), while focusing on four stages: (1) Geo Quick Scan - qualitative process test, (2) Geo Check - qualitative content and product test, (3) Geo Risk Analysis - quantitative content analysis, and (4) Implementation - Geo Risk Management as a routine work process. The risk manager (if present in the project), project leaders of the project and the contract manager have been interviewed with questions like: Is the GeoQ approach recognisable in the project? Have all six steps been fully elaborated in each project phase? Is everything done

in order to get good results from the risk management steps? Have all six steps been explicitly elaborated in each project phase?

The scan yielded six lessons, further elaborated in 19 recommendations, with a distinction to content related (C) and process related (P).

Lesson 1 - clear risk management positioning.
- Ground related risk management should be an integral part of project risk management, but with an explicit status (P);
- All specific ground related risks should be part of a project's risk register (P&C).

Lesson 2 - clear risk management responsibility.
- Appoint a coordinator responsible for ground related risk management (P);
- All ground related risk should be allocated contractually to one or more of the parties within a project (P);
- Ground related risks, completely allocated to the contractor, needs still evaluation by the client (C).

Lesson 3 - clear risk communication.
- Link explicitly the functional and technical level of project organisation to each other (C&P);
- The risk file of a client should be known by the contractor and vice versa (P);
- Tests are required on feasibility of requirements with a geotechnical scope (C).

Lesson 4 - a ground related risk register.
- Description of a risk needs to satisfy basic demands (C&P);
- All GeoQ steps should be explicitly executed step by step during each project phase (P);
- A ground related risk session should be organised in early project phases (P);
- Communication should be explicitly risk based between project and third parties (P);
- Explicit guarantee on completeness and correctness of ground related risks and analyses is necessary (P);
- Checklists are recommended as a check on the completeness of risk files (C).

Lesson 5 - risk driven site investigations.
- Site investigation should be explicitly risk based (C);
- In-situ soil and lab research should be flexible executed (C);
- Quality control of site investigations is necessary (C).

Lesson 6 - risk driven field monitoring.
- Monitoring should be used as a tool for guarantee of quality and control of risks (C);
- Ground related risks should have an explicit place in a monitoring plan (C).

These lessons seem to be generically applicable in construction projects. Ongoing application of these lessons in Dutch projects supports this conclusion.

F EXPERIENCE AND EXPERTISE: GEOBRAIN

In the current geotechnical engineering practice, the reliability is disappointing. The consequences for many works are serious, leading to cost and time overruns. The lack of reliability has caused loss of confidence in the profession and damaged the image of the construction sector. Systematic learning from case histories of completed projects is not well organised in the profession. Practicing engineers do

learn, from time to time, and they propose ad-hoc rules and equations based on experience and field observations, but no unified framework of dissemination is available to engineers. In recent years, the development of the tools of computational intelligence such as fuzzy logic and artificial neural networks make it possible for engineers to analyse experience, field and 'monitored' data of construction and truly apply 'observational' methods as recommended by codes of practice.

The concept GeoBrain, suggested by Deltares, is addressing systematic learning by developing an experience database from case histories and disseminating these experiences (Internet). This database, complemented with expert knowledge, can be used to make better predictions. It provides a toolbox for an integral approach of complex situations where the subsoil is an important risk factor, leading to a comprehensive view on the objective and reproducible consequences of choices. This development has a strong parallel with some other disciplines, like in medical science where with diagnostic systems empirical knowledge is being translated into generally applicable concepts. The present-day ICT makes this approach possible. GeoBrain forms the brain-side complementary to common physical and numerical facilities and it creates new relationships between the various knowledge sources by coupling numerical prediction models and physical tests in an objective system of data interpretations, predictions, practical experiences, expert views and test results (Fig 8.12a). It combines – so to say – hard and soft data.

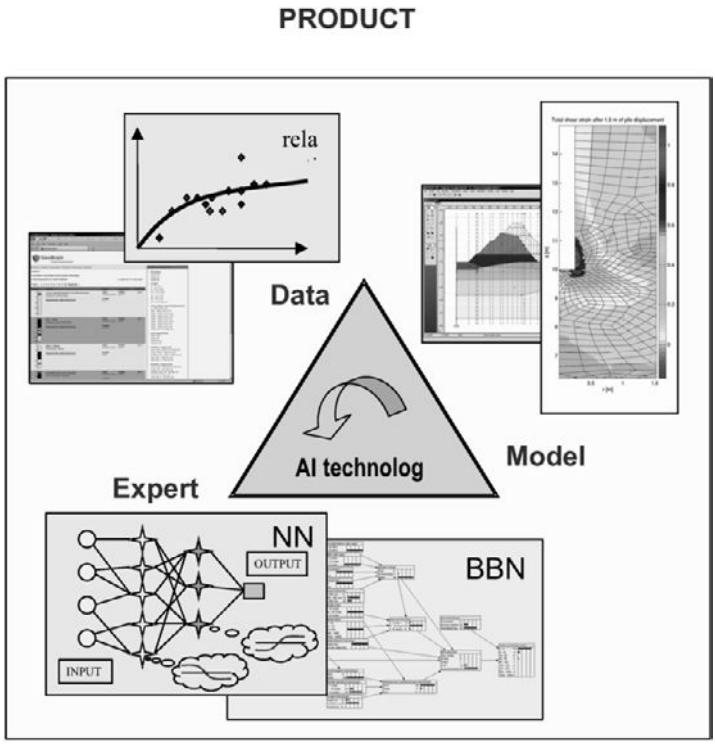

Figure 8.12a GeoBrain combines expertise, experience and efficiency

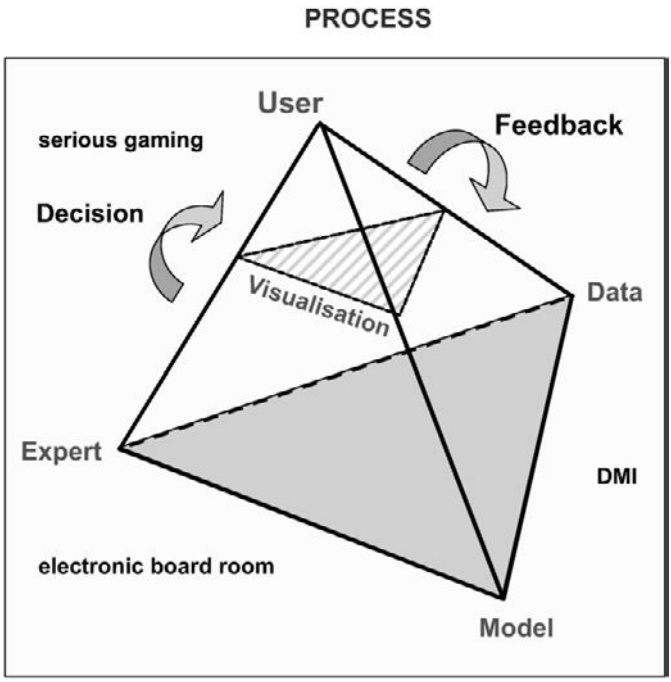

Figure 8.12b GeoBrain requires technical, process and ICT skills

GeoBrain provides opportunities for all parties to be involved at relevant stages, i.e. it creates a relation between designer and subcontractor or the geo-engineer by which decision-making and efficiency can be enhanced (Fig 8.12b). There are two kinds of output from a GeoBrain system: experiences (product) and predictions (process). Experience in its context can be objectivated using dedicated questionnaires, which have been composed together with (many) users, experts and providers. Consequences are analysed in a probabilistic fashion, i.e. an expert group defines scenarios and assigns events and their likelihood. The participating working groups for a GeoBrain implementation should consist of experienced people from contractors, consulting firms, clients, insurance companies, and scientists. Clients stimulate contractors and consultants to provide their data. Insurers provide insight in risks and the need for a shared approach. Scientists support elaboration and modelling. A proper preparation is required, since the questionnaire contains some hundreds of questions, which have to be evaluated in several scenarios. Quite a job! The Electronic Board Room and Internet are a perfect ambiance for this process. Moreover, achieving the willingness of participants to share their positive and negative experience and to create together a useful new approach requires proper preparation, convincement and special protection.

The result, objectivated expert knowledge validated by real case experiences, is properly quantified using Artificial Intelligence, e.g. Neural and Bayesian Belief Networks, see Fig 8.12a. The Internet is then an ideal medium to display experiences and results of a prediction (visualisation, serious gaming). Assigned

users can search on archetype or via a map on location. Afterwards queries can be refined. Predictions can be made on the same website.

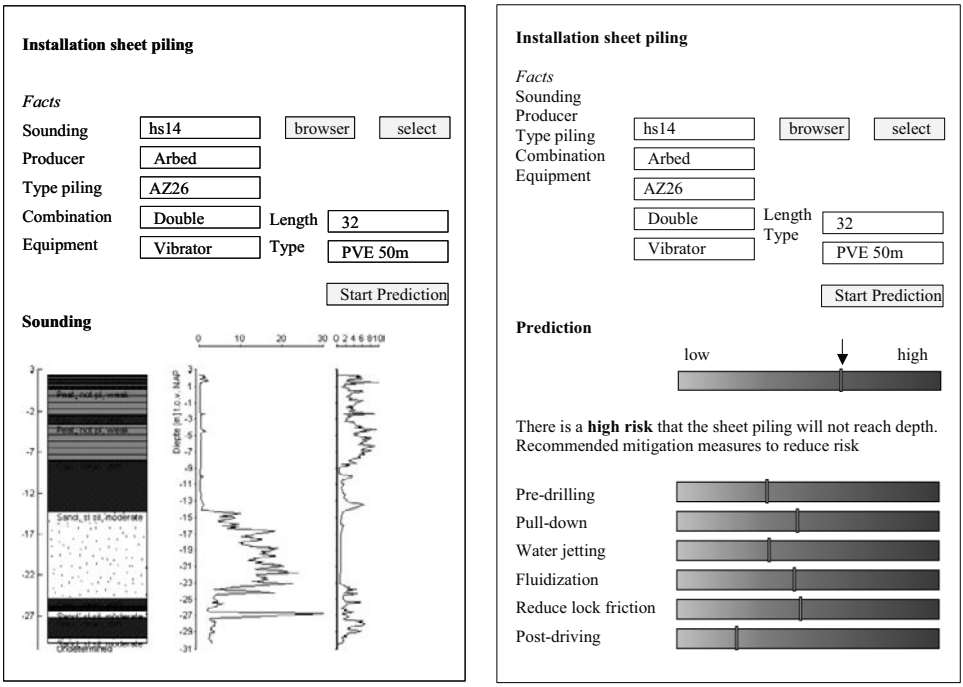

Figure 8.13 Result of a prediction using GeoBrain Foundations (installation sheet piling)

An example of the use is shown in Fig 8.13, for sheetpile installation in GeoBrain Foundations, created by Hemmen and Bles[39]. The input is a soil profile and CPT, and the choice of equipment and material. The system will then provide a prediction of the risk of malfunction, based on the probabilities in the experience database, shown by a bolt in a strip running from high to low risk. The system will also provide mitigation measures to improve the approach. Here, six potential measures are listed: predrilling, pull-down, water jetting, fluidization, reducing lock friction, or post-driving, each with their risk effect shown in a horizontal bar. This information is important for the user to estimate risk and cost, and make a final decision how to execute the work.

The use of Geobrain is restricted to members. GeoBrain Foundations proves that sharing experience is beneficial: unnecessary risks are avoided in a systematic manner.

---

[39] GeoBrain Foundations was supported by the Dutch Association for Contractors in Foundation Engineering (NVAF), ProRail, CROW, Allianz, Cunningham and Lindsey, AON and Clark Risk Management, the Ministry of Transport, Public Works and Water Management, Municipality of Rotterdam, BAM Civil Techniques, CFE, Ballast Nedam Foundation Techniques, Terracon Foundation Techniques, Voorbij, MUC and Deltares (leader).

application 8.1

Consider the situation of application 6.1. The mentioned properties in Table 6.2 have a statistical variation. Since the second (clay) and third (silty clay) layer show a significant contribution to the settlement, in particular the virginal loading part $(\sigma'_C/\sigma'_B)^{-b}$, only the effect of the variation in parameter b is considered in this example.

If the standard deviation σ_{sd} for the compressibility index C_c for the clay layer, determined by several soil tests, is 0.12 and for the silty clay (loam) layer 0.03, then the corresponding compressibility index b becomes, using (8.3), equal to 0.2413 for the clay and 0.0635 for the loam. The corresponding virginal strain increment in the clay layer becomes (top) $1 - (\sigma'_C/\sigma'_B)^{-b} = 1 - (116/66)^{-0.2413} = 0.127$ and (bottom) $1 - (\sigma'_C/\sigma'_B)^{-b} = 1 - (123/73)^{-0.2413} = 0.118$, which gives an average strain of 0.123 and a settlement of 0.123 m. The virginal strain increment in the silty clay layer becomes (top): $1 - (\sigma'_C/\sigma'_B)^{-b} = 1 - (123/73)^{-0.0535} = 0.0275$ and (bottom): $1 - (\sigma'_C/\sigma'_B)^{-b} = 1 - (163/113)^{-0.0635} = 0.0194$, which gives an average strain of 0.024 and a settlement (layer *5* m) of 0.120 m.

So, using the 95% confidence level, the contribution of the clay and loam layer to the total settlement becomes 0.243 m. If the mean values would have been used this value should be 0.185 m. In this respect the standard deviation of the settlement S, due to the considered effect is about (0.243 – 0.185)/1.64 = 0.035, or a variation coefficient V of 0.035/0.185 = 18.9%. The next step is to define and apply a proper partial safety factor. For a 95% confidence level such a partial safety factor would be: $\gamma = 1 + 1.64V = 1 + 1.64 \times 0.189 = 1.33$, and so a margin of 33%. In fact, one should include all variation aspects, which will make the variation probably in the order of 30 to 40%. Obviously, the outcome corresponds to a safety factor of 1.5 to 1.65.

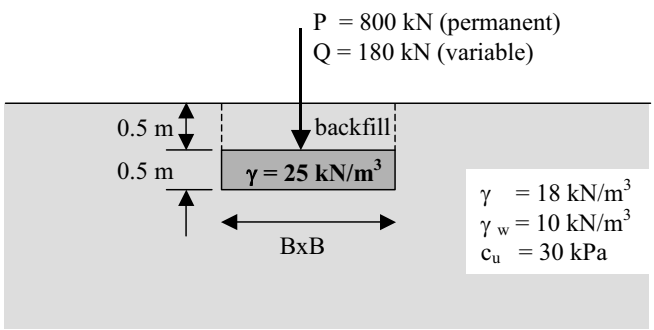

Figure 8.14 A footing design

application 8.2

The design of a square footing in undrained soil is determined using EC7 (Table 8.2). Values are shown in Fig 8.14, and partial safety factors are given in Table 8.2.

Design choice for the size of the footing B = 3.25 m. Other relevant formulas are, the weight of the foundation and backfill: $G = (3.25)^2 \times (0.5 \times 18 + 0.5 \times 25) = 227$ kN, the design value of vertical actions: $S_d = \gamma_G(P + G) + \gamma_Q Q$, the design value

of the resistance (see equations 12.3 and 12.10): $R_d = R/\gamma_R$ and $R = B^2((\pi + 2)\, c_{ud}\, s_c\, i_c + q_{0d}) = B^2\,(5.14\, c_{ud}\,(1.2)(1) + q_{0d})$, and $c_{ud} = cu/\,\gamma_M$ and $q_{0d} = q_0/\gamma_R$. Next, the safety condition $S_d < R_d$ is checked for the various design approaches.

DA1/1

$S_d = 1.35(1027) + 1.5(180) = 1656$ (kN)
$c_{ud} = 30 / 1.0 = 30$ kPa
$q_{0d} = (18 / 1.0)\,(0.5 + 0.5) = 18$ kPa
$R_d = R / 1.0 = (65.1(30) + 10.65(18) = 2145$ kN
The requirement $S_d < R_d$ is amply satisfied (over-design of 29.5%).

DA2/2

$S_d = 1.0(1027) + 1.3(180) = 1261$ kN
$c_{ud} = 30 / 1.4 = 21.4$ kPa
$q_{0d} = (18 / 1.4)\,(0.5 + 0.5) = 12.8$ kPa
$R_d = R / 1.0 = 65.1(21.4) + 10.65(12.8) = 1529$ kN
The requirement $S_d < R_d$ is amply satisfied (over-design of 21.3%).

DA2

$S_d = 1.35(1027) + 1.5(180) = 1656$ (kN)
$c_{ud} = 30 / 1.0 = 30$ kPa
$q_{0d} = (18 / 1.0)\,(0.5 + 0.5) = 18$ kPa
$R_d = R / 1.4 = (65.1(30) + 10.65(18)) / 1.4 = 1532$ kN
The requirement $S_d < R_d$ is not satisfied (under-design of 7.5%).

DA3

$S_d = 1.35(1027) + 1.5(180) = 1656$ (kN)
$c_{ud} = 30 / 1.4 = 21.4$ kPa
$q_{0d} = (18 / 1.0)\,(0.5 + 0.5) = 18$ kPa
$R_d = R / 1.0 = 65.1(21.4) + 10.65(18) = 1585$ kN
The requirement $S_d < R_d$ is not satisfied (under-design of 4.3%).

The design does not satisfy the DA2 and DA3. A wider footing will do. Which one?

9 OBSERVATION AND PREDICTION

In a world where demands for improving life and work environment are ever increasing, particularly for densely populated areas and weak soil conditions, construction in and on the underground is complex. Proper insight in the short and long-term behaviour of soils and their interaction with structural elements is inevitable for achieving reliable and sustainable works in an efficient manner. Not always straightforward design tools are sufficient and sophisticated methods are required. In the process of design and construction, two aspects are highlighted in this chapter: physical simulation and numerical simulation. For both, understanding of the concepts of adopted material behaviour (constitutive models) in a multi-dimensional fashion is essential.

A PHYSICAL SIMULATION

Besides field observation, either by monitoring a pilot test or at an unexpected failure case, the use of physical simulation is inevitable for improvement of our understanding of soil behaviour. It provides valuable information on failures (liquefaction, landslides, dams), deformations (roads, foundations, tunnels), soil-structure interface behaviour (piles, anchors), and transport (contaminants, heat). Physical simulation by means of tests and monitoring provides the means to check constitutive concepts, which form the fundaments of prediction models. In this respect physical simulation and numerical simulation are complementary. In fact, the objective of physical simulation is validation, while the objective of numerical simulation is prediction. A comprehensive evaluation of the application of physical testing methods is outlined in Chapter 3C.

A striking example of the need for physical simulation can be found from 'odd' behaviour of horizontal soil deformations due to a nearby excavation or landfill. Elastic numerical simulation will result in predicting the horizontal deformation quite well in magnitude but completely wrong in direction: the reality will show a deformation in the opposite direction! Here, the soil behaviour must be simulated with suitable calibrated constitutive models that include plasticity and/or viscosity.

Physical simulation requires special skills and experience in scaling laws (centrifuge), fabrication (sample preparation), sensors and transducers, and data elaboration (visualisation).

Scaling

Before a large, expensive object is constructed, experimentation on models (modelling) is used to determine the best properties for construction and for its functioning. One must know how to scale up the results of a model test to a full-scale prototype. Here, the concept of physical similarity is central. This concept is satisfied when values of dimensionless parameters that characterise the phenomenon of interest are equal in model and prototype.

When developing models, it is not possible to take into account all factors that influence the phenomenon of interest; some should be disregarded and those of

crucial importance should be retained. A model is in fact an idealisation of reality. With modelling, one looks for an appropriate idealisation.

Consider the consolidation process as the phenomenon of interest. The field equation is, according to (6.4)

$$c_v \partial^2 u/\partial z^2 = \partial u/\partial t \quad \text{with} \quad c_v = k/(\gamma_w \alpha) \ [\text{m}^2/\text{s}] \tag{9.1}$$

By introducing scaling in space, time and the field variables, this equation is rendered dimensionless, as follows

$$C\partial^2 F/\partial Z^2 = \partial F/\partial Y \quad \text{with} \quad F = u/u_0,\ Z = z/L,\ Y = t/T \quad \text{and} \quad C = c_v T/L^2 \tag{9.2}$$

Here, L, T and u_0 are arbitrary scaling factors, and C is a dimensionless consolidation number. Note that the field variable scale u_0 does not appear in C, because (9.1) is a linear in u. For a non-linear process the field variable scale will appear in the dimensionless number. The general solution of (9.2) in terms of consolidation degree U as function of Y, according to (6.6) with $L = h$, becomes

$$U = 1 - (8/\pi^2)\exp(-CY\pi^2/4) \tag{9.3}$$

Now, physical similarity for a model (m) and the prototype (p) is satisfied, when the number C is similar for both, i.e. $C_\text{m} = C_\text{p}$. If the same material is tested, i.e. c_v is identical, then obviously $T_\text{m}/T_\text{p} = (h_\text{p}/h_\text{m})^2$ must hold. The time in the prototype to reach the same consolidation degree as in the model will be $(h_m/h_p)^2$ faster. So, if 50% consolidation in an oedometer test of 2 cm high is reached in 0.5 day, then it takes 125 days for a layer of 5 metres in the field to reach 50% consolidation. In conclusion, it is sufficient to consider dimensionless numbers in order to achieve physical similarity.

Model tests are usually performed for situations where the solutions are not known. In most cases, the physical phenomena of interest can be described in terms of differential equations based on conservation principles (conservation of mass, momentum and/or energy) and constitutive laws. Making these dimensionless results in the physical numbers related to the different phenomena involved. Imposing similarity for all of these numbers, i.e. making them identical for model and prototype, provides the necessary scaling rules.

In centrifuge testing the gravity is significantly increased. As an example, the physical similarity for two phenomena, equilibrium and consolidation, can be elaborated. Consider the fundamental equations for both processes (for simplicity one spatial dimension is considered), as follows

$$\textit{equilibrium} \qquad \frac{\partial \sigma'}{\partial x} + \rho g = \frac{\partial u}{\partial x} \tag{9.4a}$$

$$\textit{consolidation} \qquad \frac{\partial^2 u}{\partial x^2} = \frac{\partial u}{c_v \partial t} \tag{9.4b}$$

Introducing scaling factors L for length, σ_0 for pressure, g_0 for gravity, and T for time provides

$$\frac{\partial \Sigma}{\partial X} + \left(\frac{\rho g_0 L}{\sigma_0}\right) G = \frac{\partial F}{\partial X} \qquad \text{and} \qquad \left(\frac{c_v T}{L^2}\right)\frac{\partial^2 F}{\partial X^2} = \frac{\partial F}{\partial Y} \tag{9.5}$$

$$\text{with} \qquad \Sigma = \frac{\sigma'}{\sigma_0},\ F = \frac{u}{\sigma_0},\ G = \frac{g}{g_0},\ X = \frac{x}{L},\ Y = \frac{t}{T}$$

Two dimensionless numbers occur: an acceleration number $\rho g_0 L/\sigma_0$ and a consolidation number $c_v T/L^2$. A convenient requirement is similarity of stress, $\sigma_{0m} = \sigma_{0p}$ and $u_m = u_p$. Similarity of mass, internal friction, cohesion, and compressibility by using the same materials provides identical deformation and failure states in model and prototype. The gravity is different: $g_{0m}/g_{0p} = N$, which may vary up to 100 and more, depending on the rotation speed of the centrifuge. Similarity of equilibrium is then satisfied by adopting $L_m/L_p = 1/N$. Physical similarity of consolidation involves beside length also time and the consolidation coefficient c_v. Since $c_v = k/\rho g\alpha = \kappa/\mu\alpha$ and one may adopt similarity of viscosity μ and compressibility α [40], and the fact that the intrinsic permeability κ is proportional to D^2 (D is the representative grain size), it shows that the consolidation number $c_v T/L^2$ satisfies similarity, if also the grain size is scaled according to $D_m/D_p = 1/N$. Then, time is equal in model and prototype. However, then the same material cannot be used in the model and in the prototype, and similarity of intrinsic parameters friction, cohesion, and compressibility may not hold. Usually the grain size is not scaled in centrifuge tests, and as a consequence permeability is N^2 larger and consolidation proceeds equally faster, which implies that transient boundary conditions must be faster by N^2 as well.

Implying scaling principles in modelling physical phenomena requires special expertise.

B CONSTITUTIVE MODELS

Soil is a complicated material that behaves non-linearly, anisotropic and time-dependently, when subjected to loading. It behaves differently for primary loading, unloading and reloading and it shows plastic and brittle failure behaviour. Since it is not practically possible to describe the true mechanical behaviour of saturated porous granular materials, approximate constitutive models are adopted at larger scale where soils are considered as continuous media. Though such models are commonly based on fundamental physics (continuum mechanics), the parameters involved are empirical in nature and should be verified by lab and field-testing, and in some cases monitored during construction and use. Observed phenomena, e.g. deformations, stresses, pressures and rates offer indirect information about these

[40] Note, that in reality $\alpha = \eta/\sigma'$ and therefore consolidation in (9.4) is a non-linear partial differential equation.

constitutive parameters. Thus the underlying adopted model is crucial, in this respect. The same holds for predictions of structural behaviour performed by numerical simulations, as the outcome in terms of deformations and stresses depend on model chosen, corresponding parameter values adopted and the robustness of the computational algorithm. In general five basic aspects of soil behaviour can be recognised:

- the influence of pore water and pore pressures (permeability, consolidation)
- the influences the soil stiffness (stress and strain level, stress path, anisotropy)
- irreversible deformation (plasticity, creep, preconsolidation)
- strength (loading rate, density, drained-undrained)
- compaction (contractancy, dilatancy)

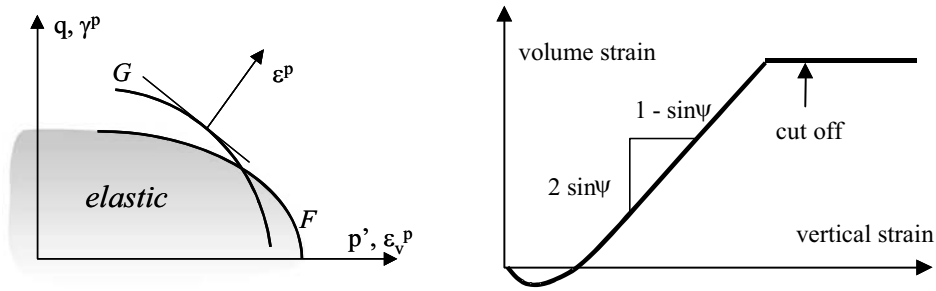

(a) flow rule F and plastic potential G *(b) dilatancy (triaxial test)*

Figure 9.1 Failure, plasticity and dilatancy concepts

Plasticity

It is assumed that plastic deformations can be represented by deformation rates $\partial\varepsilon_{ij}/\partial t$ and that these rates are zero in the elastic range and non-zero at the edge of the elastic range. A flow potential or yield surface, fully defined by effective stresses, describes the elastic range, e.g. $F(\sigma_{ij}') < 0$. At the edge of the elastic range $F = 0$. It is further assumed that the strain rates that develop at $F = 0$ are related to a plastic potential G fully defined by effective stresses, e.g. $\partial\varepsilon_{ij}/\partial t = \lambda\partial G/\partial\sigma_{ij}'$. If the flow potential F is identical to the plastic potential G the model behaves associated. If not, the behaviour is non-associated (Fig 9.1a). In soil mechanics, an associated flow rule is commonly used to model the behaviour of normally consolidated clay. A non-associated flow rule is frequently used to describe the behaviour of sands, particularly for dilation and contraction.

In geotechnical engineering many constitutive models have been suggested. Here, commonly accepted constitutive soil models are shortly outlined: for sand the Mohr-Coulomb model and for clay the Cam-Clay model. Some remarks are given for peat behaviour and a few other constitutive models are mentioned briefly.

Mohr-Coulomb model for sand

The Mohr-Coulomb model (see Chapter 7) is one of the most popular constitutive models for soil behaviour (failure). The model adopts the maximum and minimum stress in the plane of failure, such that the stress in the orthogonal direction falls somewhere in between both. It is a (linear-)elastic perfectly-plastic

model with five intrinsic parameters. The stress-strain behaves linearly in the elastic range, involving Young's modulus E and Poisson's ratio ν. Two parameters define the failure criterion (flow potential F): friction angle φ and cohesion c, by $F = |\tau| - c - \sigma' \tan\varphi$, and $G = |\tau| - c - \sigma' \tan\psi$ is the plastic potential. The dilation angle ψ applies to cover irreversible changes in volume due to shearing. In the case of associated behaviour $\varphi = \psi$ (Drucker's postulate), it is found for frictional materials that plastic deformations evolve with an increase of volume (dilatancy), which is not realistic. In the standard Mohr-Coulomb model the non-linear elasticity of soils is covered by an average linear elasticity E_{50}, representing the stress-strain rate after 50% of the failure stress. The dilation angle ψ, which describes the volume strain at failure, contributes substantially to the strength, particularly in sands. The actual friction angle and the dilation angle are interrelated, and $\varphi = \varphi_{cv} + 0.82\psi$ is used (Bolton). Here, φ_{cv} is the friction angle at constant shear-induced volume change (critical state, critical density), which is roughly equivalent to the angle of repose of a loose dry material (ranges from 30º to 37º), see Fig 3.4b. It depends on mineralogy, grading and shape, but not on the test type. A common value for sands is $\varphi_{cv} = 33^o$. In the perfectly-plastic approach the dilation angle ψ is usually kept constant. In reality, the value changes with the shear strain level, i.e. finally it tends to zero (Fig 9.1b).

The modified Mohr-Coulomb model adopts a non-linear shear modulus, according to

$$G = G_0(p'/p'_0)^{1-\beta} \tag{9.6}$$

Here, G_0 is a reference value at isotropic effective stress p'_0. The value of β is usually around 0.4. For the plastic strain dependency of the actual dilation angle ψ and the actual friction angle φ in the modified Mohr-Coulomb model, the following formulas are adopted

$$\sin\psi = \sin\psi_0 \exp(-\varepsilon_{pl}/\xi) \tag{9.7a}$$

$$\sin\varphi = (\sin\varphi_{cv}+\sin\psi)/(1+\sin\psi \sin\varphi_{cv}) \tag{9.7b}$$

Here, ψ_0 is the initial value, φ_{cv} the value at constant shear-induced volume change, ε_{pl} the equivalent plastic strain (changing during the numerical calculation) and ξ a parameter to be determined by long-duration triaxial testing (ξ is in the order of 0.07). Adopting a kinematic yield cap in the compression domain is another adjustment (see literature).

For coarse soils, Steenfelt emphasised the importance of taking the strength and dilation parameters not as an easy matter. He showed practical examples and suggested that Bolton's simplified expressions are appropriate.

$$\textit{plane: } \varphi_{pl} - \varphi_{cv} = 0.8\psi_{\max} = 5^o I_R \tag{9.8a}$$

$$\textit{triaxial: } \varphi_{tr} - \varphi_{cv} = 0.8\psi_{\max} = 3^o I_R \tag{9.8b}$$

with $I_R = D_r(Q - \ln p') - 1$. $\psi_{\max}$ is the dilation angle at failure, D_r the relative density, p' the mean normal effective stress at failure, Q a parameter accounting for mineralogy (quartz: 10, limestone: 8, anthracite: 7, chalk: 5.5), and $I_R = -d\varepsilon_v/(0.3d\varepsilon_1)$. For the projection of triaxial test results to plane symmetrical situations other empirical formulas are suggested, such as $\varphi_{pl} = \varphi_{tr}(1+0.163\ D_r)$.

Cam-Clay model for clay

Soil behaviour reveals irreversible strain and strain hardening, and plastic yielding is not synonymous with the maximum stress, as is assumed in the Mohr-Coulomb model. To cover these aspects, the soil mechanics group at Cambridge developed the Cam-Clay model (Schofield and Wroth). The Cam-Clay model is a linear-elastic plastic strain-hardening/softening model. It is based on Critical State theory, characterised by the critical state line (CSL), where soil elements can experience unlimited deformations without any changes in stress or volume. The model is able to describe deformation and failure especially for normally consolidated soft soils in applications involving loading conditions such as embankment or foundation. The adopted associated flow rule limits the simulation of undrained behaviour of sand and clay.

The state of a soil sample is characterised by three parameters: effective mean stress p', deviatoric shear stress q, and specific volume v (note: $v = 1 + e$). The change of state can be described by the isotropic compression line (loading) and swelling lines (unloading), both straight lines in the v-ln$p$ space, characterised by the compression index λ, the swelling index κ, respectively.[41] The critical state line corresponds to the failure stress and is parallel to isotropic compression line in the v-ln$p$ space. The critical-state parameter M is related to the internal friction angle φ.[42] Since the original Cam-Clay model led to too high K_0 values, the Modified Cam-Clay model adopts an ellipse for the yield cap.[43]

The cap supports a constant volume constraint at the critical state. The parameter Γ defines the critical state line at unit pressure. In Fig 9.2 two cases are worked out, one for hardening (the preconsolidation pressure increases during loading) and one for softening (the preconsolidation pressure decreases). These cases are also referred to as the wet and dry side, because the wet side (hardening), in the higher-pressure zone, causes the clay to compact resulting is wet clay (pore water expelled), while the dry side (softening), in the lower pressure zone (overconsolidated) the clay swells resulting in dry clay (water sucked in). The latter case is more difficult to model in numerical codes. Originally, cohesion is not included in the Cam-Clay model; new versions do.

---

[41] λ and κ show similarity to a amd b, mentioned in Chapter 6

[42] $M = 6\sin\varphi / (3 - \sin\phi)$ for triaxial tests

[43] The original Cam-Clay model has a logarithmic yield cap.

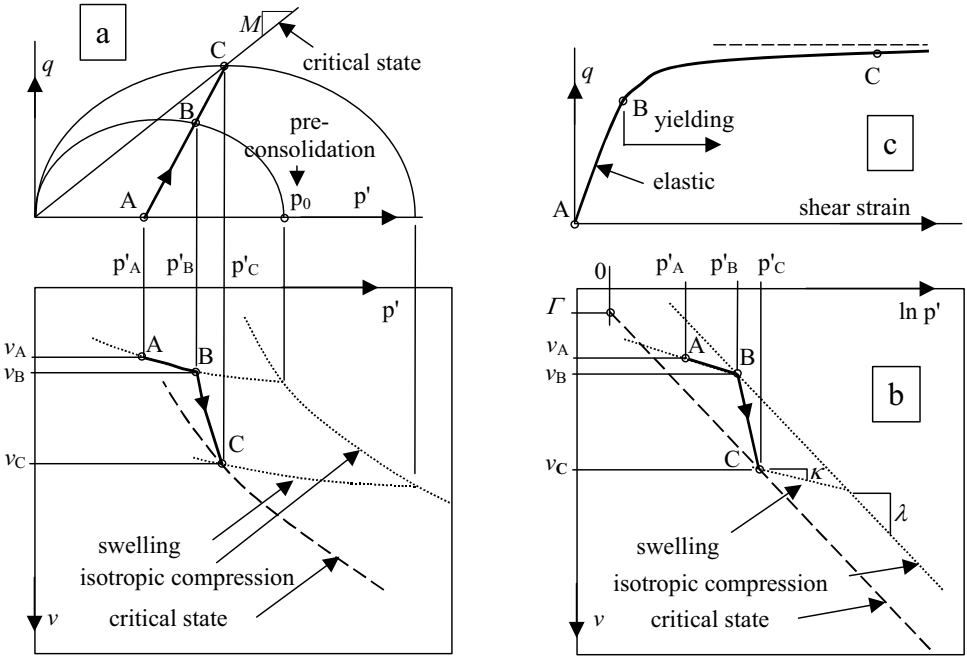

*Figure 9.2a Principle of the Modified Cam-Clay model; (a) the correspondence of the p-q space and the v-p space for a hardening stress path A-B-C, (b) the related v-*ln*p space, (c) hardening behaviour*

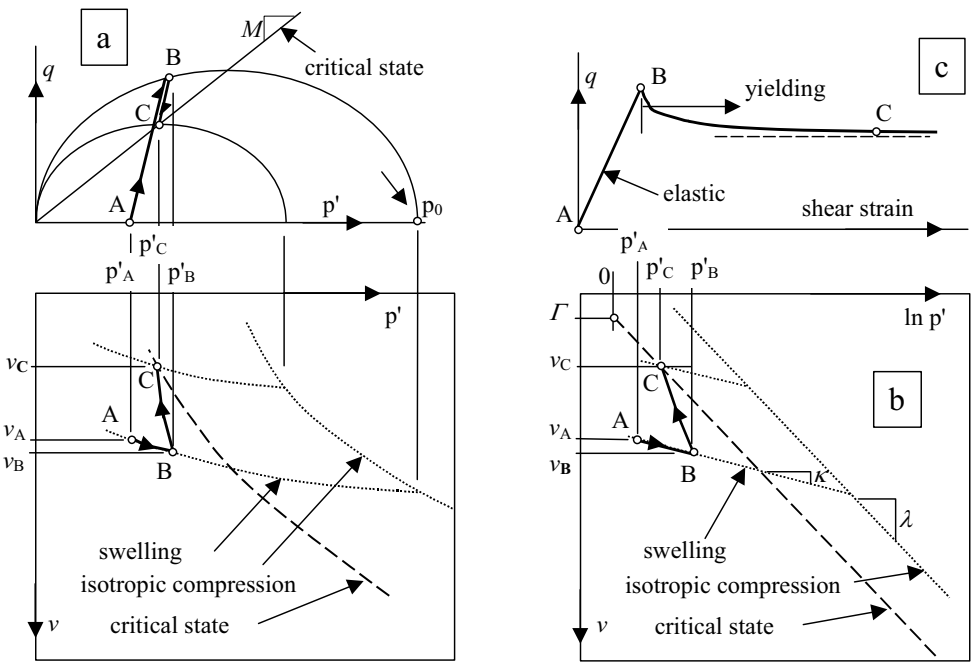

*Figure 9.2b Principle of the Modified Cam-Clay model; (a) the correspondence of the p-q space and the v-p space for a softening stress path A-B-C, (b) the related v-*ln*p space, (c) softening behaviour*

Fig 9.2a shows a hardening stress path A-B-C of the Modified Cam-Clay model. When loading starts (point A), the original yield surface is the smaller ellipse, characterised by the preconsolidation pressure p_0. The corresponding over-consolidation ratio is OCR = p_0/p'_A. At point B the material starts yielding and the corresponding yield surface grows, until the stress path reaches the critical state (failure), point C. Fig 9.2a.b shows the v-ln$p$ space, where characteristic lines becomes straight. Fig 9.2a.c shows the corresponding shear stress-strain hardening during yielding.

Fig 9.2b shows a softening stress path A-B-C of the Modified Cam-Clay model. When loading starts (point A), the original yield surface is the larger ellipse, characterised by the preconsolidation pressure p_0. The corresponding over-consolidation ratio is OCR = p_0/p'_A. The first part of the stress path A-B is elastic. At point B the material starts yielding and the corresponding yield surface diminishes, until the stress path reaches the critical state (failure), point C. Fig 9.2b.b shows the v-ln$p$ space, where characteristic lines becomes straight. Fig 9.2b.c shows the corresponding shear stress-strain softening during yielding.

Constitutive model for peat

Peat in particular behaves anisotropic related to the occurrence of fibres (organic remains) and depending on the rate of humification. Fibres are expected to mainly align horizontally, and therefore cause structural anisotropy. Since peat is a soft and very compressible, material loading may cause also induced anisotropy in stiffness. The compressibility of organic material, the main 'solid particles' in peat, is another aspect that differs from sand and clay where the solid particles are relatively incompressible. This will cause a decrease of the inter-particle stress and since equilibrium must hold, it may give rise to an additional pore pressure increase. It also affects the principle of effective stress, which becomes $\sigma = \sigma' + (1-\omega)u$, with ω the ratio between particle compressibility and bulk compressibility (Biot's coefficient). Furthermore, the large flexibility of peat may have a pronounced effect on pore pressure development during consolidation, because the permeability will change significantly with the pronounced compression. Therefore, in triaxial tests, horizontally retrieved samples may reveal differences compared to vertically retrieved samples (Zwanenburg). Conventional treatment in laboratory experiments of peat is therefore not sufficient. The constitutive behaviour of peat requires a different approach than provided in current constitutive models (Den Haan and Kruse).

Other constitutive models

A familiar elastic-plastic model is the hyperbolic model or the Duncan-Chang model, which adopts an incremental nonlinear stress-dependent concept, based on stress-strain curve in drained triaxial compression test of both cohesive and cohesion-less soil, approximated by a hyperbola (power law). The failure criterion is based on Mohr-Coulomb. The Duncan-Chang model is widely used as its soil parameters can be easily obtained directly from standard triaxial test. It is a simple enhancement of the Mohr-Coulomb model. It does not cover dilatancy, unloading behaviour and full plasticity.

For sand the Matsuoka-Nakai model is a modification between the Drucker-Prager criterion and the Mohr-Coulomb rule, and it is convenient for other stress paths than triaxial.

The Hardening Soil model (Vermeer c.s.) involves friction hardening to model the plastic shear strain in deviatoric loading and cap hardening to model the plastic volumetric strain in primary compression (see equations 9.7). Failure is defined according to Mohr-Coulomb. The model covers reduction of mean effective stress and mobilisation of shear strength. Soil dilation is covered and a power law formulation for stiffness is applied (Duncan-Chang model). This model can be used to accurately predict displacement and failure for general types of soils in various geotechnical applications. The model does not include anisotropy or creep.

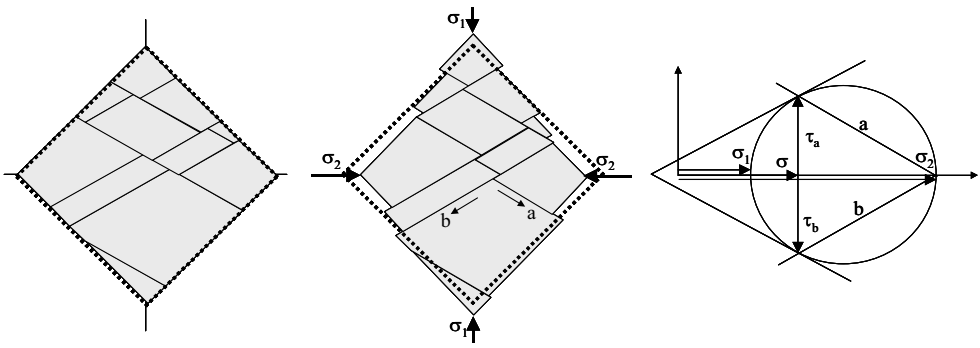

Figure 9.3 Concept of double sliding along Coulomb shear planes

The concept that the flow of granular materials is governed by shear on critical surfaces can be used to formulate an elastic-plastic model. When the elastic strains are neglected, i.e. for large strains, the model becomes identical to the rigid-plastic model of de Josselin de Jong, which he named the Double Sliding model. For the critical surfaces, he adopted the conjugate shear planes of the Mohr-Coulomb model. A typical deformation according to rigid-plastic double sliding is shown in Fig 9.3.

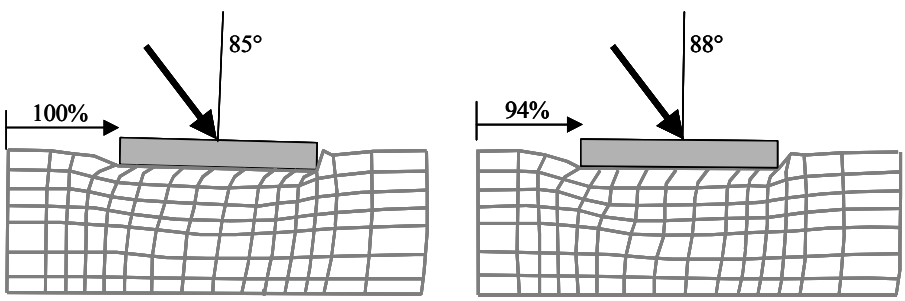

Figure 9.4 Difference of Mohr-Coulomb (left) and Double Sliding (right)

When compared to the non-associative Mohr-Coulomb model (Fig 9.4) it is shown that the rotations and displacements are somewhat different (Teunissen). The Double Shearing model predicts in general lower limit loads, because, for a

given state of stress, it allows for several possible directions of plastic flow rather than a unique direction, which coincides with one plastic potential in the Mohr-Coulomb approach. Here, a special remark is made about the use of model parameters. Since, as an example, the Mohr-Coulomb model is essentially different from the Double Sliding model, one may not use parameters obtained from laboratory tests by using Mohr-Coulomb for prediction with the Double Sliding model. This is inconsistent and may lead to erroneous results. Model parameters must be compatible with the constitutive model used for the calculation or prediction.

Hyper-elastic or Green model is suitable when the current state of stress depends on the current state of deformation and not on the history of strain. Hence, hyper-elastic materials can be characterised by a strain-energy function, assuming isotropic deformation (constant volume). Generally, it is suitable for materials that respond elastically when subjected to very large strains and under proportional loading conditions. This type of model fails to identify the inelastic and unloading behaviour.

Hypo-elastic models exhibit nonlinear, but reversible, stress strain behaviour. Similar to hyper-elasticity, the strain depends only on the stress, and not on the rate or history of loading. In this line, incremental stress-strain or piecewise linear-elastic laws are developed. Most of the plasticity models are in incremental forms similar to those of hypo-elastic models. The application of hypo-elastic models should be restricted to loading situations which do not basically differ from the experimental tests from which the material constants were determined or curve-fitted. Hypo-plastic models (Kolymbas, Gudehus) relieve the standard strain decomposition into additive elastic and plastic parts and do not use yield or potential surfaces and flow rules.

Time-dependent behaviour can be related to intrinsic viscous characteristics of soil, known as creep, relaxation, rate sensitivity and secondary compression. Viscous properties originate from the microscopic structure of soils like clay, which are composed of small clay particles with a highly active ion-water system in the micro-pores. Various visco-elastic models have been developed based on this microscopic nature (Mitchell, Sekiguchi). Macroscopic modelling of viscous behaviour follows the empirical approach, the visco-elastic approach or the visco-plastic and elasto-visco-plastic approach. Visco-elasticity consists of an elastic component and a viscous component where viscosity is a strain rate dependent on time. It has characteristics like hysteresis, stress relaxation and creep. The explicit introduction of time in an empirical approach when elaborating experimental tests violates the principle of objectivity in continuum mechanics and it is therefore limited to specific boundary and loading conditions. It is often used for one-dimensional behaviour (see Chapter 6). In the visco-elastic approach, the Maxwell model, the Voigt model and other similar arrangements are illustrative. In visco-plastic models, the key assumption is that viscous effects become pronounced when the material yields, and that the viscous effects are not essential in the elastic domain. Sekiguchi proposed an elasto-viscoplastic model for normally consolidated clay based on a non-stationary yield surface. Rate-dependent behaviour such as creep rupture is then described by a visco-plastic potential.

For cyclic loading and vibrations (earthquake) specific constitutive models have been developed, suitable to simulate pore pressure built-up, meta-stability and liquefaction.

C ASPECTS OF NUMERICAL SIMULATION

For the design of geotechnical structure, it is necessary to satisfy four basic requirements, i.e. equilibrium (stresses), compatibility (continuity of strains), material constitutive behaviour (stress-strain relation) and boundary/initial conditions (displacements and/or stresses). Since soil behaviour is rather complex, in most cases, approximations must be introduced and numerical simulations are adopted.

A simplified numerical approach used to model soil-structure interaction behaviour approximates the soil as a set of unconnected vertical and horizontal springs or represents structural supports (props or anchors) by springs. This is commonly known as the "beam-spring" approach. In the full numerical analysis approach, attempts are made to satisfy all theoretical requirements, include realistic soil constitutive models and boundary conditions. Approaches based on finite difference, boundary element and finite element methods are those most widely used and sometimes analytical element methods are applied. Their ability to accurately reflect field conditions depends on the suitability of the constitutive model to represent real soil behaviour and boundary conditions in all design stages. In this manner, the full numerical approach can contribute to efficient application of the observational method. The power of numerical analysis is that in simulations the entire geometry can be considered without trivial assumptions such as adopted in the slip circle analysis. For elasto-plastic soil behaviour, the code finds self a failure state and corresponding deformations in the surrounding. The abundant data output has to be visualised in suitable forms to provide comprehensive insight. Numerical analysis allows evaluating the typical non-linear soil behaviour. Full numerical analyses are however complex and specific experience is required for a proper use of advanced numerical codes.

Such experience is related to spatial and time discretisation, such as element shape, size, order and properties and dimensions (3D to 2D), and numerical aspects, such as non-linear iterative techniques and convergence criteria. For nonlinear constitutive soil models, a reasonable stress distribution within the element and a consistent initial state are essential. Higher order elements should be used (at least quadratic elements for elasto-plastic analysis). To improve accuracy, the discretisation should be fine at the edge of a footing or in a retaining wall and in regions where the stress and strain changes and porous flow changes are high. In transition zones and soil-structure interfaces, compatibility is properly maintained by adopting special elements with suitable interpolating functions.

The quality of calculation results depends on the stability and accuracy of the algorithms and on the constitutive model and corresponding parameter selection. Some of these parameters may have significant influence on the results. Depending on the type of soil and precision required, constitutive parameters can be determined from pressuremeter tests, dilatometer tests, CPT (lower reliability, especially for clays), SPT (lower reliability), in-situ elastic wave velocities (very

small strain) (undrained situations), oedometer test, triaxial tests (complete history of the degradation of soil stiffness with increase in strain level), simple shear test (lower reliability), and correlations with Atterberg limits (lower reliability). The initial conditions within the ground (K_0, OCR, water conditions, etc.) are important to consider when using non-linear constitutive models for the soil.

For further detailed information on the application of numerical methods reference is made to many textbooks (a.o. Potts and Zdravković), and in particular to the outcome of the EU-project GeoTechNet/design tools.[44]

Numerical and physical peculiarities

In the field of reservoir engineering numerical and physical aspects of the simulation of the mechanical interaction of pore fluids and the porous matrix is extensively studied. Basic concepts for space-time discretisation, solution techniques, numerical stability and accuracy of non-linear equations, equally valuable in geo-mechanical simulation, can be found in the work of Khalid Aziz et al. Some specific intriguing phenomena are outlined next.

Artificial dispersion

Numerical dispersion is an undesired non-physical effect inherently present in discrete time-space domain algorithms. It appears in the numerical treatment of hyperbolic or parabolic partial differential equations, e.g. for transport or dynamics in porous media. It aggravates, if processes are non-linear and at discontinuities (interfaces with a large contrast in a certain property). For time and space discretisation, Taylor series expansions are used, which have multiple terms. Generally, only the first derivative term in the expansion is used for differencing and the higher order derivative terms are neglected. Control of numerical dispersion can be accomplished by limiting the size of time steps and by increasing spatial discretisation. Also, there are numerical techniques to improve representation of the derivatives.

As an example, consider the heat transport equation (14.1)

$$D\frac{\partial^2 T}{\partial x^2} - v\frac{\partial T}{\partial x} = \frac{\partial T}{\partial t} \tag{9.9}$$

Here, $D = \alpha_L v$ is the dispersion coefficient and v the convective velocity. For the spatial derivative Taylor series is used with spatial distance d

$$\frac{\partial T}{\partial x} = \frac{T(x+d) - T(x)}{d} - \frac{d}{2}\frac{\partial^2 T}{\partial x^2} - O(d^2) \tag{9.10}$$

[44] In GeoTechNet, a EU-project during 2001-2005, 40 members of 17 countries participated in the development of a geotechnical database and in gaining insight in EC7, design tools, human and environmental impact and natural disasters in the geotechnical profession.

The first term at the right hand side is the standard finite difference approximation. The second term has the same form as the dispersive term in the fundamental equation (9.8), and therefore by using the standard approximation an error is introduced in the dispersion, D becomes

$$D = (\alpha_L + d/2)v \tag{9.11}$$

The origin of artificial dispersion is therefore introduced by truncation of approximations in the discretisation. In order to prevent the artificial effect becoming dominant over the physical process, the dicretisation should comply with $d/2 << \alpha_L$. This may lead to unpractical small spatial elements and various methods are suggested to circumvent it. Similar problems arise in dynamics, where the truncation of the damping term may pollute the mass term, causing errors in the celerity of waves.

Localisation, bifurcation and failure

Concentrated failure surfaces (localisation) can occur when the situation such allows. An example is the aspect ratio (length/width) of a triaxial sample, which is typically about twice longer than wide, otherwise the friction at the top and bottom will not allow a slip surface to develop. If a test would be performed on a shorter sample, the corresponding stress-strain curve will not exhibit softening. At certain strain the sample could be unstable, i.e. a small change in the support could yet allow a slip to suddenly develop. Such a case is referred to as bifurcation (Fig 9.5). This aspect plays a role in many geotechnical situations. Recognising the likelihood of localisation and understanding the effect of boundary constraints are important. Also numerically, softening and bifurcation are a real challenge.

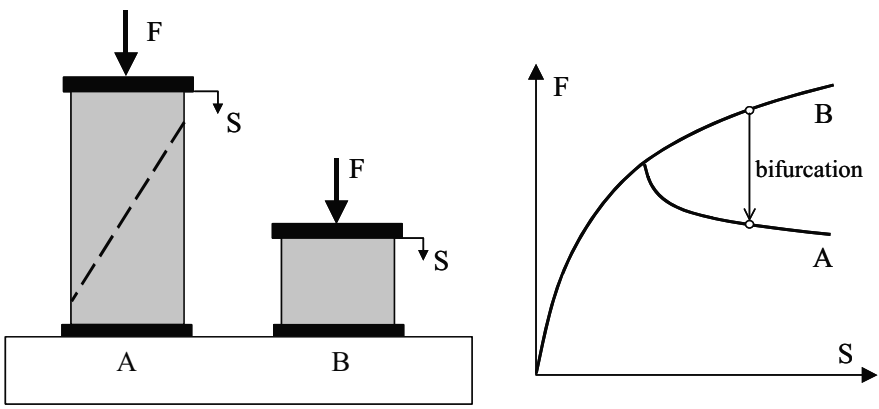

Figure 9.5 Principle of localisation and bifurcation

The previously mentioned constitutive models are developed for uniform stress and strains. The reason that these models show localisation and bifurcation is either due a plastic potential different from the yield function or to softening behaviour. The occurrence of shear bands, observed in sand, clays and peat, is essential in the description of failure in frictional materials. However, the predictability of the

formation of a shear band and its inclination is far from obvious, neither in numerical simulation nor in physical reality.

Teunissen showed an elegant and holistic way to understand this characteristic problem in geotechnical engineering. The maximum stress ratio (maximum strength) follows from the Mohr-Coulomb model (cohesion is disregarded for convenience)

$$\left(\frac{\sigma_v}{\sigma_h}\right)_{\max} = \frac{1+\sin\varphi}{1-\sin\varphi} \tag{9.12}$$

Here, the stresses σ_v and σ_h are principal stresses. Obviously, the maximum stress ratio (9.12) depends on the friction angle φ and not on the dilation angle ψ. Whether this expression gives the stress ratio for ongoing deformations (residual strength) depends on the formulation of the plastic deformations when the failure is reached.

In order to understand the ambiguity in localisation, a biaxial test where a shear plane has developed with angle α to the horizontal axis (see Fig 9.6a) will be analysed. The equilibrium conditions (in terms of forces) are expressed by

$$\sigma_h b \tan\alpha + T\cos\alpha - N\sin\alpha = 0 \tag{9.13a}$$

$$\sigma_v b - T\sin\alpha - N\cos\alpha = 0 \tag{9.13b}$$

If $R = T/N$ expresses the shear ratio, equations (9.13) results in[45]

$$\frac{\sigma_v}{\sigma_h} = \frac{\cos\alpha\sin\alpha + R\sin^2\alpha}{\cos\alpha\sin\alpha - R\cos^2\alpha} = \frac{\tan\alpha}{\tan(\alpha - \mathrm{atan}R)} \tag{9.14}$$

According to Coulomb, the lowest ratio of (9.14) is a measure for the strength of the material, referred to as critical strength, and it occurs at a specific value of α_{cr}, namely

$$R_{cr} = -\cot(2\alpha_{cr}) \quad \text{or} \quad \alpha_{cr} = 45° + ½\,\mathrm{atan}R_{cr} \tag{9.15a}$$

and it can be found that (9.14) for this value leads to the critical strength[45]

$$\left(\frac{\sigma_v}{\sigma_h}\right)_{cr} = \frac{\cos\alpha_{cr}\sin\alpha_{cr} + R_{cr}\sin^2\alpha_{cr}}{\cos\alpha_{cr}\sin\alpha_{cr} - R_{cr}\cos^2\alpha_{cr}} = \tan^2\alpha_{cr} \tag{9.15b}$$

If the same material is tested for large ongoing deformations, the ultimate shear stress ratio for a Mohr-Coulomb model can be expressed by the ratio R_{res}, according to (Davis), valid for non-associative behaviour

[45] Elaboration, see Application 9.5

$$R_{res} = \frac{\cos\psi \sin\varphi}{1 - \sin\psi \sin\varphi} \tag{9.16}$$

For given friction angle φ and given dilation angle ψ, the value of R_{res} is independent of α, and the corresponding residual strength ratio, according to equation (91.4), becomes

$$\left(\frac{\sigma_v}{\sigma_h}\right)_{res} = \frac{\cos\alpha \sin\alpha + R_{res} \sin^2\alpha}{\cos\alpha \sin\alpha - R_{res} \cos^2\alpha} \tag{9.17}$$

Note that for associative behaviour, i.e. $\varphi = \psi$, the traditional Coulomb solution is found from (9.16): $R_{cr} = \tan\varphi$, and (9.15) becomes $\alpha_{cr} = 45° + ½\varphi$, used in the familiar passive and active earth pressure coefficients, equation (7.5). Hence, for associative material behaviour, the residual, critical and maximum strength are identical. An example is worked out for $\varphi = \psi = 34°$ in Fig 9.6b. The maximum, critical and residual strength all match at $\alpha = 62°$.

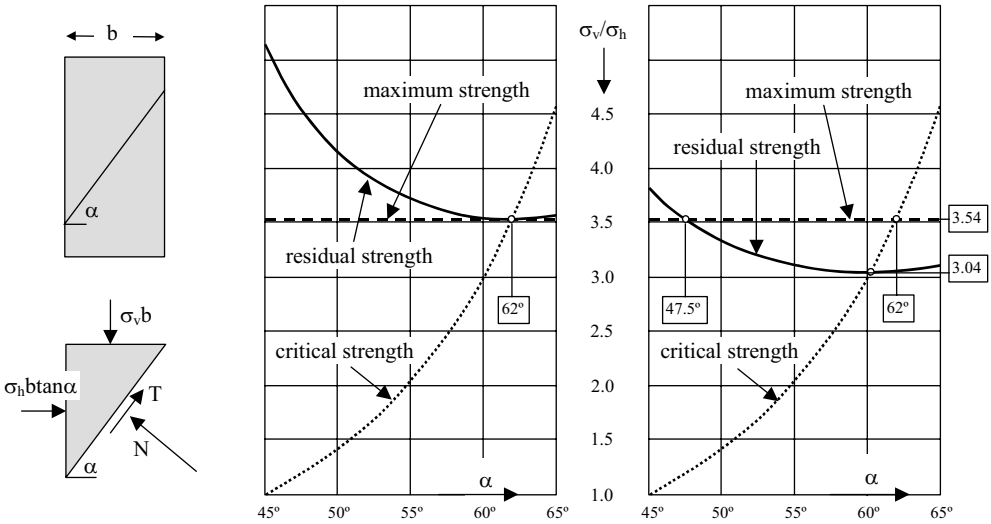

(a) test *(b) $\varphi = \psi = 34°$* *(c) $\varphi = 34°$ and $\psi = 5°$*

Figure 9.6 Biaxial test (Teunissen)

The case for $\varphi = 34°$ and $\psi = 5°$ is shown in Fig 9.6c. Here, a residual strength lower than the maximum strength and higher than the critical strength is found for shear plane orientations in a range of $47.5° < \alpha < 60.0°$, and correspondingly the residual strength is within a range of 3.04 to 3.54.

Coulomb's associative behaviour ($\varphi = \psi$) provokes unrealistic volume change. On the other hand a non-associative behaviour ($\varphi \neq \psi$) following Davis, generates unrealistic work when the stress state moves along the failure surface. This paradox, a consequence of incompleteness of Coulomb's and Davis' models, causes indeterminateness. Nature will decide. According to Teunissen, any possible

shear plane, following (9.17), under the maximum strength and above the critical strength may occur. There is no preference for any specific orientation in the corresponding range. The fact that in numerical simulations a certain shear band is found, is purely a result of calculation coincidence (numerical localisation). For a dilatation angle ψ between 0 and φ, the range of R_{cr} appears to be: $\sin\varphi < R_{cr} < \tan\varphi$. Hence, a conservative approach would be to adopt a safe friction angle $\varphi_{safe} = \mathrm{atan}(\sin\varphi)$. For $\varphi = 34°$ it yields $\varphi_{safe} = 29.2°$.

Localisation depends on the geometry and the deformation conditions. In practice, a physical trigger (e.g. a local weakness) may cause a sudden collapse (bifurcation). Hence, even with certainty about the essential parameters, the residual strength is usually uncertain. Non-associative constitutive models should be handled with care. There is need for a new comprehensive constitutive model that better incorporates stress rotations and induced anisotropy, which arise with localisation in dilatant materials.

Numerical singularities

The calculation result of a numerical model may be very accurate but not realistic. This is the case at singularity points, i.e. at locations where the discretisation does not cover the reality properly. As an example, a point well in a standard porous flow field is considered (after Kono). The real solution of the induced potential head ϕ for a well with a constant Q discharge is logarithmic. Hence the potential head ϕ between the well head ϕ_w and the head at a small distance d from the well and the corresponding discharge become

$$\phi - \phi_d = -(\phi_d - \phi_w)\frac{\ln(\frac{r}{d})}{\ln(\frac{r_w}{d})} \tag{9.18}$$

with $$Q_{real} = -2\pi\, kHr\frac{\partial\phi}{\partial r} = 2\pi\, kH\frac{(\phi_d - \phi_w)}{\ln(r_w / d)} \tag{9.19}$$

Here, kH is the transmissivity (permeability times layer height), r is the radial coordinate and r_w the actual well diameter. If in a numerical finite difference approach a linear head distribution is used, it will lead to a value ϕ_N in the well point of the square grid (grid size d) and the corresponding discharge becomes (4 neighbouring grid points contribute equally)

$$Q_{FD} = 4kH(\phi_d - \phi_N) \tag{9.20}$$

In order to achieve the same discharge, i.e. $Q_{real} = Q_{FD}$, the following must hold

$$\phi_l - \phi_w = (\phi_d - \phi_N)(-\frac{2}{\pi}\ln\frac{r_w}{d}) \tag{9.21}$$

The case that now the finite difference value ϕ_N is equal to the wellhead ϕ_w, is only correct when the well radius is $r_w = d\exp(-\pi/2) = 0.208d$ and this is not necessarily the case for an arbitrary grid size d. The best grid size near the well is $d = 4.81r_w$. If d is much larger, which is usually the case in FD-modelling, the resulting ϕ_N will be significantly larger than the real wellhead ϕ_w. A separate correction step has to be added to the numerical result.

$$\phi_w = \phi_N + \frac{2}{\pi}(\phi_d - \phi_N)\ln\frac{r_w}{d}) \tag{9.22}$$

Although the numerical finite difference calculation is accurate, the choice of a linear polynomial causes the result in singular points to be inaccurate. Similar behaviour is to be expected in the numerical analysis of mechanical problems at places of high discontinuity.

Biot effect

The storage term of a unit bulk volume can be formulated, as follows (Verruijt)

$$S = (n\beta_f + \beta_{sf}(\omega - n))du + \omega d\varepsilon \tag{9.23}$$

with β_f the fluid compressibility, β_{sf} the fluid induced grain compressibility, $\omega = 1-(1-n)\beta_{ss}/\beta$ is the Biot coefficient, β_{ss} the grain-to-grain contact compressibility, and β the soil bulk compressibility. Disregarding the term with β_{sf} and adopting Geertsma's suggestion $\omega = 1-(\beta_{sf}/\beta)$, leads to the commonly applied formula for S, which however is only consistent if $\beta_{sf} = (1-n)\beta_{ss}$.

For uniform grain compression, the micro-elastic behaviour can be expressed by $\beta_{sf}\sigma = w/R$, with σ the local average fluid stress, w the displacement, and R the grain radius. The local micro-elastic behaviour at the grain-to-grain contacts is expressed by $\beta_{ss}\sigma = w/R$, with r the grain contact area radius. For the relative grain contact r/R holds $0 < r/R < 1$. β_{ss} is related to the grain contact area. This problem is known as Herz' problem. Because of geometric constraints β_{ss} is non-linear. Elaboration[46] of Herz' solution yields $(\beta_{sf}\sigma)^2 = 0.055w/R$ and $r/R = 4.28\beta_{sf}\sigma$. Furthermore, $\beta_{ss} = \beta_{sf}$ for $r/R = 0.12$, which implies that e.g. for $n = 0.25$ and 16% relative grain contact Geertsma's suggestion holds.

A constant overburden and an effective stress concept (4.1a), according to $\sigma' = \sigma-(1-\beta_{sf}/\beta)u$, yields the following vertical strain variation (one-dimensional)

$$d\varepsilon_z = -\beta_v d\sigma' = \beta_v((1-\beta_{sf}/\beta)du - d\sigma) = \beta_v(1-\beta_{sf}/\beta)du \tag{9.24}$$

---

[46] Timosheko & Goodier (1970) Theory of Elasticity: $E = \beta_{sf}^{-1}$; $P = \pi r^2\sigma$; $3\sigma/2 = 0.388\,(PE^2/R^2)^{1/3}$; $w = 1.23\,(P^2/E^2R)^{1/3}$; $r = 1.11\,(PR/E)^{1/3}$; $\sigma/E = 0.211(w/R)(ER^2/P)^{1/3}$; $P = \pi r^2\sigma = \pi\sigma(1.11(PR/E)^{1/3})^2$; $P^{1/3} = 3.86\,\sigma(R/E)^{2/3}$;
$\sigma/E = 0.211(w/R)(ER^2/P)^{1/3} = 0.211(w/R)(ER^2/(3.86\sigma(R/E)^{2/3}))^{1/3}$; $(\sigma/E)^2 = 0.055w/R$. For $d(\sigma/E)/d(w/R) = 1$, $\beta_{ss} = \beta_{sf}$ at $\sigma/E = 0.027$; $r = \sqrt{(P/\pi\sigma)}$; $r/R = 4.28\sigma/E = 0.12$

This renders (9.23) in a vertical storage factor

$$S_v = (n\beta_f + \beta_{sf}(\omega - n) + \omega\beta_v(1-\beta_{sf}/\beta))du \qquad (9.25)$$

For a particular case, involving deep sand and silt/clay layers the Poisson ratio is estimated to $\nu = 0.30$ and the β_v becomes $\beta_v = (1+\nu)/(3(1-\nu))\beta = 0.62\beta$. Field data show $\beta_v = 3\text{x}10^{-4}$ MPa^{-1}. Thus $\beta = 4.8\text{x}10^{-4}$ MPa^{-1}. The fluid-matrix compressibility (sand/silt) is estimated to $\beta_{sf} = 0.16\text{x}10^{-4}$ MPa^{-1}. The following values are obtained for sand layers with $n = 0.25$ and 1% relative grain contact: $\omega = 1-(1-n)\beta_{ss}/\beta = 0.75$ and $S_v = (n\beta_f + 0.75\beta_v)du$. For sand layers with $n = 0.20$ and 5% relative grain contact: $\omega = 1-(1-n)\beta_{ss}/\beta = 0.87$ and $S_v = (n\beta_f + 0.88\beta_v)du$. For silt/clay with $n = 0.05$ and large relative grain contact one finds $\omega = 1-(1-n)\beta_{ss}/\beta = 0.97$ and $S_v = (n\beta_f + 0.99\beta_v)du$.

In conclusion, the Biot coefficient ω varies from 0.75 to 0.85 and higher for sand. For deep clay/silt layers it is practically 1. The previous analysis is based on elasticity. If plasticity (crushing) is involved the Biot coefficient can be lower.

D A VISCO-PLASTIC ANALYTIC ELEMENT METHOD

Many geotechnical numerical models are able to predict mechanical behaviour until the point of collapse. What happens after the moment of failure cannot be determined, except for trivial cases where a simple kinematics system is adopted. This is of particular importance for a proper evaluation of possible consequences of failure. At present, effort is devoted to improve this shortcoming. It requires an approach that includes geometric non-linearity, convective terms and rate effects. The material point method is such an approach.

Finite Element analysis approaches a failure state from the lower bound and it may underestimate the ultimate limit state sometimes by 10% or more (depending on mesh size and numerical accuracy criterion). Visco-plastic analysis approaches a vulnerable situation from the upper bound and it may overestimate sometimes by 10% or more.

Visco-plastic deformation occurs when soil is incapable of supporting deviatoric stresses. The total strains may become so large that it is acceptable to disregard elastic strains and consider only viscous strains, treating the material as a viscous fluid. Though there are numerical methods to solve complicated cases, here, the focus is on using simple analytical elementary solutions, such as the visco-plastic wedge and the Rankine wedge, as will be shown. A complex visco-plastic deformation can be composed of a consistent set of elementary solutions. Next, it will be applied to validate the effect of dike doweling, compensating for the likelihood of uplift failure.

Basic concept

During visco-plastic flow any element in a body is continuously changing in shape (in extension and distortion), translation and rotation. The time variation defines the rate of change. Plastic strain rate $\varepsilon_{ij,t}$ is defined as a tensor, the components of which are related to the derivatives of deformation velocities $u_{i,jt}$ as follows (see also Fig 7.2)

$$\varepsilon_{xx,t} = u_{x,xt}\ ;\ \varepsilon_{xy,t} = u_{x,yt}\ ;\ \varepsilon_{yx,t} = u_{y,xt}\ ;\ \varepsilon_{yy,t} = u_{y,yt} \tag{9.26}$$

Volumetric strain rate is described by $\varepsilon_{,t} = \varepsilon_{xx,t} + \varepsilon_{yy,t}$, distortion strain rate by $\gamma_{,t} = u_{x,yt} + u_{y,xt}$ and the (free body) rotation rate by $\omega_{,t} = ½(u_{x,yt} - u_{y,xt})$. For rigid plastic flow the condition of constant volume is adopted, $\varepsilon_{xx}+\varepsilon_{yy} = 0$, at any time. The deviator strain rate $D_{\varepsilon,t}$ is defined by

$$2D_{\varepsilon,t} = \sqrt{[(\varepsilon_{xx,t}-\varepsilon_{yy,t})^2 + \gamma_{,t}^2]} > 0 \tag{9.27}$$

Together with the angle β of the principal direction, the strain rate components can be expressed in terms of D, β and ω according to

$$\varepsilon_{xx,t} = -D_{\varepsilon,t}\cos(2\beta) \quad \text{and} \quad \varepsilon_{yy,t} = D_{\varepsilon,t}\cos(2\beta)\ ; \tag{9.28a}$$

$$\varepsilon_{xy,t} = D_{\varepsilon,t}\sin(2\beta)-\omega \quad \text{and} \quad \varepsilon_{yx,t} = D_{\varepsilon,t}\sin(2\beta)+\omega \tag{9.28b}$$

For a material with a von Mises yield criterion, with maximum deviator k, where k is a constant cohesion (no material friction), the related stress state is expressed in terms of the principal direction ψ, k and the isotropic stress p, according to

$$\sigma_{xx} = -p - k\cos(2\beta) \quad \text{and} \quad \sigma_{yy} = -p + k\cos(\beta) \tag{9.29a}$$

$$\sigma_{xy} = k\sin(2\beta) \quad \text{and} \quad \sigma_{yx} = k\sin(2\beta) \tag{9.29b}$$

The work rate by the plastic flow is defined by "force times corresponding distance covered in a time step". And so, for all components in all elements of volume V, the work rate is $W_{,t} = \iint \sigma_{ij}\ \varepsilon_{ij,t}\ dV$. Elaboration yields

$$\begin{aligned} W_{,t} &= \iint(-p - k\,cos(2\beta))(-D_{\varepsilon,t}\cos(2\beta)) + (-p + k\cos(2\beta))(D_{\varepsilon,t}\cos(2\beta)) + \\ &\quad + (k\sin(2\beta))(D_{\varepsilon,t}\sin(2\beta)-\omega) + (k\sin(2\beta))(D_{\varepsilon,t}\sin(2\beta)+\omega)\ dV \\ &= k\iint D_{\varepsilon,t}\,(2\cos^2(2\beta) + 2\sin^2(2\beta))\ dV \\ &= 2k\iint D_{\varepsilon,t}\ dV = k\iint\sqrt{[(\varepsilon_{xx,t}-\varepsilon_{yy,t})^2 + \gamma_{,t}^2]}\ dV \end{aligned} \tag{9.30}$$

At the border (interface A) of the plastic domain, where the adjacent boundary is rigid and the yield stress k and a jump velocity $\Delta u_{,t}$ act, the local work rate is

$$\Delta W_{,t} = k\int|\Delta u_{,t}|\ dA \tag{9.31}$$

The total internal plastic work rate is therefore expressed by $W_{,t} + \Delta W_{,t}$. This will be used in determining visco-plastic elements. Notice, that there is no effect of isotropic stress p and since $\sigma_{xy} = \sigma_{yx}$ also no effect of body rotation ω.

Plastic wedge

An important element of a steady visco-plastic motion with an analytical solution is the plastic wedge as shown in Fig 9.7. During a small rotation $\theta_{,t}\,dt$ the wedge OAB is assumed to undergo a full plastic deformation and it moves into shape OA'B', while the outside remains rigid. Along the interface OB" a slip takes place, proportional to s, in fact B"B'= $\alpha h/\cos\theta$, and P"P'= αs. The factor α is determined by considering volume constrained plastic deformation: area OAB equals area OA'B'. For convenience, the angle θ is restricted: $0 < \theta < \pi/2$, without loss of practicality. Compatibility along the interface requires (see Fig 9.7)

$$as = s\theta_{,t}\cos\theta - \alpha s\sin\theta \quad \text{and} \quad bs = s\theta_{,t}\sin\theta + \alpha s\cos\theta \tag{9.32}$$

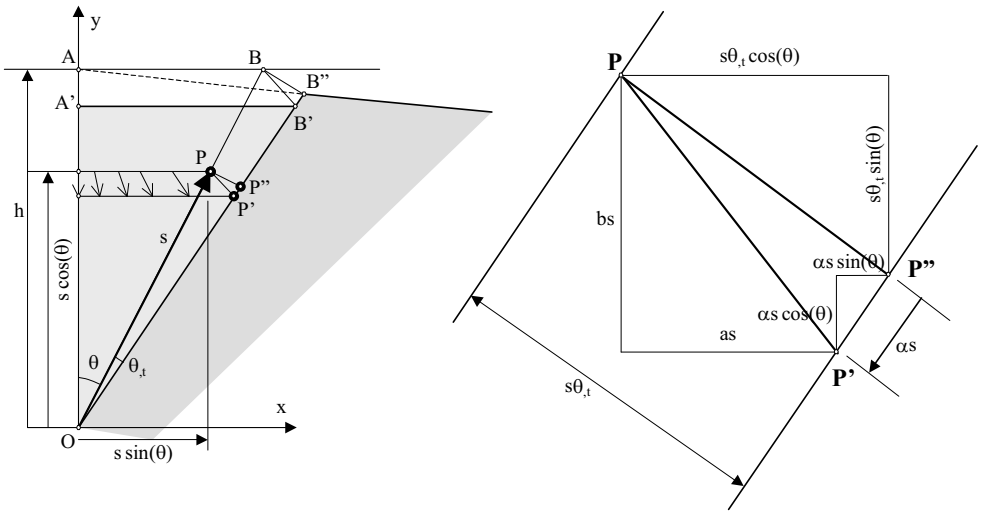

Figure 9.7 The plastic wedge

The displacements in the wedge are expressed by

$$u_{x,t} = ax/\sin\theta \quad \text{and} \quad u_{y,t} = -by/\cos\theta \tag{9.33}$$

Elaboration of the volume constraint condition yields

$$V_{OAB} = V_{OA'B'} \quad \rightarrow \quad s^2\cos\theta\sin\theta = s^2(\cos\theta - b)(\sin\theta + a)$$

$$\rightarrow \quad a\cos\theta - b\sin\theta = ab \approx 0$$

$$\rightarrow \quad \theta_{,t}\cos^2\theta - \alpha\sin\theta\cos\theta - \theta_{,t}\sin^2\theta - \alpha\cos\theta\sin\theta = 0$$

$$\rightarrow \quad \alpha = \theta_{,t}(\cos^2\theta - \sin^2\theta)/(2\sin\theta\cos\theta) =$$

$$= \theta_{,t}\cos(2\theta)/\sin(2\theta) = \theta_{,t}\,\mathrm{cotg}(2\theta) \tag{9.34}$$

And consequently

$$a = \theta_{,t}\cos\theta - \alpha\sin\theta = \theta_{,t}(\cos\theta - (\cos^2\theta - \sin^2\theta)/(2\cos\theta)) = \theta_{,t}/(2\cos\theta) \qquad (9.35a)$$

$$b = \theta_{,t}\sin\theta + \alpha\cos\theta = \theta_{,t}(\sin\theta + (\cos^2\theta - \sin^2\theta)/(2\sin\theta)) = \theta_{,t}/(2\sin\theta) \qquad (9.35b)$$

Hence, the strains in the wedge can be expressed by

$$\varepsilon_{xx,t} = u_{xx,t} = a/\sin\theta = \theta_{,t}/\sin(2\theta) \qquad (9.36a)$$

$$\varepsilon_{yy,t} = u_{yy,t} = b/\cos\theta = -\theta_{,t}/\sin(2\theta) \qquad (9.36b)$$

Easily, one may verify that for distortion $\gamma_{,t} = 0$, and for the volume constraint $\varepsilon_{xx,t} + \varepsilon_{yy,t} = 0$ holds. Next, the plastic work rate is elaborated. Inside the wedge and along the interface OB' a constant cohesion k is assumed (note, $0 < \theta < \pi/2$)

$$\begin{aligned} W_{,t} &= k \iint_{OAB} \sqrt{[(\varepsilon_{xx,t} - \varepsilon_{yy,t})^2 + \gamma_{,t}^2]}\, dV + k \int_{OB} |\alpha s|\, ds = \\ &= 2k|\theta_{,t}\sin^{-1}(2\theta)| \iint_{OAB} dV + k|\theta_{,t}\operatorname{cotg}(2\theta)| \int_{OB} s\,ds \\ &= k|\theta_{,t}\sin^{-1}(2\theta)|h^2\tan\theta + k|\theta_{,t}\operatorname{cotg}(2\theta)|h^2/2\cos^2\theta \\ &= k|\theta_{,t}|h^2\{\tan\theta/\sin(2\theta)) + |\operatorname{cotg}(2\theta)|/2\cos^2\theta\} \\ &= k|\theta_{,t}|h^2\{1 + |\operatorname{cotg}(2\theta)|\}\,(2\cos^2\theta)^{-1} \end{aligned} \qquad (9.37)$$

It can be shown that this expression is minimum for $\theta = \pi/4$. Then, $W_{,t} = k|\theta_{,t}|h^2$. If along the axis OA a rigid border is present, the work along it has to be accounted for. Assuming there a cohesion k' this contribution becomes

$$\begin{aligned} \Delta W_{,t} &= k' \int_{OA} |bs|\, ds = k'|\theta_{,t}|/(2\sin\theta) \int_{OA} s\, dy \\ &= k'|\theta_{,t}|/(2\sin\theta) \int_{OA} y/(\cos\theta)\, dy \\ &= k'|\theta_{,t}|h^2/(2\sin(2\theta)) = \tfrac{1}{2}k'|\theta_{,t}|h^2 \end{aligned} \qquad (9.38)$$

which attains a minimum at $\theta = \pi/4$. Finally, the minimum total work rate becomes

$$W_{,t} + \Delta W_{,t} = (k + \tfrac{1}{2}k')|\theta_{,t}|h^2 \qquad (9.39)$$

Rankine wedge

An important element of a visco-plastic stationary motion with an analytical solution is a Rankine wedge as shown in Fig 9.8. After a small rotation $\theta_{,t}\,dt$ the wedge OAB is supposed to undergo a plastic deformation by one-directional frictional sliding and it moves into shape OA'B, while the outside remains rigid. Along the interface OA slip takes place against a rigid border, compatible with volume constraint conditions. For convenience, the angle θ is restricted to $0 < \theta < \pi/2$, without loss of practicality. Geometric considerations yield

$$a = (h-y)/\cos\theta \quad \text{and} \quad b \approx \theta_{,t}/\sin\theta \quad \text{and} \quad c = y\theta_{,t}/\tan\theta \tag{9.40}$$

Here, b and c represent the relative inner and border displacement over dy of the wedge, while reshaping from OAB to OA'B. When assuming a constant maximum shear stress k along the θ-inclined slip lines within the volume OAB, the work rate is determined by

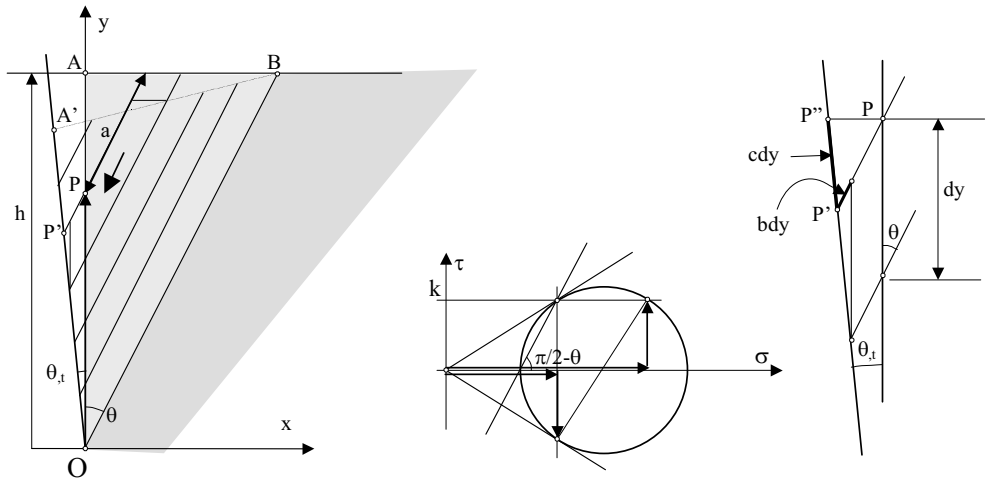

Figure 9.8 The Rankine wedge

$$W_{,t} = k\,{}_0\!\int^h a|b|dy = k\,{}_0\!\int^h 2(h-y)|\theta_{,t}|/\sin(2\theta)\,dy = k|\theta_{,t}|\,h^2/\sin(2\theta) \tag{9.41}$$

which attains a minimum at $\theta = \pi/4$: $W_{,t} = k\theta_{,t}h^2$. The additional work rate along the border line OA is added, taking into account an interface shear stress k'

$$\Delta W_{,t} = k'\int_{OA}|c|\,dy = k'\,{}_0\!\int^h y|\theta_{,t}/\tan\theta|\,dy$$

$$= k'|\theta_{,t}/\tan\theta|\,{}_0\!\int^h y dy = k'|\theta_{,t}/2\tan\theta|\,h^2 \tag{9.42}$$

Hence, the total work rate for the Rankine wedge becomes

$$W_{,t} + \Delta W_{,t} = (k/\sin[2\theta] + ½k'/\tan\theta)\,|\theta_{,t}|\,h^2 \tag{9.43}$$

For the active Rankine state: $\theta = \pi/4 - \varphi/2$ holds and for the passive Rankine state $\theta = \pi/4 + \varphi/2$, with φ the soil friction angle. For $\theta = \pi/4$ (and $\varphi = 0$) the total work rate becomes similar to the work rate for the plastic wedge, expression (9.39). The effect of gravity (soil weight) has been disregarded.

Dike doweling

In West-Netherlands a soft Holocene top layer commonly occurs on top of a relatively rigid and permeable Pleistocene sand layer. Through the sand layer high water levels in adjacent rivers may generate high pore pressures under a dike. Consequently, effective contact stresses at the layer interface decrease, eventually

to zero, giving rise to uplift (Fig 9.9b: zone B) and sliding. In the mid eighties this phenomenon was not well understood, and it caused a sudden collapse of a dike at Streefkerk (Fig 9.9a). Since then careful observation of various dikes, geo-centrifuge tests and finite element calculations have proven that uplift is a serious failure mechanism. Stability can be improved by a berm, i.e. an extra load on the leeside of the dike, an anchored sheet wall or a short unanchored buried sheet wall. The latter, referred to as a dike dowel, is being considered here.

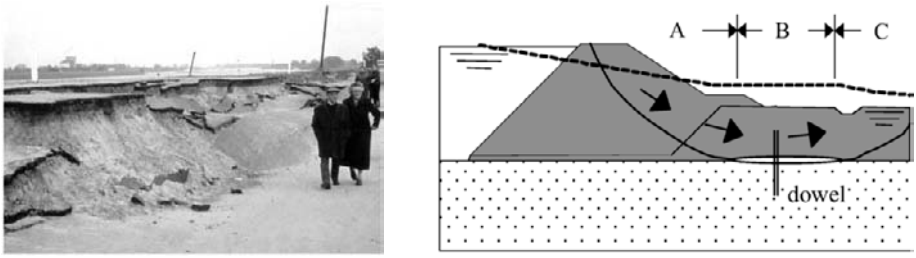

(a) *(b)*

Figure 9.9 (a) dike failure at Streefkerk, Netherlands, 1984, (b) uplift mechanism

An ultimate limit state of dike stability is represented by a compatible kinematical visco-plastic flow field. This field can be decomposed in terms of elementary solutions. A simplified method is used, considering apparent dynamic cohesion *k*, representing local shear strength under continuing deformation. The dissipation work rate during motion is considered. Two cases are considered: Case I without a dowel and Case II with a dowel.

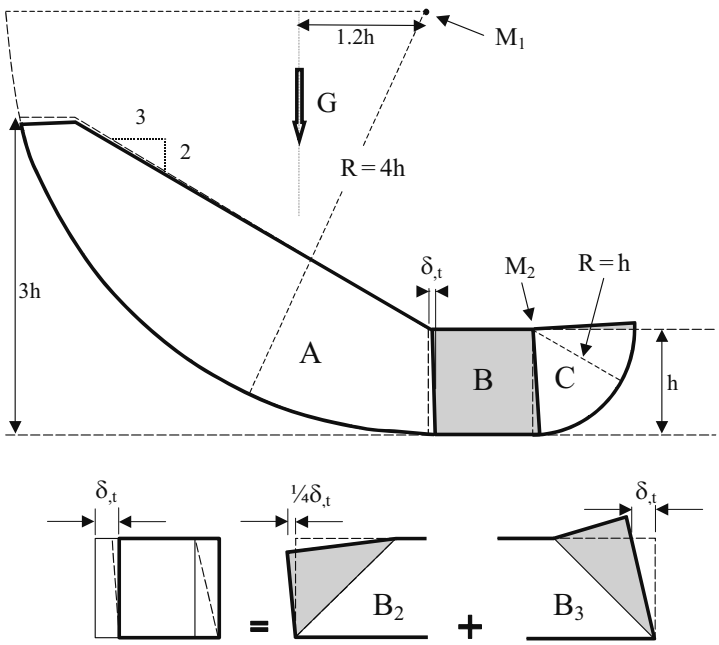

Figure 9.10 Embankment slip failure with kinematics in the uplift zone (B)

The kinematics is presented in Fig 9.10. It is essential to fit the visco-plastic subzones (wedges and rigid zones) perfectly, like a jigsaw puzzle. The motion is divided in three zones: A, B and C. Zone A and C are supposed to undergo a rigid motion of $\delta_{,t}$ along their circular slip surface, according to a rotation speed in centre M_1 or M_2. Zone B is considered as a square block with height h. The movement of zone A causes block B to move with speed $\delta_{,t}$ to the right. In Case I, the corresponding friction over the underground leads to a dissipation work of $\delta_{,t}hk'$. In order to fit the side of zone A the left side of zone B has to deform over $\frac{1}{4}\delta_{,t}$. This is achieved by assuming a plastic wedge, and the corresponding dissipation work, according to equation (9.39) with $\frac{1}{4}\delta_{,t} = \theta_{,t}h$, becomes $(k+\frac{1}{2}k')\frac{1}{4}\delta_{,t}h = \frac{3}{8}\delta_{,t}\,kh$. Here, $k = k'$ because the material of zone A and B are equal. The right hand side of block B fits rigid zone C by assuming another plastic wedge and here $\delta_{,t} = \theta_{,t}h$, which leads to a dissipation work of $(k+\frac{1}{2}k')\delta_{,t}h = \frac{3}{2}\delta_{,t}\,kh$. The total dissipation work becomes for Case I

$$W_{,t} = W_{A,t} + W_{C,t} + W_{B,t}$$

with $$W_{B,t} = \delta_{,t}\,kh\,(k'/k + \tfrac{3}{8} + \tfrac{3}{2}) = \delta_{,t}\,kh(k'/k + 1.875) \qquad (9.44)$$

Here, k is the apparent dynamic cohesion in the Holocene layer and k' at the interface in the uplift zone; k' could be taken zero because of local high excess pore pressures.

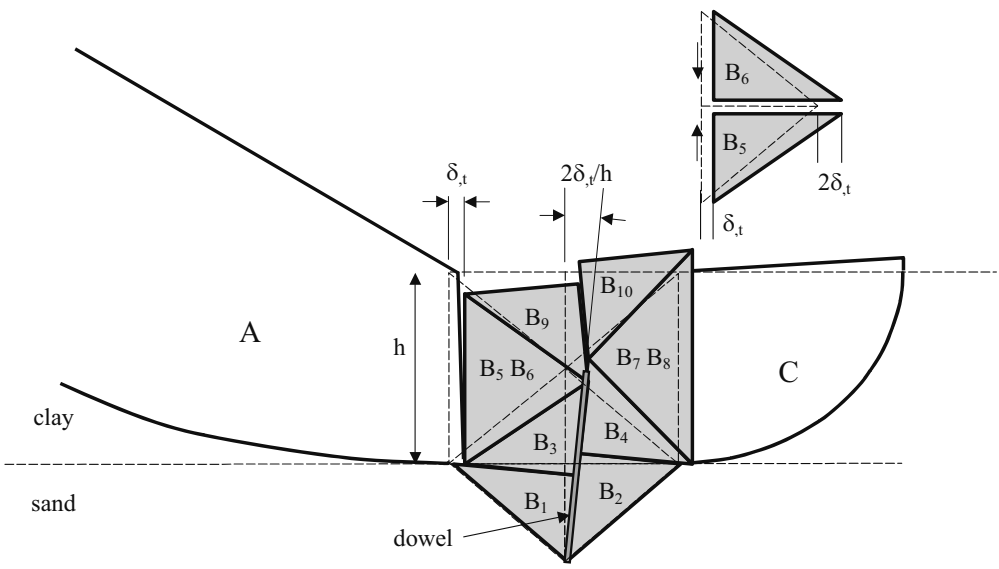

Figure 9.11 Kinematics of uplift zone B with a dowel that rotates $\delta_{,t}/2h$

In Case II, the dike stability is improved by applying a buried short sheet pile, a dowel, penetrating in the Pleistocene layer. The kinematics shown in Fig 9.11 consists of zone A and zone C, similar to the previous situation. Zone B has now 10 elementary subzones to accommodate the induced rotation of the dowel. In addition, the two wedges of Case I are superimposed to accommodate the rotations

at the sides. The corresponding dissipation work rate is elaborated and results are presented in Table 9.1 for the 10 subzones. Hence, with k_z the apparent cohesion in the Pleistocene sand layer, the dissipation work rate $W_{B,t}$ in zone B becomes for Case II

$$W_{B,t} = \delta_{,t}\, kh(\tfrac{1}{2}\, k'/k + {}^{3}/_{2}k_z/k + 6.0 + 1.875) = \delta_{,t}\, kh(7.875 + (k'+3k_z)/2k) \qquad (9.45)$$

TABLE 9.1 DISSIPATION WORK IN ZONE B DUE TO THE DOWEL

subdomain	*B1*	*B2*	*B3*	*B4*	*B5 + B6*	*B7 + B8*	*B9*	*B10*
$\Delta W_{B,t} / \delta_{,t}$ kh	¾ k_z /k	¾ k_z /k	½+¼ k'/k	½+¼ k'/k	2	2	½	½
remark	*plastic*	*plastic*	*rigid*	*rigid*	*plastic*	*plastic*	*rigid*	*rigid*

Finally the total dissipation work becomes (s_A and s_C are the lengths of the circular slip surface of zone A and zone C, respectively)

I *Without dowel* $\quad W_{,t} = \delta_{,t}\, kh(s_A k_A/kh + 1.875 + k'/k + s_C k_C/kh) \qquad (9.46a)$

II *With dowel* $\quad W_{,t} = \delta_{,t}\, kh(s_A k_A/kh + 7.875 + (k'+3k_z)/2k + s_C k_C/kh) \qquad (9.46b)$

Here, k_A and k_C represent an apparent dynamic cohesion. Adopting $k_A = 8k$ (much higher stress level and stiffness in the dike), $k' = 0$ (uplift: no effective stress), $k_C = k$, and $k_z = 2k$ (relatively low because of high pore pressures), yields with $s_A = 1\tfrac{2}{3}\pi\, h$ and $s_C = \tfrac{1}{2}\pi\, h$

I *Without dowel* $\quad W_{,t}/\delta_{,t}\, kh = (13.8\pi + 1.875) = 45.2 \qquad (9.47a)$

II *With dowel* $\quad W_{,t}/\delta_{,t}\, kh = (13.8\pi + 10.875) = 54.2 \qquad (9.47b)$

If the situation without dowel corresponds to an ultimate limit state, then the effect of the dowel is an improvement of the stability factor to 54.2/45.2 = 1.20. The stiff dowel method has been checked with centrifuge tests and FEM simulations (stability factor improvement from 1.00 to 1.10 - 1.15). At present dike dowelling is accepted as an official improvement method for dike stability in cases where space for conventional dike enlargement is limited.

The method of rigid-viscoplastic analytic elements can be used by hand and represents an elegant manner to check failure states. That it works only in two-dimensions, is a limitation.

application 9.1

The stability and accuracy of numerical calculations depends on the discretisation in space and time. For the storage equation (consolidation), which is of the type $f_{,t} = c_v f_{,xx}$, using forward time approximation and central spatial difference, the truncation error shows that the solution converges, if

$$2c_v \Delta t < (\Delta x)^2$$

There is also a minimum condition for the time step, related to the fact in a given time step Δt the storage process should be able to progress over the mesh size Δx, which leads to (see hydrodynamic period equation (6.8) for a mesh size)

$$c_v \Delta t > 2(\Delta x)^2$$

If this requirement is not met, the solution may become unstable in space. Both conditions contradict: no time step suits. By choosing for an implicit time scheme (Crank-Nicolson) there is no restriction, but for large time steps the accuracy becomes an issue.

application 9.2

A regional stationary groundwater flow with a well is calculated with a Finite Difference model with spatial discretisation (mesh size) of Δx = 25 m and linear approximation of the potential head in the mesh cells. The calculation result shows a potential head of ϕ = 7 m in the well node and ϕ = 10 m n the adjacent node. The well radius is r_w = 0.25 m. What is the true potential head in the well?

application 9.3

The result of the Direct Simple Shear test, shown in Fig 3.3b, depends on the initial stress state. This can be shown on the basis of the double sliding model. Two cases are distinguished: (A) the horizontal stress is smaller than the vertical stress, $\sigma_{xx} < \sigma_{yy}$ or $K_0 < 1$, and (B) the horizontal stress is larger than the vertical, $\sigma_{xx} > \sigma_{yy}$ or $K_0 > 1$. In the test, the vertical stress for both cases is kept equal, by adopting a similar vertical force N. The failure state for both cases, according to the associative Mohr-Coulomb model, and the corresponding principle stress direction are presented in Fig 9.12. Obviously, the measured shear force is different in both cases: $T_A < T_B$. The ratio T_A/T_B is equal to the ratio τ_A/τ_B, because the total surface of shear planes are equal in both cases. Fig 9.12 reveals that $\tau_A/\tau_B = \sigma_{xxA}/\sigma_{xxB} = (1-\sin^2\varphi)/(1+\sin^2\varphi)$. For $\varphi = 30^o$ this ratio becomes 0.6. In the DSS test, care is to be taken that the stress ratio $K_0 = \sigma_{xx}/\sigma_{yy} < 1$, so that the test result T/N gives a proper indication for $\tan\varphi$.

application 9.4

The previous example shows the stress state at the start of failure. What is the final stress state in a Direct Simple Shear test (vertical stress is kept constant), if a conventional Mohr-Coulomb model models the material? Assume

$$\cos 2\alpha = \frac{\sigma_{xx} - \sigma_{yy}}{2\tau_m} \quad \text{and} \quad \sin 2\alpha = \frac{\sigma_{xy}}{\tau_m}$$

with for the radius τ_m of the Mohr-circle complies with

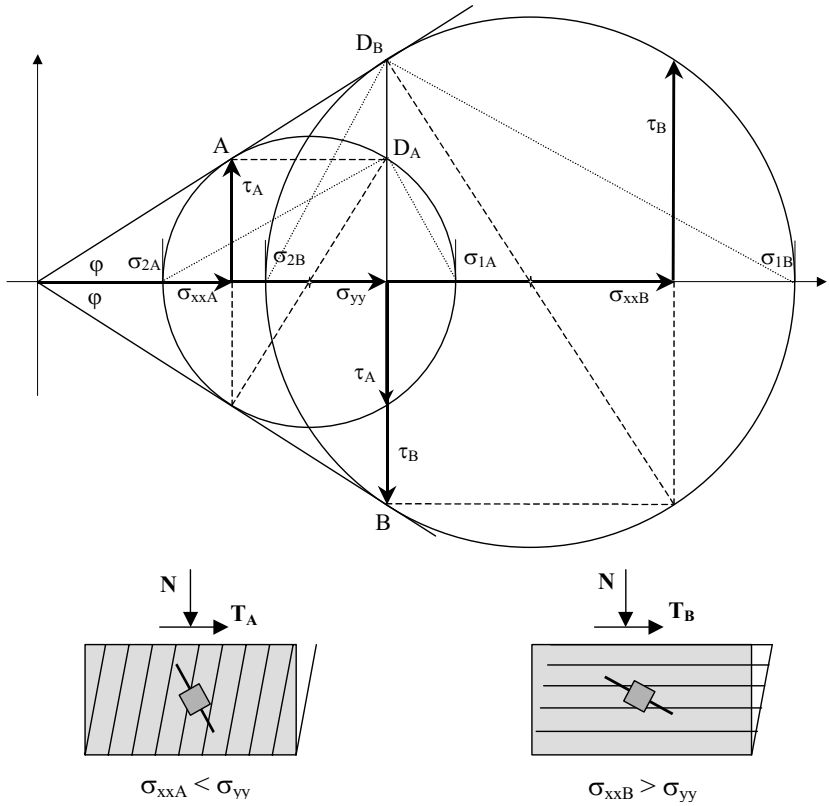

Figure 9.12 Direct simple shear test evaluated by the double sliding model

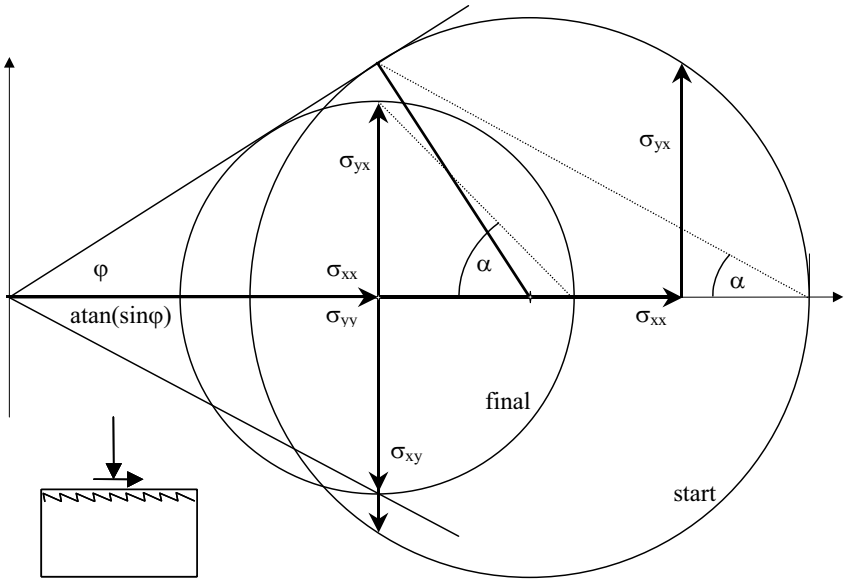

Figure 9.13 Stress rotation during simple shear

$$\tau_m{}^2 = \left(\frac{\sigma_{xx} - \sigma_{yy}}{2}\right)^2 + \sigma_{xy}{}^2$$

At the centre of the Mohr circle, the mean normal stress gives

$$\sigma_m = \frac{\sigma_{xx} + \sigma_{yy}}{2} = \frac{\sigma_{xx} - \sigma_{yy}}{2} + \sigma_{yy} = \tau_m \cos 2\alpha + \sigma_{yy}$$

The Mohr-Coulomb failure criterion states: $\tau_m = \sigma_m \sin\varphi$. This provides

$$\sigma_m = \sigma_m \sin\varphi \cos 2\alpha + \sigma_{yy} \quad \rightarrow \quad \sigma_{yy} = \sigma_m (1 - \sin\varphi \cos 2\alpha)$$

With

$$\sin 2\alpha = \frac{\sigma_{xy}}{\tau_m} \quad \rightarrow \quad \sigma_{xy} = \sigma_m \sin\varphi \sin 2\alpha$$

one obtains

$$\left|\frac{\sigma_{xy}}{\sigma_{yy}}\right| = \frac{\sin\varphi \sin 2\alpha}{1 - \sin\varphi \cos 2\alpha}$$

In similar manner one obtains

$$\left|\frac{\sigma_{xy}}{\sigma_{xx}}\right| = \frac{\sin\varphi \sin 2\alpha}{1 + \sin\varphi \cos 2\alpha}$$

For the coaxial case without dilatancy ($\psi = 0$) it follows from (9.16) for the final stage

$$R = \frac{\cos\psi \sin\varphi}{1 - \sin\psi \sin\varphi} = \sin\varphi = \frac{\sigma_{xy}}{\sigma_{yy}}$$

This complies with $\alpha = 45°$, and thus $\sigma_{xx} = \sigma_{yy}$. Obviously, the main stresses rotate from the initial state towards final state (Fig 9.13).

application 9.5

Find α_{cr} of equation (9.14) and elaborate (9.15b).

Part III

Design and Construction

This page intentionally left blank

10 STABILITY OF SLOPES

Stability of soil masses is characterised by the stability of its slopes or sides. They can be unsupported or supported by earth-retaining structures, such as geotextile, soil nailing, retaining wall, gravity wall, or strutted or anchored wall (sheetpiling), permanently or temporarily (building pit). Unsupported slopes can be created by nature (erosion) or made by man by excavating (cuttings) or by building (embankments). Cuttings cause a decrease of total stresses and embankments an increase. Particularly for cuttings the local effect on groundwater flow and corresponding pore pressures are to be considered, both during construction (pore pressures decrease by temporary drainage) and after construction (pore pressures increase again). The long-term stability of a cutting may be more critical than during construction (vanishing suction pressures). For embankments on soft soils the induced excess pore pressures in the subsoil during construction may induce collapse. In the case of water retaining dams and dikes, a critical situation may occur when the retaining water is quickly lowered, referred to as the rapid draw-down instability. Landslides are usually triggered by rainshowers.

Gravity and loading may cause movement (instability) and collapse (failure). A massive movement may take place as result of a shear failure along one or more internal slip surfaces. The soil may develop plastic zones (limit effective stress) or liquefaction (loss of effective stress). For failure one distinguishes falls (steep slopes), flow (mud), translational slides (parallel to the surface), rotational slides (short slopes), wedge failures (horizontal sliding) and collapse of retaining structures. Due to weathering and degradation many natural slopes may exist in a state of incipient failure, i.e. ultimate limit state (ULS). In this chapter the limit state of slopes is discussed.

A LIMIT ANALYSIS

The real mechanical three-dimensional state of a soil mass is usually so complex, that only approximations can be adopted. The critical condition of a soil mass, i.e. the limit of stability, is then obtained by considering an approximate limit load. There are two situations possible.

- A lower-limit load, which the soil certainly can carry, i.e. equilibrium and boundary conditions are satisfied everywhere, nowhere does the stress exceed the failure condition, but whether failure. i.e. a possible kinematic pattern, really occurs is unsure.
- An upper-limit load, under which the soil will certainly collapse according to a plausible kinematic pattern, i.e. compatibility and boundary conditions are satisfied everywhere and equilibrium conditions are satisfied for the chosen displacement pattern, but whether stress does not exceed failure conditions everywhere is unsure.

Each of these approaches has the advantage that a strict relation between stresses and strains is not required, which makes the analysis relatively simple and straightforward.

From plasticity theory it can be shown that for materials, which possess cohesion but no internal friction, the real limit load, satisfying everywhere equilibrium and

compatibility conditions, will be in between the lower and upper limit (Drucker's postulate). However, for frictional materials, such as soils, this statement may not be valid. Nevertheless, in practice, it is commonly used for evaluating soil stability. One may apply a lower-limit solution (finite element simulation) or an upper-limit solution (slip-line approach) and adopt appropriate safety factors. Well-studied examples of the limit analysis approach are the stability of (infinite) slopes, vertical excavation (Rankine's solution), and the ultimate bearing of shallow foundations (Prandtl's solution and Brinch Hansen's method).

B SLIDE ON LONG SLOPES (MICRO-STABILITY)

Slope stability can be analyzed by assuming it to be a section of a long slope, which is expected to locally slide along a slip plane parallel to its surface. Let the soil be undrained and the shear strength expressed by $|\tau| < c_u$. Critical equilibrium of forces (see Fig 10.1a), i.e. the resistance force $R = b\tau_s$, where b is the width of the section, can just counteract the tangential force $T = W\sin\beta$, related to weight $W = Hb\gamma\cos\beta$ and slope angle β, thus $R = T$ gives at depth H of the slip surface, where $\tau_s = c_u$

$$T = c_u b = R = W\sin\beta = Hb\gamma\cos\beta\sin\beta \qquad (10.1)$$

It applies for slopes $0 < \beta < 45^o$, and the depth at which the slip supposedly occurs is

$$H = c_u/(\gamma\sin\beta\cos\beta) \qquad (10.2a)$$

The corresponding stability factor is expressed by

$$F = \frac{1}{\sin\beta\cos\beta}\left(\frac{c_u}{\gamma H}\right) \qquad (10.2b)$$

Formula (10.2b) indicates for $F = 1$ a slope at the angle β under which a soil layer of thickness H is just stable. A thinner layer will be stable at a steeper slope, provided (10.2b) holds for $F \geq 1$.

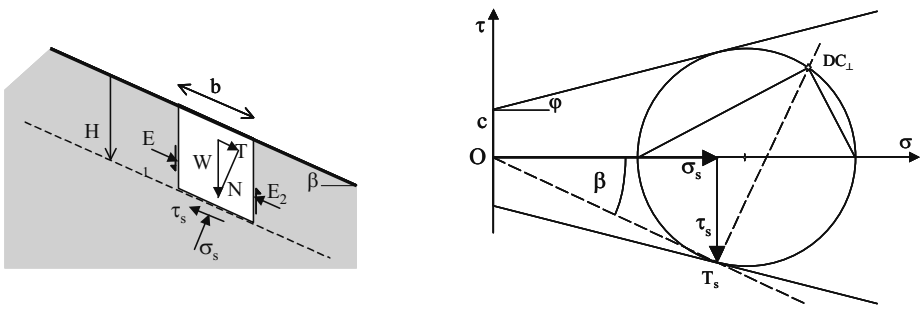

(a) (b)

Figure 10.1

Note, that the forces parallel to the slope, E_1 and E_2, are in balance, and cancel out in the equilibrium. The same holds for the shear forces on the vertical sides. Therefore, (10.2) represents a lower limit. Usually, with depth undrained strength and weight increase. Formula (10.2) is valid for shallow slip surfaces. A submerged slope under still water has the same result, except for the fact that in stead of γ the submerged weight $\gamma' = \gamma - \gamma_w$ should be used.

Let the soil be fully drained and the shear strength expressed by $|\tau| < c + \sigma' \tan\varphi$. The cohesion may allow for a steeper slope than the natural slope angle ($\beta > \varphi$), as shown by the Mohr circle in Fig 10.1b. The stress state is at limit state, expressed by point T_s, representing the normal and shear stress at the slip line. Obviously, $W = \gamma Hb\cos\beta = \sigma_s b/\cos\beta = |T_sO|b$, where $|T_sO|$ is indicated in the Mohr diagram. Hence, $|T_sO| = \gamma H\cos\beta$. From the Mohr diagram it can be shown that $|T_sO| = c\cos\varphi/\sin(\beta-\varphi)$, and a critical layer thickness is then

$$H = c\cos\varphi/(\gamma\cos\beta\sin(\beta-\varphi)) \qquad (10.3a)$$

The corresponding stability factor is expressed by

$$F = \frac{\cos\varphi}{\cos\beta\sin(\beta-\varphi)}\left(\frac{c}{\gamma H}\right) \qquad \text{with} \qquad \beta > \varphi \qquad (10.3b)$$

For $F = 1$, formula (10.3b) indicates the slope angle β, at which a soil layer of thickness H is just stable. When there is no cohesion $c = 0$, obviously $\beta = \varphi$ satisfies $F = 1$.

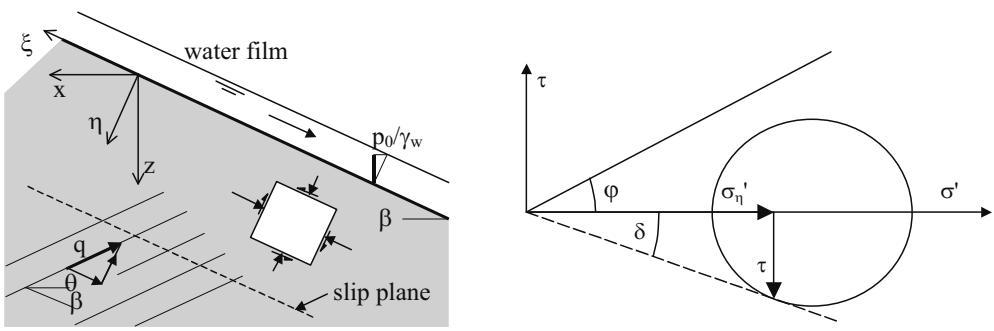

(a) (b)

Figure 10.2

For a saturated drained slope, the pore pressures induced by local groundwater flow has a pronounced effect on the stability. Let the shear strength of the soil be defined by the Mohr-Coulomb criterion: $|\tau| < \sigma' \tan\varphi$. Note, that cohesion is disregarded. Assume a local groundwater flow, with a specific discharge q inclined at an angle θ (see Fig 10.2a).

First, the corresponding pore pressure u is determined. Assume a (locally) uniform flow field, where the pore pressure is linear: or $u = A\xi + B\eta + C$. The condition that $u = p_0$ along the surface $\eta = 0$ yields $u = B\eta + p_0$. The

corresponding potential head is by definition $h = -z+u/\gamma_w$ (z is chosen positive downwards) and with $z = \eta\cos\beta - \xi\sin\beta$, we find $h = (B\eta + p_0)/\gamma_w - \eta\cos\beta + \xi\sin\beta$. The filter velocity components q_ξ *and* q_η can be expressed by Darcy's law, according to $q_\xi = -k_\xi \partial h/\partial\xi$ and $q_\eta = -k_\eta \partial h/\partial\eta$. Anisotropic permeability (fissures or layering in the subsoil) is accounted for by the ratio $\chi = k_\xi/k_\eta$. The resultant of the flow components q_ξ and q_η pointing along flow direction θ.

$$q_\eta/q_\xi = \tan(\beta+\theta) = \frac{\partial h/\partial\eta}{\chi\partial h/\partial\xi} = \frac{B/\gamma_w - \cos\beta}{\chi\sin\beta} \tag{10.4}$$

Hence, $B = \gamma_w\cos\beta(\chi\tan\beta\tan(\beta+\theta) + 1)$, and the pore pressure field becomes

$$u = (B\eta + p_0) = \eta\gamma_w\cos\beta(\chi\tan\beta\tan(\beta+\theta) + 1) + p_0 \tag{10.5}$$

Next, the equilibrium of a small soil element is considered (see Fig 10.2a). A plane uniform stress field is adopted. The general equilibrium condition, including the effect of pore pressures and the soil weight γ, is expressed in the ξ-η system as follows

$$\frac{\partial\sigma_\xi' + u}{\partial\xi} + \frac{\partial\tau}{\partial\eta} + \gamma\sin\beta = 0 \tag{10.6a}$$

$$\frac{\partial\sigma_\eta' + u}{\partial\eta} + \frac{\partial\tau}{\partial\xi} - \gamma\cos\beta = 0 \tag{10.6b}$$

Because of 'infinite' symmetry of a long slope, (10.6) is independent of ξ, and after integration, with condition at $\eta = 0$, $\sigma_\eta' = 0$, one obtains with (10.4)

$$\tau = -\gamma\eta\sin\beta \tag{10.7a}$$

$$\sigma_\eta' = \gamma\eta\cos\beta - u + p_0 = \gamma\eta\cos\beta(1 - (\gamma_w/\gamma)(\chi\tan\beta\tan(\beta+\theta) + 1)) \tag{10.7b}$$

This shows that normal stress and shear stress increase with depth, and consequently, there seems to be no specific potential slip surface. When the slope fails, it may happen in many planes parallel to the slope surface, e.g. like a mudflow. The condition $\sigma_\eta' = 0$ at $\eta = 0$ is valid for a submerged slope and the effect of p_0 cancels out. In the case of infiltration there could be a capillary pressure: $p_0 = -\gamma_w h_c$, and then $\sigma_\eta' = h_c$ at $\eta = 0$ holds, which gives an additional term h_c in (10.7b), according to

$$\sigma_\eta' = \gamma\eta\cos\beta(1 - (\gamma_w/\gamma)(\chi\tan\beta\tan(\beta+\theta) + 1)) + \gamma_w h_c \tag{10.7c}$$

Finally, the stress state has to satisfy the failure criterion $|\tau| < \sigma_\eta'\tan\varphi$. In fact, as shown by a Mohr-circle in Fig 10.2b, one can define a slope stability factor, according to

$$F = (strength)/(loading) = \tan\varphi / \tan\delta \qquad \text{with} \qquad \tan\delta = |\tau| / \sigma_\eta' \qquad (10.8)$$

Here, δ refers to the actual stress state in a potential slip plane. The slope is stable for $F > 1$, in a limit state at $F = 1$, and unstable for $F < 1$. Inserting (10.7) yields

$$F = (\tan\varphi / \tan\beta)\,[1 - (\gamma_w/\gamma)(\chi \tan\beta \tan(\beta + \theta) + 1) + \gamma_w h_c/(\gamma\eta \cos\beta)] \qquad (10.9)$$

This shows that an anisotropic permeability affects the slope stability. When $\chi = k_\xi / k_\eta < 1$ it enhances stability, i.e. perpendicular fissures may improve the stability, but permeable strata parallel to the slope reduce stability. Formula (10.9) also shows that for outflow perpendicular to the surface. i.e. $\beta + \theta = 90^o$, the slope is unstable, whereas for perpendicular inflow, i.e. $\beta + \theta = -90^o$, the slope is stable. Finally, in the case of capillary pressure head h_c the stability increases, but this effect decreases with depth. In the case of outflow, there is no capillary pressure and (10.9) with $h_c = 0$ should be applied.

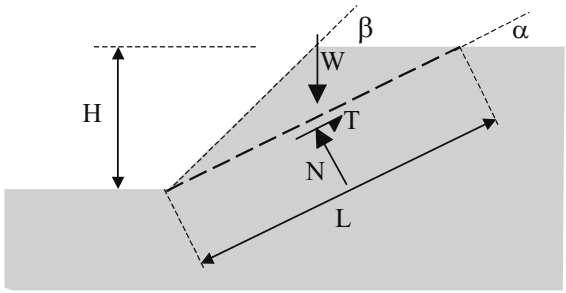

Figure 10.3 Slope sliding according to Cullmann

C SLIDE ON SHORT SLOPES (MACRO-STABILITY)

The simplest approach for sliding of a short slope, under angle β, is by considering a straight slip surface at an angle α passing through the toe of the slope (Fig 10.3), known as Cullmann's method. The weight of the sliding soil mass, $W = \gamma LH\sin(\beta-\alpha)/\sin\beta$, is counterbalanced by the normal and shear force in the slip surface, $N = W\cos\alpha$ and $T = W\sin\alpha$. Adopting the Mohr-Coulomb failure criterion, giving a maximum shear force of, $|T_{crit}| = cL + N\tan\varphi$, leads to the following stability factor

$$F = |T_{crit}|/|T| = (cL + W\cos\alpha\tan\varphi)/W\sin\alpha =$$

$$= \frac{2\sin\beta}{\sin(\beta-\alpha)\sin\alpha}\left(\frac{c}{\gamma H}\right) + \frac{\tan\varphi}{\tan\alpha} \qquad (10.11)$$

The most unfavourable angle α follows from requiring $dF/d\alpha = 0$, giving $\alpha = (\beta+\varphi)/2$. This renders (10.11) into

$$F = \frac{4\sin\beta}{\cos\varphi - \cos\beta}\left(\frac{c}{\gamma H}\right) + \frac{\tan\varphi}{\tan((\beta+\varphi)/2)} \qquad (10.12)$$

Usually slip surfaces are curved and Cullman's method overestimates the stability. Formula (10.12) is more applicable for steep slopes, in particular for undrained cohesive soils, for which, with $c = c_u$ and $\varphi = 0$, (10.12) gives

$$F = \frac{4\sin\beta}{1-\cos\beta}\left(\frac{c_u}{\gamma H}\right) \qquad (10.13)$$

For a vertical slope (10.13) yields with $F = 1$ a maximum possible height of

$$H = 4c_u/\gamma \qquad (10.14a)$$

Since the used approach is based on a plausible kinematic pattern, (10.14a) is an upper limit (failure could occur at less height). A lower limit (equilibrium solutions) can be obtained by considering the Mohr-Coulomb criterion, which states for cohesive undrained soil (with $\varphi = 0$) $\sigma_h = \sigma_v - 2c_u$. At the toe of the vertical slope, at maximum height H, the stresses are $\sigma_h = 0$ and $\sigma_v = \gamma H$, and therefore the maximum height has a lower limit (stability is guaranteed; a deeper cut may be possible). The following holds as a lower limit

$$H = 2c_u/\gamma \qquad (10.14b)$$

Studies have shown that in reality the maximum height of a vertical slope of cohesive soil is in between a lower limit of $3.64c_u/\gamma$ and an upper limit of $3.83c_u/\gamma$. Under submerged conditions (10.14) applies, with γ replaced by $\gamma - \gamma_w$. Using 'heavy water' (bentonite slurry), in fact involving a large 'γ_w', vertical slopes can be sustained to even larger depth. This method is applied to create slurry walls, diaphragm walls, and soil mixing (see Chapter 11).

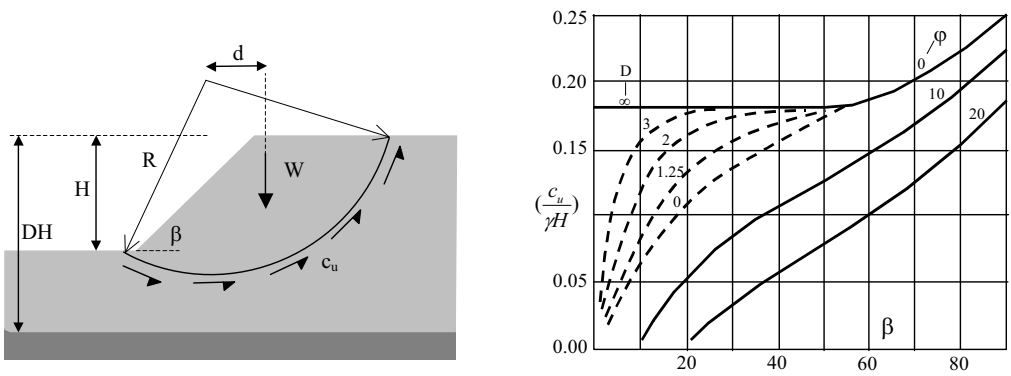

(a) (b)

Figure 10.4 Circular slip failure of cohesive slopes (Taylor)

In theory, one finds that slopes are usually curved (logarithmic spirals). The approximate approach of a circular slip surface is popular, because the kinematics is rather simple. Stability is expressed by rotational equilibrium around the circle centre (Fig 10.4a) and this yields the following stability factor for cohesive soils (W is the weight per metre longitudinal width in kN/m)

$$F = \text{(shear resistance moment)} / \text{(driving moment)} = c_u LR/Wd \qquad (10.15)$$

Here, L is the length of the circular slip surface. The most critical circle is found by trial and error. Taylor worked it out for cohesive soils in a practical diagram (Fig 10.4b). Comparison of the different methods, previously explained, shows a large variation. For a slope under an angle of $\beta = 35^o$ with a deep subsoil, Taylor's diagram gives a stability factor $F = 5.6c_u/\gamma H$. It is an upper limit and it is essential to use in addition an appropriate safety factor.

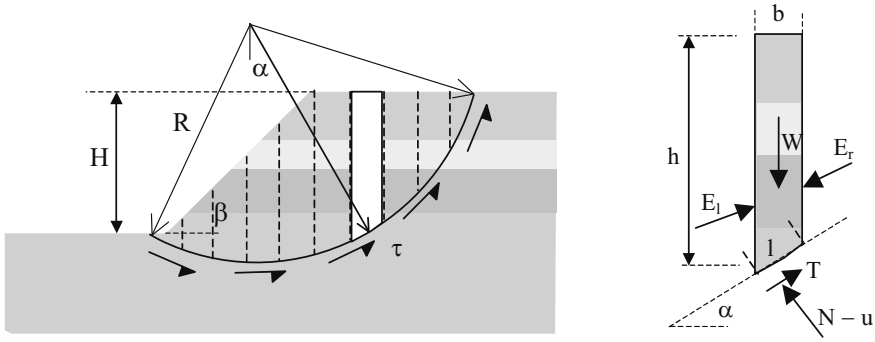

Figure 10.5 Method of slices

For layered soil and/or drained slopes the situation is more complicated, because the shear resistance varies along the slip surface and the subsoil may contain different layers. The assumed slipping soil mass is divided into vertical slices with a fixed width b and an average height h (Fig 10.5). The weight of the slice $W = \gamma bh$ is counterbalanced by the normal and shear force in the slip surface, $N = W\cos\alpha$ and $T = W\sin\alpha$. The width of the slip surface of the slice is $l = b/\cos\alpha$. The Mohr-Coulomb failure criterion yields a maximum shear force of $T_{crit} = cl + N' \tan\varphi$, with $N' = N - ul$ and with u the local pore pressure. Stability is satisfied by the rotation equilibrium of the weight of all slices and the sum of the shear forces

$$\Sigma_i G_i R \sin\alpha_i \leq \Sigma_i T_{i,crit} R \qquad (10.16a)$$

The corresponding stability factor is

$$F = \Sigma_i T_{i,crit} / \Sigma_i W_i \sin\alpha_i = \Sigma_i (cl_i + N'_i \tan\varphi) / \Sigma_i W_i \sin\alpha_i \qquad (10.16b)$$

The problem is to determine N', since the inter-slice forces E are unknown. Fellenius' method, applied for the first time in 1915, assumes that the resultant of

inter-slice forces on both sides act opposite and cancel out, giving $N' = W\cos\alpha - ul$. Fellenius' stability factor becomes

$$F_F = \Sigma_i\,[(c + (\gamma h_i \cos^2\alpha_i - u_i)\tan\varphi)/\cos\alpha_i\,] \,/\, \Sigma_i\,(\gamma h_i \sin\alpha_i) \qquad (10.16c)$$

For a straight slip line in an infinite dry slope of non-cohesive soil ($c = 0$) (10.16c) becomes $F_F = \tan\varphi/\tan\alpha$, equal to (10.11). Practice has shown that Fellenius' method yields a relatively low stability factor (less by 5% to 20%). Bishop's method assumes that the inter-slice shear forces on the vertical slice interfaces balance (their contribution to vertical equilibrium cancels), and that the same stability factor applies to every slice separately. Vertical equilibrium then yields $W = T\sin\alpha + (N'+ul)\cos\alpha$. Moreover, $T = T_{crit}/F = (cl + N'\tan\varphi)/F$. From these conditions N' can be determined in every slice. Bishop's stability factor becomes

$$F_B = \Sigma_i\,[(c + (\gamma h_i - u_i)\tan\varphi)/(\cos\alpha_i(1+\tan\alpha_i \tan\varphi/F_B))]/\Sigma_i\,(\gamma h_i \sin\alpha_i) \qquad (10.16d)$$

Since F_B appears implicitly, an iterative approach is required. For cohesive soils ($\varphi = 0$) and a straight slip surface both (10.16c) and (10.16d) become $F = c/(\gamma h\sin\alpha\cos\alpha)$, which is in accordance with (10.2b). Bishop's method is applicable for heterogeneous soils. Strong negative values of α, near the toe, may give unrealistic contributions, it is suggested then to limit α to $\varphi/2-\pi/4$. Many computer programs based on Bishop's approach are available, which search for a minimum F while varying R and the centre point of the slip circle.

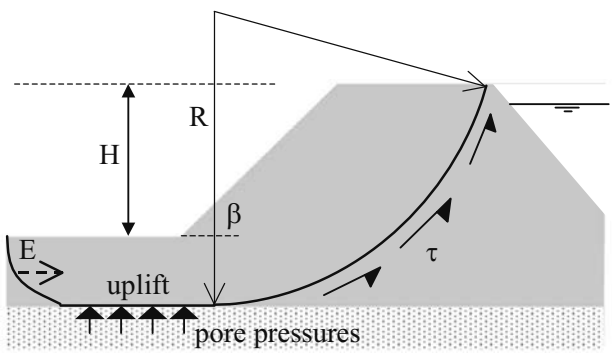

Figure 10.6 Slip surface with uplift

In some cases a circular slip surface does not fit, and one may apply a non-circular slip method, e.g. the method of Janbu, Spencer, or Morgenstern and Price. The latter rigorously solves for vertical, horizontal and moment equilibrium, both locally per slice and globally. It requires input of an arbitrary function describing the change of the angle of the interslice force in the slipping mass. Spencer simplified this by assuming a constant angle throughout, and his method is also widely used.

A specific situation occurs when pore pressures in a sandy layer under a slope of cohesive soil become so high that it lifts the overlaying soil slightly and a water film occurs in the interface. This phenomenon is called uplift (see application 4.4 and Chapter 9D)). The local shear resistance is reduced to zero in the uplift zone. An appropriate slope analysis for uplift, consisting of partly a circular and partly a straight slip surface, is suggested by Van (Fig 10.6). The passive reaction can be either an elastic force (E) as a result of large deformation or a local slip surface. A local berm or shoulder may be a solution.

Other phenomena of instability can be caused by uplift of the soil at the edges of solid (water retaining) structures induced by vertical groundwater flow, and squeezing of soft soil layers from under the edges of embankments, for which the construction phase is the most critical period. For slopes of shallow trenches and cuttings, a practical standard is used, shown in Table 10.1.

TABLE 10.1 ADMISSIBLE SLOPES FOR SHALLOW TRENCHES

soil type		*trench depth m*	*maximum slope ratio: vert / hor*
sand or loam	stiff, unremoulded	< 1.5	3.0
		1.5 – 2.5	1.5
		2.5 – 4.0	1.0
	loose or remoulded	1.0 – 4.0	1.0
clay	very stiff, unremoulded	< 1.5	vertical
		1.5 – 2.5	2.0
		2.5 – 4.0	1.25
	stiff, unremoulded	< 1.5	vertical
		1.5 – 2.5	1.5
		2.5 – 4.0	1.0
	remoulded	< 1.5	1.5
		1.5 – 4.0	1.0

application 10.1

Three specific situations are considered: (1) a dry slope, (2) a slope with flow parallel to the surface, and (3) a slope with horizontal outflow.

For a dry slope, the pore pressure is absent or $\gamma_w = 0$, which yields for (10.9) $F = \tan\varphi / \tan\beta$. Stability is guaranteed when $\beta < \varphi$. When $\beta = \varphi$, the slope is in the limit state; β is then called the natural slope angle (angle of repose). Since $F = \tan\varphi / \tan\beta$ is independent of the weight, it does not matter if the slope is submerged, under still water conditions.

For a slope with seepage flow parallel to its surface, $\theta = -\beta$, and (10.9) becomes $F = (\tan\varphi / \tan\beta)(1 - (\gamma_w/\gamma))$. Here, anisotropy in permeability does not play a role. The critical slope angle is found for $F = 1$. For an internal friction angle $\varphi = 35^o$, and a soil weight $\gamma = 18$ kN/m^3, one finds $\tan\beta_{F=1} = \tan\varphi\,(1 - (\gamma_w/\gamma)) = \tan 35^o(1 - (10/18)) = 0.31$, thus $\beta_{F=1} = 17.2^o$, about 50% of φ. Increasing the soil weight γ helps. It counts to place heavy solids on the surface (stabilising layer).

For a slope with horizontal outflow, $\theta = 0$, (10.9) becomes $F = (\tan\varphi / \tan\beta)(1 - (\gamma_w/\gamma)(\chi \tan^2\beta + 1))$, which yields for β

$$\tan\beta = ((F/f)^2+((\gamma/\gamma_w)-1)/\chi)^{0.5} - F/f \qquad \text{with} \qquad f = 2\chi\gamma_w\tan\varphi/\gamma \qquad (10.10)$$

The critical angle β is obtained for $F = 1$. One may also determine the angle for a specified safety, incorporating an overall safety factor γ_0 (see Chapter 8). Hence, F in (10.10) is replaced by $F\gamma_0$, with $F = 1$ as the limit stability factor. For example, consider a long slope (open mine pit) with a safety factor of $\gamma_0 = 1.2$. Horizontal outflow of groundwater is expected (isotropy is assumed: $\chi = 1$). With an internal friction angle of $\varphi = 35^o$, and an average soil weight of $\gamma = 18$ kN/m^3, application of (10.9) yields $f = 2\chi\gamma_w\tan\varphi/\gamma = 0.778$, and $\tan\beta = ((F\gamma_0/f)^2 + \gamma'/\gamma_w - 1)^{0.5} - F\gamma_0/f = ((1.2/0.778)^2 + 8/10 - 1)^{0.5} - 1.2/0.778 = 0.241$. Thus, $\beta_{F=1.2} = 13.5^o$. For $\gamma_0 = 1$, one would find $\beta_{F=1} = 15.7^o$. Dynamic flow conditions can aggravate the situation. Along coastlines where the sea tides and waves create dynamic conditions of which 'horizontal outflow' is determining, it is observed that slopes in the range of $\tan\beta < 0.15$ or $\beta < 10^o$ are formed.

application 10.2

Consider a water-retaining embankment, shown in Fig 10.10. The soil is fully saturated and cohesive ($\varphi = 0$). The soil properties and structural dimensions are shown in Table 10.2. The factor of safety is determined for three cases (1) stagnant water with depth H, (2) water depth zero, and (3) the effect of a tension crack in the crest of the embankment, when filled with water.

(1) stagnant water with a depth of 6 m

The sliding soil mass is divided in two zones: ABGF under the groundwater level, and GCDEF above. The weight of these zones are W_1 =144 (18–10) = 1152 kN/m and W_2 =42x18 = 756 kN/m. Applying (10.15) yields

$$F = c_uLR/\Sigma(Wd) = (30 \text{ x } 22.8^2 \text{ x } 80 \text{ x } \pi/180)/(1152 \text{ x } 4.5 + 756 \text{ x } 13) = 1.45$$

(2) water depth zero

The weight of zone ABGF becomes W_1 = 144 x 18 = 2592 kN/m. Applying (10.15) yields

$$F = (30 \text{ x } 22.8^2 \text{ x } 80 \text{ x } \pi/180)/(2592 \text{ x } 4.5 + 756 \text{ x } 13) = 1.01$$

(3) effect of a crack and hydraulic thrust

The depth of a tension crack is determined with (10.14b), which yields $z_c = 2c_u/\gamma = 2 \text{ x } 30 / 18 = 3.3$ m. The hydraulic thrust becomes $P = \gamma_w z_c^2/2 = 10 \text{ x } 3.3^2/2 = 54.5$ kN/m, and the lever arm is $z_P = 10 + 2 \text{ x } 3.3/3 = 12.2$ m. Applying (10.15) yields for case 1

$$F = (30 \text{ x } 22.8^2 \text{ x } 80 \text{ x } \pi/180)/(1152 \text{ x } 4.5 + 756 \text{ x } 13 + 54.5 \text{ x } 12.2) = 1.39$$

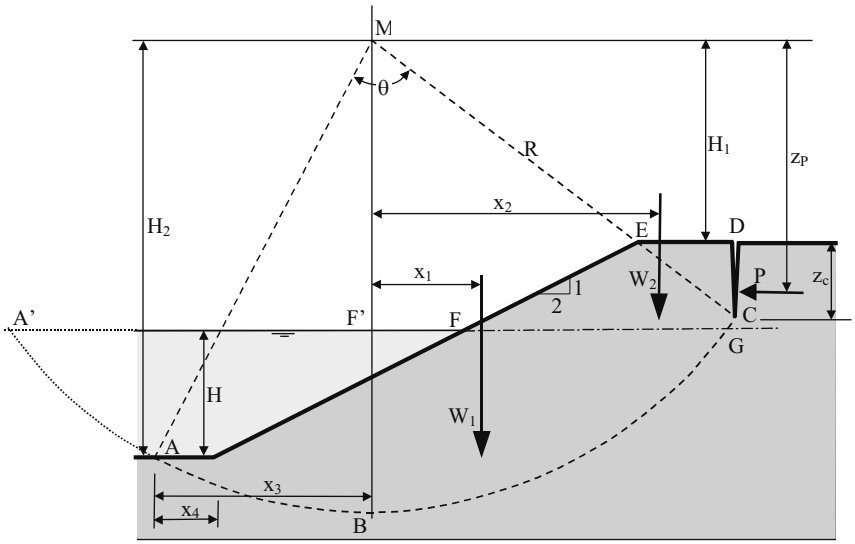

Figure 10.10

PROPERTIES

c_u	30 kPa		H_1	20 m
γ	18 kN/m^3		H_2	10 m
γ_w	10 kN/m^3		H	6 m
$Area_{ABGF}$	144 m^2		x_1	4.5 m
$Area_{GCDEF}$	42 m^2		x_2	13 m
θ	80°		x_3	11 m
R	22.80 m		x_4	3 m

Remark

For a partly submerged slope, the water pressure at the slope forms a contribution to the resistance moment. This is accounted for by considering the fact that the water weight of section A'BF' balances that of section BGF' (see Fig 10.10). Therefore, by excluding in the driving moment of the water in soil under the free water level, i.e. ABGF, accounts for the water pressure effect at the slope. Hence, taking the submerged unit weight $\gamma - \gamma_w$ for that zone incorporated this. For the remainder, the saturated soil above the free water level, the total unit weight applies. This is done in case 1. Case 2 shows that when the water level drops, the water pressures at the slope vanish, and the stability factor decreases significantly.

application 10.3

The stability factor of a translational slide of a slope, from which groundwater flows out under angle θ, is $F = (\tan\varphi / \tan\beta)(1 - (\gamma_w/\gamma)(\chi \tan(\beta)\tan(\beta+\theta) + 1)$. If the soil is isotropically permeable $\chi = 1$, then, F seems independent of the permeability. Explain why that is correct.

application 10.4

Water is seeping out of a slope which consists of horizontal thin clay and sand layers (sandwich structure). Observation shows that the actual slope angle 15.5° is just stable. Find an expression for the apparent volumetric soil weight γ (in kN/m^3) of the soil as function of the average internal friction angle φ, assuming isotropic permeability. Make a sketch of the graph. With an easily obtainable estimate of the soil weight a reasonable value for φ can be found. For example, what is φ if the wet unit soil weight is 16 kN/m^3?

application 10.5

A certain slope at an angle of 25° is stable under dry conditions. The soil volumetric weight is 19 kN/m^3. What is the reduction in the stability factor when after heavy rain the water stored in the dike and is flowing horizontally out of the slope? Assume an anisotropy factor of $\chi = 1$.

application 10.6

A long slope of a saturated soil layer of 5 m thick is just stable at 45°. The wet unit weight is 19 kN/m^3 and the friction angle $\varphi = 41°$. What is the cohesion? Does the stability factor F change when the soil becomes submerged?

application 10.7

Is Taylor's diagram for circular slip stability an upper or a lower limit approach? Indicate how you argue your answer. What additional safety factor do you recommend?

application 10.8

In Fig 10.2, the pore pressure field u increases linearly with η. However, the flow field is directed not along the η axis but at an angle θ to the horizontal. Explain the apparent discrepancy.

11 STABILITY OF EARTH-RETAINING STRUCTURES

Earth-retaining structures support vertical or near-vertical faces of a ground-surface profile. Horizontal soil pressures and groundwater pressures will act on these structures. To reduce groundwater pressure build-up (e.g. rain) proper drainage facilities are required. If a retaining wall is caused to move towards the supported soil, the horizontal pressures will increase. They are then referred to as passive pressures. If the wall moves away from the soil, horizontal pressures decrease, and are referred to as active pressures. If the wall does not move, the horizontal pressures are said to be at-rest (or neutral). The stress state can be expressed in terms of the coefficient of earth pressure, i.e. the ratio σ_h'/σ_v', and one distinguishes K_p for passive, K_a for active, and K_0 for neutral stress states. In Chapter 7 the expressions for K_i are elaborated. Only small horizontal deformations, in the order of 0.1% to 1% of the height, are sufficient to invoke an active or passive state. In practice, such deformations are quite possible.

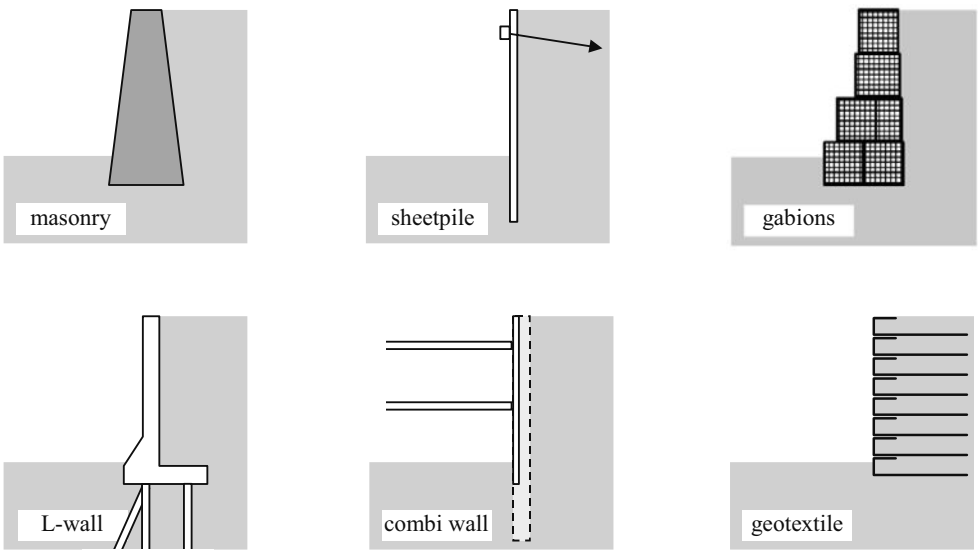

gravity walls *embedded walls* *reinforced earth*

Figure 11.1 Types of earth retaining structures

Four types of earth-retaining structures are considered in this chapter: gravity walls, embedded walls, slurry walls, and reinforced earth walls. Three of them are shown in (Fig 11.1). The stability of gravity walls depends largely on their own weight (massive walls) or on the supporting soil weight (crib walls, L-walls, T-walls, etc.). In principle, gravity walls are stiff, enforcing a rather uniform stress state, either passive, active or neutral. Embedded walls consist of driven or placed sheets or piles, which may be freestanding (cantilever wall), anchored or strutted. In principle, embedded walls are more flexible, inducing a varying stress state, depending on local deformation. Reinforced earth walls obtain their stability from inserted reinforcements, such as strips, geotextile, gabions, nails, injection or

ground anchors. For a proper behaviour the reinforcement must fit the soil type and state (compacted). A new potential method to strengthen soils uses biotechnology (cementation by bacteria), see Chapter 13.

One can imagine that there are many ways to determine the stability, since the earth-retaining structure may be stiff or flexible, the soil may be undrained or drained, and the soil-structure interface may contribute by (positive or negative) friction. Three methods are discussed: Coulomb's method for solid walls, Blum's method for sheet-pile walls, and stability aspects of soils reinforced by strips. For other structures, reference is made to codes of practice and literature.

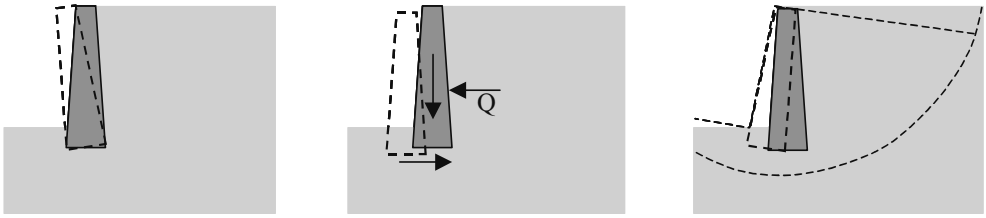

Figure 11.2 Some failure modes of gravity walls

A GRAVITY WALLS

The state of the wall itself has first to be checked, i.e. forward sliding, bearing capacity at the base, settlement, tension failure in joints, and total rotational sliding (Fig 11.2). The horizontal thrust Q has to be provided by the wall weight induced friction at the foot. A common safety factor for these failure modes is 1.5.

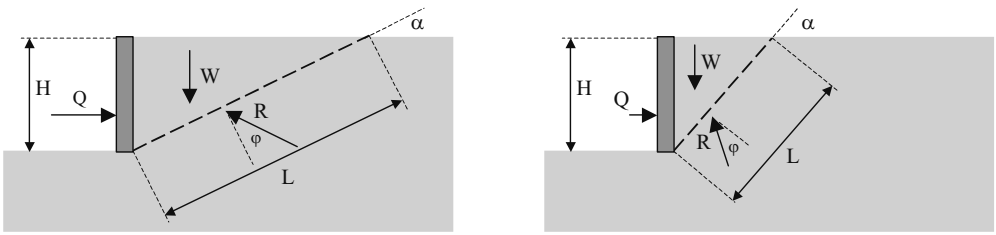

(a) passive state *(b) active state*

Figure 11.3 Coulomb's method

The horizontal soil pressure at gravity walls can be determined by the stability analysis after Coulomb that assumes dry cohesion-less soil and a straight slip surface (Fig 11.3). Equilibrium in horizontal and vertical direction yields $Q = R\sin(\alpha \pm \varphi)$ and $W = R\cos(\alpha \pm \varphi)$, and with $W = \gamma H^2/2\tan\alpha$, one obtains $Q = \gamma H^2 \tan(\alpha \pm \varphi) / 2\tan\alpha$. The plus sign in the equations refers to the passive state and the minus sign to the active state. Coulomb showed that the most unfavourable position of the slip surface can be found by posing $dQ/d\alpha = 0$. The solution is $\alpha = (\pi/4 \pm \varphi/2)$ and the corresponding thrust becomes

$$Q = \tfrac{1}{2}\gamma H^2 \tan^2(\pi/4 \pm \varphi/2) = \tfrac{1}{2}\gamma K_i H^2 \qquad (11.1)$$

When cohesion is involved, it can be shown that (11.1) becomes

$$Q = \tfrac{1}{2}\gamma K_i H^2 \pm 2cH\sqrt{K_i} \qquad (11.2)$$

Here, $K_i = K_p$ refers to the passive state, and $K_i = K_a$ to the active state, similar to equations (7.5). It should be noted that the horizontal thrust on an earth-retaining wall for an active state is only obtained when the wall allows the soil to lean on by its own. If this is not possible (not permitted because of restrictions on deformation), the thrust will be larger, which has to be considered in the design.

For rough walls Coulomb's theory of straight slip lines does not apply. The same counts for Rankine's theory (see Fig 7.4). For a plastic zone of soil, in which everywhere the limit state occurs, i.e. in every point the stress state is such that the corresponding Mohr circle touches the failure line: $\tau = c + \sigma \tan\varphi$ [47], equilibrium conditions can be elaborated along the direction of slip lines, the *s-r* system (see Fig 11.4a and Fig 11.4b). A new variable is introduced

$$\sigma_0 = \sigma + c/\tan\varphi \qquad \text{and} \qquad \tau = \sigma_0 \tan\varphi \qquad (11.3)$$

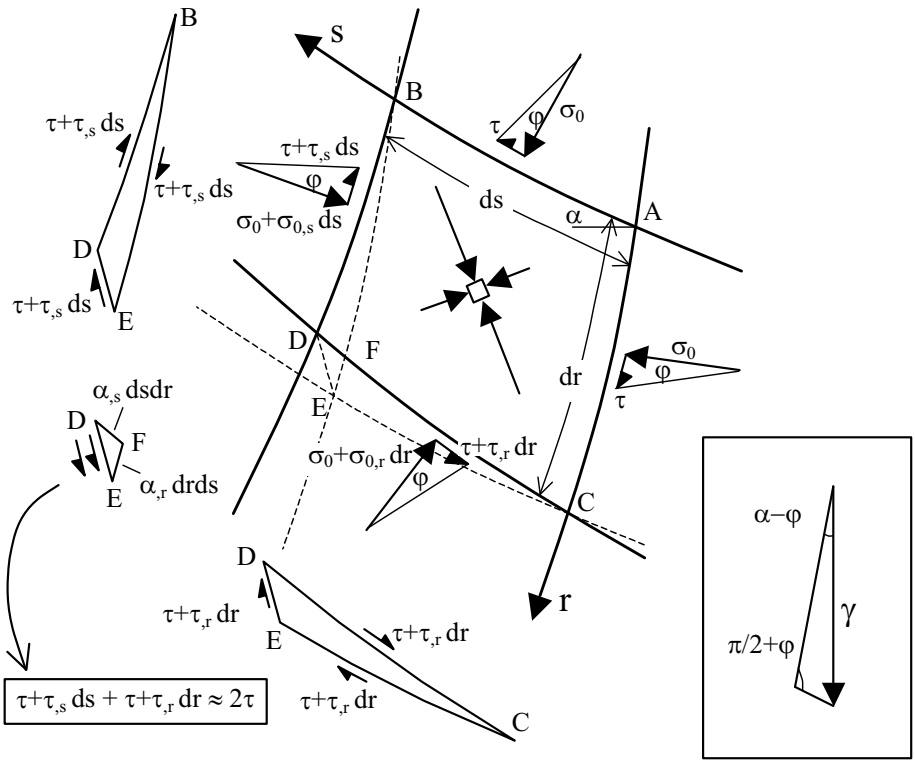

Figure 11.4a Curved slip lines or characteristic lines

[47] Note, that the formula refers to effective stresses; the dash has been omitted for convenience.

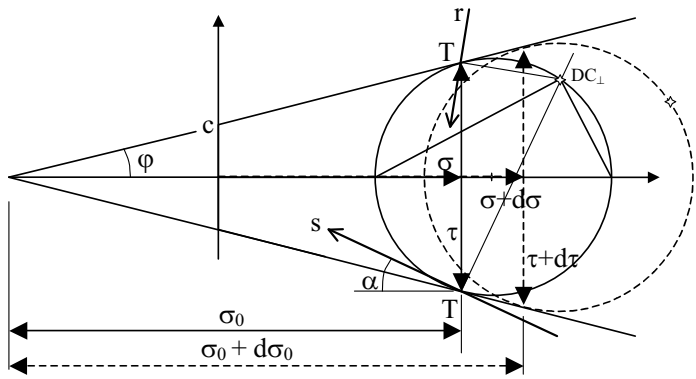

Figure 11.4b Stress states in the Mohr-Coulomb diagram

Consider an elementary curved volume in this system with normal and shear stresses and their increments, shown in Fig 11.4a. The effect of shear increments on surface BD and CD is covered by the shear stress working on ED, and components of this residual shear stress (2τ) are accounted for in the *s*- and *r*-direction. Then, equilibrium yields (note, $\tau_{,s}$ expresses $d\tau/ds$, etc.)

$$\sigma_{0,s}\, dsdr + 2\tau\, \alpha_{,s}\, dsdr + \gamma dsdr \sin(\alpha-\varphi)/\cos\varphi = 0$$

$$\sigma_{0,r}\, dsdr - 2\tau\, \alpha_{,r}\, dsdr + \gamma\, dsdr \cos\alpha/\cos\varphi = 0$$

Introducing (11.3) yields the equations of Kötter

$$\sigma_{0,s} + 2\sigma_0 \tan\phi\, \alpha_{,s} + \gamma \sin(\alpha-\varphi)/\cos\varphi = 0 \qquad \text{along direction } s \qquad (11.4a)$$

$$\sigma_{0,r} - 2\sigma_0 \tan\phi\, \alpha_{,r} + \gamma \cos\alpha/\cos\varphi = 0 \qquad \text{along direction } r \qquad (11.4b)$$

Disregarding the specific weight ($\gamma = 0$) equations (11.4) become for a cohesive soil ($\varphi = 0,\ c = c_u$)

$$\sigma_{,s} + 2c_u\alpha_{,s} = 0 \quad \text{or} \quad \sigma + 2c_u\alpha = C_s \qquad \text{along direction } s \qquad (11.5a)$$

$$\sigma_{,r} - 2c_u\alpha_{,r} = 0 \quad \text{or} \quad \sigma - 2c_u\alpha = C_r \qquad \text{along direction } r \qquad (11.5b)$$

These equations form a set of hyperbolic partial differential equations. Their solution contains so-called characteristic lines, i.e. slip lines, with changing angle α and rotating principal stresses. The same holds for drained soils ($\varphi \neq 0$), graphically shown in Fig 11.4a and Fig 11.4b.

In some cases, e.g. when there is no friction at the border of a failing zone (Rankine stress, Chapter 8), the slip lines are straight. Soil-wall friction (at the border) causes curving slip lines; some examples are shown in Fig 11.5.

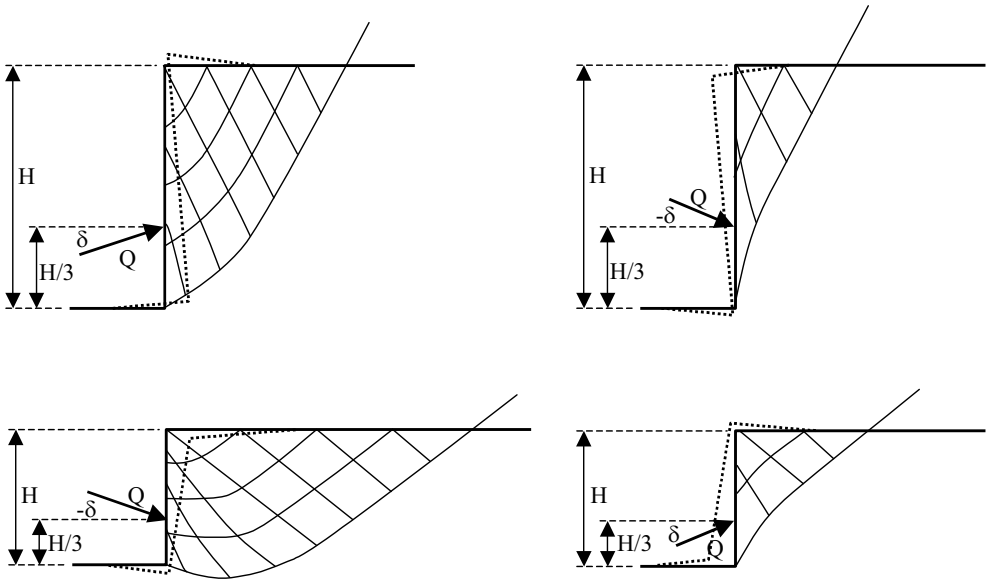

(a) passive states *(b) active states*

Figure 11.5 Curved slip lines for a rough wall +δ: the soil rises, -δ: the soil settles

Theoretical and experimental studies support the conclusion that values of active earth pressures, the lowest horizontal thrust, using Coulomb's theory, are on the safe side and only slightly deviate from results obtained by more refined methods, but values of passive earth pressure, the highest horizontal thrust, can be much higher due to wall friction. In practical guidelines one may find tables with earth pressure coefficients K_i, which incorporate cohesion, wall friction, soil weight and surface loads, and inclined surfaces.

B EMBEDDED WALLS

Embedded walls are usually installed in undisturbed soils and afterwards excavation at one side takes place. Such walls may be composed of hammered or vibrated driven sheet-piles, grouted or installed contiguous piles or slurry or diaphragm walls, acting as cantilever or supported by anchors or props (see Fig 11.1). In the stability analysis not their weight but their flexibility is essential, as embedded walls obtain support at the toe from passive resistance mobilised in the soil. Failure modes that need to be considered are rotation of the wall, slip of the anchor, buckling of the strut, excessive bending of the wall, excessive settlement behind the wall, bottom heave and overall slip failure (Fig 11.6). One may distinguish temporary and permanent structures. The latter should be designed more rigorously. Particular attention should be paid to groundwater pressures and leakage.

A freestanding (cantilever) sheet-pile wall obtains support by the depth of its embedment D. The assumption that the wall will rotate around a point B at depth d and that active and passive earth pressures will develop, as shown in Fig 11.7a, allows to define a stability factor F, according to

$$\gamma_0 F = \frac{\textit{passive moment}}{\textit{active moment}} = \frac{\frac{1}{2}\gamma K_p d^3/3}{\frac{1}{2}\gamma K_a (H+d)^3/3} = (K_p/K_a)/(1+H/d)^3 \qquad (11.6)$$

Here, cohesion is disregarded and γ_0 is the required safety factor at critical stability ($F = 1$). The earth-pressure coefficients K_p and K_a are defined in equation (7.5).

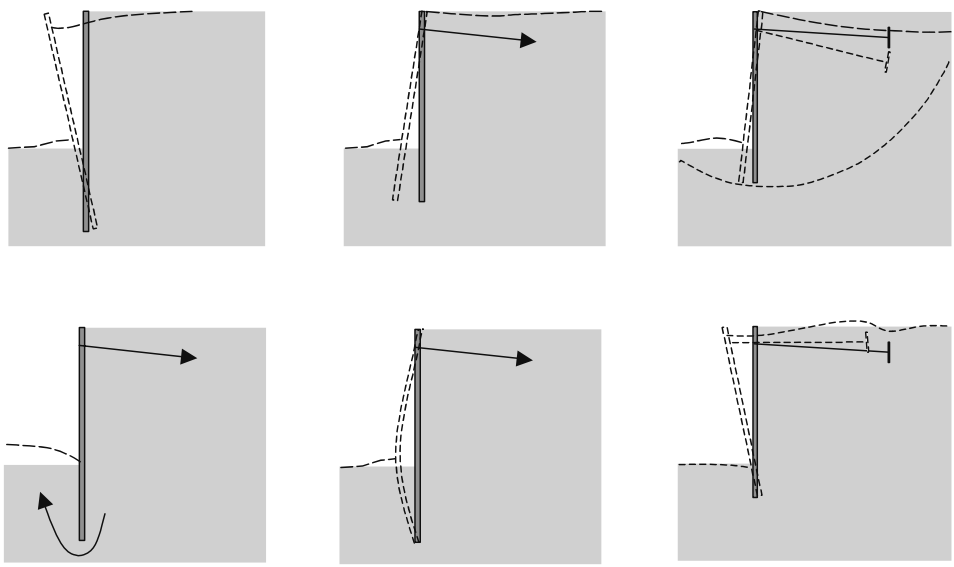

Figure 11.6 Some failure modes of embedded walls

Following Blum's approach, the contribution under the rotation point B is simplified to a force $P_B = e\,(K_p - K_a)\gamma H$, acting in the rotation point itself (a safe assumption), see Fig 11.7a. It does not affect the moments in equation (11.6). From (11.6) the value of d becomes

$$d = \frac{H}{\sqrt[3]{K_p/(\gamma_0 F K_a)} - 1} \qquad (11.7)$$

After some elaboration, horizontal equilibrium provides, including force P_B

$$e/d = \frac{\xi - (\xi/\gamma_0 F)^{2/3}}{2(\xi-1)(\xi/\gamma_0 F)^{1/3}} \qquad \text{with} \qquad \xi = K_p/K_a \qquad (11.8)$$

The required quality of the wall is determined by the maximum bending moment. The point z, measured from top, where the shear force in the sheet-pile wall is zero, and the corresponding maximum bending moment M_{max}, become, after some elaboration

$$z = H/(1-\xi^{-½}) \qquad \text{and} \qquad M_{max} = \gamma K_a z^2 H/6 \tag{11.9}$$

Usually, a safety factor of γ_0 =2.0 is applied. For a typical soil with γ = 19 kN/m^3, c = 0 and φ = 30° the ratio becomes $\xi = K_p/K_a$ = 9.0 (see equation 7.7). Then, for a stability factor F = 1 and a safety factor of γ_0 =2.0, equation (11.7) yields H/d = 0.65 and equation (11.8) yields e/d = 0.23, and the penetration depth becomes $D = d+e = 1.89H$. Applying (11.9), the point of maximum bending moment is at $z = 1.5H$ and $M_{max} = 0.238H$ KNm per metre width. Finally, for a given wall thickness and stiffness, the maximum lateral deflection at the wall top can be determined.

In practice, one applies e/d = 0.20, incorporating that Blum's approximation is at the safe side. Another method is applying a safety factor on the shear strength, i.e. $\tan\varphi_{mob} = (\tan\varphi)/\gamma_\varphi$. The corresponding earth-pressure coefficients K_p and K_a are adjusted, accordingly. One may include the wall friction, i.e. $\delta = ⅔\varphi_{mob}$ is taken for the active, and $\delta = ½\varphi_{mob}$ for the passive zone. Then, for the resulting penetration depth $D = d$ is applied, without extension e.

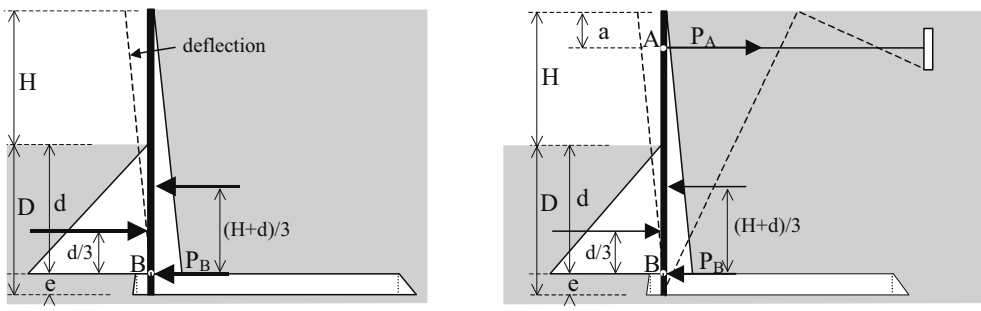

(a) cantilever wall *(b) anchored wall*

Figure 11.7 Blum's approach

Note, that for a cantilever wall the required penetration length is significantly more than retaining height H. Such wall is usually applied for supporting small excavations. By choosing a stiff wall the lateral deflections will remain small. In some cases a tension crack may be formed at the surface, which – when filled with water – may have an additional serious effect on the stability.

An anchor or a prop reduces the required length of a wall, and also the lateral deflection and bending moment. For anchored sheet-piles design the anchor force P_A is to be included (Fig 11.7b). Excluding the extra force P_B at the tip, the moment equilibrium around the anchor point A yields

$$\gamma_0 F = \frac{½\gamma K_p d^2 (H - a + 2d/3)}{½\gamma K_a (H+d)^2 (2(H+d)/3 - a)} \tag{11.10}$$

For a given safety factor, the penetration depth d can be determined iteratively from (11.10), and experience shows that d varies between 0.20H and 0.80H. Following Blum's approach, i.e. an extension of the penetration depth with zone e,

the deflections and bending moments will be reduced. The horizontal thrust P_B at the wall tip is to be included in the analysis. Then, the system needs an additional condition, which is, suggested by Blum, zero-displacement at the wall top. In case of groundwater pressures, earth pressures should be determined by considering effective soil stresses, and the groundwater pressure are included in the equilibrium analysis, separately.

In the previously discussed design method the theory of earth pressures related to the limit state (active and passive zones) has been applied, but in certain zones the displacement required to develop these horizontal earth pressures may not be realistic, and lower or higher pressures may occur. User-friendly and well-tested numerical calculation models are available that incorporate these effects and allow to make a proper design, covering different construction stages.

The anchorage system is an important aspect of the construction, and several systems are in use, such as a row of piles, a pile supported cap, grouted ground anchor, or an anchor plate or block (dead man), all equipped with tension rods or cables. It is important to locate anchors outside failure zones, as indicated by the dashed line (Fig 11.7b). The maximum anchor force is determined by evaluating the passive and active thrusts on the anchor plate. To avoid anchor-rod elongation effects, pretension may be applied. For the safety one usually applies a safety factor of 2.0.

C SLURRY WALLS

A slurry wall is a technique used to build reinforced-concrete walls in areas of soft earth close to open water or with a high groundwater table. This technique is typically used to build diaphragm (water-blocking) walls surrounding tunnels and open excavations, and to lay foundations (building pits). A trench is excavated to create a form for each wall. The trench is kept full of heavy slurry at all times. The slurry prevents the trench from collapsing by providing outward pressure which balances the ground pressures and prevents water flow into the trench. Reinforcement is then lowered in and the trench is filled with concrete, while displacing the slurry.

Excavation is done using a special clamshell-shaped digger (Fig 11.8) or a hydromill trench cutter. The excavator digs down to the design depth for the first cut. The excavator is then lifted and moved along a trench guide wall to continue the trench with successive cuts as needed. Once a particular length is reached, a reinforcing cage is lowered into the slurry-filled pit and the pit is filled with concrete from the bottom up using tremor pipes. The concrete displaces the bentonite slurry, which is pumped out and recycled. It is possible to incorporate H-beams or other structural steel elements into the freshly mixed soil, in accordance with requirements of the excavation. On

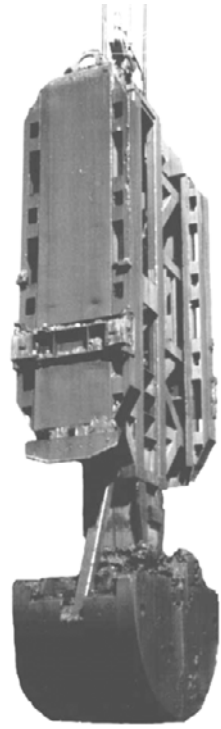

Figure 11.8 Digger

completion of concreting, digging within the now concrete wall-enclosed area can proceed. To prevent the concrete wall from collapsing into the newly open area, temporary supports such as tiebacks or thrusts are installed. Special care is required for the interconnections between successive panels and local soil intrusions. They can be traced by using monitoring techniques. Recent tests on 20-metre deep walls have shown that acoustics during construction is relatively cheap and reliable. A transmitter tube (50 kHz) and several receiver tubes near joints detect density changes which indicate improper inclusions in the concrete.

Slurry walls or cut-off trenches filled with cement-bentonite, soil-bentonite or plastic concrete may form a continuous barrier, and besides building pit walls they can also be used to limit the migration of liquid or gaseous contaminants, to allow a localised lowering of the water table or to stabilise existing and future slopes.

D REINFORCED WALLS

Earth slopes can be stabilised by the application of strips, mesh reinforcement (e.g. gabions), or soil nailing, and sometimes facing-plates are included (Fig 11.9a). It is used in retaining walls, quays, abutments, earthen dams, dikes and in temporary works. The construction is usually relatively easy and fast. The soil involved must be of suitable quality, i.e. moderate stiffness, low creep and allowing a proper connection with the reinforcement. The reinforcement should possess adequate strength, moderate (geotextile) to high stiffness (nails), low creep, proper durability and a good bond with soil. The facing plates or skin provide containment, prevent erosion, and may contribute to anchoring of the reinforcement. Grouting at anchors or facing may be added.

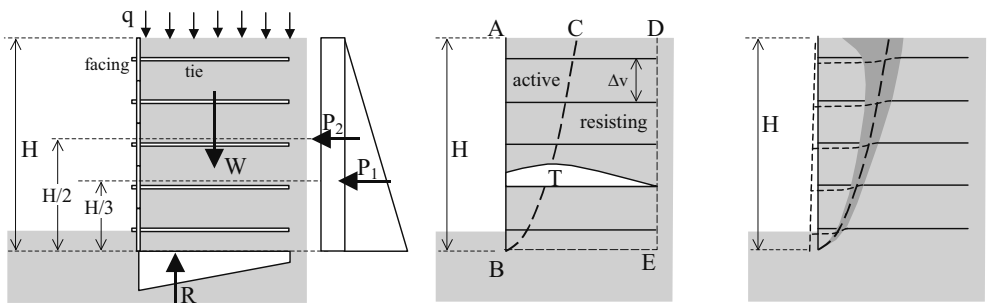

(a) external mechanical system (b) internal mechanical system (c) failure zone

Figure 11.9 Reinforced earth-retaining structures

Stability is improved by enhancing shear strength of a failure zone through compressive and tensile strains in the reinforcement. In some cases bending stiffness of the reinforcement contributes as well. In the design analysis the required forces in the reinforcement have to match allowable forces by using proper spacing and both internal and external stability must be checked. It should be noted that the development of the full shear resistance of the ties may require relatively large deformations. These residual deformations and subsequent creep should be acceptable.

The behaviour of a reinforced earth wall, constructed by subsequent layers of compacted soil of equal thickness in between reinforcement elements, shows, that tension T in the ties increases from the face (wall) to a maximum and then decreases with distance from the face. The loci of these maxima form a curved surface that separates the front part, called the active zone ABC, from the backside, which is considered stable and referred to as the resisting zone BCDE (Fig 11.9b). The tensile force T in a tie can be estimated (Schlosser) by stating that it must be able to resist the lateral pressure $\sigma_h' = K_a\sigma_v'$ in the active zone and that this force can be provided by the shear resistance (pulling out) of the tie in the resisting zone. If ties are interspaced by Δh horizontally and by Δv vertically, then stability factors can be defined, according to

$$\gamma_{yield} F_{yield} = f\, S_{tie} / (K_a \sigma_v' \Delta h \Delta v) \qquad (11.11a)$$

$$\gamma_{pullout} F_{pullout} = f\, A_{tie} L_r \tan\delta / (K_a \sigma_v' \Delta h \Delta v) \qquad (11.11b)$$

Here, f is the yield strength, S and A are the cross-section and perimeter of the tie, δ the angle of friction between the tie and the soil, and L_r the length of the tie in the resisting zone. Typical values for the safety factor are γ_{yield} = 1.5 and $\gamma_{pullout}$ = 2.0. Using ribbed strips and/or grout can raise the friction significantly. In addition, for stiff rods the bending moment and the shear force in the failure zone should be considered (Fig 11.9c). The saturation degree may influence the soil-tie friction. In practice, standard codes (NEN 3650 pipelines) are applied for designing stiff rods. For the vertical stress one usually applies $\sigma_v' = \gamma z$. This is on the safe side, as a higher stress (R: trapezoidal stress at the base) may be acting because of the overturning moment due to the earth pressures $P_1 = ½K_a\gamma H^2$ and $P_2 = K_a\, qH$ against the backside of the wall structure. Groundwater pressures have to be dealt with separately; their effect can be reduced by proper drainage facilities.

application 11.1

Consider the case of a vertical rough earth retaining wall (Fig 11.10), which supports an undrained cohesive soil mass (φ = 0, $\tau_{max} = c_u$). The value of the horizontal thrust P_a is required. A plane failure surface is assumed ending at the tip D of a tension crack CD at depth z_0, filled with water. The equilibrium of the wedge ABDC includes the following forces: weight $W = ½\gamma(H^2 - z_0^2)\cot\alpha$, normal force N_s on the slip plane, shear force at the slip plane $T_s = (H - z_0)c_u/\sin\alpha$, active thrust on the wall P_a, friction force along the wall $T_f = c_f(H - z_0)$, and the hydraulic thrust in the crack $P_w = ½\gamma_w z_0^2$. The coefficient c_f represents the soil-wall adhesion, which may vary depending on the soil stiffness. The equilibrium of the wedge ABDC is expressed by

$$N_s\cos\alpha = W - T_s\sin\alpha - T_f \quad \text{and} \quad P_a - P_w = N_s\sin\alpha - T_s\cos\alpha$$

and so $$P_a - P_w = W\tan\alpha - T_s(\sin\alpha\tan\alpha + \cos\alpha) - T_f\tan\alpha$$

Inserting the values of the forces yields

$$P_a - P_w = \tfrac{1}{2}\gamma(H^2 - z_0^2) - c_u(H - z_0)((1 + c_f/c_u)\tan\alpha + \cot\alpha)$$

Putting $\partial P_a/\partial\alpha = 0$ yields an optimum value of α. Elaboration yields

$$(1 + cf/cu)\partial(\tan\alpha)/\partial\alpha = -\partial(\cot\alpha)/\partial\alpha = -\partial(1/\tan\alpha)/\partial\alpha = \tan^{-2}\alpha\,\partial(\tan\alpha)/\partial\alpha$$

and so $\tan\alpha = (1 + c_f/c_u)^{-0.5}$

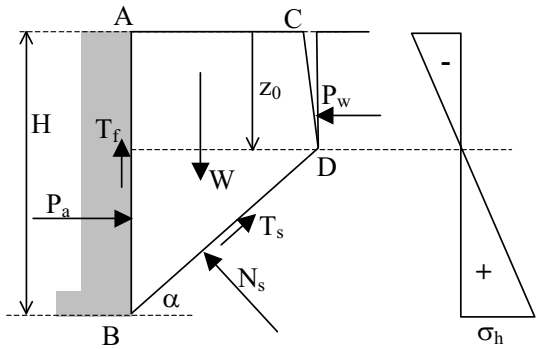

Figure 11.10

Substituting this value in the expression of P_a yields

$$P_a - P_w = \tfrac{1}{2}\gamma(H^2 - z_0^2) - 2c_u(H - z_0)(1 + c_f/c_u)^{0.5}$$

Hence, the lateral active pressure at given depth z becomes (above $z = z_0$ no effect of wall friction)

$$\sigma_h = \gamma z - 2c_u$$

At the tip of the crack $z = z_0$ the horizontal stress is zero, and therefore

$$z_0 = 2(c_u/\gamma)$$

For a wall height of $H = 8$ m, soil weight of $\gamma = 18.5$ kN/m^3, undrained strength $c_u = 30$ kPa, and adhesion $c_f = 0.5c_u$, one may find

$$\alpha = \text{atan}(1/\sqrt{(1+0.5)}) = 39.2^\circ$$

$$z_0 = 2\text{x}30/18.5 = 3.24 \text{ m}$$

$$P_w = \tfrac{1}{2}\,10\,(3.24)^2 = 52.49 \text{ kN/m}$$

$$P_a = \tfrac{1}{2}18.5\,(8^2 - (3.24)^2) - 2\text{x}30\,(8 - 3.24)\sqrt{(1+0.5)} + P_w =$$

$$= 145.11 + 52.49 = 197.60 \text{ kN/m}$$

In this case, the water in the crack adds to the active thrust for 36%. When retaining walls do not fulfil stability requirements, it is usually not because the earth pressures are inadequate, but rather because often drainage measures are (or become) ineffective.

application 11.2

Consider a stiff combi-wall which forms the side of a building pit; its length is 17 m (see Fig 11.11). A strut with horizontal force *F* is pushing against this wall, every 5m (the strut's interspace distance). Sunshine on this strut may cause extension, which can increase the force drastically. Sketch the distribution of induced horizontal stresses on the wall. Calculate the maximum value of *F*. The soil weight is γ = 18 kN/m^3, φ = 35°, c = 0.

Advice: Assume rotation point at B. Find *F* by moment around B and find F from the horizontal equilibrium. The answers may differ slightly; in fact the rotation point is a little higher.

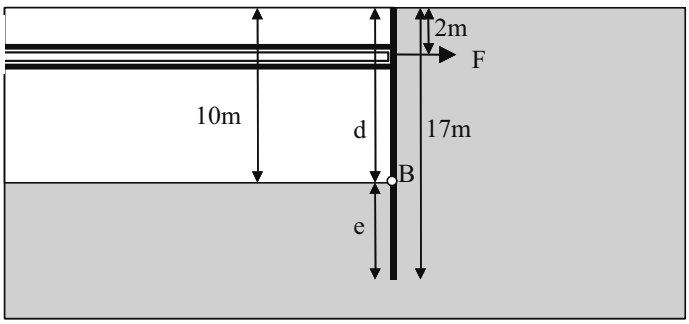

Figure 11.11

application 11.3

Does the method used in application 11.2 lead to an upper or lower limit?

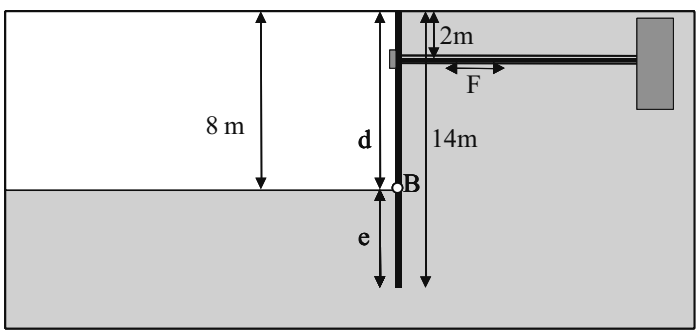

Figure 11.12

application 11.4

Consider a stiff wall which forms the side of a building pit; its length is 14 m (see Fig 11.12). An anchor, every 5m, keeps the wall on its place. At a certain moment the anchor is prestressed, which induced the anchor force F. Sketch the distribution of induced horizontal stresses on the wall. Calculate the value of F. The soil is characterised by $\gamma = 16$ kN/m^3, $\varphi = 30^o$, $c = 0$.

Advice: Assume rotation point at B and a rigid wall. Determine the horizontal earth pressures at the wall when allowing for a small rotation of the wall. Find F by considering the moment around B or by horizontal equilibrium (answers may differ; in fact the rotation point is a little higher).

application 11.5

A combi-wall is popular for building pits. A concept design is handed over without much details (see Fig 11.13). The sheet piling is a Larsson 22. What will happen when the free water suddenly drops by 3 m? Is the design robust?

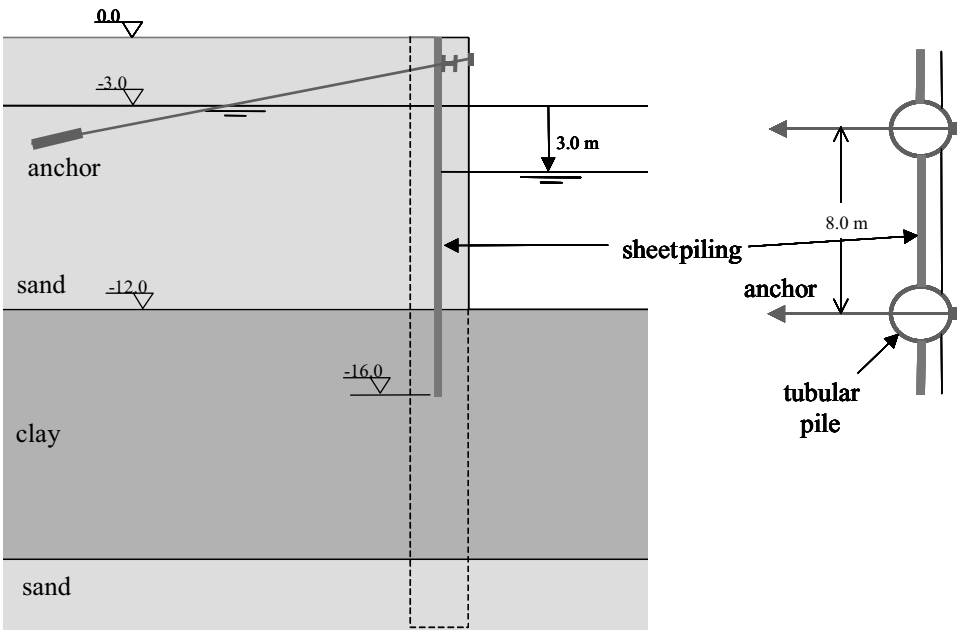

(a) vertical cross-section *(b) helicopter view*

Figure 11.13 A combi-wall

application 11.6

In Fig 11.7b a stress diagram is presented caused by an anchored rigid embedded wall. Sketch the stress diagram, if the anchor is prestressed. How much does the stability factor change because of prestressing?

application 11.7

Which of the situations in Fig 11.5 has for similar height H and soil characteristics the highest thrust Q? What will happen if the direction of this thrust is more inclined than the inclination δ?

12 FOOTINGS AND PILE FOUNDATIONS

Foundations form the interface through which structural loads are transmitted to the subsoil. In this chapter, the functioning of footings and single pile foundations will be considered in more detail. The behaviour of a foundation depends on the interaction with the structure, which it carries, and the nature of the soil in which it stands. A foundation should give sufficient bearing capacity and limited flexibility, i.e. limited settlements or other movements. It should be at a suitable depth, not vulnerable to climate changes etc., and (shear) failure should be avoided. For normal buildings 0.04 m (sand) to 0.06 m (clay) is reasonable[48] and differential settlements should be not more than 50% of these. A common overall safety factor is between 2 to 3.

A BEARING CAPACITY OF FOOTINGS

Footings, also referred to as shallow or spread foundations, include isolated slabs or pads, strip footings and rafts; their width is typically larger than their height. The ultimate bearing capacity of footings is found when a potential slip pattern or a continuous plastic zone has developed. Consider a simple example, where a strip loading with width B acts on undrained subsoil ($\varphi = 0$, $|\tau| \leq c_u$). An admissible stress field, in equilibrium and everywhere at yield, is composed of a vertical zone of width B under the strip loading with principal stresses according to $(\sigma_v, \sigma_h) = (4c_u, 2c_u)$ and the soil zones outside with $(\sigma_v, \sigma_h) = (0, 2c_u)$, see Fig 12.1a. Hence, if the loading is $q = 4c_u$, this stress field satisfies the boundary conditions. The ultimate bearing capacity is therefore $4c_u$. It is a lower limit; the real bearing capacity of the soil could be higher.

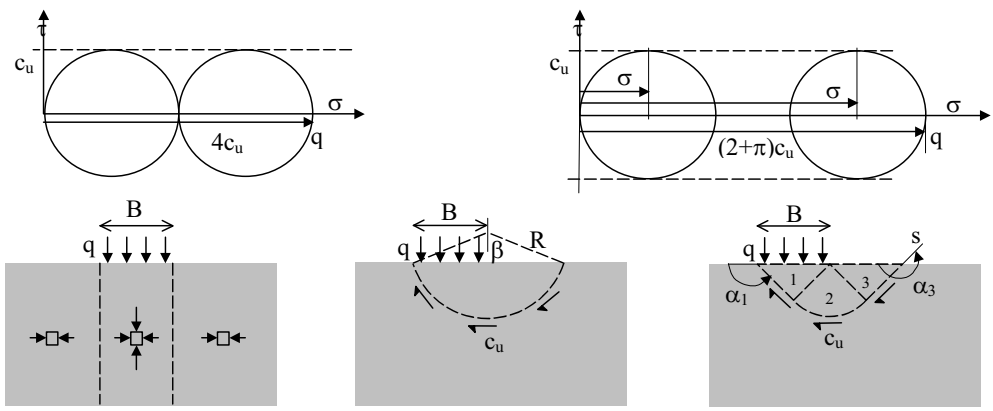

(a) admissible stress field *(b) potential failure mode* *(c) Prandtl's solution*

Figure 12.1 Ultimate bearing capacity for a strip loading on undrained soil

[48] In practice, maximum settlements of 0.15 to 0.20 is used for high-rise buildings.

Next, consider a potential failure mechanism in the form of a circular slip surface (Fig 12.1b), i.e. a kinematically admissible field. The work performed for a small rotation θ yields for the ultimate state: $\frac{1}{2} qB^2\theta = 2c_u R^2\beta\theta$. With $B = R\sin\beta$ it gives the ultimate load $q = 4c_u\beta/\sin^2\beta$, which attains a minimum for $\beta = \frac{1}{2}\tan\beta$ giving $\beta = 1.166$ radials = 66.8°. The corresponding load is then $q = 5.52c_u$. This is an upper limit; the real bearing capacity of the soil is probably lower. Thus, the real bearing capacity for a strip loading satisfies

$$4c_u < q < 5.52c_u \tag{12.1}$$

Prandtl and Reissner suggested a more comprehensive approach where the plastic area is composed of three zones; zone 1 and 3 according to a Rankine state (see Fig 7.4) and zone 2 a circular plastic wedge (Fig 12.1c). Kötter's equation for undrained soil along the *s*-direction (slip line), according to equation (11.5a), yields

$$\sigma_1 + 2c_u\alpha_1 = \sigma_3 + 2c_u\alpha_3 \qquad \text{or}$$

$$\sigma_1 = \sigma_3 + 2c_u(\alpha_3 - \alpha_1) = c_u + 2c_u(\tfrac{5}{4}\pi - \tfrac{3}{4}\pi) = (1+\pi)c_u \tag{12.2}$$

Here, σ_i represents normal stress related to the failure point of the corresponding Mohr's circle in zone *i*. The ultimate bearing capacity becomes (see Fig 12.1c)

$$q = (1+\pi)c_u + c_u = 5.14c_u \tag{12.3}$$

It can be shown that this represents both a lower limit and an upper limit; it is the real bearing capacity. Unfortunately, the example is one-of-a-kind; other similar illustrative solutions are scarce.

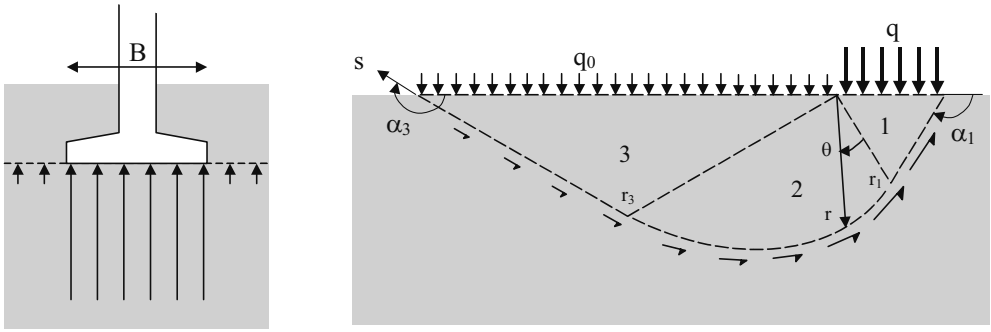

Figure 12.2a Ultimate bearing capacity for strip loading on drained soil

A similar analysis is elaborated in Fig 12.2a for drained soil ($\varphi = 30°$, $c > 0$); in principle, although not indicated, the stresses are effective stresses. Zone 1 is an active Rankine state with *s*-direction $\alpha_1 = \pi - (\frac{1}{4}\pi + \frac{1}{2}\varphi)$ and loaded with *q*, zone 3 a passive Rankine state with *s*-direction $\alpha_3 = \pi + ((\frac{1}{4}\pi - \frac{1}{2}\varphi)$ and loaded with q_0 (the weight of the soil on top of it), and zone 3 is a plastic wedge, the lower border of which is a spiral $r/r_1 = e^{\theta\tan\varphi}$, and thus: $r_3/r_1 = e^{\frac{1}{2}\pi\tan\varphi}$. The spiral is found by

considering the fact that the angle between s-direction and r-direction (radial) is constant, i.e. $\frac{1}{2}\pi + \varphi$.

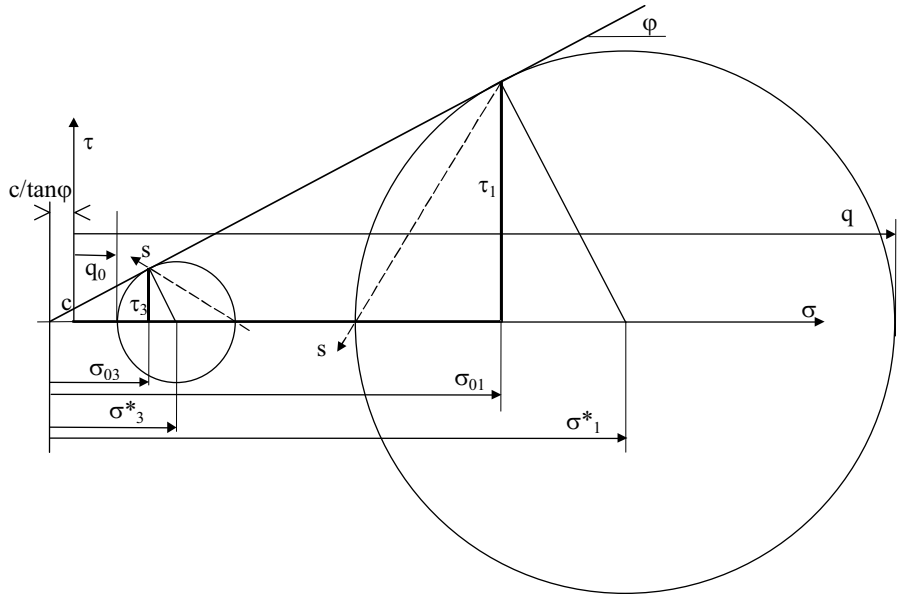

Figure 12.2b Stress state

Kötter's equation for drained soil along the s-directions, according to equation (11.4a), becomes (the soil weight of the plastic zone has been disregarded)

$$\sigma_{0,s} + 2\sigma_0\, \alpha_{,s} \tan\varphi = 0 \qquad \text{or} \qquad (\ln\sigma_0 + 2\alpha \tan\varphi)_{,s} = 0 \tag{12.4}$$

Integration yields

$$\ln\sigma_0 + 2\alpha \tan\varphi = C_s \qquad \text{in the s-direction} \tag{12.5}$$

From zone 1 to zone 3 this gives

$$\ln\sigma_{01} + 2\alpha_1 \tan\varphi = \ln\sigma_{03} + 2\alpha_3 \tan\varphi \qquad \text{or} \qquad \sigma_{01}/\sigma_{03} = e^{2(\alpha_3 - \alpha_1)\tan\varphi} \tag{12.6}$$

With $\alpha_3 - \alpha_1 = \pi/2$, $q + c/\tan\varphi = \sigma^*_1 (1+\sin\varphi)$ and $q_0 + c/\tan\varphi = \sigma^*_3 (1-\sin\varphi)$, see Fig 12.2b, keeping in mind that $\sigma_{01}/\sigma_{03} = \sigma^*_1/\sigma^*_3$, this provides the ultimate bearing capacity

$$q = N_q q_0 + N_c c \tag{12.7a}$$

$$\text{with} \qquad N_q = \frac{1+\sin\varphi}{1-\sin\varphi}\, e^{\pi \tan\varphi} \qquad \text{and} \qquad N_c = (N_q - 1)/\tan\varphi \tag{12.7b}$$

For the present case, with $\varphi = 30^o$, the bearing capacity factors become $N_q = 18.4$ and $N_c = 30.1$. In reality, the specific soil weight γ affects the pattern of slip

lines. No exact solutions including the soil weight are available. In practice, one adds in (12.7) a weight term, after Terzaghi, according to (B is the width of the footing)

$$q = N_q q_0 + N_c c + N_\gamma \gamma B \qquad (12.8)$$

For the bearing capacity factor N_γ empirical expressions are in use, e.g. $N_\gamma = 1.8(N_q-1)\tan\varphi$ (Brinch Hansen) or $N_\gamma = (N_q-1)\tan(1.4\varphi)$ (Meyerhof). In literature one may find tables with bearing capacity factor values for different situations, e.g. inclined loading, and various geometries of the loaded base.

A generalization of (12.8) for drained soils is

$$q = i_q s_q N_q q_0 + i_c s_c N_c c + i_\gamma s_\gamma N_\gamma \gamma B \qquad (12.9)$$

Here, the i-coefficients reflect inclined loading situations and the s-coefficients the shape of the foundation. The latter reflect that the previous theory of slip lines is applicable for two-dimensional situations only. The shear resistance in three-dimensional cases is usually larger, because the ratio between slip surface and slip volume is larger than in two dimensions. Table 12 shows the formulae of EC7.

TABLE 12.1a SHAPE FUNCTIONS, VERTICAL

shape	*Square or circle*	*rectangular B*L (B<L)*
s_q	$1 + \sin\varphi$	$1 + (B/L)\sin\varphi$
s_c	$(s_q N_q - 1)(N_q - 1)$	$(s_q N_q - 1)(N_q - 1)$
s_γ	0.7	$1 - 0.3(B/L)$

TABLE 12.1b SHAPE FUNCTIONS, INCLINED (COMPONENTS F_H AND F_V)

case	*F_H directed along B*	*F_H directed along L*
i_q	$(1 - 0.7\, F_H/(F_V + BLc/\tan\varphi))^3$	$(1 - F_H/(F_V + BLc/\tan\varphi))^3$
i_c	$(i_q N_q - 1)(N_q - 1)$	$(i_q N_q - 1)(N_q - 1)$
i_γ	$(1 - F_H/(F_V + BLc/\tan\phi))^3$	$(1 - F_H/(F_V + BLc/\tan\phi))^3$

For undrained soils (12.8) is generalised to

$$q = q_0 + i_c s_c (2 + \pi) c_u \qquad (12.10a)$$

with $s_c = 1 + 0.2(B/L)$ and $i_c = ½\,(1 + (1 - (F_H/BLc_u)^{½})$ (12.10b)

Beside the ultimate bearing capacity the allowable loading also depends on the deformation or stiffness, the serviceability limit state (SLS). Short-term and long-term behaviour may involve different mechanisms and the stiffness of the structure being supported may cause a redistribution of the loading on the separate foundation elements, which sometimes makes the situation more critical. The

groundwater plays a specific role, i.e. some soils swell and not necessarily uniformly, and rising groundwater decreases the bearing capacity. To establish the allowable bearing capacity special in-situ testing methods are in use, e.g. plate bearing test, California Bearing Ratio test (CBR), standard penetration test (SPT), and the cone penetration test (CPT), see Chapter 3.

B BEARING CAPACITY OF PILE FOUNDATIONS (ULTIMATE LIMIT STATE)

Piles are structural elements composed of timber, concrete and/or steel, which transmit a load Q to the soil, by skin friction (floating pile) and/or the pile point (end-bearing). The load can be vertical, horizontal, or inclined, either compressive or tensile (tension pile). Buckling of an installed slender pile is prevented by adjacent soil support, but offshore, when a pile reaches to the sea bottom, over the free-standing part buckling has to be considered. Timber piles, already in use for centuries, with a load capacity of 100 to 250 kN and a length of 10 to 25 m, are relatively cheap, well preserved under groundwater level, best suited as friction pile but vulnerable under hard driving conditions. Steel piles may carry 300 to 1000 kN with practically unlimited length, best suited as end-bearing pile, easy to splice but vulnerable to corrosion. Steel pipe piles, sometimes filled with concrete against bending, may carry 10 MN and more. Precast prestressed concrete piles, with a load capacity of 300 to 8000 kN and a length of 20 to 30 m, are not easy to splice, relatively expensive but resistant to hard driving conditions. Cast in-situ concrete piles may reach 10 to 25 m and carry up to 1000 kN. Here, quality control during construction is a major concern.

There are many different installation methods, e.g. driving by percussion (hammer blows), vibrating, drilling, casing, boring, grouting, jacking, and jetting, which all have their specific effect on the bearing capacity. In the case of pile groups and pile rafts the mutual interaction of piles during installation and during functioning has to be taken into account (Randolph, Katzenbach).

Pier foundations and caisson foundations are more or less similar to piles, but their way of installation is different. The soil at the toe is removed through the inside, and the foundation sinks gradually by its weight. This is a very old method, used to make water wells and e.g. the famous monument for queen Mumtaz, the Taj Mahal, situated on soft river sediments, is founded on this type of foundation (see Chapter 1).

Methods for estimating the bearing capacity of piles can be divided into analytical methods (stress state), on pile load testing, or on empirical methods based on in-situ measurement such as CPT. Sophisticated numerical methods are in development and not in use in practice, because numerical methods do not cover the effects of pile installation to the soil condition with proper accuracy.

Analytical approach

For an estimate of the ultimate end-bearing capacity Q_e of a pile wall with width B, length L and depth H a slip mechanism is elaborated (for a two-dimensional situation), as shown in Fig 12.3, for drained soil. Zone 1 (point 1) is an active Rankine state with $\alpha_1 = \pi - (\frac{1}{4}\pi + \frac{1}{2}\varphi)$ and a vertical stress $q_1 = Q_e/BL$. From there on, the boundary of the plastic zone develops with the spiral curve s, according to r

$= r_1\, e^{\theta \tan\varphi} = B\, e^{\theta \tan\varphi}/2\sin(\frac{1}{4}\pi - \frac{1}{2}\varphi)$, while the principal stresses rotate. At point 2 the soil reaction to the loading Q is deflected into a passive state with maximum horizontal stress and in point 4 back into an active state with a maximum vertical stress, which makes equilibrium with the local vertical weight: $\sigma_{v4} = q_4 = \gamma(H - D_4)$. From point 4 to 5 two different situations are sketched. Point 5a refers to a continuation of the spiral with in the plastic zone a positive shaft friction, and point 5b refers to a Rankine stress state with no shaft friction.

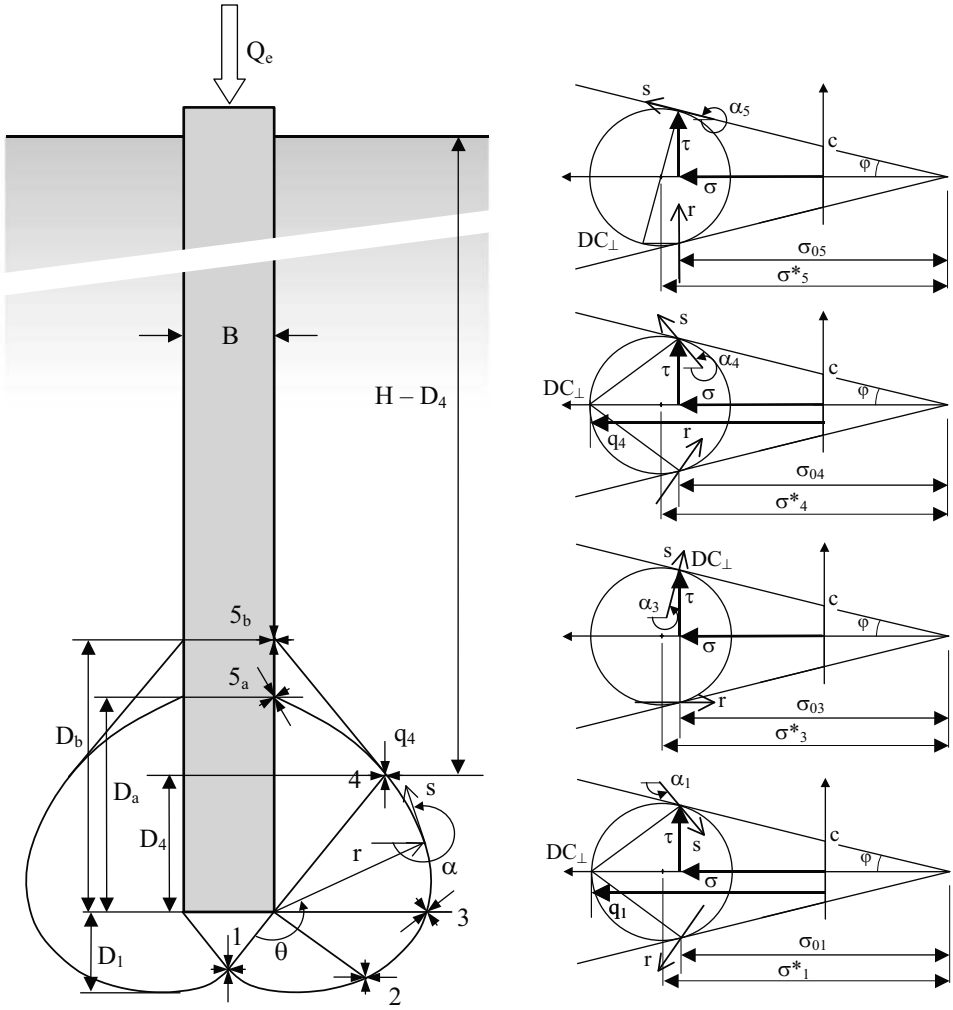

(a) failure mechanism at the pile toe *(b) Mohr circles along slip line s*

Figure 12.3 Ultimate end bearing capacity Q_e of a pile (drawn for $\phi = 15^o$)

The plastic zone shows that the soil, which plays a role in the bearing capacity, extends below the pile toe by $D_1 = B\cos\varphi\, e^{(\frac{1}{4}\pi + \frac{1}{2}\varphi)\tan\varphi}/2\sin(\frac{1}{4}\pi - \frac{1}{2}\varphi)$ and above the pile toe with $D_a = Be^{(1\frac{1}{4}\pi - \frac{1}{2}\varphi)\tan\varphi}/2\sin(\frac{1}{4}\pi - \frac{1}{2}\varphi)$ (or even higher in case of D_b). For values of $0 < \varphi < 30^o$ the corresponding depth ranges are $0.71B < D_1 < 1.59\,B$ and $0.71B < D_a < 8.30\,B$.

A value for the bearing capacity can be found by using Kötter's equation for drained soil along the s-directions, according to equation (11.4a), which from point 1 to point 4 yields

$$\sigma_{01}/\sigma_{04} = e^{2(\alpha_4 - \alpha_1)\tan\varphi} = e^{2\pi\tan\varphi} \qquad (12.11)$$

With $q_1 + c/\tan\varphi = \sigma^*_1(1+\sin\varphi)$ and $q_4 + c/\tan\varphi = \sigma^*_4(1+\sin\varphi)$, see the Mohr circles in Fig 12.3, keeping in mind that $\sigma_{01}/\sigma_{04} = \sigma^*_1/\sigma^*_4$, the ultimate end-bearing capacity Q becomes

$$Q_e = \gamma BLe^{2\pi\tan\varphi}(H - B\, e^{\pi\tan\varphi}/2\tan(\tfrac{1}{4}\pi - \tfrac{1}{2}\varphi)) + BLc(e^{2\pi\tan\varphi} - 1)/\tan\varphi \qquad (12.12)$$

For a slender wall, e.g. $B/H \approx 0.05$, and soil conditions $\varphi = 30^o$ and $c = 0$ this becomes

$$Q_e = 37.6\, BLH\gamma(1 - 5.3B/H) \approx 27.5\, BLH\gamma \qquad (12.13)$$

For $\varphi = 0$, a slightly different approach is to be used, similar to obtaining equation (12.3), and the result is, with $c = c_u$ and $c_u/\gamma L \approx 0.08$

$$Q_e = \gamma BLH(1 - \tfrac{1}{2}B/H) + 2BL\pi\, c_u \approx BLH\gamma(1+2\pi\, c_u/\gamma H) \approx 1.50\, BLH\gamma \qquad (12.14)$$

For obtaining a reasonable ultimate end-bearing capacity of a pile, equations (12.13) and (12.14) show that friction is essential. The low value (12.14) explains why pile driving in soft cohesive soils is so easy. Moreover, the point resistance is only obtained when the pile toe penetrates into the bearing layer 5 to 8 times the pile width. For that reason end-bearing piles are driven firmly into a bearing layer. Although the background of equations (12.13) is based on a kinematical approach and hence the result is to be considered as an upper bound value, it is noted that the adopted deformation and stress field is not complete, and therefore the real pile bearing capacity could be higher.

Many studies have been executed to establish a reliable approach for determining the ultimate static bearing capacity of a single pile. In general, the end-bearing capacity of a pile can be expressed, similar to (12.8), by

$$Q_e/BL = q_e = N_q\, q_0 + N_c\, c + N_\gamma\, \gamma B \qquad (12.15)$$

There are several practical sets of values for the coefficients N_q, N_c and N_γ, i.e. according to Terzaghi, Meyerhof, Vesić, or Janbu, and when applying these for a specific case it appears that results may vary up to 50%. A proper safety factor is obviously required.

The total bearing capacity Q_c (incorporating the weight of the pile itself) is found by adding the end bearing Q_e and the adhesion (friction) along the shaft Q_s. When a pile is (partly) supported by a shaft adhesion, this contribution is referred to as positive skin resistance. Thus, $Q_c = Q_e + Q_s$. However, local soil compaction and settling after installation of a pile may reverse the adhesion to negative skin

friction, with soil hanging onto the shaft. It reduces the total bearing capacity, $Q_c = Q_e - Q_s$, see Fig 12.4.

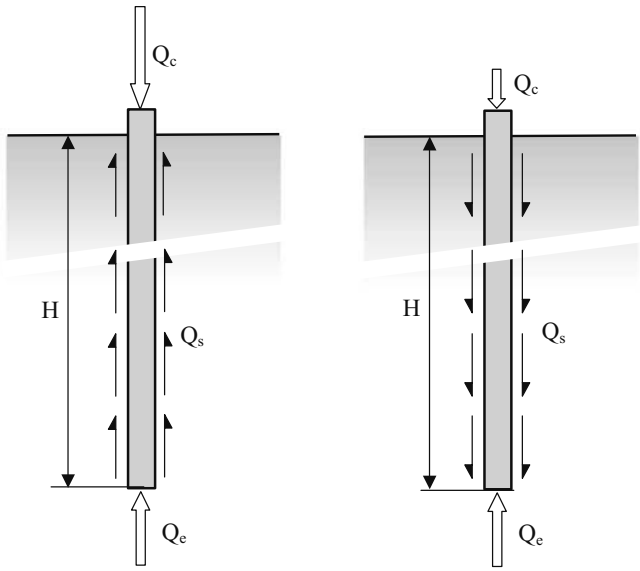

(a) positive skin resistance *(b) negative skin resistance*

Figure 12.4

The previous analysis, based on the theory of slip lines, is only applicable to two-dimensional situations. A single pile is typically three-dimensional, and resistance values may be higher than found in two-dimensional analysis. Similar analysis in three dimensions seems not possible. Therefore, validation by field tests and numerical simulation is inevitable.

Pile load testing

A reliable method is by static pile load tests. They are time consuming and expensive, but the result is a reliable load settlement curve, e.g. shown in Fig 12.5a. A common formula (hyperbolic type) approximating the curve is[49]

$$w/(Rq) = \alpha_e + w\beta/R \qquad (12.16)$$

Here, w is the settlement, R the equivalent radius, and q the ultimate vertical soil resistance. The formula expresses that the secant modulus $w/(Rq)$ increases linearly with the relative settlement w/R. For small values of w/R the parameter α_e can be obtained from the theory of elasticity, CPT or pressuremeter test. The parameter $q_u = 1/\beta$ is obtained from a pile loading test. Sometimes β cannot be achieved and then a limit pile load $Q = q_u \pi R^2$ is determined by an ultimate allowable settlement w_u.

[49] For a nice overview see: M. Jacobsen (1992) *Bearing capacity and settlements of piles*. Aalborg University, Denmark.

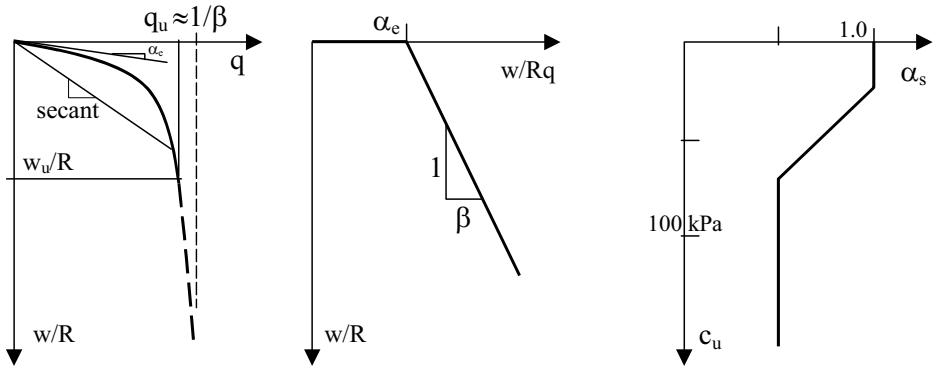

(a) load settlement curve *(b) API-code*

Figure 12.5 Pile load testing

Empirical methods

A suitable field test to determine the ultimate end bearing of a pile is the CPT test, where the cone shows some similarity with a pile, at a smaller scale (when pushed, not hammered!). A simple approximation is $q_u = 0.1q_c$. A practical method using the variation of the CPT (see Fig 3.1) was developed in Delft (NEN 6743, EC7, part 3), where the end bearing capacity Q_e is determined by the following formula[50]

$$Q_e/(\pi R^2) = q_e = c_e(q_{c1} + q_{c2} + 2q_{c3})/4 \qquad (12.17)$$

Here, q_{c1} is the smallest CPT-value obtained in a zone between 1.4R to 8R under the pile toe (related to the possibility of punching through the bearing layer), q_{c2} is the successive smallest CPT-value over that zone, and q_{c3} is the successive smallest CPT-value in the zone above the pile toe up to 16R. The coefficient c_e is related to the amount of soil displacement/replacement, see Table 12.2. New insight (Van Tol, Xu and Lehane) suggests using for c_e a value of 0.6 for percussion driven piles.

In case no negative skin resistance is expected to develop with time one may take for the shaft resistance as a first estimate not the sleeve resistance q_f but a percentage c_s (see Table 12.1) of the CPT value q_c, according to

$$Q_s/(2\pi RH) = \Sigma_i(c_s q_{ci} h_i/H) \qquad (12.18)$$

Here, h_i is the thickness of a specific soil layer. Takesu e.a. suggested a relation with pore pressure u measured during the CPT, according to $c_s = 0.8u + 0.75$ for $u < 0.3$ MPa and $c_s = 5.0u - 1.5$ for $u > 0.3$ MPa.

---

[50] Different methods are suggested in France (Bustamante, Frank), in Belgium (de Beer), in the UK: the ICP method (Jardine et al.), and in Australia (Xu and Lehane). The results of these methods may vary significantly and the uncertainty is at least 30%.

TABLE 12.2 VALUES FOR PILE FACTORS

pile type	c_e	c_s
concrete (prefab)	0.6 to 0.9*	0.012
timber	1	0.01
screw	0.8	0.0075
steel	1	0.0075
auger	0.1	0.006
bored	0.5	0.005

* depending on the way of installation: 0.6 for percussion driving

Practical design formulas for the shaft resistance are based on a large number of pile loading tests, performed on different piles in different soils and with different installation methods. Special reference is made to the API-code (American Petroleum Institute), which is widely used. It states that in undrained soil the shaft resistance q_s can be expressed by

$$q_s = Q_s / A_s = \alpha_s c_u \qquad (12.19)$$

Here, A_s is the pile shaft surface area. The API-code gives the relation between α_s and the undrained shear strength c_u (see Fig 12.5b), which may vary with the vertical soil stress. In drained soils the shaft resistance can be found from

$$q_s = K\sigma_v' \tan\delta \qquad (12.20)$$

Here, K is the earth pressure coefficient and δ the apparent skin friction angle ($\frac{1}{2}\varphi < \delta < \frac{2}{3}\varphi$). There is much to say about the value of K, as it may represent any situation between an active and a passive stress state. It may dramatically change during pile installation and partly recover afterwards. There are many practical empirical methods in use to establish the end bearing and skin resistance (Meyerhof, Vesić, Vijayvergiya, Burland, Jardine, Frank, Lehane, Xu, Van Tol).

Dynamic testing

Monitoring of the dynamic behaviour of a pile during driving can be used, in the first place, to optimise production, but also to estimate the static bearing capacity, in the case of end-bearing piles.

Pile driving data (blowcount) and static and dynamic soil investigation methods (CPT and SPT) reveal that the results show some similarity, but the differences represent a complication for precise design (Fig 12.6a).

A dynamic soil response is fundamentally different from a static response. Soil absorbs shear waves, which may decay in depth and which may run along the surface (Raleigh waves) or along interfaces of soil layers with different impedance (Stonely waves). These surface waves show relatively little damping. In principle, the soil response can be approximated with shear and/or rotational springs and dashpots (Wolf and Deeks). A comprehensive field test and sophisticated numerical simulation has shown the pattern of dynamic energy dissipation during pile driving (Fig 12.6b). While analysing the dynamic response during pile driving, it may give information about the static bearing capacity, but soil variation (layering) and soil constitution (friction, plasticity) make a reliable analogy a rarity.

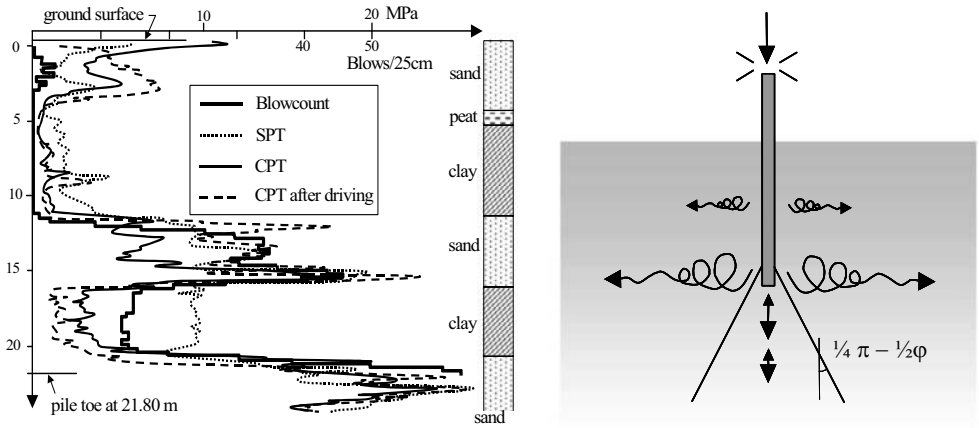

(a) survey methods and driving data *(b) dynamic energy dissipation (Hölscher)*

Figure 12.6 Energy dissipation during pile driving

In general dynamic measurements are not a reliable substitute for static pile load tests. On a specific job site, however, a dynamic analysis (CAPWAP, PDA) can be efficient, when a calibration with local static tests is possible. The STATNAMIC method is in principle a dynamic impact pile testing method, but it succeeds in drawing out the length of the impact far beyond other dynamic methods, and can yield reliable estimates of pile capacity in many cases. Very large units are available, for high pile capacities, up to 30 MN.

C DEFORMATION OF FOUNDATIONS (SERVICEABILITY LIMIT STATE)

Besides a failure criterion, the functioning of a foundation is also determined by the deformation. The serviceability may be insufficient, if deformations exceed a certain threshold, conditioned by the structure itself or the environment, e.g. adjacent infrastructure and buildings. Deformations of the subsoil induced by a loaded foundation are controlled by the corresponding induced stresses, which involves the entire area and requires boundary conditions, equilibrium conditions and compatibility conditions. The stiffness of the structure plays a role and the theory of a flexible plate on elastic subsoil may provide an answer. However, their use is limited (valid for relatively small strains), since soil behaviour is markedly non-linear. For a realistic non-linear analysis sophisticated computational models are available, which can simulate multi-dimensional complex situations.

A classic solution is the case of a single force Q on semi-infinite subsoil, attributed to Boussinesq. The axi-symmetrical stress field due to the load is described by the following set, with r the radial coordinate, z the vertical coordinate, $R^2 = r^2 + z^2$, and ν the Poisson ratio

$$\sigma_v = \frac{3Qz^3}{2\pi R^5} \qquad (12.21a)$$

$$\sigma_{rr} = \frac{Q}{2\pi}\left[\frac{3r^2 z}{R^5} - \frac{1-2\nu}{R(R+z)}\right] \tag{12.21b}$$

$$\sigma_{\theta\theta} = \frac{Q}{2\pi}\frac{1-2\nu}{R^2}\left[\frac{r}{R+z} - \frac{z}{R}\right] \tag{12.21c}$$

$$\tau = \frac{3Qrz^2}{2\pi R^5} \tag{12.21d}$$

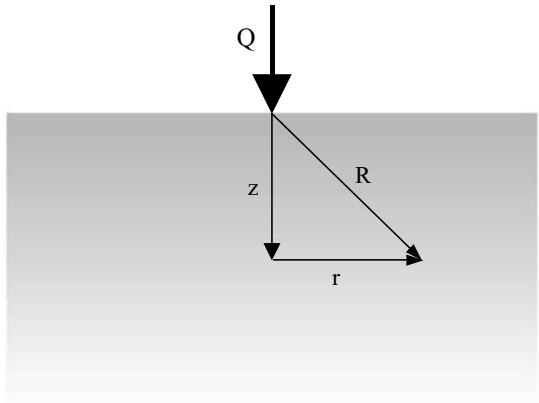

Figure12.7 Boussinesq's problem

Corresponding strains and deformations can be determined by using the elastic stress-strain relation, according to (5.2). Elaboration shows that the vertical displacement w due to the load Q in the centre becomes

$$w = \frac{Q(1+\nu)}{2\pi ER}\left[2(1-\nu) + \frac{z^2}{R^2}\right] \tag{12.22}$$

This expression shows that under the load at the surface the displacement becomes infinite, which is a practical inconvenience. In practice, (12.21a) is used in the following form

$$\Delta\sigma_v = QN/\pi z^2 \qquad \text{with} \qquad N = 3/2\,(1+r^2/z^2)^{-5/2} \tag{12.23}$$

If one assumes an influence area in the underground limited by an expanding cone under 45°, implying that at depth z the load is mainly carried in a zone restricted to πz^2, then $N = 1$. Boussinesq's solution can be used for superposition. For a uniform load q in a circle with radius r_0 and the vertical displacement in the centre becomes

$$w = 2qr_0(1-\nu^2)/E = 2Q/\pi r_0 E_e \qquad \text{with} \qquad E_e = E/(1-\nu^2) \tag{12.24a}$$

Various other shapes have been worked out, e.g. line or strip load (Flamant) and arbitrary shape (Newmark). Westergaard elaborated elastic solutions for anisotropic soils (limited horizontal deformation), which gives stresses less than Boussinesq. The reality may be in between. Deformations in layered non-linear subsoils are more complicated and numerical computation is the only possible way.

Pile deflections behave non-linearly (see Fig 12.5). Fahey and Carter suggested a practical method for the vertical pile settlement, based on elastic continuum theory, by adding a factor $(1-q/q_u)^{-0.3}$ related to the degradation of the elastic modulus with increasing strain. In this regard, the vertical deformation w of a pile under axial loading Q becomes

$$w = (1-q/q_u)^{-0.3}\, QI/(2r_0 E_e) \qquad (12.24b)$$

Here, I is an empirical factor (see Mayne, Poulos, Randolph), and E_e is the equivalent elastic modulus along the pile at the toe. Piles when installed may be subjected to horizontal forces due to inclined loading or deformations of the soil they are placed in. This topic is not further elaborated in this book.

D DYNAMIC SOIL RESPONSE

Soil response to vibrations

The dynamic soil response under shaking or rocking loading can be represented by a set of springs and dashpots. Several methods have been developed, such as elastic half space theory, a cone model, analytical solutions, and dynamic finite element methods, each with its limitations. Sophisticated tests have been undertaken to validate the methods. Here, we consider the cone model, developed by Ehlers (1942) for homogeneous subsoils.

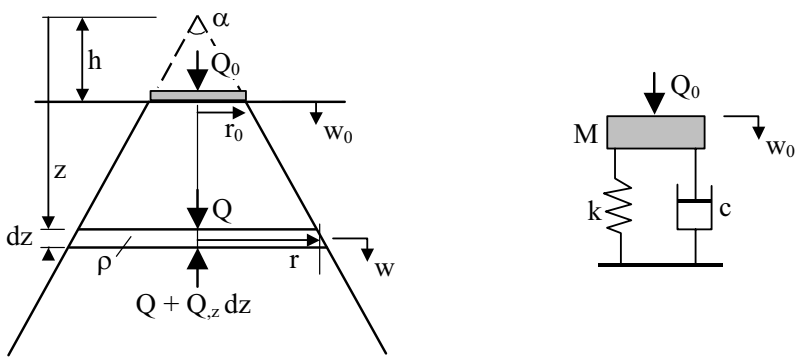

(a) Ehlers' model *(b) mass-spring-dashpot model*

Figure 12.8

The harmonic vertical displacement u of a rigid mass-less circular foundation disk with radius r_0 and surface $A_0 = \pi r_0^2$ on the surface of a homogeneous soil is addressed (Fig 12.8a). The cone, expanding with depth with apex α, has a cross-section $A = \pi r^2$, increasing with depth proportional to z^2. At depth z the induced

pressure distribution is approximated as a uniform pressure q over the cone cross-section. No energy is assumed to be transmitted outside the cone and therefore the induced soil pressures decrease proportional to depth squared. Also Boussinesq's solution has this trend, see equation (12.23). Adopting elastic soil, i.e. elasticity E and absence of lateral deformation ($\nu = 0$), the vertical force acting in the cone becomes

$$Q = qA_0(z/h)^2 = -EA_0(z/h)^2 w_{,z} \qquad (12.25)$$

Dynamic equilibrium of a thin disk out of the cone at depth z, having mass density ρ, is expressed in terms of the vertical displacement w by

$$\rho A_0(z/h)^2\, w_{,tt} = (EA_0(z/h)^2 w_{,z})_{,z} \quad \text{or} \quad w_{,tt} = a^2(2w_{,z}/z + w_{,zz}) \qquad (12.26)$$

Here, $a = \sqrt{(E/\rho)}$ is the vertical (compression) wave celerity within the cone.

This equation can be solved for harmonic oscillation, using complex algebra. The harmonic motion is expressed by $w = Ue^{i\omega t} = U\,[\cos(\omega t) + i\sin(\omega t)]$, where U is the amplitude, a function of z only. This renders (12.26) into

$$-\omega^2 U = a^2(2U_{,z}/z + U_{,zz}) \qquad (12.27)$$

A solution of this equation is sought for $U = Be^{i\beta z}/z$. Substitution yields $-\omega^2/z = a^2(-\beta^2/z)$, which is valid for all values of z, and gives $\beta = \pm\,\omega/a$. The solution is $U = Be^{-i\omega z/a}/z$, which satisfies $U = 0$ for $z \to \infty$. The value at the surface becomes $U_0 = Be^{-\omega h/a}/h, \to B = U_0\, he^{i\omega h/a} \to U = U_0\, he^{-i\omega(z-h)/a}/z$. The displacement becomes

$$w = Ue^{i\omega t} = U_0\, he^{i\omega(t-(z-h)/a)}/z =$$

$$= (U_0\, h/z)\,[\cos(\omega(t-(z-h)/a)) + i\sin(\omega(t-(z-h)/a))] \qquad (12.28)$$

For the real motion, only the real part of (12.28) should be considered, which is

$$w = U_0\,(h/z)\cos(\omega(t-(z-h)/a)) \qquad (12.29)$$

The corresponding force Q can be elaborated from (12.25)

$$Q = EA_0(z/h)^2 w_{,z} =$$

$$= EA_0(z/h)^2 U_0 h\,[-(1/z^2)\cos(\omega(t-(z-h)/a)) + (\omega/za)\sin(\omega(t-(z-h)/a))]$$

$$= EA_0U_0/h\,[-\cos(\omega(t-(z-h)/a)) + (\omega z/a)\sin(\omega(t-(z-h)/a))] =$$

$$= EA_0U_0/h\,(1 + (\omega z/a)^2)^{1/2}\cos(\omega(t-(z-h)/a) + \eta)$$

$$= U_0\, EA_0\cos(\omega(t-(z-h)/a) + \eta)\,/\,(h\cos\eta) \quad \text{with} \quad \tan\eta = \omega z/a \qquad (12.30)$$

Finally, at the surface Ehlers' model yields for the displacement and the force

$$w_0 = U_0 \cos(\omega t) \tag{12.31a}$$

$$Q_0 = U_0 (EA_0/h) \cos(\omega t + \eta) / \cos\eta \quad \text{with} \quad \tan\eta = \omega h/a \tag{12.31b}$$

Next consider the Kelvin-Voigt model: a spring-dashpot model (Fig 12.8b) without mass. Harmonic displacement $w = U_0 e^{i\omega t}$ for a weightless system (mass $M = 0$) is described by the following equilibrium

$$cw_{0,t} + kw_0 = Q_0 = Q_{00} e^{i\omega t} \quad \text{or} \quad (i\omega c + k)U_0 = Q_{00} \tag{12.32}$$

Here, c is the dashpot constant and k the spring constant. Hence

$$Q_0 = Q_{00} e^{i\omega t} = U_0 (i\omega c + k) (\cos(\omega t) + i\sin(\omega t)) =$$

$$U_0 (k\cos(\omega t) - c\omega\sin(\omega t) + ik\sin(\omega t) + ic\omega\cos(\omega t)) \tag{12.33}$$

For the real motion, the real part of (12.33) must be considered

$$Q_0 = U_0 (k\cos(\omega t) - c\omega\sin(\omega t)) = U_0 (k^2 + (c\omega)^2)^{½} \cos(\omega t + \delta)$$

$$= kU_0 (1 + (c\omega/k)^2)^{½} \cos(\omega t + \delta) =$$

$$= kU_0 \cos(\omega t + \delta) / \cos\delta \quad \text{with} \quad \tan\delta = c\omega/k \tag{12.34}$$

Thus, the system's motion of a weightless spring-dashpot system is described by

$$w_0 = U_0 \cos(\omega t) \tag{12.35a}$$

$$Q_0 = kU_0 \cos(\omega t + \delta) / \cos\delta \quad \text{with} \quad \tan\delta = c\omega/k \tag{12.35b}$$

Perfect similarity with Ehlers' model (12.31) is obtained by putting

$$k = EA_0/h \quad \text{and} \quad c = EA_0/a = A_0(\rho E)^{½} \tag{12.36}$$

The conclusion is that for dynamic oscillations the subsoil, with uniform stress within a cone, can be represented by a simple spring-dashpot system, the coefficients of which can be related to intrinsic soil properties, according to (12.36). Here, the geometric factor h is related to the apex of the cone, which is a choice: the apex α is incorporated through $h = r_0\tan(\alpha/2)$. A common choice is $\alpha = 90^o$, so $h = r_0$. The dashpot constant c of (12.36) is equivalent to expressions in literature, e.g. Verruijt: $c = \pi A_0(\rho G)^{½}/2m$ with $m^2=(1-2\nu)/(2(1-\nu)$.

Next, mass is incorporated. Following the mass-spring-dashpot theory, a harmonically oscillating circular disk with mass M, representing the mass of a foundation (and structure on it), will induce a response at the interface between soil and foundation, according to

$$w_0 = U_0 \cos(\omega t) \tag{12.37a}$$

$$Q_0 = kU_0 \cos(\omega t + \theta) / \cos\theta \quad \text{with} \quad \tan\theta = (c\omega/k) / (1 - M\omega^2/k) \qquad (12.37b)$$

Adopting Ehlers' model this becomes in terms of soil properties with (12.36)

$$w_0 = U_0 \cos(\omega t) \qquad (12.38a)$$

$$Q_0 = U_0 (EA_0/h) \cos(\omega t + \theta) / \cos\theta$$

$$\text{with} \quad \tan\theta = (h\omega/a) / (1 - Mh\omega^2/EA_0) \qquad (12.38b)$$

Soil response to an impact loading

In case of a shock load the eigen frequency ω_1 of this system will dominate. For this type of loading the equilibrium of the mass-spring-dashpot system is described by

$$Mw_{0,tt} + cw_{0,t} + kw_0 = Q_{00}\, \delta(t) \quad \text{with} \quad \delta(t) \text{ the Dirac delta function} \qquad (12.39)$$

Laplace transformation gives

$$\int_0^\infty w_0 e^{-st} dt = Q_{00}/(Ms^2 + cs + k) \qquad (12.40)$$

Solving with Heaviside's theorem leads to

$$w_0 = Q_{00}\, e^{-ct/2M} \sinh(\omega_1 t) / \omega_1^2 \quad \text{with} \quad \omega_1 = ((c/2M)^2 - k/M)^{½} \qquad (12.41)$$

This shows that for $D = c/2(kM)^{½} > 1$ the system shows smooth damping, and for $D < 1$ it is oscillating and damping (resonance). The critical damping is therefore expressed by $D = 1$, which leads to

$$c = 2(kM)^{½} \rightarrow EA_0/a = 2(EA_0 Mh)^{½}$$

$$\rightarrow EA_0/(E/\rho)^{½} = 2(EA_0 M/h)^{½} \rightarrow A_0 h\rho = 4M$$

This gives

$$A_0 h\gamma = 4Mg = 4W = 4A_0 \sigma_0 \rightarrow \sigma_0 = ¼h\gamma \qquad (12.42)$$

Here, W is the weight of the foundation (and structure above it) and σ_0 the static contact pressure between the foundation and the soil. For $\sigma_0 > ¼h\gamma$ oscillations will occur, and for $\sigma_0 < ¼h\gamma$ the system will only show smooth damping. Here, the choice of h plays a role.

Static case determined from dynamics

Solution (12.38) shows for the static case, i.e. $M = 0$, $c = 0$ and thus $\theta = 0$, that at the surface the displacement and force are described by

$$Q_0 = (EA_0/h)w_0 = kw_0 \quad \text{or} \quad q_0 = Q_0/A_0 = (E/h)\, w_0 = kw_0/A_0 \tag{12.43}$$

This is the known as Winkler's model. The soil at the surface reacts at the surface as a simple spring, and the spring constant is $k = EA_0/h$. The choice of h is related to the choice of the representative cone, within which the soil stresses are absorbed. Adopting Rankine stress states, i.e. active or passive, the value of h is given by

$$r_0/\tan(\tfrac{1}{4}\pi + \tfrac{1}{2}\varphi) < h < r_0/\tan(\tfrac{1}{4}\pi - \tfrac{1}{2}\varphi) \tag{12.44}$$

Here, r_0 is the (apparent) radius of the foundation and φ the internal soil friction angle. For cohesive soil ($\varphi = 0$) one finds $h = r_0$ corresponding to a cone apex of $\alpha = 90^o$.

The previous theory applies for axi-symmetric systems. The same holds for plane two-dimensional systems, if one adopts the soil elasticity increasing proportionally to z. Thus, E is proportional to z and for a two-dimensional cone A is also proportional to z, so that EA is proportional to z^2, and the previous elaboration applies. This model is known as a Gibson soil. Gibson showed that in this case at the surface Winkler's model is satisfied. It seems realistic, since experiments show that elasticity increases with depth. For a one-dimensional case, i.e. A is constant, the same solutions may hold, if E is proportional to z^2.

Soil response to a dynamic load moving along a 'beam'

The response of subsoil to dynamic loading Q_0 can be approximated by a bending beam on springs (Fig 12.9). The equilibrium is described by

$$EIw_{0,xxxx} + \rho A w_{0,tt} + (k/B)w_0 = Q_0/B \tag{12.45}$$

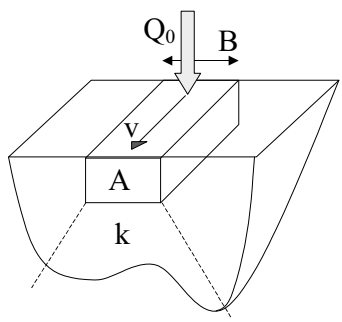

Figure 12.9 Schematization of a HSL railway embankment

Here, w_0 is the surface displacement under the load, EI the bending stiffness, ρA the mass/m of the beam, and k is the spring constant of the supporting soil. The material damping, which affects the amplitude of the induced vibrations during resonance, has been disregarded. When the load is moving at a constant velocity v, equation (12.45) can be reformulated with a convective coordinate $\xi = x - vt$, according to

$$EIw_{0,\xi\xi\xi\xi} + \rho A v^2 w_{0,\xi\xi} + k/B\, w_0 = Q_0/B \qquad (12.46)$$

The load Q_0 is acting at $\xi = 0$. The harmonic solution of (12.46) can be found by trying $w_0 = U_0\, e^{a\xi}$, and the corresponding characteristic equation is

$$EIa^4 + \rho A v^2 a^2 + k/B = 0 \qquad (12.47)$$

The roots of this equation are

$$a = \pm\sqrt{\frac{-\rho A v^2 \pm \sqrt{(\rho A v^2)^2 - 4kEI/B}}{2EI}} \qquad (12.48)$$

The general solution is therefore $w_0 = \Sigma\, U_{0i} e^{ai\xi}$. From (12.48) one may distinguish four independent roots. One may recognise a critical velocity when $(\rho A v^2)^2 - 4kEI/B = 0$ or

$$v_c = \sqrt[4]{\frac{4kEI}{\rho^2 A^2 B}} \qquad (12.49)$$

Elaboration shows that for $v > v_c$ all the roots a_i are purely imaginary, representing undamped vibrations. For $v < v_c$ all the roots are complex, representing attenuating vibrations. Therefore, the critical velocity represents a characteristic value, essential for the design of foundations, which must sustain dynamic loads.

The previous analysis is a simplification of the reality; it considers bending waves in the beam and approximated pressure waves in the subsoil, while material damping is disregarded. Dynamic response of soils contains vibrations related to three types of acoustic waves, i.e. pressure waves, shear waves and interface waves, e.g. Rayleigh wave along a surface, each travelling with a specific celerity, for pressure waves the celerity is $\sqrt{(K/\rho)}$, for shear waves $\sqrt{(G/\rho)}$, and for surface waves slightly less than $\sqrt{(G/\rho)}$. The most disturbing wave is usually the Rayleigh wave. It carries most of the dynamic energy relatively far. The practical implementation of dynamics in (rail)way embankments, particularly at specific construction elements, is rather complex (Degrande, Hölscher, Powri).

Soil response including damping

Verruijt introduced a special form of damping: hysteretic damping, which is based on frictional damping. It may be more realistic in granular soils than viscous damping. From (12.41) it can be seen that the resonance frequency (eigen frequency) for the undamped system is

$$\omega_1 = (k/M)^{1/2} \qquad (12.50)$$

Here, k is the spring constant and M the mass. The damping ratio is dependent on the frequency

$$D = c/2(kM)^{1/2} = c/2M\omega_1 \qquad (12.51)$$

Hysteretic damping assumes that the factor $c\omega/k$ is constant (residual deformations under cyclic loading are independent of the frequency), which renders the damping ratio into a constant

$$D_h = \frac{c}{2\sqrt{kM}} = \frac{c\omega_1}{2k}\frac{k}{\omega_1\sqrt{kM}} = \frac{c\omega_1}{2k}\frac{k}{\sqrt{k/M}\sqrt{kM}} = \frac{c\omega_1}{2k} \qquad (12.51)$$

Hence, the damping ratio is constant, independent of the speed or frequency of the loading. There is no critical damping in soils with hysteretic damping.

application 12.1

A steel pipe pile with length H = 30 m, radius R = 0.7 m and wall thickness d = 4 cm is driven through a thick clay layer with c_u = 50 kPa down to a rigid sand bed with CPT value of q_c = 20 MPa. An estimate of the elasticity modulus E can be obtained from the CPT value by the formula $E \approx q_c/\beta$ with β an empirical constant. The bearing capacity Q_c consists of the shaft resistance Q_s and the point resistance Q_e. The shaft friction includes the inner and outer side and using (12.19) one finds

$$Q_s = 2\pi H(R + R - d)\alpha_s c_u \approx 4\pi RH \text{ x } 0.7 \text{ x } 50 = 9.24 \text{ MN}$$

The point bearing Q_e is due to the point cross-section, i.e. a cylindrical strip. Thus $Q_e \approx 2\pi R d q_e$, with q_e the local uniform pressure. The maximum value of q_e can be related to the CPT value by $q_e = 1.3q_c$, where the coefficient 1.3 is a shape factor (strip load versus point load). Hence, the end-bearing capacity becomes

$$Q_e = 2\pi R d q_e = 2.6\pi R d q_c = 2.6\pi\, 0.7 \text{ x } 0.04 \text{ x } 20 = 4.67 \text{ MN}$$

The total bearing capacity becomes $Q_c = Q_s + Q_e$ = 13.9 MN with the main contribution from the shaft friction.

Using solution (12.24) the displacement can be approximated by subtracting an opposite cylindrical load with radius R-d. Under ultimate loading the vertical displacement w can be approximated by

$$w = 2q_e d(1-\nu^2)/E = 2.6q_c d(1-\nu^2)/(q_c/\beta) = 2.6\beta(1-\nu^2)d$$

For the empirical constant $\beta \approx 0.1$ (for sand) is chosen and for the Poisson ratio the value $\nu = 0.35$ is adopted. Then, the vertical displacement becomes $w = 0.23d$ = 0.009 m, i.e. 9 mm, which is quite acceptable. In compacting soils, the side friction may give rise to additional settlement. Often a plug of compacted soil may stick firmly in the pile toe, which changes the situation drastically.

application 12.2

Consider a fast moving train with velocity v on a rail bed on soft soil. The question is what is the maximum speed, where induced surface vibrations will be damped, i.e. the critical velocity. The rail bed is composed of a relatively thin gravel layer on a sand embankment on clay subsoil. The gravel-sand body is considered to act as a beam with bending stiffness E_sI and mass ρA per metre length, and the dynamic behaviour of the subsoil is characterised by a spring with constant k. The elasticity modulus is E_s = 200 MPa for sand and E_c = 60 MPa for clay. The mass of the sand is ρ = 2000 kg/m^3. The sand embankment is 10 m wide (B) and 5 m high (H), which gives A = 50 m^2 and $I = BH^3/12$ = 104 m^4.

The spring constant is, according to equation (12.36) adopted for two dimensions, $k = E_cB/h$, and for h the value $B/2$ = 5 m is taken (apex of the dynamic cone is 90°). This yields k = 30 MN/m. However, the attention is focused on surface waves, and therefore, instead of E_c the shear modulus should be inserted $G = E/2(1+\nu) \approx E/3$, thus k = 15 MN/m applies. Equation (12.49) defines the critical velocity

$$v_c = (4kEI/\rho^2A^2B)^{1/4} = (4\text{x}15\text{x}10^6\text{x}200\text{x}10^6\text{x}104\text{x}(2000)^{-2}(10\text{x}8\text{x}10)^{-2})^{0.25}$$

$$= 42.5 \text{ m/s} = 153 \text{ km/hr}$$

This result indicates that for a high speed train the structure of a rail bed on soft soil should be different than standard. Cement-soil mixed piles in the clay or a (partly buried) concrete bridge founded on piles is a solution in this case.

application 12.3

A circular footing with radius R = 5 m is placed on a sandy sea bottom. The soil has a strength of c = 0 kPa and φ = 25°, and a submerged weight of γ' = 9 kN/m^3. By using EC7 code determine the bearing capacity q when the load inclination is F_v / F_h = 2. So, what is $F_{v,max}$?

application 12.4

Is the result of a pile-loading test a lower or an upper bound value?

application 12.5

A concrete element with a weight of 10 kN falls on the ground; its surface touching the ground is 1 m^2. The soil unit weight is 18 kN/m^3. What is the response of the soil? Does it vibrate?

application 12.6

Fig 12.8 shows Ehlers' model, which can be applied for dynamic and static soil response. The apex α is related to active, neutral (shear strength is not mobilised) or passive soil states. What is the value of α, if a neutral soil state is adopted? For a passive soil state, does α increase or not, and how much (for a cohesion-less soil)?

application 12.7

A concrete pile of 25 m length and equivalent diameter of 40 cm is driven into the soil until end-bearing is achieved in a deeper sand layer. On top the soil is soft with unit weight 18 kPa/m and undrained strength of 50 kPa. The CPT of the sand is 20 MPa. Determine the total bearing capacity of the pile. Is it wise to include shaft friction and which safety factor would you suggest. So, finally what is the design value for the bearing capacity?

application 12.8

The foundation of a strip footing with width 3 metres can be designed with Prandtl's solution. The footing is placed 2 metre under the soil surface. The undrained strength of the soil is 25 kPa and the unit weight is 14 kPa/m. What is the bearing capacity q? Note that q_0 is not zero! What controls the Prandtl wedge being at the left or at the right side? If the strip footing is not long, dimensional effects play a role. Does the bearing capacity increase or decrease under three-dimensional effects?

application 12.9

In soft soil regions pile foundations support buildings, the older buildings on traditional wooden piles. When the road in front is raised to compensate for the compaction of the underground, the added sand weight may exert a horizontal pressure on these piles. In the end, the piles may be pushed aside from the walls they should support. As a consequence severe settlement may occur (Fig 12.10). Which possible measure could be taken to prevent this from happening?

Figure 12.10

This page intentionally left blank

13 METHODS OF GROUND IMPROVEMENT

Soft soil is often improved prior to building on/in it. This can be motivated by the otherwise excessive settlement of foundations, which would compromise serviceability and would require excessive maintenance, and by saving on otherwise heavy foundations. Many methods of ground improvement have been developed, and quite often various choices are available in a given situation to obtain the desired level of performance of the structure.

Ground improvement methods can be grouped according to how the soft soil is treated: displacement, replacement, mass improvement and improvement by stiff inclusions. Pile foundations essentially fit into the latter group, but are not usually viewed as being a method of ground improvement. Rather, they allow to by-pass the soft soils altogether and transfer the foundation loads to deeper more competent strata (see Chapter 12). Biological treatment of soil is in the development stage and methods of application could eventually fall into either the mass treatment category or that of the stiff inclusions. They are treated separately here.

A GRAVITY DISPLACEMENT METHODS

In the gravity displacement method, the soft soils are displaced by failure of a sand-fill, which is placed on the surface. The fill is applied rather quickly and is increased until failure of the soft soil occurs. The latter is pushed aside and the fill settles to replace it. This method was applied on a large scale in the Netherlands for road and railway construction up to approximately the 1950's. It had a number of disadvantages: the density of the settled sand was usually quite low, soft soil was often trapped by the fill before it could be displaced, and it caused large lateral displacements. Fill could penetrate horizontally into the soft soil and flow laterally to quite large distances, resulting in unexpected heave of the surroundings.

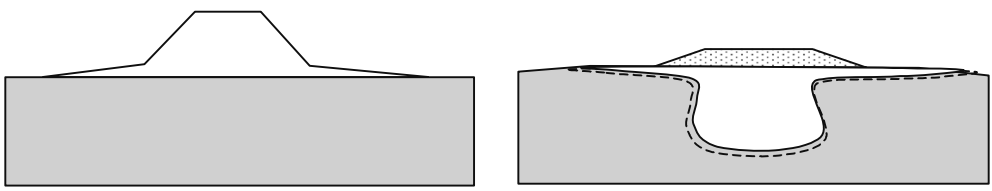

(a) initial situation *(b) final situation*

Figure 13.1 Gravity displacement

In the present time where much old infrastructure is being widened or crossed by new infrastructure, it is often problematic to deal with the loose sand of old gravity displacements. An example is the crossing of the Gouda railway line in Rotterdam by a tunnel for the RandstadRail light-rail to Zoetermeer. Any disturbance of the loose sand by the tunnel construction could result in its densification and consequently subsidence of the Gouda line (see also Fig 8.9).

Approximate analyses were performed with the finite element method to relate increases of pore pressure in the sand to increases of settlement and shear

deformation. It was considered that an increase of pore pressure by 50% of the initial vertical total stress σ_{v0} was a safe estimate, but this was found to result in shear strains of more than 10%, and a settlement of more than 0.1 m. Undrained triaxial tests on the loose sand revealed that at pore pressures of $0.5\sigma_{v0}$, the shear strain reached about 5%. That is, the support by the soft clay and peat (adjacent to the sand body), which was accounted for in the calculations did not succeed in reducing shear deformation to levels below those of the unsupported material in the triaxial test, and therefore liquefaction of the sand and large deformations could occur. A solution is to increase the effective stresses by adding an overburden on the clay and peat layers and to lower the groundwater table in the sand layer. This reduced calculated shear strains to about 1 to 2% at the design level of excess pore pressure of $0.5\sigma_{v0}$ and thus no liquefaction is expected with those measures.

Figure 13.2 A surprise; pile driving caused unexpected sand bed densification

B REPLACEMENT METHODS

Cunette method

Replacing bad foundation soil with better material has always been a popular method. The cunette method was widely applied to infrastructure in the Netherlands, where advantage of the high groundwater table was taken by dredging a trench or "cunette" (deep ditch) and later filling it with sand. This sand too is usually quite loose, just as with the gravity displacement method. The widening of existing roads and railways, where this method was used in the past, is problematic. An illustration of the difficulties is shown in Fig 13.2, where the loose sand underneath the A15 highway near Sliedrecht was densified when a sheet pile was driven into it, and the road surface was seriously damaged.

Fig 13.3 illustrates the problem of "squeezing" of a thin, weak and compressible layer such as peat underneath a replacement cunette. This leads to additional deformations, which in many cases are time-dependent and significantly increase maintenance costs.

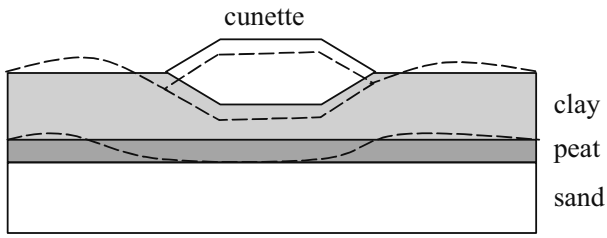

Figure 13.3 Squeezing below a back-filled cunette

Lightweight fill

Lightweight fill as a replacement material has the advantage that the increase of load on the soft soils is limited or completely prevented. This method too has old roots, e.g. road construction in peat areas by excavating the top few metres of bad soil and replacing it by bales of horticultural peat. As long as the peat bales remain below the groundwater table, this is an enduring solution. Sawdust, expanded clay beads, lava products and shredded automobile tyres are other examples of lightweight fill materials. Expanded polystyrene (EPS), also known as geofoam, is becoming the preferred material for lightweight fill. It is very light, only 15 to 30 kg/m^3, and is used in large blocks which can be easily trimmed on site. They are also used in embankment construction (Fig 13.4), and make fast construction possible with little or no effect on neighbouring structures and utilities. Where space is limited, vertical walls are possible by applying a facing. Geofoam has poor chemical resistance and must be protected against spillage of chemicals.

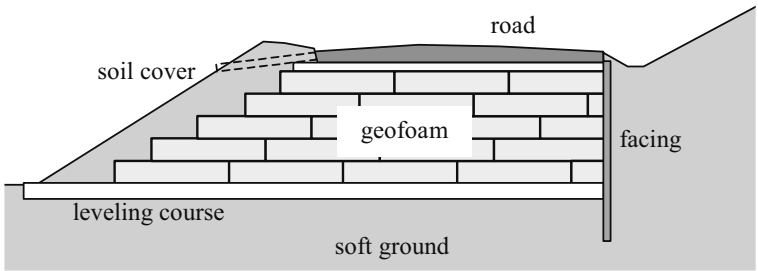

Figure 13.4 Lightweight fill (geofoam) application in an embankment slope

C MASS IMPROVEMENT

Dynamic compaction

Densification or solidification can be applied to the entire mass of soft soil. Menard's method of Deep Dynamic Densification consists of dropping weights onto the surface of the soil. Weights up to 190 tons and drop heights up to 25 m are used. The site is covered in a grid of drop points. Large craters can form, which can either be backfilled or levelled with surrounding fill. The method relies mainly on expelling air from the soil and is therefore effective only in non-cohesive soils. It is often used to compact loose fill material, but also for compaction of waste. Very

heavy tamping may fissure the soil, helping water to escape, and may therefore be effective in fine-grained soils. The depth of influence H is estimated as $H = n\sqrt{(Mh)}$, where M is mass in tons and h is the drop height in m. The empirical constant n varies from 0.5 to 0.9 in sand, and from 0.3 to 0.5 in silt and slightly clayey soils. In a final "ironing" phase, the upper metre is densified. Bearing capacities up to 250 kPa can be reached, allowing simple spread footing foundations.

Vibro-compaction

A vibrating poker also known as a vibroflot is used to densify cohesionless soil. Applied in a grid, mass improvement is achieved. The relative density of sand can be raised between 70 to 85%.

Mass stabilisation

Solidification of the entire soil mass can be brought about by mixing stabilising agents such as cement into it. This method has been developed in Finland to mass-stabilise peat and soft clays and silts up to a depth of 4 m. A mixing tool is moved through the upper part of the soft soil horizontally as well as vertically. At the same time a chemical binder, usually cement, is injected near the mixing tool, and the soil eventually hardens. Settlements are reduced and stability improved. The method is mainly used in infrastructure projects.

Vertical drainage

Artificial drainage of soft soils consolidating under applied overburden is also a mass improvement method. Embankments built over soft soil, and extensive sand fills on marshy (polder) areas, call for such enhanced drainage, and the method of vertical drainage by means of wick drains is much used for this purpose. The method is sometimes designated as Prefabricated Vertical Drains (PVD). The drains consist of a core of polypropylene with grooves (castle board or fish-bone) and a filter fabric as wrapping. They are pressed into the soil by a mandrel, and are repeated at distances of between 1 to 3 m. Stressed pore water in the soft layers passes through the filter fabric into the grooves and travels upwards to the surface where excess pressure is absent. From there it is drained off to ditches, etc. Hence, the soil consolidates and settles more rapidly.

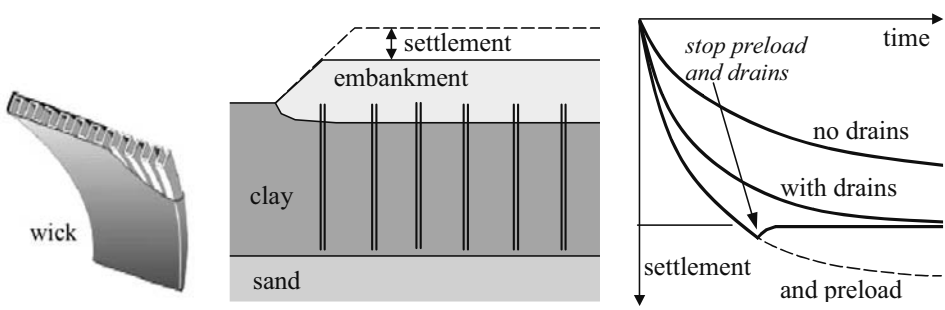

Figure 13.5 Vertical drainage applied for widening a highroad on soft soil

Drainage can also occur downwards to a draining layer of sand. This is quite possible in the Netherlands where the Pleistocene sands underlying the soft Holocene deposits usually have potential heads equal to or even lower than the surface ditch levels. However, the pore water in the Pleistocene often communicates with seawater and can be silty. If potential head in the Pleistocene can equal or exceed the polder levels, the drains are usually terminated 1 to 1.5 m above the Pleistocene, to prevent upward seepage of silty water (Fig 13.5).

The flow of water escaping from the soft soil is predominantly horizontal when vertical drains are present. The length of flow in the soft soil is drastically reduced by the vertical drains, to at most one-half of the centre-to-centre distance of the drains. A simple but rather approximate rule is that the duration of consolidation is proportional to the square of the maximum drainage distance. If drains are centered at 1.5 m in soft layers 10 m thick, the period of drainage is $10^2/1.5^2 = 45$ times shorter. Vertical drainage is designed to obtain the necessary consolidation in a period of less than 6 to 12 months. Sustainability of the soil and groundwater is of special concern when vertical drains have been used. The drains remain in the soil and they may provide an easy way for pollutants from the surface (industry plant) to reach sandy layers and cause groundwater contamination.

The effect of the vertical drainage can be incorporated into the consolidation equations. This was first achieved by Barron (1947). The (average) pore pressure u dissipating around a vertical drain (Fig 13.6a) during a consolidation process, triggered by a sudden loading σ_0, is, according to Barron, when assuming uniform (vertical) strain

$$u = \sigma_0 \exp(-8T_h/F(\delta)) \qquad (13.1)$$

Here[51], $T_h = c_v t/4R^2$, $2R$ is drain spacing and $F(\delta) \approx \ln(\delta) - ¾$, for $\delta = R/r_0 > 8$, with r_0 the (equivalent) drain radius. Approximation of $\ln(\delta)$ yields (see Fig 13.6b)

$$\ln(\delta) \approx 0.16\delta + ¾ \qquad \text{for} \qquad 5 < \delta < 20 \qquad (13.2)$$

Hence, Barron's formula can be rewritten into

$$u = \sigma_0 \exp(-8T_h/F(\delta)) = \sigma_0 \exp(-t/\theta_B) \quad \text{and} \quad \theta_B = R^3/(12.5 r_0 c_v) \qquad (13.3)$$

The condition of uniform strain, which Barron imposed, is fundamental to this solution.[52] In reality, induced horizontal stress gradients may cause a redistribution

---

[51] In fact, Barron wrote $T_h = c_v(1+e)t/4R^2$, voids ratio $e = n/(1-n)$. The introduction of the voids ratio was in Barron's time generally in use after Terzaghi's suggestion to define strains with reference to the solid part of the height. The parameter c_v is found accordingly. Presently, one refers to the bulk height, and the corresponding parameter c_v is found. Hence, the factor $(1+e)$ can be disregarded.

[52] For shallow layers the deformation is stress-conditioned, allowing for differential settlements. For deep layers the overburden works like a stiff beam and the deformation is strain-controlled (uniform), inducing stress redistribution. This causes additional horizontal pressure gradients. In the oil/gas industry this phenomenon is called compaction drive.

of pore pressures resulting in changes in the pore pressure gradient, and for large interspaces between the vertical drains, i.e. $R > h$, the assumption of uniform strains does not hold. In practice, for designing vertical drainage systems, one uses simple diagrams, which are based on formula (13.3).

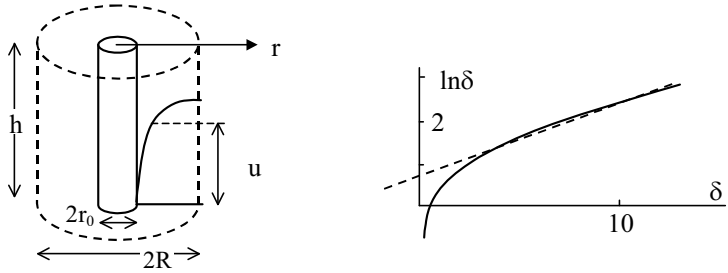

(a) process around one drain *(b) approximation*

Figure 13.6 Consolidation by vertical drains

Vacuum drainage

Newer methods have been developed making use of vacuum drainage. The method was actually first developed in China. The vacuum can be applied to a sand fill, which is covered by impervious membranes, thereby drawing the pore water up to the surface. Vertical drains enhance the action. Sometimes the lateral boundaries of the area are sealed off by e.g. slurry walls to prevent drawing in water from the vicinity.

One of such methods (Beaudrain) applies the vacuum directly to vertical drains, and another method (IFCO) uses a hydro-mill trench cutter to bury horizontal drains at the bottom of the trench, which is back-filled with sand (Fig 13.7). Vacuum is then applied to the drains, which connect to the surface. The trenches are about 0.25 m wide, up to 5 m deep and are repeated at e.g. every 3 m. Here, vacuum pressure in the vertical drains or trenches is applied to enhance the settlement process. The vacuum pressure, maintained by isolating the underground from the atmosphere with a (local) impervious sealing at the surface or just above the drains, works similar as a preloading.

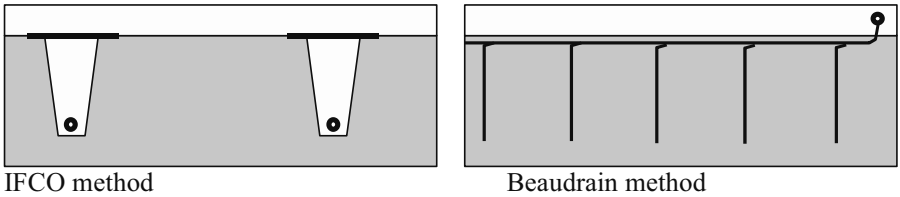

Figure 13.7 Vacuum consolidation

These methods have in common that the amount of applied vacuum increases the hydraulic gradient, which determines the rate of flow of pore water from the soil. When sufficient consolidation has been achieved, the vacuum pumps are turned off, and slight swelling of the soil may occur as water is drawn back into the soil. During swelling, the reload stiffness applies, and as it is higher than the virgin

compressive stiffness, swelling is limited. The reduction of potential head within the soil mass by the vacuum has the added advantage of increasing the stability of the sides of the embankment.

Preloading

Preloading is a commonly used technique to speed up consolidation of embankments and extensive sand fills on soft soils. The applied overburden is increased temporarily (II) to a thickness above what is eventually needed (III), and is removed after settlements have increased sufficiently (Fig 13.8). The idea behind achieving more settlement in the construction period is that a "period of grace" is obtained during which very little settlement occurs. This period is the beginning of the service life of the structure (road, railway, embankment, etc) and, if it can be made to last long enough, reduces maintenance costs drastically.

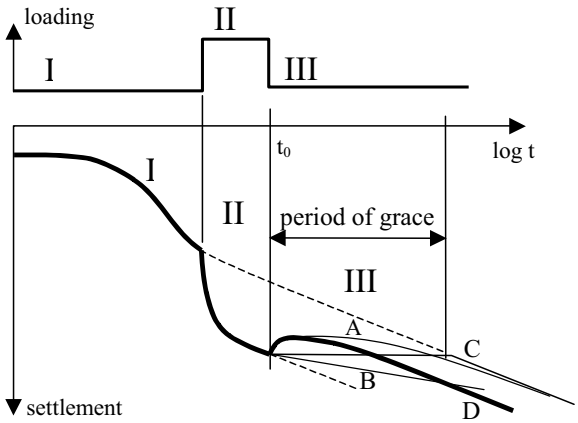

Figure 13.8 Stages during preloading

There are various views with regard to the duration of the period of grace, and whether or not swelling occurs when the preload is removed. View C in Fig 13.8 expects settlements to completely cease until the time it would have taken load III to achieve the same settlement. This is certainly too optimistic. View A incorporates swelling due to the unloading, but is otherwise equal to view C. It is also optimistic. View D is the most likely behaviour: first swelling occurs due to reversed consolidation, and then creep reasserts itself, more quickly than expected in view C. The curve B may occur if the preloading is very minor or is removed too quickly. Then swelling may not occur. Applying vertical drains in the preloading period helps to more quickly transform the extra overburden into effective stresses. Then a longer period of grace is obtained.

The isotache model or abc-model (see Chapter 6) is useful to design preloading. Such models predict a behaviour according to curve A, because the virgin isotaches (i.e. the relationship between effective stress, incurred strain and creep rate of strain in virgin conditions) are also applied to the unloading and the recompression after swelling. During the unloading however, the virgin isotaches are disturbed, and higher rates of compression occur after the end of swelling than predicted by

the virgin isotaches. It will be necessary to account for this, when more accurate predictions of post preloading behaviour are available. In the meantime, a simple expedience is to reduce the amount of unloading in the calculations to some empirically decided percentage of the actual unloading.

It should be realised that the central issue in preloading design is creating a period of grace of sufficient length. Some methods of calculation focus on the latter part of the post preload curve (the "recompression" curve) and are less accurate with regard to the period of grace. Unfortunately, no accurate methods presently exist for the latter.

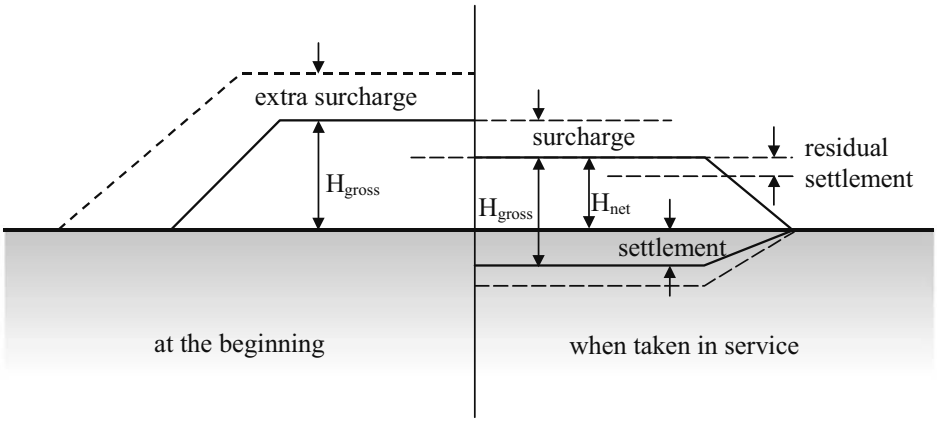

Figure 13.9 Definitions for preloading design

There is perpetual confusion about the terminology surrounding preloading. The word surcharge is often used in the same meaning.[53] The prefix *pre* may denote either a load that is applied earlier to obtain reduced settlements later, or denote load that is removed. The prefix *sur* may denote a height of fill that is applied to compensate for settlements due to the fill itself, or the extra load that is later removed. A Dutch committee has solved this matter by a new set of definitions shown in Fig 13.9. Surcharge is now the load applied to compensate for settlements, and extra surcharge is the load, which is eventually removed. The word preload is avoided. In the paragraphs above therefore, preload would become "extra surcharge".

D STIFF INCLUSIONS

The group of ground improvement methods that apply stiff elements into the soft soil, is quite large and varied. The following methods are discussed: compound wooden columns, stone columns, deep mixed columns, compaction grouting, compensation grouting, and geotextiles.

[53] The same unclarity occurs in Dutch: “voorbelasting” respectively “overhoogte”.

Compound wooden column

An interesting historic ground improvement is shown in Fig 13.10. It dates back to the 17th century. Probably the technique is much older. In very soft saturated soil (peat and clay) a foundation was made on a series of compound wooden columns, called "hui" (the word does not occur in dictionaries any longer, probably is meant "hat"), each of which at a mutual distance of about 2 m consisted of a bundle of short poles of about 3 to 4 m, kept together by half a cask. A double hoop held the staves of the cask. On these columns with their head just above groundwater level a massive wooden beam was placed, upon which the masonry of the foundation started. This foundation was well preserved in the saturated peat and clay.

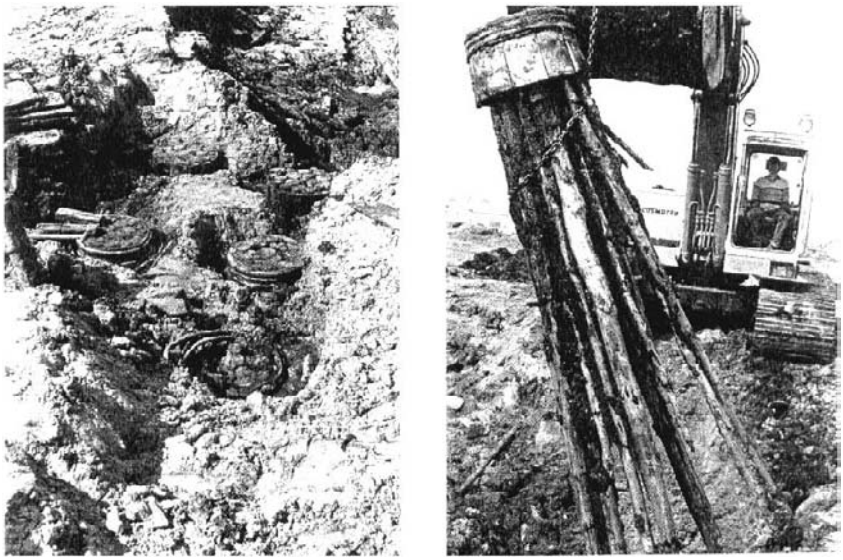

Figure 13.10 Historical compound wooden column; a 'hat'

Stone columns

Both vibro-compaction and vibro-replacement use a vibrating poker to make a hole in the ground. Soil is displaced sideways, not removed from the ground. For vibro-compaction in coarse-grained soils the poker may be removed slowly while still vibrating. This causes the sides of the hole to collapse and results in a depression in the ground surface. For vibro-replacement in fine-grained soils it is usual to fill the hole with coarse aggregate (up to 50 mm). The poker may be used to compact the stone column in layers. A typical column might be 5 m deep and 0.5 m diameter. A line of such columns at say 3 m centres can be used to support a reinforced concrete raft or beam effectively, producing a kind of piled foundation.

Deep mixed columns

Deep mixed columns, also known as lime-cement columns, mixed-in-place columns, dry-jet-mixed columns and soil-cement columns, were developed independently in Sweden and Japan from the 1960's onwards. A mixing tool fixed to the end of a kelly bar is moved vertically through the soil, and a binding agent is injected near the mixing tool and mixed into the soil. A hardened column of soil

results. Columns are applied in grids, in walls (Fig 13.11), and occasionally overlapping on all sides to achieve mass stabilization. Binder powder can be transported to the mixing tool by air (dry mixing), or it can be slurried (wet mixing). Column diameters are typically 50 cm, and lengths can be up to 60 m (Japan, offshore). The Scandinavian method applied unslaked lime (CaOH) sometimes with Portland cement in a 1:1 ratio, and was limited to soft, inorganic clay. Typical binder dosage is in the order of 60 to 100 kg per m^3 of treated soil.

Figure 13.11 Application of mixed column walls for a large building pit

Recently it has proven possible to apply the method in organic clays and even in peat. Lime does not harden well in these soils, but blast furnace cement has been found to give satisfactory results, albeit that high dosages in the order of 250 kg/m^3 are needed. The latter development has brought the method into focus in the Netherlands, covered as it is liberally with soft organic soils. It was trial tested since 1998 at a number of locations, and has been since used in a number of projects, all of which happen to be train tunnel approaches: Botlek train tunnel, Randstadrail tunnel, Groene Hart tunnel. Its use is being contemplated for stability enhancement of river dikes as a space-efficient alternative to berm widening (the INSIDE concept), see Chapter 17.

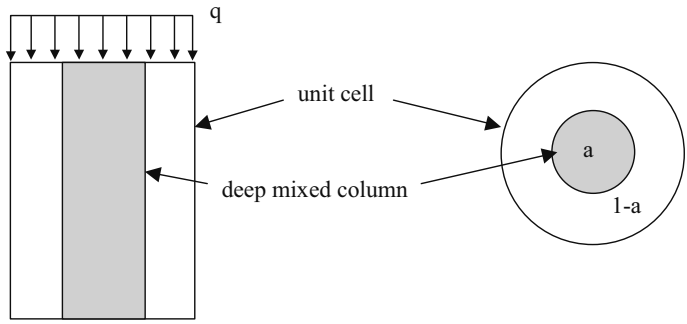

Figure 13.12 Schematization of a deep mixed column

The columns perform best under vertical load and can reduce settlements considerably, e.g. of embankments on soft soil. They are also used to increase stability of slopes, embankments and excavations. However the shear strength of the columns is low for horizontal and passive states, and large safety factors must be applied. The columns are therefore generally placed in overlapping as walls or in lines of blocks perpendicular to the sliding direction.

The settlement reduction in soft soil relies on the stiffening effect of the columns. The 'equal strain assumption' is often adopted: equal vertical strain is assumed in the column and in the surrounding untreated soil. If the mixed soil is α times stiffer than the natural soil, $\alpha = E_c / E_s$ (E is one-dimensional stiffness modulus), the columns have an area ratio of a (cross section of column as ratio of the cross section of a unit cell containing one column), and the soil is loaded at the surface by q, then at each depth it follows that $\sigma'_c / \sigma'_s = \alpha$, where σ'_c is the stress in the columns and σ'_s is the stress in the soil due to the surface load q. Accounting for the area ratios, the columns carry $q_c = a\sigma'_c$ and the soil carries $q_s = (1-a)\sigma'_s$. With $q_c / q_s = \alpha\, a/(1-a)$, the bearing capacity becomes

$$q = q_c + q_s = \frac{1 + a(\alpha - 1)}{(1-a)} q_s \qquad (13.4)$$

Commonly, an area ratio in the order of $a = 0.2$ is used, so that $q_c / q_s \approx \alpha/4$. The stiffening ratio can be in the order of $\alpha \approx 20$ to 50, so that quite a large proportion of the load is attracted by the columns (about tenfold). In the equal strain theory no transfer of load occurs between the soil and the columns by interface shear, and in practice this is quite likely to happen. Any settlement of the ground surface below the head of the columns will result in the columns attracting more load from the fill. Arching will occur if the fill is granular and has sufficient thickness. Consolidation and creep effects in the soft soil must also be accounted for. The columns may act as large vertical drains if binder dosage is limited and the soil is not very fine-grained.

Grouting

Injection of viscous liquids into the soil by grouting serves a number of purposes, the most common being reduction of permeability, strengthening of soil, compaction and expansion. In permeation grouting, the liquid invades the soil and hardens. Permeability can be reduced and voids filled. It is not applicable in fine-grained soils.

Compaction grouting

Injecting cementitious material into a soil mass tends to reduce permeability, cause swelling and may increase strength. Grout injection into fractured rock, which forms the foundation of a dam is possibly the oldest and best-known application. Grout injection has been used successfully to strengthen and reduce permeability of soil around a basement excavation below the water table. It has been used to control the settlement of structures adjacent to tunnel excavations in London Jubilee line: predicted settlements of 60 mm, which would have caused

extensive damage to old buildings, were limited to 10 mm. Compaction grouting uses displacement to effect densification of the soil. Highly viscous grout is used. Large voids as in karstic soil, loose fill (e.g. rubble), etc. can be compacted. Grout bulbs are formed from an injection point. A sequence of primary, secondary and tertiary bulb locations is sometimes applied to achieve fuller coverage.

Compensation grouting

In this application, grout slurry is used to fracture the soil thereby effecting expansion and heave. It can be used to compensate the settlement of a foundation when a tunnel is being passed below it, or to rectify or reduce differential settlements of foundations. Elaborate deformation and injection pressure monitoring and control are required.

Jet grouting

Jet grouting has increasingly become one of the ground improvement technologies used to address leakage and to provide strength improvement to soils. The technique of jet grouting uses high pressure/velocity jet fluids to erode the existing soil and then to mix the cuttings with cement slurry, a binder (at lower pressure), to form 'soilcrete' (see picture: cement-soil mixer). Excess slurry or spoil is ejected to the surface. Alternative methods apply a jet of slurry (single fluid method) or envelope the water jet by air (triple fluid method) to enhance erosion. The latter method is effective in cohesive soil. Not only are jet grout columns or sheets used for load carrying, but when applied in overlapping grids, impermeable seals can be formed, e.g. between sheet piles to allow the excavation of watertight spaces, or underground bulwarks for slope stabilisation. If the native soil is not completely mixed with slurry, the resulting columns will have soil inclusions, which can reduce the strength of the column and/or increase the permeability of the column. Monitoring and control are required.

cement-soil mixer

Geo-textiles

Geo-textiles can be used for segregation of layers. Rock-fill being laid on soft ground to form a road or embankment base can be prevented from punching into the soil below using a geotextile underlay. It can provide tensile strength. Horizontal membranes can be used to provide tensile reinforcement and reduce settlement. It can act as drainage layer, either as a water-conductor or as a filter to reduce the migration of fine particles into a granular soil drain, or it can act as an impermeable barrier preventing or controlling the flow of contaminated groundwater from or in landfill sites. As a tensile support there are two difficulties: aligning the membrane in the direction of the principal tensile stress, which is

probably not horizontal, and the fact that geotextiles have a low modulus of elasticity and are plastic and therefore tend to creep.

Pile-mattress

The pile mattress (Fig 13.13) is a type of load relief structure. The ground pressure is reduced by a system of mat and piles that carry a part of the loading to deeper-seated bearing layers. The mat may consist of a geotextile or reinforced grid (chicken-foot system) which transfers the load to the pile heads, after a certain settlement has taken place. As an alternative for the mat a mattress of reinforced soil can be used, where the load transfer is realised by arching. The design of load relief structures involves many aspects of geotechnical engineering: pile behaviour (end-bearing and/or friction), settlements, horizontal deformation, arching, geogrid strength and flexibility, durability and safety factors. Since 2005, a pile mattress with a geogrid reinforcement and a sludge mixture (renewable material) as fill has been tested as a relatively cheap and environmentally friendly method for road foundation on very soft soils (Kyoto Road). The results are positive. The reduction of the ground pressure is 50%, arching effects increase with time, and the various available design methods predict reasonably well (van Eekelen).

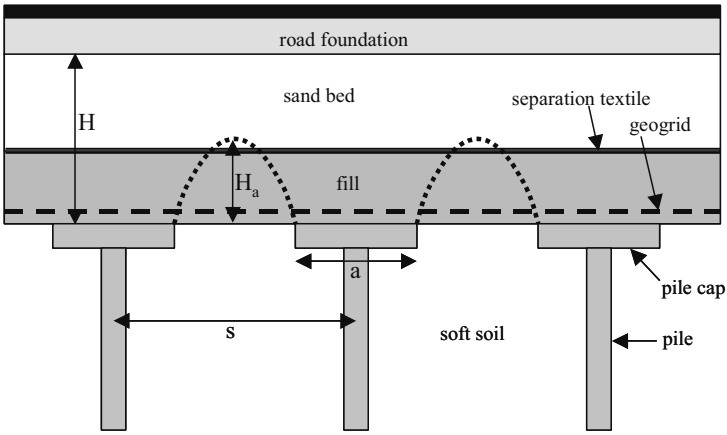

Figure 13.13 Pile mattress

E BIO-CHEMICAL TREATMENT

SmartSoils® are technologies, launched by Deltares, that can direct the localisation and rate of natural soil processes that influence soil properties. By influencing these processes, there is real potential to alter the properties of the soil (for example, permeability and stiffness). Thus, by means of specific biological and chemical technologies, one can generate soil to suit a desired purpose, such as changing the natural soil to make it suitable as a foundation for construction. Some successful examples are:

- Self-cleaning Road. A unique road construction for transformation and remediation of contaminated dredged material over the lifetime of the road.
- Biosealing. A natural biological process for self-detection and sealing of leakage in water impermeable barriers.

- Biogrout. In-situ cementation of permeable soils for strength improvement with retention of permeability.
- Black Clay. Active carbon/clay organic barrier for isolating material from the environment.
- Drillmix. Fluid for horizontal directional drilling that is suitable for use in salt-water.
- ETAC. Two-component grout system with an adaptable hardening time for efficient tunnel boring, even in impermeable soils.

The core of biological treatment is using specific bacteria and chemicals in the soil, and enhancing the activities with appropriate treatment (nutrients), which results in required changes, such as permeability (Biosealing: 10 to 50 fold reduction is possible in sands) and strength (Biogrout: up to 5 to 10 times increment is possible in sand), see Fig 13.14.

In organic clay and peat-containing soils, contaminated and uncontaminated dredged sludge the improvement of soil properties via biological methods is under investigation. This field of 'pore-space engineering' is a relatively new branch in geotechnical engineering: it involves different disciplines and offers many challenges.

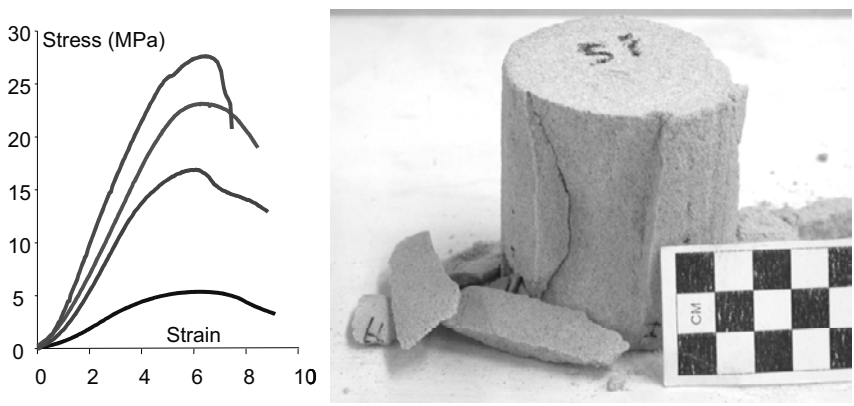

Figure 13.14 Biogrout: compression strength after successive bio-flushings

application 13.1

Consider a soft saturated clay layer with a height of h = 5 m. Vertical drains are installed. The consolidation coefficient is determined in the laboratory: $c_v = 2\text{x}10^{-6}$ m^2/s. An additional permanent ground layer (weight γ = 18 kN/m^3) to be placed on top involves an extra total vertical stress of σ kPa in the clay layer. To reduce the consolidation period $T_{hd} = 2h^2/c_v$ (see equation 6.8), in this case $2(5)^2/2\text{x}10^{-6} = 25\text{x}10^6$ s =9.7 months, a vacuum pressure of v kPa is applied. Which vacuum pressure reduces the consolidation period by a factor 4, to about 2.5 months, and what maximum height of the additional soil layer can be handled?

The total stress σ is counter balanced by with time decreasing pore pressure u and increasing effective stress σ', and the corresponding settlement S increases proportional to the effective stress. Hence, the progress of the degree of consolidation U (see equation 6.6) is conformal to the pore pressure development,

shown in Fig 13.15. The value of U at the end of consolidation at $S \approx S_\infty$ is 0.994, when $t = T_{hd}$, and at 1/4th of this period $U = 0.764$.

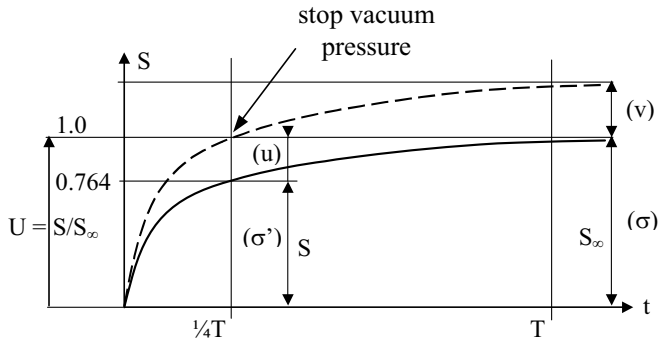

Figure 13.15

A vacuum pressure is simply additive and, therefore, its value causing a reduction of the consolidation period by a factor 4 can be obtained by proportionality, according to

$$v/(v+\sigma) = u_{t=\frac{1}{4}T}/\sigma = (1-0.764) = 0.236 \qquad \text{or} \qquad v = 0.31\sigma$$

In this analysis the vacuum pressure is assumed uniformly distributed in the clay layer, which is not usually the case. In the pipes and/or drains the vacuum pressure is significantly lower, and there a practical lowest value is about 70% of the atmospheric pressure (~100 kPa), which limits the extent of the vacuum method. In this case, with $v_{max} \approx 40$ kPa, the maximum load which can be dealt with for a reduction of 4 times is $\sigma = 40/0.31 \approx 130$ kPa, or a height of 130/18 = 7.2 m. This shows that vacuum consolidation can be effective.

application 13.2

Calculate the required spacing of vertical drains in a soft soil deposit to achieve a reduction of excess pore pressures to 30% of an applied surface load within 5 months. Data: prefabricated drains, width 150 mm, thickness of 6 mm. Consolidation coefficient of soft soil $2\text{x}10^{-8}$ m^2/sec.

application 13.3

Calculate the time required to obtain a degree of consolidation of 90% using vertical drains in a soft soil deposit to which a surface fill is applied, using the following data: prefabricated drains, width 150 mm, thickness 6 mm, spacing = 2 m on a rectangular grid. Consolidation coefficient of soft soil $2\text{x}10^{-8}$ m^2/sec. Is the period you find acceptable in practice? Determine the dependency between this period and the drain spacing. From this, give the drain spacing needed to fulfil the specification within 1 year.

application 13.4

A soft clay site is to be prepared for development by applying a surcharge sand fill of 2m thick. Thickness soft clay is 6m. Groundwater level: 1m below surface. The wet unit weight soft clay is 14 kN/m^3, the dry unit weight sand: 16 kN/m^3, and porosity is 40%. Determine the required vacuum to be applied to prefabricated vertical drains to obtain 80% consolidation in 4 months. With what means could such a vacuum be applied? Drain distance $2R$ = 1.4 m; drain diameter $2r_0$ = 0.07 m. Coefficient of consolidation c_v = 2x10^{-7} m^2/sec.

application 13.5

Prefabricated vertical drains with vacuum are applied to drain a site with a very low c_v. Determine the required vacuum to be applied to the vertical drains to obtain 80% consolidation in 120 days. Surface load is 32 kPa. Coefficient of consolidation: c_v = 2x10^{-8} m^2/s. Drain distance $2R$ = 1.4 m. Drain diameter $2r_0$ = 0.07 m

application 13.6

Fig 13.8 shows settlement stages during preloading. Given $C_c/(1+e_0)$ = 0.5, $C_\alpha/(1+e_0)$ = 0.025, t_0 = 180 days, σ'_{II} = 120 kPa, σ'_{III} = 80 kPa, the most optimistic estimate of the period of grace is given. This is too optimistic, as explained in the notes. Find a more realistic estimate by assuming the unloading is only effective for 50%.

application 13.7

A fill, which imposes a load of 50 kN/m^2, compresses a clay layer of 5 m thick. Vertical drains are installed to accelerate the consolidation process. The drain width is 0.1 m, drain thickness is 0.01 m.

Determine an equivalent drain radius r_0, based on surface similarity.

Calculate the degree of consolidation U after 6 month, given c_v = 2x10^{-7} m^2/s, drain spacing $2R$ = 2 m (see Fig 12.6).

Calculate the time required to obtain the same degree of consolidation if vertical drains are not used, and only vertical consolidation occurs to the ground surface.

14 ENVIRONMENTAL ENGINEERING

Environmental engineering in the geotechnical profession can be seen as a part of eco-engineering or geo-engineering, which has become a new and important topic to retain the best possible living ambience on earth. The vastly increasing population and its affluence and technology is affecting the earth on a global scale, and if no changes occur, humans could become the reason of a sixth catastrophic mass extinction of plants and animals. Geologists debate to refer to this global impact as a new geological period: the Anthropocene. A fact is that humans are transforming the world and altering the planet through farming (40% of the land is used for agriculture) and by building cities (soon 80% of the expected 9 billion humans will live in large metropoles in fertile and vulnerable lowland areas). In a lecture about eco-engineering in 2010, Rijnaarts showed that the balance of depletion and accumulation in the natural biological system is at stake: the fresh water cycle is for 65% exhausted, the phosphorus cycle for 82%, the CO_2 cycle is with 110% beyond its balance boundary and nitrogen even with 400%, while the status of chemical pollution and the carbon balance are not known. Important minerals, like phosphor, may become extinct bringing life in real danger. There is hope that with growing awareness also readiness for a drastic change of human habits will increase.

The ground is an important buffer, a flywheel of society's wealth. Its protection is vital and geotechnical engineers should contribute their part in preserving the best conditions, in particular when building cities and their infrastructure and when exploiting transport processes in the underground. Environmental engineering in the geotechnical field usually considers the impact of (underground) construction to the surroundings (Chapter 15) and pollution of the underground, i.e. contamination of the ground, hazardous to flora and fauna (this Chapter).

It is not easy to distinguish pollution amongst the many natural processes that take place, more so as most are beneficial for controlling ground functions in a way to stimulate health and life in upper soil. The air and water in soil are volatile, but ground itself is solid. The knowledge of physical, chemical and biological interactions in the underground is important in order to understand not so much the presence of contaminants, but rather their effect. In environmental engineering, the effect of (human) action on the main functions of ground are studied. These functions are agriculture (food), filter (groundwater) and ecology (bio-cycles). Air pollution (heavy metals), water pollution (rivers), or solid pollution (dung, dump, spill, leakage) are widespread threats to the local ground quality. A modern way of treating polluted areas is Flexible Emission Control (Van Meurs) that involves impact containment and stimulation of natural bio-chemical cleansing.

A PHYSICAL-CHEMICAL CHARACTERISTICS OF SOIL

The upper soil can be considered as a three-phase system: solid, liquid and gas. The global average distribution of these components is: air 26%, water 24%, organic matter 5% and minerals 45%. In deltaic areas this distribution is different: air 5%, water 33%, organic matter 7% and minerals 55%. In these sedimentary

soils the solid phase consists of grains with intermediate space (pores) filled with gas or/and water. The density and constitution of these components have been discussed in chapter 2.

Solid phase

The mineral part of the soil is subdivided into sand (60 – 2000μm), silt (2 – 60μm) and lute or clay (< 2μm). The sand fraction is mainly quartz (SiO_2); adsorption is very small because quartz is electrically neutral. Pure sand has relatively large pores.

The silt fraction also has little adsorptive capacity. The lute fraction consists mainly of clay minerals. Clay minerals are usually aluminium-silicates composed of SiO_2-tetraeders and $Al(OH)_6$ – octahedran, where sometimes Si^{4+} is replaced by Al^{3+}, and Al^{3+} by Mg^{2+} or Fe^{2+} ions. This creates an electrically negative value and it has influence on the adsorptive capacity (cation exchange capacity). Other non-crystal matter consists of oxides, hydroxides and oxi-hydroxides of Al, Fe and Si and Al and Fe silicates. Fe oxides and organic matter usually determine the soil colour. Fe oxides may have a large specific surface area and play an important role in cementation or fixing of phosphate, molybdate or silicate, and also tracer elements Cu, Pb, V, Zn, Co, etc. The organic matter consists of remnants of flora and fauna. It plays a role in binding and buffering minerals and creates 'structure' (smaller and larger pores).

Neutral adsorption (a-polar binding) is inversely proportional to the 6th power of the distance (VanderWaals forces). Adsorption of electrolytes at internal (micro)-surfaces occur following Coulomb's law, i.e. binding forces are inversely proportional to the square of the distance. Replacement adsorption (exchange of ions) may work actively or weakly. The exchange capacity is determined by the ratio of the ions and follows a certain order, such as Li < Na < K < Rb < Cs < H. The adsorption capacity is essential for buffering nutrients for ecological processes in soils. Adsorption by organic matter is strongly dependent on the acidity (*pH*) of the soil, and may be significantly higher than by clay minerals.

Liquid phase

The liquid in soil is water, which may have various conditions (e.g. temperature, gas bubbles) and it may contain many solvents (salts, humus). It enters the soil by infiltration (rains, rivers) or by intrusion (density driven). Osmosis or capillarity may bind the liquid. Movement of the liquid through soil is controlled by gravity, osmotic and capillary forces. Binding forces between ground and groundwater are determined by mutual interaction of water molecules (hydration, usually a layer of a few molecules), osmotic water (electric ion concentration), and capillary water (combination of cohesive and adhesive forces). Bound water causes pressure gradients, which influences the adsorption by plant roots. Bound water above the groundwater table is called hanging or pendulous water. In time, it evaporates, is absorbed by roots or precipitates towards the groundwater table.

The water in the ground under the phreatic water table is referred to as groundwater. The phreatic or groundwater table is a hypothetical surface where the pressure is equal to the atmospheric pressure. The actual groundwater surface

cannot be sharply specified due to saturation, capillarity, and pore structure of the soil. The groundwater table usually follows the soil surface relief. Capillarity in sands is in the order of centimetres. In fine soils (clay) it can be metres. The groundwater table forms the border below which normally no plant roots grow (lack of oxygen). Groundwater extends in the subsoil in different layers, since the pore structure in coarse and fine soils are interconnected. The flow of water in various soil layers may differ significantly (permeability).

For a practical characterisation of the presence of water in the soil, i.e. the humidity, the *pF*-curve is used. It is the logarithm of the suction-tension (in mBar), i.e. a measure of the force of binding of water to the soil. In Fig 14.1a, some *pF*-curves are presented as a function of the saturation θ for various soil types.

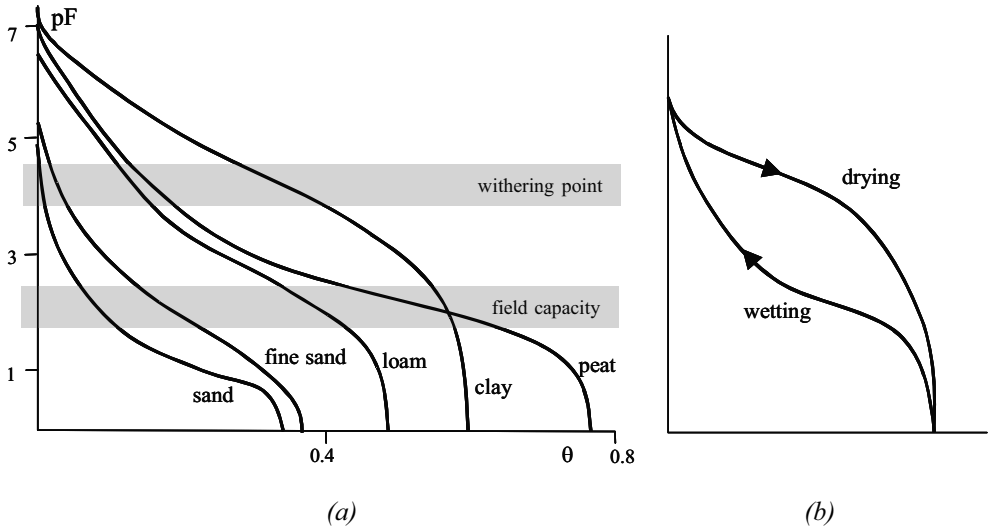

Figure 14.1 pF-curves

Two characteristic values are distinguished: the field capacity and the withering point, in between which the soil provides humid for plants. The field capacity is related to the absorption capacity of the soil for heavy rain. Usually at $pF = 3$ (equal to 1 Bar) all capillary water has vanished. The field capacity varies normally between 1.8 and 2.5. The withering point is around $pF = 4.2$ (equal to 16 Bar), where plant roots cannot obtain water anymore, although some arid and alpine plants species can exert suctions up to 60 Bar. The behaviour for wetting (adsorption) or drying (desorption) is hysteretic (see Fig 14.1b). It causes a larger *pF* value at drying than wetting for the same saturation.

Gas phase

The most common gas in soil is air (oxygen, nitrogen and carbon dioxide). The amount of gas is determined by the porosity and the humidity (saturation). The composition of the gas in soil is controlled by biological activities and the atmospheric air composition. Usually the CO_2 concentration in soil is higher than in the atmosphere, and the opposite holds for oxygen. A diffusion process triggered by the concentration gradient will cause transport from and to the soil. Diffusion in

gas is about 10,000 times faster than in fluid and therefore the diffusion speed is mainly determined by the saturation degree. After strong and long rain periods the diffusion will be significantly less. In the air, the sum of oxygen and carbon dioxide is about 21%, both in soil and atmosphere; the nitrogen concentration in soil is about equal to the atmosphere. The oxygen concentration in soil rarely drops under 15%, and CO_2 content rarely rises above 6%.

B PHYSICAL-CHEMICAL PROCESSES IN SOIL

Transport in soil

Transport in soil is mainly caused by groundwater movement. Permeability and pressure differences control the groundwater flow. Three aspects of transport by groundwater flow are considered: convection, diffusion and dispersion. The largest amount of transportation in the soil is by groundwater convection of dissolved or suspended matter. It is expressed as qc, where q is the groundwater discharge velocity and c the concentration of the dissolved or suspended matter.

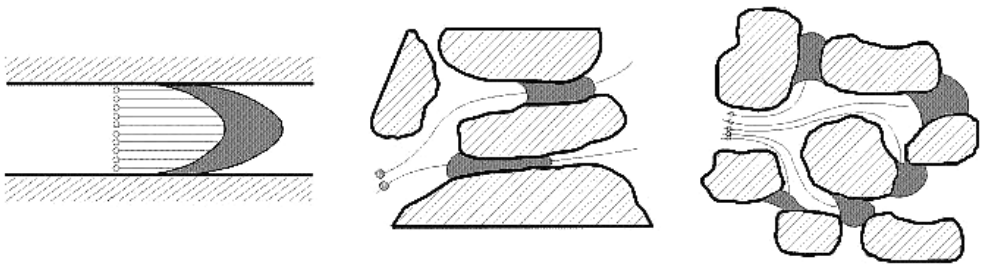

(a) velocity inside a pore *(b) variation of pore diameter* *(c) variation of direction*

Figure 14.2 Dispersion by groundwater flow at micro level

Diffusion and dispersion

In the transport process diverse scales are used. Microscopically, grains and pores exist and the concept of porosity does not apply. In case the concentration is not uniform, molecules will move differentially, driven by the concentration gradient. This mode of transport is called diffusion and described by Fick's law: $wc = D_d \nabla c$, where w is the local fluid velocity in a pore, and D_d the molecular diffusion coefficient. The value of D_d in pure water is in the range of 10^{-8} to 10^{-11} m^2/s. The transport is also affected by convection, characterised by microscopic velocity profiles. Suspended particles in 'favoured' flow lines will move faster than in more stagnant flow lines (Fig 14.2). Because of these microscopic differences in velocity in the pore structure extra spread occurs, referred to by dispersion (Bear, De Josselin de Jong, Strack, Hassanizadeh).

At a larger scale, at macroscopic level (multiple of pores), the transport is described by a law similar to Fick's law with a dispersion coefficient D, related to the average fluid velocity $v = q/n$ (porosity and Darcy velocity q exist). It contains a longitudinal term $D_L = D_d + \alpha_L v$ and a transversal term $D_T = \alpha_T v$, where α_L and α_T are dispersivity parameters with dimension of length.

The use of analytic elements for numerical studies of the phenomenon of macroscopic dispersion has advanced significantly in the last years. By applying the principle of superposition, computational performance could be increased by special solvers and parallel processing. Supercomputer clusters analyze ground water flow and transport through hundreds of thousands of particles, allowing stochastic experiments to examine effective conductivity and dispersion coefficients for heterogeneous formations, describing detailed variations at various levels. One peculiar result of such analysis is the additional effect of microscopic torque flow on dispersion in three-dimensional simulations, which is not observed in two-dimensional flow (Jankovic).

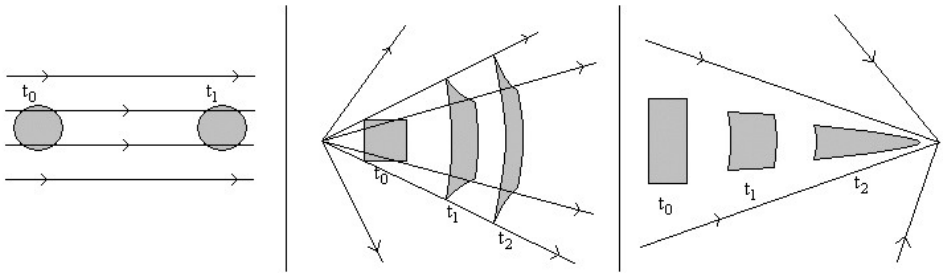

Figure 14.3 Dispersion by groundwater flow at meso-level

At a larger scale, at mesoscopic level, the velocity field itself is non-uniform (Fig 14.3) and the concentration may change accordingly with a dispersion coefficient of a different scale and the dispersivity should attain a value according to the length scale of the flow field characteristics.

If one considers regional differences, the megascopic scale, i.e. soil layers with different permeability and usually with horizontal dimensions significantly larger than vertical ones, the transport process could be characterised with a dispersivity of a regional length scale. (Fig 14.4).

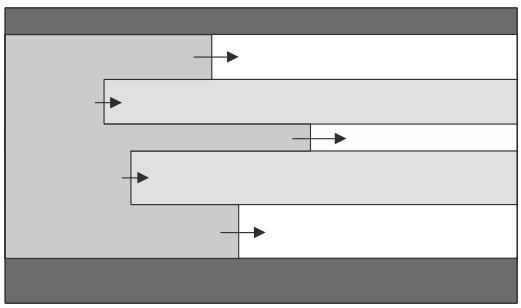

Figure 14.4 Mega-dispersion

The transport of a concentration of a solute of suspended material in a plane uniform groundwater flow at velocity v (convection) is described by the so-called transport equation at macroscopic level, according to

$$D_L \frac{\partial^2 c}{\partial x^2} + D_T \frac{\partial^2 c}{\partial y^2} - v\frac{\partial c}{\partial x} = R\frac{\partial c}{\partial t} + \mu c \qquad (14.1a)$$

Here, $R \geq 1$ is the retardation factor which expresses the 'loss' of solute due to absorption at or in the solids of the porous matrix, and μ is an autonomous decay factor, expressing that the solute vanishes according to $\exp(-\mu t/R)$. For a constant groundwater discharge, equation (14.1a) can be reformulated into

$$D_L\left(\frac{\partial^2 C}{\partial \xi^2} + \frac{\partial^2 C}{\partial \eta^2}\right) = \frac{\partial C}{\partial \tau} \qquad (14.1b)$$

with $C = c\,e^{\mu\tau},\ \xi = x - v\tau,\ \eta = \beta y,\ \tau = t/R,\ \beta^2 = D_L/D_T$

The solution for a point injection of intensity A becomes

$$C(\xi,\eta,\tau) = \frac{A}{4\tau\pi}\exp\left(-\frac{\xi^2+\eta^2}{4D_L\tau}\right) \qquad (14.2)$$

The maximum concentration is found at $(\xi,\eta) = (0,0)$, equal to $A/(4\tau\pi)$. Because at the location of the maximum $x = v\tau$ holds, $C_{max} = Av/(4x\pi)$. Inserting $C = c\exp\mu t$, leads then to $c_{max} = Ave^{-x\mu/v}/(4x\pi)$. The spreading due to dispersion is expressed by the standard deviation $\sigma_L = (2D_L\tau)^{0.5}$ and $\sigma_T = (2D_T\tau)^{0.5}$. The trend of decay and spreading is shown in Fig 14.5.

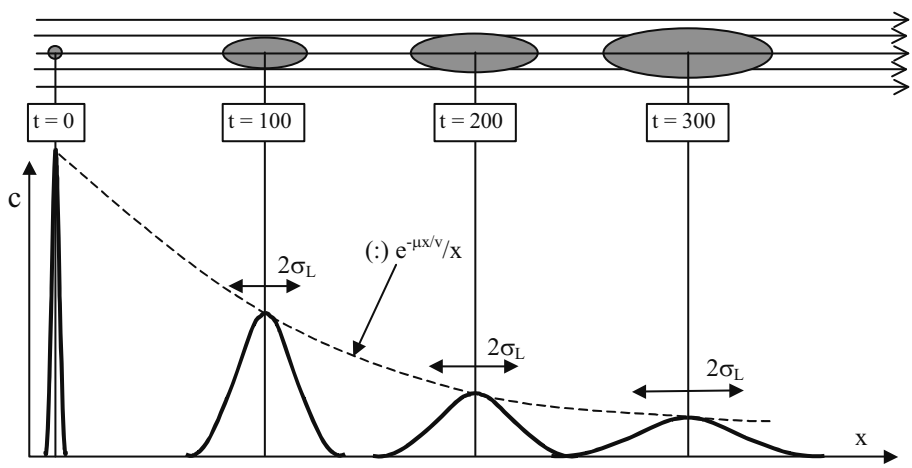

Figure 14.5 The decay and delay of a point injection in a 2D uniform flow

Adsorption and desorption

The amount of adsorbed matter (adsorbate) depends on the concentration (adsorbens). Several formulas describe this behaviour (Freunlich, Langmuir). The process is usually temperature dependent. For electrolytes other aspects have to be accounted for as well. In general one can state that all aromatic matter is strongly

adsorbed, and all aliphatic organic matter and inorganic matter are weakly adsorbed, with the exception of chlorine, brome and iodine. If during convective transport a part of the matter is being adsorbed, it shows up by the changes in concentration occurring slower; one speaks of a retardation effect, which can be incorporated as a time factor.

Chemical equilibrium

Chemical processes represent another significant aspect of changes in concentration in soils. Such processes are related to the chemical equilibrium of solid matter, i.e. the dissolution in water, of different fluids and fluid-gas, i.e. solution of gas in the fluid. Because of suspension and solution, these processes determine the mobility of specific matter. Many such processes may run parallel and interact, making the system complex.

Specific chemical reactions mostly depend on the *pH* of the soil fluid, the CO_2-tension in soil and the redox potential. The redox potential reflects that oxidation is always coupled to a reduction and expresses the potential of electron exchange during oxidation. Important elements in soil are calcium, iron and aluminium. In calcium-rich soils (with low ventilation) there is little to no (micro)biological activity and the *pH* may reach 10 (maximum). If such a soil is well ventilated (CO_2) the *pH* drops to 8. If the CO_2-tension increases the *pH* becomes even lower, down to 6.7, due to which more $CaCO_3$ dissolves. Iron is present in soil as oxide or hydroxides and as organic and inorganic complexes. Both the ions and the Fe^{3+} may occur; their activity is determined by the *pH* value. Aluminium is present in Feldspath, and oxides and hydroxides, both crystalline and amorphous. Under low *pH* Al and Fe oxides can dissolve, infiltrate to lower regimes and precipitate again.

C BIO-CHEMICAL PROCESSES IN SOIL

Biologically induced chemical processes in rock, including soil, are due to the activity of flora and fauna within it, much of which is microbial. Mould, yeast, and most of the microbes, such as bacteria are heterotrophic, i.e. they obtain carbon for their growth from organic materials. Microorganisms such as algae and other bacteria obtain carbon from CO_2 or CH_4, and are called autotrophic. The energy for heterotrophic life is obtained from oxidation-reduction reactions. Beside aerobic breakdown with oxygen as electron acceptor, anaerobic breakdown occurs with many kinds of organic or inorganic matter as electron acceptor (notably sulphates, nitrates, Fe^{3+}). The redox potential is a measure of the likelihood of such reactions. Bacteria and notably archea can prosper under large ranges of redox potential, acidity (*pH*), temperature and pressure.

For about 3 billion years microbial life existed on earth before complex multi-cellular life forms arose, only about 600 million years ago. About 2.5 billion years ago oxygen entered the oceans after the rise of cyano-bacteria, which give oxygen as a waste product; oxigen eventually also entered the atmosphere. Bacteria and archea have contributed significantly to the present-day atmosphere, hydrosphere and biosphere. They occur in unsaturated soil, but also in groundwater, and in oil and gas reservoirs at depths over 5 km, in oceans to over 10 km deep and under conditions of 100° C. They catalyse many chemical reactions in the

geohydrosphere including dissolution of silicates, oxides, sulphides, and carbonates (weathering), and form a variety of minerals, notably sulphides, carbonates, and generate hydrocarbons. As a consequence, these reactions change the subsoil drastically.

In this respect, it is important to know whether certain soil pollution can be a part of a 'natural' cycle, and is therefore in principle not a negative aspect of the soil condition. Bacteria and archea play a main role in the present day cycles of oxygen, nitrogen, sulphur and carbon. Oxygen is important for biodegradation of pollutants like carbohydrates and organo-chlorine matter.

Since bacteria also contribute to soil structure (e.g. dissolution and cementation) their activity can be used to modify soil properties to meet our needs. There is great potential in using natural processes without harm (building with nature). In some cases, there is also potential to recycle waste materials and turn them into new construction materials. In this respect, SmartSoils® are technologies that can direct the localisation and rate of natural soil processes that influence soil properties. By influencing these processes, there is real potential to alter the properties of the soil (permeability, porosity, stiffness and strength, see Chapter 13E).

D HEAT / COLD TRANSPORT IN SOIL

Storage of solar energy and industrial heat at shallow depth and using it for heating is known as heat-and-cold storage. At greater depth, in search for sustainable energy, the exploitation of geothermal energy from underground hot reservoirs becomes opportune. The process of heat/cold transport in saturated porous media involves conduction, convection, dispersion and bleeding (conduction into the surroundings). Convection is the heat transport by the pore fluid motion and bleeding is the heat/cold loss by conduction into adjacent semi-pervious formations.

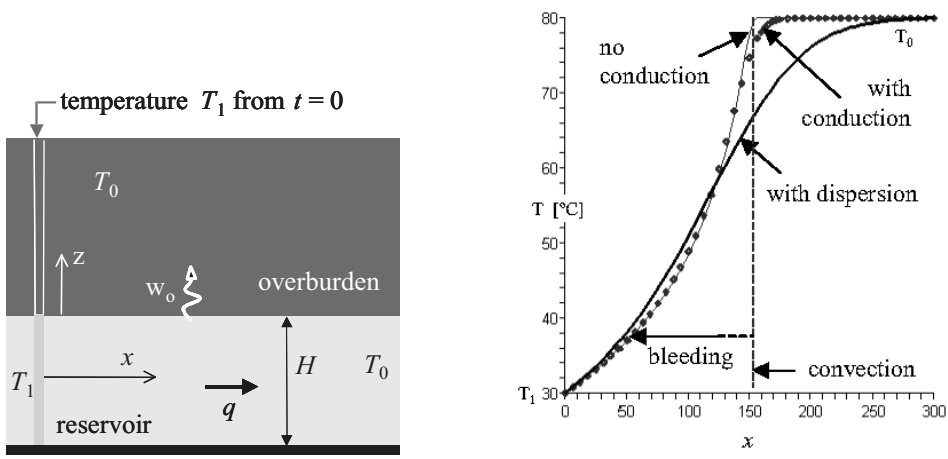

(a) Schematisation *(b) Cold front in the reservoir*

Figure 14.6 Cold transport in a uniform sand layer with constant groundwater flow

Linear model

The heat transport in a single layer (reservoir) with thickness H and in a uniform steady groundwater flow at initial temperature T_0 of 80 °C is considered (Fig 14.6a). At time t = 0, water of temperature T_1 of 30 °C is injected at constant volume rate Q. In this example, the lower boundary of the reservoir is sealed for water and heat, and the upper boundary is sealed for water, but it can conduct heat (thermal bleeding). If vertical temperature gradients in the reservoir are disregarded, assuming the heat in the reservoir is uniform over the height, the process is described by:

in the reservoir

$$\frac{\partial}{\partial x}\rho c D_L \frac{\partial T}{\partial x} + \frac{\partial}{\partial y}\rho c D_T \frac{\partial T}{\partial y} - \rho c v \frac{\partial T}{\partial x} = \rho c \frac{\partial T}{\partial t} + \frac{w_o}{H} \qquad (14.3a)$$

in the overburden

$$\frac{\partial}{\partial z}(\rho c)' D' \frac{\partial T'}{\partial z} = (\rho c)' \frac{\partial T'}{\partial t} \qquad (14.3b)$$

thermal bleeding (heat leakage)

$$w_o = -\lambda' \left.\frac{\partial T'}{\partial z}\right|_{z\downarrow 0} \qquad (14.3c)$$

at the interface $z = 0$

$$T = T' \qquad (14.3d)$$

Here, the parameters are: reservoir thermal longitudinal dispersion-diffusion coefficient $D_L = \lambda/\rho c + a_L v$ [m^2/s], reservoir thermal transversal dispersion-diffusion coefficient $D_T = a_T v$ [m^2/s], overburden thermal diffusion coefficient $D' = \lambda'/(\rho c)'$, thermal convection velocity $v = q(\rho c)_f/(\rho c)$, soil heat capacity $\rho c = n(\rho c)_f + (1-n)(\rho c)_s$ [J/m^{3}K], thermal conduction coefficient λ [J/msK] in the reservoir and λ' in the overburden, Darcy velocity q, density ρ, specific heat capacity c [J/kgK], $h' = (\rho c)'/\rho c$, longitudinal mechanical dispersivity a_L [m], transversal mechanical dispersivity a_T [m] and porosity n. The dash characterises the overburden and the suffix f refers to pore fluid and s to the soil matrix. The heat leakage at the interface $z = 0$, the thermal bleeding, is characterised by the heat flux w_o [J/m^{2}s]. In this approach, the parameters ρ, c, D_L, D_T, D', a_L, h', q and H are considered constant. Usually, the diffusion effect is significantly smaller than the convection effect.

The reservoir temperature T becomes in this case (no vertical temperature gradient in the reservoir)

$$T - T_0 = (T_1 - T_0)\, erfc\left(\frac{h' x}{H}\sqrt{\frac{D'}{4v(vt - x(1-\delta))}}\right. \qquad (14.4)$$

with $\delta = D_L D'(\frac{h'}{vH})^2 < 0.2$ and $h' = \frac{(\rho c)'}{\rho c}$

In principle, this solution represents a moving heat front in the reservoir at a speed about two times slower than the true groundwater velocity (faster than the Darcy velocity), since some energy is required to heat the solid matrix. Fig 14.6b shows effects of conduction, dispersion and bleeding for a particular situation.

Equation (14.3a) can also be reformulated into

$$\frac{1}{Pe}\frac{\partial^2\Theta}{\partial\xi^2}-\frac{\partial\Theta}{\partial\xi}=\frac{\partial\Theta}{\partial\tau}+Bl\Theta \qquad (14.5)$$

with $$\Theta=\frac{T-T_0}{T_1-T_0},\quad \xi=\frac{x}{L},\quad \tau=\frac{tv}{L},\quad Pe=\frac{vL}{D},\quad Bl=\frac{2h'L}{\sqrt{\pi}H}\sqrt{\frac{D'}{vL}} \qquad (14.6)$$

Two numbers characterise the heat transfer process. The Peclet number *Pe* gives the ratio between convection and conduction in the reservoir. The thermal bleeding number *Bl* gives the ratio between bleeding (conduction in the overburden) and convection. For practical situations, *Pe* and *Bl* can be evaluated straightforwardly, and they provide the reasoning when simplifying the transport equation by eliminating partial processes of lesser importance. Fig 14.7 shows some numerical examples of heat transport, radial flow from a well, plane flow, and the effect of convection and conduction.

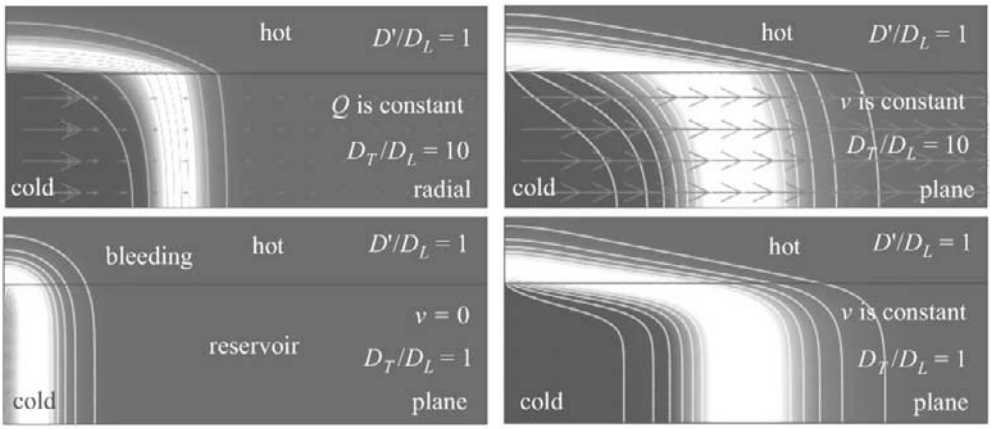

Figure 14.7 Numerical examples of heat transport (after Saeid); (upper left) radial situation representing flow from a single well with a constant discharge; (upper right) plane symmetric situation, approaching formula (14.4) with $D_T = 10D_L$; (lower left) pure conduction (no groundwater flow); (lower right) with convection and $D_T = D_L$.

Scaling the heat transport in porous media can be performed in a geocentrifuge (see Chapter 9). The larger convection velocity *v* coincides with the equally smaller spatial dimension *L*, while the similarity of each of physical numbers *Pe* and *Bl* is preserved (see equation 14.6). However, the mechanical dispersion will not maintain similarity, but its effect is minor for high Peclet numbers, which is the case in many practical situations.

Non-linear aspects

The viscosity, density and heat conduction are not constant with temperature, but the specific heat capacity of water or soil between 0°C and 100°C is rather a constant. Related aspects, such as permeability, retardation and potental drop are therefore influenced by the change of temperature and the development of heat transfer creates heterogeneity and affects convection and the life cycle of a geothermal system. For many fluids, viscosity is less sensitive to pressure (it is usually ignored), but it shows a pronounced variation with temperature; for water $\nu_{20°C}/\nu_{70°C} \approx 2.5$. The density of water is slightly dependent on temperature, and less sensitive to pressure (water without air bubbles is usually considered relatively incompressible); for water $\rho_{20°C}/\rho_{70°C} \approx 1.03$. Furthermore, density changes may cause free convection. A test may clarify these aspects.

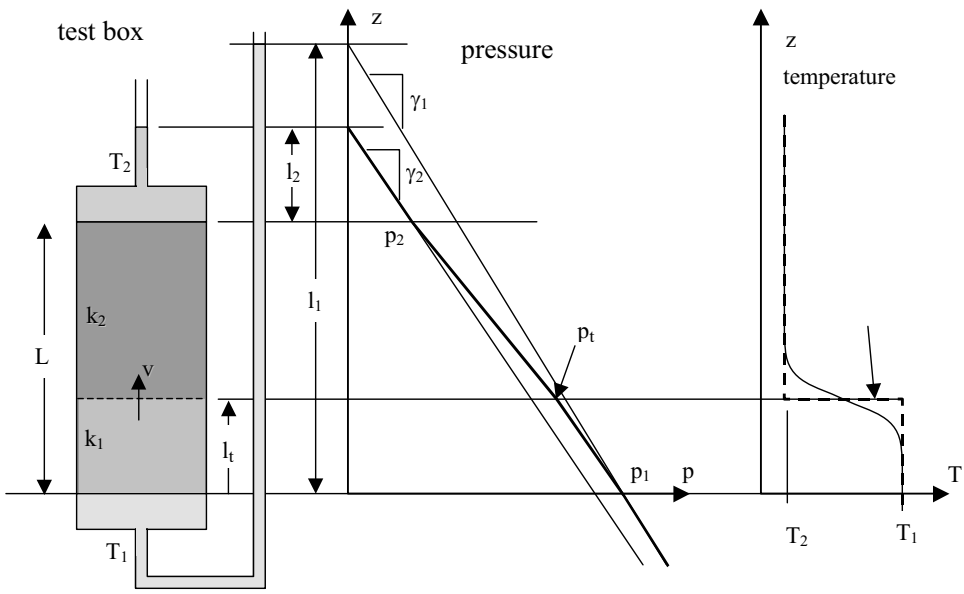

Figure 14.8 Test on heat transport; non-linear effects

Consider a vertical tube filled with cold saturated sand with height L and with initial temperature T_2, see Fig 14.8. From time $t = 0$, hot water with temperature T_1 is infiltrated, driven by a constant pressure drop $p_1 - p_2 = \gamma_1 l_1 - \gamma_2 l_2$. Note that the volumetric weight of hot water and cold water differs. The heat is transported by the induced pore water flow (retarded by the energy loss for heating up the grains) and it spreads by conduction (and dispersion). Because of symmetry in the spreading, a sharp heat front can be considered. It moves with velocity $v = Rw = Rq/n$, where w is the true pore water velocity, R the heat retardation factor (about 0.4), q the Darcy velocity and n the porosity. At time t, the heat front has progressed over $l_t = vt$. The heated area of the sand column has permeability k_1 and the cold part k_2. The permeability ratio is $k_2/k_1 = (\kappa g/\nu_2)/(\kappa g/\nu_1) = \nu_1/\nu_2$, where κ is the intrinsic permeability (not affected by heat), g the gravity acceleration and ν the kinematic viscosity. Since the permeability changes due to the temperature change

with time, the specific discharge q increases with time, and so does the heat front velocity v and position l_t.

Considering mass conservation between the hot and cold area at any moment, leads to

$$q = q_1 = \frac{k_1}{\gamma_1}\frac{p_1 - p_t}{l_t} = q_2 = \frac{k_2}{\gamma_2}\frac{p_t - p_2}{L - l_t} \quad \rightarrow \quad p_t = \frac{\frac{k_1}{\gamma_1}\frac{p_1}{l_t} + \frac{k_2}{\gamma_2}\frac{p_2}{L - l_t}}{\frac{k_1}{\gamma_1 l_t} + \frac{k_2}{\gamma_2 (L - l_t)}}$$

$$\rightarrow \quad q = \frac{\frac{k_2}{L}(\frac{\rho_1}{\rho_2} l_1 - l_2)}{1 + (\frac{\rho_1 \nu_1}{\rho_2 \nu_2} - 1)\frac{l_t}{L}} \tag{14.7}$$

One may recognise the density and viscosity effect. Next, $l_t = \lambda L$ and q are calculated.

$$\partial l_t = v \partial t = \frac{Rq}{n}\partial t \qquad \rightarrow \qquad (1 + (\frac{\rho_1 \nu_1}{\rho_2 \nu_2} - 1)\lambda)\partial\lambda = \frac{Rk_2}{nL^2}(\frac{\rho_1}{\rho_2} l_1 - l_2)\partial t$$

$$\rightarrow \qquad \lambda + \frac{1}{2}(\frac{\rho_1 \nu_1}{\rho_2 \nu_2} - 1)\lambda^2 = \frac{Rk_2}{nL^2}(\frac{\rho_1}{\rho_2} l_1 - l_2)t \qquad \rightarrow \qquad \frac{l_t}{L} = \lambda = \frac{-1 + \sqrt{1 + 2\varepsilon t}}{(\frac{\rho_1 \nu_1}{\rho_2 \nu_2} - 1)}$$

$$\rightarrow \qquad q = \frac{\frac{k_2}{L}(\frac{\rho_1}{\rho_2} l_1 - l_2)}{\sqrt{1 + 2\varepsilon t}} \tag{14.8}$$

with $\quad \varepsilon = (\frac{\rho_1 \nu_1}{\rho_2 \nu_2} - 1)\frac{Rk_2}{nL^2}(\frac{\rho_1}{\rho_2} l_1 - l_2)$

Since $\rho_1 \nu_1 / \rho_2 \nu_2 < 1$, this result indeed shows that q increases with time when hot water is injected. Obviously, when cold water is injected in a hot aquifer, the discharge will decrease with time. For a temperature drop of 50°C, this increase or decrease can be in the order of 40% (significant!).

The viscosity and density effect in heat dispersion is shown in Fig 14.9. In reality, the heat front is not uniform and preferential channels can be formed, particularly in horizontal flow, where the density change will cause two-dimensional free convection (warm water tends to move upward). Here, numerical simulation is required. Practically, the density effect is marginal for geothermal systems. The viscosity effect is however pronounced. If disregarded, it may lead to underestimation of the life cycle of deep geothermal systems and for cyclic shallow

heat and cold storage and the viscosity effect causes cold injection to require more energy than heat injection.

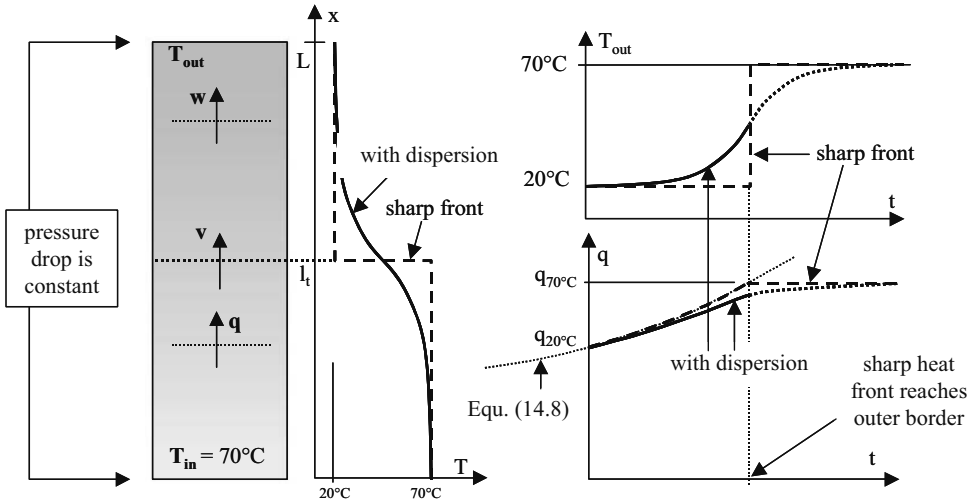

Figure 14.9 The viscosity effect with and without heat dispersion

E LAND SUBSIDENCE

Fluid withdrawal from the underground induces land subsidence at the surface above, which has effects for the surface water management and infrastructure, particularly in lowland areas and deltas. Notorious subsidence due to extensive groundwater withdrawal is observed in lowland cities, such as Bangkok, Djakarta, New Orleans, Houston, San Jose, Mexico City, Shanghai, Tianjin, Osaka, Tokyo, HoChiMinh City, Venice, Ravenna, and many others. Similar effects are known in case of oil/gas withdrawal. Flooding is the major adverse effect of subsidence. Other effects include tilting, well-casing failure, lowering infrastructure (roads, bridges), faulting and (small) earthquakes. Methods to stop subsidence are control of groundwater pumping, development of aqueducts, groundwater recharge, and the construction of extensive networks of dikes and sea walls, locks, and pumping stations. In the light of expected climate change and population growth, the problem of land subsidence is aggravating. Here, a well function for groundwater extraction induced subsidence and a Dutch protocol for mitigating oil and gas exploitation effects are discussed.

Well systems are also in use for temporary dewatering of building pits. The induced pore pressure decline in adjacent soil layers is a notorious culprit for damage to the surroundings, in terms of subsidence, differential settlements of buildings and desiccation of agricultural fields.

There is a principle difference in the physical system of water-withdrawal and oil/gas withdrawal. Water withdrawal takes place from relatively shallow permeable aquifers (water conveying sand layers) that are confined by less pervious layers (aquitards). The pore pressure lowering causes effective stress increase and volume decrease. In shallow formations the major contribution to the

shrinkage noticed as surface subsidence comes from the aquitards, which are relatively more compressible. In the aquitards, in fact, a process of consolidation is triggered by the water withdrawal. Oil/gas withdrawal takes place from relatively deep reservoirs (sandstone, shales), which are confined by impermeable rock layers (salt, claystone). Sometimes there is a connected adjacent aquifer. The pressure drop here is significantly higher than for shallow water withdrawal, causing the reservoir itself to compact, which results in land subsidence. So, for water withdrawal the storage effect is in the adjacent layers, while for oil/gas withdrawal it is in the reservoir itself.

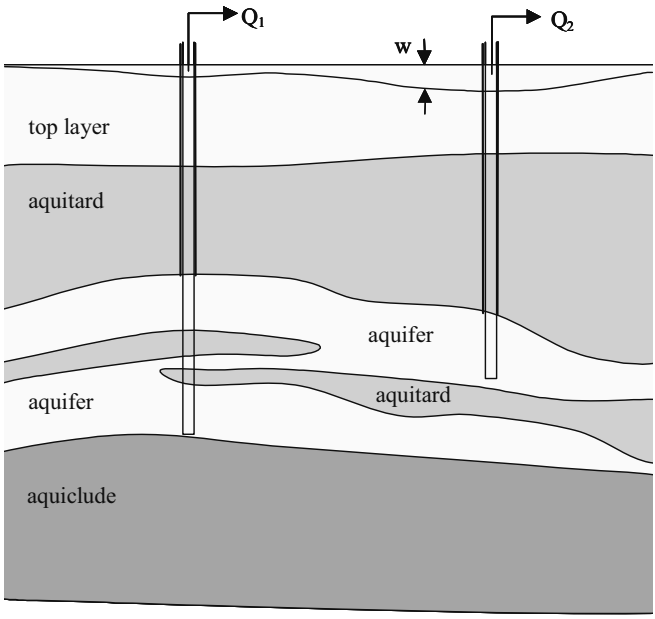

Figure 14.10 Geological system and a production well

Water withdrawal

The geohydrological system from which groundwater is recovered consists of aquifers (permeable reservoir) and aquitards (semi-pervious confining layer) or aquicludes (impervious confining layer), see Fig 14.10. The drawdown (pore pressure head lowering in the aquifer) s at time t at distance r from a production well with constant discharge Q is formulated by

$$s = \frac{Q}{4\pi kH} W(r,t) \tag{14.9}$$

Here, kH represents the aquifer transmissivity (permeability x height) and W is a well-function. For a confined aquifer the well-function is (Theis)[54]

[54] Horizontal strains are disregarded.

$$W(r,t) = W(u) = \int_u^\infty \exp(-y)\frac{dy}{y}, \quad u = \frac{r^2 S}{4tkH} \tag{14.10}$$

with S the aquifer storativity. For $u < 0.01$ the formula simplifies to $W(u) = -0.5772 - \ln(u)$. The transmissivity kH can be obtained from the gradient of s and $\log(t)$. It is difficult to obtain a reliable value for the storativity S. One usually adopts $S = 0.001$.

For a semi-confined aquifer the well-function is given by Hantush[55]

$$W(r,t) = W(u,\beta) = \int_u^\infty \exp(-y - \frac{\beta^2}{4y})\frac{dy}{y}, \quad \beta = \frac{r}{\lambda}, \quad \lambda = \sqrt{kHC} \tag{14.11}$$

with λ the leakage factor, and $C = H'/k'$ the hydraulic resistance of the semi-confining layer (H' the height and k' the permeability). It is commonly applied by geohydrologists. Note that in equation (14.11) an instantaneous leakage without consolidation is adopted from a (rigid) aquitard. In fact, such a system is quite unrealistic for shallow systems.

Besides some modifications (well storage, skin effect, anisotropy, partial penetration) these well-functions comprise the core of the state of the art for pumping tests and water well systems. If one includes time-dependent consolidation in the aquitard, the well function becomes, adopting a semi two-dimensional process (Barends)

$$W(r,t) = W(u,\beta,\tau) = \int_u^\infty \exp(-y - \frac{\beta^2 f_i}{4y})\frac{dy}{y} \tag{14.12}$$

with $\quad f_i = f_i(\xi), \quad \xi^2 = \tau/(1 - \frac{u}{y}), \quad \tau = \frac{H'^2}{c_v t}$

Here, c_v is the consolidation coefficient of the aquitard. (14.12) is based on an approximate Laplace inverse technique; the error involved is less than 1%. The function f_i depends on the condition of the adjacent aquitard. Three situations can be considered

1 (infinite) thick aquitard $\quad f_1 = \xi$ *(14.13a)*

2 finite aquitard drained at the outside $\quad f_2 = \xi \coth(\xi)$ *(14.13b)*

3 internal aquitard $\quad f_3 = \xi \tanh(\xi/2)$ *(14.13c)*

---

[55] For large value of time t Hantush' function transforms to a Bessel function, $W(0,\beta) = 2K_0(\beta)$. Other simplifications lead to $K_0(\beta) = \sqrt{(\pi/2\beta)}\exp(-\beta)$, for $\beta >> 1$, and $K_0(\beta) = -\ln(\beta/1.123)$, for $\beta << 1$.

If the reservoir has more adjacent aquitards with different conditions their effects accumulate in the aquifer, and they can be summarised in the well-function, as follows

$$W_m(r,t) = W_m(u,\beta,\tau) = \int_u^\infty \exp(-y - \frac{\sum_m \beta_m^2 f_{mi}}{4y}) \frac{dy}{y} \qquad (14.13d)$$

with m referring to the aquitard and i to its condition. Formula (14.13d) shows that the effect of time-dependent consolidation or leakage is embodied in the factor f. For $f = 1$ equation (14.13d) becomes equal to the Hantush well-function (14.11). It suits only $c_v = \infty$, which corresponds to a rigid porous aquitard.

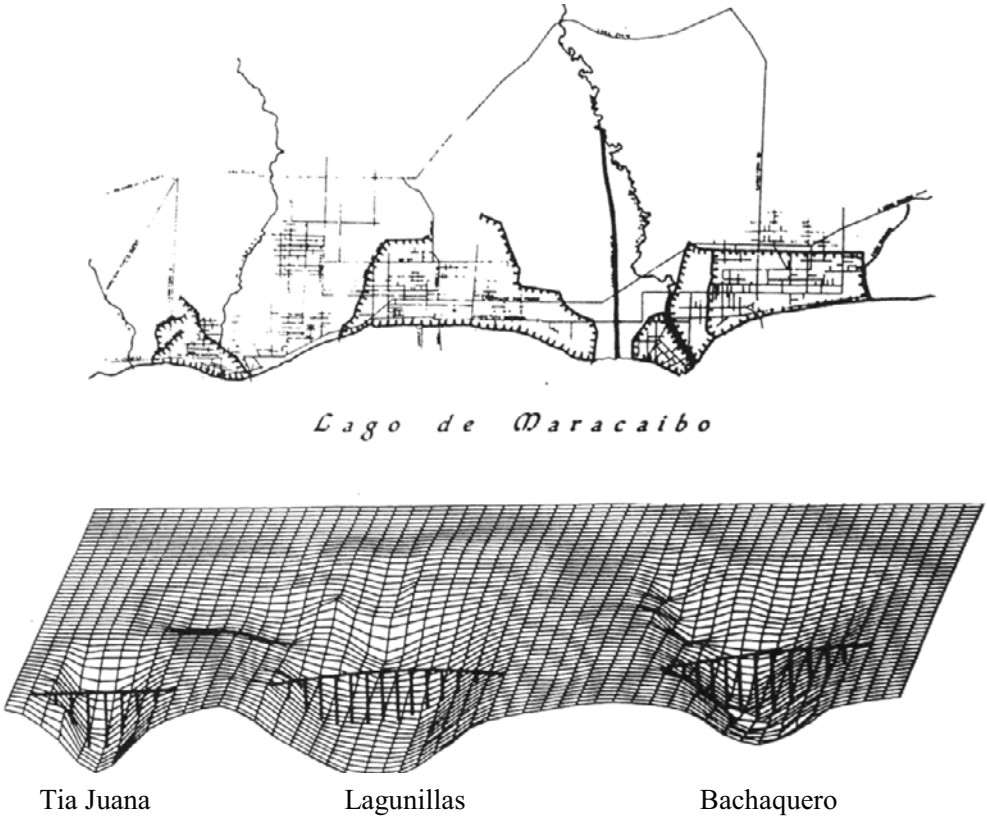

Figure 14.11 Land subsidence by gas/oil withdrawal from about 1600 wells

The corresponding land subsidence w is found by combining the aquifer compaction and the consolidation in the aquitards

$$w = \frac{Q}{4\pi kH}(S + \sum_m \left[\frac{k'H'}{c_v} \frac{\tanh(\sqrt{\tau/2}}{\sqrt{\tau/2}} \right]_m) W_m(u,\beta,\tau) \qquad (14.14)$$

Here, superposition m refers to the number of aquitards (type 2 and 3, see 14.13) per vertical position r. The Hantush well-function, commonly used in geohydrology, is not suitable for land subsidence. The well-function (14.13d) and the corresponding subsidence (14.14) can be used in complex situations (multiple well systems), since the principle of superposition holds. It has been successfully applied for the simulation of land subsidence at the Bolivar coast in Venezuela (Fig 14.11), reaching at the coast up to 5 metre subsidence in 2010.

Peat oxidation

Peatlands cover an estimated area of 3% of the Earth's land surface. Most of it is in the northern hemisphere, covering large areas in North America, Russia and Europe. Tropical peatlands occur in mainland East Asia, Southeast Asia, the Caribbean and Central America, South America and southern Africa where the current estimate of undisturbed peatland is 10-12% of the global peatland resource (International Peat Society). Agriculture (drainage for agricultural practices enhances the loss of mass due to oxidation of organic matter), forestry and peat extraction for fuel and horticultural use are the major causes of peatland disappearance. As these land-use changes require alteration of peatland hydrology, peat oxidation results leading to land subsidence, which could reach 2-3 cm per year. This subsidence causes increased pumping and drainage costs.

An empirical formula to quantify the effect of water table depth on subsidence due to peat oxidation per year is (Stephens)

$$S = 0.01(a + bh)\, 2^{(T-5)/10} \quad \text{[m/yr]} \qquad (14.15)$$

with $a \approx -0.1$ and $b \approx 1.5$ are empirical constants, h is actual groundwater depth in metre, and T the temperature in °C at 0.1 m depth.

Peatland restoration is receiving attention in Europe and North America. It is also recognised in tropical peatland areas. While peatland restoration is primarily designed for global biodiversity protection, it can also play an important role in reducing CO_2 emissions.

Oil and gas recovery

The standard process, applied internationally by the gas and oil mining industry for subsidence prediction, may be considered as being divided broadly into two steps

- Reservoir modelling. This step is used to simulate the flow processes of hydrocarbons and water in the porous layers and to compute the pressure and saturation changes that take place during hydrocarbon extraction.
- Geomechanical modelling. This step is used to compute the deformation (including the compaction and resulting subsidence) of the porous layers and to compute the change in stresses and porosity due to fluid pressure changes, e.g. as a consequence of hydrocarbon extraction.

There are many factors that influence the magnitude and aerial extent of subsidence associated with gas production. The key factors are compressibility of reservoir formation, thickness, depth and radius of reservoir, influence of adjacent water aquifers, and volume of gas production and related pressure drop. The sediment

compressibility c_m is a measure of the deformability of the sediment when subjected to a change in the applied stress, such as the change in pore fluid pressure induced by fluid extraction. c_m is therefore a measure of stiffness, relating a stress increment to the resulting increment of deformation.

Reservoir model

Development of the reservoir model generally comprises two stages: (1) a static study (i.e. development of the geological model), and (2) a dynamic study (i.e. development of the flow model). Development of the geological model requires an interpretation of the main structural features (e.g. faults), the geometry of all the porous levels forming the reservoir and their petrophysical characterization. For the dynamic study (i.e. flow model) two different models are accepted as best practice internationally: the material balance model and a 3D model.

A material balance or 'single cell' model was the first approach developed for simulating the production of hydrocarbon reservoirs. Material balance models are considered to be a well-established and sound approach and have been used worldwide in reservoir engineering studies for over 70 years. In these models it is assumed that the pressure is spatially constant throughout the reservoir or 'cell', changing only as a function of production, i.e. with time. A 3D model is currently considered the most advanced technology for studying and simulating reservoir behaviour, and therefore for evaluating the spatial and temporal distribution of fluid pressure and saturations inside a reservoir body. By discretising the model into multiple small elements for the purpose of the analysis, a more realistic picture of the distribution of the pressure change at different locations in the reservoir can be developed.

The predictive accuracy of a reservoir model is related to the quality and quantity of the available data. In studies for new small-medium sized gas field development projects the amount of geological/geophysical information available is inevitably limited and no past history data is available for any calibration. In this case the use of a simple reservoir model, such as a material balance or 'single cell' model, to simulate the future behaviour of the reservoir is considered to be a sound technical approach, fully adequate in terms of the reliability of the results obtained.

Geomechanical Model

Internationally, the following three different approaches to the development of a geomechanical model are accepted as good practice.

- Geertsma cylinder-shaped model. Geertsma's analytical solution for the evaluation of the surface subsidence induced by the depressurisation of a reservoir level was published in 1973. The reservoir geometry Geertsma considered is a cylinder-shaped layer, with petrophysical and mechanical properties assumed to be homogeneous and isotropic, and behaving linear-elastically when stressed. In his analysis, the formations surrounding the reservoir level (over-, side-, and under-burden) is considered to be homogeneous and isotropic, with mechanical properties equal to those of the reservoir rock.
- Geertsma semi-analytical model. The second approach is known as the Geertsma semi-analytical model and is a natural evolution of the Geertsma cylinder-shaped model. This version of Geertsma is usually applied when a 3D reservoir model is available. The model is based upon the same basic assumptions as the

full Geertsma model, with similar rock properties for the reservoir and the surrounding formations. However, as the reservoir is discretised into the same 3D cells as the reservoir model, the resulting prediction gives a more realistic distribution of subsidence because it can more accurately reflect the real geometry of the reservoir and actual depressurisation field.

- Finite Element Model. Use of Finite Elements is the most accurate (but also most complex) tool for the assessment of subsidence. The reliability and accuracy of a Finite Element model depend on the availability of a large amount of data describing both the geological setting and the mechanical properties of the reservoir rocks and of the surrounding formations.

The choice of any one particular model depends largely on the availability of data and whether the assumptions inherent in the model can reasonably accurately represent the physical situation. The proper use of simple models, such as those developed by Geertsma, can often provide realistic estimates of the subsidence magnitude. In practice, if the reservoir is small, of limited thickness and remote from subsidence-sensitive objects, industrial practice considers the analytical Geertsma-type model adequate for the assessment of subsidence.

Sediment compaction coefficient c_m

The sediment compaction (vertical compressibility) coefficient c_m can be measured via laboratory experiments (e.g. by oedometer tests), or by in situ monitoring (using markers). Geotechnical engineering practice favours in situ tests as a source of compressibility data because these tests can be made with a minimum of soil disturbance and, by definition, will take into account the integrated effect of the full layer rather than relying on the extrapolation of properties derived from a small element test. This preference has led to the development of an industry of field-testing, with numerous methods and test tools. For deep sediment compressibility, radio-active borehole marker measurements have become standard practice internationally. However, in cases where marker measurements are not available or limited, laboratory experiments based on second-cycle compressibility derived from oedometer testing is considered to be the only practical alternative. Experience suggests that the second-cycle compressibility is generally quite reliable as an average value.

Geertsma's analytical solution

The internationally accepted approach used by industry to assess the approximate order of magnitude of the expected subsidence is to apply the following standard formula, which relates the approximate maximum subsidence to the geometric properties of the reservoir (depth, radius), the thickness, compressibility and expected pressure drop, according to

$$S_{max} = 2(1-\nu)\,(1 - C/(1+C^2)^{0.5})\; h\, c_m\, \Delta p \qquad (14.16)$$

With S_{max} maximum settlement in the subsidence bowl, ν Poisson ratio, C reservoir factor $C = D/R$, D approximate depth of the reservoir, R approximate radius of the reservoir, h average reservoir thickness, c_m average compressibility of the reservoir, and Δp average pressure drop in the reservoir.

The variance in the parameters is estimated: for C about 25%, for h 20%, for c_m at least 50% depending on tests applied and monitoring available, for R, D, Δp and ν usually no significant uncertainty, giving a variance in S_{max} of about 100%. If adjacent aquifers are active, the variance could be more. Therefore, Geertsma's formula can be used as a first approximation. When exploitation takes place monitoring of the induced land subsidence is common practice, and the obtained data is used to calibrate towards a better prediction model.

<u>Retardation effect</u>

Observations show that induced land subsidence starts later than the start of the exploitation and when the production is stopped it will lag. These periods are referred to as retardation. It can be described by the following empirical formula, valid for a sudden constant reservoir pressure drop of Δp

$$S = S_{max}\,(1 - \exp(-t/T_r)) \qquad (14.17a)$$

Here, T_r is the retardation time. Observation of small reservoirs shows a value for T_r of about one year, but sometimes it is significantly longer, related to the type of reservoir rock. In case the reservoir depletion is performed with a constant pressure drop gradient, such that after a production period of T_p at abandonment the total pressure drop is Δp, then the retardation can be found by convolution of (14.17a), yielding

$$S = (S_{max}/T_p)\,(r - T_r\,(\exp(-(r-t)/T_r) - \exp(-t/T_r)) \qquad (14.17b)$$

with $r = t$ if $t < T_p$ and $r = T_p$ if $t > T_p$.

Geodetic evaluation

In a geodetic campaign at time t_i height differences are measured: $dh_{ti}^{A\text{-}B}$. These differences are improved (closed loop control) and converted to actual heights h_{ti}^{A} and h_{ti}^{B} by using a unique stable reference benchmark (Fig 14.12a). The collected heights h_{ti} are called an epoch t_i. Commonly epochs are used for subsidence evaluation. Using all epochs in an integral way provides better noise and error handling (Houtenbos).

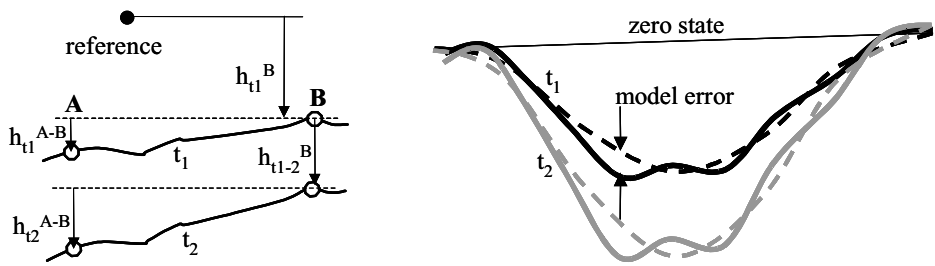

(a) Definition of height and height differences. *(b) Incorporation of the model error*

Figure 14.12

The measured time change in height difference in the period t_1 to t_2 is: $dh_{t2}^{A\text{-}B} - dh_{t1}^{A\text{-}B}$. In this value the effect of a uniform additional height change or a uniform height change in time (subsidence rate) is not distinguishable. The time change in height is in practice obtained from collected heights h_{t1} and h_{t2} as they have been elaborated with respect to the unique stable reference benchmark. Hence, time changes in the reference benchmark will affect the absolute height differences, unnoticed. In some campaigns different reference benchmarks are used, which gives space to additional errors if these reference benchmarks are subjected to relative changes. Four types of errors can be distinguished

- measurement noise; no correlation/trend in space and time;
- benchmark motion; no correlation in space, a noticeable trend in time;
- model error; a noticeable correlation/trend in space and time;
- reference benchmark motion.

Usually the first epoch is used as a zero state. The model error is determined in time and place using an integral error analysis and since it contains consistent information it should be added to the signal (Fig 14.12b).

As an example, the development of a local subsidence bowl in five epochs is considered. Benchmarks are selected above an expected subsidence bowl (Fig 14.13a). The relative benchmark heights per epoch as a function of the distance to the bowl centre. Clearly in benchmark B something went wrong. Fitting congruent bowls shapes in time provides a sound way to extract the most probable subsidence (Fig 14.13b).

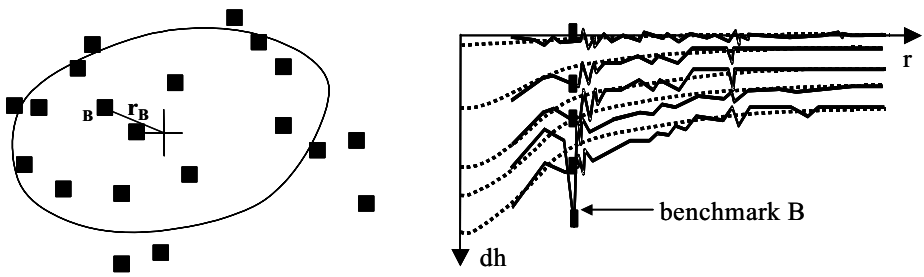

(a) selected benchmarks *(b) Fitting a standard congruent bowl shape*

Figure 14.13

Modern methods for geodetic surveys involve GPS and InSAR (Hanssen). Gravity force measurements allow to determine height changes in absolute sense. GPS uses specific reflecting benchmarks. InSAR is based on radar-interferometrics. Both use satellites. For InSAR reflection and scatter are crucial factors, and not all surfaces are suitable (agricultural fields). Nowadays, in accuracy and instant availability GPS and InSAR can compete with spirit levelling, the traditional method.

application 14.1

In an area with uniform groundwater flow the groundwater appears to be contaminated by a leak in a gas tank of a petrol station. By installing a well downstream all the contaminants are caught, because, as calculation show, all

contaminated streamlines end up in the well. However years later the groundwater downstream beyond the well shows contamination. Why?

application 14.2

If the groundwater table in a peat land is at 0.35 m depth, what is the expected land subsidence per year, if the ground temperature at 10 cm depth is 15 °C?

application 14.3

A proper Environmental Impact Assessment (EIA) related to oil and gas recovery involves the evaluation/prediction of deep effects (pressure decline in adjacent aquifers), surface effects (land subsidence, vibrations, and water management), and a monitoring plan. The following example is worked out for a small reservoir that will be exploited for 25 years.

The compaction coefficient is obtained from general data of sandstone: c_m = 6x10^{-9} Pa^{-1}. The reservoir has been preloaded in the glacial periods (ice-cap) and a factor 5 is adopted to account for the re-loading: c_{mr} = 1.2x10^{-9} Pa^{-1}. The maximum pressure drop in the reservoir is Δp = 20 MPa. The reservoir height involves the net height: h_{net} = 50 m, gross height: h = 100 m (including shales, etc.). The maximum (ultimate) reservoir compaction becomes $\Delta h = c_{mr}\ h\ \Delta p$ = 1.2x10^{-9}×100×20 10^{6} = 2.4 m. The choice of h and not h_{net} is appropriate, if the intermittent shales also compact finally.

For the maximum subsidence S_{max} at the surface the rebound of the underburden is considered for 20%, yielding and effective reservoir compaction of Δh_{eff} = 0.8×2.4 = 1.92 m. The arching: overburden is incorporated in formula (14.15) $S_{max} = 2(1-\nu)[1-C/\sqrt{(1+C^2)}]\ \Delta h$, with $C = D/R$. The reservoir depth is D = 2000 m, the reservoir apparent radius is R = 4000 m, and Poisson's ratio is ν = 0.3. Hence, $S_{max} = 2(1-0.3)[1-0.5/(1.25)^{0.5}]\ 1.92$ = 1.79 m. The subsidence bowl will have a radius of about $R + 2D$ = 8000 m. The compaction of the intermittent shales (consolidation) gives another retardation effect. The direct subsidence can be found by using $\Delta h_{dir} = h_{net}/h\ \Delta h$ = 0.5×2.4 = 1.2 m, which leads to S_{max} = 0.895 m. Moreover, this subsidence will become manifest at a later stage due to the retardation time (viscous effects at the start), which could be 2 years.

Monitoring and a mitigation plan are therefore important. They should include measuring the zero state (before exploitation), and regularly thereafter by levelling and/or InSAR / GPS.

15 UNDERGROUND ENGINEERING

A DEEP BUILDING PITS

The infrastructure in highly populated areas is essential for social and economic development. In deltaic regions, such as the western part of the Netherlands, it is characterised by many complex river and canal crossings, a great variety of viaducts, aqueducts, ecoducts, tunnels and pipelines, each representing a sound engineering achievement because of soft soil conditions and high water tables (Fig 15.1a).

Figure 15.1a Deep building pit

Because of lack of space in urban areas and growing mobility, and the demand for a healthy urban life and nature protection, the number of other underground structures is gradually increasing in recent years, such as metro stations, car parks, shopping centres, museums, concert halls, water treatment facilities, etc. Special techniques have been developed, such as massive earth retaining walls (up to 40 metre depth), in-situ fabricated grout column screens in difficult locations, and remote-controlled small diameter borings, directional drilling (Fig 15.1b), to maintain and extend the immense network of underground cables and pipelines. Large and deep building pits are required for rebuilding old city centres, such as in Berlin (Lehrter Bahnhof building pit was 40.000 m^2 and 18m deep), in London (Jubilee Line Extension in the Docklands area), in Amsterdam (North South Metroline under the monumental central railway station), and in many other metropoles in the world. In such locations the groundwater level cannot be controlled using dewatering systems because of the large environmental effect. In the soft-soil conditions, a system of anchored and strutted earth retaining structures with artificial basement sealing is then necessary within strict environmental regulations. Managing the influence of external conditions for such situations and minimising lateral movements and settlements requires the best skills and the latest experience.

Figure 15.1b A directional drilling is completed

Tunnels under waterways were originally constructed in open excavations reaching a depth of 25 m. The required groundwater drainage caused significant damage in the surroundings (settlements, desiccation) and the method was abandoned. The immersion method (Fig 15.2), applying prefabricated caissons, which were floated to their location, was successfully used and further improved. In urban areas the cut-and-cover method, applying watertight screens (diaphragm walls) and a 'roof' on which the daily life continues, is used, but disturbance to traffic and living, and damage induced by partial groundwater drainage, even with a recharge system, is always there, usually reaching an additional 10% or much more in unexpected situations, above the planned construction cost.

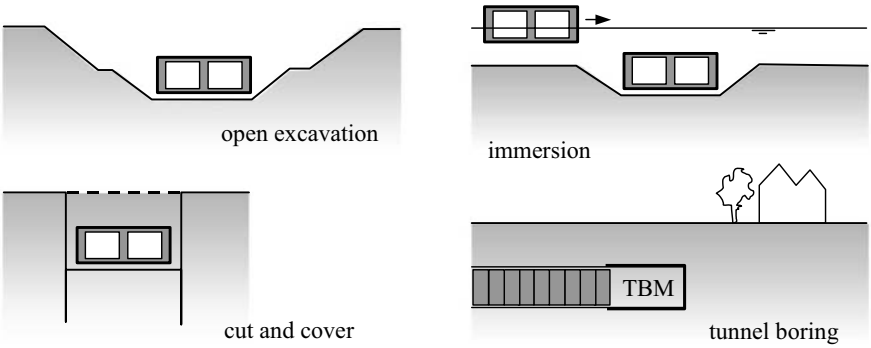

Figure 15.2 Tunnel techniques

During recent decennia shield-boring machines have come in use to construct underground tunnels with less disturbance at the surface. Here, the challenge is to keep the tunnelling process stable and efficient in the soft and variable soil with high water levels. At present, about 30 of these complex transportation crossings have been constructed in the Netherlands, with a length varying from 300 to 6500 m, the longest reaching a depth of 60 m, and they function well.

Moving underground

Decisions about infrastructure policy form an integral process where political and social consensus should be achieved at an early stage on issues related to planning and procedures, finance and economy, environment and construction techniques. Underground construction is usually conceived as relatively expensive, but if for above ground construction additional costs related to environmental impact and traffic congestion during construction are taken into account, the difference between the aboveground and underground alternatives is significantly reduced. Moreover, when the potential for dual use of the ground in urban areas is considered, the underground option even becomes attractive.

Relevant conditions for the decision-making process for large-scale infrastructural projects are usually not clearly formulated and the selection and rejection of alternatives is generally not based on well-defined procedures. In this respect, three main issues are important: transparent information about advantages and disadvantages of underground construction for the short term and the long term, a methodology to weigh all 'hard and soft' aspects in an integral manner, and an inventory of missing knowledge with a corresponding research agenda.

There are many parties involved: governmental institutes, authorities, research institutes and universities, engineering and consulting companies, contractors and manufacturers, and research-coordinating offices and professional organisations. The disciplines relevant to realising the underground infrastructure are manifold: civil engineering (construction, geotechnics, dynamics, hydraulics, building physics, materials, traffic technology, planning), mining engineering (rock mechanics, geology), mechanical engineering (excavation technology, ventilation, aerodynamics, control technique, vehicle/rail technology, installation technique), electrical engineering (light/signal technique, safety-monitoring, air condition), mathematics (informatics, risk analysis), chemical engineering (soil chemistry, ground freezing), economy (transport, finance, logistics, management and exploitation), equity and law (deprivation, allowances, labour inspection, contract, liability, insurance), planning (city planning, architecture, aesthetics, landscape), cultural technology (history, archaeology, social development), social science (public relations, psychology, sociology, media technique), and environmental sciences (ecology, biology, natural history). The geotechnical engineer needs skills beyond his technical education (see Chapter 8 and Annex III) to play a proper role.

Ground movements due to excavations and tunnelling

In geotechnical engineering the induced deformations in the surroundings of construction sites due to building activities is referred to as undesired environmental effect. For large projects where deep excavations are used or where tunnel machines are used, environmental effects are almost inevitable. The removal of ground causes a change in the soil stresses in the neighbourhood. Artificial groundwater lowering is sometimes used to create a safe building ground in the pit (bottom heave), but it causes settlements due to consolidation of soft soil layers in the adjacent areas. Building pit walls either strutted or anchored will deflect and in unfortunate cases loss of soil by seepage through improper wall plate connections may occur. During tunnelling an oversize drilling compared to the lining is applied

which is to a major part compensated by grout injection. All these aspects cause deformations in the direct environment, and they have to be taken into account in a project design. During construction, specific monitoring is required to take timely measures to prevent serious damage.

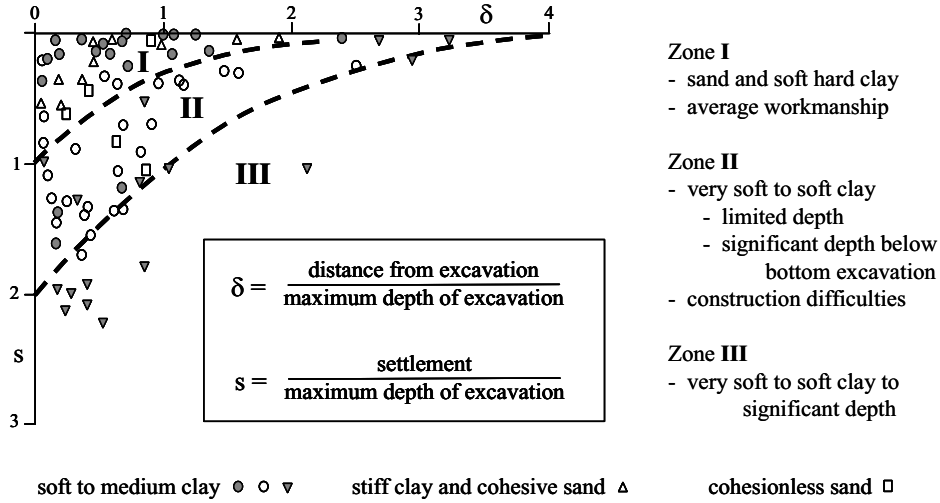

Figure 15.3 Environmental effect: settlements near excavations (Peck)

Since this environmental effect is rather case specific, only some general views are available from experience. Peck (1969) has collected information of many projects in the past and for the settlement adjacent to open cuts as a function of the distance from the excavation, he suggested distinguishing three cases related to the type of soil, shown in Fig 15.3. The data refer to excavations with a depth varying between 6 and 23 metre where standard piles or sheet piles with cross bracing and tiebacks have been used. Rankin (1988) published a comprehensive overview of various empirical approaches for the assessment of surface movements due to soft-ground tunnelling. In general, he adopts a Gaussian-curved bowl shape characterised by a maximum depth, a length and a width. The position of the centre of the bowl is $2z_0$ behind the tunnel face, and the border of the bowl is $2z_0$ ahead of the tunnel face, where z_0 is the depth of the tunnel. For cohesive soils, the maximum settlement w_{max} is assumed to be related to the volume loss into the tunnel. It does not hold for granular soils or stiff clays (see Fig 15.4). An approximate trend can be obtained from case history data: $w_{max} = (0.1R^2/z_0)^{1.18}$, where R is the tunnel radius and z_0 the depth of the tunnel axis. However the experience so far with tunnelling induced surface settlements reveals a large scatter. A recent state of the art review is presented by Mair (2011)

B SOFT-GROUND TUNNELLING TECHNIQUES

There are various tunnelling techniques. In rigid soils, one may apply an open boring front and even use explosives, but in soft permeable soils a shield is required to keep soil and water under control and retain the front by a (pressure)

buffer of slurry or air, or by a solid frame, referred to as earth-pressure balance shield (EPB). The tunnel-boring machines (TBM) are large, complex and impressive semi-automatic robots. Beside the shield and the cutting wheel at the front, the size of which may reach more than 15 m, cut soil has to be removed, tunnel lining elements have to be transported and installed, and the machine has to be maintained (replacing chisels, removing obstacles). The design and operation of a tunnelling project is multi-disciplinary, since the involvement of technical, legislative, social, communicational and even political skills are required.

Soil behaviour

Two main aspects with regard to soil behaviour are considered in a TBM operation: the front stability and the soil response on the lining. The front stability is complex and a different behaviour is to be expected in sandy soil and in clayey soil. Internal friction in sand may cause arching, which may induce more favourable stress redistribution (see Fig 15.4). The slurry pressure at the front must not be too low to disturb the cutting process and not too high to cause a blow-out towards the surface. Careful monitoring is constantly required. Large obstacles (boulders, buried trees, remnants of old foundations) may hamper the production seriously, and they must be removed.

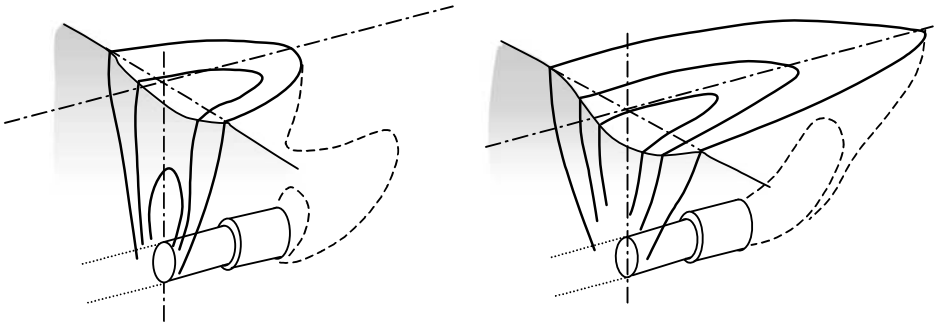

(a) frictional soil *(b) cohesive soil*

Figure 15.4 Schematic soil deformations during tunnel boring

Along the lining, for directional drilling, the soil may be compressed, while for large diameter drilling over-cutting (the cutting wheel is usually slightly larger than the external tunnel-lining diameter) will let soil locally expand, even if high pressure grouting at the tail of the shield fills this space. Furthermore, the hole which the TBM creates in the soil, will, according to Archimedes law, result in a tendency of lifting, and this has led to instability during tunnelling through very soft layers (peat) and dilatant layers (sand). All these aspects change the original stress state of the soil and invoke pressures on the TBM and the tunnel lining. Induced deformation and friction must be within limits in every stage to make the operation a success.

A fundamental soil problem related to tunnelling, boring or in-situ wall installation is what happens to a hole in the ground. Two aspects will be discussed,

i.e. the effects of a cylindrical cavity in a uniform infinite soil and a cavity in a semi-infinite soil.

C A CYLINDRICAL CAVITY IN A UNIFORM INFINITE SOIL

Consider a cylindrical cavity with a radius r_0 and an internal pressure q in a 3D elastic soil (Fig 15.5a). Equilibrium is expressed in terms of effective radial stress σ_r' and effective tangential stress σ_θ' and pore pressure u by

$$\sigma_{r,r}' + (\sigma_r' - \sigma_\theta')/r = u_{,r} \qquad (15.1)$$

The axial stress is $\sigma_z' = \nu\,(\sigma_r' - \sigma_\theta')$. It can be shown that the induced deformation involves only shear and that no volumetric deformation occurs (no dilation is assumed)[56]. Hence, no pore pressure are generated, i.e. $u = 0$, and a total or effective stress approach makes no difference. Consider a zone $r > r_p$ where the soil response is linear-elastic and described by the shear modulus G only. The soil expands or contracts radially due to a boundary stress σ_p at $r = r_p$ and the following stresses and radial displacement w comply with this state

$$\sigma_r = q\,(r_p/r)^2 = 2Gw/r = 2Gw_p\,r_p/r^2 \quad \text{and} \quad \sigma_\theta = -\sigma_r \quad \text{and} \quad \sigma_z = 0 \qquad (15.2a)$$

$$w = qr_p^2/2Gr \quad \text{and} \quad w_p = qr_p/2G \qquad (15.2b)$$

Here, q is the cavity pressure. The displacements are relatively small, i.e. $|w| << r$.

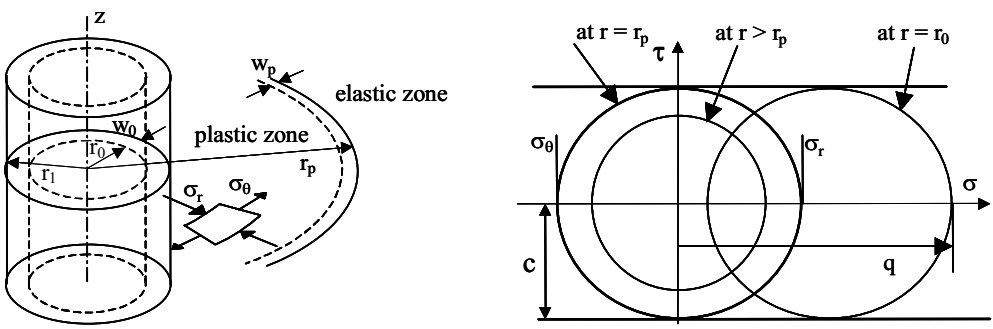

(a) cylindrical cavity *(b) Mohr circle*

Figure 15.5 An expanding cylindrical cavity in cohesive soil

Under higher pressures the soil may behave non-linear in a zone $r_0 < r < r_p$ where r_p is the radius of the interface between the plastic and elastic region. Assume a cohesive soil ($\varphi = 0$) with no volume change in the plastic zone (also no

[56] If no dilation may hold, the pore pressure is not affected. Hence, the dash indicating effective stresses is omitted for convenience. It may hold for clay. However, in sands dilation / contraction is not negligible and pore pressures will be involved.

shear induced dilation is assumed). Equilibrium is expressed by (15.1). The yield criterion demands (see Fig 15.5b)

$$\sigma_r - \sigma_\theta = |2c_u| \qquad \text{and} \qquad |\sigma_\theta| < |\sigma_z| < |\sigma_r| \tag{15.3}$$

Here, c_u is the undrained strength (or apparent cohesion). Two situations may occur: an expanding cavity in soil in a passive state with $\sigma_r > \sigma_\theta$ and $q > 0$ and a contracting cavity in soil in an active state with $\sigma_r < \sigma_\theta$ and $q < 0$.

Expanding cavity

For the plastic zone distinction is made between two cases: (1) a large cavity or relatively small deformations, i.e. $w_0 << r_0$ and (2) a small cavity or relatively large deformations, i.e. $w \approx r_0$.

In the case of a large expanding cavity or relatively small deformations, i.e. $w << r_0$, elaboration of (15.1) with yield condition (15.3) and boundary condition $\sigma_r = q$ at $r = r_0$ gives

$$\sigma_r = q - 2c_u \ln(r/r_0) \tag{15.4}$$

At the plastic-elastic interface $r = r_p$ both the elastic equilibrium condition $\sigma_r = -\sigma_\theta$ and the plastic equilibrium condition $\sigma_r - \sigma_\theta = 2c_u$ hold, which leads to $\sigma_r = c_u$ and $\sigma_\theta = -c_u$. Therefore, with (15.4) one finds $\sigma_r = c_u = q - 2c_u \ln(r_p/r_0)$ or

$$r_p = r_0\, e^{(q - c_u)/2c_u} \tag{15.5}$$

This result shows that the induced plastic region increases exponentially with q. Moreover, because $r_p \geq r_0$, the cavity pressure satisfies $q \geq c_u$. In the plastic zone the radial stress satisfies $q > \sigma_r > c_u$, but the difference $\sigma_r - \sigma_\theta$ remains c_u throughout the plastic region. This implies that for $0 < q < c_u$ there is no plastic zone; then the soil behaves elastically everywhere.

The corresponding displacement can be found using the condition of constant volume: $dV = 2\pi r_0 w_0 = 2\pi r_p w_p$, which gives $w_0/w_p = r_p/r_0$. Equation (15.2a) yields at $r = r_p$ for the radial stress $\sigma_r = 2Gw_p/r_p$, and since the plastic zone demands $\sigma_r = c_u$ also $w_p = c_u r_p/2G$ must hold, so that $w_0 = r_p^2 c_u/(2Gr_0)$. Hence, with (15.5) one finds

$$w_0 = r_p^2 c_u/(2Gr_0) = c_u r_0\, e^{(q - c_u)/c_u}/2G \qquad \text{for} \qquad w_0 << r_0 \tag{15.6}$$

In the case of a small expanding cylindrical cavity or relatively large displacements in the plastic zone, i.e. $w_0 \approx r_0$, the approach of Vesić is applied. He suggested to account for the displacing soil and incorporate the convective motion, i.e. using $r_1 = r_0 + w_0$ instead of r_0 (see Fig 15.5a). Elaborating the equilibrium according to (15.1), the radial stress in the plastic zone $r_1 < r < r_p$ with boundary condition $\sigma_r = q$ at $r = r_1$ becomes

$$\sigma_r = q - 2c_u \ln(r/r_1) \tag{15.7}$$

At the interface $r = r_p$, beyond which the elastic zone starts, the displacement is relatively small and also here $\sigma_r = c_u$ and $w_p = c_u r_p/2G$. This gives with (15.7)

$$q = c_u(1 + 2\ln(r_p/r_1)) \tag{15.8}$$

Using constant volume (Vesić): $dV = 2\pi(r_1^2 - r_0^2) = 2\pi(r_p^2 - (r_p - w_p)^2)$, which gives approximately $r_1^2 = 2w_p r_p$, omitting terms r_0^2 and w_p^2. With $w_p = r_p c_u/2G$ on finds $r_1^2 = (c_u/G)r_p^2$ or

$$(r_p/r_1)^2 = G/c_u = I_r \tag{15.9}$$

The ratio I_r is called the rigidity index. Expressions (15.8) and (15.9) provide the corresponding cavity maximum pressure, beyond which the system collapses, i.e.

$$q_{crit} = c_u(1 + \ln I_r) \tag{15.11}$$

If, for example, G = 20 MPa and c_u = 50 kPa, then for q = 50(1+ ln(20000/50)) = 350 kPa, a cohesive soil behaves fully plastic in a region with a radius $r_p = r_1 I_r^{1/2}$ = 20 r_1. This represents more or less a case, where a concrete foundation pile is driven through this soil. Here, r_1 can be associated with the pile radius. Its weight causes a pressure at least ten times more than 350 kPa and the pile will sink easily down by its own weight, see Fig 12.6, which shows a blow count zero from soil depth of 3 to 12 m.

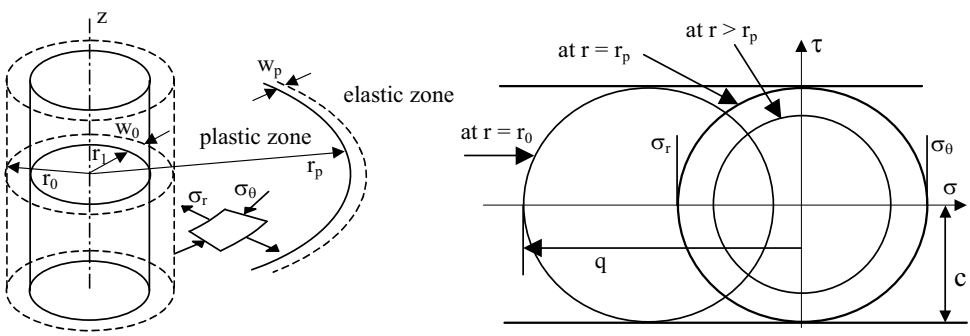

(a) cylindrical cavity *(b) Mohr circle*

Figure 15.6 A contracting cylindrical cavity in cohesive soil

Contracting cavity

There may be a zone where soil behaviour is plastic. In this plastic zone, $r_0 < r < r_p$, the larger tangential stresses σ_θ will squeeze the soil into the cavity by a radial plastic flow until the cavity is closed (Fig 15.6). Also here, for the plastic zone $r_0 < r < r_p$ distinction is made between two cases: (1) a large cavity or relatively small deformations, i.e. $|w_0| << r_0$ and (2) a small cavity or relatively large deformations, i.e. $|w_0| \sim r_0$.

In the case of a large contracting cavity or relatively small deformations, i.e. $|w_0| << r_0$, elaboration of (15.1) with yield condition (15.3) and boundary condition $\sigma_r = q$ at $r = r_0$ gives

$$\sigma_r = q + 2c_u \ln(r/r_0) \tag{15.12}$$

At the plastic-elastic interface $\sigma_r = -c_u$ and $\sigma_\theta = c_u$. Therefore, with (15.12) one finds

$$r_p = r_0\, e^{-(q+c_u)/2c_u} \tag{15.13}$$

This result shows that the induced plastic region increases exponentially with q. Moreover, because $r_p \geq r_0$, the cavity pressure satisfies $q \leq -c_u$. Note, q is negative (tension). This implies that for $-c_u < q < 0$ there is no plastic zone and the soil behaves elastically everywhere.

The corresponding displacement can be found using the condition of constant volume: $dV = 2\pi\, r_0 w_0 = 2\pi\, r_p w_p$, which gives $w_0/w_p = r_p/r_0$. Equation (15.2a) yields at $r = r_p$ for the radial stress $\sigma_r = 2Gw_p/r_p$, and since the plastic zone demands $\sigma_r = -c_u$, also $w_p = -c_u r_p/2G$ must hold, so that $w_0 = -r_p^2 c_u/(2Gr_0)$. Hence, with (15.13) one finds

$$w_0 = -r_p^2 c_u/(2Gr_0) = -c_u\, r_0\, e^{-(q+c_u)/c_u}/2G \qquad \text{for} \qquad |w_0| << r_0 \tag{15.14}$$

In the case of a small contracting cylindrical cavity or relatively large displacements in the plastic zone, i.e. $|w_0| \approx r_0$, Vesić's method also applies. Using $r_1 = r_0 + w_0$ instead of r_0 (see Fig 15.6) and elaborating the equilibrium according to (15.1), the radial stress in the plastic zone $r_1 < r < r_p$ with boundary condition $\sigma_r = q$ at $r = r_1$ becomes

$$\sigma_r = q + 2c_u \ln(r/r_1) \tag{15.15}$$

At the interface $r = r_p$, beyond which the elastic zone starts, the displacement is relatively small and also here $\sigma_r = -c_u$ and $w_p = -c_u r_p/2G$. This gives with (15.15)

$$q = -c_u(1 + 2\ln(r_p/r_1)) \tag{15.16}$$

Using constant volume: $dV = 2\pi(r_1^2 - r_0^2) = 2\pi(r_p^2 - (r_p - w_p)^2)$, which gives $-r_0^2 = 2w_p r_p$, omitting terms r_1^2 (note, $r_1 < r_0$) and w_p^2. With $w_p = -r_p c/2G$ one finds, similar to (15.9)

$$(r_p/r_1)^2 = G/c_u = I_r \tag{15.17}$$

And with (15.16) the maximum cavity maximum pressure

$$q_{crit} = -c_u(1 + \ln I_r) \tag{15.18}$$

Cavities in frictional soils

A fluid pressure in the cavity, e.g. the borehole contains water or slurry, may keep the cavity stable for a while. A low permeability provides the effective stresses to be large initially, but as consolidation proceeds they will become lower and plasticity may start.

In case of non-cohesive soils ($\varphi \neq 0$) the tangential stress can become much larger and maintain a cavity under relatively quite low pressures. This effect is referred to as arching (see Fig 15.7).

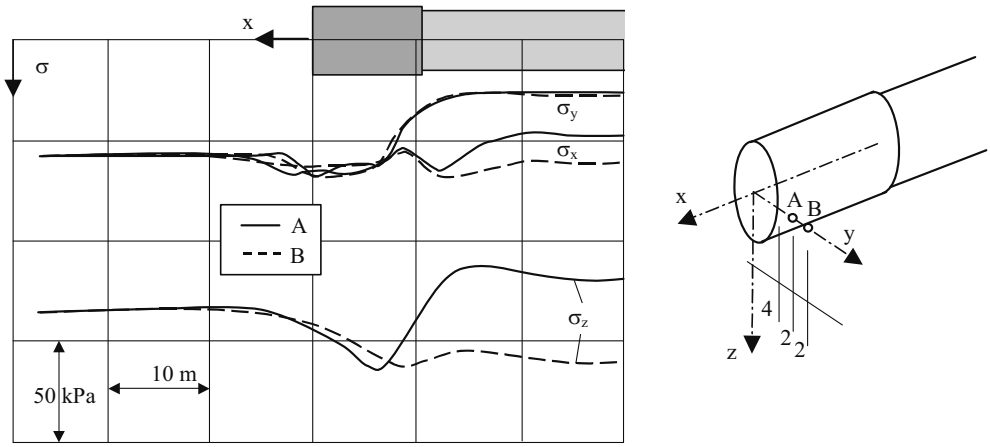

Figure 15.7 3D simulation of arching effects: vertical stress in A is smaller than in B.

Vesić developed formulae for expanding cavities in cohesive or frictional soils, both for spherical and cylindrical situations and valid for Mohr-Coulomb behaviour, including initial isotropic stress, soil weight and volume change Δ in the plastic zone (dilatancy). He expressed his results in the following form

$$q = cF_c + \sigma_0 F_\sigma \tag{15.19}$$

Here, σ_0 is the initial stress and F_c and F_σ are cylindrical cavity expansion factors, each of them a function of I_r , φ and Δ. For these functions tables and graphs have been prepared for practical use. They are applicable for small cavities or relatively large displacements, i.e. $|w| \approx r_0$. The previous analysis explains that Vesić's approach may be applied for contracting cavities as well. For tunnels, which can be conceived as large horizontal cavities, the situation may be more complex, but fundamentals discussed here do apply to some extent.

D A HORIZONTAL CYLINDRICAL CAVITY IN A UNIFORM SEMI-INFINITE SOIL

A typical example of a horizontal cylindrical cavity in soil is a pipeline or a tunnel. Such a structure will induce a change of local soil stresses, because the weight is different from the soil weight. Also the boring process will induce changes in local stresses particularly at the boring front due to slurry pressures and over-cutting. In cohesive soils or in frictional soils the response will be different (e.g. see Fig 15.4) and also groundwater may play an important role. Furthermore, over time, induced stresses will relax due to consolidation and creep. During all these processes the soil deforms and at the surface settlements may occur, which could affect nearby buildings and infrastructure. Insight in the stress distribution is essential and a simple approximation after Verruijt is discussed here.

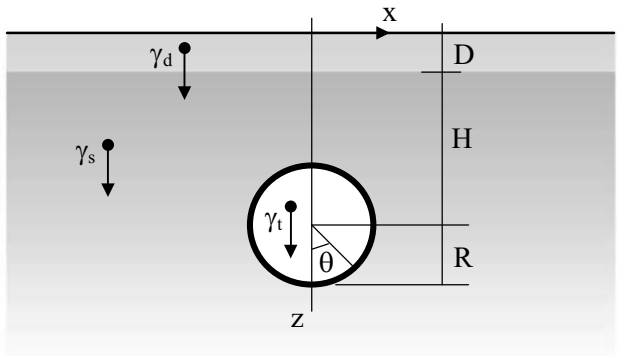

Figure 15.8 Situation of a tunnel lining in a semi-saturated soil

The stresses around a rigid circular cylindrical cavity with radius R at a depth $D+H$ can be evaluated in semi-saturated uniform subsoil (Fig 15.8), when adopting that shear σ_{xz} remains zero and no gap exists between soil and structure, thereby excluding all effects of the boring process and construction. The initial vertical stress state (without the cavity) at the location of the projected cavity perimeter can be expressed by

$$\sigma_z = \gamma_d D + \gamma_s(H - R) + \gamma_s R(1+\cos\theta) \qquad (15.20)$$

Here, the first term is due to the unsaturated soil weight; the second due to the weight of the saturated part above the crest of the cavity and the third is the stress along the perimeter, as a function of θ. Incorporating the local hydrostatic pore pressure $p = \gamma_w(H + R\cos\theta)$ yields for the effective stress

$$\sigma_z' = \gamma_d D + (\gamma_s - \gamma_w)(H + R\cos\theta) \qquad (15.21)$$

The horizontal effective stress, with a constant stress ratio coefficient K_0, becomes

$$\sigma_x' = K_0(\gamma_d D + (\gamma_s - \gamma_w)(H + R\cos\theta)) \qquad (15.22)$$

Adding the pore pressure gives the total horizontal stress

$$\sigma_x = K_0\gamma_d D + (\gamma_w + K_0(\gamma_s - \gamma_w)(H + R\cos\theta) \qquad (15.23)$$

When the rigid cavity is installed, Verruijt assumes that horizontal stresses remain unchanged and vertical stresses change, i.e. the specific weight of the third term of (1) is changed from γ_s to γ_t, where γ_t is the average specific weight of the cavity (weight per cross-section and length). This gives

$$\sigma_z = \gamma_d D + \gamma_s(H - R) + \gamma_t R(1+\cos\theta) \qquad (15.24)$$

The resulting force of this approximate stress distribution is worked out; the components are

$$Q_x = {}_0\int^{2\pi} \sigma_x \sin\theta \, R d\theta = 0 \qquad (15.25a)$$

$$Q_z = {}_0\int^{2\pi} \sigma_z \cos\theta \, R d\theta = -\gamma_t \pi R^2 \qquad (15.25b)$$

It shows that the force Q corresponds to the cavity weight. Verruijt showed by comparison of this approximate stress state according to (15.23) and (15.24) to an exact analytical solution for a rigid cavity with a vertical force in a semi-infinite elastic space that it reveals good agreement for cavity depths $H > R$. The evaluation of induced stresses during boring is, however, more complicated. During this process extensive monitoring, proper understanding of the measured data and adequate mitigating measures are therefore inevitable.

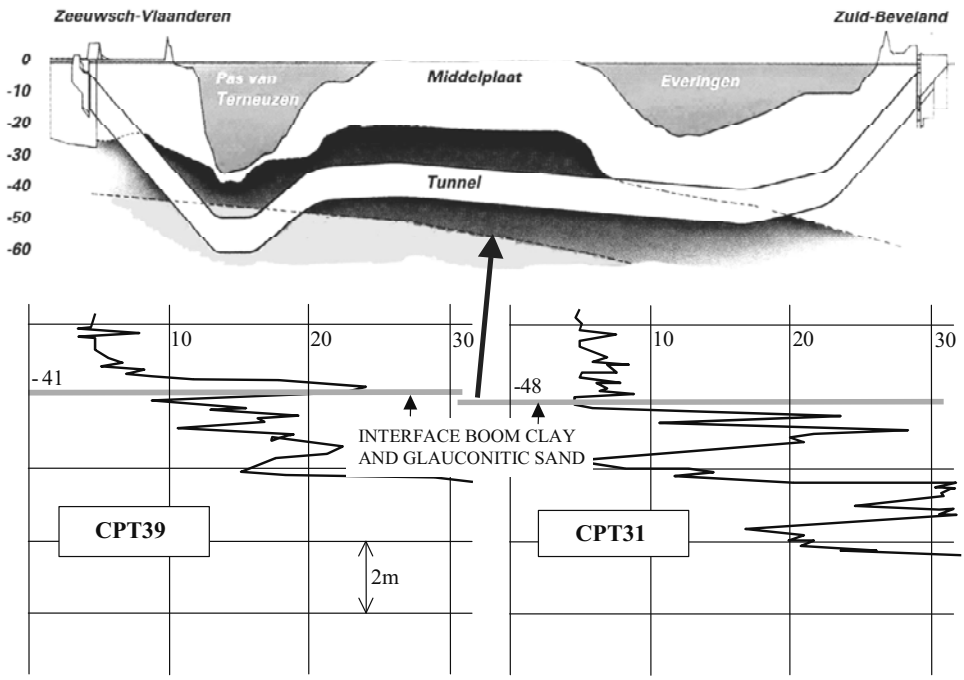

Figure 15.9 Western Scheldt Tunnel alignment; geological-geotechnical conditions

E TUNNEL BORING DESIGN AND CONSTRUCTION

The design and the construction of the Western Schelde tunnel in the Netherlands opened in March 2003, started in 1995. It was at the limits of the state of the art: a bored twin tunnel of 6600m length with diameters of 11m reaching as deep as 60m below sea level under difficult geological conditions, in particular the loose sands and stiff clays of extraordinary composition (Fig 15.9). The public-private nature of the consortium, with the private organisation NV Westerschelde (NVW), responsible for the construction and access roads, as well as for the

technical management, maintenance and operation for a period of 30 years, the Dutch Government acting as shareholder, and the contractor known as KMW, who designed and built the tunnel, according to a design-build contract, was quite exceptional. The budget of about 750 million euro was exceeded by only 6%.

In many respects the construction was a pioneering project. The logistics were a great challenge since the civil fitting out of the tunnel immediately followed the boring process, including the 26 cross-connections, which were constructed using ground freezing techniques under extreme conditions. A bored tunnel at this depth had not previously been realised in partly soft and partly stiff sediments. Soil investigations included unprecedented deep cone penetration tests reaching 65m below sea level through the Boom clay into tertiary glauconitic sands. Soundings in these sands showed a resistance with significant variation between 5 MPa and 35 MPa (Fig 15.9). This has a serious implication on the soil bedding of the tunnel shield and lining as is demonstrated next.

The boring started in 1999 with two TBMs. In May 2000 in the Tertiary glauconitic sand, serious deformations at the tail of the shields of both TBMs were noticed and some equipment damage occurred. The theoretical free space measured between the TBM and the tunnel lining was 85 mm. Deformation measurements showed that at a number of spots the tail of the shield almost touched the lining. Over a length of 4.5 to 5 m (in the longitudinal direction of the shield, total length of 11.55 m) the boring shield of the east TBM showed severe irregular deformations (buckling). The maximal deformation of the west shield was 40/50 mm and the maximal deformation of the east shield was 52 mm. Finally the west TBM and the east TBM stopped near the deepest point in the glauconitic sand (Fig 15.9). The TBMs seemed almost to be lost and the project would be a disaster. Fortunately, proper measures could be taken and boring continued. Despite these measures the deformations of the TBM increased to a maximum of 60 mm. As soon as the TBM went up, back into the Boom clay, these deformations decreased. Boring in glauconitic sands was a new experience.

The stagnation had cost serious delay and additional costs reaching 35 million euro. An investigation started to find possible causes and work out who should finance the unexpected loss. Concerning the ground conditions and design approach the following observations were made. The design of the tunnel shield is based on Duddeck's method (Fig 15.10), which is a common state of the art. Original calculations showed sufficient soil bedding support for the shield stability (buckling risk) under the extreme high water pressures (60 m below sea level), when adopting low soil stiffness. This was the basis for the tunnel shield design. However, when adopting high soil stiffness, there is locally no soil bedding, meaning that under the very high pore pressures shield deformations (buckling) may occur. The soundings (CPT's in Fig 15.9) show that the soil stiffness is strongly non-uniform and it is known that, particularly when there is significant silt or clay content, it is possible for cavities to remain unsupported in sands. Furthermore, a few case histories of tunnels constructed in loose clay-silt sands show that radial effective stresses may become very low.

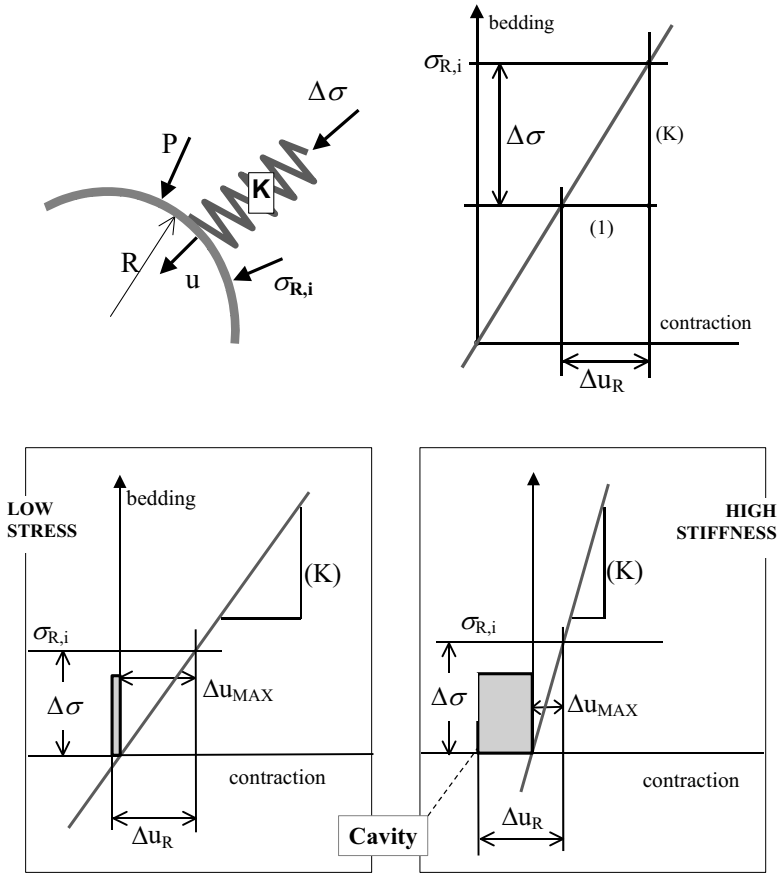

Figure 15.10 Tunnel shield design:
(above) soil effect simulated by a simple spring (Duddeck's method);
(below) soil stiffness: low stiffness (left), high stiffness (right); the grey box shows the corresponding cavity (free space between soil and shield); Δu_R is the oversize of the drill wheel with respect to the shield .

Tertiary glauconitic sands can show much greater variation than one may imagine. Temporarily, a void can arise, where the shield contact is released, or a very stiff reaction is generated, where the shield contact is intensified. Similar experience is found in pipe jacking: the boring hole is rather stable, but steering corrections are hardly possible. The clay content and sand density determine this behaviour. A combination of facts contributed to the excessive shield deformation: drift, glauconitic sand and high water pressure. The soil stiffness chosen in the design did not reflect the most critical condition at the lowest position. The extreme bedding (cavity) and high pore pressure condition there could have been foreseen, when the available soil data and experience had been considered with sufficient care. However, the execution of specific on-site soil investigation was extremely difficult and the apparent high horizontal stresses (high K_0-value) were unexpected. Fortunately, the project was finished with almost no delay and a successful tunnel is now in fine operation.

F UNSEEN LEAKAGE

It is remarkable that the groundwater is such a common factor in failure cases. It may gradually change the local conditions, particularly when large pore pressure drops are involved. The collapse of a temporary retaining wall of a building pit in Rotterdam in 1995, is such an example.

A grout-column retaining wall protecting a deep building pit near a river collapsed, unforeseen, after months of satisfactory performance. A new metro station was being built around an existing metro tunnel while train services continued uninterrupted, at more than 10 meter below groundwater level. Investigations after the event revealed that a combination of several factors gradually caused a critical situation: leakage, consolidation, erosion, piping, pump failure, and column fracture. Pore pressures had been measured continuously. They reveal the unseen gradual process of local deterioration, which took place along the interface of the existing metro tunnel and the subsoil. The leakage and a possible small deformation of the deeper clay layer due to the deep pumping system (head drop of about 12m), may have given place to regressive erosion of the sand under the existing tunnel (piping), which was founded on piles into the sand layer underneath the clay. Small water and sand inflows would hardly be noticed during the excavation and construction works (open pit, it rained regularly).

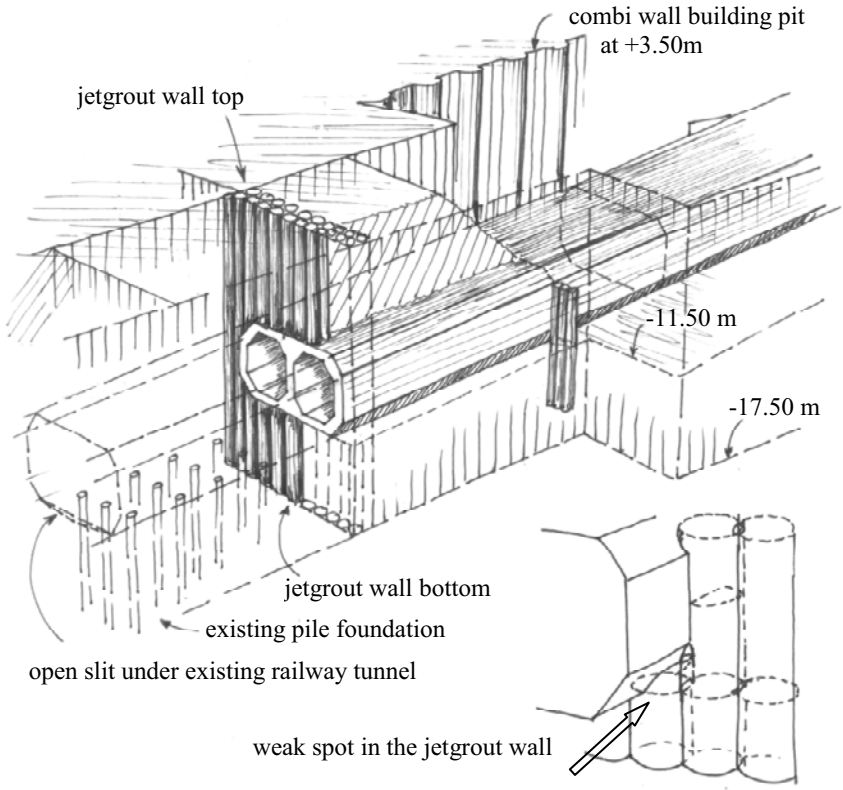

Figure 15.11 Building pit metro station Wilhelmina Pier, Rotterdam

Then in February 1995, after five months of uneventful performance, suddenly a strong leakage was observed. Next, a pump broke down, a pronounced sand inflow was noticed, and after a temporary repair the grout-column wall locally collapsed (Fig 15.11). The subsequent mud and water inflow could not be stopped. In the end, the building pit had to be put under water in order to repair the grout-column wall. Total damage was about 5 MEuro. It is worthwhile to mention, that, if the ongoing erosion process would have been modest another two months, nothing would have been noticed and no damage would have happened, as by then the construction of the metro station basement would have been completed.

application 15.1

Consider a cylindrical vertical borehole with a radius r_0 = 0.25 m in a soft cohesive soil with undrained strength c_u = 20 kPa, shear modulus G = 400 kPa, saturated weight γ = 14 kN/m^3. The soil has a low permeability. The hole is filled with water. At a depth of 5 m the situation is considered. Here the pore pressure is u = 50 kPa. The total stress was 70 kPa, so a cavity pressure of q = –20 kPa is representative and the cavity is contracting.

Applying (15.13) gives a plastic zone $r_p = r_0\, e^{-(q+c)/2c} = r_0$, implying that there is just no plastic zone. (15.14) gives the local displacement $w_0 = -cr_0\, e^{-(q+c)/c}/2G$ = –20x0.25 x$e^{-(-20+20)/20}$/(2x400) = – 0.00625 m = – 0.6 cm. Rather small.

Next, the water is taken out. Hence the representative cavity pressure is q = –70 kPa, which gives $r_p = r_0\, e^{-(q+c)/2c}$ =0.25 $e^{-(-70+20)/40}$ = 0.88 m; in a ring wide 0.88 – 0.25 = 0.63 m around the cavity the soil is in a plastic state. The corresponding displacement is $w_0 = -cr_0\, e^{-(q+c)/c}/2G$ = –20x0.25 $e^{-(-70+20)/20}$/(2x400) = – 0.076 m = –7.6 cm. Quite large!

A critical situation occurs when, with (15.17), $q = -c(1+\ln I_r)$ = –20(1+ ln(400/20) = –79.9 kPa. At a depth of *5* m the cavity will not collapse, but at a depth 79.9/14 = 5.7 m it will. Here, the soil weight will play a role.

application 15.2

Consider a tunnel lining with radius R at a depth H under the ground surface. The groundwater table is at the surface, i.e. D = 0 in Fig 15.8. Let K_0 = 4 (a highly over-consolidated soil), R/H = 1/3, γ_s = 20 kN/m^3, γ_w = 10 kN/m^3, and γ_t = 0 (the tunnel lining is rigid and relatively weightless). The components of the traction t at the lining surface, i.e. the normal pressure induced by the local soil stress, is described by its components (see Fig 15.11)

$$t_x = \sin^2\theta\,\sigma_x + \cos\theta\sin\theta\,\sigma_z \quad \text{and} \quad t_z = \sin\theta\cos\theta\,\sigma_x + \cos^2\theta\,\sigma_z$$

Application of the approximate soil stress according to (15.23) and (15.24) to this situation yields

$$\sigma_x/\gamma_s H = (K_0\gamma_d D + (\gamma_w + K_0(\gamma_s - \gamma_w)(H + R\cos\theta)/\gamma_s H = 3/2 + ½\cos\theta$$

$$\sigma_z/\gamma_s H = (\gamma_d D + \gamma_s(H - R))/\gamma_s H = ⅔$$

And the traction components become

$$t_x = \sin^2\theta\,(3/2+\tfrac{1}{2}\cos\theta) + \tfrac{2}{3}\cos\theta\sin\theta$$

$$t_z = \sin\theta\cos\theta\,(3/2+\tfrac{1}{2}\cos\theta) + \tfrac{2}{3}\cos^2\theta$$

In Fig 15.11 a graph is presented of the traction components. Also the results for K_0 = 0.5 (normally consolidated soil) are presented in the graph. The value of K_0 makes a difference.

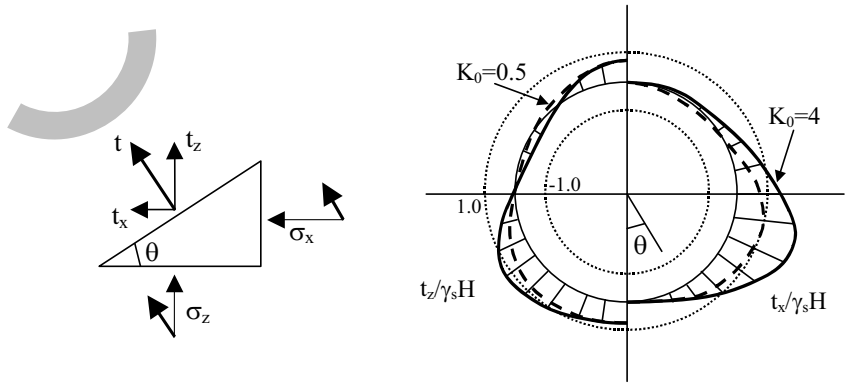

Figure 15.11

application 15.3

The lining of a tunnel with radius R = 5 m can buckle under local soil and water pressures. A practical approach for the calculation is by adopting springs on the lining. These springs represent the ground stiffness. The springs can be determined using the theory of an elastic half space. The spring constant is then: $k = EA_0/h$ (equation 12.36). At the depth of the tunnel the soil elasticity E is 10 MPa. Explain how you would interpret A_0 and h, and determine the corresponding spring constant value k.

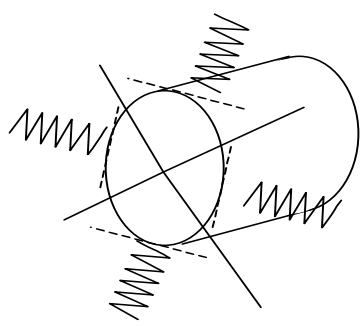

Figure 15.12

application 15.4

Arching effects may occur when boring a tunnel.
What is the arching effect?
In which type of soils is this most likely to occur?
Is arching good or bad? Give an example.

16 COASTAL ENGINEERING

A HYDRO-GEODYNAMICS

Hydro-geodynamics in porous media refers to the mechanical response of granular sediments when exposed to hydro-dynamic loading, i.e. water waves, wave impacts, tides and earthquakes. Geotechnical aspects under such conditions include: critical cross-sections and material parameters, wave/earthquake loading, dynamic pore pressures, excess pore pressures, pore pressure build-up and liquefaction, hydraulic (internal) filter stability, dynamic stability and residual deformation. In this chapter these aspects are outlined to some extent.

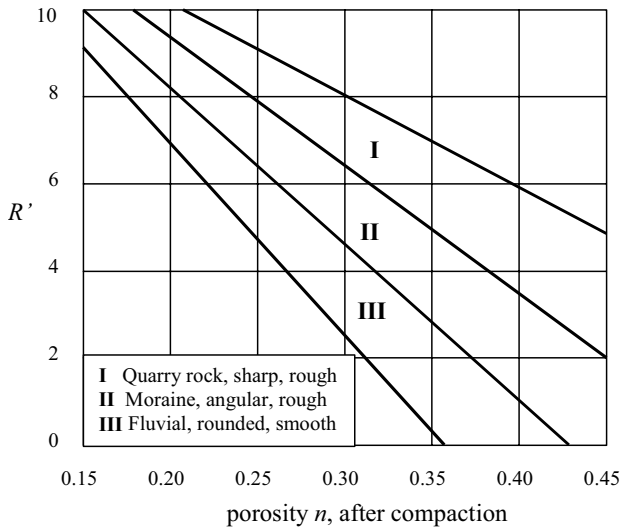

Figure 16.1a Equivalent roughness R'

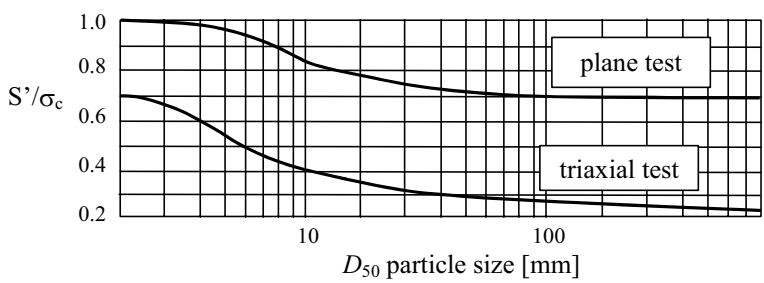

Figure 16.1b Equivalent strength S'; σ_c is the uniaxial rock compression strength

Rock friction

Since coastal structures usually involve coarse filter layers (stones and rock) the corresponding internal friction angle needs some concern. Barton's formula reads

$$\varphi = \varphi_0 + R' \log (S'/\sigma') \qquad (16.1)$$

Here, φ_0 is the basic friction coefficient between polished surfaces (range between 27° and 33°), R' is the equivalent roughness related to rock type, shape and packing (Fig 16.1a), S' is the normalised equivalent strength (Fig 16.1b) and σ' the actual in situ effective stress.

Densification

The natural densification (settlement) of rock fill subjected to gravity, hydraulic or earthquake loading may be important. Cohesionless materials dumped or discharged through water will be in a loose state. For earth reservoir dams usually 0.2 to 0.5% densification is assumed together with careful placement during construction. In marine structures, controlled densification is rarely performed. Loose dumped gravel and rock fill can be densified by specific methods (falling weight, shaking plate). The Menard method is popular and densifications to depths of 10 m are reported. For gravel 10-15% densification can be achieved and for rock fill 10-60 kg about 15%. For larger stones heavier equipment may cause crushing. For comparison, densification machines produce accelerations up to 10g, earthquakes may produce 2g in the entire structure (leading to 2-4% densification). Large slamming waves cause 1g acceleration, locally under concentrated impact, which can be observed along coastal defence structures around the storm water line (see page 284).

Turbulent porous flow

Porous flow in coarse granular media (stones and rock beds) develops under inertial effects and partial turbulence (Forchheimer's law), in accordance to

$$u_{,i}/\gamma_w = -cq_{,t} - (a + b|q|)q_i \qquad (16.2)$$

with $a = 160\ \nu(1-n^2)/(gD_{15}^2 n^3)$ and $b = 2/(gn^2 D_{15})$

Here, c is a mass factor, and a and b are permeability parameters with ν the kinematical viscosity, n porosity, g gravity acceleration and D_{15} the characteristic pore size dimension. Here, $u_{,i}/\gamma_w$ represents the pressure head gradient. The expressions for a and b are empirical (Hannoura and Barends).

Turbulence effects may be expected to start in granular soils with a $D_{50} > 5$ mm, depending on the grain size distribution. Sea gravel often has a flow regime intermediate between linear and turbulent. For turbulent flow one may adopt an apparent permeability, applying $k = (a/2 + (a^2/4 + b|u_{,i}|/\gamma_w)^{0.5})^{-1}$. Formula (16.2) shows that the apparent permeability in the linear regime ($b = 0$) is proportional to D^2 and in the turbulent regime proportional to $D^{0.5}$, showing a dependence of four orders. The flow regime depends on the actual pore pressure gradient, which will vary in space and time under wave loading conditions. Scaling difficulties seem unavoidable in physical modelling of the linear-turbulent porous flow field.

Filter rules

In stratified filter layers, local pore fluid velocities may convey fine particles through the pores. This may lead to internal erosion and can become the onset of

the structure's malfunctioning. The occurrence of these phenomena is covered by the so-called filter rules, which defines limits of adjacent coarse and fine granular grain sizes. For uniform materials the non-migrating filter rule states $D_{50f}/D_{50b} < 5$ to 10, and for wide graded materials three conditions are to be satisfied: (1) $D_{15f}/D_{85b} < 4$ to 9, and $D_{50f}/D_{50b} < 12$ to 18, and for preventing clogging $D_{20f}/D_{20b} > 5$. Suffix f stands for the coarse filter and b for the base material. For wide graded material suffusion or colmation is likely to happen.

If a filter is subjected to dynamic pore pressure gradients (a gradient of 20% is considered significant) an extra norm should be considered: $N_f = n_f D_{15f}/D_{50b} < 1$ to 5. Artificial armour and rock fill degenerate with time, breaks at intergranular contacts and fines are washed out or accumulate (blocking). This process is characterised as material fatigue. Water may convey free sediments that settle in the pores and change the hydraulic permeability. It may become a serious problem under critical loading conditions. Growth of marine organisms in pores may have a similar effect.

An adequate thickness of a filter layer is at least 3 times D_{85} or 20 cm, or 30 cm when placement occurs under water. In literature, refined filter rules can be found for other materials (geotextiles).

Liquefaction

The sensitivity of granular material becoming liquefied is expressed by the so-called liquefaction potential, which can be determined by special laboratory tests (cyclic shear or cyclic triaxial test) on samples from the site at various manufactured densities. Results should be calibrated with the in-situ density, which is difficult to measure, unfortunately. Under critical dynamic loading excess pore pressures may arise depending on the slope angle, the wave period and the drainage capacity. When the excess pore pressure reaches the actual effective stress level, the granular structure collapses into a mud: liquefaction. Particularly fine loose sands ($D_{50} < 300\mu$) are sensitive to this excess pore pressure generation. When sands are densely packed, negative pore pressures may arise, which create a temporary additional strength. This can be of significant influence in dredging operations.

When locally the soil liquefies, it behaves suddenly as a heavy liquid. Immediately, induced additional pore pressures in the surroundings will arise (Fig 16.2), jeopardising structures by drastic reduction of required shear strength. When a liquefied sand is covered, sand fountains at the surface may occur, sometimes observed during earthquakes. Also fresh deposited hydraulic fill may suddenly fail due to liquefaction. The air content is crucial for the liquefaction potential. Small air content in the pore water (> 2%) may drastically reduce the likelihood of liquefaction, because it damps the excess pore pressure generation significantly. A light cementation of loose sands is a remedy against liquefaction, and here is a potential for the application of biotechnology (see Chapter 13).

In Fig 16.2 a column test shows that after a shock the loosely packed top sand layer suddenly liquefies and behaves like a heavy fluid. The pore pressures have been measured by 6 sensors, equally spaced along the vertical. The weight of liquefied mass is directly felt as excess pore pressures in the densely packed sand

layer underneath. These excess pore pressures dissipate in accordance with the sedimentation process of the liquefied layer. The expelled water due to densification appears on top of the sand column (after 8 shocks it reached about 8% of the height of the top layer). This test is performed by successive equal shocks, and each time a liquefaction occurred in the top layer and the following sedimentation proceeds each time about 25% faster than after the previous shock. The increase of relative density D_r and the decrease of porosity n of the top layer is shown in the inset of Fig 16.2 (the critical density is 0.65). The lower layer had a high density and did not liquefy.

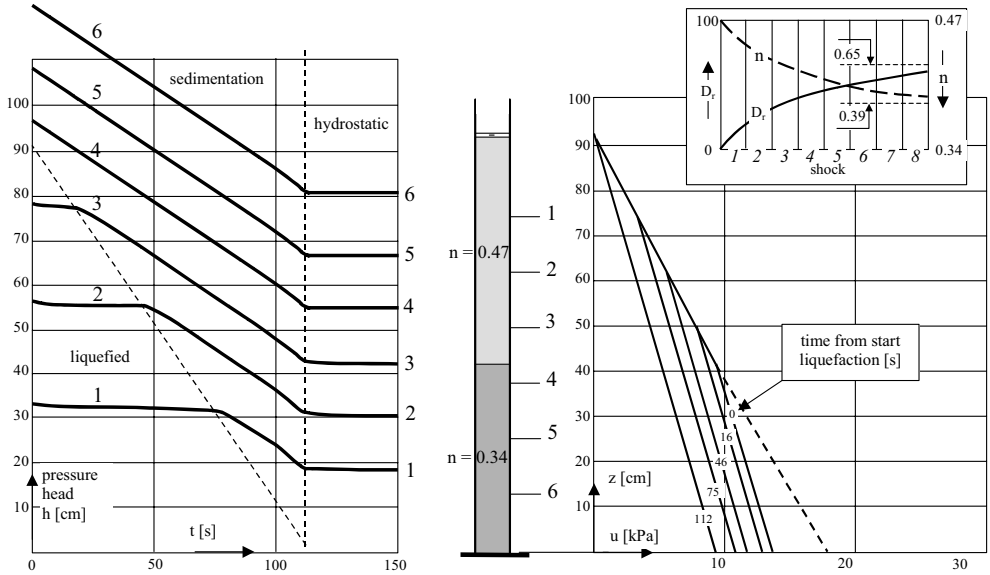

(a) measurements first shock (b) test set-up (c) actual pore pressures first shock
Figure 16.2 The effect of liquefaction to the direct surroundings

In multi-dimensional situations the induced excess pore pressures may dissipate alongside the liquefied zone. The expelled water has also to dissipate through the sides and above the liquefied zone, creating excess pore pressures there as well. This process is governed by the transport and storage capacity of the direct surroundings of the liquefied zone. The related consolidation is in the order of minutes. During this period the shear strength of the soil is seriously reduced. It is important to realise that the influence of liquefaction may reach far beyond the liquefied zone itself.

Liquefaction of a land fill

The recent harbour enlargement in Barcelona included two new large breakwaters and a wharf for a container terminal, covering 934 hectare and 1500 metres quay wall (Fig 16.3a). The quay wall of the wharf consisted of large pre-cast reinforced sand-filled caissons (each 17.5 metre high, 18.5 metre wide and 40 metre long) based on a rubble mound sill in a dredged trench. Land reclamation of the area behind the quay wall was performed by hydraulic fill.

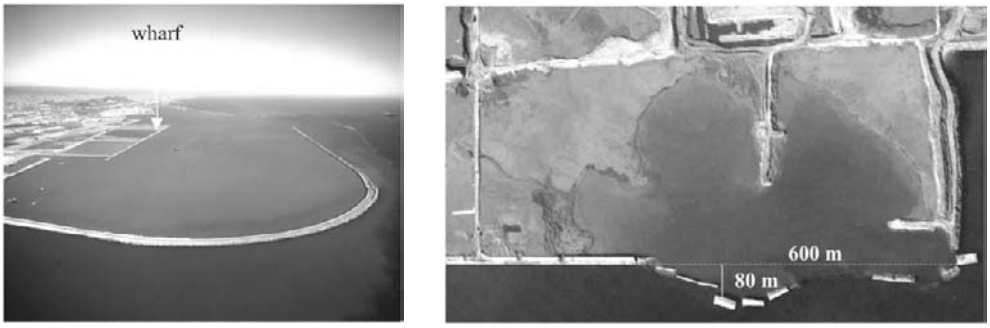

(a) position of the new wharf *(b) after the liquefaction*

Figure 16.3 Barcelona harbour

On 1 January 2007 a sudden unexpected collapse took place: 600 metre of the quay wall and a large part of the fill, already well advanced, disappeared (Fig 16.3b). Eyewitnesses reported that 16 massive caissons were displaced, some over 80 metres within a few minutes.

In general, hydraulic fill mud settles slowly. Particularly for fine soils, it may take days. During filling a settling mud slope advances in a dynamic way with successive local sliding. The mud may have a temporary density significantly higher than water, at times even up to 1800 kg/m^3. Such mud fluid induces additional excess pore pressures in the subsoil. Accordingly, local shear resistance will decrease, making the soil's stability vulnerable.

The massive slide, which occurred at the end of the fill operations, was most probably caused by high mud level, while the front slope of the fresh mud reached its deepest and steepest size, and excess pore pressures in adjacent zones due to the mud weight were at their peak. Because an advancing sedimentation front during hydraulic fill is unstable, successive small slides took place, one of which may have triggered the massive slide. Some caissons became instable, mud penetrating under the tilting caissons working as a lubricant, and next gravity caused the fluidised mass to move and expand, taking with it many more caissons into the recently deepened harbour. It is essential to include the mud-weight induced pore pressure effect in the surroundings in the design of temporary works.

B WAVES ON SEABED

The transient pore pressure generation in a stratified seabed due to waves is not trivial. The variance in permeability and compressibility of submerged soil layers may give rise to locally unexpected effective stress changes and in some locations excess pore pressures that exceed common limits and seem to have a negative retardation. It may reduce the local seabed stability and resistance against erosion or liquefaction. Some of these phenomena are explained.

One-dimensional cyclic consolidation

A method that provides straightforward solutions is the method of harmonic oscillation. A cyclic loading is applied and the response after many cycles (the steady cyclic state) is considered. The method is based on complex algebra. It will

be explained with an example that deals with the response of a vertical soil column to cyclic loading.

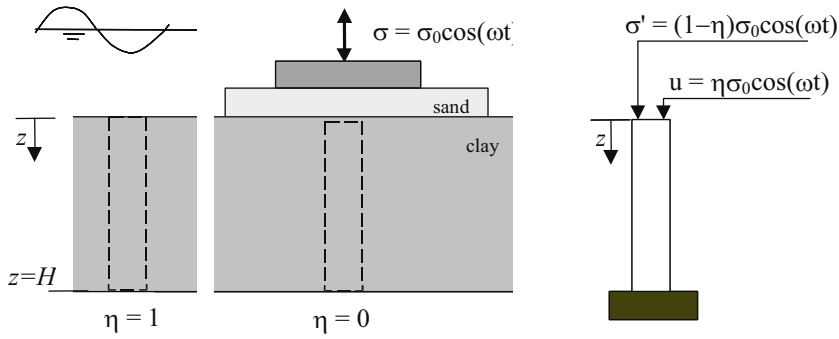

Figure 16.4a Cyclic vertical consolidation

At the surface $z = 0$ the conditions $\sigma = \sigma_0\cos(\omega t)$ and $u = \eta\sigma_0\cos(\omega t)$ hold. With Terzaghi's law, this yields for the effective stress at the surface $\sigma' = \sigma - u = (1-\eta)\sigma_0\cos(\omega t)$. Here, η is some constant $0 < \eta < 1$, which expresses a situation between two extremes: for $\eta = 1$ it refers to free waves on a seabed, for $\eta = 0$ a loaded shallow submerged footing on a drained layer (Fig 16.4a). For this situation the consolidation process in the soil is described by [57]

$$c_v u_{,zz} = u_{,t} - a\sigma_{,t} \quad \text{with} \quad a = (1+n\beta/\alpha)^{-1} \tag{16.3}$$

Here, α is the compressibility for the soil matrix and β for the pore fluid. Equilibrium at the bottom yields $\sigma = \sigma_0 \cos(\omega t)$, since at the bottom there is no relative motion between both phases. Hence, the flow term becomes zero, which yields, applying equation (16.3), $u_{,t} - a\sigma_{,t} = 0$ or $u = a\sigma + constant$. The constant can be identified with the effect of volumetric weight (hydrostatic pressure). Because, here, excess pore pressures are considered, this constant is zero. The internal stress state at the bottom becomes

$$u = a\sigma_0 \cos(\omega t) \quad \text{and} \quad \sigma' = \sigma - u = (1 - a)\, \sigma_0 \cos(\omega t) \tag{16.4}$$

Introduction of the variable $w = a\sigma - u$ yields for equation (16.3), keeping in mind that σ is only a function of t and not of z

$$cw_{,zz} = w_{,t} \tag{16.5}$$

with boundary conditions

$$z = 0, \quad w = a\sigma - u = (a-\eta)\sigma_0 \cos(\omega t)$$

[57] Suffix $,zz$ refers to a second partial derivative to the space coordinate z and $,t$ to a first partial derivative to the time coordinate t.

$z = H, \quad w = a\sigma - u = 0$

An harmonic solution is found by considering the response of the system to the complex excitation: $\exp(i\omega t)$, by stating that $w(z,t) = W(z)\exp(i\omega t)$. Inserting this into equation (16.5) yields

$$cW_{,zz} = i\omega W \tag{16.6}$$

which has a general solution according to $W = (a-\eta)\sigma_0 \exp[-z\sqrt{(i\omega/c)}]$. Here, for convenience, it is assumed that the bottom is relatively deep, which implies that there $z\sqrt{(i\omega/c)}$ is large, or $H >> \sqrt{(c/\omega)}$. The total solution is found by combination, i.e. $w = (a-\eta)\sigma_0 \exp[i\omega t - z\sqrt{(i\omega/c)}]$. Splitting this formula into a real and an imaginary part yields with $\sqrt{i} = (1+i)/\sqrt{2}$ and $\zeta = z\sqrt{(\omega/2c)}$

$$w = (a-\eta)\sigma_0 \exp(-\zeta + i(\omega t - \zeta))$$

$$= (a-\eta)\sigma_0 \exp(-\zeta)\,(\mathrm{os}(\omega t-\zeta) + i\sin(\omega t-\zeta)) \tag{16.7}$$

The real part is the response to the real part of the loading: $w=(a-\eta)\sigma_0 \cos(\omega t)$. The final solution therefore becomes

$$w = (a-\eta)\sigma_0 \exp(-\zeta)\cos(\omega t-\zeta) \tag{16.8}$$

The corresponding pore pressure and effective stress become

$$u = a\sigma - w = a\sigma_0\,[\cos(\omega t) - (1-\eta/a)\exp(-\zeta)\cos(\omega t-\zeta)] \tag{16.9a}$$

$$\sigma' = \sigma - u = \sigma_0\,[(1-a)\cos(\omega t) + (1-\eta/a)\exp(-\zeta)\cos(\omega t-\zeta)] \tag{16.9b}$$

To investigate the behaviour of the pore pressure and the effective stress formulae (16.9) are rewritten in the form of an amplitude U and a (negative) phase shift ψ, according to $u = U\cos(\omega t + \psi)$. Elaboration with $\xi=1-\eta/a$ gives

$$u = a\sigma_0\,[\cos(\omega t) - \xi\exp(-\zeta)(\cos(\omega t)\cos(\zeta)+\sin(\omega t)\sin(\zeta)]$$

$$= a\sigma_0\,[(1-\xi\exp(-\zeta)\cos(\zeta))\cos(\omega t) - (\xi\exp(-\zeta)\sin(\zeta)\sin(\omega t)]$$

With $A = 1-\xi\exp(-\zeta)\cos(\zeta)$ and $B = \xi\exp(-\zeta)\sin(\zeta)$ and $\psi = \mathrm{atan}(B/A)$ this becomes

$$u = a\sigma_0\,[A\cos(\omega t) - B\sin(\omega t)]$$

$$= a\sigma_0\sqrt{(A^2+B^2)}[(A/\sqrt{(A^2+B^2)})\cos(\omega t) - (B/\sqrt{(A^2+B^2)})\sin(\omega t)]$$

$$= a\sigma_0\sqrt{(A^2+B^2)}[\cos\psi\cos(\omega t) - \sin\psi\sin(\omega t)]$$

$$= a\sigma_0\sqrt{(A^2+B^2)}\cos(\omega t + \psi)$$

Note from B/A that for $\zeta < \pi$ the phase shift is negative ($\psi > 0$). Finally, the amplitude and phase shift become

$$U = a\sigma_0 \sqrt{(A^2+B^2)} = a\sigma_0 \sqrt{(1 - 2\xi \exp(-\zeta)\cos(\zeta) + \xi^2 \exp(-2\zeta))} \qquad (16.10a)$$

$$\psi = \mathrm{atan}(B/A) = \mathrm{atan}[\xi \sin(\zeta)/(\exp(\zeta) - \xi \cos(\zeta))] \qquad (16.10b)$$

The graphical representation of these formulas is given in Fig 16.4b, for various values of η. The cases for $\eta < 1$, shown in Fig 16.4b, reveals that at certain depth $\zeta > 1.45$ or $z > 2.06\sqrt{(c_v/\omega)}$ the amplitude U becomes larger than the partial loading $a\sigma_0$. A maximum is found at $z = 3.25\sqrt{(c_v/\omega)}$ of $1.07a\sigma_0$, for $\eta = 0$ (see Fig 16.4a). In case of incompressible water, the pore pressure is then 7% larger than the total loading σ_0! The phase shift ψ shows that in the area $0 < z < \pi\sqrt{(2c_v/\omega)}$ the local maximum of U arrives before the maximum of the loading, in fact a negative phase shift or a negative retardation! For $z = 0$ this negative phase shift is at maximum $\pi/4$, with a local amplitude equal to zero. The negative phase shift is small, about 0.03π, when U reaches its maximum at $z = 3.25\sqrt{(c_v/\omega)}$. The maximum pore pressure response and the maximum loading will hardly show any phase shift.

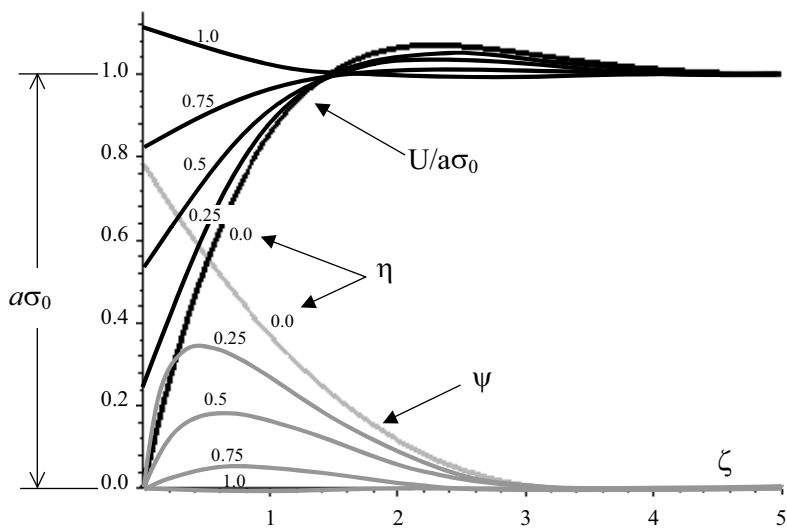

Figure 16.4b The pore-pressure amplitude and phase shift

A set of isochrones for the induced pore pressure for the case of a fully drained surface ($\eta = 0$) including the effect of pore fluid compressibility, i.e. for $a = 0.9$ and $a = 1.0$, is presented in Fig 16.5a.

The value $\sqrt{(c_v/\omega)}$ has dimension of length. For sand: $c_v \approx 0.01$ m^2/s and for clay: $c_v \approx 10^{-5}$ m^2/s. For tidal loading $\omega \approx 1.45\text{x}10^{-4}$ 1/s, the length $\sqrt{(c_v/\omega)}$ becomes for sand 8.3 m, and clay 0.26 m. For large waves with a period of $T = 10$ s (Note $\omega = 2\pi/T$=0.63 rad), the length $\sqrt{(c_v/\omega)}$ becomes for sand 0.13 m, and for clay 0.003 m. Hence, consolidation takes place near the seabed surface, and the assumption of a

one-dimensional schematisation is valid, because the wave length is in both cases much larger than the consolidating zone. The effective stress σ' can be treated in the same way. The amplitude is the counterpart of u because at any moment their sum is equal to the loading amplitude $a\sigma_0$. Hence. the effective stress amplitude σ' can be obtained from the graph of Fig 16.4b. In a zone beyond $z = 2.06\sqrt{(c_v/\omega)}$ the induced effective stress becomes negative (tensile). Because of hydrostatic stress (gravity is not included in this analysis) tensile stresses may not occur, but lower effective stress does occur.

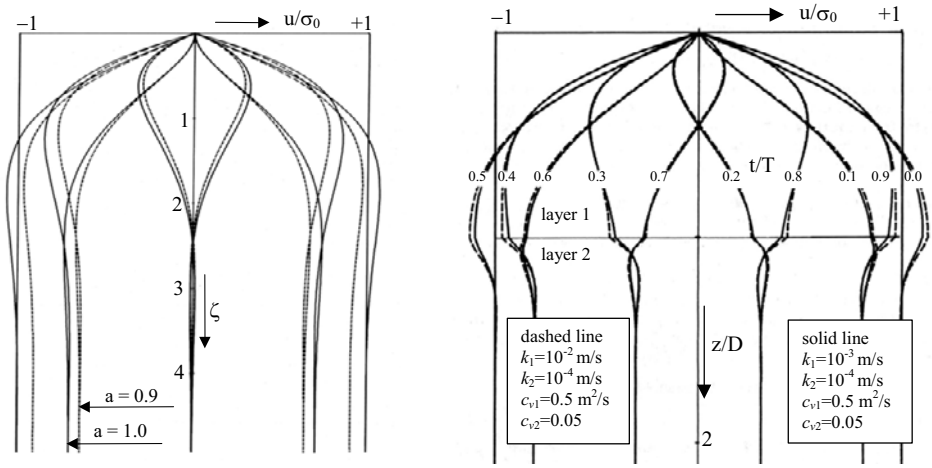

(a) cyclic pore pressures uniform seabed *(b) cyclic pore pressures layered seabed*

Figure 16.5

This particular example shows three typical effects of cyclic consolidation: (1) the maximum pore pressure at some moments may exceed the maximum total loading, (2) the generated effective stresses may decrease (become zero), and (3) there is a negative delay in the response. Moreover, these phenomena may take place in a relatively small zone near the border, which with regard to the wavelength supports the validity of the one-dimensional approach.

Next, consider a stratified subsoil, i.e. a two-layer system. The upper layer is defined in the range $0 < z < D$, and the second layer in the range $z > D$. At the boundary $z = 0$ a cyclic loading is imposed, according to Fig 16.4a. The elaboration is tedious and not presented here. In Fig 16.5b the solution for two situations is presented (incompressible pore water). Note, that the maximum pore pressure occurs at the layer separation and is in the order of $1.11\sigma_0$, exceeding the loading by 11%.

The gradient $u_{,z}$ in the second layer at the interface is of particular interest. It is expressed by

$$u_{,z} = \sigma_0\sqrt{(\omega/c_{v2})}\cos(\omega t - \psi + \pi/4)/\sqrt{(A^2+B^2)} \qquad (16.11)$$

$$A = \cos(D\sqrt{(\omega/2c_{v1})})(\cosh(D\sqrt{(\omega/2c_{v1})} + \delta\sinh(D\sqrt{(\omega/2c_{v1})})$$

$$B = \sin(D\sqrt{(\omega/2c_{v1})})(\sinh(D\sqrt{(\omega/2c_{v1})} + \delta\cosh(D\sqrt{(\omega/2c_{v1})})$$

$$\delta = (k_2\sqrt{(\omega/2c_{v2})} / (k_1\sqrt{(\omega/2c_{v1})}$$

This particular example shows that, in a two-layered stratified porous medium, maximum cyclic pore pressures take place at the interface and they may exceed the total loading up to ~15%, and that pore fluid gradients at the interface in the finer bed are relatively large. The latter implies that filter instability is more likely.

In practice, one commonly interprets cyclic pore pressures by applying the standard formula for cyclic-damped response from the theory of heat conduction, which states

$$u = u_0 \exp(-\zeta) \cos(\omega t - \zeta) \qquad (16.12)$$

This is not correct for the examples discussed previously. It violates the principle of effective stress and the fact that the total loading by waves, tides or rocking submerged structures is transferred as a body force instead of a boundary force.

Travelling water waves on a seabed

The previous situation describes standing water waves. The solution for travelling water waves on a seabed is extensively discussed in literature (see Verruijt). The principle elastic solution for the pore pressures response in a seabed subjected to long wave loading $\underline{u} = A\cos(i\omega t - \lambda x)$ at $z = 0$ is

$$u = A\cos(\omega t - \lambda x)\,(\exp(-\lambda z) + m\theta\exp(-\alpha z))/(1+ m\theta) \qquad (16.13)$$

with $\alpha = \lambda(1 + i\psi(1+\theta+m\theta))^{0.5}$, $\theta = 2(1+\nu)n\beta_f/E$, $m = 1/(1-2\nu)$, $\psi = L^2/(2\pi c_v T)$, $\lambda = 2\pi/L$, and $T = 2\pi/\omega$, where L and T are the wave length and wave period, and E and ν are the elastic constants. Because α is complex it will give rise to a phase shift, which will rapidly attenuate with depth, since the real part of α is large compared to λ. In case the pore water is incompressible, $\theta = 0$ holds and (16.13) becomes $u = A\exp(-\lambda z)\cos(\omega t - \lambda x)$, showing that there is no phase lag and the induced pore pressures attenuate with depth. For large waves, Verruijt also gives an expression for the shear stress amplitude: $\hat{\tau} = A\,\lambda z\exp(-\lambda z)$, which for $\lambda z < 1$ is linear with depth. Hence, the shear stress ratio $\hat{\tau}/\sigma'_0$ is a constant in the top of the seabed. When this ratio approaches $\tan\varphi$, the seabed may become unstable.

Water waves on rigid structures

A semi-submerged coastal structure, founded on a filter bed and subjected to wave loading, will rock on its foundation. These movements will cause deformation in the seabed and hence induced pore pressures in the subsoil. The situation at the edges of the foundation involves two phenomena; in fact, a combination of the two situations presented in Fig 16.4a. For $\eta = 1$ (free-standing wave loading) and $\eta = 0$ (effective drained loading under the structure), in a 2-D setting, see Fig 16.6. Although the cyclic character of this induced phenomenon will probably not create serious pore water flow, large local pore water gradients

may occur occasionally, which invoke migration of particles (dynamic piping), and without proper measures it may affect the stability of the structure.

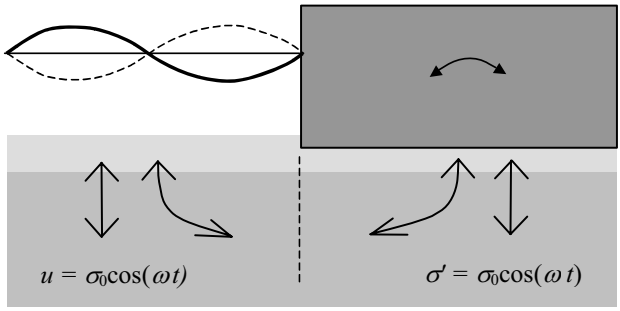

Figure 16.6 Combined conditions at the edge of a coastal structure

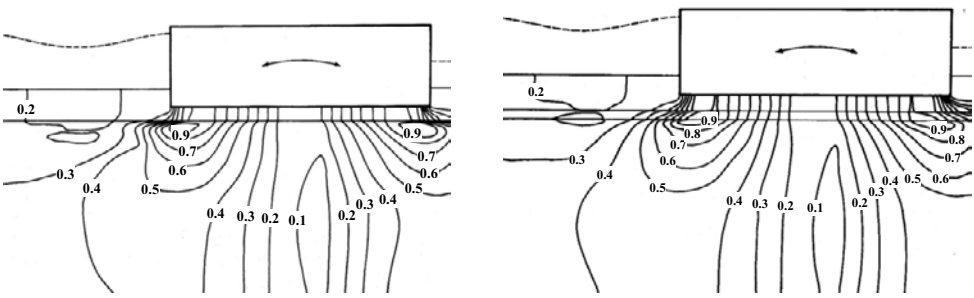

(a) two-layer foundation *(b) three-layer foundation*

Figure 16.7

An example of a numerical simulation of a two-dimensional cyclic consolidation process involving the previously described condition at the edge of a rocking coastal structure, on a shallow foundation and subjected to wave loading, is presented in Fig 16.7, case (a) with a soft seabed with on top one coarse, relatively stiff and permeable filter layer, and case (b) with a soft seabed, with on top a two-layer filter bed consisting of coarse and finer softer material. The pore water is assumed slightly compressible (some air intrusion due to wave action).

In Fig 16.7 isobar lines are presented, tagged with a number that shows the excess pore pressure amplitude relative to the loading amplitude by the rocking structure (rocking is significantly more severe than the wave itself). Local zones of high pressures are observed, in agreement with aspects previously discussed. Proper modelling of local gradients in these zones near interfaces of the filter bed is achieved by a very fine FEM mesh. These gradients are essential in the design of a stable filter bed under extreme loading conditions.

Multi-dimensional cyclic consolidation

The specific solution of cyclic consolidation problems in three dimensions requires advanced mathematics. For stationary consolidation the volumetric averaging method has been elaborated in Chapter 6E. Here, the same is used for cyclic consolidation. Consider a general porous medium with volume V and surface

$S = A_1 + A_2$, where A_1 is a drained surface (pore pressure is constant $u = 0$) and A_2 is closed surface (no flow condition). Adopting a volumetric approach, i.e. volume strain ε and mean effective stress σ' are related through a bulk modulus K: $\sigma' = K\varepsilon$, the general storage equation, expressed by[58]

$$\nabla\cdot\nabla u = (1/c_v)\,\partial\,(u - \sigma)/\partial t \quad \text{with} \quad c_v = kK/\gamma_w \tag{16.14}$$

Two cases are considered: a cyclic pore pressure u at boundary A_1 and a cyclic loading σ on the entire volume.

The first case implies that the loading σ is constant, and at the drained boundary A_1 a harmonic loading is applied $u_1 = U_1\cos(\omega t)$. The harmonic solution, employing complex algebra, seeks the real part of the complex response, subjected to the complex extension of the loading $u_1 = U_1\exp(i\omega t)$. Since a harmonic response is considered, everywhere the pore pressure has identical frequency. Thus, $u = U \exp(i\omega t)$, where the amplitude U is only a function of space. Equation (16.14) becomes

$$c_v\nabla^2 U = i\omega\, U \tag{16.15}$$

A simple solution is sought by averaging over space (see Chapter 6E), rendering (16.15) into,

$$c_v \iiint \nabla^2 U dV = i\omega \iiint U dV \tag{16.16}$$

Introduction of average field pressures

$$\underline{U} = \iiint U dV / V \quad \text{and} \quad \underline{u} = \iiint u dV / V \tag{16.17}$$

and adopting an approximate two-dimensional parabolic distribution of the field pressure, shown in Fig 16.8, so that

$$\iiint \nabla^2 U dV = \iint \nabla U dA = 3(U_1 - \underline{U})\, A_1 / L_1 \tag{16.18}$$

where, A_1 is the drained surface and L_1 the relevant flow path, renders (16.16) into

$$\underline{U} = U_1\,(1 - i\alpha)/(1+\alpha^2) \tag{16.19}$$

with $\alpha = \omega\, L_1 L_2 / 3c_v$ and $L_2 = V/A_1$, the hydraulic radius (drainage capacity). The total harmonic response is therefore

$$\underline{u} = \underline{U}\exp(i\omega\, t) = U_1 \exp(i\omega\, t)\,(1 - i\alpha)/(1+\alpha^2) \tag{16.20}$$

The real part of this expression, the real response, becomes after some elaboration

---

[58] The compressibility of the pore fluid β can be included by adopting $c_v = kK/(\gamma_w + n\beta K)$

$$\mathrm{Re}(\underline{u}) = U_1 \cos(\omega t - \theta) / \sqrt{(1+\alpha^2)} \qquad (16.21)$$

where $\theta = \arctan(\alpha)$. Solution (16.21) represents a response with a decay of $1/\sqrt{(1+\alpha^2)}$ and a delay of θ/ω, as shown in Fig 16.9.

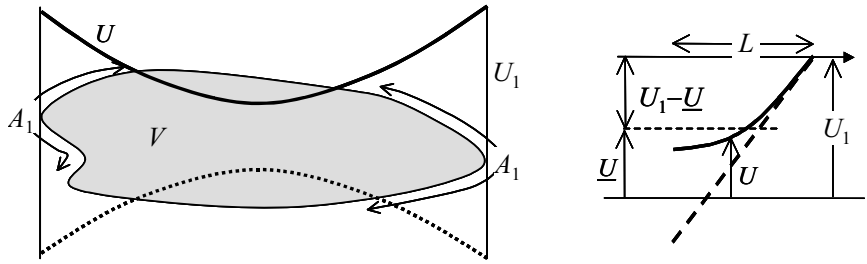

Figure 16.8

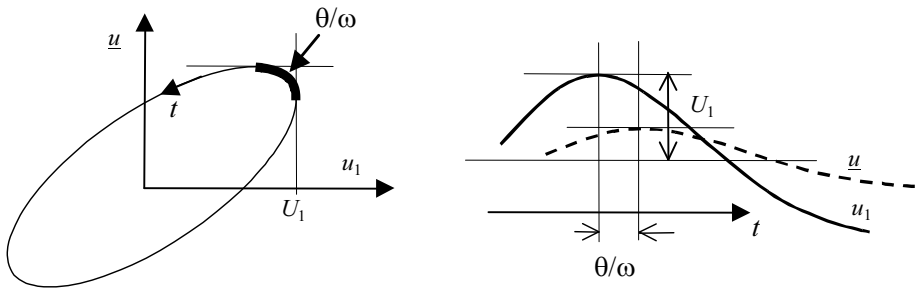

Figure 16.9 Harmonic average response to cyclic boundary loading

The second case defines at the drained boundary A_1 a pore pressure $u_1 = 0$, and on the entire volume an harmonic loading $\sigma = S_1\cos(\omega t)$. The harmonic solution, employing complex algebra, seeks the real part of the complex response, subjected to the complex extension of the loading $\sigma = S_1\exp(i\omega t)$. Since a harmonic response is considered, everywhere the pore pressure has identical frequency. Thus, $u = U \exp[i\omega t]$, where the amplitude U is a function of space. Then, the field response (16.14) is described by

$$c_v \nabla^2 U = i\omega\,(U - S_1) \qquad (16.22)$$

Volume average yields

$$c_v \iiint \nabla^2 U dV = i\omega \iiint (U - S_1) dV \qquad (16.23)$$

Introduction of average field pressures according to (16.17), and adopting an approximate two-dimensional parabolic distribution of the field pressure, shown in Fig 16.10, gives

$$\iiint \nabla^2 U dV = \iint \nabla U dA = -3\underline{U}A_1/L_1 \qquad (16.24)$$

This renders (16.22) into

$$\underline{U} = S_1\, i\alpha\,(1-\mathrm{i}\alpha)/(1+\alpha^2) \qquad (16.25)$$

The total harmonic response is therefore

$$\underline{u} = \underline{U}\exp(i\omega t) = S_1\exp(i\omega t)\, i\alpha\,(1-i\alpha)/(1+\alpha^2) \qquad (16.26)$$

The real part of this expression yields

$$\mathrm{Re}(\underline{u}) = S_1\,\alpha\cos(\omega t + \pi/4 - \theta)\,/\sqrt{(1+\alpha^2)} \qquad (16.27)$$

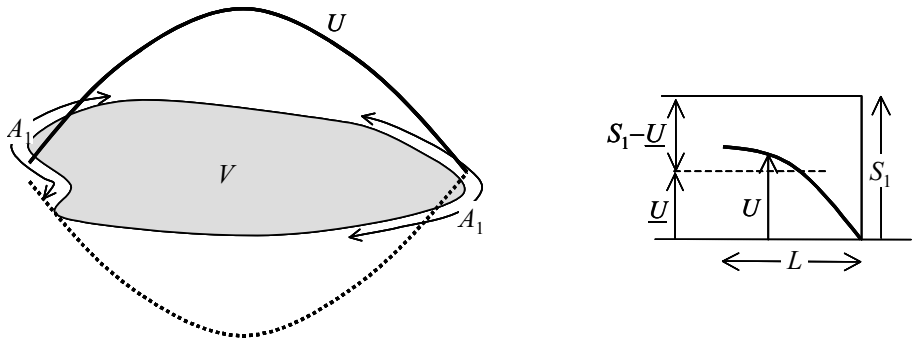

Figure 16.10

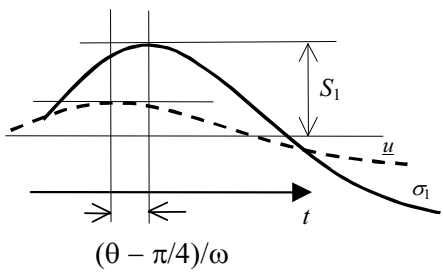

Figure 16.11 Harmonic average response to cyclic total loading, showing negative retardation

Solution (16.27) presents a response with a decay of $\alpha/\sqrt{(1+\alpha^2)}$, and a delay of $(-\pi/4+\theta)/\omega$, which is a negative delay for $\theta > \pi/4$, see Fig 16.11. The condition $\theta > \pi/4$ yields $\alpha = \omega L_1 L_2/3c_v < 1$. For a sandy seabed, under cyclic loading with a period in the order of $T = 10$ s or $\omega = 2\pi/T = 0.63$, and length scales L_1 and L_2 in the order of decimetres (vertical consolidation of thin layers), the condition of negative delay, i.e. $\alpha < 1$, is met for a seabed consolidation coefficient c_v larger than the order of $\omega L_1 L_2/3 = 2\text{x}10^{-3}$ m^2/s, which is also likely in many cases.

For a thicker soft clayey seabed, the length scales L_1 and L_2 are normally in the order of decametres and the corresponding consolidation coefficient c_v is usually in the order of 10^{-5} m^2/s, or smaller. In this case the condition of negative delay, i.e. $\alpha < 1$, is met for slower waves, like tidal waves, where ω is in the order of 10^{-4} rad/s.

The observed transient excess pore pressure response in coastal zones due to tidal water level changes shows a damped response with, indeed, a negative delay

(the peak response occurs earlier than the peak loading). Already in 1904 Honda noticed a negative delay in the potential tidal response in Yokohama and in 1916 Friedrich observed the same in Lubeck. Unknown subsoil water streams were thought to be the cause! In 1933 a similar behaviour was noticed during construction of the Park sluice in Rotterdam. No explanation was offered then. Today, the phenomenon can be understood after a close inspection of the physical process that takes place; in fact, it is a consequence of the effective stress principle.

C WAVES ON BREAKWATERS

Internal set-up

Regular storm waves and tides characterised by amplitude H and period T generate groundwater flow and transient pore pressures in porous dams and dikes. The induced internal water table height h shows a decay and delay, which are usually expressed by the well-known cyclic solution for a dam with a permeability k and effective porosity n, according to

$$h = H\exp(-x/\lambda_\omega)\cos(\omega t - x/\lambda_\omega) \qquad (16.28)$$

with the cyclic leakage factor $\lambda_\omega = (KDT/(n\pi))^{0.5}$, and wave period $T = 2\pi/\omega$.

This formula explains that at distance x from the boundary (outer slope), where the free water moves with $H\cos(\omega t)$, the local amplitude decays with $H\exp(-x/\lambda_\omega)$ and delays with $t = x/\lambda\omega$. The average still water level D remains unchanged in this example (Fig 16.12).

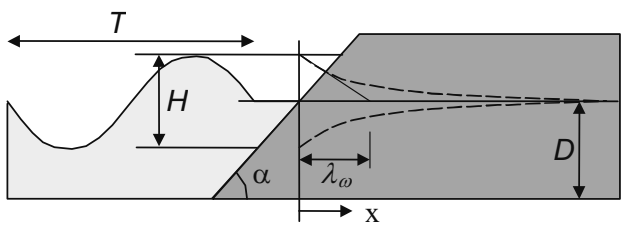

Figure 16.12 Cyclic porous flow in a breakwater

Geometric nonlinear effects occur which are related to the water depth D and the angle α of the outer slope of the dam or dike. They may cause the average water level h inside the dam to rise significantly more than expected, according to equation (16.28), which is addressed as internal set-up (Barends). The inflow surface along a slope at the moment of high water level (wave top) is significantly larger than the outflow surface at the moment of low water level (wave trough). Moreover, the average seepage path for inflow is significantly shorter that the outflow path. Hence, during cyclic water level changes, water will enter the structure more easily than it will leave. Consequently, there will be a state in which the corresponding inflow surplus is balanced with an extra outflow drive, i.e. by a groundwater table set-up.

The following formula for this internal set-up S is suggested

For small amplitudes *(H << D)* $S/H = \xi F/2$ *(16.29a)*

For large amplitudes *(H ~ D)* $S/H = (1+\xi F)^{0.5} - 1$ *(16.29b)*

Note, that S represents the average water table inside the breakwater, upon which the cyclic part has to be superimposed. Here, D is the still water depth, H the wave amplitude, S the set-up, $\xi = c_a H^2/(2\pi\lambda_\omega D\tan\alpha)$, c_a the air-intrusion factor[59], α the slope angle, λ_ω the cyclic penetration length ($\lambda_\omega = \sqrt{(kDT/n\pi)}$), k the permeability, T the wave amplitude and n the porosity. The factor F depends on the width of the structure L and the inner boundary condition (open or closed), see Fig 16.13.

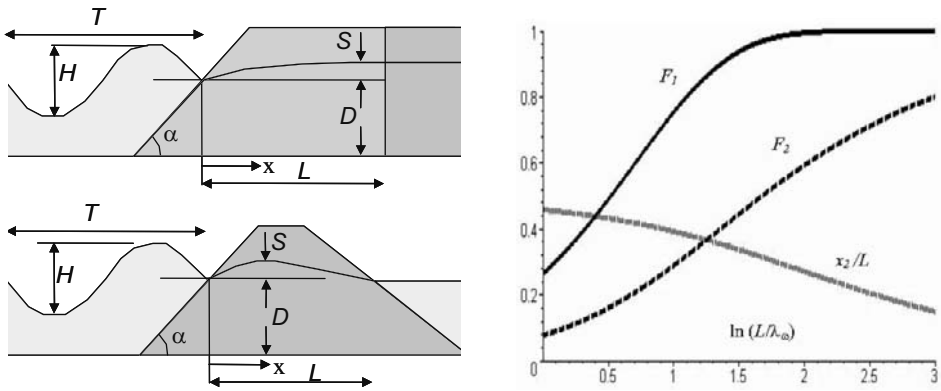

Figure 16.13 Internal set-up for closed end (F_1), open end (F_2) and S_{max} at L or x_2

Dynamic slope stability

Cyclic wave induced effects on the slope stability cause a variation in the stability factor, related to the variation of the free water level. Two typical situations, i.e. at the moment of a wave top at the slope and of a wave trough at the slope, are shown in Fig 16.14. In both situations the inner water table (B) follows the outer one (A) with a retardation. The actual porous flow fields and the corresponding critical cyclic slip surfaces reveal that the dynamic stability factor F_d is lowest, just before the wave trough, because then pore water is flowing out of the slope.

A sensitivity analysis, varying the characteristic parameters, such as wave height, slope angle, internal friction angle and average water depth over a wide range, results in $F_{d\,min}/F_s \approx 0.8 \pm 0.1$ (F_s is the static stability factor), allowing a general statement, that significant dynamic wave effects decrease the static slope stability with 20% to 30%.

---

[59] Air intrusion is entrapped air during inflow, for waves on coarse structures c_a may reach up to 4; for tides $c_a = 1$.

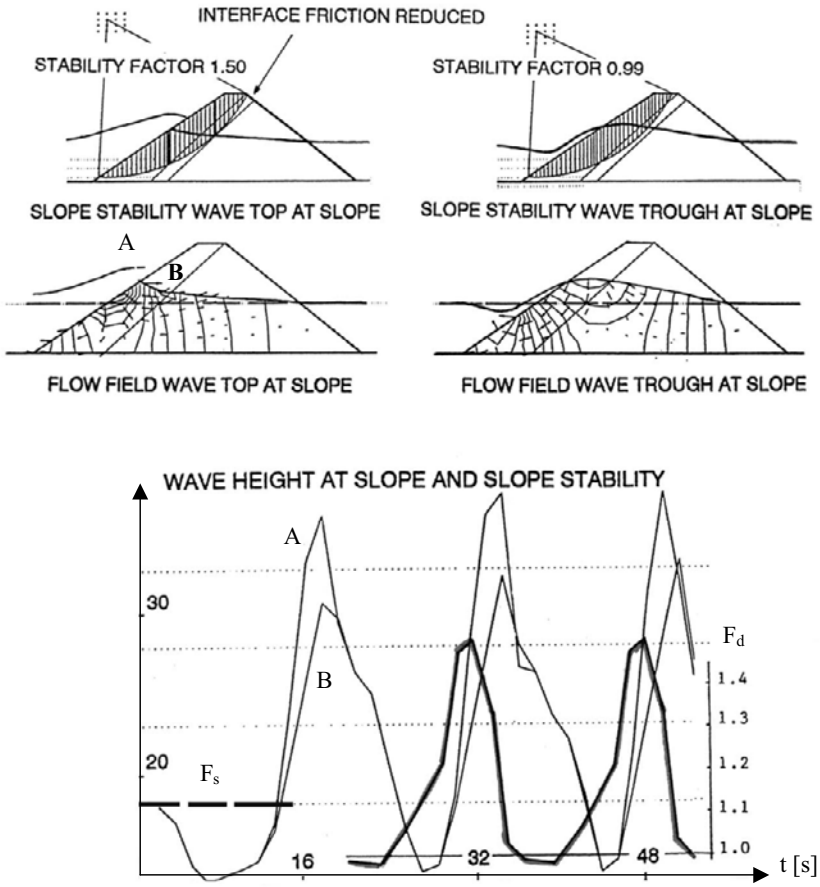

Figure 16.14 Wave induced effects on dynamic slope stability

Earthquake impact

Earthquakes and water waves cause a dynamic response of earth slopes. Earthquakes manifest at the surface as a volumetric force related to the soil mass. For impermeable soils the saturated soil mass will be triggered, and the effect can be incorporated as a dynamic addition to the static soil gravity. For permeable soils the pore water may partly be triggered (via drag forces at micro-scale)

The dynamic energy will mostly be transferred to the solid part. Hence the effect should be incorporated as a dynamic addition to the gravity of the solid part. Fig 16.15 shows the dynamic response of a large breakwater subjected to a heavy earthquake, simulated by a numerical simulation model. The response reveals residual displacements and plastic deformation at the lee side due to pore pressure build-up. The local weakening of the toe of the lee-side slope may cause the slope to shift down, allowing waves to erode the core and finally inducing collapse of the entire structure.

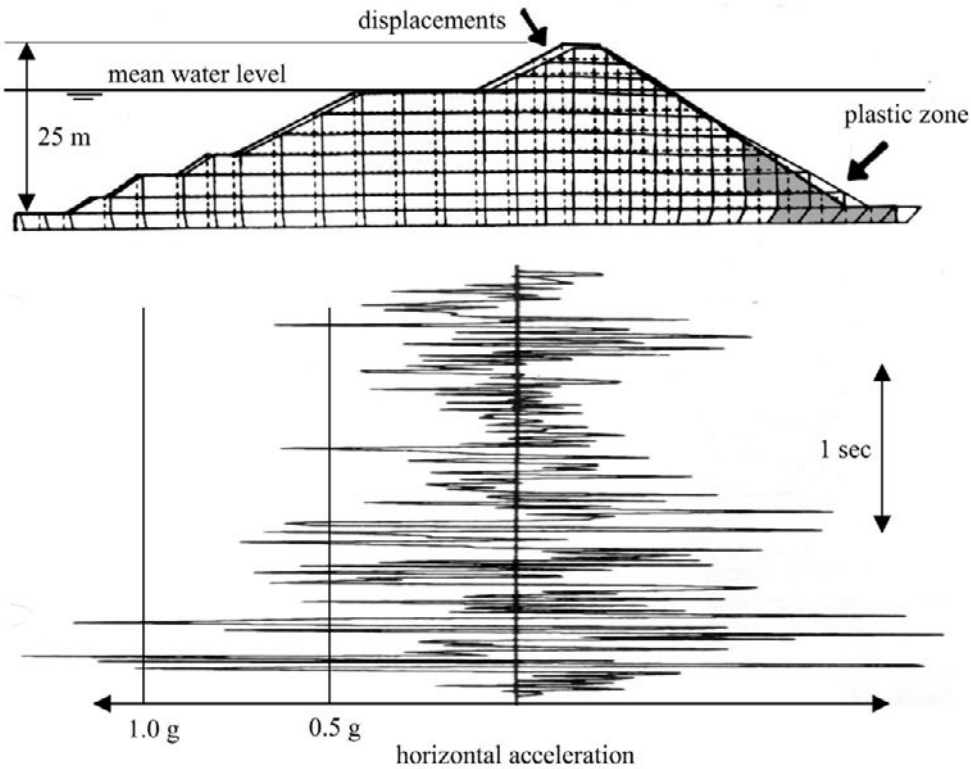

Figure 16.15 Earthquake induced effects to a large breakwater (Teunissen)

Wave impact on a slope

Shock effects by a heavy water wave slamming into a slope cause acoustic wave effects in the pore water and the porous matrix of the soil. The dynamic porous flow field remains rather local due to viscous forces (Fig 16.16b), and the dynamic energy is mainly dissipating through the saturated soil in the form of fluid-solid coupled deformations by surface waves (Raleigh waves), shown in Fig 16.16a, calculated by a numerical code that incorporates the dynamic Biot theory (Hölscher). The moments of extension (tension) occur along the surface just under the impact and they are critical to local revetment stability, see picture at the right (Bezuijen).

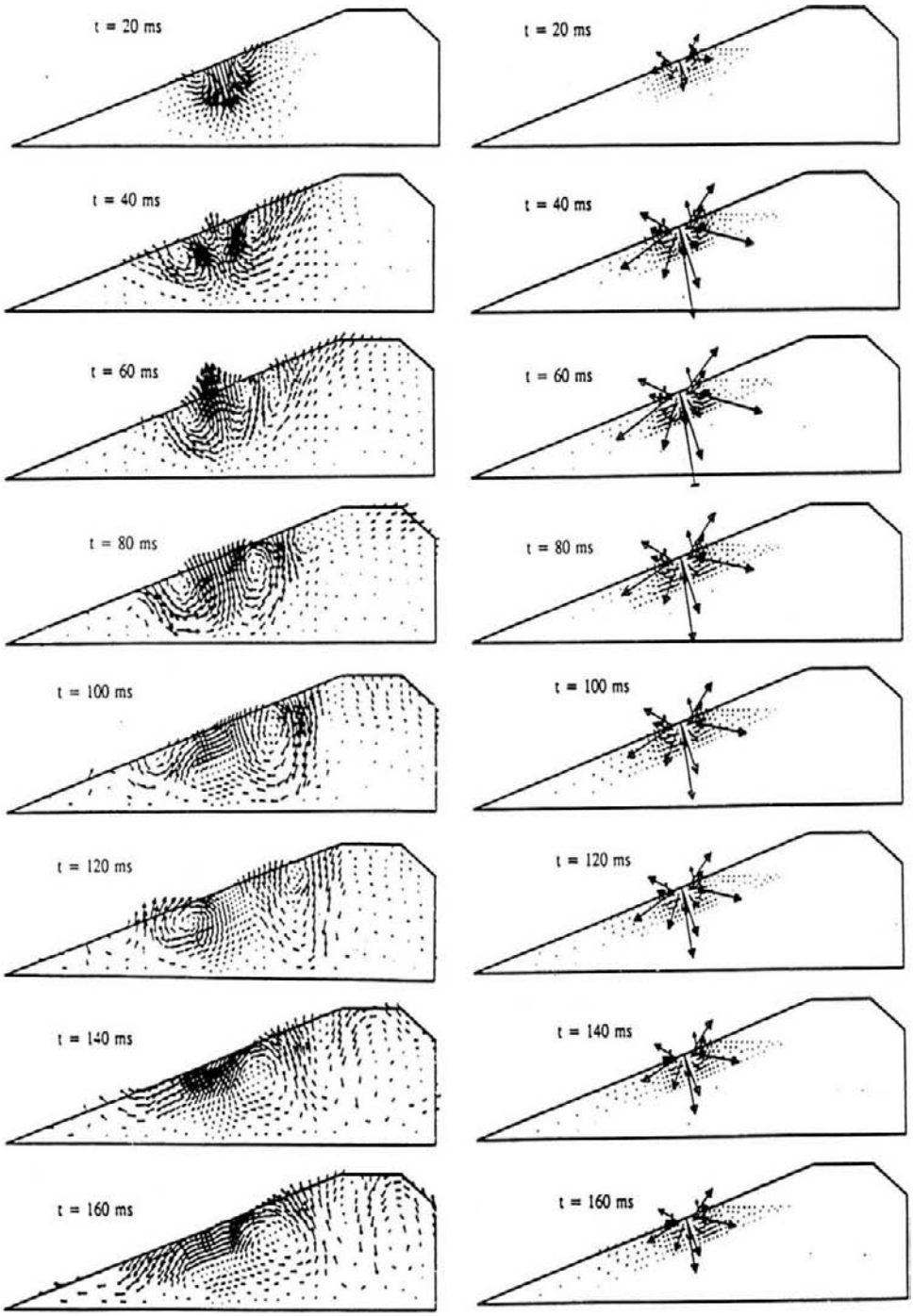

(a) coupled motion *(b) relative motion*

Figure 16.16 Wave-slamming on a slope showing the pore fluid and porous matrix response (Hölscher)

D A LIQUEFACTION MODEL

The sudden change of constitution of a sand or clay layer into a heavy mud usually occurs due to a dynamic trigger, an earthquake or a heavy vibration by wave impact or human action (pile driving). Two specific situations are considered: a slope and a horizontal layer.

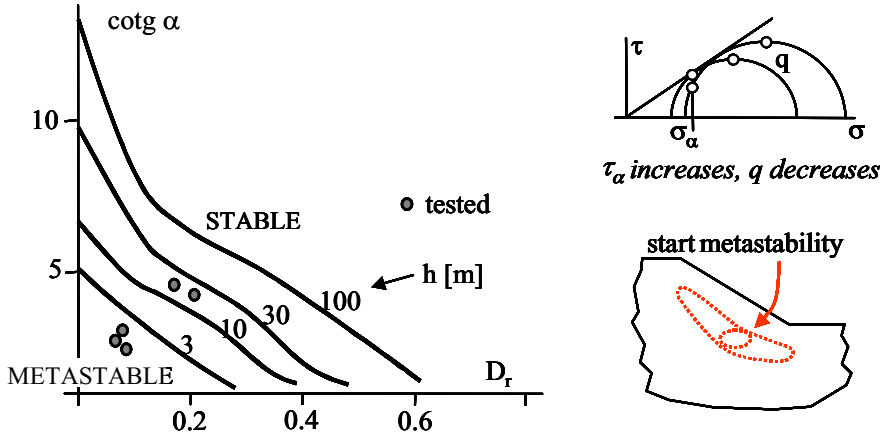

Figure 16.17 Metastable submerged slopes tested and simulated by 3D numerical model

Static liquefaction

The situation of a slope is characterised by the shear resistance. The slope may seem stable, but if the layer is loosely packed (contractant) then sudden failure (bifurcation) may occur, since the residual shear strength is less then the actual shear stress state. A trigger can cause the layer to liquefy (static liquefaction). If the slope is in such a critical situation, it is called metastable. It is difficult in practice to determine whether a slope is metastable. Sandy underwater slopes are at certain depth metastable, and a trigger may cause an semi-undrained response of sudden large excess pore pressures.

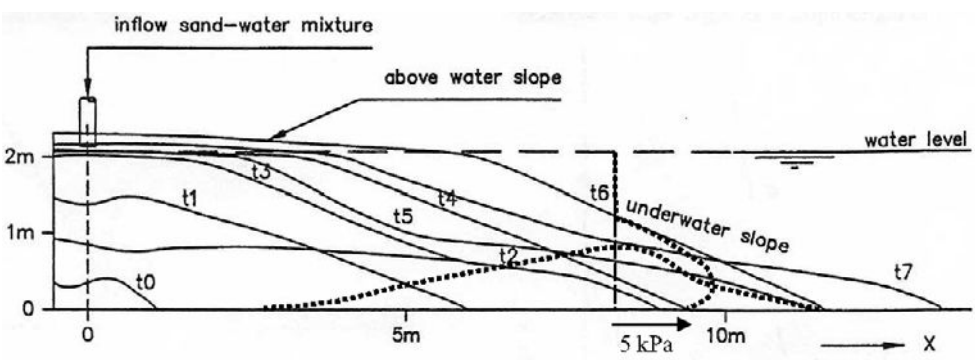

Figure 16.18 Large scale model test hydraulic fill
Advancing slopes during hydraulic fill (D_{50}=135mu, U=1.5). Slides are noticed at t1 > t2, t4 > t5, and t6 > t7; Excess pore pressures just before slide t6 (dotted line).

Tests and theory (Fig 16.17) reveal that the susceptibility of a loose sand slope to initiate a flow slide decreases with density, and increasing with slope steepness and height (Stoutjesdijk, de Groot and Lindenberg). Hydraulic fill progresses usually with local slides and induced high pore pressures (Fig 16.18). For a natural slope severe rains may cause instability (see application 7.1), and in unfortunate circumstances a dangerous mud flow may be triggered.

The liquefaction of a (steep) slope of dense sand follows a different process. The density has to decrease (dilation) to the critical density before sliding of a thin zone at the surface occurs. In fact the slope is moving into the sand. The corresponding negative excess pore pressure keeps the sand inside temporarily stable. This process can be described by a moving storage equation (van Os, Verruijt). The velocity of the slope motion v is expressed by

$$v = k\frac{1-n}{|\Delta n|}(G_s - 1)\cos\alpha\left(\frac{\tan\alpha}{\tan\varphi} - 1\right) \qquad (16.30)$$

where k is the permeability, $|\Delta n|$ is the porosity change from actual density to critical density, G_s is the specific solid gravity, and α is the slope angle. Note that for $\alpha < \varphi$ no flowing sand zone at the surface of a dense sand slope occurs (natural slope at $\alpha = \varphi = \varphi_{cv}$). The velocity of the slope motion (16.30) characterises the speed of breach growth and is essential in the estimation of dregding production.

Cyclic liquefaction

In the situation of a horizontal layer of loosely packed sand a cyclic dynamic trigger (waves, earthquake) may cause excess pore pressure build up and eventually liquefaction (cyclic liquefaction). If a coastal structure is positioned on such a layer the available shear strength (on the edges) will decrease and this may be the onset of collapse. For this situation a simple liquefaction model is presented.

Under cyclic loading, residual deformations may change the stiffness, the strength and the permeability of sand. The corresponding change in density is also referred to as preloading or preshearing. If the cycles are fast enough the pore water in a drained soil can only partly dissipate and pore pressures will rise. This pore-pressure rise u can be characterised by four parameters: u_0, ψ_0, θ and δ. The first one u_0 is the initial set-up (see Fig 16.19), the second one ψ_0 represents the so-called liquefaction potential (capacity of pore pressure rise under undrained conditions), the third one θ is related to drainage capacity (related to dissipation of excess pore pressures) and the fourth one δ to preshearing or densification (the liquefaction is less likely when the soil gradually densifies).

Three situations can be described by these parameters (Fig 16.19a): undrained (A), drained (B), and presheared (C). For a one-dimensional (vertical) situation the average excess pore pressure $\underline{u}$ satisfies

$$\underline{u} = u_0 \exp(-\theta t) + \psi_0(\exp(-\delta t) - \exp(-\theta t))/(\theta - \delta) \qquad (16.31a)$$

Here, averaging has been applied over the loose-sand layer height. The moment t_m of maximum pore pressure becomes (Fig 16.19b)

$$t_m = (\ln(\omega\theta) - \ln(\delta))/(\theta - \delta) \quad \text{with} \quad \omega = 1 - u_0\,(\theta - \delta)/\psi_0 \qquad (16.31b)$$

Thereafter, the pore pressure attenuates to zero. The parameters u_0, ψ_0, and θ can be determined by special laboratory tests and δ by a special field test. In detail, $\theta = 3c_v/d^2$ with c_v the consolidation coefficient and d the layer thickness.

Here, $\delta = (1-n)\psi_0\alpha/\Delta n$ with n the porosity, $\Delta n = n_{field} - n_{crit}$ the densification[60], and α the compressibility. $\psi_0 = f_N\, r\, \psi'\sigma'_0/N_l$ with ψ' is obtained from tests (see Fig 16.19c) and $f_N = 1/T_c$ is the cyclic frequency. The factor r =0.65 relates the triaxial stress configuration to the one-dimensional situation. N_l is the number of cycles when liquefaction in the undrained triaxial test occurs. It depends on the loading intensity characterised by the stress ration $\hat{\tau}/\sigma'_0$ ($\hat{\tau}$ is the amplitude of shear loading). In Fig 16.19c, 4 such tests are shown. Here, sand samples from a location are prepared under various densities; initial porosity in test (1) is 0.40, in (2) 0.38, in (3) 0.42, and in (4) 0.39.

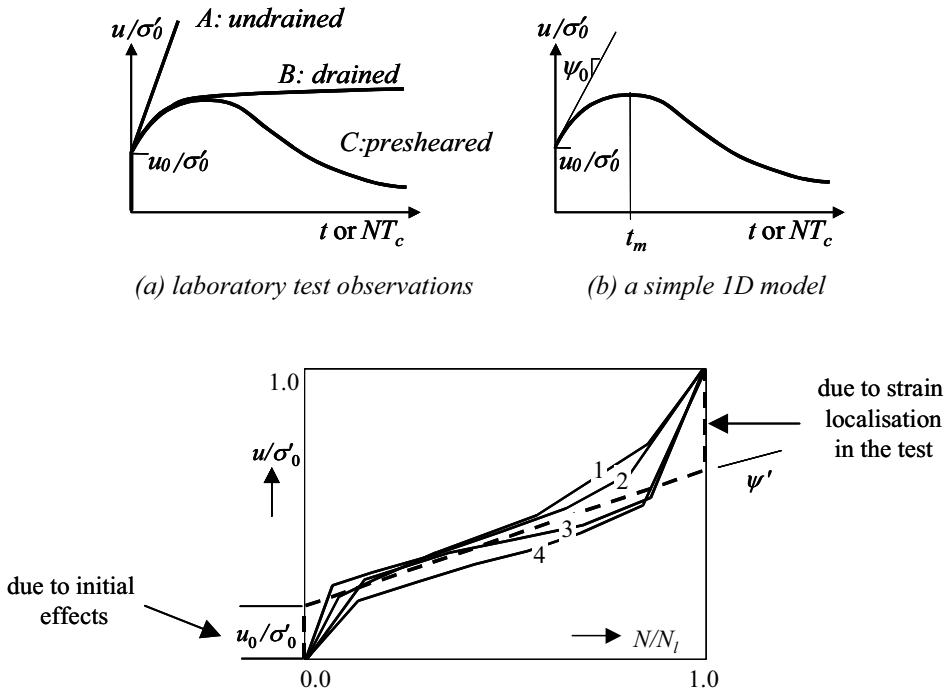

(a) laboratory test observations *(b) a simple 1D model*

(c) cyclic undrained triaxial tests at specific value of $\hat{\tau}/\sigma'_0$; N number of cycles, N_l number at liquefaction

Figure 16.19 Liquefaction phenomena

---

[60] n_{crit} the density at zero contraction/dilation, can be measured in the lab. In fact, $\delta = (1-n)\psi_0\alpha'/\Delta n$ with α' the ratio of volume strain rate and ψ_0.
The assumption $\alpha' = \alpha$ probably is a safe approximation.

The sensitivity to pore pressure generation under cyclic loading is measured and represented in a graph, normalised with respect to the applied initial effective stress σ'_0 and the cycle number N_l for which liquefaction is observed; N_l values found in test 1 to 4 are 200, 35, 200, 150, respectively. For wave generation over a loose seabed sand layer based on a relatively stiff substratum, a two-dimensional fully-coupled two-phase numerical analysis shows that the stress ratio $\hat{\tau}/\sigma'_0$ is then about constant (see also the discussion under equation (16.13)). It implies that N_l measured in the test can be applied in the field at any depth in the sand bed.[61]

In most sands the hydrodynamic period (consolidation time) is relatively short, except when the drainage path is long due to a specific geological situation, such as a sand layer partly sealed off by a clay layer. It is suggested in that to use case $\delta = 0$. The average excess pore-pressure generation then becomes for $\theta t << 1$

$$u = u_0 \exp[-\theta t] + \psi_0(1 - \exp[-\theta t])/\theta = u_0 + \psi_0 t \qquad (16.32)$$

This complies well with case A (undrained, see Fig 16.19a). When the initial pore pressure and cyclic pore pressure rise together and have reached a value equal to the total stress, the corresponding effective stress will be zero, and then the soil has lost its structure. It is in a state of liquefaction, like a mud. Any shear resistance will be completely lost. Also during the process of pore pressure rise, shear resistance is already decaying. This phenomenon is important for land reclamation, landslides, and coastal and offshore foundations.

Liquefaction of the seafloor

Because of morphological dynamics the top few metres of a sandy seafloor is usually loose, and in the sand cyclic pore pressure increase or liquefaction may occur due to wave or earthquake agitation. An example is worked out for the slope stability of a large breakwater during a storm. Waves cause small shear deformation which in loose sand (contractancy) gradually result in excess pore pressures. Local effective stresses will decrease, accordingly. In Fig 16.20 the situation is shown for the critical moment of a design wave on the slope. The effect of the momentary actual water pressures on and in the structure and the seabed, excluding or including the effect of gradual excess pore pressure increase (using 16.31), is reflected in the slope stability factor (slip circle approach) as shown in Table 16.1.

TABLE 16.1 EFFECT OF EXCESS PORE PRESSURES ON THE SLOPE STABILITY

excess u	*Not included*	*Yes included*
factor F_1	1.21	1.03
factor F_2	1.47	0.94

[61] If no information on N_l is available it may be determined from the shear stress ratio. Experiments imply that the relation between N_l and $\hat{\tau}/\sigma'_0$ can be expressed by an empirical relation, including a threshold shear amplitude $\hat{\tau}_0$: $N_l = b(\hat{\tau}/\sigma'_0 - \hat{\tau}_0/\sigma'_0)^a$ for $\hat{\tau} > \hat{\tau}_0$. The empirical constants a and b are dependent on the type of sand and its density. For the 4 tests in Fig 16.12c a constant value: $a = -0.13$ was found and b varied with density (porosity).

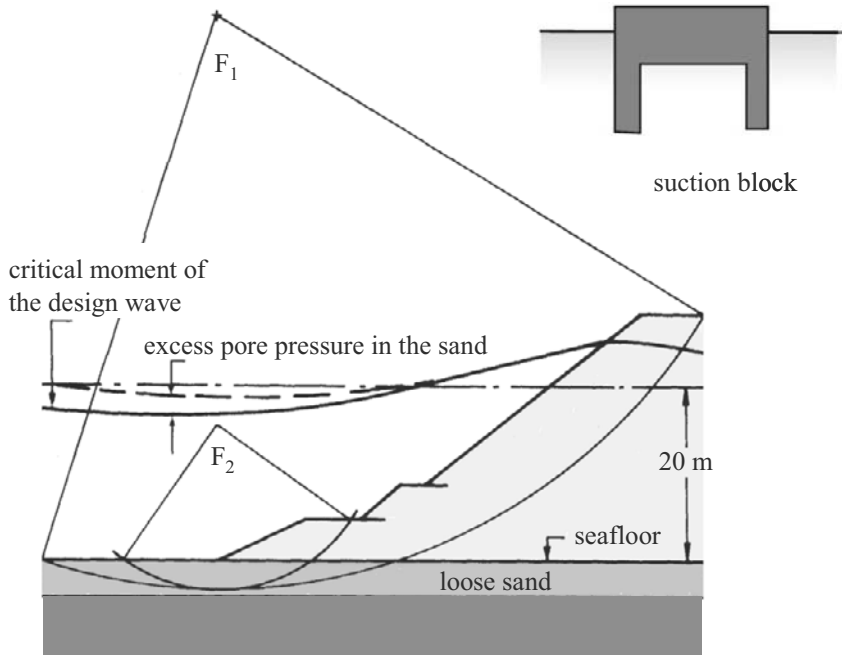

Figure 16.20 Local and total stability under storm wave attack

Obviously, the local toe may fail, causing the armour layer above to shift down and expose the core behind to wave attack and erosion. This failure mechanism can be prevented by extending the toe structure (adding rock) or by applying special structure elements, such as a geotextile with rock on top or a suction block mattress (Zen). If just rock is placed before the toe, it is assumed that during storms they get submerged in the sand and form a stable metaskeleton.

E SQUEEZING

If an embedded soil layer is liquefied it may be squeezed by the overburden load. The analysis of squeezing of soft layers is rather complicated, but a simple approximation method is sufficient in many cases. This method evaluates the horizontal equilibrium of a soil column (Fig 16.21). The active earth pressure produces a force E_a. The resisting force is E_p and an intermediate shear force E_s. The safety against sliding is expressed by the ratio $F = (E_p + E_s)/E_a$, which can be determined by evaluating the following formulas

$$E_a = \int_0^H K_a(\sigma_v + \Delta\sigma) - 2c\sqrt{K_a}\,dz\,,\ E_p = \int_0^H K_p\sigma_v + 2c\sqrt{K_p}\,dz\,,\ E_s = \int_0^L \tau\,dx \quad (16.33)$$

Here, K_a is the coefficient of active earth pressure (see Chapter 7), K_p the coefficient of passive earth pressure, σ_v the original vertical effective stress, $\Delta\sigma$ the load increment, c the cohesion and τ the shear stress.

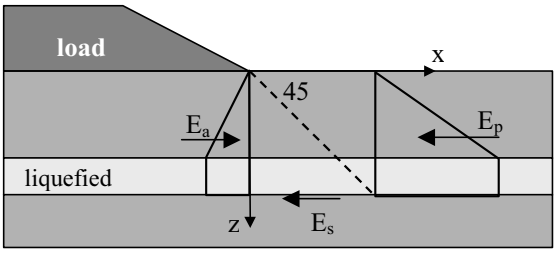

Figure 16.21 Stability against squeezing

application 16.1

Two large breakwaters protect a new harbour extension, with at the leeside a landfill (Fig 16.22a). At the connection between breakwater and fill, a drain (filter) is placed to dispose overtopping water through the breakwater core, during storms. It appeared that this drainage system did not work as expected, and the cause was found to be internal set-up due to geometric nonlinear effects.

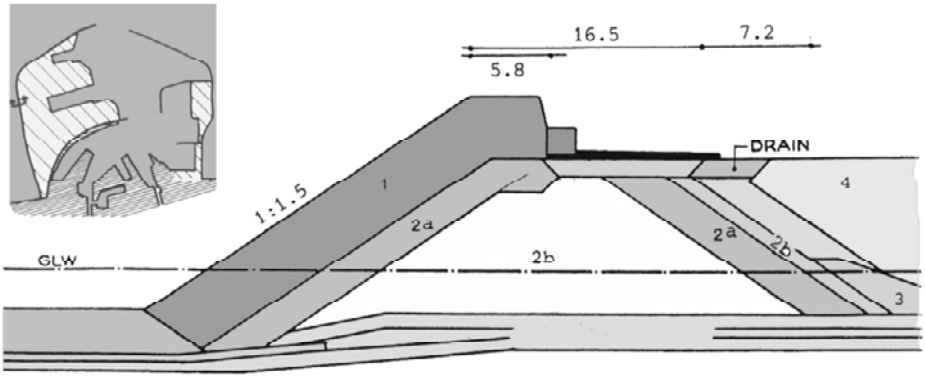

1	armour	25 ton	concrete cube
2	filter a	1 – 3 ton	rock
	filter b	0.1 – 0.3 ton	rock
3	filter	seagravel	wide grading
4	fill	sand	geo-textile face

Figure 16.22a Harbour breakwater, cross-section and leeside landfill

As to incorporate for the geometric non-linearity a sophisticated numerical model was developed accounting for free wave action and the induced turbulent groundwater flow, based on momentum, mass conservation and interface continuity. Various waves and wind set-up scenarios were simulated.

A typical result shown in Fig 16.21b presents isochrones at each $T/8$ moments during the once in 500 year significant wave $H_s = 6.5$ m, for two cases; (1) for the situation shown in Fig 16.21a and (2) with an open core (filter 2b replaced by material 2a). The focus is at the leeside, on the set-up S and the local water table

oscillations H_b. Note, that the average free water level is lower, because of wave deformation on the shallow zone before the breakwater slope (trochoidal form), and the average water level at the back side is high due to internal set-up.

From Fig 16.21b one observes that the maximum head gradient is in the range of 20%. This leads to $0.20 = bq^2$, or $q = (0.20/1.73)^{0.5} = 0.20k$, which gives for the apparent (linear) permeability $k = 1.7$ m/s. In a similar manner the apparent permeability of 0.1 to 0.3 rock (filter 2b) becomes $k = 1.2$ m/s. Because of air intrusion during high water a reduction is required, and for the 1 to 3 ton rock (filter 2a) an approximate permeability of $k = 0.9$ m/s is assumed.

In case 2 the effective still water depth is $D = 11$ m, and in case 1 the finer core is simulated by a reduced effective depth of $D = 5.5$ m. The dam width is $L = 35$ m, the slope 34°, the porosity is $n = 0.4$, the wave height is 6.5 m, the wave period $T = 20$ s, and the air intrusion coefficient is taken as $c_a = 4$ (large waves are considered). Results of formula (16.29) for case 1 and case 2 are given in the table in Fig 16.22a, and they are in reasonable agreement with the results of the numerical values, shown in Fig 16.22b. H_b is significantly lower than found by numerical simulation, particularly for case 2, probably due to reflection (closed-end) and the assumption of a uniform velocity field over depth in the formulae.

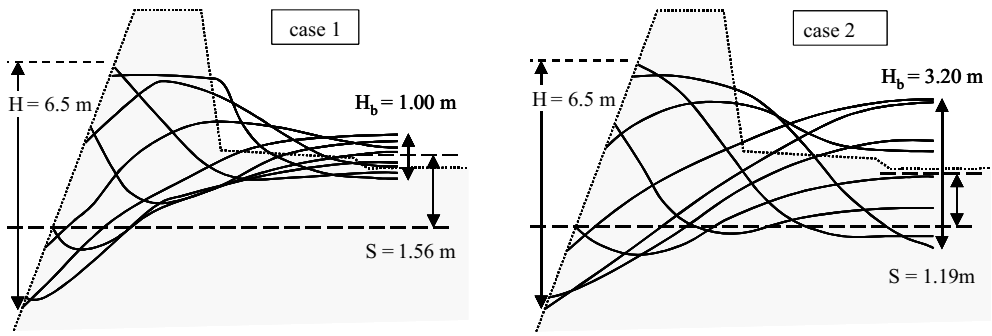

Figure 16.22b Isochrones of cyclic internal water table response by numerical simulation

		case (1)	case (2)
S by formula (16.29) H_b by formula (16.28)	D m	5.5	11.0
	λ_ω m	8.9	12.6
	F_1	0.90	0.77
	ξ	0.82	0.29
	S m	1.75	1.17
	H_b m	0.91	1.91
numerical	S m	1.56	1.19
	H_b m	1.00	3.20

application 16.2

A dam is constructed on a permeable stratum of about 20m underlain by an impermeable rock (Fig 16.23). A sheet piling of 10 metre height is installed at the upstream face. The permeability is 50 m/day. Some streamlines are given. Sketch the equipotential lines and determine the total discharge Q in m^3/hr under the

structure. Determine the pressure directly behind the sheet piling under the dam in kPa. Determine the horizontal force in KN on the sheet piling per m width.

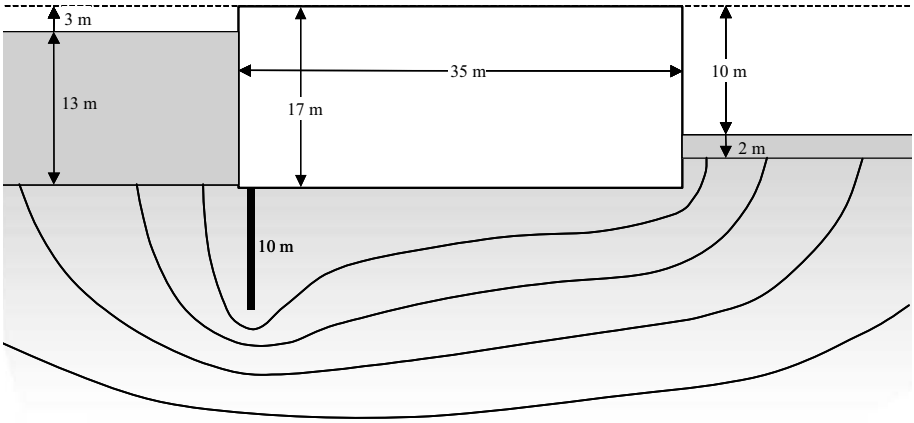

Figure 16.23

application 16.3

A cofferdam is constructed on a permeable cutting underlain by rigid rock (Fig 16.24). A row of sheet piles is installed at the up and down stream face, connected by an anchor. The permeability of the sand is 140 m/day. The unit weight of the water is 10 kN/m^3. Determine the total discharge Q in m^3/hr through the structure. Determine the pressure at position B outside and inside the cofferdam, in kPa. Determine the part of the anchor force produced by the water pressure.

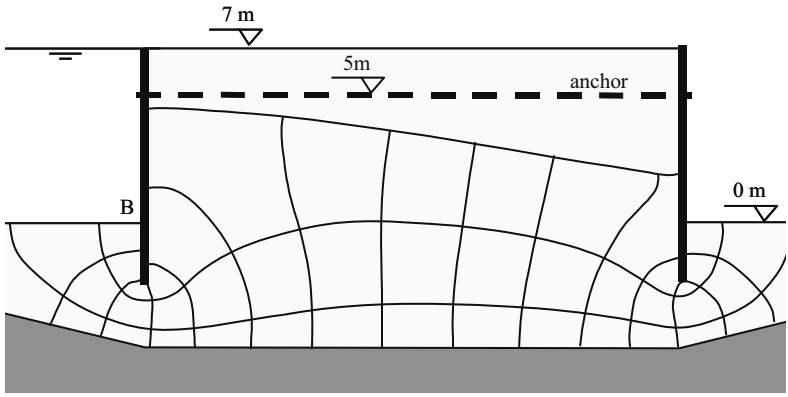

Figure 16.24

application 16.4

An example of the application of the classic filter rules is shown (Fig 16.25). For several types of granular materials (SA: sand, GR: sea gravel, QW: quarry waste 0 – 2 kg stone, QR: quarry run 2 – 300 kg stone, FI: filter 1 – 3 ton, AM: concrete

armour cube 25 ton) the grain size distribution curve is presented (with some scatter). Compose the best possible filter structure, from AM to SA.

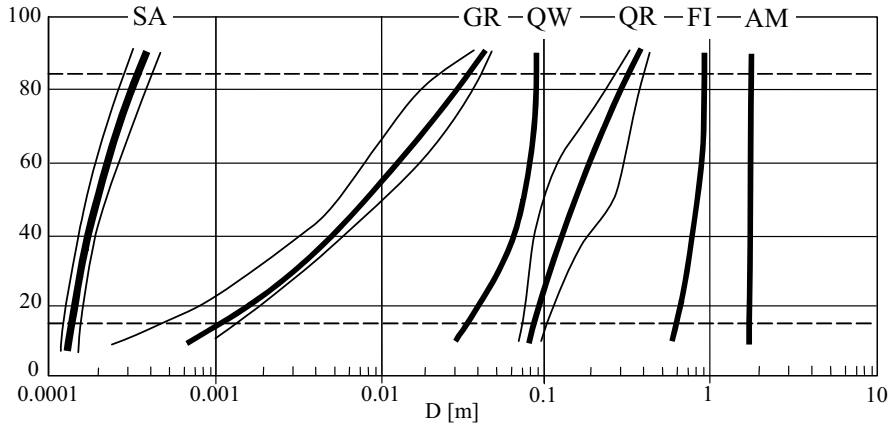

Figure 16.25

application 16.5

Determine the maximum cyclic excess pore pressure for a sand layer subjected to a storm surge with a wave train of 200 large waves. The following data is provided: layer thickness d = 4 m, submerged unit weight γ' = 10 kN/m^3, wave period T_c = 8 s, porosity at the site n = 0.4, permeability $k = 2\text{x}10^{-4}$ m/s, compressibility $\alpha = 10^{-5}$ m^2/N. In an undrained test in the lab: liquefaction number N_l = 50, ψ'= 0.3, initial set-up u_0 = 0.0, critical density n_c = 0.38.

application 16.6

Determine the internal set-up in a breakwater for a wave with amplitude of 6 m and a period of 12 s. At the rear side of the breakwater a solid ground body exists (closed end); at the average water height the breakwater is 10 m wide. Other numerical data are: average water depth is 10 m, porosity 0.4, permeability 0.1 m/s, and the slope angle 40º. There is no air intrusion (c_a = 1).

17 DIKE ENGINEERING

A DELTAS IN THE WORLD

A scan through the world reveals that there are about 75 large delta areas (Africa 13, Asia 26, Australia 9, Europe 8, America 19), which all differ due to the associated environmental processes. About 500 million people in the world live and work in these river deltas, and this number is rapidly increasing (Fig 17.1a). Deltas are centres of nature (wildlife), agriculture and economy. The safeguarding and sustainable development of these areas should receive the highest priority. Geotechnical aspects related to the management of a delta region concerns land subsidence (sinking) and flood protection under changing climate conditions.

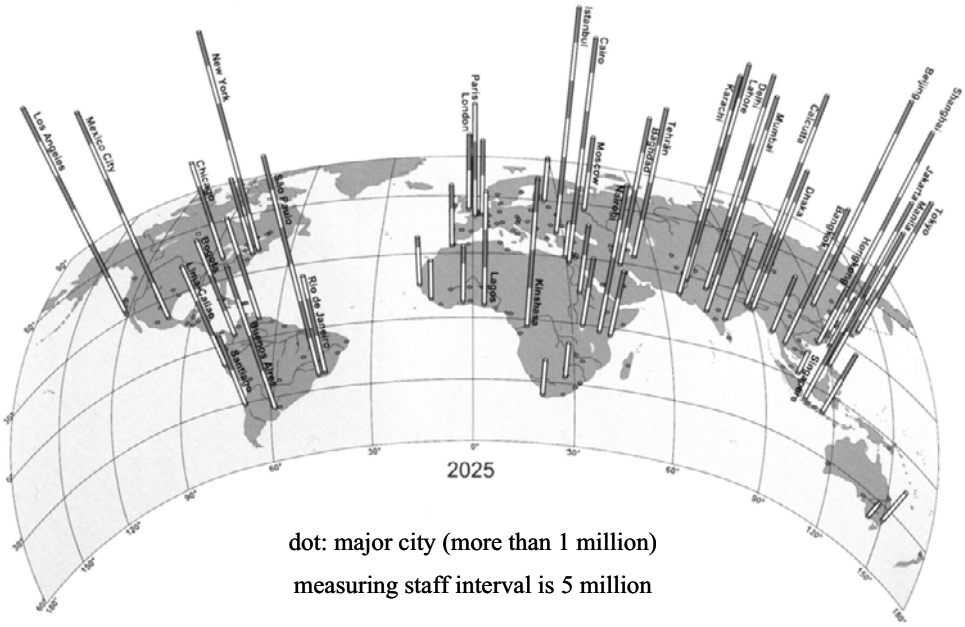

Figure 17.1a Large deltas and mega-cities in the world (Waterman)

While the 2007 Intergovernmental Panel on Climate Change (IPCC) report concluded many river deltas are at risk from sea level rise, recent studies indicates other factors are causing deltas to sink significantly. The sinking of deltas is accelerated by the upstream trapping of sediments by reservoirs and dams, man-made channels and levees that sweep sediment beyond coastal floodplains, and the compaction caused by the extraction of groundwater and natural gas and oil. One third of the world's major deltas is sinking and 85 percent regularly experience severe flooding. Intensive storms, rains and flooding result in temporary submergence of vast areas with huge damage. Fig 17.1b shows an example of the global floods in the year 2003, notably not a particular year.

Under current prediction of 0.45 m in sea level rise by the end of the 21st century as forecast by the IPCC-report, global delta flooding could increase by 50 percent. Hurricane Katrina may be an illustrative example, but flooding in the Asian deltas of Irrawaddy in Myanmar and the Ganges-Brahmaputra in India and Bangladesh, and the earthquake invoked tsunamis that recently struck Thailand, Indonesia and Japan have claimed thousands of lives. Similar disasters could occur in the Pearl River delta in China and the Mekong River delta in Vietnam, where thousands of square miles are below sea level and the regions are hit by periodic typhoons.

From a geotechnical point of view, a contribution can come from smart dike and coastal engineering, both in a proper context and with proper knowledge management. How this is organised in the Rhine delta is explained.

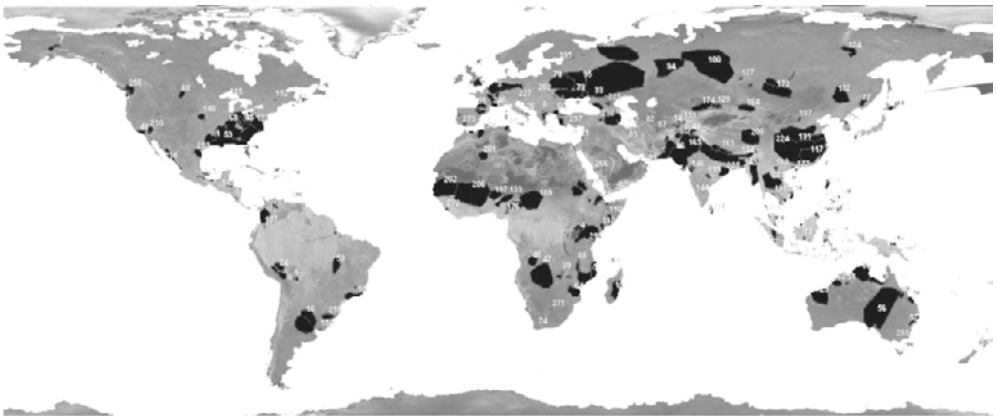

Figure 17.1b Global flooding in 2003 (black areas with large damage and casualties); annual recording by Dartmouth Flood Observatory

The Rhine delta

The Rhine delta hosts the Netherlands, which for a large part was created during the last millennium by land cultivation, by flood protection against sea and rivers and permanent water drainage from lowland and polder areas. Some large cities developed, including an intricate infrastructure of roads, railways, waterways and pipelines for sewerage, gas, and water and for underground transport. The main ports for shipping in Rotterdam and air transport in Amsterdam are a cradle for international industry and commerce. The protection of commercial and social values in the lowland demands a continuous engineering effort. Tens of thousands of kilometres of sea dikes, river dikes and canal embankments, numerous sluices, bridges, harbours, tunnels, dams and closures and sophisticated monitoring and control systems form the backbone of the lowland flood protection. The engineering skill could develop during centuries within a special legislative, social and political frame. The expertise, the backbone of delta technology, has now settled in a wide range of laws, guidelines, handbooks and codes.

At present new developments are required meeting the demands of the society of today. Demands related to multiple functioning and integral values. Moreover, the expectation of climate changes in terms of sea level rise, increasing rain intensity

and high-peaked river discharges rings the warning bell for risk engineering in design and integral maintenance of water-defence structures.

B HISTORY OF DUTCH DIKE ENGINEERING

Before building dikes

A large part of the Netherlands is situated under sea level. Without dunes and dikes half the country would be submerged. In general, one speaks of lowlands and the name "Netherlands" is appropriate. Since the last glacial period, which ended about 10,000 year ago, the sea level is rising and the coastline receding. This process took place intermittently. Repeatedly, the sea was aggressive (transgression period), and other times relatively quiet (regression period). During the transgression periods the sea intruded deeply into the inland. During the regression periods large peat areas developed in the eroded parts (Holland, Utrecht).

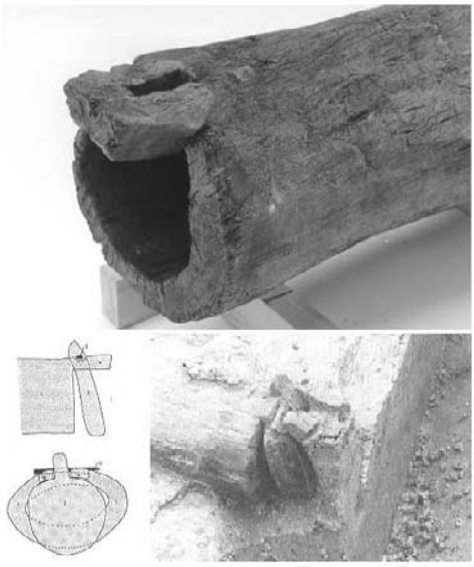

Figure17.2a Ancient valve-sluice, Roman period (Schiedam, Netherlands)

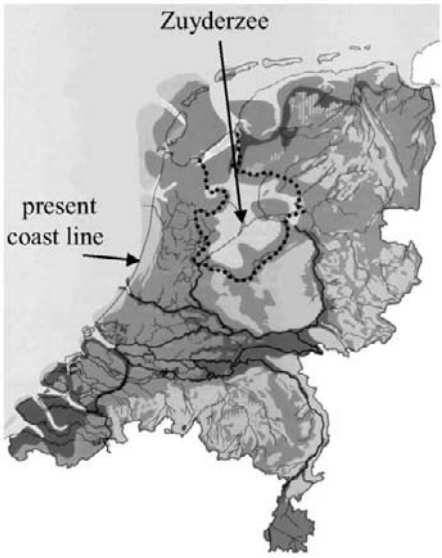

Figure 17.2b The Netherlands ~ 800 AD light: sand, medium: peat; dark: clay

Natural sea walls along the coast could withstand the high storm surges, although the sea swallowed large areas. In the Roman era the possibilities for land cultivation improved and small villages arose at the borders of the peat marshes and inland creeks. One of the known gullies in that time was the Gantel running from the river Maes to the north, passing Delft. Shipping became feasible when in 12 AD Drusus ordered channels to be built from the Rhine northwards, and in 47 AD the Roman warlord Corbulo ordered the digging of a southern channel connection to the river Rhine. Remnants of small dams and valve-sluices made from hollow trees were found in the area (Fig 17.2). The higher dunes ascended only ten centuries ago. In the late Middle Ages, the sea became more dangerous

and aggressive. In the twelfth century, an enormous gap was made in the Netherlands. The small lake Almere in the centre was enlarged into a substantial inland sea (Fig 17.2b), the Zuyderzee. In that disaster many villages drowned.

Early dike building

The oldest dike made from sods of turf was found in Friesland in 1996 and it is several hundreds metres long and dates from 200 AD. The reclamation and exploitation of large peat-lands in the west and middle of the country created many large lakes, which are clearly shown on maps of the 16th and 17th century. In the 17th century large-scale land reclamation started to dry these lakes. Dikes surrounded low-lying areas and surplus water was drained out during low tides, or eventually by windmill power. These areas are called polders.

In those times the discharges of the main rivers had increased significantly. Annual inundations and floods had serious consequences. Since the 11th century large efforts were undertaken to create defences against the rising water. In many parts of the country dikes were build. The probability of inundation decreased and man started to settle in previously uninhabitable places. Formerly, this was only possible on hand-made mounds and sandbanks.

Yet the danger of inundation was not over. Particularly, poor or unsystematic maintenance of the dikes frequently caused flooding. Pools along these dikes recall the many dike bursts. Frequently, enormous amounts of ice accumulated against the dikes often causing collapse.

Not always was the water regarded as dangerous. In war times, one breached the dikes deliberately to prohibit passage for the enemy. The Spanish and French, in particular, have experienced this strategic inundation during their invasions. The region Holland remained safeguarded against occupation. Until after the World War II this Holland Water Line was maintained. In 1939, Germany managed by spying during inundation exercises to attack at weak spots along this water-defence line (Grebbeberg). At present, parts of it are a tourist attraction.

Land subsidence and sea-level rise

It is by no means certain that the Netherlands will always be inhabitable, as it is now, for a large working population. Some believe a time will come when the sea will again inundate most of the Netherlands, as it already has on more than one occasion in the distant past. The level of the sea is rising, slowly but surely. If climatic change causes the polar ice caps to melt faster than at present, the rate at which the sea is now rising could increase and rapidly create a critical situation. It would only take one-tenth of today's polar ice to produce enough water to heighten the level of the sea by three metres.

At present, measurements indicate a rise of about 0.50 m per century, but it is not only a case of rise in sea level. Ground levels are getting lower at the same time. Besides a small tectonic subsidence, the weight of the upper layers of soil is compressing the softer peat ground underneath, and the intensified use of groundwater means the ground is getting dryer, and dry soil compresses faster than wet soil. Dry peat oxidises and vanishes. So the difference between sea level and ground level is increasing. In total, the lowlands in the Netherlands may face an

average of 0.25 metre additional subsidence in this century, up to 1.0 metre in some locations.

The Dutch approach

The method of flood defence that the inhabitants of the Netherlands have developed and applied - with varying degrees of success - throughout the centuries is dike building. Ever since the eleventh century, when the earliest primitive dikes and embankments were built, the task of keeping the hungry sea and rivers at arm's length has been a matter of dogged perseverance and trial and error. Since then the main outlines of the Dutch coast have changed very little. The Dutch success resulted in 1113 in a contract of the King-Bishop Frederik I of Bremen with a group of Dutchmen under leadership of Priest Heinricus to reclaim Northwest German lowlands in a Dutch style. Dutch engineers invited by the Japanese Emperor (Ming dynasty) assisted in the regulation of water management problems and land reclamation (Johannes de Rijke). As military history has demonstrated, the shorter the lines, the stronger the defences. The first real major improvement in the Dutch coastal defences came in 1932, when the Afsluitdijk (Zuyderzee Barrier Dam) was built, linking the coasts of the provinces of North Holland and Friesland. This dike shortened the 1900-km coastline to 1300 km. It was a flood disaster in 1916 that gave the final impetus to the decision to link up the two coasts. After 1945 new plans were made to improve the country's defences against the sea and major rivers. But governments learn slowly, and it took another disaster to give the impetus to carry the Delta plan into the execution stage.

Figure 17.3 Maeslandt Barrier; the gates are as long as the Eiffel tower is high

The Delta-sea project

In February 1953 the dikes of the delta area in the southwest Netherlands were breached during a severe storm. 1835 people lost their lives and the material damage was enormous. The following Delta Act in 1956 provided for reinforcing the dikes and completely damming off the largest estuaries. Only the Western

Scheldt was excepted, as it connects the sea with the harbour of Antwerp. In 1976 under the influence of the environmental lobby, which was then at the height of its strength, it has been decided to keep the Eastern Scheldt partially open in order to conserve the tidal environment of this estuary. This was realised by building a very costly open dam. In 1983, the government wanted to cut public expenditure by back-pedalling on the river-dikes reinforcement program. There were sincere protests all round, but the most vociferous opposition came from the water boards, the public authorities responsible for managing the sea and river defences. To relieve the cost of continuous inland dike maintenance the government decided to construct a moveable closure, the Maeslandt Barrier (Fig 17.3), in the main entrance canal to the harbour of Rotterdam, the only vulnerable open sea connection left. This closure has been completed in 1996. The government has kept its promise made in 1953 that the sea defences will be of the required height and strength. The project took 40 years! Billions of guilders have been spent on the job and a gigantic amount of work has been done.

The Delta-river project

The struggle against the water continues. Several hundreds of kilometre of river embankments, lake and canal dikes are waiting in turn for proper improvement. New insight uncovered the fact that design water levels have risen significantly. In the last decades, public opinion changed. Landscape, natural and cultural values should be preserved in balance with safety requirements. The public protested fiercely against sacrificing old villages to dike enforcement measures. Several governmental Committees advised the parliament about acceptable lower norms and suggested development of sophisticated smart redesign methods and construction. Dike enforcement became subject to law, the Environmental Impact Assessment Act, which delayed the river dike improvement program drastically. water boards did not posses enough money, wanted to save maintenance costs and preferred a less expensive conventional technology. Latent danger laid in waiting! When in 1995 and 1996 high-river water levels threatened again to destroy the weak dikes and a massive evacuation of some hundreds of thousands of man and cattle had to be undertaken, the government reacted quickly with special legislation. The Delta Act Large Rivers was launched, and 370-km primary river dikes were reinforced in an accelerated tempo with a more integral design approach. With costs varying from 5 million euro per kilometre (conventional groundwork) to 15 million euro per kilometre (‘smart‘ methods) this project required an investment of more than ten billion guilders; it was completed in 2000.

Besides, the attention also focuses on problems related to polluted river beds, storage of contaminated sludge, restoring the natural habitat of rivers, estuary dikes, unstable sea-dike slope protection, introduction of the new integral approach and the development of a broad public and politic platform for a modern and consistent safety norm, i.e. not just the likelihood of flood but also incorporating the subsequent damage by inundation. A continuous great effort is dedicated to the improvement of the Dutch water-defence system by exploring new methods and ways, by developing new insight and experience and by inspiring a true and balanced political and social awareness about the matter of safety (see Fig 17.7). There is consensus that a water-defence structure represents a multi-functional

element, and that the safety demand – one of the primary functions - should be considered in relation with other aspects.

C THE PHILOSOPHY BEHIND THE DUTCH WATER DEFENCE

Organisation of water management

The unique form of self-government - the Water Board - that may be regarded as having fostered the independent spirit of the western part of the Netherlands, began to emerge in the first half of the twelfth century. The water boards are authorised to 'manage' water levels in the western lowlands by building and maintaining embankments, dikes and sluices. The water boards have continued to function in much the same form to this day, when water has become a crucial factor in many aspects of life such as industry and recreation and their attendant problems, like water quality control. The water boards exercise authority over 3500 kilometres of primary dikes (sea dikes, river dikes (Fig 17.4b), compartment dikes), some 2000 water defence structures or facilities (Fig 17.3), and about 17,000 km secondary bosom dikes and embankments (Fig 17.4a).

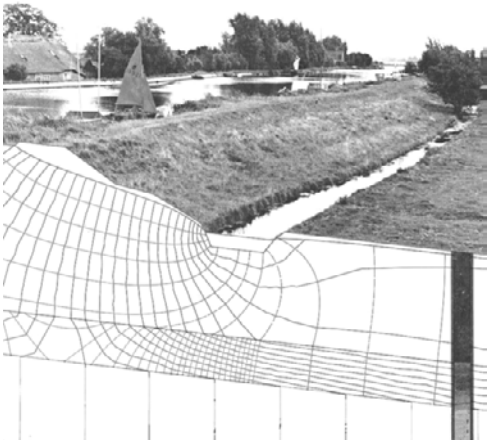

Figure 17.4a Bosom dike; the soil stratification top-down includes peat, clay and sand; the groundwater flow is steady; the height of the dike is 4 m

Figure 17.4b River dike; high water level; houses built in the river basin are inundated; water percolates through and under the dike; the height of the dike is 6 m

A water board's regulations mostly include detailed provisions for the recruiting and the functioning of the dike 'army'. When danger threatens, the 'troops' must be on alert, patrolling the dike and standing by with sandbags and equipment to stop occurring breaks. Members of the 'army' must be instilled with the need to defend their families, community and country and have an intimate knowledge of the lie of the land. Originally, by law, all male residents aged between 18 and 60 have if urgent to report for duty. At present, this urgency force has been professionalised. An administrative and a technical department carry on the Board's everyday work.

The administrative department prepares policy and gives legal and financial direction to all the work of water management to be carried out by the technical department. The technical department cares for the design, execution and management of dikes, pumping stations, purification plant, roads and buildings.

Dike types

There are, roughly speaking, four types of dikes in the Netherlands: river, coastal, estuarine dikes and the embankments around bosom waters, i.e. the canals and lakes used as storage basins to regulate polder water levels. These four types differ in design and construction. When, in the past, the authorities had to decide how high to build a dike, they took the highest known level as their standard. The many erosion holes, scoured out by water swirling through breaches, now to be seen as pools along the lines of the dikes, bear silent witness to our forefathers' failure to get their calculations right. After the devastating 1953 flood, the authorities decided that the height to which the dikes ought to be raised, should conform, as far as possible, to scientifically calculated criteria.

Their basic principle was not that flood water levels should never be able to exceed the height of the dike, since this would be impossible to finance, but rather that the likelihood of floodwater overflowing the dike would be quite small. This principle was laid down in the Delta Plan, drawn up in 1953. In some areas, for example, an inundation risk of once in four thousand years is acceptable. The heights derived from these base levels are known as draft levels. Besides the draft level, the effect of surf rolling up the seaward slope must be taken into account when calculating the height of the dike crest. This seaward slope will, if properly designed, break the surf so it does not surge as high. Dikes in very exposed places are designed with a 'sill' built into the slope at storm tide level.

The body of the dike must be protected against the force of the waves and the effect of tidal currents. Dikes are mostly faced with turf as a basic covering. Depending on the angle of the slope and the force of the waves' attack, basalt, concrete blocks and/or asphalt are used as revetment. Fortunately, high tide levels never last long. A normal tide cycle lasts twelve hours; consequently the water hardly ever gets a chance to percolate deep into the dike so the angle of the inland slope can be allowed to be fairly steep, provided the subsoil allows it.

Water levels on the non-estuarine upper reaches of the rivers are determined by weather conditions upstream, such as rainfall and thaw. These days, the necessity of dike improvement is based on exceeding a certain river discharge occurring about once in two thousand years, a figure derived from statistics. High water on the upper river reaches lasts considerably longer than in a storm tide area, and waves do not generally play as great a role. These two factors are reflected in the design of the most desirable river dike cross-section. The riverside slope may, consequently, be angled more steeply and the revetment need not be of heavy quality as on the coast. The angle of the slope may not, however, be too steep for growth of proper grass cover or for a stone revetment to be satisfactorily placed. The longer periods of high water give the groundwater table within the body of the dike more opportunity to rise. In order to prevent seepage, the inland side of the dike is often given a gentler slope.

A peculiar phenomenon is uplift, occurring when groundwater pressures are high enough to lift the covering ground layer at the lee side slope toe. In some cases, local erosion arises in the form of sand boils, which undermine the foundation (piping). Another criterion is the overtopping, water gulping over the dike crest and loss of stability by subsequent erosion of the lee side.

The bosom embankments are the smallest of all the four types of dike. They are mostly constructed of clay and peat. The core below the crest often consists of a great variety of materials as, in the course of time, local authorities have used sand, rubble, and clay as available to add to the dike's height. The strain that bosom embankments have to withstand differs from other types of dike. They are subjected to a practically constant high water level. Their groundwater table is, consequently fairly high. The subsequent saturation forms a hazard, especially during periods of high rainfall, as earth-slides occurring along the inland slope might inflict inundation.

Dike design

Already since prehistoric time, dams and dikes showed two distinct functions: stability by the two parallel outer embankments of rock and mortar, and imperviousness by the central filling of materials of the bed of the wadi (Jawa dam, Kafara dam, Ma'arib dam). In ancient Netherlands, a consistent dike design was developed by monks; it also consisted of the two separate functions: an impermeable part by densified sea weed, and a stabile part by an earth body of clay, reinforced by coupled rows of short wooden piles and a carefully placed stone toe against wave attack. Until 1850 dikes were made symmetric, just like the Kafara, with slopes of about 1:2.5. At present, a Dutch dike is faced with an impermeable layer. This is mostly clay but sometimes supplemented by asphalt or stone revetment. Apart from being impermeable, the layer must also resist scouring. A grass cover with a healthy layer of turf is usually sufficient for dikes on non-tidal river reaches. Dikes subjected to heavier attack are usually given a revetment of stone or concrete blocks. The core of a dike 'bears' the dike. It must provide support for the clay layer and give the whole dike sufficient volume and weight to resist the pressure of the water piled against it.

It is hardly seen or felt, but a dike displaces horizontally for several decimetres when subjected to high water. Shear forces in the underground provide a further slip. Other than the clay facing, the core should be permeable. Any water that does manage to percolate through must be allowed to flow away safely so the body of the dike does not become saturated and weaker, as higher saturation significantly decreases soil shear resistance. On the inland side the sand core is again faced with clay to prevent it being washed away, either by rain or by water overtopping the crest. Provision is made along the foot of the inland slope to allow water, which has penetrated the core to drain away safely. Such drainage is vital for the safety of the dike. It is to be said that many old river dikes have a clay core.

These general features may vary from place to place. Much depends on local factors, which can differ widely such as the type of ground below the dike, the materials available in the past, the pressure the dike must withstand, and the traditions and customs of the area. The evaluation of the relative importance of the various criteria of dike construction or dike improvement and subsequently the

assessment of an economically optimal design is achieved by the application of the probabilistic approach, which involves a close inspection of water levels and corresponding failure mechanisms, their probability and their coherence. This approach has gained support in the last twenty years and has become the accepted design philosophy of modern dike design and maintenance in the Netherlands.

Dike-ring approach

The strength of the chain of defences is never greater than their weakest link. This anticipates a safety norm of an area protected by a sequence of dikes, referred to as a dike-ring. For each zone surrounded by a dike-ring the safety norm is related to the economic, social and environmental values assigned to the protected area. Hence, the probability of local dike failure is connected to the likelihood of damage to the protected assets, i.e. risk = probability of failure x consequences. Dike technology is therefore based on three major elements:

- The safety philosophy; the dike-ring approach, application of probabilistic methods, and research on economically and ecologically sound ways to retain the water, in balance with the protected values.
- The design and the control of functions of water-defence systems; control-guidelines, technical elaboration of various failure mechanisms, and research on new ways of realisation of structural elements.
- Rational maintenance; methods for preventive maintenance, methods for error detection and monitoring, and efficient techniques of maintenance.

Safety philosophy

Disasters due to technical failure seem to be socially less acceptable than natural catastrophes. An important question is whether disasters due to technical failure can be avoided and whether damage due to natural catastrophes can be minimised. An observation is that in a society full with sophisticated technical systems disasters are unavoidable. Accidents are the logic consequence of a society that "lives" on technology. The discussion about safety mainly deals with probability theory and social acceptance. In a society that is full of technical systems, there exists an apparent subjective safety during a period of absence of accidents. Safety assessment therefore comprises the evaluation of risk sensation involving objective personal and social acceptance and the analysis of probability of failure involving various realistic events. The new Water Retainment Act provides the possibility to base the safety philosophy on likelihood of inundation. Three risk-components determine the relation between safety level and a probability of failure or malfunctioning: (1) personally acceptable risk, (2) optimised economic risk, and (3) socially acceptable risk.

The indivudually acceptable risk is the probability of a casualty during an action while considering the personal factor (voluntary or involuntary activity). The optimised economic risk is the probability of exceeding expected cost of damage/maintenance, which may include the number of casualties in case of failure (inundation). The socially acceptable risk is related to a balance of social costs and benefits, including cultural, ethical and environmental aspects. The most critical or

a combination of these three criteria is taken as the target reliability. This approach is still a subject of national debate.

Functional analysis

The basic function of a dike is to retain the water. Various elements can be distinguished each playing a characteristic role in the functioning of the dike. These principal elements are (see Fig 17.6)

- The crest height should be above the design water level.
- Outer slope: a watertight cover in order to keep the inner groundwater table and leakage low and resistant against rapid draw down, ice and earthquake.
- The core of the dike conveys the horizontal load due to the water to the subsoil.
- Inner slope: a permeable cover to keep groundwater table and leakage low and stable under overtopping and earthquake.
- The subsoil provides suitable stability and has a water retaining function.

In urban areas existing buildings in and on the dike can jeopardise its function. The watertight cover is locally interrupted, differential settlements can cause cracks and maintenance becomes more complicated. Using functional analysis two principal solutions can be defined for the situation of buildings on a dike: fully integrated, when the buildings and their foundations are also the water retaining structure or building and dike are functionally separated. This can be achieved by various measures. In these solutions the effects on the elements of the dike must be considered precisely and in detail (leakage, stability, erosion, etc.). For trees, cables and pipelines on and in the dike the same holds. They are admitted when they do not interfere with the principal dike function (separation and evaluation of functions). If the problems related to buildings and trees can be solved in a technical way, the question of control and maintenance is to be solved. When the water retaining function and building are fully integrated, frequent inspection is necessary. Uncontrolled changes in the buildings by their owners may be a danger to the dike function and a threat to the safety. It is recommended to plan the design for a period of 100 year. If buildings are outside the technical dike profile the inspection is more complicated, particularly when the fundamental elements (watertight screen) are not directly visible. The quality can be checked by adequate measurements during high waters. For buildings in the lee-side area a regular inspection of the cellars and the maintenance of the lee-side slope is required. The present-day development of houses in the river forelands, although officially prohibited, became lucrative and popular, but it raises a serious new political issue, as safety is at stake during high river discharges.

Dike maintenance

The technical component of management is daily maintenance, which consists of inspection, taking measures and allocation of personnel, materials and equipment. The condition of a water-defence system will degenerate in the course of time. Moreover, the loading conditions may change, and new insight in the evaluation of strength of elements in the system may arise. Two fundamental activities, periodic inspection and taking measures in time, form the backbone of a proper maintenance policy. Periodic inspection implies a comparison between actual

condition and the minimum condition requested. The important question is how the system will behave until the next moment of inspection.

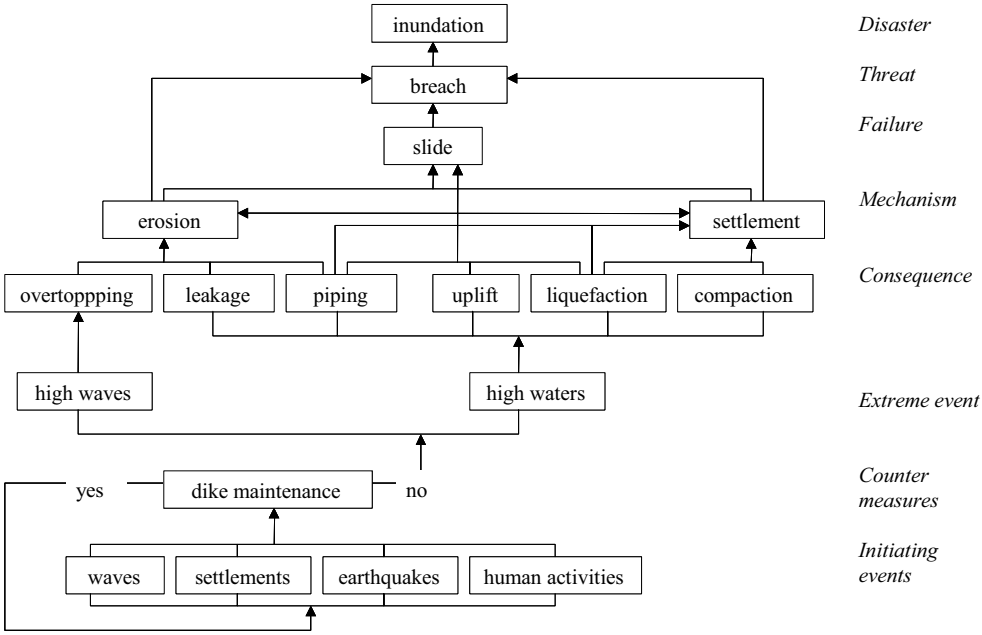

Figure 17.5 Event tree for flooding

principal element	*link*	*principal limit states*
height		overtopping
		wave overtopping
outer slope		erosion outer slope
		instability outer slope
core		leakage
		settlement
inner slope		erosion inner slope
		instability inner slope
subsoil		uplift
		piping

Figure 17.6 Dike system; relation between functions and failure modes

The following steps are distinguished: determination of functional demands, evaluation of the condition until the next inspection, comparison with the norms, choice of measures, and optimisation. Therefore, besides the daily maintenance an overall check, every 6 years according to the Water Retainment Act, leads to an actual High Water Protection Program, which will be executed in the following 6 years. Important aspects in this procedure are the concept of fixed and variable data, the degeneration model and the system of diagnosis. How to determine the actual strength of an existing dike? Pilot studies have been performed to clarify the

approach for practical purposes. Preliminary results are compiled in a concept control-guideline for a try out.

Failure mechanisms or malfunctioning

For a typical dike cross-section various failure mechanisms (limit states) can be distinguished (Fig 17.5). Traditionally, much attention is given to the mechanism of overtopping and wave overtopping. By the selection of a proper crest height with respect to the exceedence of design water levels and wave heights a safe dike profile can be accomplished. Breaches in the past have proved that overtopping was not always the cause of inundation. Piping, micro-instability and slope-slides have induced flood disasters. Also situations that did not happen so far could be added, such as collision during high water by a large ship. A similar consideration applies to structures in the dike (sluices, floodgates, locks, pumping stations), when they participate in the water-retaining function of the dike. Excess loading may also exceed the bearing capacity of the foundation causing large unacceptable displacements. History shows that structures in dikes present a major threat. An aspect of special concern is the human factor, i.e. the manual operation of sluices, locks and floodgates during high waters. In the analysis, the probability of the human error should be considered. For a dike-ring the probability of failure of any dike section and of any structure may lead to inundation of the area, as the total strength is not greater than its weakest link. The probability of inundation increases with the length of dikes in a dike-ring. Usually, a dike, which is well designed and performs the required functions, also satisfies the safety conditions of various failure mechanisms. The function "water-retaining" demands a suitable "crest height", a suitable "water tightness" of the dike body and subsoil, a suitable "stability" to transfer the water level induced shear force, and a suitable "resistance" of the dike to all forces which are related to its existence (current forces, wave loading, tourist and cattle damage). If the principal elements are well designed, i.e. the crest height, the outer slope, the core, the inner slope, and the subsoil, the principal limit states or failure mechanisms are dealt with automatically.

Dealing with uncertainties

The safety of a certain mechanism is controlled by investigation of the critical situation, the limit state[62], where loading and mobilised strength is in equilibrium, and any increase of loading causes collapse. Sometimes a limit state cannot be assessed by calculations. Physical tests and pilot tests or engineering experience is used. The probability method, in fact, elucidates and quantifies the relative importance of uncertainties. It is here, that conventional deterministic calculation methods apply as a cornerstone in an integral approach. Uncertainties are classified as intrinsic (related to nature: time, stochastic water levels, and space, soil heterogeneity) and epistemic (related to models: statistics, incomplete data,

[62] A distinction is made between ultimate limit state and service limit state. The former is the extreme situation when breaching occurs, the latter when any designed function is being jeopardised.

inaccuracy, scale). This is practically possible by the definition of dike-rings. For each ring a safety norm is determined and the safety norm of all other elements in the dike-ring system are related to this norm. The scheme shown in Fig 17.7 clarifies the relation between the conventional inundation safety approach and the new way as foreseen in the New Water Retainment Act. Four different levels are distinguished: water level exceedence, inundation likelihood, inundation risk, and inundation safety. They are interconnected in a comprehensive manner, and they will give place to evaluating required and actual safety. Hence, the inundation approach comprises the following aspects

- Loading (tides, waves, earthquakes);
- Mechanisms (failure mechanisms per type of structure and element);
- Calculation methods (probabilistic models, partial safety factors);
- Inundation scenarios, damage evaluation;
- Decision models accounting for "values" and "loss" (damage).

The dike-ring approach is essentially different from the traditional dike building method. The original dike improvement concept, applied until the first Delta law, after the flood of 1953, was raising the height of the dike by one metre above the latest highest water level (Fig 17.7a). Here the only strength aspect considered was the height. Flood safety was based on intuition and calamity.

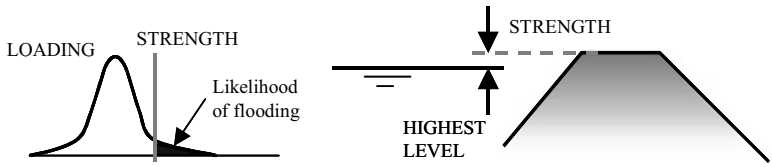

Figure 17.7a Dike building approach before 1953

During the flood of 1953, it was noticed that in many cases the dike inner slope had failed, and the first following Delta Law distinguished the likelihood of different failure mechanisms. The probability of flooding was therefore redefined into: inundation likelihood = water level exceedance (loading) ⊗ failure likelihood (strength). The symbol ⊗ refers to convolution of stochastic loading (water level / waves) and each dike ring, each case and each failure mode, such as overtopping, wave overtopping, erosion outer slope, instability outer slope, leakage, settlement, erosion inner slope, instability inner slope, uplift, and/or piping (see Fig 17.5 and 17.6). The approach is shown in Fig 17.7b in a schematic way.

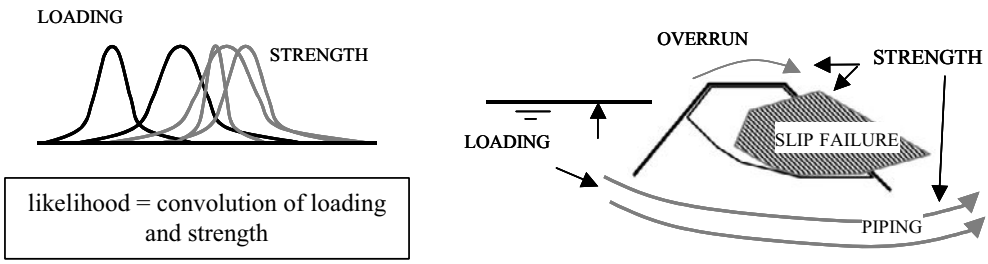

Figure 17.7b Dike building approach after the first Delta law.

Recently, the approach of dike building is changing because of a growing awareness that the protected assets are not the same everywhere, and the cost of ever improving dike systems should be looked at. The approach is characterised by: inundation risk = inundation likelihood ⊗ consequences (damage per dike ring), see Fig 17.7c.

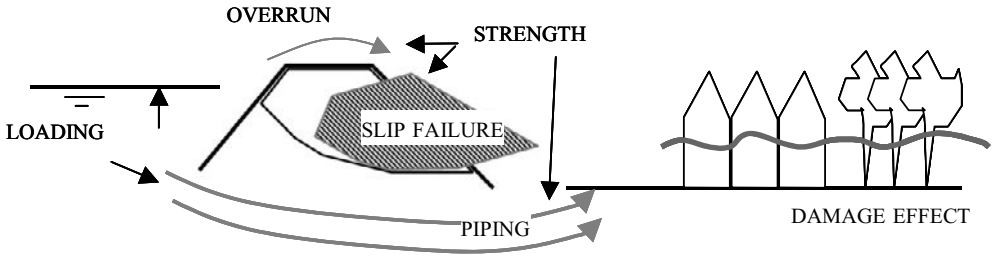

Figure 17.7c Latest development of the risk approach on flood protection

This inundation approach requires the evaluation of the economic, social, and cultural damage caused by inundation. It requires awareness for natural and environmental values and a social acceptance of a change of the role that existing water-defence systems may play. A serious social-political problem yet to solve is how to cope with the principle of equity in the constitution and the different probability of drowning in the various dike-rings, and how to manage with the valuation of the difference of the economic value in the various dike-rings, from 6 to 30 billion euro (total is estimated at 280 billion euro and the dike-ring average is about 10 billion euro). The amount of potential damage should become, in fact, a guiding principle for the effort one should implement to keep the probability of this failure low. The calculation methods and decision models will define how the information obtained can be used to make a rational decision. This concept is defined as: inundation safety = *boolean* (inundation risk < accepted inundation risk). Mere intuition and experience have in the past, addressed uncertainties. Today, it is possible to more objectively quantify and qualify uncertainties for yet inexperienced but well-described scenarios. Societies call for this approach confronted as they are with climate change and an increasing pressure on space allocation for work and living for a growing population with altering needs. In the coming decades the Dutch will face the issue how to handle uncertainties in an integral policy and decision making process for a prosperous development of their lowlands.

D STATE OF THE ART

After completion of the Delta-river project, a workshop was organised to identify needed innovation directions, in an open discussion in the style of the British parliament. In introductions, sharp inspiring statements on social versus scientific matters were prepared to stimulate a debate. Over eighty delegates from building, government and education communities participated as 'civilian' seated in the society bench, seated opposite in the scientific bench, or in the public seats behind a jury. The discussion took place between society and science, the public

showed acclamation, while a small selected jury of conscious men summarised and ascertained. Central themes were time and risk management, as the general goal is the establishment of optimum environments in a safe and fast manner. This fits well in the geotechnical discipline with a focus on dike technology, road and railway design, underground construction, foundation, and soil-quality management. The workshop evoked memorable sayings, still valid today

- The troubles are lying on the street. Due to the soft ground condition and an old-fashioned ownership structure cities are caught up with lingering costs for inefficient maintenance of roads and sewerage, spending millions of guilders yearly.
- A firm coupling between social demand and scientific technology is essential. The social profit of R&D efforts can be guaranteed in the new form of collective research programs.
- The conventional structural separation of budget and responsibility for building and maintenance prohibits an integral approach.
- For the involvement of calculation and monitoring results as practical engineering tools, it is the question how the behaviour in the construction stage can be reliably extrapolated to the behaviour of the structure in use.
- The present-day monitoring is too much static. In fact, not the absolute results are important, but the effects and alterations in measured data. An appeal is made for dynamic monitoring.

The discussion and debate were lively and pleasant. The popular subject was monitoring, which has a great potential seen in the light of the modern information technology. The workshop contributed to a consensus on social effects, scientific importance, objective priorities and a consciousness to cooperate. Conclusions stated by the jury are

- Monitoring in the construction and in-use stage makes sense only if possibilities exist to interfere in case of malfunctioning.
- Monitoring or close inspection by experts during the building phase may provide valuable information about weak links in the process.
- Monitoring might enhance building methods as new opportunities and innovations that may otherwise not come to life. This, in turn, may emphasise the value of monitoring.
- Parallel monitoring of specific vital parts of a construction process will provide new knowledge and information, which can be generalised in conceptual prediction models.
- Better performance later by monitoring now; knowledge investment for future quality is a timeless wisdom.
- Knowing about or being involved in risks makes a great difference. Dedicated communication and clear information, dealing with social and political innocence and ignorance, is of essential importance. The geotechnical profession needs more visualisation (social visibility).
- Legislation is decisive and fateful. A once fixed norm is inflexible and it can create its own rigid environment.
- Safety against inundation is not a commercial commodity. The responsibility should always lie with the central authority, i.e. the government and the parliament.

Recent achievements in expertise and experience

Some of the most valuable achievements are compiled in comprehensive manuals and guidelines. They refer to earth and rubble stone dams and dikes constructed on soft ground.

Soft ground engineering

CUR report 162 – Building on Soft Soils (1996). The Dutch knowledge and experience is gathered on design and construction of earth structures on and into highly compressible soils of low bearing capacity. The design process, including soil investigation, probabilistic methods and mechanical behaviour, is extensively discussed, and the construction, including fill materials, building methods and maintenance and management, are outlined. Special information is given on parameter correlations, software codes and validation methods of calculations, and practical cases are worked out. A special chapter deals with behaviour of peat and organic clays.

Rubble mounds and stone revetments

CUR/CIRIA Report 154 – Manual on the Use of Rock in Coastal and ShoreLine Engineering (1991). Knowledge and experience obtained from several large projects, like the Delta Works, has been gathered by British and Dutch engineers. The manual includes data collection, design, construction and maintenance aspects. Chapter 4 describes the dynamic hydro-geotechnical stability of rubble mound structures and stone covers, in particular when exposed to wave attack and earthquakes. The manual contains various practical design concepts and formulae, and elaborated examples on the probabilistic approach. It also describes instruments and numerical tools, and the corresponding legislation.

Dike technology

A long list of guidelines and manuals, technical reports and fundamental studies is available, mostly published under the auspices of the ENW (Expertise Network Water Defences, formerly TAW, founded in 1965), a committee that advises the ministry in charge of water management. Amongst its members are representatives of the ministry, governmental departments, the water boards, the provinces, the universities, and knowledge institutes.

Technical guidelines, manuals and regulations are coherently organised and regularly updated for the use by the water boards for the six-annual evaluation. The actual list of main guidelines and regulations includes

- Fundamentals for Water Defence (1998);
- Regulation Hydraulic Boundary Conditions (2007);
- Regulation Safety Evaluation Primary Water Defence Systems (2007);
- Guide line Environmental Effect Report;
- Guide line River Dike Design, part I, lower river regime (1985);
- Guide line River Dike Design, part II, upper river regime (1989);
- Guide line Rivers (2007);
- Guide line Sandy Coasts (2002);
- Guide line Sea and Estuary Dikes (1999);
- Guide line Water Defence Special Structures (2003);
- Manual Actual Strength of Dikes (2009);

- Manual Aspects of Clay (1996);
- Manual Asphalt as Cover (2002);
- Manual Classification of Peat (1994);
- Manual Cofferdams and Deep Walls in Water Defence Systems (2004);
- Manual Inventory and Valuing LNC (Landscape, Nature, Culture) (1994);
- Manual Stone Revetments (2003);
- Manual Sand Boils (1999);
- Manual Water Defence Ground Structures (2001);
- Manual Water Pressures in Dikes (2004);
- Manual Wave Run-up and Overtopping (2002).

There is an annual budget of about 100 million euros for a research program to update the guidelines with a frequency of six years, parallel to the once in six-year evaluation of all primary dikes and water defence structures. The outcome of the last three evaluations shows that about 50% of the flood defence is sufficient to good, about 30% is undetermined (lack of data, lack of knowledge), and about 20% is insufficient and needs to be improved. After every evaluation a comprehensive dike-improvement program is defined: for the undetermined a focus on collection of missing data, and for the insufficient a redesign. For this effort the Dutch government spends 1 to 1.5 billion euros a year. The work is executed by the water boards under supervision of the provincial authorities and the ministry in charge. The lack of knowledge is addressed in the research program. The money spent for safety looks much, but compared to the national budget and the national product is not more than a few percent. One may wonder if that is sufficient when the value at stake is considered. Flooding damage is not easily insurable!

E LATEST DEVELOPMENTS

The thousand-year experience in eliminating high water threat to the Dutch lowlands is by no means complete and sufficient. A comprehensive study for coastal zone extension has been completed (Waterman), and progress is made to natural supported coastal developments at several locations. Observation indicates that natural sand transport guided by local hard elements creates the planned coastal zones, in due time.

After the devastating sea storm of 1953, the government installed a Delta Committee and its advice became the basis for flood protection: a system for regular dike repair and evaluation, founded in the Water Defence Act. Extensive works have been performed since, amongst which the Delta project, completed in 1986. The dramatic high river levels of 1993 and 1995, which led to a massive evacuation have called for a national focus on river dike improvement (the Delta River project) completed in 2000. In the same period, several weak spots on the seacoast defence have been improved. Recent information about climate change with sea level rise and more intense river discharges gave rise to national concern about flooding safety in the future. The government installed a new Delta Committee, which came with an integral advice in 2008 that will protect the lowlands for a long time and calls for working together *with* the water. The flooding threat is not acute but yet urgent. The advice is a new Delta program that comprises twelve recommendations

1. Flooding safety of dike rings must be ten times higher.
2. The load of new investments on unfavourable locations must be carried by those who have the benefit and not the society as a whole.
3. Developments in river beds may not disturb the discharge capacity.
4. Use the concept building with nature for the North Sea coastal protection (sand nourishment.
5. Protection of the Wadden mud flats (nature protectorate) in an international context.
6. In due time, replacement of the Eastern Scheldt barrier with improving the tidal climate in the estuary.
7. Western Scheldt remains open and dikes will be strengthened accordingly.
8. Furnish the closed south-west estuaries for river water retention to decrease salt intrusion.
9. Complete the space-for-river projects accommodating higher river discharges.
10. A Rhine river closure system.
11. Improvements of coastal infrastructure allowing for a level rise of 1.5 m in the lake Ijssel.
12. Political: a special governmental task manager and a parliamentary theme committee charged with the execution of the plan (expected period 2010 – 2050), financial: a special Delta fund (expected an extra 1 to 2 billion euro per year), and judicial: essential issues laid down in a special Delta law.

In 2009, following up the recommendations, the government installed a Delta Commissioner for a period of 7 year with the mandate to execute the complex Delta program in close cooperation with ministries, water boards, provinces and municipalities. The works involved will undoubtedly ask the best skills and experience of the geotechnical profession.

Space for the river

The residents in the river region experienced anxious times in 1993 and 1995. The water levels were extremely high and the dikes just managed to hold. A quarter of a million people had to be evacuated. Extremely high river discharges will occur more frequently in the future and for this reason, it was decided to ensure that the rivers could discharge the forecast greater volumes of water without flooding. In 2007, the Government approved the Space for the River Plan, carried by 17 partners (provinces, water boards, municipalities, RWS) under responsibility of the Ministry. Total cost is 2.3 billion euros. This Plan has the following objectives:

- By 2015, the branches of the Rhine will cope with a discharge capacity of 16,000 m^3 of water per second without flooding.
- Measures implemented to increase safety will also improve the overall environmental quality of the river region.
- The extra room the rivers will need in the coming decades to cope with higher discharges due to the forecast climate changes, will remain permanently available.

At 39 locations in the Rhine delta, one or more of the following measures is being implemented to create more space for the river and reduce high water levels

1. Lowering of floodplains. Lowering (excavating) an area of the floodplain increases the space for the river at high water levels.
2. Dike relocation. Relocating a dike land inwards increases the width of the floodplains and provides more space for the river.
3. De-poldering. The dike on the river side of a polder is relocated land inwards and water can flood the area at high water levels.
4. Deepening summer bed. The river bed is deepened by excavating the surface layer of the river bed. The deepened river bed provides more space for the river.
5. Lowering groynes. Groynes stabilise the location of the river and ensure that the river remains at the correct depth. However, at high water levels groynes can form an obstruction to the flow of water in the river. Lowering groynes increases the flow rate of the water in the river.
6. Removing obstacles. Removing or modifying obstacles in the river bed where possible, or modifying them, increases the flow rate of the water in the river.
7. Water storage. The Volkerak-Zoommeer lake provides for temporary water storage when exceptional conditions result in the combination of a closed storm surge barrier and high river discharges to the sea.
8. High-water channel. A high-water channel is a embanked area that branches off from the main river to discharge some of the water via a separate route.
9. Strengthening dikes. Dikes are strengthened in areas in which creating more space for the river is not an option.
10. With regard to measures 5 and 9 special attention is to be paid to the local geohydrology. Since the geological stratification in the area exists of a low-pervious top layer (Holocene) and a sandy pervious second layer (Pleistocene), the corresponding lowering of the hydraulic resistance of the top layer by implementing the measure may provoke higher groundwater pressures in the hinterland during high rivers. The measure may invoke the need to strengthening the dike for higher pore pressures, particularly at the lee side.

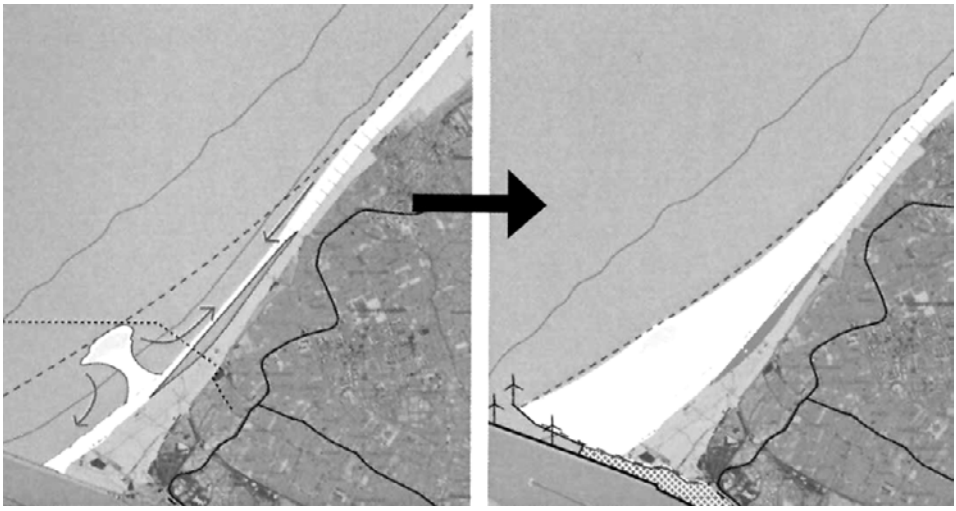

Figure 17.8 Sand motor (erosion island) at the coast (Stive); start and finale

Dynamic coastal protection

In accordance with recommendation (4) of the Delta program, the 50 million euro pilot project Sand Motor started in 2010. At a strategic location along the North Sea coast 20 million m^3 of sands dredged from 20 km in sea is positioned before the coast in the form of a hook (erosion island, Fig 17.8). With time, this sand will be spread along the coast by wind, waves and sea currents, and provides effective beach nourishment and more. With this innovative method, using natural forces (building with nature) extra space for nature and recreation is created and it contributes to safety against flooding, erosion and sea level rise. The expectation is that the sand motor will disappear in a period of 20 years and supports a shoreline progression of 100 metre over 20 kilometres coast, to the north.

Overtopping and erosion

An important dike failure mechanism is inner slope sliding due to overtopping. Due to alternate dehydration and saturation, the top layer loses strength. In fact, this is how most of the dikes in the southwest of The Netherlands failed during the 1953 flood disaster. The amount and the frequency of overtopping a dike is a topic of research. Clearly, it determines the height of the dike crest above the design water level (the freeboard or excess height), and hence influences the cost level of the flood defence system. As this freeboard can be different in different countries, it may lead to complications in case of trans-national rivers. e.g. the debate about the maximum possible discharge that can reach the Netherlands via the Rhine.

If a dike crest is too low and there is no space for a higher dike, a superstructure is built. Some examples are concrete Muralt superstructures, T-walls (on levees in New Orleans) and sheet piling (Pettemer Sea Dike). Their purpose is to reduce overtopping. Recent events in New Orleans have shown that these superstructures may fail under extreme conditions and destabilise the dike. The probable causes, as understood from tests, are a combination of geotechnical and hydraulic processes, such as heavy overtopping, local scour, wall rotation, hydraulic shortcuts, piping and extreme soft soil deformation (peat layers). A proper design of such structures requires an intense interaction of expertise in surface water hydraulics, geohydrology and geotechnics.

In the Netherlands, the crest height of a dike is traditionally designed to allow a small amount of overtopping, for instance 2% of the waves may overtop during a storm, or a small average overtopping discharge of 0.1 to 1 [l/sm] (litre per second per metre width) is allowed. The method to determine the overtopping discharge is described in the Eur0top wave-overtopping manual. For example, for a significant wave height of 1 metre, a free board is required of 3 metre for limiting overtopping to 0.1 l/sm, 2.2 metre for 1 l/sm and 1.4 metre for 10 l/sm. For higher waves, the differences in the required free board for various overtopping levels become larger.

Dike grass cover stability under overtopping conditions is based on constant overflow tests. In case of wave overtopping, however, individual overtopping volumes can be large, generating flow velocities up to 9 m/s for short periods of time. Since 2007, a wave-overtopping simulator (Fig 17.9a) is used to test the strength of grass covers against erosion. It has a 4 m wide water container, during testing being filled with a constant discharge to provide the random overtopping

discharge to be tested. At irregular time intervals, the valve is opened, releasing a water volume over the inner slope in such a way that a realistic storm is simulated. The drop height of the water volume is calibrated to generate the correct flow velocity at the dike crest for the large overtopping volumes.

(a) wave-overtopping simulator (van der Meer) *(b) infiltration tests*

Figure 17.9

Twenty-five wave-overtopping tests were performed on actual dikes at 8 locations in the Netherlands and Belgium, in winter when the grass is relatively weak and the probability of storm conditions is high. The tests show a strong erosion resistance of the grass cover. Most covers did not fail until an average overtopping discharge beyond 50 l/sm. Hence, small overtopping volumes (as in standard practice today) will cause no significant damage. If there are no mole and rat holes, only the largest overtopping volumes produce damage.

Parallel to the research in the erosion resistance, sliding of the cover layer was investigated. The mechanism is governed by the shear strength of the cover layer, the fixation to the dike core, and the accumulation of induced pore pressures in and underneath the cover layer. Field infiltration tests (Fig 17.9b) were performed on the same locations where the overtopping tests were conducted. Based on the test results, a simple model was created for the assessment of the pore pressure build-up taking into account the infiltration capacity of cover layers and the overtopping characteristics.

With the tendency of increasing hydraulic loads to be considered in dike design due to (anticipation of) expected climate change and the desire for higher safety levels without more expenses, the acceptance of more overtopping becomes opportune. In some cases, the acceptance of a lower crest and more overtopping can be a real option, particularly if space to build or extend the dike is limited.

Peat dikes

In the summer of 2003 a peat embankment suddenly slid away with a loud snap, after months of severe drought. The water of the canal inundated a village. The responsible water board took immediate action, dammed the canal and evacuated part of the population. No one drowned, but the damage was later put at 60 million euro. During that period some 15 other similar embankments were also found to be in danger, showing local collapse, cracks and leakage. Even after a century of soil mechanics in the Netherlands, particularly on dike technology, this was unforeseen.

The lowlands of Holland seems in jeopardy by water from four different fronts: by high rivers, stormy seas, heavy rains, and also from drought.

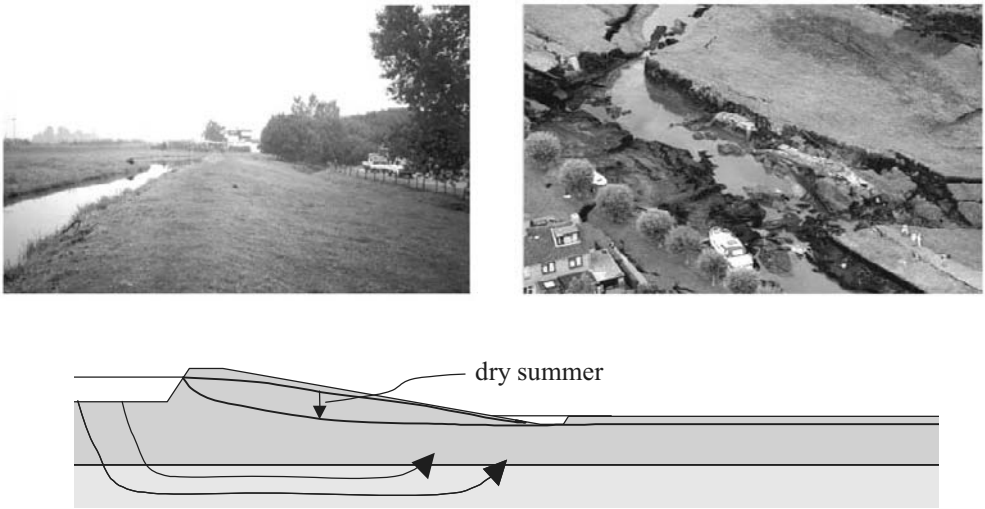

Figure 17.10 Bosom embankment of peat; collapse during a dry summer, in 2003

These secondary embankments are of a typical construction, built from peat and organic clay centuries ago in the original swamps, embedding a lowland canal to which the surplus water of the area was and is being pumped and transported to the sea. These dikes served peat mining for salt production and turf. When the peat mining stopped the resulting lowland, called polder, was used for cattle. At present, these regions settled about 1.4 metres below canal level and are developed into modern living areas. A peaty embankment has a typically moderate slope, around 1:10 (Fig 17.10). Peat is light and if not compressed it is relatively permeable. To perform its function it must be saturated, and usually the infiltration from a steady canal level provides sufficient recharge to maintain the water content. In fact, the water retaining capacity comes from the groundwater weight. When peat dries out, however, it shrinks significantly and it becomes like cork. Investigation after the event revealed that shrinkage and uplift triggered the slide. Following this failure, it became clear that our knowledge of the mechanical and chemo-biological behaviour of peat is poor. Before, no one thought to consider dry embankment behaviour. Nature may have still many surprises. Our knowledge of peat and organic clay needs improvement.

Liquefaction and piping

In case of high water levels, the latest dike evaluation has shown that piping induces relatively large failure probabilities. The process may involve micro-liquefaction and whether coarse sand is less vulnerable is yet uncertain. In low-density sands, recent small-scale tests show that a different erosion process may occur, i.e. the pipe starts upstream and moves downstream by local densification. In addition, the likelihood of flooding is not well predictable in areas with loosely packed sands. The measurement of the local density (porosity) in the field is

difficult due to unavoidable sample disturbance and this leads to a rather conservative attitude: too many dikes may get the qualification unsafe. Not only in the Netherlands is this problem prevalent. In China, for more than 50% of the flood disasters along the Yangtze River, piping is the culprit. The many sand boils along the Mississippi also show the relevance of piping. During recent storms, large problems by piping occurred in California and New Orleans.

The demand for fundamental insight in the piping process and in the liquefaction phenomenon is urgent. A suitable prediction model for piping and/or liquefaction in loose sands is clearly needed and sound investigation, including time effects, may prove that temporary higher water levels are not that dangerous. A major issue is the localisation of weak (geological) spots in the dike rings and a sound method for the determination of the local density. A promising innovation seems using biogrout (bacteria that cement the sand) in order to fix loose sand preventing liquefaction and piping or to avoid sample disturbance during in-situ testing the density. The ultimate goal is a thorough knowledge of the phenomena and practical and adequate prediction tools, by which the safety of flood defence systems can be guaranteed without unnecessary over-sizing.

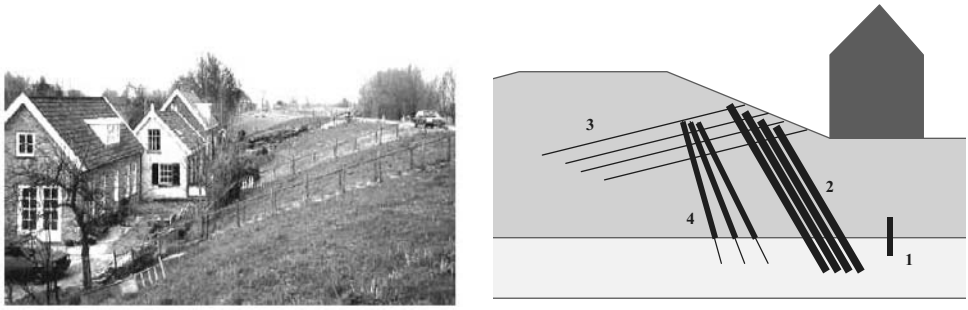

Figure 17.11 Four inside-dike enforcement techniques

Inside

Four innovative dike redesign methods have been evaluated by different consortia: (1) short sheet dowel, (2) mixed in place, (3) nailing, and (4) pin doweling. The challenge is to strengthen existing dikes without occupying more space, because in many situations the existing buildings and infrastructure do not allow expanding the dike geometry. Each of the consortia consisted of participants from contractors, consulting firms, institutes, universities and governmental authorities. The different techniques have been investigated by physical tests, numerical predictions and field-testing. Environmental aspects, sustainability and economics have been an important part of the studies as well. For these methods a pilot test has been performed focusing on construction, quality and monitoring. The methods are judged to be sufficiently mature to be applied in practice.

Flood control of urban areas

As shown in Fig 17.1 most of the world's large cities are positioned in delta areas, and their size and number is expected to increase in the near future. The vulnerability of these areas to flooding and the complexity of flood prevention and

calamity control in urban regions calls for a review of the actual situation and knowledge of the weak spots in the safety systems. In this respect, two actions are mentioned, FloodProbe and FloodControl.

FloodProbe[63] is a European research project running from 2009 to 2013 addressing technologies for improved safety of the built environment in relation to flood events, with a focus on impacts of damage to networks and assets with a high value density, on flood-proofing of the urban environment, and on construction technologies and concepts to support holistic flood risk management strategies. The results will be implemented in the EU Flood Directive.

FloodControl 2015 is a Dutch public-private collaboration in the field of crisis management during (the threat of) flooding. Current flood protection is extremely fragmented. Weather forecasts, dike strengths, water levels, they are all assessed separately. The result is that uncertainties are added in a cumulative way. Current flood protection is primarily concerned with strong dikes. But the greatest gain lies in making the total system smarter, i.e. the dike, the decision-maker, and their environment. Flood Control 2015 addresses this. Specialists[64] in the field of water management, ICT and crisis management combine their expertise and experience to integrate these three aspects in advanced forecasting- and decision-supporting systems, involving serious gaming. But also new sensors that provide direct information are required. Flood protection then becomes more transparent, quicker, better, and more efficient. It will support new design and maintenance methods leading to solid and sustainable solutions in line with social requests and continuously changing natural conditions.

[63] FloodProbe partners are Deltares, HR Wallingford, Cemagref, SINTEF, EIVP/LGUEH, Regional Environmental Center, Oxford Brookes University, Dura Vermeer, Acciona, Samui Design and Management Ltd, Mostostal Warszawa SA, Laboratoire Central de Ponts et Chaussees, DeltaSync b.v., and Solintel M&P SL.

[64] Partners in FloodControl 2015 are Arcadis, Fugro, Royal Haskoning, IBM, HKV, TNO, Deltares, ITC, IJkdijk.

This page intentionally left blank

ANSWERS

answer 2.1

Standard testing involves measuring W and V of (semi-)saturated soil, and after drying in an oven W_s and V_s (by pycnometer). Elaboration: $W_w = W–W_s$, hence, $V_w = W_w/\gamma_w$. $V_p = V–V_s$. Hence, $s = V_w/V_p$. $\gamma_s = W_s/V_s$, $G_s = \gamma_s/\gamma_w$ and $v = 1+e = 1/(1-n) = V/V_s$. Dealing with organic matter is treated separately (ashing).

answer 2.2 (another test)

Measured data: W_w = 20.26 gr, W_s = 48.75 gr, b = 8.0 cc, c_1 = 31.5 cc (before mixing) and c = 31.0 cc (after mixing), d = 20.5 cc. Note, c is slightly different after mixing because of density changes.

Elaboration: $a + d = b + c$. Hence, a = 18.5 cc. Note, c = 31.0 cc is chosen (the mixture). Next, $(1–n)\ c = a$ or $(1–n)\ 31.0 = 18.5$. Hence, n = 0.403 (porosity is 40.3%). Total weight of the mixture is 20.26 + 48.75 = 69.01 gr. The weight of saturated soil is found by subtracting the free water above (after sedimentation): volume b cc.

Pay attention to units!

$W = 69.01 – b\gamma_w/g$ = 69.01 [gr] – 8.0 [cc] 10 [kN/m^3] / 10 [m/s^2] =
= 69.01 [gr] – 8.0x10^{-6} [m^3] 10^4 [N/m^3] / 10 [m/s^2] =
= 69.01 [gr] – 8.0x10^{-3} [Nm/s^2] = 69.01 [gr] – 8.0x10^{-3} [kg]
= 69.01 [gr] – 8.0 [gr] = 61.01 [gr]

Note, $b\gamma_w/g$ is [gr], if we insert b in [cc], γ_w in kN/m^3 and g in [m/s^2]!

Next, $W = W_w + W_s = ((1–n)\gamma_s + n\gamma_w)\ c / g$.

Hence, 61.01 = ((1-0.403)γ_s + 0.403x10) 31.0 / 10. This gives γ_s = 26.2 kN/m^3.

Since $\gamma = Wg/c$, it follows that γ = 61.01x10/31.0 = 19.68 kN/m^3.

answer 2.3

The value of c and c_1 differ (see Fig 2.6). The water will not saturate the dry sand sample because of air entrapment.

answer 2.4

Clay silty high plasticity.

answer 2.5

By $V_p = V–V_s$ and $W_w = W–W_s$ giving $V_w = W_w/\gamma_w$, makes $s = V_w/V_p$ known.

answer 2.6

W = 160g = 0.160x9.82=1.571 N; W_s = 110g = 0.110x9,82 = 1.080 N;
W_w = 1.571–1.080 = 0.491 N. Water content: $w = W_w/W_s$ = 0.491/1.080 = 0.455;
$V_p = V–V_s$ = 125–65=60 cm^3= 0.60x10^{-4} m^3; porosity $n = V_p/V$ = 60/125 = 0.480;
Volume of pore water: $V_w = W_w/\gamma_w$ = 0.491/(1000g) = 0.491/9820 = 0.50x10^{-4} m^3;

Saturation degree: $s = V_w/V_p = 0.50\text{x}10^{-4}/0.60\text{x}10^{-4} = 0.833$;
Specific solid gravity $G = 110/65 = 1.692$;
Organic content 0.634;
Highly organic clay (as in the oedometer practical)

answer 2.7

$W = 193\text{g} = 0.193\text{x}9.82 = 1.895$ N; $W_s = 158\text{g} = 0.158\text{x}9{,}82 = 1.551$ N;
$W_w = 1.895–1.551 = 0.344$ N. Water content: $w = W_w/W_s = 0.344/1.551 = 0.222$;
$V_p = V–V_s = 100–60 = 40$ cm^3 = $40.0\text{x}10^{-6}$ m^3; porosity $n = V_p/V = 40/100 = 0.400$;
Volume of pore water: $V_w = W_w/\gamma_w = 0.344/(1000\text{g}) = 0.344/9820 = 35.0\text{x}10^{-6}$ m^3;
Saturation degree: $s = V_w/V_p = 35.0\text{x}10^{-6}/40.0\text{x}10^{-6} = 0.875$;
Specific solid gravity $G_s = 158/60 = 2.63$;
It is sand or silt

answer 2.8

$w = se/G_s$ and $e = n/(1\text{-}n)$; $w = 0.347$, $w_l = 0.406$ and $w_p = 0.302$, $I_p = 0.104$. Silt (Casagrande), $I_l = 0.439$ and $c_u = 20$ kPa (varies between 8 and 35 kPa, Fig 2.3).

answer 2.9

$\gamma = \gamma_s(1+w_0)(1–n_0) \rightarrow n_0 = 0.360$; $w_0 = s_0 n_0 \gamma_w/\gamma_s/(1–n_0) \rightarrow s_0 = 0.72$; $(1–s_0)n_0 = 0.101$; rise is 1/10/0.110 = 0.992m; phreatic level rises to 0.992m above base.
pV = constant; $p_{initial}$ is atmospheric, $V_{initial} = 10\text{x}5\text{x}0.110$ m^3/m, $V_{final} = V_{initial} – 1$ m^3/m, $p_{final} = V_i/(V_i–1) = 1.247$ bar. Required thickness 24.7/18 = 1.37m

If $\gamma_w = 10$kN/m^3 rather than 9.81kN/m^3 is taken, then respectively 0.945m and 1.30m is found.

answer 3.1

Terzaghi's cohesion is independent on stress. Taylor's interlocking depends on stress.

answer 3.2

Both apparatus measure only the normal stress and shear stress, so Mohr's circle can not be constructed. DS gives a discrete failure plane and so mimics failure planes in-situ. SS gives a parallellogram which probably is closer to field failure in many cases. Thin weak layers dominate in SS but may be missed in DS.

answer 3.3

The cell pressure is uniform (isotropic stress): $\sigma_v = \sigma_h = p$. The axial stress is just added to the vertical stress component: $\sigma_v = p + q$ and $\sigma_h = p$. In the stress circle of Mohr the radius is $(\sigma_v - \sigma_h)/2$ is equal to the maximum shear stress τ_{max}. Hence, $\tau_{max} = q/2$.

answer 3.4

The soil is likely to be unsaturated and will swell as the moisture content increases. Uniform swelling will only cause heave of the buildings, but non-uniform swelling is more likely and will result in distress to foundations, floors and walls such as fissuring, bending and breaking.

An oedometer test could be performed on the undisturbed material, noting the amount of swelling and the reduction of suction as a function of change in water content of the soil.

The swelling parameter (e.g. a in the abc-model) can characterise this behaviour. In confined conditions, swelling cannot occur and a swelling pressure will develop. This can be measured by adding water and increasing load such that deformation of the sample is zero.

answer 3.5

SPT uses percussion and CPT pushes with slow velocity a cone into the soil; SPT is preferred in stiffer soils.

answer 4.1

Free water level increase may cause an increase of effective stress in a submerged soil with a pore fluid with gas bubbles. Because the pore fluid is compressed, the pore volume decreases and grains are therefore compacting, unless sufficient additional water can flow into the pores (dependent on dissipation time of pore fluid with regard to the period of the level change). In the case of a fully saturated submerged soil with relatively soft soil particles, a free water level increase may decrease the effective stress, because the pore fluid pressure increase will compress the soil particles and therefore the intergranular forces (effective stress) will become less.

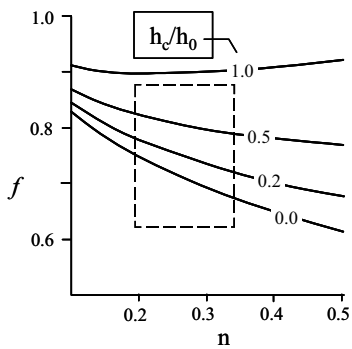

(a) Relation f(n) for 4 values of h_c/h

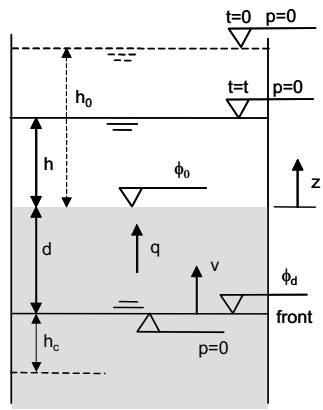

(b) Infiltration with capillarity effect

answer 4.2

The time of infiltration increases with capillary head. For infiltration the effective porosity should be used (about 0.7n), see dashed window in (a), above.

answer 4.3

The discharge of the large-scale virtual well is Q = 4x10x5x1.2/3 = 80 m^3/day. The discharge of the northern well is Q = 3x10x5x0.6/3 = 30 m^3/day, the discharge of the south-western well is Q = 3.5x10x5x0.6/3 = 35 m^3/day, and the discharge of the east southern well is Q = 2.5x10x5x0.6/3 = 25 m^3/day. The sum of these three wells is 90 m^3/day, a bit more than the large-scale value. The difference is due to the limited accuracy of estimating the relevant flow tubes.

answer 4.4

The potential head at location B, which balances the local total stress of 40 kPa at the interface due to the saturated soil weight of the clay layer, is $u_B = (D+h_B)\gamma_w = 40$ or $h_B = 4 - 2.5 = 1.5$ m, a reduction of 25% with respect to the earlier measured h_B of 2.0 m. Therefore, the corresponding waterlevel in the river also reduces with 25% to 3.0 m. The effect of this riverlevel, though it does not cause uplift, is yet significant for the shear strength, because at the interface the local vertical effective stress at location B is zero, and only cohesion remains to uphold the required shear resistance to support the dike against the high river.

answer 4.5

Estimate $k = 0.1 - 0.5\text{x}10^{-3}$ m/s. $Q = (M/N)k\Delta h$=(4/10) k (7)=2.8 k m^3/sm^1. Advise the highest value to the client ($k = 0.5\text{x}10^{-3}$): $Q = 0.5\text{x}10^{-3}$ x 2.8=1.4x10^{-3} m^3/sm^1=121 m^3/day m^1.

answer 4.6

Estimate k = 1 m/day. $Q = (M/N)k\Delta h$ = (6.5/8) 1 (5) = 4.06 k. [m^2/day].
The potential head along FE and ED is $\phi = z - p/\gamma_w = z$, because $p = p_{atm} = 0$.
The total drop is ΔH = 5 m. Thus $\Delta\Phi = k\Delta H/N = 5k/8$. Hence, $\Delta\phi = 5/8 = 0.625$ m.
In point A (the first equipotential line): $\phi_A = 1\text{x}\Delta\phi = 0.625$ m. The position is: z_A = 4 m. Thus $p_A = \gamma_w (\phi_A + z_A) = 10^4 (0.625 + 4) = 46.25$ kPa.
The vertical total stress in point A due to the bulk weight is σ_v = 4x11 = 44 kPa.
Since the pore pressure exceeds the total stress, the peat layer will be lifted up.

answer 4.8

$Q_1/K = 1.1$, $Q_2/K = 0.51$, $Q_2/Q_1 = 0.46$, $s_2/s_1 = 0.01$; A small leak already has a significant discharge.

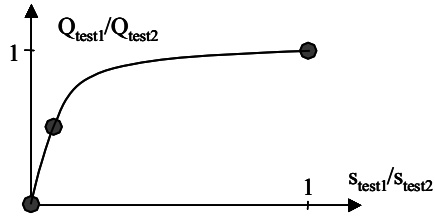

answer 5.2

Assume groundwater level at the surface.
σ'_0 = 2.5x15 – 2.5x10 = 12.5 kPa; σ' = 12.5+50 = 62.5;
$(1-\varepsilon_l) = (62.5/12.5)^{-0.2} = 0.725$; $\varepsilon_l = 0.275$; S = 5x0.275 = 1.38 m
layer 1: σ'_{01} = 1.25x15 – 1.25x10 = 6.25 kPa; σ'_1 = 6.25+50 = 56.25;
$(1-\varepsilon_{l1}) = (56{,}25/6.25)^{-0.2} = 0.644$; $\varepsilon_{l1} = 0.355$; S_1 = 2.5x0.355 = 0.889 m;
layer 2: σ'_{02} = 3.75x15 – 3.75x10 = 18.75 kPa; σ'_2 = 18.75+50 = 68.75;
$(1-\varepsilon_{l2}) = (68.75/18.75)^{-0.2} = 0.771$; $\varepsilon_{l2} = 0.229$; S_2 = 2.5x0.229 = 0.572 m;
So: $S = S_1 + S_2$ = 1.46 m

answer 5.3

It leads to less compression, e.g. a numerical value of 0.3 corresponds for natural strain to a compression of 1−exp(−0.3) = 0.26. Likewise, a value of 1.0 results in a compression of only 0.63. Pitfall: equal compression gives a larger numerical value of natural strain, but conversely, equal numerical value gives less compression for natural strain.

answer 5.4

$1.20 = -\ln(1-\varepsilon_l)$, from which follows $\varepsilon_l = 0.70$; so 70%.

answer 5.5

Answer: Reload compressibility C_c' determines settlement. Initial $\sigma_v'_0$ is 16x1+10x1+6x2.5 = 41 kPa; $\Delta\sigma'_v$ = 100 kPa; $\varepsilon_{l,soft} = C_c'/(1+e_0)\ \log_{10}(1+\Delta\sigma'/\sigma_v'_0)$ = 0.0054; $S = H_{soft}\ \varepsilon_l$ = 0.027 m.

answer 5.6

$S = C_c/(1+e_0)\ h\ \log_{10}(1+\Delta\sigma/\sigma_v'_0)$; $\sigma_v'_0 = h\gamma'_1/2 + x/L\ (H-h)\ \gamma'_2$; (Left, Centre, Right) $\sigma_v'_0$ = (270, 970, 1670 kPa) S = (0.22, 0.065, 0.038 m). Observe a logarithmic trend due to increasing initial stress.

answer 5.7

σ'_0 = 1x14 + 1x4=18 kPa;
$\Delta\sigma$ = 2x16=32 kPa; $\Delta z = H_{clay}\ \varepsilon_l = 6(1-(1+32/18)^{-0.15})$= 6x0.142=0.85 m;
$\Delta\sigma_2$ = 32-0.85x10=23.5 kPa; $\Delta z_2 = 6(1-(1+23.5/18)^{-0.15})$= 0.71 m;
Average 0.78 m; Grade −1+2−0.78 = 0.22 m + N.A.P.

answer 6.1

Switching the layers 2 and 3 leads to the following results.

TABLE 6.2 DATA PROVIDED

H [m]	n	γ_d	$\gamma = \gamma_{sat}$	C_r	C_c	C_α
1	0.40	16	20	0.001	0.006	0.0
5	0.35	14.0	18	0.04	0.14	0.002
1	0.42	12.8	17	0.12	0.76	0.005

TABLE 6.3 ELABORATION FOR $\Delta\sigma = \Delta\sigma' = 100$ kPa AND PRECONSOLIDATION STRESS OF 50 kPa

layer	e_0	a	b	I	σ_A kPa	u kPa	σ'_A kPa	σ'_B kPa	σ'_C kPa	$-\varepsilon_l$	S_{total} m	S_{creep} m
1	0.667	0.0003	0.0016	0	8	0	8	58	108	0.0015	0.001	0.0
2	0.538	0.0113	0.0396	0.0006	16	0	16	66	116	0.0462	0.175	0.025
					106	50	56	106	156	0.0273		
3	0.724	0.0303	0.1917	0.0013	106	50	56	106	156	0.0997	0.097	0.105
					123	60	63	113	163	0.0947		
											total 0.274	*total* 0.036

answer 6.3

Asaoka's method gives: $\tan\theta = (S_3 - S_2)/(S_2 - S_1) = 0.75$; $h = 5$ m; $c_v = 4h^2(1-0.75)/\pi^2\Delta t = 9.77\text{x}10^{-7}$ m^2/s; $T_e = 2h^2/c_v/86400 = 592$ days; $t_{0.2} = 59$ days $< t_1$ so settlement data are valid; $m = S_2 - S_1\tan\theta = 0.45$; $S_\infty = m/(1-\tan\theta) = 1.8$ m.

answer 6.4

$\varepsilon_l = 0.05/10 = 0.005 = 1 - (50/40)^{-c}$; $c = -\ln(0.995)/\ln(5/4) = 0.0225$

answer 6.5

$\sigma'_A = 6/3\text{x}(15\text{-}10)=10$ kPa; $\sigma'_B = 25$ kPa; $\sigma'_C = 10+2\text{x}16 = 42$ kPa; $\varepsilon_l = 1 - (25/10)^{-0.01}\ (42/25)^{-0.1}(10^4/1)^{-0.005} = 0.10$; $Z_{max} = 0.60$ m. Reduction of load 10x0.60x(1-0.4) = 3.6 kPa; $\sigma'_C = 42 - 3.6 = 38.4$ kPa; $\varepsilon_l = 1 - (25/10)^{-0.01}(38.4/25)^{-0.1}(10^4/1)^{-0.005} = 0.093$; $Z_{min} = 0.56$ m. Variation $(0.60 - 0.56)/(0.60 + 0.56)*2 \approx 8\%$, acceptable.

answer 6.6

Consolidation plays no role anymore. No creep: $0.0005(t - 200) = 0.20 \rightarrow t = 600$ AD. With creep: $0.0005(t - 200) = 0.20 - 3(1 - (t/200)^{-0.0225})$; by iteration $t = 482$ AD; 118 years earlier due to creep.

answer 6.7

$C_r = 2.3\ a\,(1+e_0)$

answer 6.8

$$\lambda_t = \left[\frac{S}{2tkD} + \frac{d_1/\sqrt{2tc_{v1}}\coth(d_1/\sqrt{2tc_{v1}})}{\lambda^2} + \frac{d_2/\sqrt{2tc_{v2}}\coth(d_2/\sqrt{2tc_{v2}})}{\lambda^2} \right]^{-0.5}$$

provided that at outer boundary $z = d_2$, $\phi = 0$ holds.

answer 6.9

The consolidation zone is $3\sqrt{(2c_v t)} = 3\sqrt{(2\text{x}10^{-6}\text{x}604800)} = 3.30$ m (at the edge of the zone, at $z = 3.3$ m the potential in the clay is about 5% of the potential change in the aquifer). The storage effect is $Sc_v/k'd = 0.0025$, very small.

answer 7.1

Using goniometric analysis it can be shown that the effective stress circle in Fig 7.8 can move to the left by 4.26 kPa before it touches the strength envelope AB. So, $\Delta\sigma_v' = 5\ kPa$. The effective stress change under groundwater level changes (see answer 4.1) is $\Delta\sigma_v' = (1 - n)\gamma_w \Delta h$. Hence, $\Delta h = \Delta\sigma_v'/(1- n)\gamma_w = 4.26/(1- 0.35)10 = 0.66$ m. Thus, the slope will collapse when the groundwater level rises 66 cm.

answer 7.2

From the stress values corresponding Mohr circles can be drawn (Fig 7.9). They confirm the obtained value for the friction angle φ. In this case the cohesion c is zero.

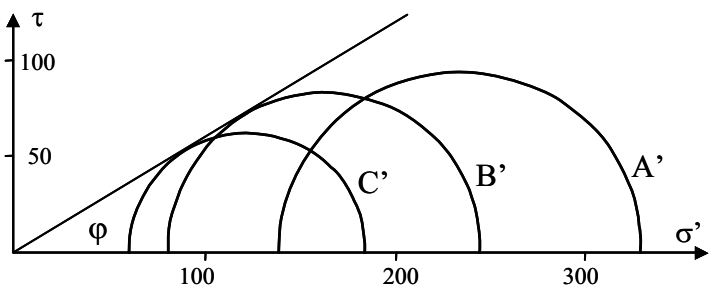

answer 7.3

Because of (2-D or 3-D) volume-constraint shear deformation is possible at the edges.

answer 7.4

By pore pressure increase the circle size does not change, but moves to the right until touching the measured (lab) envelope (failure line); Fig 7.9 shows a shift of $\Delta\sigma' = 4.26$ kPa is possible. Using equation 4.1 (relation rising groundwater Δh and corresponding effective stress) gives $\Delta h = \Delta\sigma'/(1–n)\ \gamma_w = 0.707$ m. For a rain of 0.05 m/day this rise is realised in $0.707n/0.05 = 5.66$ days. Rise speed 70.783/5.66

= 12.5 cm/day must be less than k_v (maximum possible infiltration), which is not correct. Hence, rise is realised in 70.7/8 = 8.8 days, assuming it is raining all the time.

answer 7.5

The directions of critical shear planes are related to the points where the Mohr-circle touches the failure envelope, observed from the DC (direction centre). The angles are $\alpha + 45^o = 112^o$, and $\alpha - 45^o = 12^o$.

answer 7.6

φ is about 21^o(precise 20.8^o) and passive major stress is about 200 (precise 201.1) kPa.

answer 7.7

$M = 6\sin\varphi/(3\text{-}\sin\varphi) = 1.42$; $a = 6\ c\cos\varphi/(3\text{-}\sin\varphi) = 30.4$ kPa. $\Delta q/\Delta p$ of tsp (total stress path) follows from $\Delta\sigma_3 = 0 \rightarrow$ slope at 3 : 1.

For esp (effective stress path) $B = 0$ (*in*saturation $\Delta u = 0$): esp = tsp.

$B = 1$ (complete saturation): from (7.18) and (7.20) follows $\Delta u = \Delta p + (A-1/3)\Delta q$, and $\Delta p' = -(A-1/3)\Delta q$.

And so, $\Delta q\ /\Delta p' = -1/(A-1/3) = -3/2$, given $A = 1$.

Intersections with failure envelop is found at resp. at $q = 2c_u = 326.6$ kPa and 88.6 kPa. So, for tsp: $c_u = 163.3$ kPa and for esp (saturated): $c_u = 44.3$ kPa.

Influence of B: esp closer to tsp as B decreases to zero.

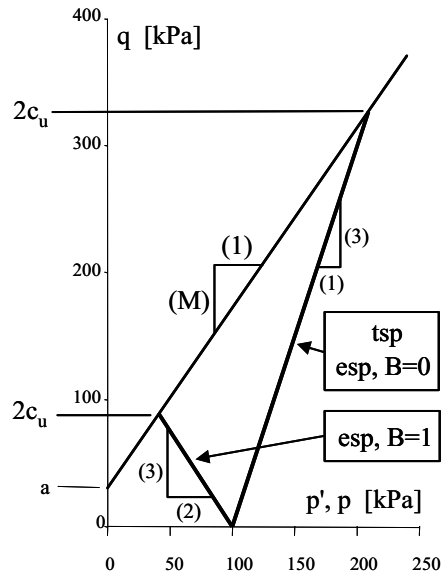

answer 8.2

B = 3.41 m

answer 9.2

Use formula (9.22): $\phi_w = 10 - (2/\pi)\ \ln(25/0.25)\ (10 - 7) = 1.2$ m, quite different than 7 m!

answer 9.5

With $\sin(2\alpha) = 2\sin\alpha\cos\alpha$ and $\cos(2\alpha) = 1-2\sin^2(\alpha) = 2\cos^2(\alpha)-1$ equation (9.14) becomes with $\beta = 2\alpha$

$$F = \frac{\sigma_v}{\sigma_h} = \frac{\sin\beta + R(1-\cos\beta)}{\sin\beta - R(1+\cos\beta)}$$

The minimum of σ_v/σ_h is found by $\partial F/\partial\beta = 0$, which yields

$$0 = \frac{\cos\beta + R\sin\beta}{\sin\beta - R(1+\cos\beta)}\left[1 - \frac{\sin\beta + R(1-\cos\beta)}{\sin\beta - R(1+\cos\beta)}\right] = \frac{\cos\beta + R\sin\beta}{\sin\beta - R(1+\cos\beta)}(1-F)$$

Since obviously $1-F \neq 0$, the numerator $\cos\beta + R\sin\beta$ must be 0, which yields

$$R = -\frac{\cos\beta}{\sin\beta} = -\cot(\beta) = -\cot(2\alpha) = +\tan(2\alpha - \pi/2)$$

Thus $\alpha = \pi/4 + ½ \operatorname{atan} R$ gives a minimum for F.

Elaboration of F give the following simplification, with $R = \tan(\theta)$ and $\beta = 2\alpha$

$$F = \frac{\sigma_v}{\sigma_h} = \frac{\sin\beta + R(1-\cos\beta)}{\sin\beta - R(1+\cos\beta)} = \frac{\cos\theta\sin\beta - \sin\theta\cos\beta + \sin\theta}{\cos\theta\sin\beta - \sin\theta\cos\beta - \sin\theta} =$$

$$= \frac{\cos\theta\sin\beta - \sin\theta\cos\beta + \sin\theta}{\cos\theta\sin\beta - \sin\theta\cos\beta - \sin\theta} = \frac{\sin(\beta-\theta) + \sin\theta}{\sin(\beta-\theta) - \sin\theta} =$$

$$= \frac{\sin(\alpha)\cos(\alpha-\theta)}{\cos(\alpha)\sin(\alpha-\theta)} = \frac{\tan(\alpha)}{\tan(\alpha - \operatorname{atan} R)}$$

Elaboration of (9.15b) with $\beta = 2\alpha$ and $R = -\cot(\beta)$ yields

$$\frac{\sigma_h}{\sigma_v} = \frac{\sin\alpha\cos\alpha + R\sin^2\alpha}{\sin\alpha\cos\alpha - R\cos^2\alpha} = \frac{2\sin\alpha\cos\alpha + 2R\sin^2\alpha}{2\sin\alpha\cos\alpha - 2R\cos^2\alpha} = \frac{\sin\beta - \cot\beta(1-\cos\beta)}{\sin\beta + \cot\beta(1+\cos\beta)} =$$

$$= \frac{\sin^2\beta - \cos\beta(1-\cos\beta)}{\sin^2\beta + \cos\beta(1+\cos\beta)} = \frac{1-\cos\beta}{1+\cos\beta} = \tan^2\frac{\beta}{2} = \tan^2\alpha$$

answer 10.3

A pore pressure field (homogeneous permeability), conditioned by only boundary pressures (no flux condition), is always independent of permeability. Since (slope) stability in question is affected by pore pressures, therefore, k does not appear in the formula.

answer 10.4

Use formula 10.9. Because of the soil layering the groundwater flow must be horizontal: $\theta = 0$. Observed: $\beta = 15.5^{\circ}$, or $\tan\beta = 0.277$. Just stable: $F = 1.0$.

Hence, formula (10.9) gives $1.0 = (\tan\varphi /0.277)(1-(9.82/\gamma)(0.277^2 +1))$ or $\gamma = 10.58 \tan\varphi (\tan\varphi - 0.277)^{-1}$. For $\gamma = 16$, it follows then that $\varphi = 39.3^o$.

answer 10.5

Use formula 10.9. The reduction is determined by $1-(\gamma_w/\gamma)[\tan^2\beta+1] = 1-(10/19)[\tan^2 25+1] = 0.64$. Thus, only 36% of the original safety factor is left.

answer 10.6

Using formula (10.3b) gives for $F = 1$, $c = \gamma H \cos\beta \cos(\beta-\varphi) / \cos\beta = 6.2$ kPa. If the soil becomes submerged, replacing γ by γ', shows the stability should increases.

answer 10.7

Answer: For $\varphi = 0$ and $\beta = 90^o$ the graph is similar to formula (10.14a) and so Taylor's graph is an upper limit; an additional safety factor of at least 1.2 should be adequate (depending on the risk of sub- sequential damage).

answer 10.8

For an infinite slope there is no pore pressure dependency in the slope ξ-direction. Therefore pore pressure must increase (or decrease) linearly with η. Due to gravity, the ξ component of flow is always constant at $q_\xi = -k_\xi \sin\beta$ and directed downhill. Therefore flow will always have a component off the η direction.

answer 11.2

$d = 10$m; e = 7m; $K_a = 0.27$; $K_p = 3.7$; Moment around B: $d^3\gamma K_p/6 - e^2(3d+2e)\gamma K_a/6 + e^3\gamma K_p\, 2/6 = F(d-2)/5$ or $F = 10.57$ MN.
Horizontal equilibrium: $d^2\gamma K_p/2 + e\,(2d + e)\gamma K_a/2 - e^2\gamma K_p/2 = F/5$ or $F = 10.77$ MN.
Exact location of rotation point is 0.06 m above bottom, giving $F = 10.59$ MN.

answer 11.3

An upper, since Rankine slip line states are assumed (admissible kinematic system); whether the stress state at the tip outside the slip zone is admissible is not known.

answer 11.4

$d = 8$m; $e = 6$m; $K_a = 033$; $K_p = 3.0$; Moment around B: $d^3\gamma K_p/6 - e^2(3d+2e)\gamma K_a/6 + e^3\gamma K_p\, 2/6 = F(d-2)/5$ or $F = 5.33$ MN.
Horizontal equilibrium: $d^2\gamma K_p/2 + e\,(2d+e)\gamma K_a/2 - e^2\gamma K_p/2 = F/5$ or $F = 5.12$ MN
Exact location of rotation point is 0.105 m below bottom, giving $F = 5.30$ MN

answer 11.5

The weak point is the shortness and flexibility of the sheet piling. The middle of the toe can move slightly to the outside due to space in the sheet pile locks, and it can give room to sand intrusion at the left side of the toe. Hence, a higher inside groundwater pressure can act without much reduction at the toe, giving rise to heave of the submerged clay layer at the right side, and subsequently erosion will cause sink holes at the quay surface.

answer 11.6

Assuming the retaining wall is rigid, prestressing the anchor causes the wall to rotate to the right (in the book it is assumed to rotate around point B to the left). Hence, the diagrams of horizontal stress will change from passive to active and from active to passive state. If adopting formula (11.10), then by replacing K_p by K_a and K_a by K_p will cause a drastic increase in stability (81 times!). It has to be said that the wall is usually not rigid. It bends and local deformations will define the stress state. Also the rotation point B will change when prestressing the anchor.

answer 11.7

Left with Q pointing downwards; the wall will be pushed into the soil, if Q is more inclined than δ.

answer 12.3

$q_0 = 0$ (no loading on the soil surface at the sides) and $c = 0$
$N_q = ((1+\sin\varphi)/(1-\sin\varphi)) \exp(\pi \tan\varphi) = 10.67$
$N_\gamma = 1.8(N_q-1) \tan\phi = 8.12$
$i_\gamma = (1-(F_H/F_V))^3 = (1-0.5)^3 = 0.125$
$s_\gamma = 0.7$
So, $q = i_\gamma s_\gamma N_\gamma \gamma = 0.125\text{x}0.7\text{x}8.12\text{x}9 = 6.4$ kPa and $F_{v,max} = qA = 6.4\text{x}\pi 5^2 = 502$ kN.

answer 12.4

The test is performed until failure (large deformation); hence, the result is just reality (under testing conditions) and it is neither an upper nor a lower bound.

answer 12.5

Apparent radius surface $R = \pi^{-0.5} = 0{,}56$ m; assume apex 45°; $h = 0.56$m. Equation (13.42) gives stress for critical damping $\sigma_0 = 2.52$ kPa. Dead weight contact stress $W/A_0 = 10$ kPa $> \sigma_0$, so the ground will vibrate.

answer 12.6

$\alpha = 90^\circ$. Passive soil reaction occurs when the soil is being pushed and more resistance is being generated; the apex becomes $\alpha = 90^\circ + \varphi$.

Note, $\alpha = 90^o$ refers to $K_0 = 1$ (or $\sigma_h = \sigma_v$); neutral stress state usually refers to undisturbed soil states where $K_0 = 1-\sin\varphi$ (and $\sigma_h \neq \sigma_v$) is adopted as an approximation (then shear stresses are mobilised).

answer 12.7

In case of settling soil, negative shaft friction should be considered.

$Q_s = 2\pi RH\alpha_s c_u = 2\pi$x0.2x25x0.7x50 = 1.08 MN, $Q_e = \pi R^2 q_e = \pi(0.2)^2$x20=2.5 MN, so, the end bearing is Q_c = 2.5–1.08=1.42 MN, a safety factor 3 would be appropriate; the design capacity becomes about 0.47 MN.

answer 12.8

$q = q_0 + 5.14c_u$ = 2 x 14 + 5.14 x 25 = 156.5 kN/m. Note: width of footing is irrelevant for undrained case. Any irregularity of the loading in terms of inclination or moment, and any inhomogeneity of the soil leads to a left or right motion if the structure on top allows for the induced rotation. If no rotation is possible, two equal wedges will originate. 3D effect increases the bearing capacity, because shape factor $s_c > 1$.

answer 12.9

Use lightweight fill material (see Fig 13.4).

answer 13.2

$r_0 = 0.156/\pi \approx 0.05$ m; $\theta_B = R^3/12.5/0.05/2\text{x}10^{-8} = 8\ 10^7 R^3$ sec;
$u/\sigma_0 = 0.3 = \exp(-3\text{x}30\text{x}24\text{x}3600/8\ 10^7/R^3)$; $R = 0.51$ m

answer 13.3

$r_0 = 0.156/\pi \approx 0.05$m; $\pi R^2 = 4$; $R = 1.128$m; $\theta_B = 1.128^3/12.5/0.05/2\text{x}10^{-8} = 1.15\text{x}10^8$ sec; $u/\sigma' = 0.1 = \exp(-t/1.15\text{x}10^8)$; $t = 2.65\text{x}10^8$ sec = 8.4 yr. Much too long! The relation between t and R is: t is proportional to R^3; so,
$R_2 = R_1(t_2/t_1)^{1/3}$. which gives $R_2 = 2\ (1/8.4)^{1/3} = 0.98$m.

answer 13.4

Without vertical drains consolidation for $U = 0.8$ makes $U = 1-(8/\pi^2)\exp(-\pi^2 c_v t/4h^2)$ which gives t = 39.4 month or 3.2 years. With vertical drains and no vacuum pressure: $U = (1-u/\sigma_0) = 0.8 = 1-\exp(-12.5c_v t r_0/R^3)$ which gives t = 73 days or 2.4 months. There is no need for vacuum pressure, normal drains will do.

answer 13.5

$\theta_B = 0.7^3/12.5/0.035/2\text{x}10^{-8} = 3.92\ 10^7$ sec; t = 120*24*3600=1.0368 10^7 sec;
$\exp(-t/\theta_B) = 0.768$; σ_0=32 kPa; the pore pressure under surcharge and vacuum load (σ_0+v) has to reduce to ($0.2\sigma_0+v$) to accomplish a reduction of 80%, and this in 120 days ; this gives $(0.2\sigma_0+v) = (\sigma_0+v)\exp(-t/\theta_B)$, which leads to $v = 2.45\sigma_0$ = 78 kPa ;

so, after 120 days the vacuum pump is stopped and a reduction of pore pressure by $0.8\sigma_0$ is reached.

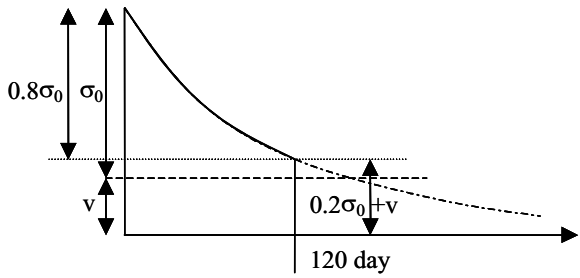

answer 13.6

$C_\alpha/(1+e_0)\log(1+t_{grace}/t_0) = C_c/(1+e_0)\log(\sigma'_{II}/\sigma'_{III})$; $t_{grace} = t_0[(\sigma'_{II}/\sigma'_{III})^{Cc/C\alpha}-1] = 180[1.5^{20}-1] = 6\ 10^5$ days. Not realistic because creep rates are higher after unloading. More realistic $t_{grace} = 180[1.2^{20}-1] = 6720$ days.

answer 13.7

$2x0.1+2x0.01 = 2\pi r_0$ So: $r_0 = 0.035$ m; $\theta = R^3/(12.5r_0c_v) = 1/(12.5x0.035x2x10^{-7}) = 11.4\ 10^6$ s; $t = 6$ month $= 15.6\ 10^6$ s
$u = \sigma_0 \exp(-t/\theta) = 50\ \exp(-1.37) = 50x0.254 = 12.7$ kPa So: $U = 1-u/\sigma_0 = 1-0.254 = 0.746$; $U = 0.746 = 1 - (8/\pi^2)\exp(-c_v t(\pi/2h)^2)$;
$t = -(2h/\pi)^2/c_v \ln(0.254\pi^2/8) = -(2x5/\pi)2/2x10^{-7}\ (-1.16) = 58.8E6 = 680$ days.

answer 14.1

Due to transverse dispersion.

answer 14.2

$S = 100(a + bh)\ 2^{(T-5)/10} = 0.01(-0.1 + 1.5x0.35)x2^{(15-5)/10} = 0.0085$ m

answer 15.3

The constant h in the cone-shape dynamic soil model for a circular tunnel lining is best chosen equal to the radius, because then no overlapping or opening with neighbouring cones along the surface occurs. So, $h = R = 5$ m. For a quarter of the circular perimeter and per metre axial length the spring constant is: $k = A_0E/R = (\pi R/2)E/R = \pi E/2 = 15.7$ MN/m

answer 15.4

Arching may occur in sand (non-cohesive soils): due to friction stress is diverted to the sides. For temporary situation arching may be useful (standing borehole); on the long run it will vanish.

answer 16.2

Choose the reference at the dashed line: $z = 0$ (pointing upwards), and take there the reference for the potential head: $\phi = 0$. The base of the structure is taken at $z = -17$ (1 m lower than the soil bottom in front). The total discharge under the structure is calculated by the graphical method of square net (Chapter 4): $Q = Mk\Delta H/N$, where $M = 5$ is the number of flow tubes, $k = 50$ m/day = 2.08 m/s, $\Delta H = 7$ is the drop over the structure, and a sketch provides $N = 17$, the number of potential intervals. Hence, $Q = 4.28$ m^3/m.hr. The pressure under the structure behind the sheet piling is defined by $p = \gamma\,(\phi - z)$. Here, $\gamma = 10$ kPa/m the volumetric water weight, $\phi = -3 - 8\Delta\phi = -3-8\text{x}7/17 = -6.3$ m, and $z = -17$ m. This yields $p = 10(-6.3+17) = 107$ kPa. In the same manner is found that before the sheetpile $p = 130$ kPa. The groundwater pressure difference between both positions becomes 23 kPa. At 5 m down along the sheetpiling the pore pressure at the left side becomes 10(–3–2x7/17+22) = 182 kPa and 10(–3–7.5x7/17+22) = 159 kPa at the right side. This gives a pressure difference of 23 kPa. At the sheetpiling tip the pressure is 10(–3–4x7/17+27) = 223.5 kPa, equal at the left and right side. Hence the horizontal force due to groundwater pressures becomes 5x23 + 5x23/2 = 172.5 kPa/m, pointing to the right.

answer 16.3

$Q = Mk\Delta H/N = 2.5\text{x}140\text{x}7/15 = 163$ m^3/mday = 6.8 m^3/mhr.

$p_{B,out} = 70$ kPa; $p_{B,in} = 70-4.7\text{x}7\text{x}10/15 = 48.1$ kPa.

The water pressures at the left sheetpiling are compensated by the soil pressure. The water pressure at the right side has to be compensated by the anchor force. That part is calculated as the resulting force determined by the average pressures in the squares at either side of the sheet piling. It gives about 85 kN/m

answer 16.4

The characteristic D-values are given underneath; porosity is estimated.

D_{xx} [m]	SA	GR	QW	QR	FI	AM
15%	0.0001	0.0010	0.033	0.08	0.6	1.7
20%	0.0001	0.0017	0.040	0.09	0.6	1.7
50%	0.0002	0.0080	0.080	0.20	0.8	1.7
85%	0.0003	0.0370	0.090	0.30	0.9	1.7
porosity n	0.37	0.35	0.40	0.42	0.42	0.43
$D_{60}/D_{10} < 2$	graded	graded	uniform	graded	uniform	uniform

For the classic non-migration rule: graded $D_{15f}/D_{85b} < 4$ to 9

D_{15f}/D_{85b}	FI	QR	QW	GR	SA
AM	1.89	5.67	> 10		
FI		2.00	6.67	> 10	
QR			0.89	2.16	> 10
QW				0.89	> 10
GR					3.33

For the classic non-migration rule: uniform D_{50f}/D_{50b} < 5 to 10 or graded D_{50f}/D_{50b} < 12-18

D_{50f}/D_{50b}	FI	QR	QW	GR	SA
AM	2.13	8.5	> 18		
FI		4.00	10.0	> 18	
QR			2.50	> 18	
QW				10.0	> 18
GR					> 18

For the permeability rule $D_{20f}/D_{20b} > 5$ for graded material

D_{20f}/D_{20b}	FI	QR	QW	GR	SA
AM		18.9			
FI		6.67			
QR			2.25	52.9	
QW				23.5	
GR					12.1

For the dynamic loading norm $N_f = n_f D_{15f}/D_{50b}$ < 1 to 5

N_f	FI	QR	QW	GR	SA
AM	0.91	3.65	> 5		
FI		1.26	3.15	> 5	
QR			0.42	4.20	> 5
QW				1.65	> 5
GR					1.75

From these tables one may compose an adequate filter structure. The combinations QW-SA and FI-QW are not unconditionally stable. Four filters systems are possible

1) AM FI QR QW GR SA
2) AM FI QR GR SA
3) AM QR QW GR SA
4) AM QR GR SA

Number 4 is probably the cheapest, and the thinnest; except for the armour layer, the thickness of two filter layers of combination 4 becomes 3x0.3 + 0.3 = 1.2 m.

answer 16.5

The storm surge takes t = 8x200 = 1600 s {equal to 26.6 minutes). The required data are

- $c_v = k/\gamma_w\alpha = 0.002$ m^2/s
- $\theta = 3c_v/d^2 = 3.75$E-4 s^{-1}
- $\sigma'_0 = 20000$ N/m^2 (the average stress at 2 m depth)
- $\psi_0 = f_N\, r\psi'\sigma'_0/N_l$ =0.125x0.65x0.3x20000/50 = 9.75 N/sm^2
- $\delta = (1-n)\psi 0\alpha/\Delta n$ = 0.6x9.75xE-5/0.02 = 2.93E-3 s-1

Three situations are considered.

1. Undrained: $\theta = \delta = 0$. According to (16.28) the average excess pore pressure after the storm surge at t = 1600 s becomes $u_m = \psi_0$ = 9.75x1600 = 15600 N/m^2, which is 78% of the average initial effective stress.

2. Drained without preshearing: $\delta = 0$. There is no t_m. The average excess pore pressure after the storm surge at t = 1600 s becomes $u_m = \psi_0(1 - \exp(-\theta t_m))/\theta$ = 9.75(1− exp(−3.75E-4x1600))/ 3.75E-4 = 11730 N/m^2, which is 59% of the average initial effective stress.

3. Drained and preshearing. $t_m = \ln(\theta/\delta)/(\theta-\delta)$= ln(3.75E-4/2.93E-3)/(3.75E-4−2.93E-3) = 805 s. So, a maximum average pore pressure occurs during the wave train, and becomes $u_m = \psi_0(\exp(-\delta t_m) - \exp(-\theta t_m)/(\theta - \delta)$ = 9.75(exp(−2.93E-3x805)− exp(−3.75E-4x805))/ (3.75E-4−2.93E-3) = 2460 N/m^2, which is 12.3% of the average initial effective stress.

Finally, there will be no liquefaction. The shear strength is decreased by circa 12%, a maximum reached after 15 minutes from the start of the heavy wave attack.

answer 16.6

$\lambda_\omega = (KDT/n\pi)^{0.5}$ = (0.1x10x12/0.4xπ)$^{0.5}$ = 3.09 m
$\xi = c_a H^2/(2\pi\lambda_\omega D\tan\alpha)$ = 1x6^2 / (2πx3.09x10x0.839) = 0.221
From Fig 16.2: $\ln(L/\lambda_\omega)$ = ln(10/3.09) = 1.174 → F = 0.84
$S/H = (1+\xi F)^{0.5} - 1$ = (1+0.221x0.84)$^{0.5}$ – 1 = 0.0889 → S = 0.889x6 = 0.53 m

RECOMMENDED LITERATURE

The text of this introductory book is for a significant part based on input from a wide range of comprehensive textbooks and some trend-setting articles and reports, which are mentioned in this recommended reference list.

Aziz, K., and Settari, T. (1997) *Petroleum reservoir simulation.* Appl Science Pub, 475 pages.

Azizi, F. (1999) *Applied analysis in geotechnics.* Spon Press, London. 776 pages.

Barends, F.B.J. (2005) *Associating with Advancing Insight*. Terzaghi Oration, Proc XVI-ICSMGE Osaka, Millpress Rotterdam, Vol 1, p217-248.

Bear, J. (1972) *Dynamics of fluids in porous media.* Elsevier PC, Amsterdam, 764 pages.

Bolton, M.D. (1986) *The strength and dilatancy of sands.* Géotechnique 36(1), p65-78.

Bowles, J.E. (1988) *Foundation analysis and design.* 4th ed. McGraw-Hill BC Int., 1004 pages.

Coduto, D.P., Yeung M-C.R., and Kitch, W.A. (2011) *Geotechnical engineering; principles and practice*. Pearson Edu., New Yersey, 2nd ed., 814 pages.

Craig, R.F. (1992) *Soil mechanics*. 6th ed. E & FN Spon, 432 pages.

CUR (1996) *Building on soft soil*. Balkema Pub. 386 pages.

Frank, R., Bauduin, C., Driscoll, R., Kavvadas, M., Krebs Ovesen, N., Orr, T., and Schuppener, B. (editors) (2004). *Designers' guide to EN 1997-1 Eurocode 7: Geotechnical design - General rules*. Thomas Telford, 232 pages.

GeoTechNet (2006) WP3: *Innovative design methods in geotechnical engineering, background document on the use of finite element and finite difference methods in geotechnical engineering.* www.geotechnet.org, 90 pages

Haan, E.J. den, Termaat, R., and Edil, T.B. (eds) (1994) *Advances in understanding and modelling the mechanical behaviour of peat.* Int. Workshop Delft, Balkema Rotterdam, 428 pages.

Haan, E.J. den, and Kruse, G.A.M. (2007) *Characterisation and engineering properties of Dutch peats.* Proc. IC on Characterisation and Engineering Properties of Natural Soils (eds Hight and Leroueil). Taylor and Francis, London, p:2101-2133

Hanson, J.L.R., and Termaat, R.J. (2001) *Soft ground technology*. ASCE Geotechnical Special, Nr 112, 500 pages.

Josselin de Jong, G. De (1988) *Elasto-plastic version of the double sliding model in undrained simple shear tests.* Géotechnique, 38(4), p533-555.

Kerisel, J. (1991) *Down to Earth, Foundations Past and Present, the Invisible Art of the Builder*. Balkema, Rotterdam, 150 pages

Kroonenberg, S.B. (2006) *The human scale (de menselijke maat), the earth ten thousand years from now*. Atlas Publisher, 334 pages.

Lambe, T.W., and Whitman, R.V. (1969) *Soil mechanics.* John Wiley Inc., London, 553 pages.

Lancellotta, R. (1987) *Geotechnical engineering.* Balkema, Rotterdam, 436 pages.

Leroueil, S., Magnan J-P., and Tavenas, F. (1990) *Embankments on soft clays.* Ellis Horwood Pub. 360 pages.

Mair, R. (2011) *Tunnelling and deep excavations; ground movements and their effects*. Keynote Lecture, XV ECSMGE Athens, IOSS Press.

Mayne, P.W., Coop, M.R., Springman, S.M., Huang, A-B., and Zornberg, J.G. (2009) *Geomaterial behaviour and testing.* Proc. XVII ICSMGE (eds Hamza et all), IOS Press, p2777-2872.

Muni Budhu (2007) *Soil mechanics and foundations.* 2nd ed. John Wiley & Sons, New York. 634 pages.

Nicholson, D., Tse, C, and Penny, C. (1999) *The observational method in ground engineering; principles and applications.* Report 185, CIRIA, London.

Pilarczyk, K.W. (2000) *Geosynthetics and geo-systems in hydraulic and coastal engineering*. Balkema R'dam, 913 pages.

Potts, M.D., and Zdravković, L. (1999 & 2001) *Finite element analysis in geotechnical engineering.* Thomas Telford Pub, 2 Volumes, 440 & 420 pages.

Powri, W. (2004) *Soil mechanics, concepts and applications.* 2nd ed. Spon Press, London. 704 pages.

Schofield, A. (2005) *Disturbed soil properties.* Thomas Telford, London. 142 pages.

Schotting, R.J., van Duin, C.J., and Verruijt, A. (editors) (2006) *Soil mechanics and transport in porous media; selected works of G. de Josselin de Jong.* Springer, 362 pages.

Springman, S. (editor) (2002) *Constitutive and centrifuge modelling: two extremes.* Workshop at Monte Verità, Balkema, 379 pages.

Steenfelt, J.S. (2004) *Guestimate of φ', c' and ψ for coarse soils.* Danish National Lecture – NGM, Ystad, Sweden, 14 pages.

Terzaghi, K., Peck, R.B., and Mesri, G. (1996) *Soil mechanics in engineering practice.* John Wiley Inc., London, 553 pages.

Teunissen, J.A.M. (2007) *On double shearing in frictional materials*. Int. J. Numerical and Analytical Methods in Geomechics, 2007; 31:23–51.

Tsuchida, T., Watabe, Y., Kang, M., Kusakabe, O., and Terahsi, M. (editors) (2003) *Soft ground engineering in coastal areas.* Nakase Memorial Symposium. Balkema, Rotterdam, 423 pages

Vaníček, I., and Vaníček, M. (2008) *Earth structures in transport, water and environmental engineering.* Springer, 637 pages.

Van Staveren, M.Th. (2006) *Uncertainty and ground conditions – a risk management approach*, Elsevier Publishers, Oxford, 321 pages.

Verruijt, A. (1995) *Computational Geomechanics*. Kluwer Academic Pub., 383 pages.

Verruijt, A. (1999) *Grondmechanica*. 5th edition, VSSD Delft, 295 pages.

Verruijt, A. (2010) *An introduction to Soil Dynamics.* SpringerS+B Media BV, 433 pages.

Waterman, R.E. (2008) *Towards an integrated coastal policy via building with nature*. Printed by Opmeer, the Hague, 450 pages.

Whitlow, R. (1996) *Basic soil mechanics*. 3d edition, Longman Malaysia, 559 pages.

Wolf, J.P., and Deeks, A,J, (2004) *Foundation vibration analysis: a strength of material approach*. Elsevier PC, 240 pages.

Wood, D.M. (1991) *Soil behaviour and critical state soil mechanics*. Cambridge University Press, 486 pages.

ABOUT THE AUTHOR

The author of this book, Frans B. J. Barends, born in Arnhem the Netherlands, in 1946, grew up as eldest son with four sisters and four brothers, completed the Gymnasium in 1965 and M-Sc Civil Engineering at the Technical University Delft in 1971, topic theoretical soil mechanics. After some years, as research fellow in the group of De Josselin de Jong and Verruijt and a scholarship at the Technion Haifa under Bear. Thereafter, he joined the Laboratory of Soil Mechanics in Delft, in 1974. He married Echlaas Zoabi and they got three children.

As a young engineer, Frans Barends was involved in the Delta project, a huge national effort to protect the lowlands of the Netherlands against the sea after the devastating storm of 1953. His career developed typically along two paths, management and science, as a scientific engineer.

Manager of the Mathematics and Informatics Department in the period 1979 to 1988 during the boost of computer model development, Head of the Research Department, Director Scientific affairs, and since 2008 Member of the Science Council of Deltares, into which the geotechnical institute merged in 2008. Deltares' task is the translation of ideas and concepts for practical application, in the field of delta technology. Its slogan is Enabling Delta Life.

In 1980, Frans Barends achieved the title Doctor in Technical Sciences with a thesis on Non-Linearity in Groundwater Flow. He lectured groundwater flow at IHE Institute for Water Education in Delft from 1980 to 1988, and became in 1988 part-time Professor in Groundwater Mechanics at the Department of Civil Engineering of the Technical University Delft, one-day a week until 2010, where he taught three courses: Groundwater Flow, Theory of Consolidation and Introduction to Soft Soils Geotechnique. Under his guidance, 10 Ph-D candidates performed their studies on various topics

Evert den Haan, *Vertical Compression of Soils*, TUD1994 (copromotor)
Paul Hölscher, *Dynamic Response of Saturated and Dry Soils*, TUD1995
Amro ElFeki, *Stochastic Characterization of Geological Heterogeneity*, TUD1996
Bernadette Wichman, *Consolidation Behaviour of Gassy Mud*, TUD1999 (partly)
Xiaohui Cheng, *Localisation in Dutch Dune Sand and Organic Clay*, TUD2004
Cor Zwanenburg, *The Influence of Anisotropy on the Behaviour of Peat*, TUD2005
John van Esch, *Adaptive Multiscale FEM for Surface Flow Simulation*, TUD2010
Bruno Coelho, *Dynamics of Railway Transition Zones in Soft Soils*, TUD2011
Sanaz Saied, *Transport aspects of Geothermal Energy*, TUD2012
Vera van Beek, *Displacement and Erosion Piping*, TUD2014

Through active guidance and teaching, and the involvement in many challenging projects Prof. Dr. Frans B. J. Barends became an expert in the field of geotechnical engineering. As a specialist in groundwater mechanics, transport phenomena and consolidation in soils, he wrote/edited eighteen books and published over 200 articles and reports. He was assigned to dozens of appealing projects, such as

2008-2011: Restoration of canal dike systems in Egypt, for NWRI-CRi.

2007-2009: Claim damage Barcelona Harbour, for Generali, London.

2002-2011: Land subsidence and environmental impact gas fields, for Eni Italy.

2004-2008: Coastline stability in The Netherlands, for RWS.

2000-2003: Claim stagnation Western Scheldt TBM, for Min VenW.

1998-2000: Geomechanical Aspects in the Dutch Mining Law, for Min Econ. Affairs.

1996-1997: Damage claim Wilhelmina Metro Tunnel, Rotterdam, for GWR.

1992-1996: National R&D-program Underground Construction, for RWS

1992-1994: Relation earthquakes/gas production, BOA committee, Dutch Government.

1991-1992: Embankment Stability Assessment Study, for Shimizu Corporation, Japan.

1986-1989: Assessment transient seepage in dike design and maintenance, for RWS.

1983-1985: Computer simulation in probabilistic design of breakwaters, for CUR.

1980-1987: Land subsidence by oil/gas production, Bolivar Coast, for Maraven.

1980-1983: Evaluation breakwaters: Sines (Portugal), Tripoli (Libya), Arzew (Algeria).

1974-1980: Geo-hydraulic stability, Eastern Scheldt Storm Surge Barrier, for RWS.

Professor Barends presented many lectures, amongst these the prestigious Terzaghi Oration at the XVI ICSMGE (2005), the Prague Geotechnical Lecture (2007) and the Keverling Buisman Lecture (2009). He taught at IHE in Delft, in La Sapienza Rome, in DRPI Kyoto, and in the Bundes Anstalt für Wasserbau, Neurenberg. He received a medallion of his work for the Eastern Scheldt Barrier 1986, the Dutch Geo-Oscar award 2006 GT, an award by USACE-ERDC (Vicksburg) in 2008 for help in New-Orleans after Katrina hurricane, and the Royal Institute of Engineers (KIVI) Research Prize 2008.

Professor Barends is member of the Dutch Governmental Technical Committee on Land Movement (TCBB), member of the Dutch Governmental Technical Committee on Land Protection (TCB), former member of the Dutch governmental committee on flood defence structures (ENW), founder of the European Large Geotechnical Institutes Platform (ELGIP) and member of the UNESCO Working Group on land subsidence.

List of books, supported by professor Barends

2011: *Introduction to Soft Soil Geotechnique, Content, Context and Application* (author), IOS Press, 364p.

2008: *Land Subsidence at the Dutch Coast; state of the art* (editors Barends, Dillingh, Hanssen and Van Onselen), IOS Press, 300p.

2005: *Multi-disciplinary Assessment of Subsidence Phenomena on the Ravenna Area* (editors Barends, Carbognin, Gambolati and Steedman), Special Proceedings SISOLS 2005, Millpress, 171p.

2003: *Measuring Land Subsidence* (editors Barends, Kenselaar and Schröder) (Dutch), Proceedings Symposium Monitoring Landsubsidence in the Netherlands, NCG (KNAW) 39, Delft, Netherlands. 91p.

2002: *Learned and applied; Soil mechanics out of Delft* (editors: Barends and Steijger), Tribute to Professor Verruijt, Balkema, 218p.

2000: *The Role of Experimental Research in the International World* (organisor), International Workshop, GeoDelft, 150p.

1999: *Geotechnical Engineering for Transportation Infrastructure* (editors Barends, Lindenberg, Luger, de Quelerij and Verruijt), Proceedings XII ECSMGE 1999 Amsterdam, Balkema, 4 Volumes, ca 2500p.

1997: *Groundwater Contaminant Transport; Impact of Heterogeneous Characterization and a New View on Dispersion* (authors Elfeki, Uffink and Barends), Balkema Rotterdam, 316p.

1995: *River, Coastal and Shoreline Protection: Erosion Control using RipRap and Armour Stone* (editors Thorne, Abt, Barends, Maynard and Pilarczyk), Wiley, New York, 784p.

1995: *Land Subsidence* (editors Barends, Brouwer and Schröder), Proceedings FISOLS 95, IAHS-Press, Wallingford, nr 234, Volume I, 492p, and Balkema Rotterdam, Volume II, 409p.

1993: *Physical Processes and Design Tools, Geotechnical Interactions* (author), Chapter in Coastal, Estuarial and Harbour Engineering Reference Book, Chapman Pub, London, 24p.

1992: (editor) Proceedings IV International Conference on Stress Wave Theory to Piles, Balkema PC, Rotterdam, 710p.

1989: *Hydro-Mechanics in Porous Media in the Marine Environment* (author), Chapter in Handbook Marine Structures, CUR-CIRIA, London, 43p.

1985: *Computer aided evaluation of the reliability of a breakwater design* (editor), CIAD, 124p.

1981: *Flow and Transport in Porous Media* (editors Verruijt and Barends), EuroMech Balkema Rotterdam, 232p.

1980: *Tribute to Professor De Josselin de Jong* (editor), LGM-Mededelingen XIX-2, 96p.

1980: *Non-Linearity in Groundwater Flow* (author), Dr-Thesis, TU Delft, LGM-Mededelingen XXI-1 ,120p.

1978: *Advanced Methods in Groundwater Flow Computation* (author), LGM-Mededelingen XIX, 145p.

THE MAGIC OF GEOTECHNICS[65]

In the Terzaghi Oration at the 16th ICSMGE in Osaka, September 2005, Prof Dr F.B.J. Barends addressed the role of knowledge in modern societies and the different way technicians must adopt to become and remain a successful contributing partner in protecting and improving quality of life at our planet. Here some highlights from the Terzaghi Oration. The main message is: expose your knowledge and skills.

UNCERTAIN GEOTECHNIQUE

Uncertainty is characteristic for geotechnique, much more than in other branches of technique, but societies are less inclined to accept that we (geotechnical

[65] Author: Jurjen van Deen, 2006, Geotechniek, January 2006, 16-17

engineers) do not know. This creates a tension between geotechnical profession and society. The fact that engineers are not consistent with systematically handling uncertainty, makes the situation even worse. It is essential that we communicate with the world around us how we can manage the uncertainty in a societal context, in a broader risk perception and control. Barends' slogan is: from uncertain safety to safe uncertainty. Here, knowledge plays an important role and the communication of the value of this knowledge is a challenge for the geotechnical engineers of today.

TECHNOLOGY CYCLE

Knowledge we gained in a technical ambience – civil engineering, or more precisely geotechnical engineering – is developed in a cycle. According to Barends this cycle has four essential elements: field testing, lab testing, modelling, led by 'man'. Field tests provide practical experience, sometimes really in the form of loading tests, but more often by just doing: make a design, execute its construction, and observe that it works just slightly differently than anticipated. Phenomena not understood are investigated by experiments in model tests in the laboratory. They lead to new concepts and new designs. The models are usually precipitated in numerical calculation codes, in the silicon of chips in a PC.

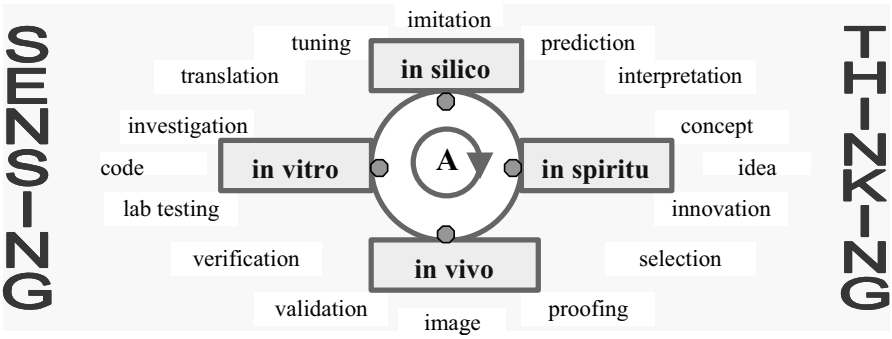

Figure III.1 The knowledge innovation cycle

With a wink to the medical profession one could state that field tests are 'in vivo' (life), model tests are 'in vitro' (test tube), and numerical models 'in silico' (in the chips). At last, for the creation of technical innovations a process of observation, association and thinking 'in spiritu' in the human mind is required. Since the developments in knowledge management and ICT are so rapid and have such an impact in coming years, the element 'in silico' needs much attention.

knowledge		*general perspectives*		
		feature	*appearance*	*feeling*
mode	1	facts	data	veni
	2	experience	meaning	vidi
	3	wisdom	value	vici

Following Barends, knowledge has various forms of appearance: facts, experience and wisdom. At the level of 'facts' an abundance of data is available (internet, Google). However, it is still a challenge to catch reality by facts, i.e. to make facts transparent, consistent and complete, stored in a collective memory. A step further is 'experience' or expert knowledge. Facts elaborated into insights are compiled in handbooks, encyclopaedia, theses, publications and software. We should make effort to store this information electronically in 'collective brains' with a structure that is logical and communicative, and above all associative. Expertise-bases are the answer with which a free traffic of ideas and expertise become possible in selective networks and groups. A nice example is the concept GeoBrain, recently launched by Deltares. The biggest challenge for knowledge management is the creation of the coupling with value concepts. The ever increasing interlacing of technique and society requests therefore that ecological, social, cultural and economical values play a role in knowledge development. Barends introduced for this 'value-base' as the new carrier. In future societies will demand this form of ICT support for many issues.

CONTEXTUALISATION

The interlacing of technique and society, or the contextualisation, is a crucial point. The systematic development of knowledge has to be implemented in the society as well, so that the technical innovation also leads to societal innovation. It is convenient to use a model for societal innovation. The World Bank recognises three key factors: economy, culture and nature. As a fourth key factor Barends adds science (or technology), which remarkably is missing in the list of the World Bank. Science and technology seem not to be recognised, even worse, not to be respected. To achieve this recognition again, the engineer needs to bring the value of his contribution in societal spotlights.

In the past the development of science and technology was an autonomous process, devoted to knowledge, with its own truth, not influenced by political or economical reflections. Independence was considered essential in order to give a rational and objective support to political, economical and cultural processes. In the present-day society the integration of authority, market, culture and science has become so intense that independent science and technology cannot anymore provide solutions for societal problems. Think about pollution, biotechnology, medical-ethical issues, and weapons. Societal questions and doubts became an integral part of scientific research and technological innovations. This change has far reaching consequences for the functioning, the image and the justification of science and technology. Classic criteria for validation of scientific efforts, such as accuracy, objectivity and truth, are supplemented by societal and practical robustness criteria. Truth becomes negotiable. Decisions are taken in a new agora, a virtual market where public and private interests meet, differences in views flourish, and where – if they want to be recognised – researchers must raise their voice. This is the modern context for technique and science.

The question is how (geo)engineers can make themselves understandable. To let others listen it is essential to know the wishes and concerns of the listener and to phrase the arguments in corresponding terms. Politicians are not interested in cost

reduction, the industry has no need for perfection, and managers do not like probabilities or risks. Authorities choose an incremental approach, while technicians prefer an integral total solution. It is ironic that technicians and managers call the other slow and non-reactant. But managers and politicians are the deciders. Hence, technicians must learn to speak in managerial terms. To carry the message the media are crucial. They have at present a dominant role in determining the societal agenda, and in prioritising investments.

How can we cross this knowledge barrier, how make science and technology transparent and society robust without concessions to technical quality and reliability? At European level a start has been made by formulation of a mission statement for the sector, carried by new networks of which ELGIP (European Large Geotechnical Institutes Platform) represents the geo-engineering branch. ELGIP formulated the mission in four items

- Geo-engineering plays a key role in society, because every building and element of the infrastructure stands in or on ground.
- Ground is a natural product. Uncertainties in material behaviour and spatial variation have therefore led to a profession with an intrinsically empirical feature.
- Societal and economical damage by natural hazards (floods, earthquakes, landslides, storms) are underestimated and efforts to prevent damage are marginal.
- The geo-engineering challenge is to bring its value under the spotlights in order to guarantee more safety and sustainability for a higher quality of life.

Barends' vision may be partly impaired, but it can work as a stimulator, as a sketch of the roadmap where everyone can find his way. For geo-engineers a lot of 'value' has to be disseminated. Networks inside, but much more outside, are crucial because the interlacing of technique and society will only increase. As a metaphor for creating a roadmap Barends uses a real spider web and he writes:

The spider is showing us how to network
Using fabulous art and unbelievable skill
With daily maintenance, no energy spilled
Crossing inaccessible gaps and gorges
By using just gravity and natural wind.

SYMBOLS, STANDARDS, UNITS, KEYWORDS

TABLE IV.1 A LIST OF COMMONLY USED SYMBOLS

bar	(gas)pressure;	100 kPa		p	pressure; stress	kPa
a b c	modelparameters	1		p'	effective stress	kPa
c	cohesion	kPa=kN/m^2		*psi*	pounds per square inch	6.9kPa
c	damping constant	Ns/m		Q	discharge	m^3/s
C_c	compression index	1		Q	bearing capacity (piles)	kN
CPT	cone penetration test	-		q	seepage velocity	m/s
C_α	creep index	1		q	uniform load	kPa
c_v	consolidation coefficient	m^2/s		q	shear stress in p-q diagram	kPa
c_u, s_u	undrained shear strength	kPa		S	settlement, set-up	m
dyne	unit for force	10^{-5} N		s, θ	saturation degree	1
E	elasticity modulus	MPa		*SPT*	standard penetration test	-
E_m	pressiometer modulus	MPa		*SLS*	service limit state	
e	voids ratio	1		T	waver period	s
F	symbol for force	N		*ULS*	ultimate limit state	
F	stability factor	1		U	uniformity coefficient	1
f	frequency	Hz: 1cycle/s		U	degree of consolidation	1
G	shear modulus	MPa		u	pore water pressure	kPa
g	gravity acceleration	m/s^2		v	specific volume	1+e
h, ϕ	potential head	m		w	water content	1
h_p	pressure head	m		α	uniaxial compressibility	1/kPa
h_c	capillary head	m		γ	shear strain (distortion)	rad
I_l	liquidity index	1		γ	unit weight; = ρg	kN/m^3
I_p	plasticity index	1		γ_i	(partial) safety factor	1
i	hydraulic gradient	1		δ	wall friction angle	^{o}
K	bulk modulus	MPa		ε	strain	1
K_a	active lateral stress ratio	1		ε_v	volumetric strain	1
K_0	neutral lateral stress ratio	1		η	compressibility index; = b	1
K_p	passive lateral stress ratio	1		κ	intrinsic permeability	m^2
k	(hydraulic) permeability	m/s		κ	unloading index; = a	1
K	spring constant	N/m		λ	compressibility index; = b	1
I_l, I_p	Liquidity, Plasticity index	1		μ	dynamic viscosity	Ns/m^2
lb	pound	4.448 N		ν	kinematic viscosity	m^2/s
m_v	coeff. (vert) volume strain	m^2/N		ν	Poisson ratio	1
N	blowcount (SPT)	1		ρ	mass density	kg/m^3
N_q	bearing capacity coeff.	1		σ	normal stress	kPa
n	porosity	1		σ'	normal effective stress	kPa
Pa	unit of stress (Pascal)	N/m^2		τ	shear stress	kPa
OCR	overconsolidation ratio	1		φ	internal friction angle	^{o}

Internationally accepted standards are found in codes of practice, such as NEN (Dutch norms): 6740 (basics), 6702 (loading), 6743 (piles), 6744 (shallow foundation), 6745 (loading tests), BS (British Standards Institution, 1981), ASTM (American Society for Testing Materials, 1995-2005), DIN (Deutsches Institut für Normierung, 1985), ISO norms for field and lab testing, and in Eurocode 7. Units should follow the SI-metric system (Système Internationale des Poids et Mesures), which is in terms of length (m), mass (kg) and seconds (s). If applicable prefixed notations are used, such as μ (micro = *10^{-6}), k (kilo = *10^3), and M (= * 10^6), and in soil mechanics sometimes non-SI units are

used, such as μ (micron, instead of μm), Atmosphere (≈ 1.014 bar = 0.1 MN/m^2), day (= 24 hrs) and ^{o} for angles (= π/180 rad).

TABLE IV.2 COMMONLY USED GEOTECHNICAL KEYWORDS

Structure	*Objective*	*Method*	*Process*
Airfield	Biology	Boring	Adsorption
Anchor	Chemistry	Cement mixing	Arching
Barrier	Clay	Centrifuge test	Biodegradation
Breakwater	Communication	CPT	Cohesion
Bridge	Damage	Database	Collapse
Building pit	Design	Drains	Conductivity
Coastal structure	Durability	Dredging	Consolidation
Dam	Economy	Drilling	Contraction
Dike	Education	Excavation	Creep
Disposal	Environment	Field test	Deformation
Earth work	Evaluation	Foam	Dilatancy
Embankment	Geology	Geotextile	Dispersion
Foundation	Knowledge	GIS	Drainage
Harbour	Legislation	GPS	Dynamics
Land fill	Maintenance	Ground radar	Earthquake
Reclamation	Management	Grouting	Elasticity
Offshore structure	Mechanism	ICT	Erosion
Pile	Nature	InSAR	Failure
Pipeline	Optimization	Image processing	Flooding
Plate	Organic soil	Injection	Fracturing
Quay	Parameter	Inversion	Freezing
Raft	Peat	Isolation	Friction
Railway	Policy	Laboratory test	Infiltration
Reinforced earth	Process	Literature	Interaction
Reservoir	Purification	Model test	Leaching
Retaining wall	Quality control	Mixing	Leakage
Revetment	Recovery	Monitoring	Liquefaction
Road	Risk	Numerical analysis	Migration
Sheetpiling	Rock	Observation	Piping
Slope	Safety	Prediction	Plasticity
Sluice	Sand	Preloading	Pore pressure
Soil protection	Sanitation	Probabilistics	Pressure
Trench	Scale effect	Probe test	Sedimentation
Tunnel	Site	Reinforcement	Settlement
Underground	Stability	Remediation	Shear
Wall	Temperature	Sand column	Sliding
Waste	Theory	Sealing	Statistics
Waterway	Time effect	Seismic	Strength
Weir	Two-phase	Software	Stress
	Uncertainty	Sounding	Swell
	Validation		Transport
	Wave		Wear

For the characterisation of geotechnical activities keywords are commonly applied. Table 1V.2 compiles a keyword vocabulary distinguishing 4 items: geotechnical structures, objectives, methods and physical processes. A process, product, publication or other can be best characterised by choosing from each item not more than two keywords. This table can also be applied by searching a specific topic on the Internet.

NAME INDEX

Specific references are not given. This name index compiles the specialists mentioned in this book. The reader looking for detailed information may consult Internet with the name and some keywords related to the specific topic.

Steven Abt 341
Eduardo Alonso 46
Samuel Amar 46
Andreas Anagnostopoulos 46
Knut Andersen 46
Akira Asaoka 83
Khalid Aziz 144, 337
Frans Barends 46, 86, 109, 113, 123, 241, 268, 281, 285, 339
Jacob Bear 230, 337
Reginald Barron 215
Nick Barton 267
Vera van Beek 339
Edouard de Beer 197
Ulf Bergdahl 46
Adam Bezuijen 284
Maurice Biot 21, 51, 140, 149
Alan Bishop 170
Thomas Bles 126,130
William Bligh 61
Reint de Boer 19
Malcolm Bolton 137, 337
Joseph Valentin Boussinesq 14, 200
Joseph Bowles 337
Heinz Brandl 46
Henrico Brignoli 46
Jørgen Brinch Hansen 164, 192
Frits Brouwer 341
Muni Budhu 338
John Burland 16, 198
M. Bustamante 197
Laura Carbognin 340
John Carter 201
Arthur Casagrande 28, 83
Xiaohui Cheng 339
Bruno Coelho 339
Charles-Augustin Coulomb 14, 44, 176
Man-chu Conduto 337
Matthew Coop 337
Robert Craig 337
Karl Cullman 167
David Cummings 37
Henry Darcy 15, 55
Neil Davis 146
Andrew Deeks 198
Jurjen van Deen 343
Geert Degrande 206
Douwe Dillingh 340
Heinz Duddeck 262
Hans van Duin 338
Tuncer Edil 337
Victor Ehlers 201
Suzanne van Eekelen 223
Amro Elfeki 339, 341
John van Esch 339
Martin Fahey 201
Eric Farell 46
Wolmar Fellenius 169
Adolf Fick 230
Paul Fillunger 19
Roger Frank 198, 337
Giuseppe Gambolati 340
Gideon Gartner 109
John Garlanger 77
Jacques Garnier 46
Jan Geertsma 149, 244
Robert Gibson 205
Antonio Gomes Correia 46
Maarten de Groot 287
Gerd Gudehus 142
Evert den Haan 77, 140, 337, 339
Alim Hannoura 268
Ramon Hansen 237, 340
James Hanson 337
Mahdi Hantush 113, 241
Majid Hassanizadeh 230
Bas Hemmen 130
Adolf Herz 149
Paul Hölscher 199, 206, 284, 339
Adriaan Houtenbos 246
A-B Huang 337
Viacheslav Ilychev 46
William van Impe 46
Emöke Imre 46
Kenji Ishihara 46
Moust Jacobsen 196
Michael Jamiolkowski 29, 46
Jilmar Janbu 70, 170, 195
Igor Jankovic 231
Richard Jardine 197

Gerard de Josselin de Jong 19, 22, 141, 230, 337, 341
Minsoo Kang 338
Rolf Katzenbach 193
Michael Kavvadas 46
Frank Kenton 37
Frank Kenselaar 340
Jean Kerisel 337
Albert S. Keverling Buisman 18
William Kitch 337
Helmut Kobus 46
Ichiro Kono 148
Fritz Kötter 181, 189
Dimitrios Kolymbas 142
Salle Kroonenberg 337
Gerard Kruse 140, 337
Osamu Kusakabe 338
T. William Lambe 337
Suzanne Lacasse 46
Renato Lancelotta 337
Barry Lehane 197
Serge Leroueil 337
Jaap Lindenberg 287, 341
Andrew Littlejohn 37
Dirk Luger 341
Jean-Pierre Magnan 337
Robert Mair 252, 337
Iacinto Manoliu 46
Rainer Massarch 46
Stephen Maynord 341
Paul Mayne 201, 337
Jentsje van der Meer 316, 338
Gholamreza Mesri 46, 338
Gerard van Meurs 227
Otto Meyerhof 192, 198
Peter Mitchell 142
Frans Molenkamp 46
Norbert Morgenstern 170
Nathan Newmark 201
Duncan Nicholson 337
Manfred Nussbaumer 46
Kyra Van Onselen 340
Trevor Orr 46
Ad van Os 287
Hocine Oumeraci 46
Ralph Peck 252, 338
Jean Claude Eugène Péclet 236
Charles Penny 338
Kristian Pilarczyk 337, 341
David Potts 144, 338
Harry Poulos 201
William Powri 206, 338
K Prakash 83
Ludwig Prandtl 164, 189
David Price 170
Louis de Quelerij 341
Mark Randolph 201
William Rankin 252
William John Macquorn Rankine 44
Eric Reissner 190
Huub Rijnaarts 227
Bengt Rydell 46
Cesar Sagaseta 46
Sanaz Saied 236, 339
Jean Claude Barré de Saint-Venant 51
Frans Schröder 340, 341
Andrew Schofield 44, 138, 338
Ruud Schotting 338
Timo Schweckendiek 118
Pedro Sêco e Pinto 46
Hideo Sekiguchi 46, 142
Hans Sellmeijer 61
Toni Settari 337
Alec Skempton 102
V.V. Sokolovski 14
Eric Spencer 170
Sarah Springman 46, 337, 338
Asuri Sridharan 83
Martin van Staveren 124, 338
Jørgen Steenfelt 46, 137, 338
Scott Steedman 340
Paula Steiger 340
John Stephens 243
Simon Stevin 12
Marcel Stive 314
Theo Stoutjesdijk 287
Otto Strack 230
Francois Tavenas 337
Neils Taylor 46
Donald Taylor 44, 83, 168
Masaaki Terashi 338
Ruud Termaat 337
Karl Terzaghi 18, 51, 72, 81, 192, 338
Hans Teunissen 142, 146, 284, 338
Charles Vernon Theis 113, 240
Colin Thorne 341
Ergün Togrol 46
Frits van Tol 124, 197
Che-Ming Tse 338
Takashi Tsuchida 338
Gerard Uffink 341
Meindert Van 171
Johannes Diederik van der Waals 228
Ivan Vaníček 338

Martin Vaníček 338
Ben Veltman 46
Pieter Vermeer 46, 141
Arnold Verruijt 22, 46, 84, 149, 203, 206, 258, 276, 287, 338, 341
Aleksandar Vesić 195, 198, 257, 258
Vitruvius 8
Yoichi Watabe 348
Ronald Waterman 312, 338
Bram van Weele 114
Roy Whitlow 338
Robert Whitman 337
Bernadette Wichman 339
Emil Oscar Winkler 205
John Wolf 198
Reinhard Woltman 14
David Muir Wood 29, 338
Peter Wroth 29, 138
Xiangtao Xu 197
Ronald Yeung 337
Lidija Zdravković 144, 337
Kouki Zen 290
Jorge Zornberg 337
Cor Zwanenburg 140, 339

This page intentionally left blank

SUBJECT INDEX

A and B factor 102
abc-model 78
Adsorption 228, 232
Ageing 69, 77, 80
Anisotropy 59, 102, 140
API code 198
Apparent cohesion 96
Aquiclude 53, 240
Aquifer 53, 86, 240
Aquitard 53, 86, 240
Archimedes 7
… Law 52
Arching effect 258
Artificial dispersion 144
Artificial Neural Network (ANN) 61
(Non)-associative behaviour 136, 147
Atterberg limits 28
Bearing capacity 192, 197
Benchmark 247
Bifurcation 145, 286
Bio-chemical process 233
BioGrout 224
BioSealing 223
Biot coefficient 51, 140, 149
Bishop slope stability 170
Bleeding number 236
Blum's method 181
Boiling 59
Bosom dike 301
Boussinesq's problem 200
Breach growth 289
Building pit 124, 249
Camclay model 138
Capillarity 53, 64, 166, 229
Characteristics 25, 177, 227
Chemical equilibrium 233
Circle of Mohr 14, 95
Creep 20, 42, 78, 142, 217
Critical density 45, 137, 270
Coastal structure 277
Coefficient of earth pressure 97
Cofferdam 292
Colmation 269
Column
Deep mixed 219
Compensation grouting 222
Compaction grouting 221
Jet grouting 222
Stone 219
Wooden 219
Compaction coefficient 245
Compatibility 87, 143, 163
Compression 93
Index 29, 70, 73, 77, 138
Uniaxial 72
Cone Penetration Test 38
Consolidation
Coefficient 82, 241
Multi-dimensional 84, 267
One dimensional 80
Process 81
Constitutive
Behaviour 112
Model 135
Contextualisation 345
Continuous sampler 39
Contractancy 45, 93, 103, 136
Convection 32, 230, 234
Coulomb's method 176
Coupled motion 286
Critical damping 204
Critical velocity 206
Cyclic consolidation 271, 277
Cyclic pore pressures 275
Cylindrical cavity
Contracting 256
Expanding 254
Darcy's law 54, 82, 166
Decay factor 232
Deformation 71, 111, 119, 199
Degree of consolidation 82
Deltas of the world 295
Delta Sea project 299
Delta River project 300
Densification 268
Desorption 232
Deviator 95
Deviatoric shear stress 138
Diffusion 230
Dike
Building 298
Design 303
Doweling 153
Enforcement inside 318
Engineering 297
Maintenance 305
Ring approach 304
Technology 311
Dilatancy 16, 45, 93, 103, 136
Dilation angle 94, 137, 146

Dilation parameter 103
Direct Simple Shear 43, 158
Directional drilling 250, 253
Dispersion 230, 235
Dispersivity 230, 235
Distortion 93
Double sliding 141, 158
Drainage capacity 287
Drying 229
Duddeck's method 262
Duncan-Chang model 140
Dupuit's formula 59
Dynamic
  Compaction 213
  Response 198, 201
  Slope stability 282
Earth pressure coefficient 97, 98, 99
Earth retaining wall 175
Earthquake impact 283
Effective
  Stress 51
  Mean stress 138
Ehler's model 201
Elasticity modulus 43
Embedded wall 180
Engineering factor 116
Environmental engineering 227
Environmental effect 252
Eurocode 119
Event tree 306
Excavation 178, 252, 263
Experimental model facility 49
Failure mode 306
Fick's law 230
Filter rule 268, 293
Flow rule 136
Footing 189
Free convection 237
Friction angle 14, 29. 44, 101, 137,146
Functional analysis 304
Gas phase 229
Geological strength 26
GeoBrain 127
Geofoam 213
Geodesy 246
Geological system 240
GeoQ 124
Geomechanic modelling 243
Geotextile 222
Gibson soil 205
GPS 247
Gravimetric data 26
Gravity wall 176
Ground improvement
  Bio-chemical 223
  Cunette method 212
  Gravity displacement 211
  Mass stabilisation 214
  Replacement 212
  Stiff inclusion 218
Ground movement 251
Groundwater
  Flow 52, 54
  Gradient 54
  Head 53
  Square flow net 56
Hardening 139
Heat/cold transport 234
Heave 43, 60, 66, 211
Heterogeneity 59
Hydraulic resistance 86, 241, 314
Hydrodynamic period 83, 90, 289
Hydro-geodynamics 267
Hype curve 109
Hysteretic damping 206
Impact loading 204
Index
  Compression 73, 77, 138
  Creep 77, 78
  Inelastic compression 77
  Recompression 73, 77
  Swelling 73, 138
Infiltration test 64
Innovation cycle 342
InSAR 247
Internal set-up 281
Isotache model 78
Kafara Dam 5
Kötter equations 178, 191
Knowledge 109, 116, 124, 129, 342
Laboratory testing
  Density 45
  Falling head 57
  Hele-Shaw 58
  Oedometer 42
  Permeability 42, 53, 57, 68
  Shear box 43
  Triaxial 16, 44, 105, 136, 288
Land fill 103, 270
Land subsidence 239, 241, 298
Lawrence Church 11
Leakage factor 66, 86, 113, 241, 281
Lightweight fill 213
Linear strain 71

Liquefaction 269, 283, 286, 317
Liquefaction potential 269, 287
Liquid phase 228
Limit analysis 163
  Lower limit 163
  Upper limit 163
Localisation 145, 223, 339
Macro dispersion 231
Maxwell's dashpot 80
Ma'arib Dam 6
Method of slices 169
Micro dispersion 230
Mohr-Coulomb model 44, 96, 136
Monitoring 41, 122
Natural strain 71
Negative retardation 280
Numerical
  Simulation 143
  Singularity 148
Observational method 120, 143
Overconsolidation ratio 80
Overtopping 315
Partial safety factor 116, 120
Particle size distribution 27
Peat
  Constitutive model 140
  Dike 316
  Oxidation 243, 298
  Structure 30
Peclet number 236
Period of grace 217
Permeability 31, 68, 83, 135, 224, 268
  Intrinsic 55
  Test 57
pF-curve 229
Physical
  Model testing 46, 133
  Process 113
  Similarity 133
  Simulation 133
Plastic potential 136
Plastic wedge 151
Plasticity 28, 69, 136
Piezometer 54
Pile
  End bearing capacity 195
  Factor 198
  Foundation 193
  Load test 114, 196
  Mattress 223
  Toe 194
Piping 60, 62, 317
Pore pressure 52
pq-diagram 100
Prandtl's solution 189
Preloading 217
Preshearing 287
Principal direction 95
Principle of precaution 121
Pumping
  System 65
  Test 113
Railway embankment 205
Rankine
  Stress state 97
  Wedge 153
Reconnaissance survey 37
Relative density 26, 30, 45, 138, 270
Relative motion 286
Reliability 109
Reservoir modelling 243
Retardation 232, 237, 246, 280
Revetment 311
Risk Management 125
  Dealing with risk 121, 309
Rock strength 267
Rock friction 267
Safety philosophy 304
Saturation 26, 52, 229, 303
Sea-level rise 298
Sea floor liquefaction 289
Scaling 133
Sedimentation 270
Serviceability limit state 119, 163
Shallow trench 171
Sheet piling 115, 130, 187, 292
Site investigation 37
Skempton factors 102
Skin friction 196
Slide
  Cicular 167
  Slope 104
  Translational 164
Slope stability 115, 164, 168
Smartsoils® 223, 234
Softening 69, 139, 145
Soil
  Classification 31
  Investigation 37, 110
  Quality survey 40
Solid phase 228
Specific solid gravity 26
Specific volume 26, 72, 138
Spring-dashpot 201

Squeezing 26, 116, 171, 212, 290
Standard deviation 128
Standard Penetration Test 37
Strain concept 70
Strength
  Critical 146
  Maximum 146
  Residual 146
Stiffness 69
Storativity 87, 113, 241
Stress ratio K_0 70, 146
Strip loading 190
Suction 229
Suction block 289
Suffusion 269
Swelling index 138
Taj Mahal 11
Tortuosity 32
Transient leakage 70, 86
Transport in soil 230
Transport equation 231
Tresca model 96
Triaxial
  Cell 45, 99
  Stress 93
  Test 44, 99
Tunnelling 122, 250, 252, 253, 260
Turbulent porous flow 268
Ultimate limit state 119, 163
Uncertainty 109, 307
Undrained strength 30, 96, 101
Uniaxial compression 71
Uplift 170
Vacuum drainage 216
VanderWaals force 228
Variation coefficient 117
Vertical drainage 214
Vertical stress 52
Vibration 201
Vibro-compaction 214
Viscous behaviour 142
Visco-plasticity 151
Void ratio 26, 71
Wall
  Combi 175, 187, 263
  Diaphragm 122, 168, 182
  Embedded 179
  Gravity 176
  Reinforced 183
  Rough wall 179
  Slurry 168, 182, 216
Water withdrawal 240
Wave
  Impact 284, 285
  On breakwater 281
  On seabed 271
  On structure 276
Wetting 229
Winkler's model 205